Unclassified **NEA/CSNI/R(2005)7**

Organisation de Coopération et de Développement Economiques
Organisation for Economic Co-operation and Development

11-Oct-2005

English text only

NUCLEAR ENERGY AGENCY
COMMITTEE ON THE SAFETY OF NUCLEAR INSTALLATIONS

NEA/CSNI/R(2005)7
Unclassified

INTERNATIONAL STANDARD PROBLEM 48
ANALYSIS OF 1:4-SCALE PRESTRESSED CONCRETE CONTAINMENT VESSEL MODEL UNDER SEVERE ACCIDENT CONDITIONS

Lyon, France
6-7 April 2005

The CD-Rom enclosed in the Synthesis Report contains full papers and presentations.

The complete document is only available in pdf format.

JT00191530

Document complet disponible sur OLIS dans son format d'origine
Complete document available on OLIS in its original format

English text only

ORGANISATION FOR ECONOMIC CO-OPERATION AND DEVELOPMENT

Pursuant to Article 1 of the Convention signed in Paris on 14th December 1960, and which came into force on 30th September 1961, the Organisation for Economic Co-operation and Development (OECD) shall promote policies designed:

- to achieve the highest sustainable economic growth and employment and a rising standard of living in member countries, while maintaining financial stability, and thus to contribute to the development of the world economy;
- to contribute to sound economic expansion in member as well as non-member countries in the process of economic development; and
- to contribute to the expansion of world trade on a multilateral, non-discriminatory basis in accordance with international obligations.

The original member countries of the OECD are Austria, Belgium, Canada, Denmark, France, Germany, Greece, Iceland, Ireland, Italy, Luxembourg, the Netherlands, Norway, Portugal, Spain, Sweden, Switzerland, Turkey, the United Kingdom and the United States. The following countries became members subsequently through accession at the dates indicated hereafter: Japan (28th April 1964), Finland (28th January 1969), Australia (7th June 1971), New Zealand (29th May 1973), Mexico (18th May 1994), the Czech Republic (21st December 1995), Hungary (7th May 1996), Poland (22nd November 1996), Korea (12th December 1996) and the Slovak Republic (14 December 2000). The Commission of the European Communities takes part in the work of the OECD (Article 13 of the OECD Convention).

NUCLEAR ENERGY AGENCY

The OECD Nuclear Energy Agency (NEA) was established on 1st February 1958 under the name of the OEEC European Nuclear Energy Agency. It received its present designation on 20th April 1972, when Japan became its first non-European full member. NEA membership today consists of 28 OECD member countries: Australia, Austria, Belgium, Canada, the Czech Republic, Denmark, Finland, France, Germany, Greece, Hungary, Iceland, Ireland, Italy, Japan, Luxembourg, Mexico, the Netherlands, Norway, Portugal, Republic of Korea, the Slovak Republic, Spain, Sweden, Switzerland, Turkey, the United Kingdom and the United States. The Commission of the European Communities also takes part in the work of the Agency.

The mission of the NEA is:

- to assist its member countries in maintaining and further developing, through international co-operation, the scientific, technological and legal bases required for a safe, environmentally friendly and economical use of nuclear energy for peaceful purposes, as well as
- to provide authoritative assessments and to forge common understandings on key issues, as input to government decisions on nuclear energy policy and to broader OECD policy analyses in areas such as energy and sustainable development.

Specific areas of competence of the NEA include safety and regulation of nuclear activities, radioactive waste management, radiological protection, nuclear science, economic and technical analyses of the nuclear fuel cycle, nuclear law and liability, and public information. The NEA Data Bank provides nuclear data and computer program services for participating countries.

In these and related tasks, the NEA works in close collaboration with the International Atomic Energy Agency in Vienna, with which it has a Co-operation Agreement, as well as with other international organisations in the nuclear field.

© OECD 2005

Permission to reproduce a portion of this work for non-commercial purposes or classroom use should be obtained through the Centre français d'exploitation du droit de copie (CCF), 20, rue des Grands-Augustins, 75006 Paris, France, Tel. (33-1) 44 07 47 70, Fax (33-1) 46 34 67 19, for every country except the United States. In the United States permission should be obtained through the Copyright Clearance Center, Customer Service, (508)750-8400, 222 Rosewood Drive, Danvers, MA 01923, USA, or CCC Online: http://www.copyright.com/. All other applications for permission to reproduce or translate all or part of this book should be made to OECD Publications, 2, rue André-Pascal, 75775 Paris Cedex 16, France.

COMMITTEE ON THE SAFETY OF NUCLEAR INSTALLATIONS

The NEA Committee on the Safety of Nuclear Installations (CSNI) is an international committee made up of senior scientists and engineers, with broad responsibilities for safety technology and research programmes, and representatives from regulatory authorities. It was set up in 1973 to develop and co-ordinate the activities of the NEA concerning the technical aspects of the design, construction and operation of nuclear installations insofar as they affect the safety of such installations.

The committee's purpose is to foster international co-operation in nuclear safety amongst the OECD member countries. The CSNI's main tasks are to exchange technical information and to promote collaboration between research, development, engineering and regulatory organisations; to review operating experience and the state of knowledge on selected topics of nuclear safety technology and safety assessment; to initiate and conduct programmes to overcome discrepancies, develop improvements and research consensus on technical issues; to promote the coordination of work that serve maintaining competence in the nuclear safety matters, including the establishment of joint undertakings.

The committee shall focus primarily on existing power reactors and other nuclear installations; it shall also consider the safety implications of scientific and technical developments of new reactor designs.

In implementing its programme, the CSNI establishes co-operative mechanisms with NEA's Committee on Nuclear Regulatory Activities (CNRA) responsible for the program of the Agency concerning the regulation, licensing and inspection of nuclear installations with regard to safety. It also co-operates with NEA's Committee on Radiation Protection and Public Health (CRPPH), NEA's Radioactive Waste Management Committee (RWMC) and NEA's Nuclear Science Committee (NSC) on matters of common interest.

FOREWORD

At the CSNI meeting in June 2002, the proposal for an International Standard Problem on containment integrity (ISP 48) based on the NRC/NUPEC/Sandia test was approved. Objectives were to extend the understanding of capacities of actual containment structures based on results of the recent PCCV Model test and other previous research. The ISP was sponsored by the USNRC, and results had been made available thanks to NUPEC and to the USNRC. Sandia National Laboratory was contracted to manage the technical aspects of the ISP.

At the end of the ISP48, a workshop was organized in Lyon, France on April 6-7, 2005 hosted by Electricite de France. Its overall objective was to present results obtained by participants in the ISP 48 and to assess the current practices and the state of the art with respect to the calculation of concrete structures under severe accident conditions. Experience from other areas in civil engineering related to the modelling of complex structures was greatly beneficial to all. Information obtained as a result of this assessment were utilized to develop a consensus on these calculations and identify issues or "gaps" in the present knowledge for the primary purpose of formulating and prioritizing research needs on this topic.

The ISP48 exercise was published in the report referenced NEA/CSNI/R(2005)5 in 3 volumes. Volume 1 contains the synthesis of the exercise; Volumes 2 and 3 contain individual contributions of participating organizations.

The CSNI Working Group on the Integrity and Ageing and in particular its sub-group on the behaviour of concrete structures has produced extensive material over the last few years. The complete list of references is given below.

- NEA/CSNI/R(2005)5 – Vol 1 to 3 - International Standard Problem No.48 - Containment Capacity. Synthesis Report - Results of Pressure Loading Analysis
- NEA/CSNI/R(2004)11 International Standard Problem No.48 - Containment Capacity. Phase 2 Report - Results of Pressure Loading Analysis
- NEA/CSNI/R(2004)8 Proceedings of the CSNI/RILEM Workshop on Use and Performance of Concrete in NPP Fuel Cycle Facilities - Hosted by Instituto de Ciencias de la Construcciòn, Eduardo Torroja, Madrid, Spain, on 15-16 March 2004
- NEA/CSNI/R(2002)21 Electrochemical techniques to detect corrosion in concrete structures in nuclear installations - Technical Note
- NEA/CSNI/R(2002)14 Report of the task group reviewing activities in the area of ageing of concrete structures used to construct nuclear power plant fuel-cyle facilities
- NEA/CSNI/R(2002)13 Finite element analysis of ageing reinforced and prestressed concrete structures in nuclear power plants - An international review of current capabilities and priorities for future developments

- NEA/CSNI/R(2002)7 OECD-NEA Workshop on the Evaluation of Defects, Repair Criteria & Methods of Repair for Concrete Structures in Nuclear Power Plants – GRS, Berlin 10/11 April 2002 (Volume I - Volume II)
- NEA/CSNI/R(2000)15 Proceedings of the Workshop on Instrumentation and Monitoring of Concrete Structures, Tractebel, Brussels, 22-23 March 2000
- NEA/CSNI/R(1999)11 Tendon Prestress Loss in NPP Containments (EdF, Poitiers)
- NEA/CSNI/R(1999)1 Proceedings of Workshop on Finite Element Analysis of Degraded Concrete Structures (BNL New York/Oct5. 1998)

The complete list of CSNI reports, and the text of reports from 1993 onwards, is available on http://www.nea.fr/html/nsd/docs/

ACKNOWLEDGMENTS

Gratitude is expressed to Electricite de France, France for hosting the workshop and to the Scientific Committee members for their guidance, expertise and support.

Mr. Michael Hessheimer	SNL	USA
Mr Jean-Luc Valfort	EdF	FR
Dr. Nam-Ho LEE	KOPEC	KR
Mr. Eric MATHET	OECD-NEA	International

The Scientific Committee would like to thank Dr Claude Duval, Mr Etienne Gallitre, Mr Alexis Courtois, Mr Bertrand Perracino and Prof Pierre Labbe of EdF for their support.

TABLE OF CONTENTS

-Summary of NUPEC/NRC 1:4-Scale PCCV Model Tests and
-Summary of ISP48 – Main Results and Conclusions..15
Dr. M. Hessheimer (Sandia National Laboratories- USA)

-Papers on Containment Performance, Finite Element Modeling and Other Issues········· 61
Chairpersons: Dr. Michael Hessheimer (SNL- USA), Mr. Eric Mathet (OECD/NEA-FR)

Contributions:

-Effect of Thermal Loading on Containment Capacity for the International Standard Problem (ISP - 48) Phase 3
Dr. N. K. Prinja and Mr. J. A. Curley (NNC Ltd- UK)
-Paper...**63**
-Presentation...**78**

-FE modelling of reactor containments - some relevant topics
Mr. O. Jovall and Mr. J.-A. Larsson (Scanscot Technology- SWD)
-Paper...**103**
-Presentation...**108**

-Statistical assessment of the prestress level based on in-service inspections of unbonded tendons
Mr. P. Anderson (Lund Uni.- SWD)
-Paper...**115**
-Presentation...**125**

-Probability Nonlinear Analysis of Reinforced Concrete Containment Integrity Considering Degradation Effects and High Internal -Overpressure
Prof. J. Králik (STU- SK)
Department of Structural Analysis, Faculty of Civil Engineering STU in Bratislava, Slovakia
-Paper...**131**

-Analysis of 1:4 scale prestressed concrete containment vessel (PCCV) model subject to pressure and thermal loading
Dr. N.-H. Lee and I.-H. Moon (KOPEC- KR)
-Paper...**143**
-Presentation...**158**

-Indirect Consideration of Unbonded Tendons in 1/4 PCCV Model
H.-G. Kwak, Mr. J. H. Kim (KAIST), Mr. S.-H. Kim (Youngdong Uni.) and Dr. Y.-S. Chung, (KINS- KR)
-Paper...**173**

- Mechanical behavior of containment building PWR 900MW under severe accident «global model »
G. Nahas - JM Rambach - IRSN, France
-Presentation..**183**

-Mechanical behavior of containment building PWR 900MW under severe accident «local model »
B. Ciree - G. Nahas - JM Rambach - IRSN, France
-Presentation..**195**

-The Creep of Confinement Building's Elements, Finite Element Analysis on Confinement, Ageing Program
Mr. C. Nyárádi (NPPP- HUN)
-Paper..**207**
-Presentation..**218**

-GRS calculations on large scale experiments of SANDIA pre-stressed concrete containment model
Dr. H. Grebner and Dr. J. Sievers (GRS- GER)
-Paper..**227**
-Presentation..**255**

-Posttest Analysis of a 1:4 Scale PCCV Model - Effects of Pressure and Temperature Loading
Mr. J. Stepan (NRI Rez- CR)
-Paper..**271**
-Presentation..**300**

-Experimental Studies on the Failure Behaviors of a Prestressed Concrete Containment Building
Dr. Y.S. Choun (KAERI), N.S.Cho (HICTD), and Dr. J.-M. Seo, (KAERI- KR)
-Paper..**309**
-Presentation..**327**

-*A* Summary of Complex Evaluation of the Status of Deliveries for the Mochovce NPP Units 3 and 4
Dr. Juraj Nozdrovický (VÚEZ- SK) and Dr. Martin Moravčík (UTC-SK)
-Paper..**335**

-Topical discussions **343**

Contributions:

-Evaluation and modeling of the ageing of the structure over its lifetime - How does finite element analysis fit in an ageing management program?
Moderator: J.P. Touret (Edf, FR) **345**
Panel Members: O. Jovall (Scanscot Technology,SWD)..**347**
P. Lenkei (Paks NPP, HUN)..**351**

-Suitability of current analytical tools/methods and required model(s) fidelity for realistic capacity estimates - Applicability of standard material test methods for derivation of material constitutive models for large structures subjected to severe damage states. Scale effects between material specimens and structures. Use of laboratory test results for design and performance assessment.

Moderator: *N. Prinja* *(NNC, Ltd, UK)* **353**
Panel Members: *J. Stepan* *(UJV ReZ, CR)* **359**
O. Jovall *(Scanscot Technology,SWD)* **361**

-Application of damage or functional performance criteria, e.g. leakage, to numerical simulations. Consensus on surrogate performance/failure criteria, e.g. strain, for statutory performance criteria. Model dependency of surrogate failure criteria.

Moderator: *M. Hessheimer* *(SNL, USA)* **363**
Panel Members: *J-M. Seo* *(KAERI, KR)* **369**
H. Grebner *(GRS, GER)* **371**
JM. Rambach (IRSN, FR)

-Leak vs. Catastrophic rupture: consequences and design implications

Moderator: *J. Rashid* *(ANATECH, USA)* **373**
Panel Members: J. Gustavsson (Ringhals AB, SWD), *J. Curley* *(NNC, Ltd, UK)* **379**
P. Varpasuo *(Fortum NS, FIN)* **381**

-Integration of best estimate containment capacity/behavior in PRA models and quantification of uncertainties

Moderator: *S. Ali* *(USNRC, USA)* **383**
Panel members: *S. Basha* *(NNC, Ltd, UK)* **389**
N. Lee *(KOPEC, KR)* **393**

-Research needs for advanced and next generation plants, e.g. long term high temperature behavior, confinement (leakage/venting) vs. containment

Moderator: *M. Elgohary* *(AECL, CAN)* **395**
Panel Members: C. Nyaradi (Paks, HUN), *T. Ogata* *(Obayashi Corp., JPN)* **399**

List of participants **403**

The enclosed CD-ROM contains papers and presentations.

Summary of NUPEC/NRC 1:4-Scale PCCV Model Tests

Summary of ISP48 - Main Results and Conclusions

April 6, 2005

Mike Hessheimer
Sandia National Laboratories
Albuquerque, NM USA

Cooperative Containment Research Program Overview

- Program Scope and Objectives:
  - Sponsors:
    - Nuclear Power Engineering Corporation (NUPEC) of Japan
    - U.S. Nuclear Regulatory Commission (NRC), Office of Nuclear Regulatory Research.
  - This research program consisted of testing two scale models: a steel containment vessel (SCV) model (tested in 1996) and a prestressed concrete containment vessel (PCCV) model.
  - The objective of the program is to investigate the response of representative scale models of nuclear containments to pressure loading beyond the design basis accident and to compare analytical predictions to measured behavior.
  - This objective is accomplished by conducting static, pneumatic over-pressurization tests of scale models at ambient temperature.

Project Milestones

• NUPEC-DOE Funds-in Agreement Signed	25 June 91
• PCCV Model Construction Started	3 Jan 97
• First Basemat Pour F1	12 Feb 97
• First Liner Panel Installed	19 June 97
• Final Dome Pour (D3)	15 Apr 99
• PCCV Pretest RR Meeting	12-14 Oct 99
• PCCV Prestressing	8 Mar – 3 May 00
• PCCV Construction Completed	25 June 00
• PCCV Structural Integrity & Integrated Leak Rate Test	12-14 Sep 00
• PCCV Limit State Test	27-28 Sep 00
• PCCV Posttest RR Meeting	22 Aug 01
• PCCV SFMT	14 Nov 02
• PCCV Demolition and Site Restoration Completed	3 May 02

Prestressed Concrete Containment Vessel Model

- Model of the containment structure of Ohi Nuclear Power Station, a large, dry PWR prestressed containment vessel
  - Design pressure is 0.39 MPa (57 psig) :
  - Geometry: configuration and overall dimensions (height, radius, thickness) scaled 1:4.

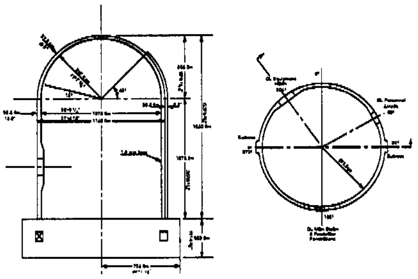

PCCV Pretest Round Robin Participants

- Argonne National Laboratory (ANL)
- Atomic Energy of Canada Limited (AECL)
- Commisariat A L'Energie Atomique/Saclay/DRN (CEA)-presented by IPSN
- Electricite de France/Sechaud et Metz (EDF)
- Institute of Nuclear Energy Research (INER)*
- Institut de Protection et de Sûreté Nucléaire (IPSN)
- Japan Atomic Energy Research Institute/Mitsubishi Heavy Industries (JAERI)*
- Japan Atomic Power Company/PWR Utility Research Group (JAPC)
- Korea Institute of Nuclear Safety (KINS)
- Korea Power Engineering Company (KOPEC)
- H. M. Nuclear Installations Inspectorate/NNC (NII)
- Nuclear Power Engineering Corporation (NUPEC)
- Nuclear Safety Institute (IBRAE)*
- PRINCIPIA-EQE SA
- Russian International Nuclear Safety Center (RINSC)-presented by ANL
- ANATECH/Sandia National Laboratories
- University of Glasgow

* Submitted analysis results, not attending pretest meeting

Low Pressure Testing

- System Functionality Test:
  - The SFT was used to check for leaks in the model and penetrations and verify the functionality of the pressurization system, the installed instruments and the data acquisition system. Leak rate measurement instrumentation was also calibrated during depressurization using calibrated orifice plate.
- Structural Integrity and Integrated Leak Rate Tests
  - The SIT/ILRT reproduced the pre-operational tests conducted at the prototype plant and allow for a comparison of the model's elastic response characteristics and leak behavior with the prototype and pretest analyses.
  - Procedures incorporated a combination of Japanese standards (JEAC 4203-1994, SIT and ILRT) and US requirements (ASME B&PV Code, Section III, Division 2, Article CC-6000 for SIT; 10CFR50, Appendix J "Primary Reactor Containment Leakage Testing for Water-Cooled Power Reactors" for ILRT)

SIT/ILRT (September 12-14, 2001)

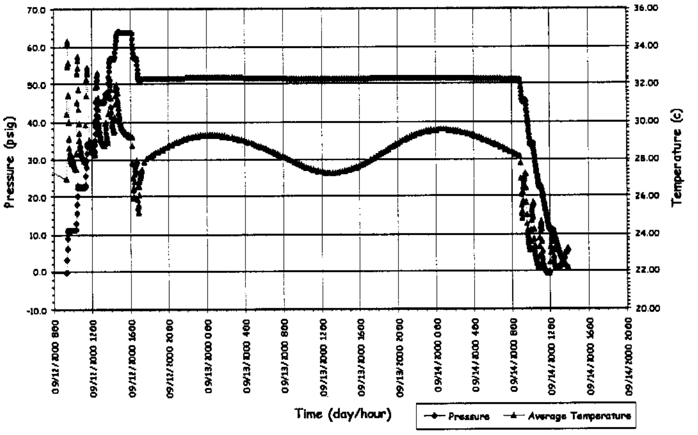

Sandia
National
Laboratories

ILRT Leak Rate Measurement

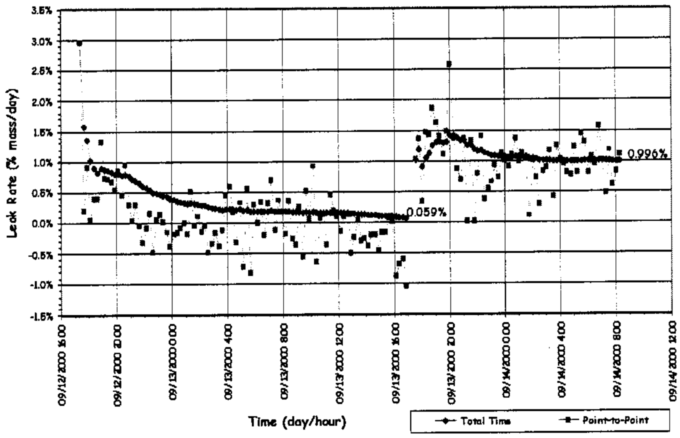

Sandia
National
Laboratories

Limit State Test Conduct & Results

- **The LST fulfilled(?) the primary objectives of the PCCV test program, i.e. to investigate the response of representative models of nuclear containment structures to pressure loading beyond the design basis accident and to compare analytical predictions to measured behavior.**
- **Test Sequence:**
  - **Initial Pressurization: matched SIT pressurization sequence**
  - **Stability Criteria for Data-of-Record:**

$$\frac{Q_t - Q_{t-\Delta t}}{Q_{t-\Delta t}} \le 0.02$$

  - **Pre-planned Leak Checks at 1.5Pd, 2.0Pd and 2.5Pd, estimated after 2.5Pd (PCCV was not isolated during 'rapid' pressurization)**
  - **Termination Criteria: pressure reached the operational limit of the pressurization system, 5000 scfm at approximately 3.3 P_d (1.3 MPa or 188 psig)**

Sandia National Laboratories

LST Pressure & Temperature Time Histories

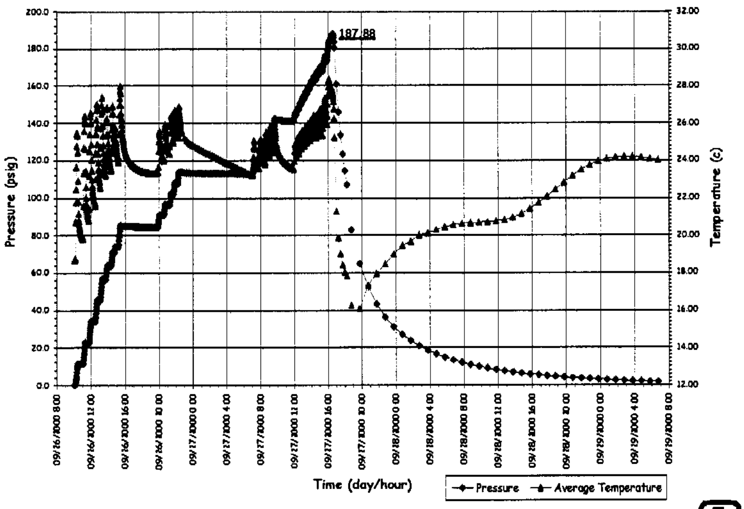

Sandia National Laboratories

PCCV LST - Calculated Leak Rate

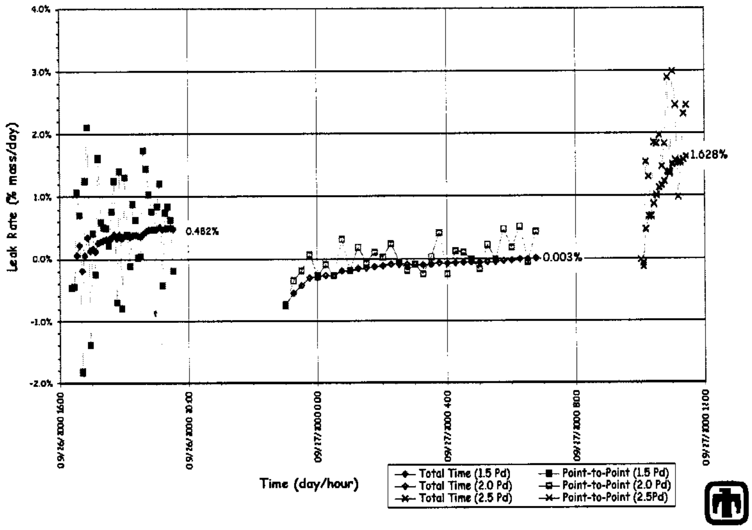

Sandia
National
Laboratories

PCCV LST - Estimated Leak Rates (2.5-3.1 Pd)

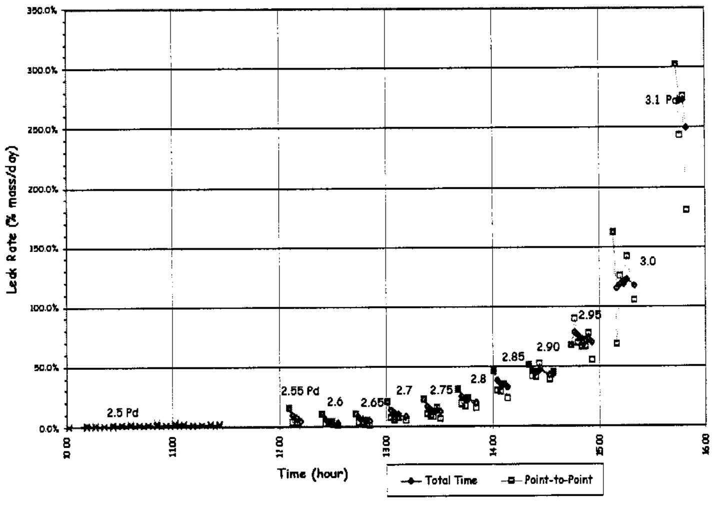

Sandia
National
Laboratories

PCCV LST - Calculated Leak Rate

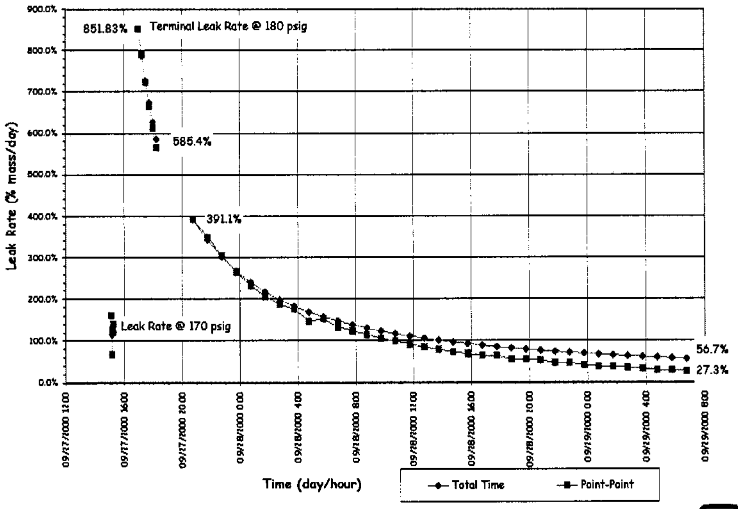

Sandia
National
Laboratories

Displacement Profiles

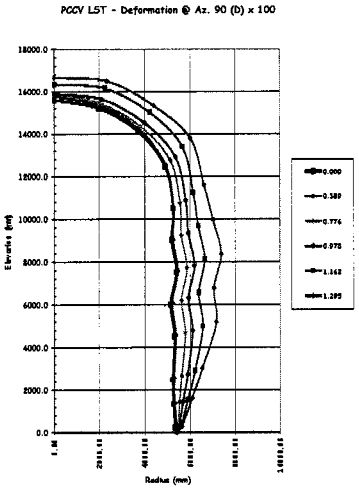

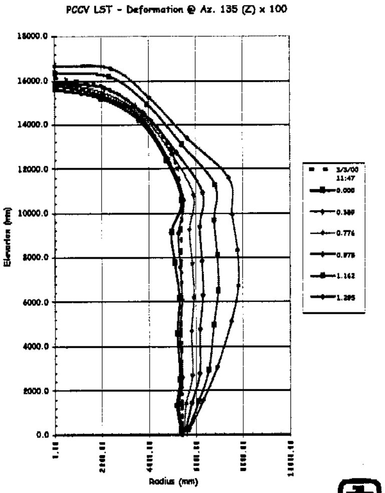

Sandia
National
Laboratories

Displacement Profiles

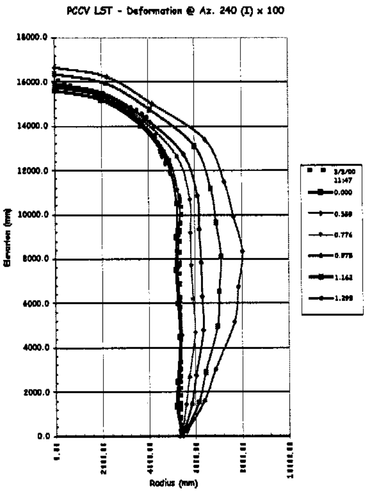

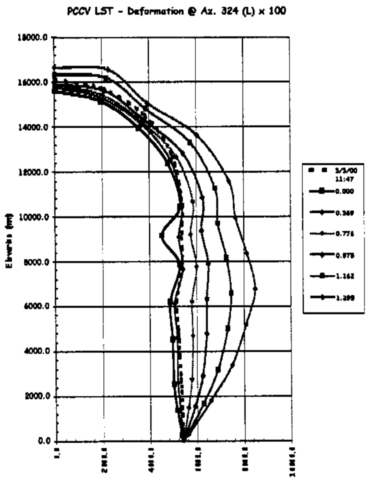

Sandia National Laboratories

PCCV LST - Deformation @ El 4680 (5) x100

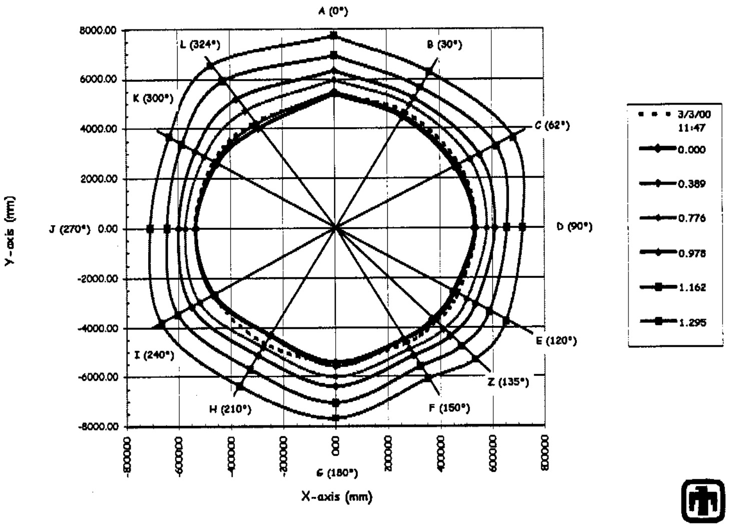

Sandia National Laboratories

Liner Strains - Summary

• Maximum Free Field Hoop Strain	0.90%
• Maximum Free Field Meridional Strain	0.14%
• Maximum Free Field Meridional Anchor Strain	0.10%
• Maximum Equipment Hatch Strain	3.88%
• Maximum Personnel Airlock Strain	0.75%
• Maximum Main Steam Penetration Strain	4.54%
• Maximum Feedwater Penetration Strain	6.39%
• Maximum Wall-Base Junction Strain	1.97%
• Maximum Miscellaneous Liner Detail Strain	5.75%

Rebar Strain Summary

• Maximum Free Field Hoop Rebar Strain	1.68%
• Maximum Free Field Meridonal Rebar Strain	0.47%
– Initial Strain at start of LST = 5.85%	*6.11%
– Maximum Delta	0.27%
• Maximum Free Field Radial Rebar Strain	0.88%
• Maximum Basemat Rebar Strain	0.84%
• Maximum Rebar Strain @ E/H	1.62%
• Maximum Rebar Strain @ A/L	1.50%

Acoustic System Response

- Acoustic System Goals:
  - Tendon/Wire Failure
  - Concrete Crack Development and Location
  - Kaiser Effect Cracking
  - Leak Development and Location
- Acoustic System:
  - Soundprint® by Pure Technologies, Ltd.
- Acoustic System Results:
  - No Tendon Failures were detected
  - Concrete Cracking was detected and sources located as the test progressed
  - Kaiser Effect cracking rates changed as pressure increased
  - First Leak was detected at 2.4 Pd

Acoustic Sensors at E/H

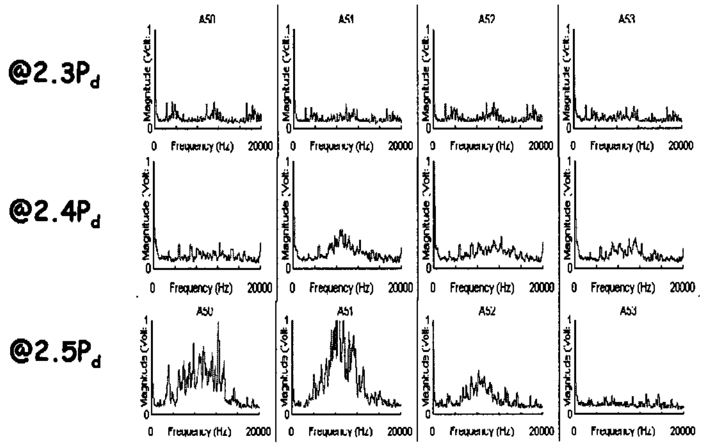

Posttest Inspection

- **Liner Inspection**
  - **In-situ examination (photos/paint removal, thickness measurement, etc.)**
  - **Destructive examination in progress:**
    - **25 specimens removed from the model**
    - **18 specimens currently undergoing metallographic analysis.**
    - **Remaining specimens along with additional liner samples being shipped to NUPEC (MHI) for further testing/examination.**
  - **Preliminary Metallographic Analysis Results**
- **Crack Mapping and Photos**
- **Posttest Measurements**
  - **Residual Displacements around Equipment Hatch**
  - **Posttest Survey of Cardinal Coordinates will not be done**
    - **Of limited value and results perturbed by liner buckling.**

Sandia
National
Laboratories

Liner Tears and Acoustic Events

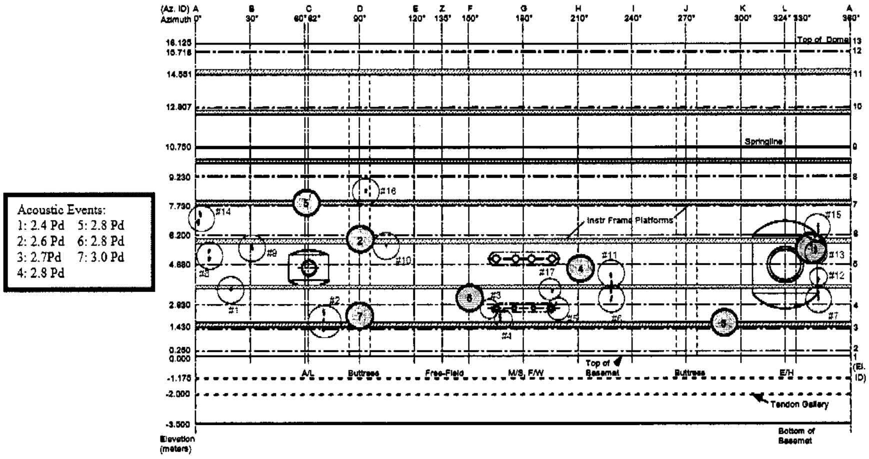
Acoustic Events:
1: 2.4 Pd
2: 2.6 Pd
3: 2.7Pd
4: 2.8 Pd
5: 2.8 Pd
6: 2.8 Pd
7: 3.0 Pd
(Az. ID) A B C D E Z F G H I J K L A
Azimuth 0° 30° 60° 62° 90° 120° 135° 150° 180° 210° 240° 270° 300° 324° 330° 360°
16.125
15.718
14.551
12.807
10.750
9.230
7.730
6.200
4.680
2.930
1.430
0.250
0.000
-1.175
-2.000
-3.500
Elevation (meters)
13
12
11
10
9
8
7
6
5
4
3
2
1
(El. ID)
Top of Dome
Springline
Instr Frame Platforms
#1
#2
#3
#4
#5
#6
#7
#8
#9
#10
#11
#12
#13
#14
#15
#16
#17
A/L
Buttress
Free-Field
M/S, F/W
Top of Basemat
Buttress
E/H
Tendon Gallery
Bottom of Basemat

Sandia
National
Laboratories

Liner Tear 7 @ E/H

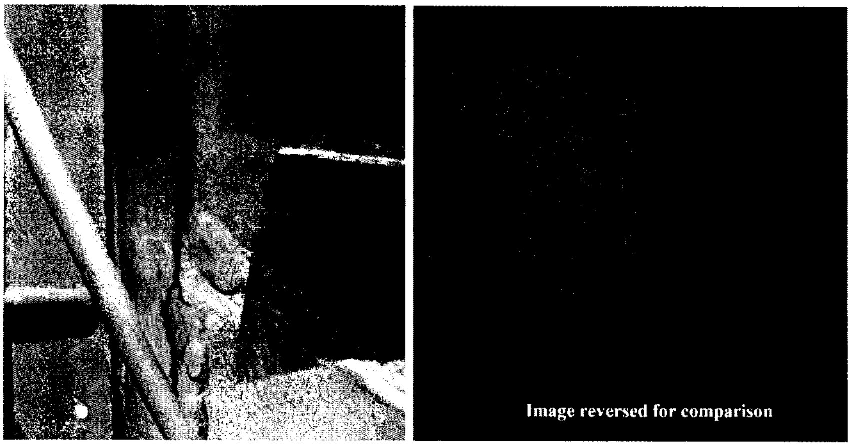
Image reversed for comparison

Sandia National Laboratories

Liner Tear 2-3 ~ Free-Field

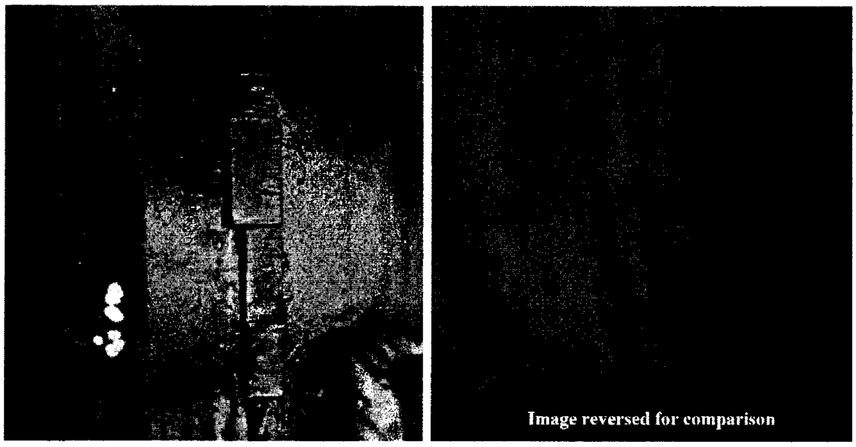
Image reversed for comparison

Sandia National Laboratories

Summary of PCCV RR Pretest Results

	Pressure (MPa)	Failure Mode
• ANL	1.51-1.62	local liner tear/hoop tendon failure @ El. 6.4 m
• AECL	0.94-1.24	complete cracking/axisymmetric yield
• CEA	1.60-1.70	numerically unstable
• EDF	1.95	
• INER	0.81	
• JAERI		buckling @ dome or local fracture by bending in cylinder
• JAPC	1.45-1.55	hoop tendon/rebar/liner rupture @ El. 7 m
• KINS	1.25-1.44	tendon rupture
• KOPEC	1.30-1.51	tendon rupture (@3.55% strain)
• HSE/NNC	1.98	liner tear w/ extensive concrete cracking @ buttress
• NUPEC	1.49-1.57	tendon rupture
• IBRAE	1.26	tendon rupture
• Principia	1.30	tendon yielding
• RINSC	1.50	hoop failure of vessel
• ANATECH/SNL	1.25	liner tearing (16%) @ E/H
	1.40	tendon rupture
● Test	0.98	1.5% mass/day leak through liner tear @ E/H
	1.30	limit of pressurization capacity during LST
	1.42	hoop tendon and rebar rupture during SFMT

Sandia National Laboratories

Summary of SFMT Results

- Structural Failure Mechanism Test (SFMT):
  - Justification: LST did not completely satisfy pre-test objective of providing data to validate response predictions 'well into the in-elastic regime'.
- Procedure:
  - Sprayed-on polyurethane elastomeric liner (200 mil min. thickness) applied to interior surface of model.
  - Pneumatic leak test conducted Oct. 3, 2001
    - Leak rate at 30 psi was ~70% mass/day
  - Model filled with water beginning November 6, 2001 after initial data scan and continued to November 8.
  - SFMT started at 10:00, Nov. 14, 2001 with an initial pressurization rate of 5 psi/min, scanning continuously (approximately every 30 seconds).

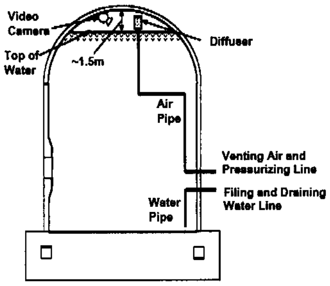
Video Camera
Top of Water
~1.5m
Diffuser
Air Pipe
Venting Air and Pressurizing Line
Filling and Draining Water Line
Water Pipe

Sandia National Laboratories

Pressure Time History

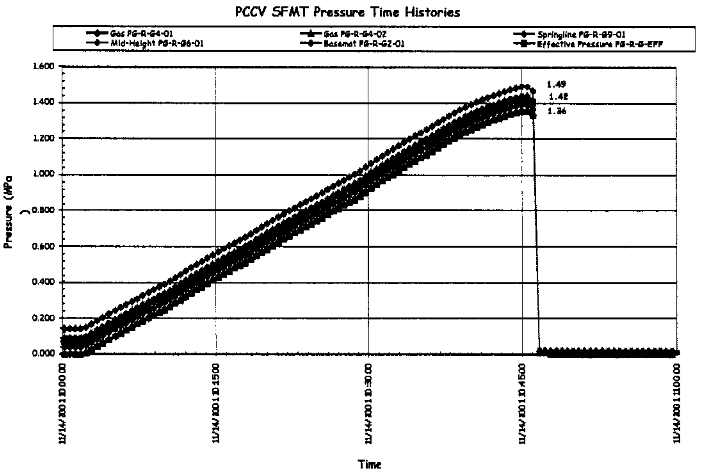

Sandia
National
Laboratories

PCCV Model Structural Failure Mode Test

November 14, 2002, 10:46:12 AM

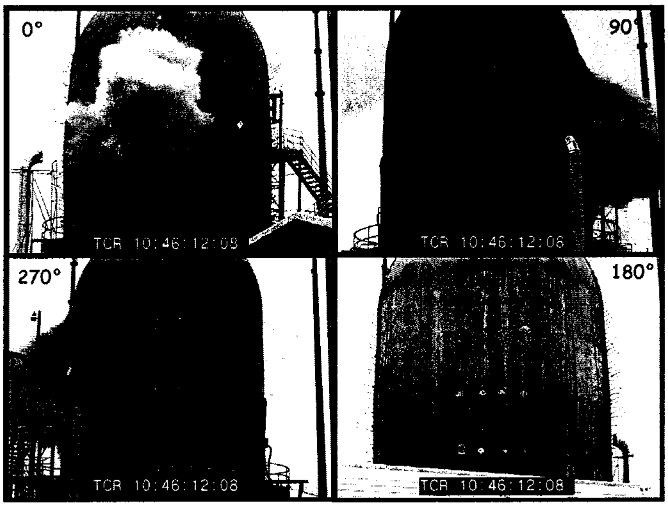
0°
90°
270°
180°
TCR 10:46:12:08
TCR 10:46:12:08
TCR 10:46:12:08
TCR 10:46:12:08

Sandia
National
Laboratories

PCCV Model after SFMT

November 14, 2002

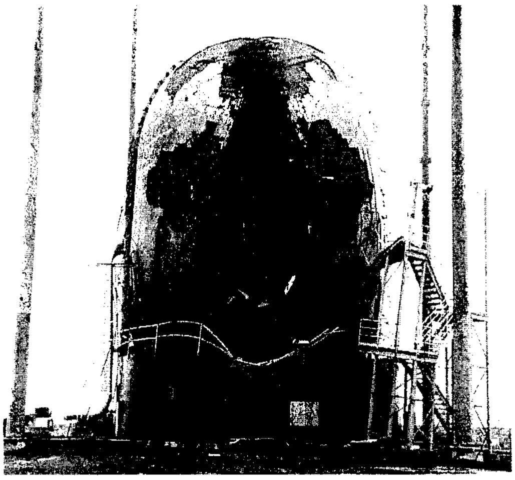

Sandia National Laboratories

PCCV SFMT

- Posttest Observations:
  - Water level inside model appeared to drop shortly before the rupture of the PCCV.
  - 4 to 6 tendons were observed to 'fail' in the final minute before the vessel ruptured.
  - Rupture initiated at approximately mid-height of the cylinder at Azimuth 6°, radiated vertically in both directions then radiated circumferentially approximately 7' above the top of the basemat. Vessel 'telescoped' over stem of cylinder wall and came to rest on the instrumentation frame.
  - Approximately 12 tendon segments were completely ejected from the model (all remained within test site boundaries)
  - Hoop tendons and rebar at the rupture line exhibited significant necking indicating that rupture was essentially ductile in nature.
  - Model displaced 3" horizontally and tipped in the opposite direction of the rupture.

Sandia National Laboratories

Rupture Map

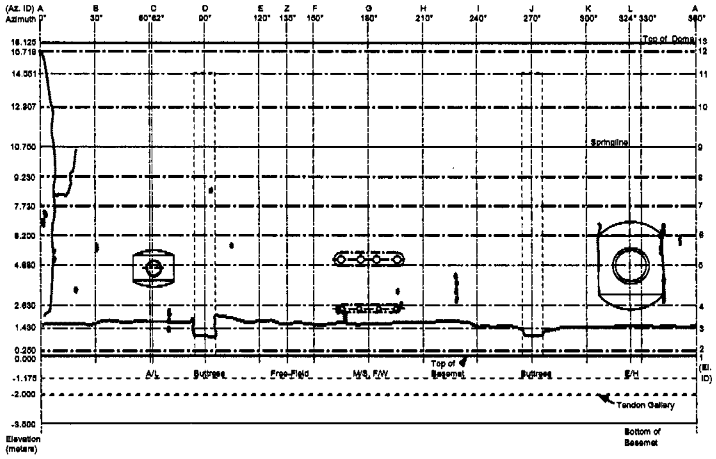
(Az. ID)
Azimuth
A 0°
B 30°
C 60°62°
D 90°
E 120°
Z 135°
F 150°
G 180°
H 210°
I 240°
J 270°
K 300°
L 324°
330°
A 360°
16.125
15.718
14.551
12.807
10.750
9.230
7.730
6.200
4.680
2.630
1.430
0.250
0.000
-1.175
-2.000
-3.500
Elevation (meters)
13
12
11
10
9
8
7
6
5
4
3
2
1
(El. ID)
Top of Dome
Springline
A/L
Buttress
Free-Field
M/S, F/W
Top of Basemat
Buttress
E/H
Tendon Gallery
Bottom of Basemat

Rebar and Tendons

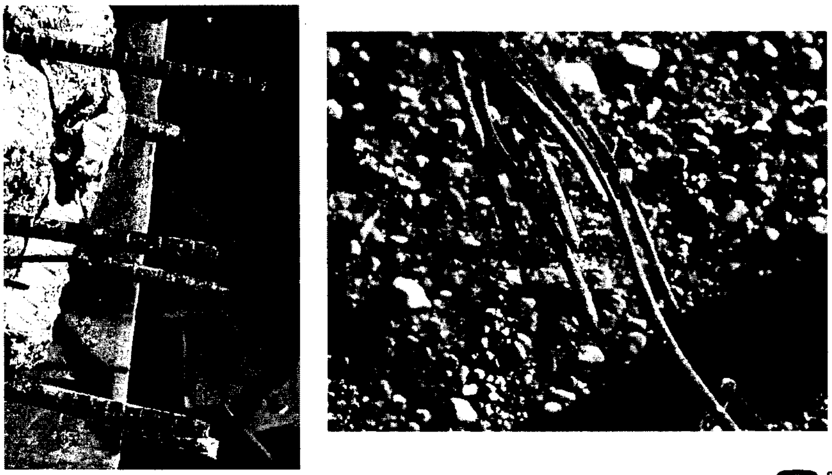

Model Displacement

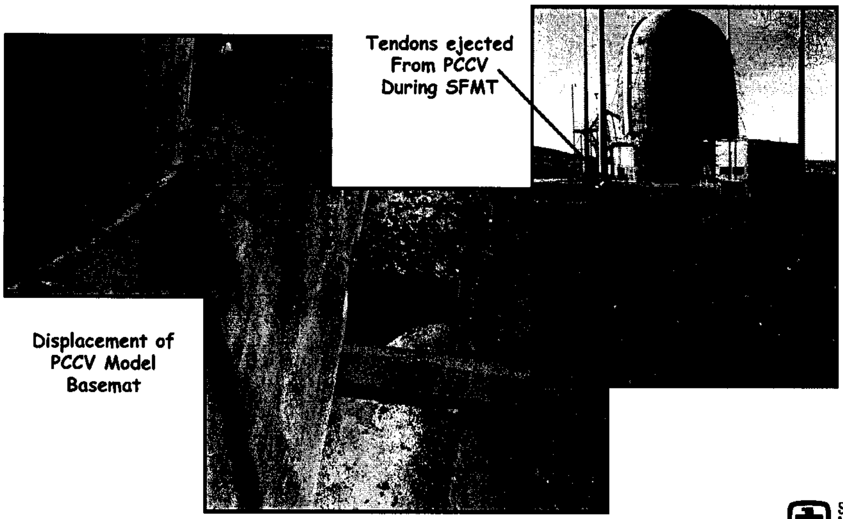

Tendons ejected From PCCV During SFMT

Displacement of PCCV Model Basemat

Sandia National Laboratories

Acoustic Response

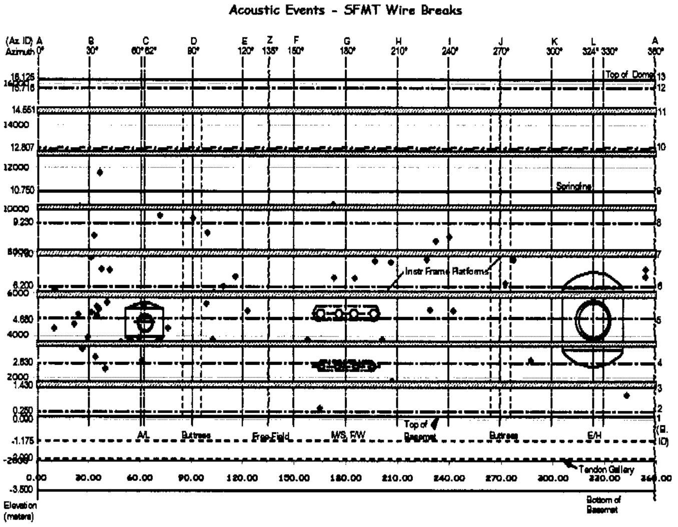

Sandia National Laboratories

Acoustic Response

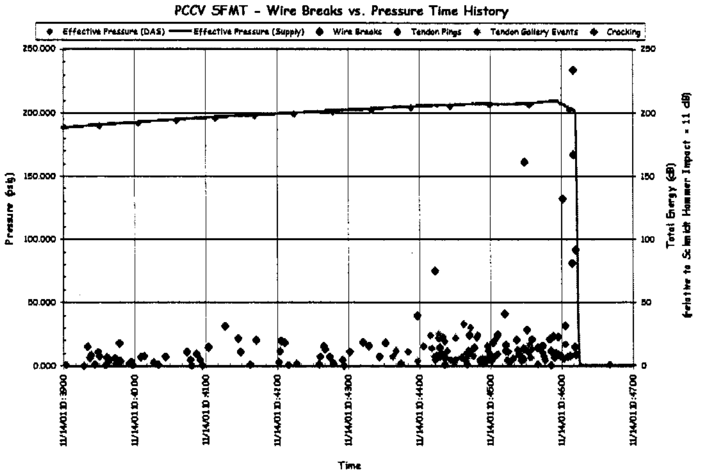

Strain Summary

- Displacements:
  - Δr/R = 1.4% @ 4680 (Level 5)
- Exterior Liner Strains
  - Gages @ Wall-Base Junction appear to have failed at 0.5Pd
  - Maximum Free-field Hoop Liner strain: 1.5% @ Z6, 1.9% @Z5
- Rebar Strain
  - Max Free-field Hoop Rebar strain: 1.4% (RS-C-Z6-02)
  - Gage Bar strain data: all gages appear to have failed prior to 0.5 Pd
- Concrete Strain (SOFO):
  - Max Free-field Hoop strain: 1.1% (CE-C-Z6-01)

Displacements

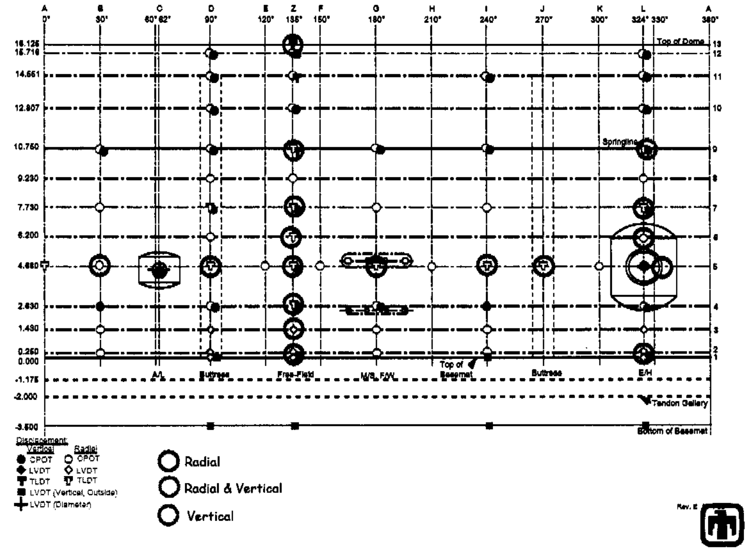
A
B
C
D
E
Z
F
G
H
I
J
K
L
A
0°
30°
60° 62°
90°
120°
135°
150°
180°
210°
240°
270°
300°
324° 330°
360°
16.125
15.716
14.551
12.807
10.750
9.230
7.730
6.200
4.680
2.630
1.430
0.250
0.000
-1.175
-2.000
-3.500
Top of Dome
Springline
13
12
11
10
9
8
7
6
5
4
3
2
1
A/L
Buttress
Free-Field
M/S, F/W
Top of Basemat
Buttress
E/H
Tendon Gallery
Bottom of Basemat
Displacement
Vertical
● CPOT
◆ LVDT
TLDT
■ LVDT (Vertical, Outside)
+ LVDT (Diameter)
Radial
○ CPOT
◇ LVDT
TLDT
Radial
Radial & Vertical
Vertical

Rev. E

Sandia
National
Laboratories

Displacements

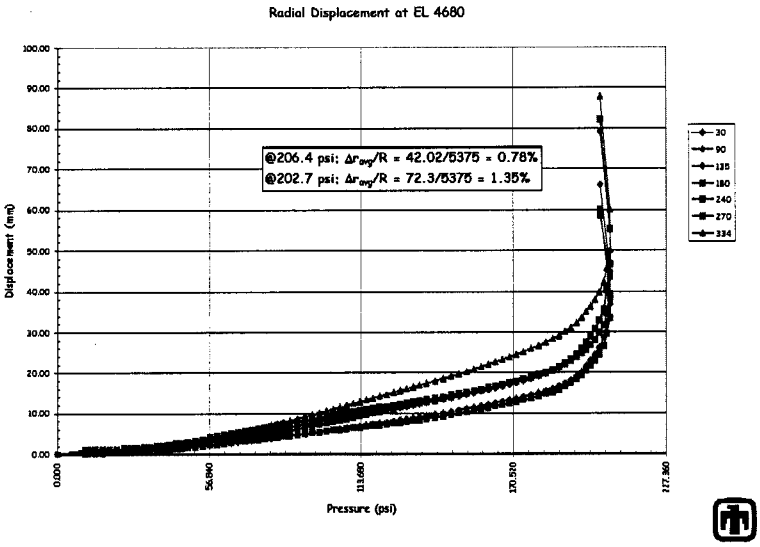

Sandia
National
Laboratories

Displacements

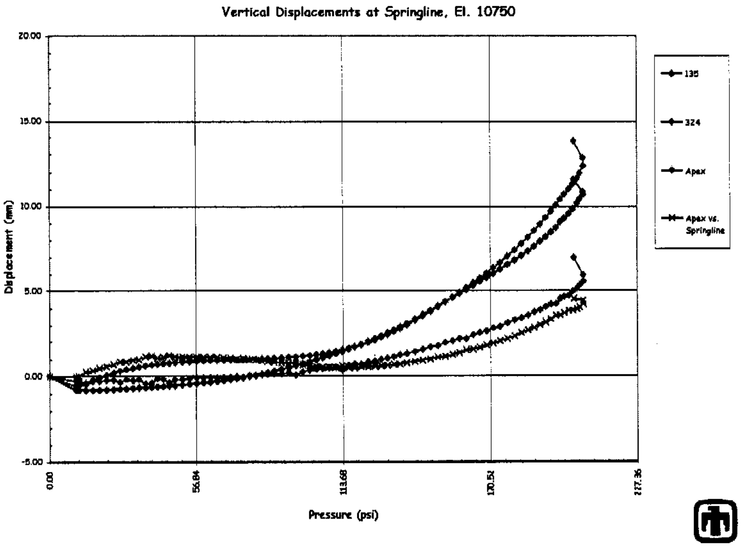

Sandia National Laboratories

Displacements

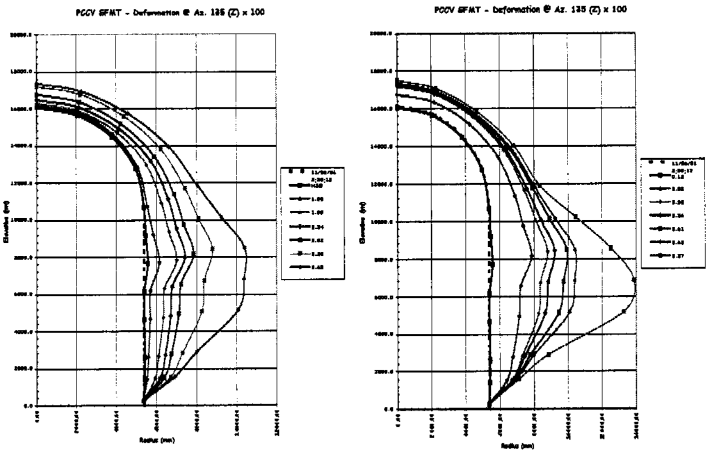

Sandia National Laboratories

Displacements

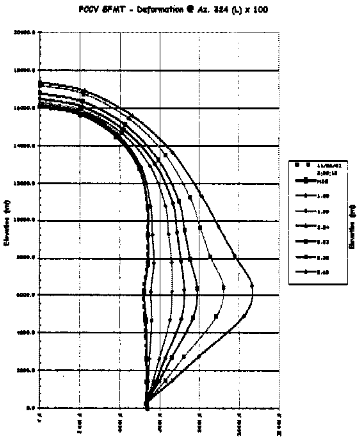

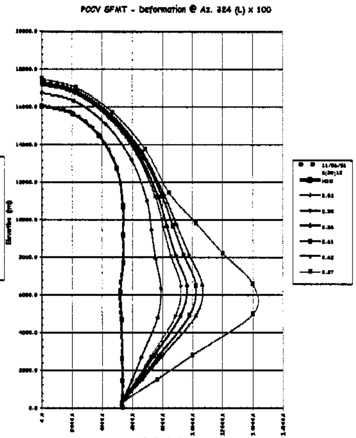

Displacements

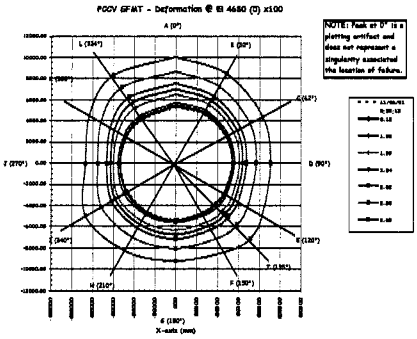

NOTE: Peak at 0° is a plotting artifact and does not represent a singularity associated the location of failure.

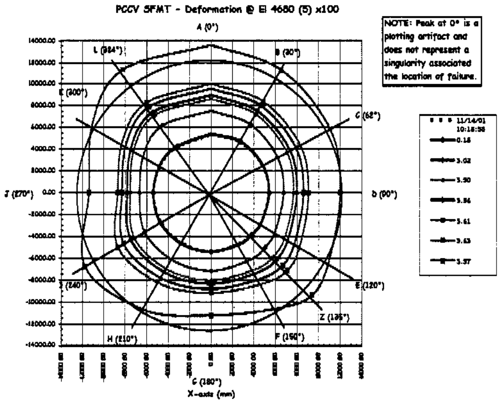

NOTE: Peak at 0° is a plotting artifact and does not represent a singularity associated the location of failure.

Liner Strains

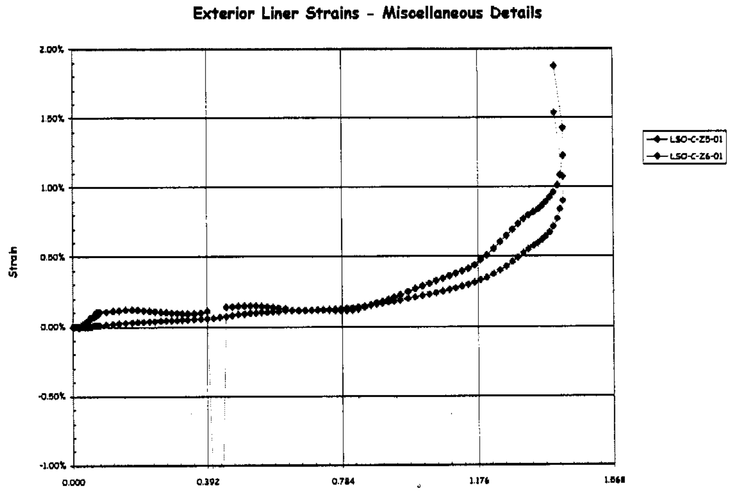

Sandia National Laboratories

Rebar Strains

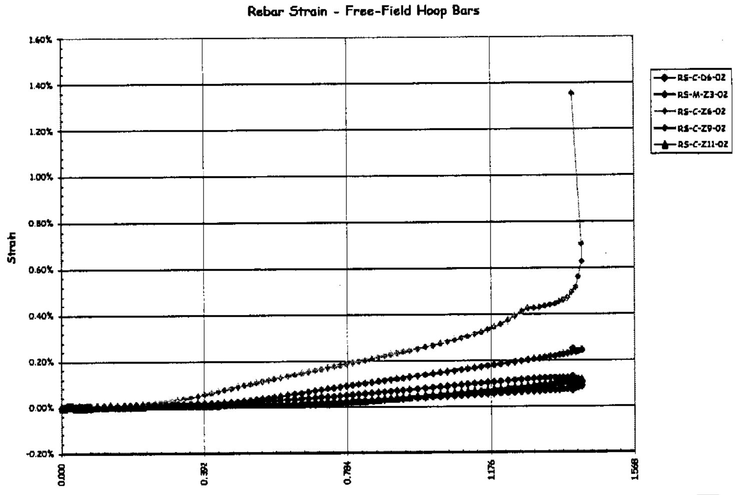

Sandia National Laboratories

Concrete Strains

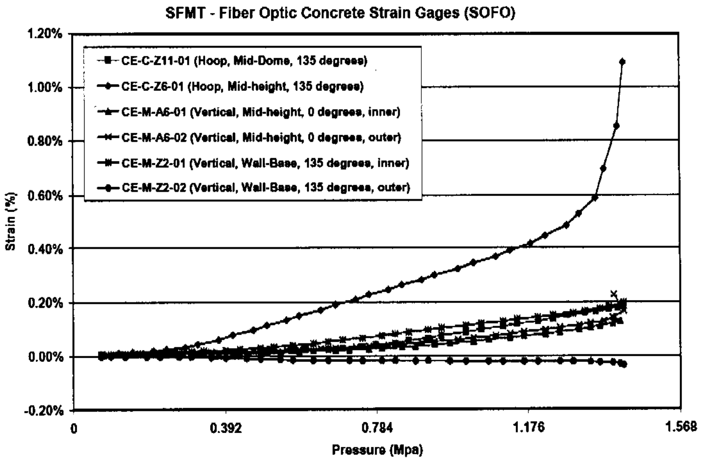

Tendon Forces

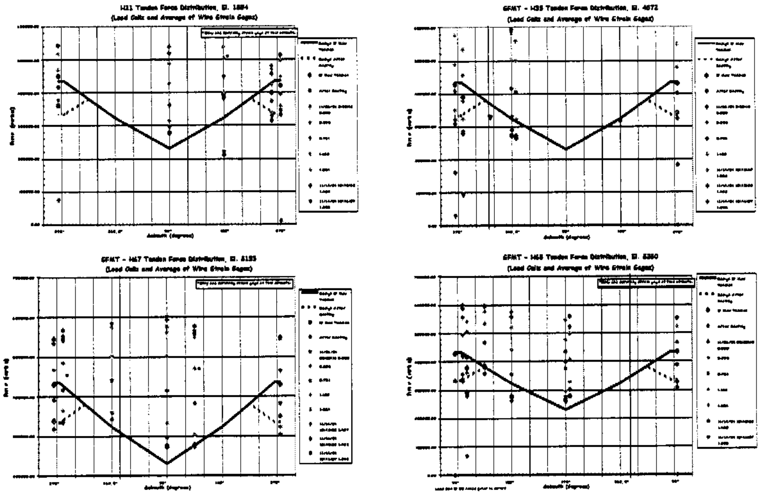

Tendon Forces

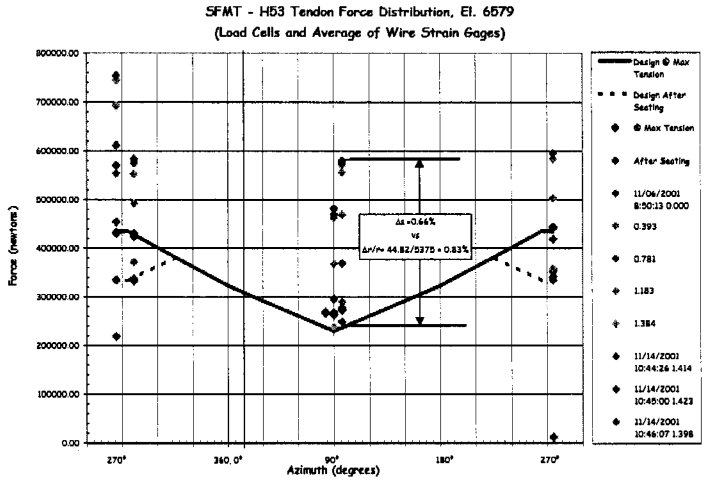

Sandia National Laboratories

Tendon Forces

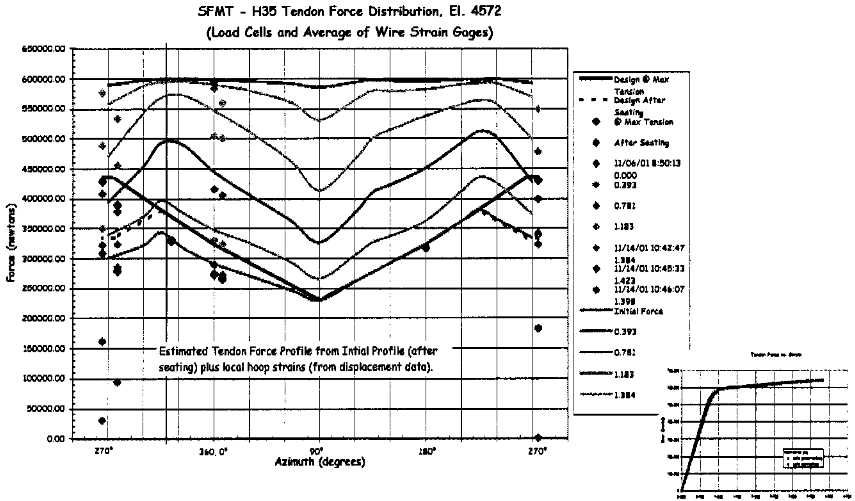

Sandia National Laboratories

Round Robin Predictions

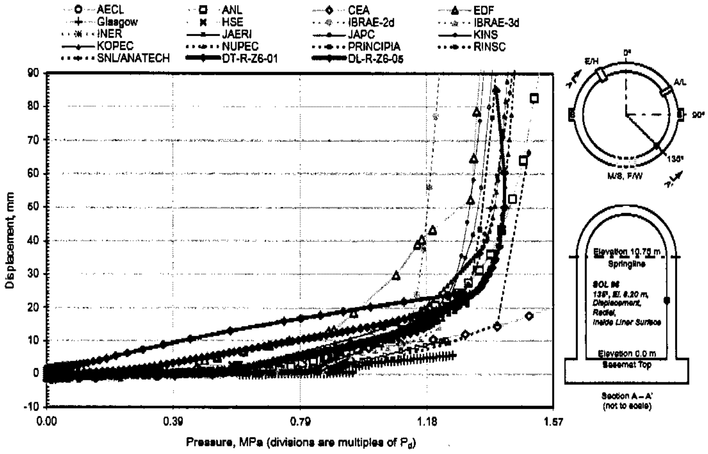

SFMT Conclusions

- **SFMT objectives were met:**
  - **–Additional data on the response of the PCCV model 'well beyond' the elastic limit were obtained.**
  - **–Structural failure mode was demonstrated.**
  - **–Structural failure mode does not appear to be a result of any flaw in the structure but appears to represent a true structural limit.**

PCCV Model Demolition

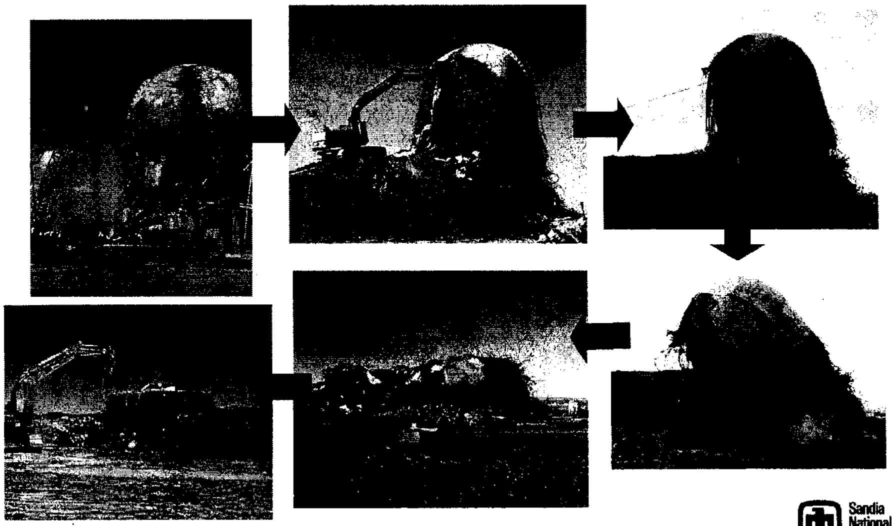

Sandia National Laboratories

(Former) Containment Technology Test Facility

May 3, 2002

Sandia National Laboratories

OECD/NEA/CSNI International Standard Problem #48

- Objective:
  - Extend the understanding of capacities of actual containment structures based on results of the recent PCCV Model Test and other previous research.
- Issues:
  - The PCCV Model Test results showed a leakage failure that began at about 2.5 times the design pressure. The subsequent failure mode test (SFMT) showed a global failure due to exceeding hoop tendon capacity at about 3.6 times design pressure. Two questions about actual (full size and thickness) structures are obvious:
  - *(1) Would the onset of leakage be later and much closer to the burst pressure?*
  - *(2) How would including the effect(s) of accident temperatures change* the outcome?
- Scope:
  - Review differences between PCCV model and prototype.
  - Utilizing models built for PCCV analysis, modify to more accurately reflect prototype
  - Reanalyze model to include more realistic severe accident loads, esp. temperature.

Sandia
National
Laboratories

1st Meeting of ISP48 (Stockholm, Nov. 2002)

- Although there was no test supporting this calculation, the group agreed that an increased in temperature was better and more realistic than a constant temperature. They thus approved the proposal made by IRSN to use the pressure and thermal loadings as defined in WASH1400. IRSN will provide the group with the evolution of temperature and pressure versus time by the end of March 2003.

Sandia
National
Laboratories

1st Meeting of ISP48 (continued)

- The group decided to discuss thoroughly thermal hypothesis and data to be used during Phase 2 meeting. Nevertheless, the following were agreed upon:
  - Temperature will be applied on the surface of the liner;
  - Contact (i.e. no air gap) will be assumed between the liner and the concrete. The transfer coefficient will be specified;
  - Boundary conditions will be the same for all participants and will be specified;
  - Calculation should be performed up to 24 hours or up to rupture whichever comes first;
  - As to results, it was decided to compare, at several times to be defined:
    - the temperature profile through the thickness;
    - tendon, liner stresses (to be determined);
    - displacements (less points that in phase 2 will be selected based on phase 2 results);
    - crack patterns;
    - etc.

ISP48 Participant Summary

	Phase 2	Phase 3
• BE/NII/NNC	X	X
• EDF	-	-
• EGP	X	X
• GRS	X	X
• FORTUM	-	X
• IRSN/CEA	X	X
• JPRG	-	X
• KAERI	X	-
• KOPEC	X	X
• NRC/SNL/DEA	X	X
• SCANSCOT	-	X

ISP48 References

- NUPEC/NRC Cooperative Containment Program:
  - PCCV Test Report (SNL)
  - http://www.nrc.gov/reading-rm/doc-collections/nuregs/contract/cr6810/
  - PCCV Posttest Analysis Report (ANATECH)
  - http://www.nrc.gov/reading-rm/doc-collections/nuregs/contract/cr6809/
- OECD/NEA/CNSI Phase 2 Report
  - http://www.nea.fr/html/nsd/workshops/ISP48/index.html

  - Username:
  - Password:

2nd Meeting of ISP48 (Madrid, March 2004)

- Review results of Phase 2 calculations
  - Pressure only analysis for comparison with PCCV test results
- Finalize Phase 2 report
- Plan Scope of Phase 3
  - Pressure plus temperature analysis

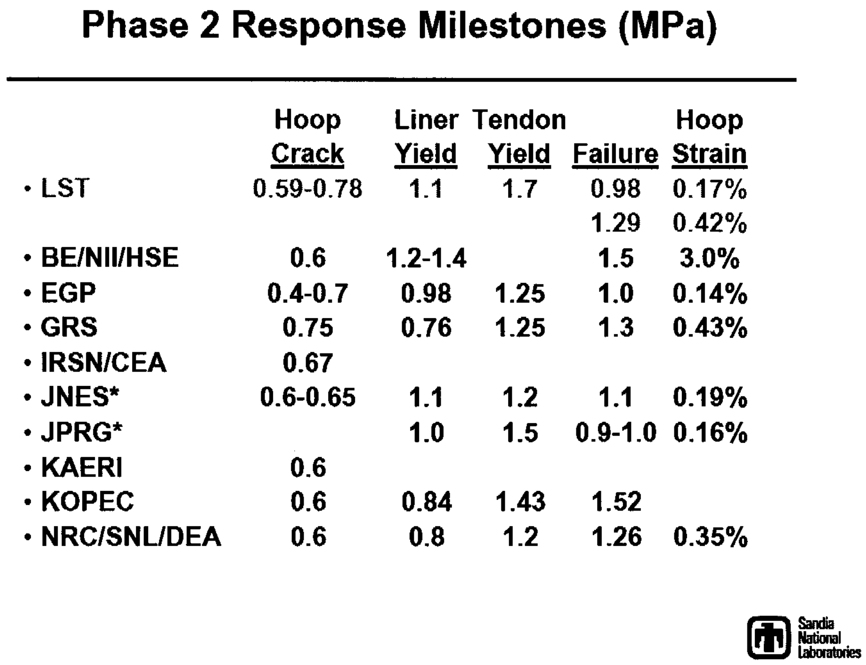

Phase 2 Response Milestones (MPa)

	Hoop Crack	Liner Yield	Tendon Yield	Failure	Hoop Strain
• LST	0.59-0.78	1.1	1.7	0.98	0.17%
				1.29	0.42%
• BE/NII/HSE	0.6	1.2-1.4		1.5	3.0%
• EGP	0.4-0.7	0.98	1.25	1.0	0.14%
• GRS	0.75	0.76	1.25	1.3	0.43%
• IRSN/CEA	0.67				
• JNES*	0.6-0.65	1.1	1.2	1.1	0.19%
• JPRG*		1.0	1.5	0.9-1.0	0.16%
• KAERI	0.6				
• KOPEC	0.6	0.84	1.43	1.52	
• NRC/SNL/DEA	0.6	0.8	1.2	1.26	0.35%

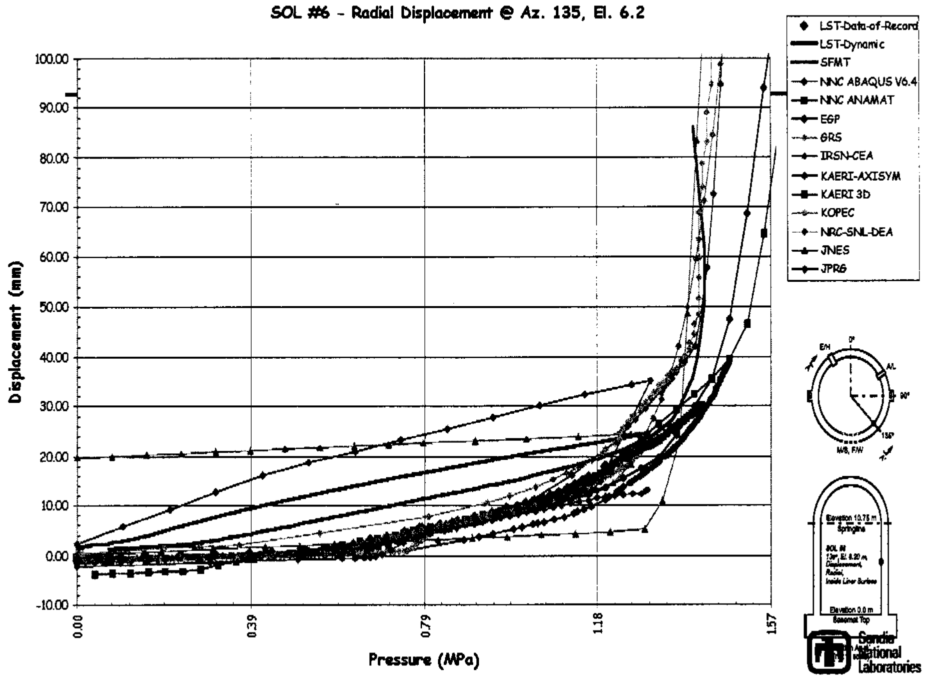

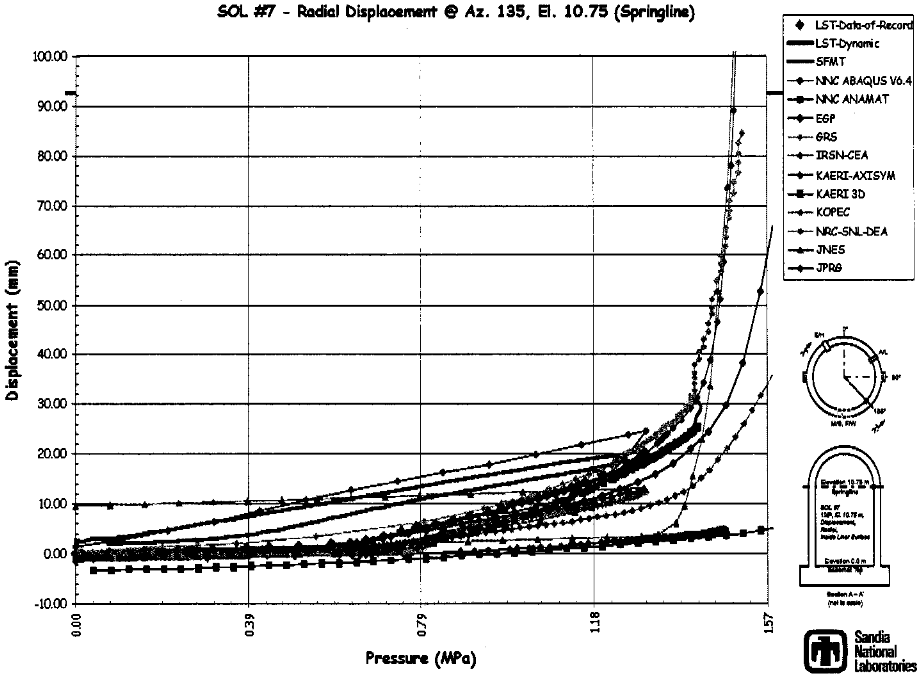
SOL #7 - Radial Displacement @ Az. 135, El. 10.75 (Springline)

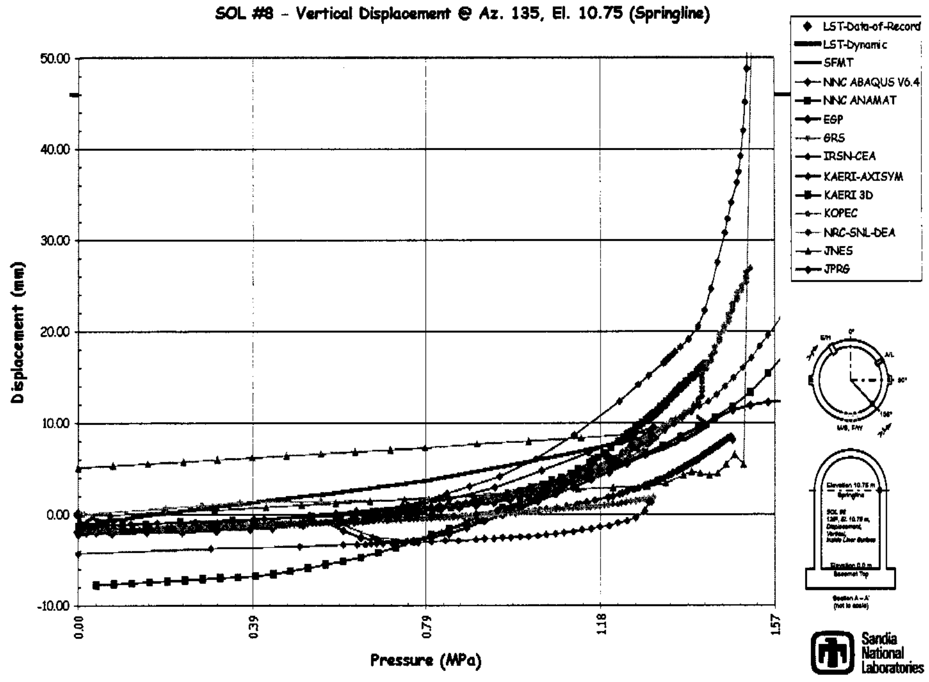
SOL #8 - Vertical Displacement @ Az. 135, El. 10.75 (Springline)

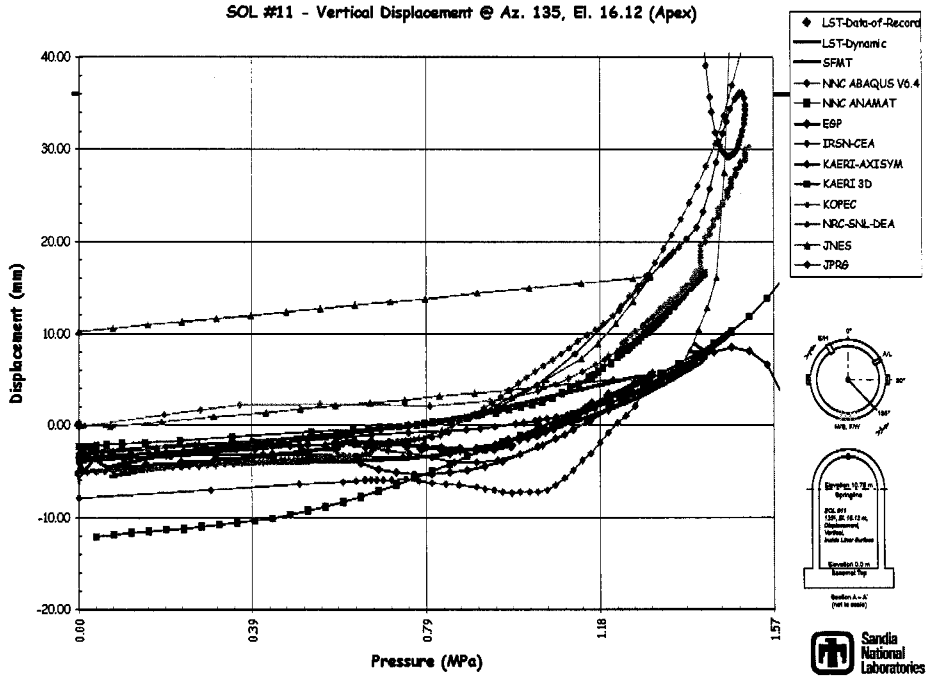
SOL #11 - Vertical Displacement @ Az. 135, El. 16.12 (Apex)
Displacement (mm)
40.00
30.00
20.00
10.00
0.00
-10.00
-20.00
Pressure (MPa)
0.00
0.39
0.79
1.18
1.57
LST-Data-of-Record
LST-Dynamic
SFMT
NNC ABAQUS V6.4
NNC ANAMAT
EGP
IRSN-CEA
KAERI-AXISYM
KAERI 3D
KOPEC
NRC-SNL-DEA
JNES
JPRG
0°
E/H
A/L
90°
Sandia National Laboratories

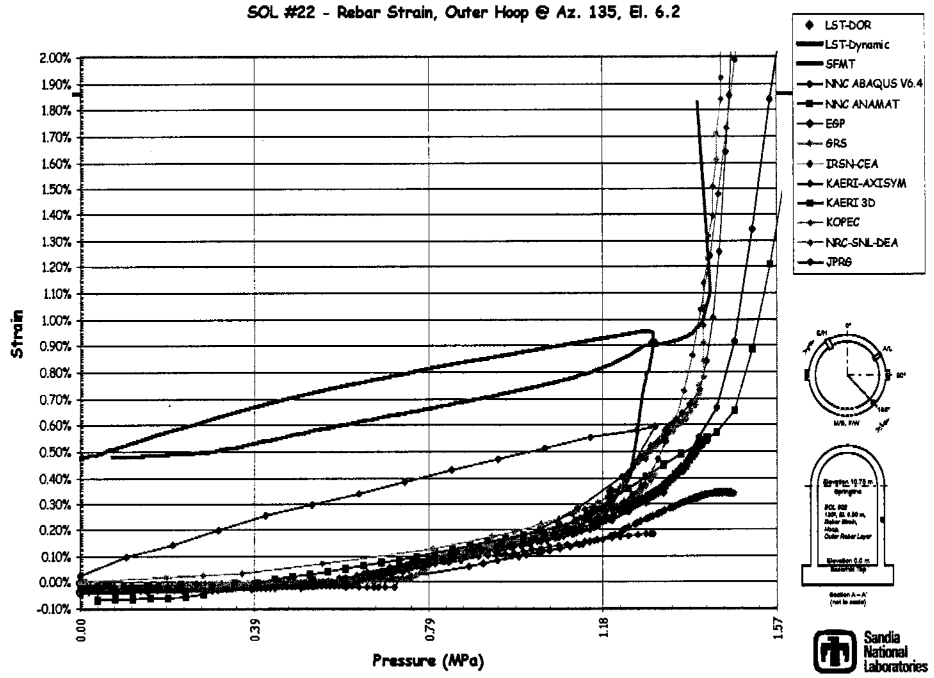
SOL #22 - Rebar Strain, Outer Hoop @ Az. 135, El. 6.2
Strain
2.00%
1.90%
1.80%
1.70%
1.60%
1.50%
1.40%
1.30%
1.20%
1.10%
1.00%
0.90%
0.80%
0.70%
0.60%
0.50%
0.40%
0.30%
0.20%
0.10%
0.00%
-0.10%
Pressure (MPa)
0.00
0.39
0.79
1.18
1.57
LST-DOR
LST-Dynamic
SFMT
NNC ABAQUS V6.4
NNC ANAMAT
EGP
GRS
IRSN-CEA
KAERI-AXISYM
KAERI 3D
KOPEC
NRC-SNL-DEA
JPRG
0°
E/H
A/L
90°
Sandia National Laboratories

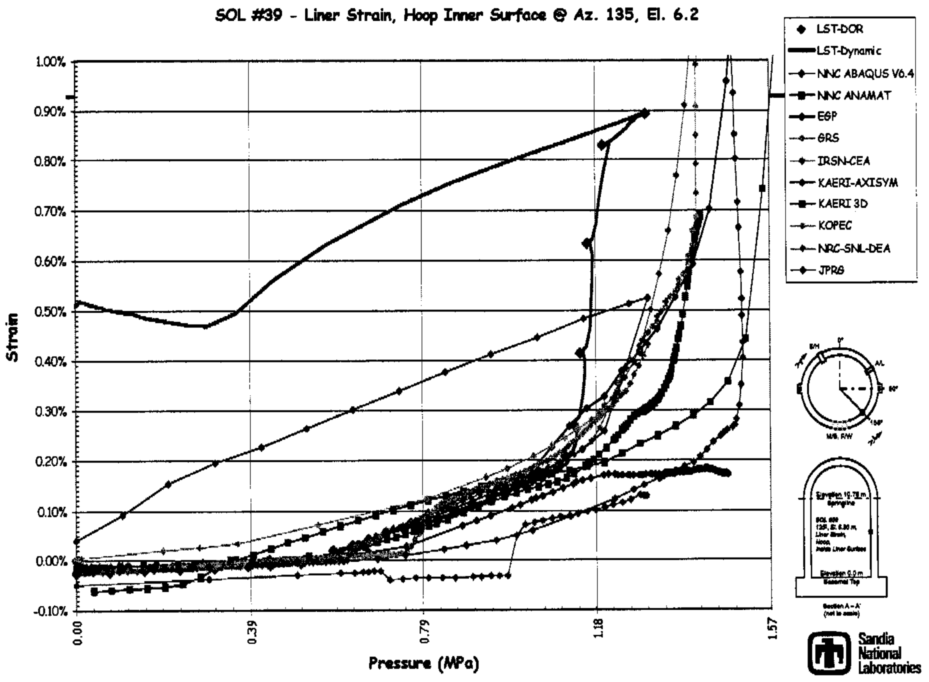
SOL #39 - Liner Strain, Hoop Inner Surface @ Az. 135, El. 6.2
Strain
1.00%
0.90%
0.80%
0.70%
0.60%
0.50%
0.40%
0.30%
0.20%
0.10%
0.00%
-0.10%
0.00
0.39
0.79
1.18
1.57
Pressure (MPa)
LST-DOR
LST-Dynamic
NNC ABAQUS V6.4
NNC ANAMAT
EGP
GRS
IRSN-CEA
KAERI-AXISYM
KAERI 3D
KOPEC
NRC-SNL-DEA
JPRG
Sandia National Laboratories

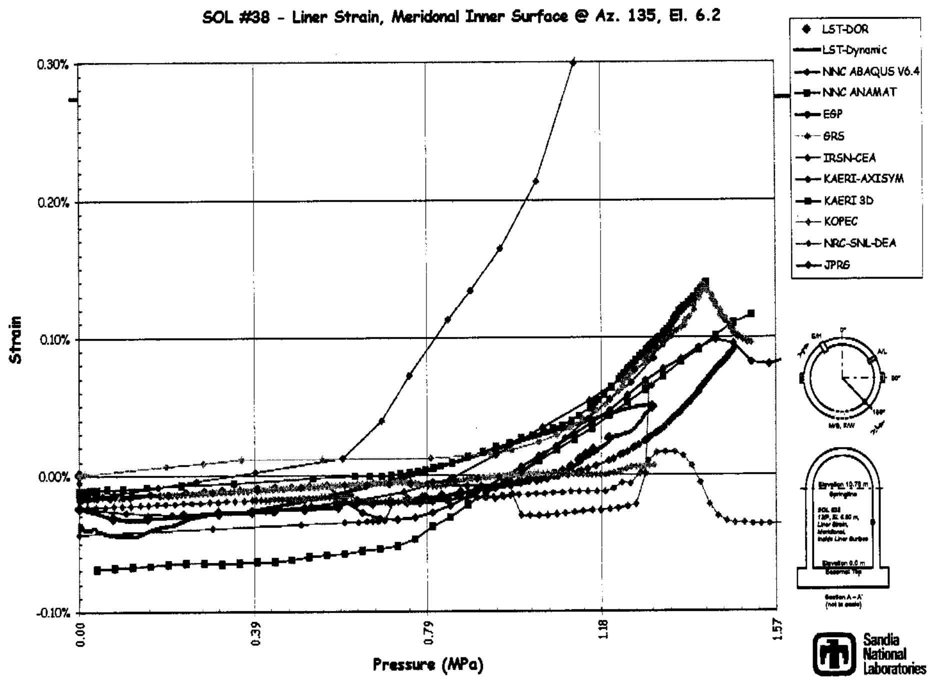
SOL #38 - Liner Strain, Meridonal Inner Surface @ Az. 135, El. 6.2
Strain
0.30%
0.20%
0.10%
0.00%
-0.10%
0.00
0.39
0.79
1.18
1.57
Pressure (MPa)
LST-DOR
LST-Dynamic
NNC ABAQUS V6.4
NNC ANAMAT
EGP
GRS
IRSN-CEA
KAERI-AXISYM
KAERI 3D
KOPEC
NRC-SNL-DEA
JPRG
Sandia National Laboratories

Phase 2 Summary/Conclusions

- Displacements
  - Radial displacement at mid-height of cylinder in good agreement with data and each other.
  - Poorer agreement near discontinuities
- Rebar strains:
  - Capture bending at wall-base junction(?)
  - Consistent with displacement based strains at mid-height of cylinder.
- Liner strains:
  - Inconsistent
- Tendon strain/force:
  - Increase due to pressure consistent and in agreement with test.
  - Prestressing behavior highly inconsistent.
  - Vertical prestressing not affected by pressure, hoop prestressing carries most of pressure load.

Sandia
National
Laboratories

NRC/SNL/DEA Proposal for Phase 3

- Define Pressure and Temperature time history based on Station Blackout (SBO) analysis for Large, Dry PWR.
- (NRC/SNL/DEA will) perform transient thermal analysis to define thermal gradients at several cross-sections.
  - ABAQUS semi-coupled Heat Transfer
- Time-dependent thermal gradients will be provided to all ISP48 participants for analysis of combined thermal-mechanical loading.

Sandia
National
Laboratories

Phase 3 Plan

- Per 2nd Meeting of ISP 48 Participants (Madrid, 19 Mar '04):
  - Case 1
    - Monotonically increasing static pressure and temperature (saturated steam)
    - Each participant performs heat transfer calculations or reads gradients provided by SNL.
  - Case 2
    - Station Blackout Scenario (NRC/SNL/DEA proposal plus hydrogen detonation defined by IRSN)
    - SNL will perform heat transfer calculation using full-scale axisymmetric model w/ 12 nodes through the thickness.
    - Apply resulting gradients to 1:4-scale model

Sandia National Laboratories

Case 1: Pressure-Temperature Relationship

- Saturated Steam

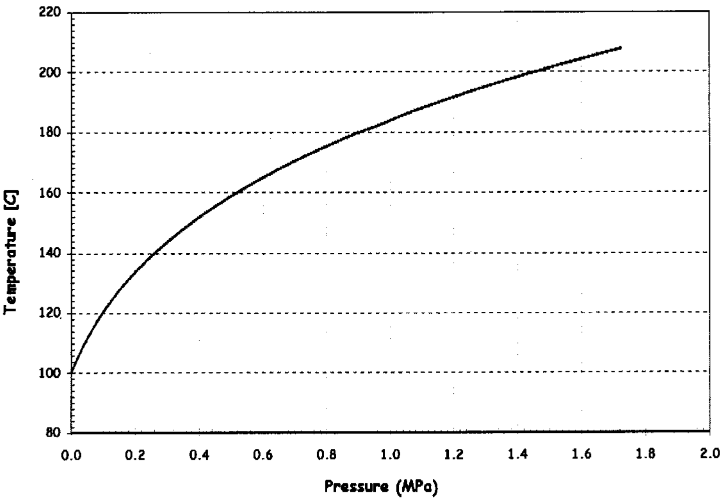

Sandia National Laboratories

Case 1: Pressure-Temperature Time Histories

- **Saturated Steam**
  - **Pseudo-time history based on SFMT pressurization rate (5 psi/min)**

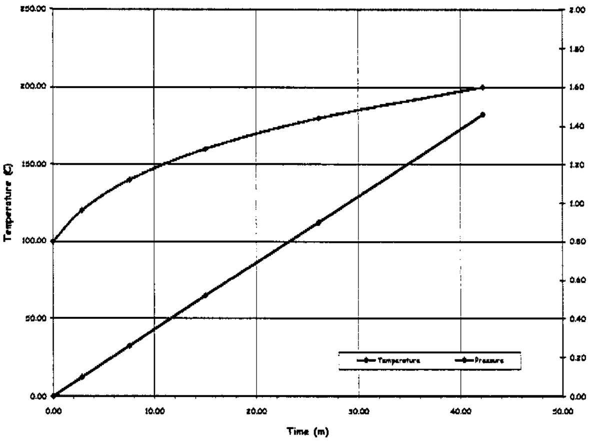

Sandia National Laboratories

Case 2: Pressure-Temperature Time Histories

- **Large, Dry PWR SBO, no containment leakage**

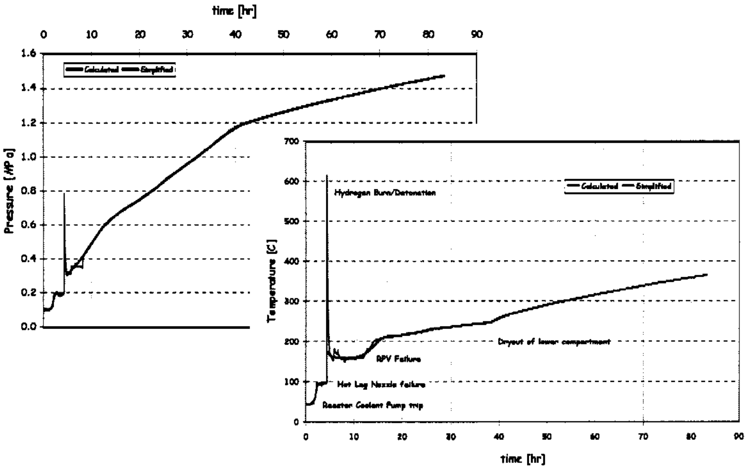

Sandia National Laboratories

Thermal Analysis

- **Model: Full-scale Axisymmetric with additional nodes throughout cylinder and dome - 12 through-thickness**
- **Material Properties: based on typical data**
- **Thermal Gradient calculation locations:**
  - **See figure**
- **Boundary Conditions:**
  - **Liner: Uniformly applied temperature; quasi-static, but transient**
  - **Dome & Cylinder: convection to air**
  - **Basemat/soil: conduction**
- **Reference:**

Dameron, et. al., "Analysis of Axisymmetric Presstressed Concrete Containment Vessel (PCCV) Including Thermal Effects", May, 2004

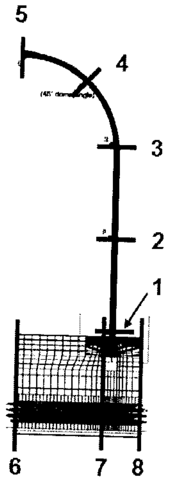

Case 1 Thermal Time Histories @ Section 2

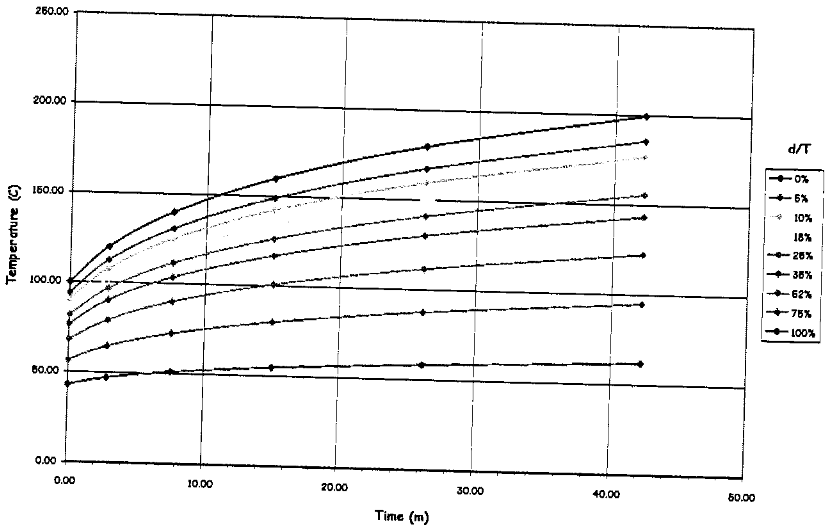

Case 1 Gradients @ Section 2

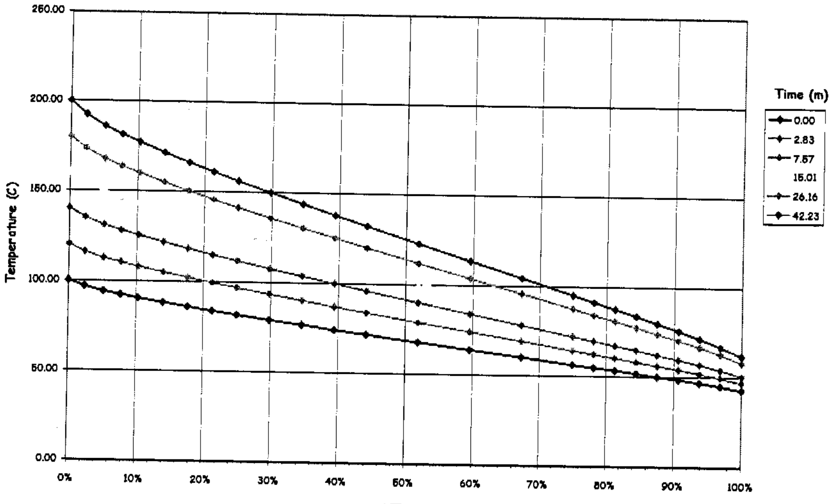

Case 1 Contours

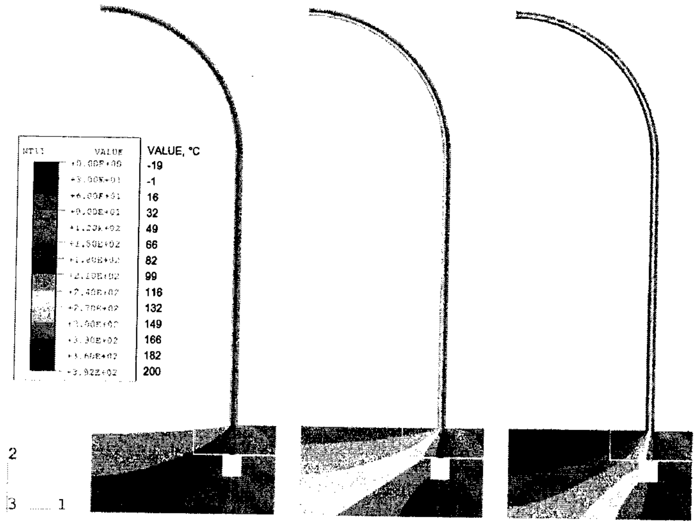
NT11
VALUE
+0.00E+00
+3.00E+01
+6.00E+01
+9.00E+01
+1.20E+02
+1.50E+02
+1.80E+02
+2.10E+02
+2.40E+02
+2.70E+02
+3.00E+02
+3.30E+02
+3.60E+02
+3.92E+02
VALUE, °C
-19
-1
16
32
49
66
82
99
116
132
149
166
182
200
2
3
1

Time = 3.83 Minutes

Time = 16.01 Minutes

Time = 43.23 Minutes

Case 2 Thermal Time Histories @ Section 2

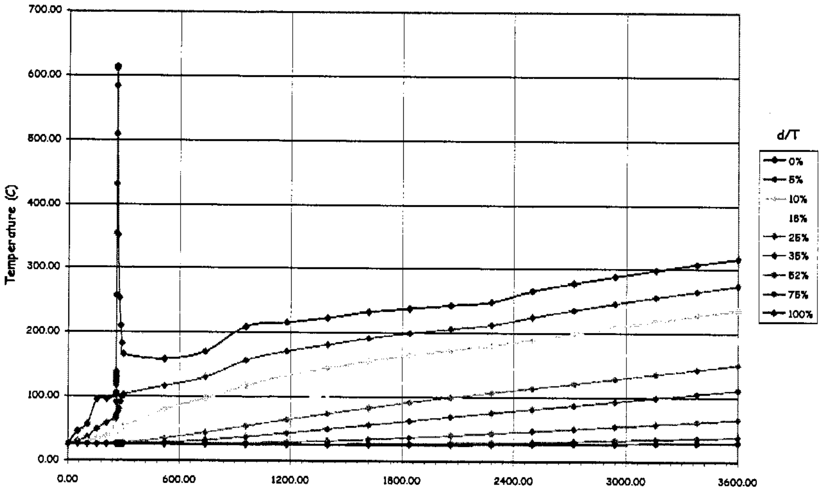

Sandia National Laboratories

Case 2 Gradients @ Section 2

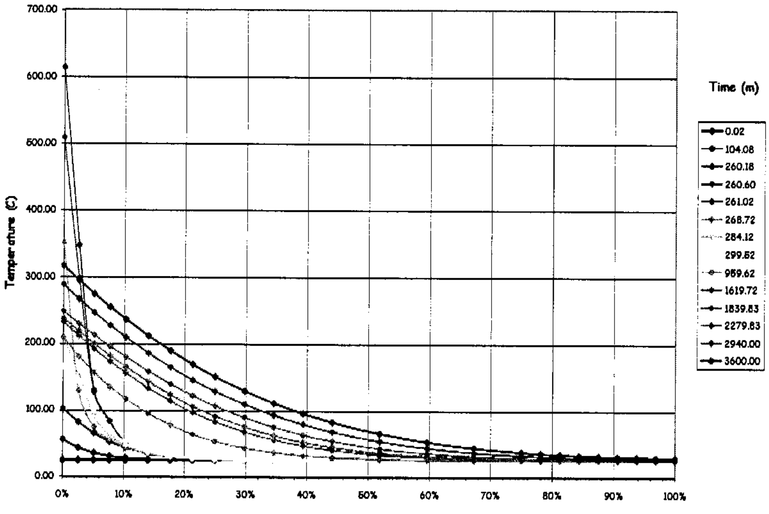

Sandia National Laboratories

Case 2 Contours

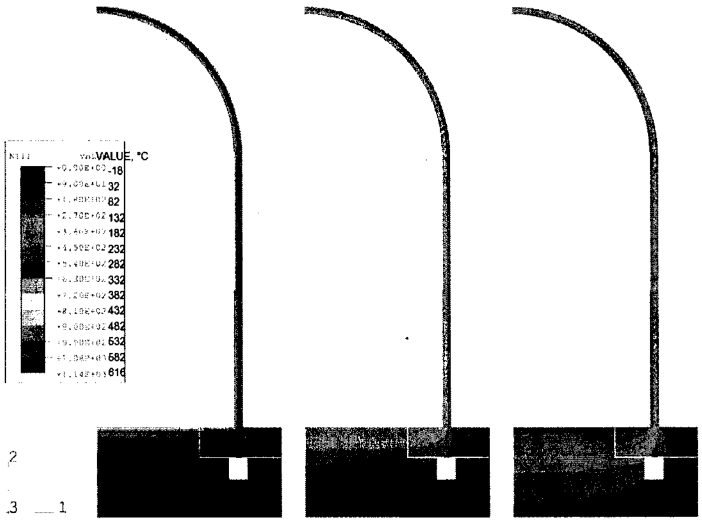
VALUE, °C
-18
32
82
132
182
232
282
332
382
432
482
532
582
616
2
3
1

Time = 260 Minutes

Time = 960 Minutes

Time = 3600 Minutes

Concrete Degradation due to Temperature

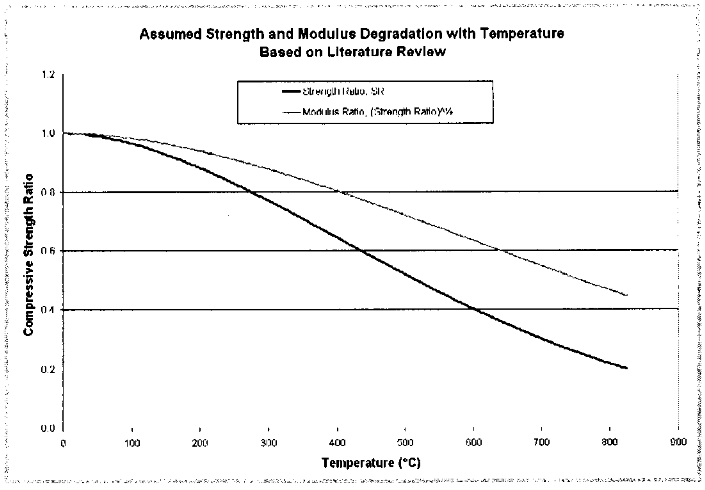

Steel Degradation due to Temperature

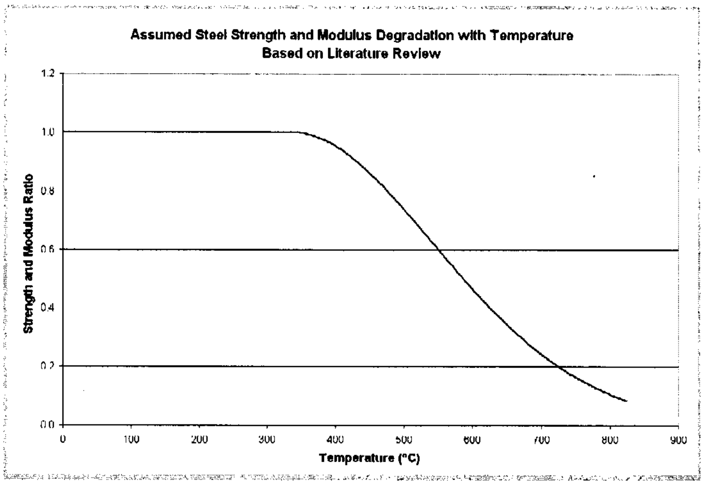

Schedule Status

✓Complete definition of Phase 3 loading Mar '04
✓Complete transient thermal analysis Apr '04
✓Transmit time-dependent gradients May '04
✓Mechanical-Thermal Analysis May-Dec '04
✓Submit Phase 3 Reports/Results Dec '04

- **Compile Draft Final Synthesis Report Apr '05**

Meetings at EdF in Lyon, France:

- **ISP48 Participant Meeting Apr 4-5, 2005**
- **Containment Capacity Workshop Apr 6-7, 2005**
- **IAGE Concrete sub-group Apr 8, 2005**

Meetings at OECD, Paris, France:

- IAGE Metal and Seismic sub-groups (in parallel) Apr 11-12, 2005
- IAGE Main group Apr 13, 2005
- **Publish Final Synthesis Report June '05**

Reporting

- Format for Phase 3 Reports
  - Summary reports
    - Analysis focuses on fundamental questions about temperature effects on PCCVs not addressed in previous research:
      - a.With addition of temperature, would the onset of leakage occur later in the pressure history and, possibly, closer to the burst pressure?
      - b.How would including the effect(s) of accident temperatures change the prediction of failure location and failure mode?
  - Comparison of responses
    - Reduced set of Standard Output Locations
      - Displacements: 1, 6, 7, 8, 11,12, 13, 14
      - Rebar Strains: 18, 19, 22, 23, 32, 33
      - Liner Strains: 38, 39, 42, 45,
      - Tendon Strains: 48, 50
      - Tendon Forces: 54, 55
    - Profiles

Reporting (continued)

- Summary of Response Milestones

  Specify pressure/temperature/time at which event occurs. Include range, confidence limits
  - Cracking (include location and estimate of crack size
    - Hoop
    - Meridional
  - Liner Yield
  - Liner Rupture
  - Rebar Yield
    - Hoop
    - Meridonal
  - Hoop Tendon Strain
    - Yield
    - 2%
    - Rupture
  - @ Failure
    - Pressure
    - Free Field Hoop Strain
    - Radial Displacement
  - Mode

Analysis Comparison

- **Summary Tables**
- **Comparison Plots**
- **Profiles**

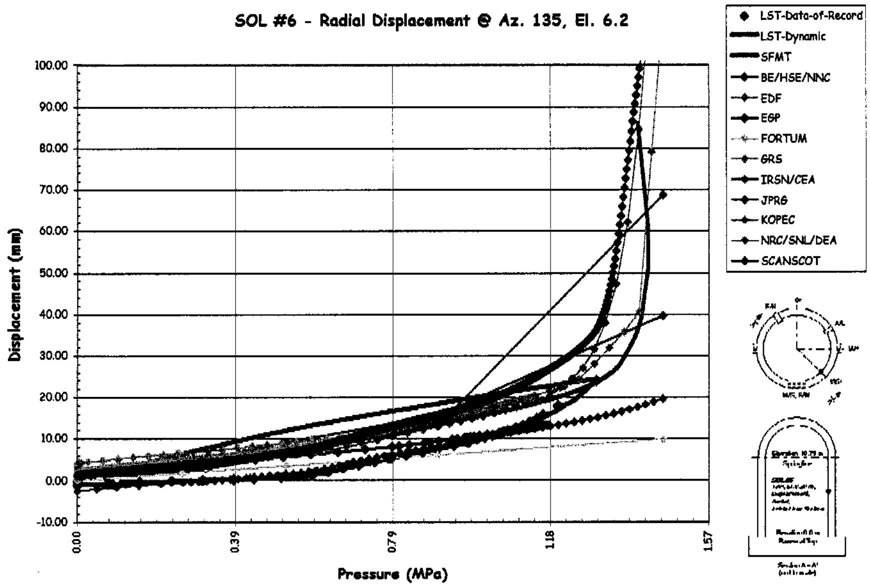

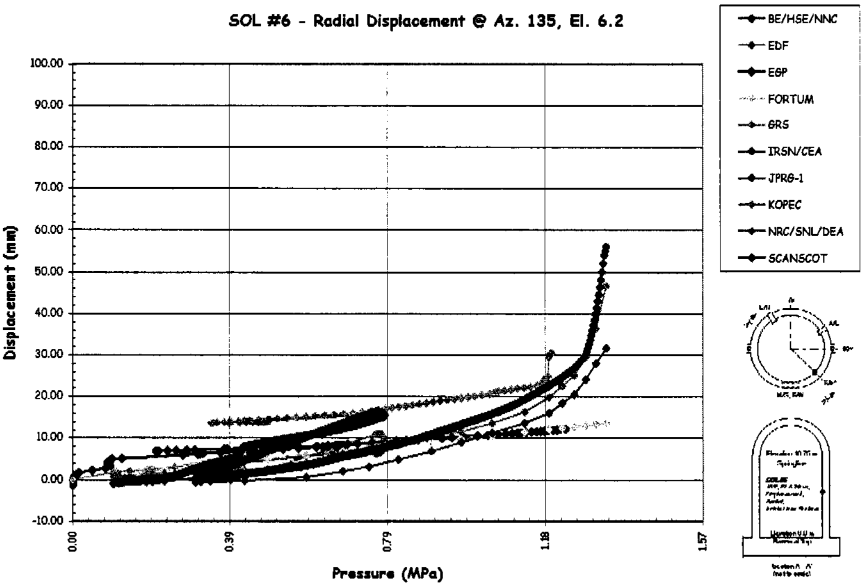
SOL #6 - Radial Displacement @ Az. 135, El. 6.2
Displacement (mm)
100.00
90.00
80.00
70.00
60.00
50.00
40.00
30.00
20.00
10.00
0.00
-10.00
0.00
0.39
0.79
1.18
1.57
Pressure (MPa)
BE/HSE/NNC
EDF
EGP
FORTUM
GRS
IRSN/CEA
JPRG-1
KOPEC
NRC/SNL/DEA
SCANSCOT

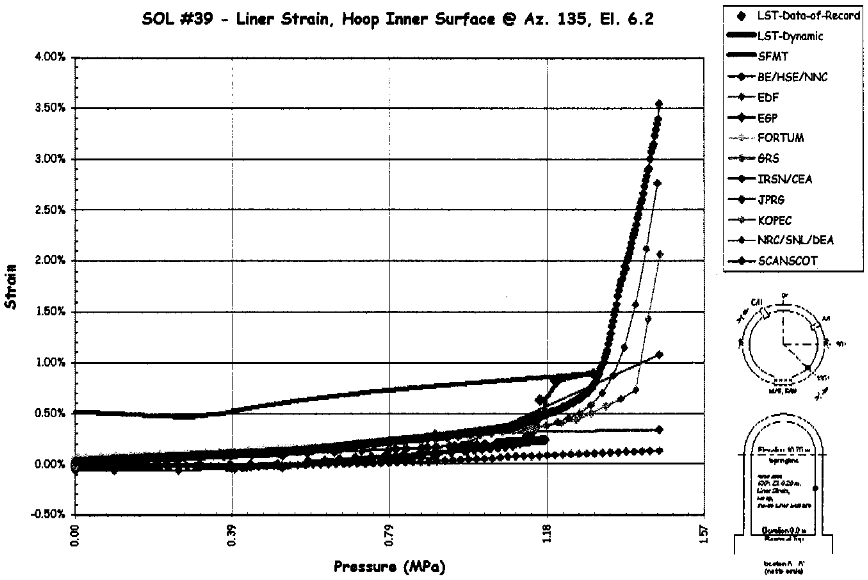
SOL #39 - Liner Strain, Hoop Inner Surface @ Az. 135, El. 6.2
Strain
4.00%
3.50%
3.00%
2.50%
2.00%
1.50%
1.00%
0.50%
0.00%
-0.50%
0.00
0.39
0.79
1.18
1.57
Pressure (MPa)
LST-Data-of-Record
LST-Dynamic
SFMT
BE/HSE/NNC
EDF
EGP
FORTUM
GRS
IRSN/CEA
JPRG
KOPEC
NRC/SNL/DEA
SCANSCOT

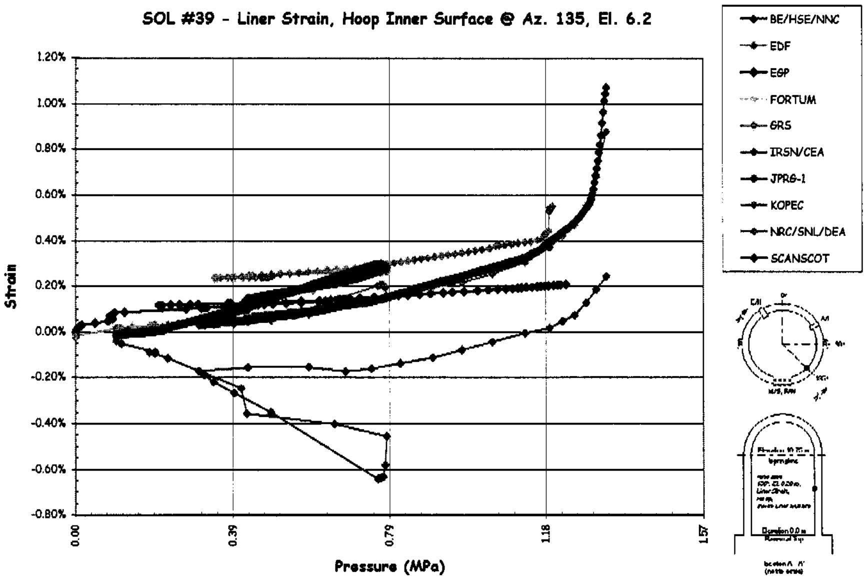

Summary

---

a. ***With addition of temperature, would the onset of leakage occur later in the pressure history and, possibly, closer to the burst pressure?***

b. ***How would including the effect(s) of accident temperatures change the prediction of failure location and failure mode?***

-Papers and Presentations on Containment Performance, Finite Element Modeling and Other Issues

Dr. M. Hessheimer (Sandia National Lab.- USA) and Mr. E. Mathet (OECD/ NEA - FR)

Contributions:

-Effect of Thermal Loading on Containment Capacity for the International Standard Problem (ISP - 48) Phase 3

Dr. N. K. Prinja and Mr. J. A. Curley (NNC Ltd- UK)

-Paper........63
-Presentation........78

-FE modelling of reactor containments - some relevant topics

Mr. O. Jovall and Mr. J.-A. Larsson (Scanscot Technology- SWD)

-Paper........103
-Presentation........108

-Statistical assessment of the prestress level based on in-service inspections of unbonded tendons

Mr. P. Anderson (Lund Uni.- SWD)

-Paper........115
-Presentation........125

-Probability Nonlinear Analysis of Reinforced Concrete Containment Integrity Considering Degradation Effects and High Internal -Overpressure

Prof. J. Králik (STU- SK)

Department of Structural Analysis, Faculty of Civil Engineering STU in Bratislava, Slovakia

-Paper........131

-Analysis of 1:4 scale prestressed concrete containment vessel (PCCV) model subject to pressure and thermal loading

Dr. N.-H. Lee and I.-H. Moon (KOPEC- KR)

-Paper........143
-Presentation........158

-Indirect Consideration of Unbonded Tendons in 1/4 PCCV Model

H.-G. Kwak, Mr. J. H. Kim (KAIST), Mr. S.-H. Kim (Youngdong Uni.) and Dr. Y.-S. Chung, (KINS- KR)

-Paper........173

- Mechanical behavior of containment building PWR 900MW under severe accident «global model »

G. Nahas - JM Rambach - IRSN, France

-Presentation........183

-Mechanical behavior of containment building PWR 900MW under severe accident «local model »

B. Ciree - G. Nahas - JM Rambach - IRSN, France

-Presentation........195

-The Creep of Confinement Building's Elements, Finite Element Analysis on Confinement, Ageing Program
Mr. C. Nyárádi (NPPP- HUN)
-Paper..**207**
-Presentation..**218**

-GRS calculations on large scale experiments of SANDIA pre-stressed concrete containment model
Dr. H. Grebner and Dr. J. Sievers (GRS- GER)
-Paper..**227**
-Presentation..**255**

-Posttest Analysis of a 1:4 Scale PCCV Model - Effects of Pressure and Temperature Loading
Mr. J. Stepan (NRI Rez- CR)
-Paper..**271**
-Presentation..**300**

-Experimental Studies on the Failure Behaviors of a Prestressed Concrete Containment Building
Dr. Y.S. Choun (KAERI), N.S.Cho (HICTD), and Dr. J.-M. Seo, (KAERI- KR)
-Paper..**309**
-Presentation..**327**

-*A* Summary of Complex Evaluation of the Status of Deliveries for the Mochovce NPP Units 3 and 4
Dr. Juraj Nozdrovický (VÚEZ- SK) and Dr. Martin Moravčík (UTC-SK)
-Paper..**335**

EFFECT OF THERMAL LOADING ON CONTAINMENT CAPACITY FOR THE INTERNATIONAL STANDARD PROBLEM (ISP - 48) PHASE 3

Dr N K Prinja, BSc, MSc, PhD, FIMechE, NNC Limited, UK
J. A. Curley, BSc, NNC Limited, UK

Abstract

This paper presents the assessment of concrete containment capacity for phase 3 of the International Standard Problem, ISP 48. The mandatory load case for phase 3 (Case 1) involving saturated steam conditions was analysed by using a full 3D global model of the containment structure. Heat transfer and nonlinear stress analysis was conducted using version 6.4 of ABAQUS to study the influence of thermal loading on the containment capacity. In addition, the effects of Thermal Transient Creep (TTC) in concrete at elevated temperatures have been investigated. It is concluded that the thermal straining of the liner results in rupture at approximately 1.25MPa, which is 14% higher than the rupture pressure of 1.1MPa obtained from the limit state test. The structural collapse dictated by the failure of the pre-loaded tendons also increases by 7% from 1.4MPa to 1.5MPa. Inclusion of thermal loading and temperature dependent effect of TTC show that the margin between the liner rupture and the structural collapse decreases.

Introduction

NRC/NUPEC sponsored tests of the ¼ scale pre-stressed concrete containment vessel (PCCV) which have been executed at Sandia National Laboratories (SNL) in the USA [1]. The Limit State Test (LST) executed during September 2000 was based on pneumatic pressurisation of the vessel and achieved a maximum pressure of 1.3MPa (3.3 times the design pressure). The objectives of the ISP48 are to extend the understanding of capacities of actual containment structures based on the results of the PCCV LST and any other sources of available research.

NNC participated in the LST round robin exercise and completed the analysis [2] to predict the limit load of the vessel. Predictions from all the participants of the round robin were collated and published by SNL in August 2000[3]. The LST identified liner tearing as the mode of failure. Whilst there was no visible damage to the PCCV structure, the breach of the pressure boundary dictated the limit load due to excessive leakage rate. It can be seen from Ref 3 that out of the total 17 participants, the NNC/HSE model is one of only four that successfully predicted liner tearing as the mode of failure. It was recognised at the international pre-test round robin meeting in October 1999 that the NNC/HSE model was one of the most sophisticated 3D full global models, which took account of the interaction between all the main structural features.

Following the pre-test round robin, NNC carried out the post-test analysis under HSE contract CE/GNSR/1 and the work was presented in Ref 4. This work consisted of a comparison between the FE analysis and the test results to give an assessment of the accuracy and reliability in predicting the failure modes and limit loads of PCCV structures using finite element analysis. It also included analysis of the Structural Failure Mode Test (SFMT) executed in November 2001, in which hydraulic pressure was used to over pressurise the containment to total structural collapse. The results of the over pressurisation test have been published by SNL[3]. The analysis carried out in Ref 2 predicted the failure location and the behaviour up to collapse with good accuracy.

All the previous test and analysis work done has shown that leakage occurs before the burst pressure but in these studies only the mechanical loading (gravity, prestress and internal pressure) was considered and thermal loading was ignored. In real containments, increase in internal pressure is associated with thermal loading. One of the aims of Phase 3 of the ISP48 project is to study the effects of accident temperatures and see if the onset of leakage is closer to the burst pressure in full size containments.

The 2nd meeting of the ISP48 project held in Spain in March 2004, reviewed Phase 2 results and finalised the combination of mechanical and thermal loadings for Phase 3[5]. The mandatory Case 1 consists of applying saturated steam conditions as steady state static loading and recommended Case 2 simulates Station Blackout pressure and temperature transients. This work covers only Case 1 of Phase 3.

PCCV Finite Element Model

Description of global model

Figure 1 shows the 3D global model of the PCCV model. All the Concrete components of the vessel are represented with the eight-noded solid elements type C3D8 [6]. The eight-node solid element includes smeared steel reinforcements. At a minority of locations, due to meshing requirements, six-node linear prism elements (C3D6) were used. Six-node prism elements do not support reinforcement capability. Within the cylinder, all solid elements are fully integrated, while the basemat and dome elements have reduced integration.

The origin of the FE model is at the centre of the top surface of the basemat. Directions 1, 2 and 3 are X, Y and Z respectively. X is along the 90° azimuth, Y is vertical and Z is along the 180° azimuth.

Cylinder wall and dome

The mesh density of the cylinder wall and dome in the circumferential direction was driven by the requirement to model each vertical post-tensioning tendons explicitly. The resulting layout consists of a cylinder and dome wall mesh with elements at approximately 2° intervals in the circumferential direction. Three elements were employed in the wall-thickness direction of the cylinder and dome.

The mesh density in the vertical direction was influenced by the specification of the hoop tendons in the concrete elements. The cylinder hoop tendons were arranged at vertical intervals of 112.7mm. The solid element nodes are meshed vertically to correspond with the spacing of the hoop tendons.

The buttresses at the 90° and the 270° azimuths are reinforced columns onto which the hoop tendons are anchored. The stiffness of the cylinder and the dome at the 90° and 270° azimuths is enhanced by the restraining effect of the buttresses. The reinforcement scheme of the buttresses comprises vertical, radial and trim bars. Additional stiffening is provided by the steel plates at the tendon anchorage end-blocks. The buttresses and their reinforcement have been modelled explicitly.

The cylinder wall penetrations and their immediate vicinity have been modelled in detail. Structural features within the penetration area that are represented explicitly in the model are the enhanced reinforcement stiffening, thickened wall section (airlock and equipment hatch penetrations), steel plates lining the penetration cavity, the penetrations cover plates, the deviation in the layout of the vertical and hoop tendons, internal vessel liner and the liner anchorage.

Basemat

The basemat is a thick concrete reinforced slab supporting the vessel superstructure within which the vertical tendons are anchored. It is heavily reinforced at its top and bottom surfaces. The top surface reinforcement consists of a layer of hoop rebars sandwiched between two grids of radially spanning rebars. The bottom surface is reinforced with a rectangular grid of cross rebars. Additional reinforcement is provided in the vicinity of the tendon anchorage gallery. The flexural reinforcements were defined as smeared layers within each solid element. The basemat shear reinforcements were not modelled.

The Prestressing system

The post-tensioning tendons have been modelled using two different approaches. The vertical tendons were modelled explicitly using the two-node, linear truss element T3D2. For each tendon, nodes have been generated coincident to the solid element concrete nodes along the tendon path. Typically, in the non-penetrated areas a vertical tendon consists of up to 220 elements, depending upon its location within the vessel. Each vertical tendon node lying within the cylinder of the vessel is constrained in the horizontal degrees of freedom (i.e. the X and Z directions) to the coincident concrete nodes. The vertical degree of freedom (Y) of tendon nodes within the cylinder were left unconstrained, allowing relative sliding of the tendons and concrete in the vertical direction. Within the cylinder, friction at the concrete/tendon interface is assumed to be negligible and has not been modelled. However, within the dome, the curved trajectory of the tendon causes appreciable friction at the concrete/tendon interface, resulting in a non-uniform variation of load in the tendon. Although interface behaviour has not been explicitly modelled, the non-uniform distribution of load in the vertical tendons over the dome is allowed for by constraining all coincident tendon and concrete nodal degrees of freedom.

The hoop tendons are modelled as single rebars embedded within concrete elements. The concrete elements were defined such that an element edge lies along the path of the hoop tendon as this facilitated the placement of the hoop tendons with the elements. Each hoop tendon starts at one face of the buttress, completes a 360° loop around the vessel and is anchored at the opposite face on the same buttress. Alternative tendons are anchored at opposite buttresses. Interface behaviour between the concrete and the tendon has not been modelled. Frictional loss in the hoop tendons is discussed in the section below.

The load distribution within the tendons was non-uniform because of friction between the tendons and ducts. This was taken into account during the analysis by using the design values of the anchorage loads of 350kN and 471kN for the hoop and vertical tendons respectively. Variation in the tendon loads due to frictional loss was obtained by applying the following Equation 1.

$$P = P_{1,2}\, e^{(-\mu\beta - 0.001L)} \qquad (1)$$

Where

$P_{1,2}$ = Load at the tensioning end 1 or 2.
β = Change of angle from tensioning end.
P = Load at β from tensioning end.
μ = Friction Coefficient. (taken as 0.21)
L = Length of Tendon.

The average seating loss of 24757N was taken from the PCCV test results, and was included in the calculations for the pre-loads. The modelling assumed that the seating loss was linear throughout the 90° segment.

Internal liner and liner anchorages

The thicker insert plates surrounding the main steam and feed water penetrations are simulated with the shell element S4R and the general area of the liner with membrane type M3D4R elements.

The liner-to-concrete anchorage was modelled by connecting the liner node to the corresponding coincident concrete node with three linear spring elements at each node, representing the radial, hoop and axial anchorage plate stiffness. Given that the pitch of the horizontal and vertical liner anchorage plates is not uniform, no attempt was made to simulate the anchorage plates at their exact locations. The spring stiffness values are derived from test results for the pullout of anchorage plates in tensile and shear modes [1].

Concrete reinforcements

The grid of reinforcing bars in the vessel has been represented as rebar smeared within the parent solid elements. The orientation, cross-sectional area, spacing and material properties are taken from the construction drawings [7].

The duct-supporting steel frame construction is modelled as single rebars within the parent solid elements. The properties of the steel frame are given in Ref 5.

PCCV support conditions

The basemat is constructed on a 150mm thick un-reinforced slab which itself is supported on an engineered sand and gravel subgrade. The soil stiffness was characterised as exhibiting a settlement of less than 25mm due to a bearing pressure of 3.11kN/m^2 [7].

The soil was represented using grounded spring elements (SPRING1). Each node on the bottom surface of the basemat was supported on a spring element. The spring stiffness was computed based on the influence area of each spring node. The vessel was constrained to eliminate rigid body translations and rotations at four nodal positions on the top surface of the basemat in the horizontal degrees of freedom.

Thermal property data supplied by SNL

The additional data package from SNL provided thermal properties for the PCCV model, these included:-

- Surface film coefficients for convection to free air for the cylinder, dome & basemat.
- Surface film coefficients for conduction into the soil from the basemat.
- Specific heat capacity of the concrete.
- Thermal conductivity for the concrete.

The actual values of the above properties can be found in Table 1.

Loading data supplied by SNL

The temperature loading for Case 1 is a steady state non-linear increase from 100°C to 200°C (Figure 2). The temperature loading was defined over a period of approximately 42 minutes, which was a pseudo time step as this heat transfer analysis was performed at steady state increments of temperature.

The pressure loading was a linear increase from 0MPa to 1.46MPa over the 42 minute pseudo time step.

Heat transfer modelling

The global PCCV model that was used for Phases 1 & 2[8] was updated for heat transfer analysis. In order for the model to be used for heat transfer analysis some modifications were required. These are highlighted below.

All concrete solid elements were replaced with corresponding heat transfer DC3D8 and DC3D6 elements, these include both the full and reduced integration continuum elements. This is because there are no reduced integration heat transfer elements available for 8 noded continuum elements.

The Liner elements (which were M3D4 & M3D3 membrane elements) were replaced by S4 and S3 shell elements respectively. Even though the shell elements provide an in plane stiffness this was satisfactory as the stiffness can be neglected for heat transfer analysis.

The vertical tendons were previously modelled using T3D2 truss elements, for heat transfer analysis the element type had to be modified to DC1D2 (1D solid) elements. These elements were then attached to the concrete using equations to couple the temperature degrees of freedom. The hoop tendons and rebars were previously smeared into the solid elements using the *REBAR facility within ABAQUS. This type of element cannot be used during heat transfer and as there was no direct solution to this problem the hoop tendons and rebars were omitted for the heat transfer analysis. However the nodal temperatures are applied to the rebars and tendons during the stress analysis.

Boundary conditions

Boundary conditions applied are as follows:-

- Sink Temperature of 25°C outside the PCCV.
- Convection from the outer surfaces of the cylinder, dome and exposed sections of the basemat concrete to free air.
- Convection from the insulated bottom surface of the basemat to the soil.

Conduction between liner and inner concrete

To facilitate Conduction between the Liner and the concrete, surfaces were created on the outer surface of the liner and the inner surface of the concrete so that a gap conduction could be set up. Gap conductivity uses the two surfaces and a specified conductivity depending upon distance between the two surfaces. The conductivity was set as a perfect thermal contact. Therefore between the two surfaces the thermal conductivity was defined as being the same as the conductivity of steel irrespective of distance between the surfaces.

Convection from outer concrete surfaces

Two separate regions were specified for the convection from the outer surface of the concrete. Firstly one region was defined for the dome, cylinder and exposed sections of the basemat (i.e. top and sides) to allow for standard convection. Secondly the base of the basemat was defined as a surface to simulate conduction from the basemat into the soil. The equations for the convection from the outer surfaces were provided by SNL and are shown below:-

Convection to free air

$$h = 4.80 * (\square T)^{1/3} \text{ W/m}^0\text{K}$$

Convection into soil

$$h = 0.0724 \text{ W/m}^0\text{K}$$

Effects of radiation have been ignored.

Thermal Loading

The heat transfer analysis was completed in two steps. The first step was a steady state heat transfer step in which the liner temperature was raised from 20°C to 100°C.

The second step raised the liner temperature in accordance with the temperature profile (Figure 2) distributed by SNL. Each increment of the second step was converged as a steady state using the 42.23 minute pseudo time step as defined in the original SNL heat transfer analysis. By performing the heat transfer analysis in this way the pressure loading can be run as a time history using steady state temperatures at each increment of pressure.

Analysis Procedure

The stress analysis model was loaded as follows:-

Step 1 – Application of prestressing
Step 2 – Increase model temperature from 20°C to 100°C steady state
Step 3 – Apply temperature and pressure loading as defined by SNL (Figure 2)

Steps 2 & 3 of the stress analysis model read in the nodal temperatures from the heat transfer analysis and are applied at each increment as a steady state temperature.

Results and Assessment

For the ISP 48 project the number of standard output locations have been reduced to 23 locations. For each location, the following results were obtained from the following are plotted:

- LST test results (pressure only) from Ref 1.
- FE analysis pressure only.
- FE analysis pressure plus temperature.
- FE analysis pressure plus temperature with TTC.

For sake of brevity, results at standard output location 39 and 53 are presented in Figures 3 to 5.

The results are plotted against pressure which is related to temperature as shown in Figure 2.

The finite element model have the initial values reset to line up with the Limit State Test results.

The radial deformation at 135 degrees azimuth for various loading stages is shown in Figure 8.

Assessment of liner

The primary function of the steel liner is to act as the pressure boundary for the containment. Therefore it is important to know the pressure it can sustain before rupture. It is the design intent that liner rupture and pressure leakage occurs at levels below that required to cause catastrophic failure of the concrete containment. The limit state test [1] demonstrated this design feature. Liner rupture was the first failure mode and the high leak rates seen ensured the concrete containment did not fail catastrophically.

The limit state test [1] did not consider the effects of accident temperature transients. Under such conditions, liner thermal expansion could influence the limit load before rupture. If liner thermal expansion is constrained by the concrete containment, compressive strains may be induced in the liner that increases the pressure required to cause rupture. From a design viewpoint, the concern is that the pressure required for liner rupture may increase to levels above that which causes structural failure of the vessel.

Figure 3(location 39) presents the mechanical strain (total strain – thermal strain) in liner in the hoop direction midway up the cylinder wall, at the 135° azimuth. This figure highlights decreased strains are calculated in the liner when the thermal loading is included. These are indicative of compressive stress developed in the liner (see Figure 4) due to the differential thermal expansion.

Assuming the liner rupture strain the same as that observed during LST(0.0015), the data indicates that the rupture pressure is increases by 0.15MPa when thermal expansion is included (see Figure 3). The results indicates that as expected, the liner is under compression initially due to the differential thermal expansion but begins to experience tensile stress after the cracking of the concrete.

Tendon Assessment

Ultimate structural collapse of the PCCV test model was initiated by failure of hoop tendons located in the free field region, approximately mid-height to the cylinder wall. Tendon failures resulted in a loss of pre-load to the concrete in this region and a breach of the wall ensued. It is therefore important to assess if the application of accident temperatures reduces the pressure at which rupture of the tendons occurs. Two aspects are assessed.

The first aspect is the temperature of the tendons during the fault. A significant increase could lower the material yield strength. Figure 7 presents a profile of the temperature distribution through the cylinder wall of the vessel. This shows the peak fault temperature of 200°C is transferred through the liner to the inner surface of the wall. However, the temperature quickly reduces through the wall thickness due to the insulating properties of the concrete. The hoop tendons are located in the wall, approximately 216mm from the inner surface. At this location the temperature approximates to a range between 100°C to 130°C and therefore is well below the level required to reduce the material yield strength [9].

The second aspect of vessel response considered is its global response when accident temperatures are included. Thermal expansion of the vessel could increase the prestress in the tendons and increases the pressure required to cause rupture. Figure 5 presents the mechanical strain(total strain – thermal strain) histories for the hoop tendon located at an elevation of 4.57m, mid-way between the equipment and airlock hatches. This is the region of vessel rupture from the structural failure test. The figure highlights that at the vessel rupture pressure of 1.4MPa, a tendon strain of 0.0034 is induced when only pressure is applied. For the pressure plus temperature case, a tendon strain of 0.0034 equates to a pressure limit of 1.5MPa. This is an increase in the vessel capacity by 7%. The results are summarised in Table 2

The load distribution along the hoop tendon at different stages of vessel pressurisation, during Case 1, is presented in Figure 6. This shows how the tendon loads redistribute as the vessel pressure increases. At the pre-stressing load, the tendon profile is as expected. High loads occur at the anchor points at the 90° and 270° azimuths. The loads then reduce to a minimum at the mid-length due to friction losses between the tendon and concrete wall. As the vessel pressure increases, the loads redistribute such that the maximum shifts to the mid-length of the tendon. This coincides with the tendon failures and containment breach at the 0° azimuth during the LST. It is the vessels deformation that causes load concentration in the tendons that leads to tendon failure near the 0° azimuth.

Thermal transient creep

For the thermal transient investigated, the impact of TTC on strain levels is shown to be small. Comparison of the inner wall strain distributions highlight there is very little change when TTC is simulated [10]. A nominal reduction is observed in the E11 (i.e. radial at this location) tensile strain at the top of the buttress on the 270° azimuth [10]. The level of TTC activity in concrete is temperature dependant. Creep initiation occurs at levels above 85°C and activity increases with respect to temperatures in excess of this. However, for the fault transient investigated low temperature distributions dominate, particularly through the thickness of the containment concrete boundary. Hence significant strain re-distribution is not witnessed.

The inclusion of TTC has an effect on vessel displacements. The effects are most pronounced for the radial displacements. TTC is simulated using an effective Young's modulus approach to reduce the material stiffness of the concrete. Thus the restraining effects of the pre-tensioning tendons become more dominant as the concrete stiffness reduces. The increasing dominance of the compressive pre-loading results in the reduced displacements calculated for the TTC analysis.

This investigation considers a fault transient based on a loss of cooling accident for a typical PWR containment. However, for British Advanced Gas-cooled Reactors (AGR), the pre-stressed concrete pressure vessels (PCPV) are expected to experience more elevated and sustained thermal transients. Thus TTC can be expected to be of more significance to the AGRs.

Conclusions

When the effects of accident temperatures on concrete containments are considered, the following conclusions can be made.

- The elevated temperatures induce significant thermal expansion of the steel liner. The thermal straining of the liner results in rupture at approximately 1.25MPa. This is 14% higher than the rupture pressure of 1.1MPa obtained from the mechanical loading of the limit state test.
- The pre-loaded tendons are well insulated from the peak temperatures experienced in the accident transient. However, the global response of the PCCV increases the pressure required to induce tendon failure from 1.4MPa to approximately 1.50MPa. This is an increase of approximately 7% compared to the limit state test.
- For the accident condition investigated, liner rupture is the initial failure mode. The design intent of liner rupture before catastrophic failure of the containment is maintained.
- If the margin between tendon failure and liner rupture is defined as the ratio of vessel pressurisation required to cause the failures, the margin decreases from 1.27 for pressure only to 1.2 for pressure plus temperature loads.
- The temperature dependent effect of TTC in concrete is simulated using an effective modulus approach. For the accident condition investigated TTC is shown to have a small effect on PCCV strain distributions, but reduced vessel displacements are witnessed.

References

[1] Overpressurisation Test of a 1:4 Scale Prestress Concrete Containment Vessel Model, Sandia National Lab., NUREG/CR-6810, SAND2003-0840P, Project Report No. R-SN-P-010, March 2003.
[2] HSE/NNC Pretest Analysis Report for ¼ Scale PCCV Model, NNC Report C5769/TR/002.
[3] Pretest Round Robin Analysis of a Prestressed Concrete Containment Vessel, Sandia National Lab., NUREG/CR-6678, SANDE 00-1535, August 2000.
[4] HSE/NNC PCCV Round Robin Post Test Analysis, NNC Report C6635/TR/001, Issue 01, Dec 2002.

[5] Summary Records of the 2nd meeting of the ISP48 Exercise on Containment Capacity. Madrid, Spain, 19 March 2004. OECD Nuclear Energy Agency IAGE-CONC/ISP48/(04)1. 2 April 2004.
[6] ABAQUS/Standard Version 6.4, ABAQUS/CAE, ABAQUS/Viewer, ABAQUS Inc., USA.
[7] Obayashi Corporation package of construction drawings of PCCV model.
[8] International Standard Problem on Containment Capacity (ISP-48) Phases 1 & 2 NNC Report C11248/TR/001 Issue 2 April 2004.
[9] Structural Performance of PCPV's at Elevated Temperatures. Nuclear Electric plc, EWI-17275/R/008, December 1996.
[10] International Standard Problem on Containment Capacity (ISP-48) Phases 1 & 2 NNC Report C11248/TR/002 Issue 01 December 2004.
[11] An Engineering Data Book – J R Calvert & R A Farrar, 1999.

Acknowledgements

The Authors are grateful for the support and encouragement which they have received from Mr Graham Doughty (British Energy) and Dave Shepherd (NII, HSE). It is through their good offices that this analysis work at NNC has commenced.

Table 1 Heat Transfer Material Properties

Heat Transfer Property	**Steel (Liner & Tendons)**	**Concrete**
Conductivity (W/mmK)	50 (Ref 11)	1.0-1.6 (SNL)
Specific Heat Capacity (Nmm/tonneK)	$4.6*10^8$ (Ref 11)	$0.879*10^9$ (SNL)
Expansion (mm/mm°C)	$10.8*10^{-6}$ (Ref 11)	$10*10^{-6}$ (Ref 11)

Table 2 Summary of Results: Calculated Pressures (MPa) and Strains (%)

Loading	Cracking		Liner Yield	Liner Rupture	Hoop Tendon Stress		Pressure @ Failure	Free Field Hoop Strain**	Max Radial Displacement***	Mode
	Hoop	Meridional			Yield[+]	Rupture				
Pressure	0.6	0.6	0.75	1.1*	1.16	1.4[!]	1.4	0.12%	38.8mm	Liner tearing causing high leakage rates.
Pressure + Temperature	0.6	0.6	0.83	1.25	0.96	1.5	1.25 1.50	0.18%	49.4mm	Liner tearing. Hoop Tendon failure.
Pressure + Temperature with TTC	0.6	0.6	0.82	-	-	-	-	-	-	
LST Test Results	0.59	-	-	0.98	1.02	-	0.98 1.295	0.17% -	28.30mm	Liner Tearing, 1% mass/day leak. Max. Pressure @ 1000% mass/day leak
SFMT Test Results	-	-	-	-	-	1.4	1.4	-	86mm	Structural collapse

* Liner strain of 0.0017 reached at SOL39

! Hoop tendon strain of 0.0034 at the maximum SFMT pressure in tendon H53

** Strains at SOL39 @0.98Mpa

*** Displacement at SOL 14 @1.295Mpa

+ Assumed yield strain of 0.2% obtained from tendon testing at SOL50

Figure 1 Finite Element model of PCCV

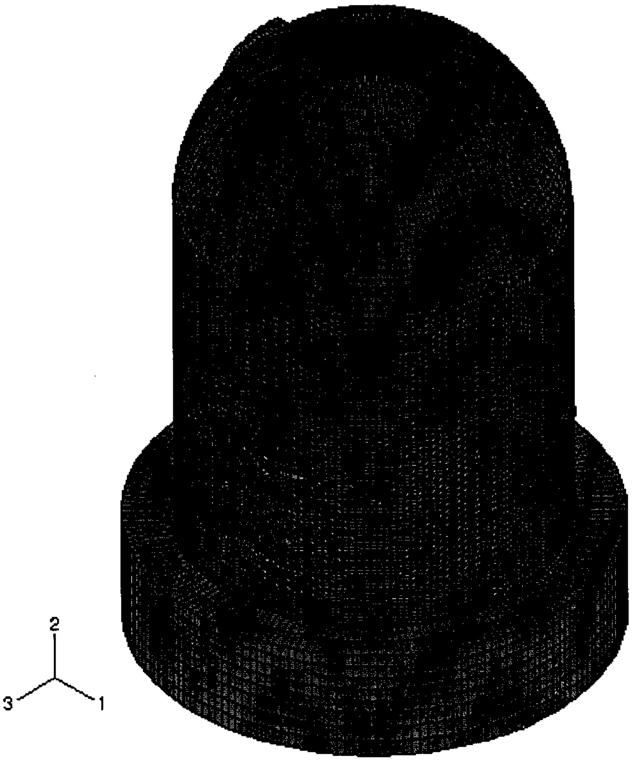

Figure 2 Pressure vs temperature from SNL

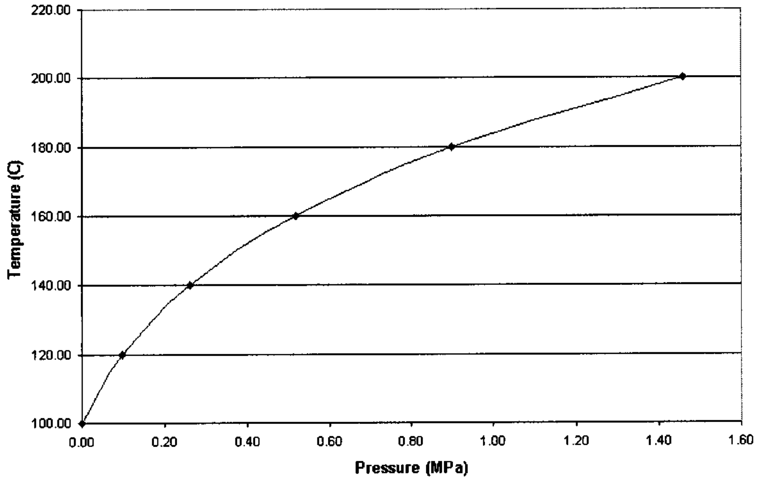

Figure 3 Standard Output Location 39 Hoop Liner Mechanical Strain

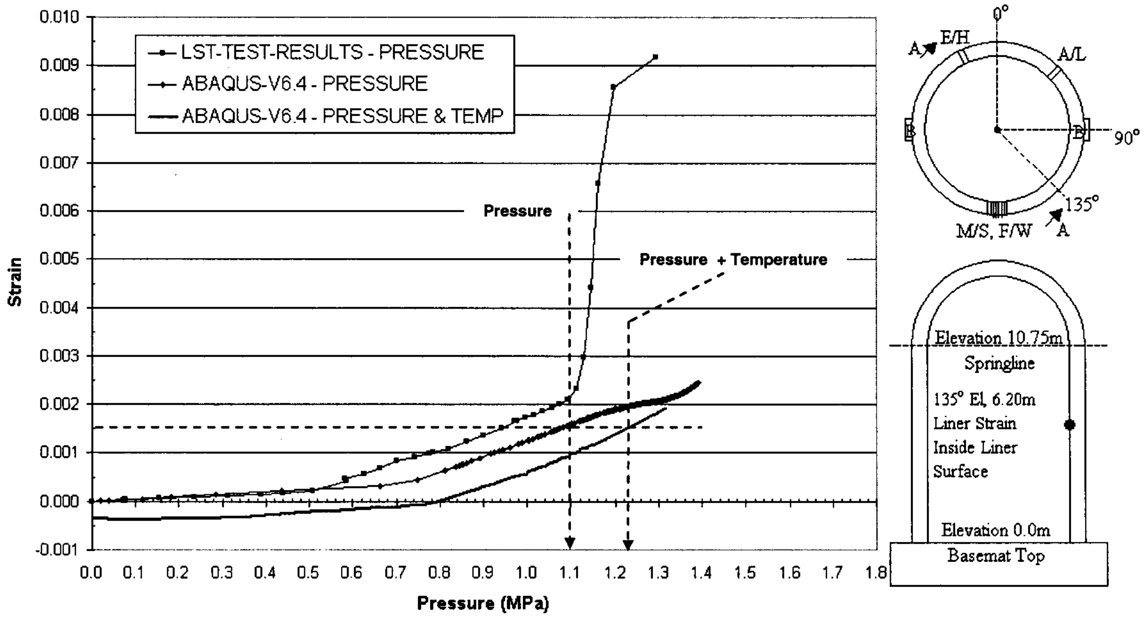

Figure 4 Standard Output Location 39 Hoop Liner Stress

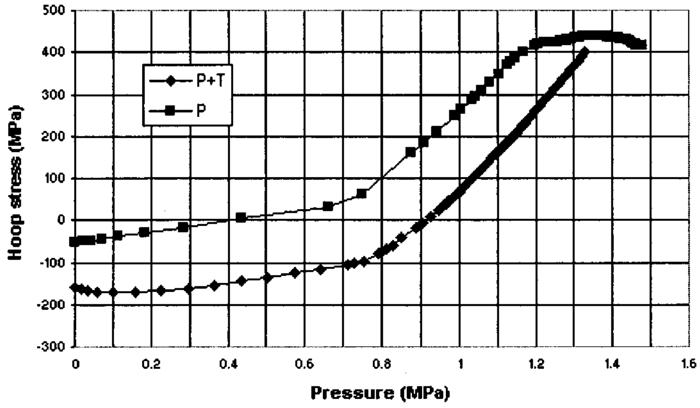

Figure 5 Standard Output Location 53 Hoop Tendon Mechanical Strain

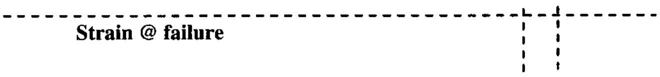

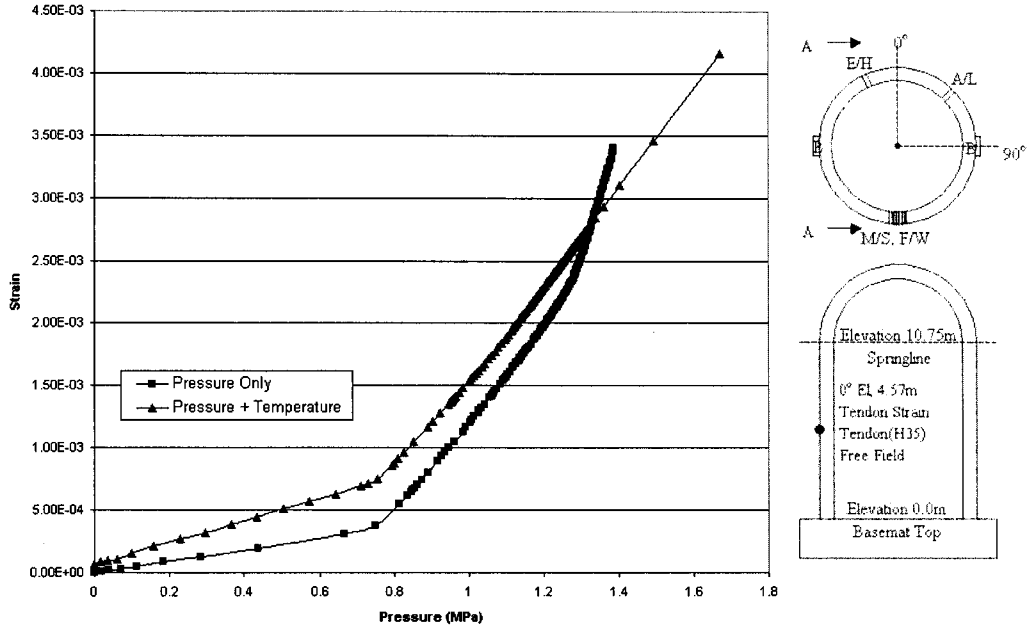

Figure 6 Tendon Load Profile During Vessel Pressurisation and Heat-Up

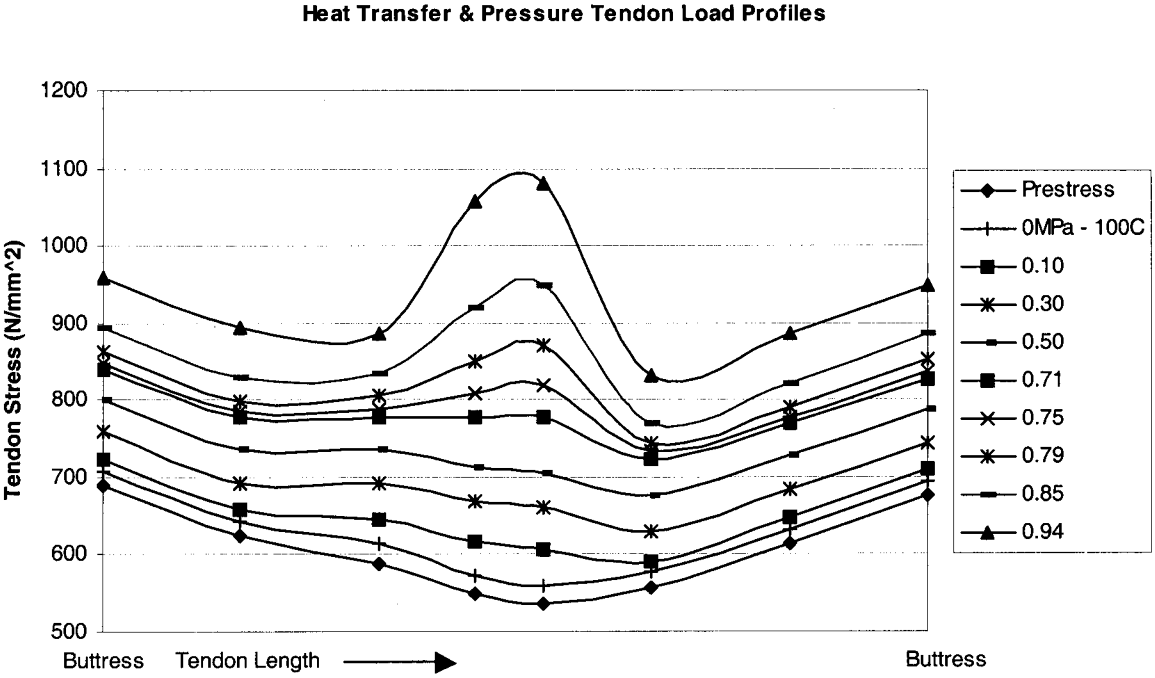

Figure 7 Temperature contour profiles through the cylinder wall thickness

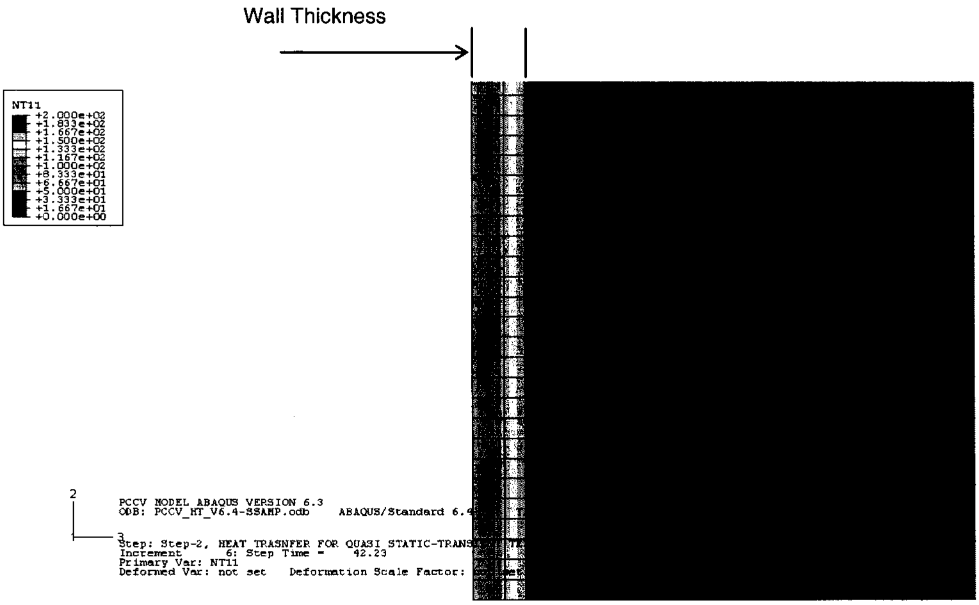
Wall Thickness
NT11
+2.000e+02
+1.833e+02
+1.667e+02
+1.500e+02
+1.333e+02
+1.167e+02
+1.000e+02
+8.333e+01
+6.667e+01
+5.000e+01
+3.333e+01
+1.667e+01
+0.000e+00
2
3
PCCV MODEL ABAQUS VERSION 6.3
ODB: PCCV_HT_V6.4-SSAMP.odb ABAQUS/Standard 6.4
Step: Step-2, HEAT TRASNFER FOR QUASI STATIC-TRANS
Increment 6: Step Time = 42.23
Primary Var: NT11
Deformed Var: not set Deformation Scale Factor:

Figure 8 PCCV deformation at Az @ 135 x 100 at outer surface

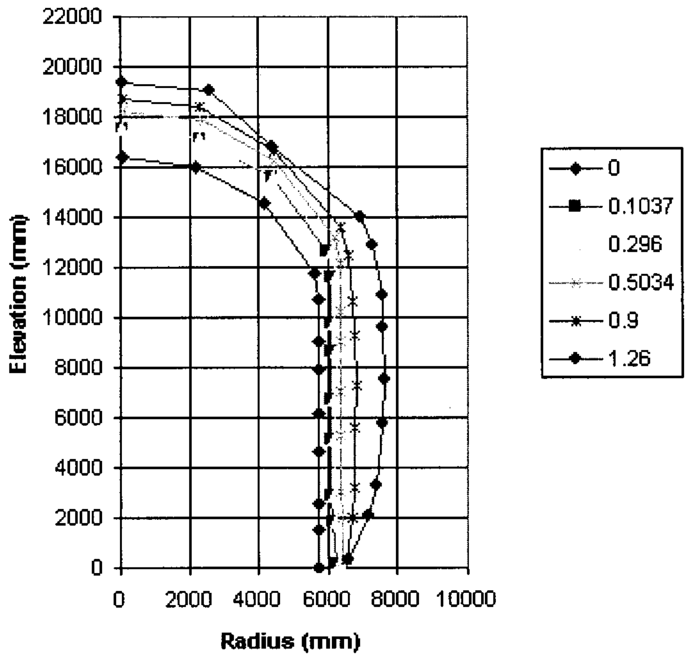

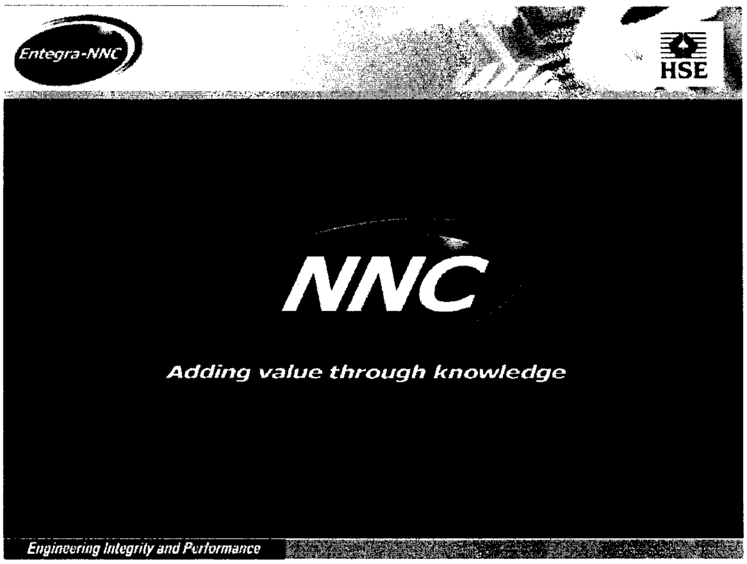

Entegra-NNC

HSE

NNC

Adding value through knowledge

Engineering Integrity and Performance

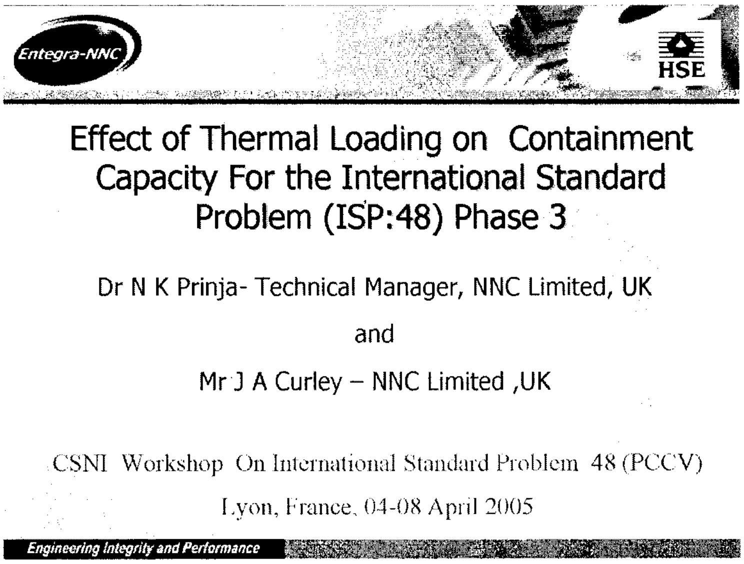

Entegra-NNC

HSE

Effect of Thermal Loading on Containment Capacity For the International Standard Problem (ISP:48) Phase 3

Dr N K Prinja- Technical Manager, NNC Limited, UK

and

Mr J A Curley – NNC Limited ,UK

CSNI Workshop On International Standard Problem 48 (PCCV)

Lyon, France, 04-08 April 2005

Engineering Integrity and Performance

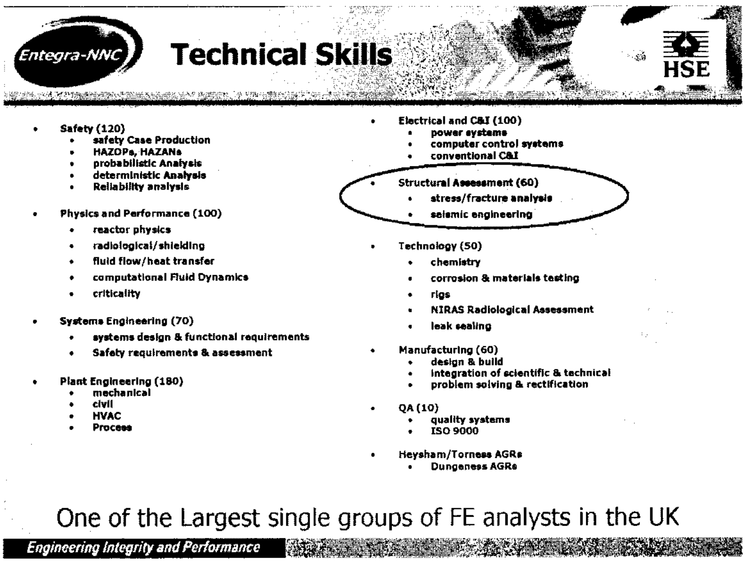

Entegra-NNC

HSE

Technical Skills

- Safety (120)
  - safety Case Production
  - HAZOPs, HAZANs
  - probabilistic Analysis
  - deterministic Analysis
  - Reliability analysis
- Physics and Performance (100)
  - reactor physics
  - radiological/shielding
  - fluid flow/heat transfer
  - computational Fluid Dynamics
  - criticality
- Systems Engineering (70)
  - systems design & functional requirements
  - Safety requirements & assessment
- Plant Engineering (180)
  - mechanical
  - civil
  - HVAC
  - Process
- Electrical and C&I (100)
  - power systems
  - computer control systems
  - conventional C&I
- Structural Assessment (60)
  - stress/fracture analysis
  - seismic engineering
- Technology (50)
  - chemistry
  - corrosion & materials testing
  - rigs
  - NIRAS Radiological Assessment
  - leak sealing
- Manufacturing (60)
  - design & build
  - integration of scientific & technical
  - problem solving & rectification
- QA (10)
  - quality systems
  - ISO 9000
- Heysham/Torness AGRs
  - Dungeness AGRs

One of the Largest single groups of FE analysts in the UK

Engineering Integrity and Performance

The ISP Analysis Team

British Energy

Mr Graham Doughty

HSE

Mr Dave Shepherd, Technical Officer

NNC

Dr Nawal Prinja, Technical Manager

Mr Jim Curley, Technical Lead, Structural Analysis.

Commonwealth Scholar

Mr S.M.Basha, BARC, India

Engineering Integrity and Performance

The ISP Challenge

1/4 scale model of OHI-3 PWR in Japan

What effects does thermal loading have on;

- The PCCV Failure Pressure?
- The PCCV Failure Mode?

NNC sponsored by British Energy

Engineering Integrity and Performance

PCCV 1/4 Scale Model at Sandia Labs., Albuquerque, USA

ISP Reporting Requirements

- 23 Output Locations
- Output Results
  - Displacements
  - Reinforcement strains
  - Liner strains
  - Tendon loads
  - Liner stresses

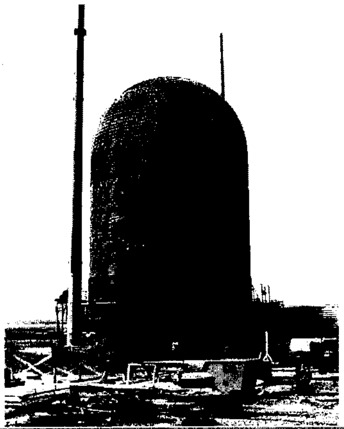

Engineering Integrity and Performance

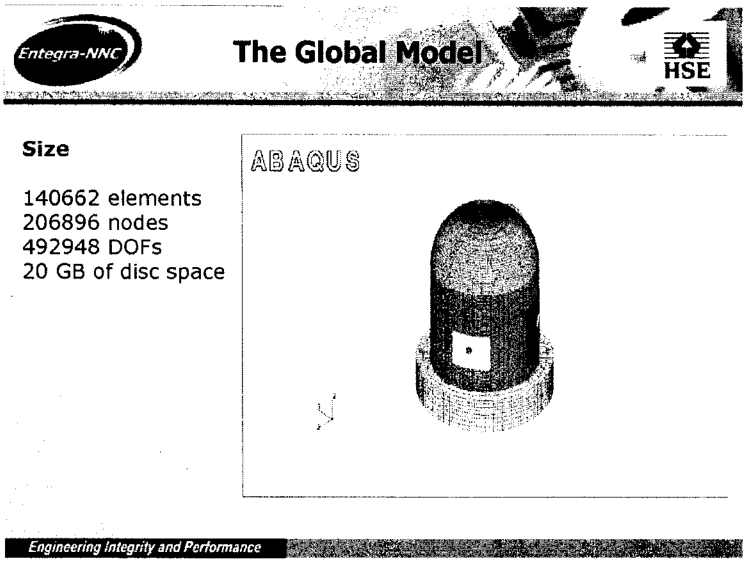
Entegra-NNC
HSE
ABAQUS

The Global Model

Size

140662 elements
206896 nodes
492948 DOFs
20 GB of disc space

Engineering Integrity and Performance

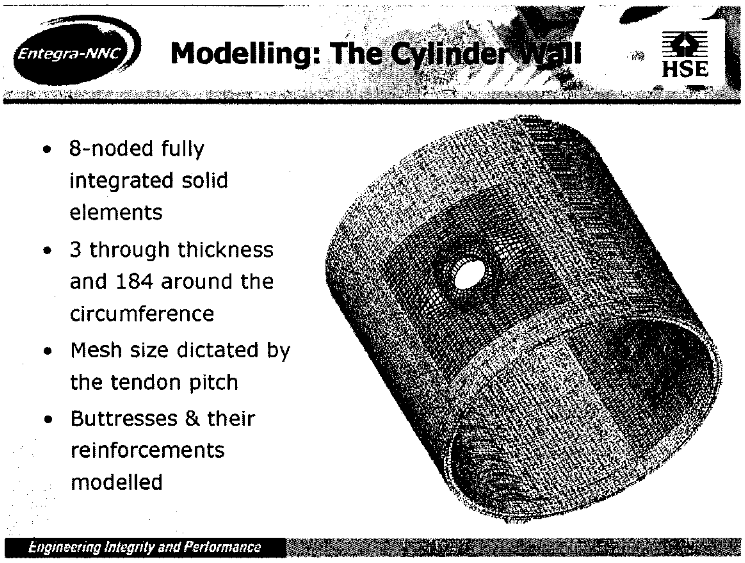
Entegra-NNC
HSE

Modelling: The Cylinder Wall

- 8-noded fully integrated solid elements
- 3 through thickness and 184 around the circumference
- Mesh size dictated by the tendon pitch
- Buttresses & their reinforcements modelled

Engineering Integrity and Performance

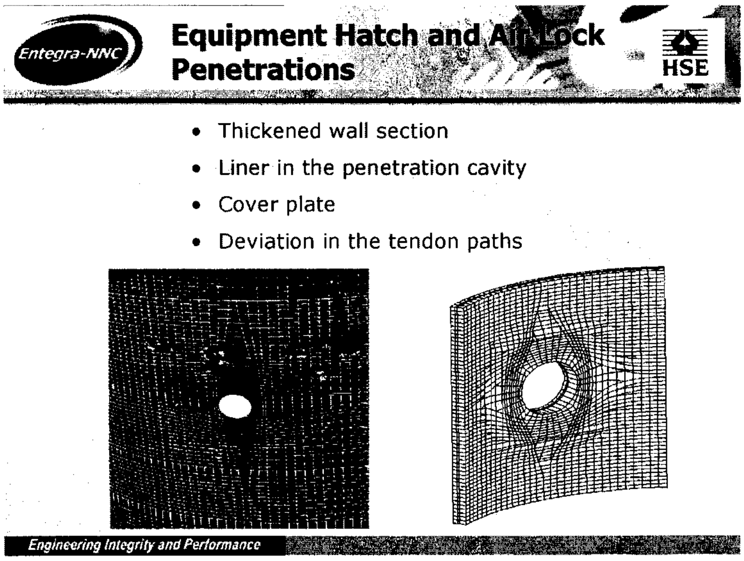
Entegra-NNC
HSE

Equipment Hatch and Air Lock Penetrations

- Thickened wall section
- Liner in the penetration cavity
- Cover plate
- Deviation in the tendon paths

Engineering Integrity and Performance

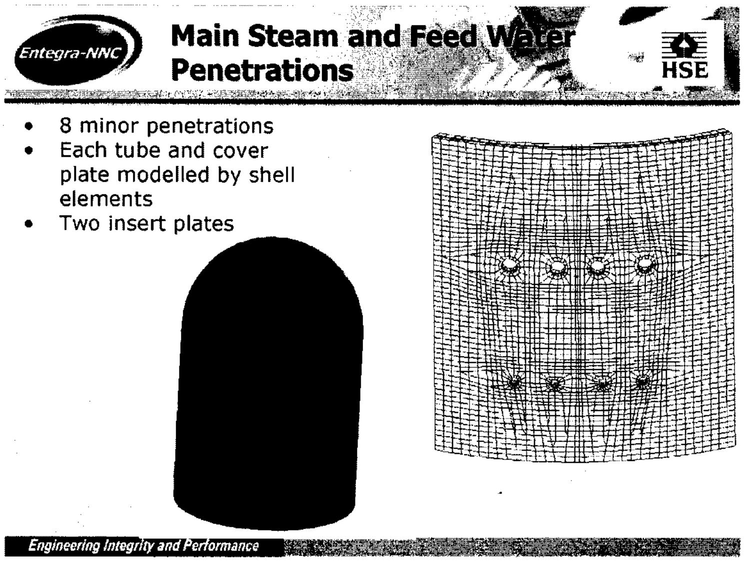

Main Steam and Feed Water Penetrations

- 8 minor penetrations
- Each tube and cover plate modelled by shell elements
- Two insert plates

Engineering Integrity and Performance

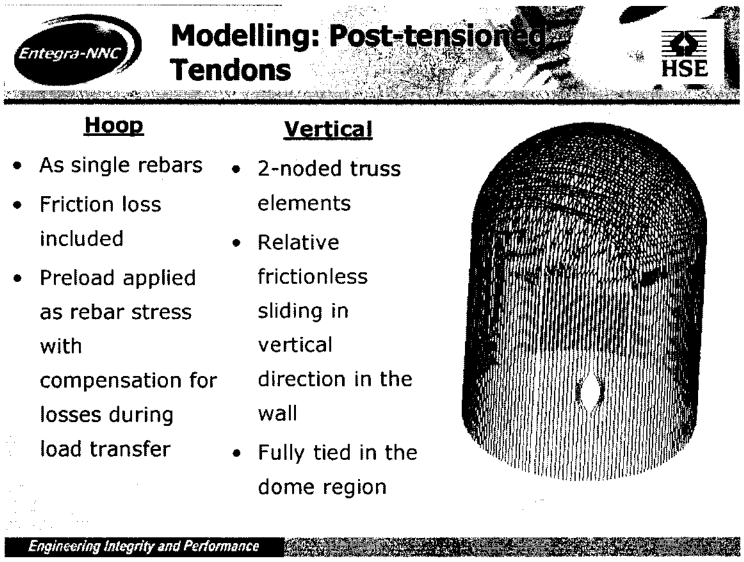

Modelling: Post-tensioned Tendons

Hoop

- As single rebars
- Friction loss included
- Preload applied as rebar stress with compensation for losses during load transfer

Vertical

- 2-noded truss elements
- Relative frictionless sliding in vertical direction in the wall
- Fully tied in the dome region

Engineering Integrity and Performance

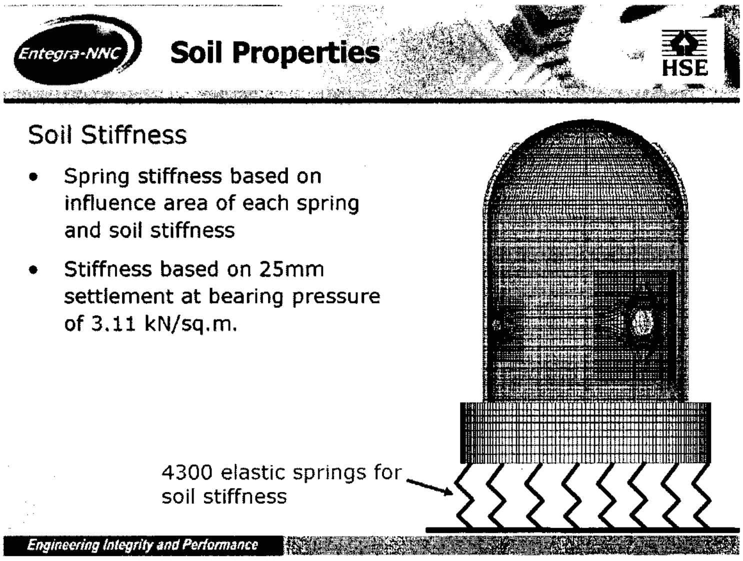

Soil Properties

Soil Stiffness

- Spring stiffness based on influence area of each spring and soil stiffness
- Stiffness based on 25mm settlement at bearing pressure of 3.11 kN/sq.m.

4300 elastic springs for soil stiffness

Engineering Integrity and Performance

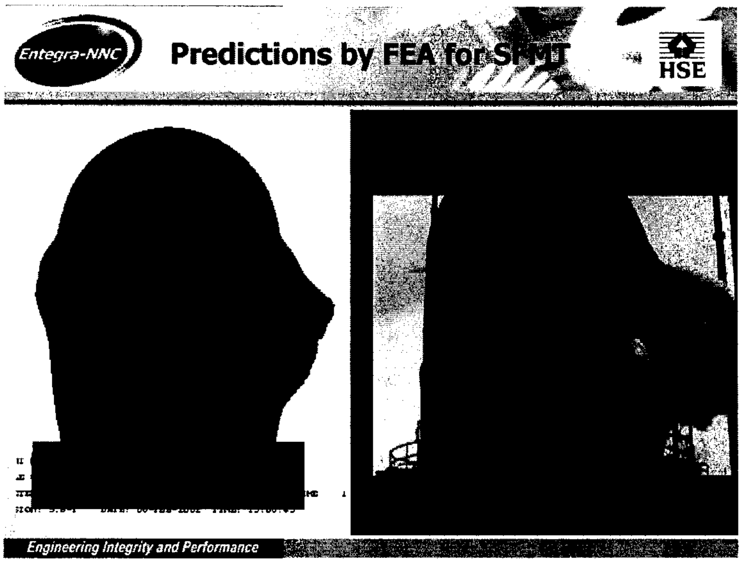

Predictions by FEA for SFMT

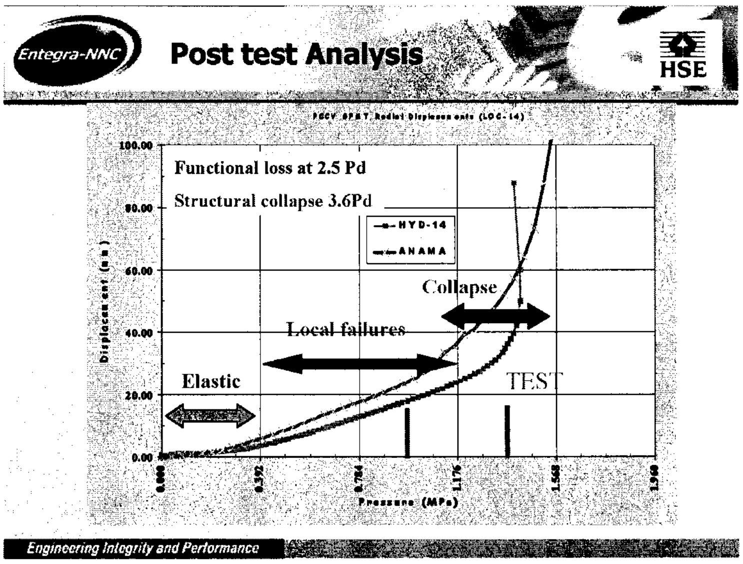

Post test Analysis

Project Sequence of ISP48

The ISP consisted of four phases over a period of 2 years

- Phase 1: Data Collection and Identification
- Phase 2: Calculation of the Limit State Test (LST), i.e. static pressure loading
- Phase 3:
  - Saturated steam condition case (Case1)
  - Station blackout scenario(Case2)- Not Analysed
  - Investigate effects of Transient Thermal Creep in High Temperature Concrete (Case 1)- Additional study
- Phase 4: Reporting Workshop

Entegra-NNC

HSE

Engineering Integrity and Performance

Entegra-NNC

Transient Thermal creep

HSE

- What is TTC ?
  - TTC is defined as the strain in excess of the creep at a constant temperature and load.
  - Is a function of temperature alone.
  - Only occurs on 1st load cycle when the concrete is heated beyond a temperature previously experienced.
  - Has been found to be irrecoverable.

Engineering Integrity and Performance

Entegra-NNC

Concrete Material Model

HSE

- The ANAMAT concrete material model could not model thermal strain with concrete cracking
- The ABAQUS concrete model could not combine creep with concrete cracking
- The effective modulus approach is used with ABAQUS
- Young's modus for the concrete is specified for a range of temperatures between 85°C and 200°C.

Engineering Integrity and Performance

Entegra-NNC

Limit Loads

HSE

- 1- Extensive cracking leading to nonlinear response
- 2- Integrity of pressure boundary lost leading to unacceptable leakage
- 3- Structural collapse

Engineering Integrity and Performance

Entegra-NNC

Heat Transfer Analysis – Case 1 Loading

HSE

- Heat Transfer completed in 2 steps.
  - Step 1 – Steady state with Liner @ 100°C.
  - Step 2 – Further increase in Temperature with Pressure for Saturated Steam Condition.

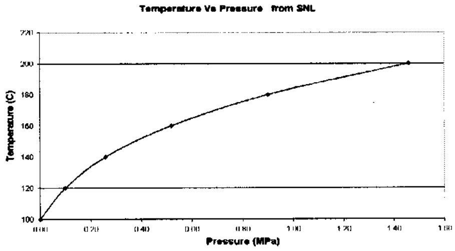

Engineering Integrity and Performance

Entegra-NNC

Heat Transfer Material Properties

HSE

Heat Transfer Property	Steel (Liner & Tendons)#	Concrete
Conductivity (W/mmK)	50	1.0-1.6 (SNL)
Specific Heat Capacity (Nmm/tonneK)	$4.6*10^8$	$0.879*10^9$ (SNL)
Coefficient of Expansion (mm/mm°C)	$10.8*10^{-6}$	$10*10^{-6}$

Values adopted from 'An Engineering Data Book' – J R Calvert & R A Farrar 1999

Engineering Integrity and Performance

Entegra-NNC

Heat Transfer Modelling of PCCV

HSE

Element Types

Element types were required to be changed for heat transfer analysis. These were

•Concrete Elements	C3D8	DC3D8
•Liner Elements	M3D4	S4
	M3D3	S3
•Vertical Tendons	T3D2	DC1D2(1D solids- Heat Transfer links)

Tendons and rebar elements using *rebar command has to be removed due to incompatibility

Engineering Integrity and Performance

Heat Transfer Modelling of PCCV

Generation of HT surfaces

Heat transfer surfaces have been defined on various sections of the PCCV these are:

- Outer surface of Liner
- Inner surface of Concrete
- Outer surface of Concrete

Heat Transfer Modelling of PCCV

HT Boundaries

- The boundary temperature is applied to the liner
- Gap conductance is used between the outer liner surface and the inner concrete surface

Two different 'h' values are used

  - Convection with air for outer surface of cylinder,dome and exposed section of basemat,

    $h = 0.0153(\Delta T)^{0.3}$ lbf/in-s-°F

  - Conduction at basemat and soil interface,

    $h = 2.3\times10^{-4}$ lbf/in-s-°F

Case 1 Heat Transfer Analysis Comparison

- Comparison between NNC, SNL & Hand Calculation show good agreement.

Analysis	Temperature (°C)
NNC FE	56.66
SNL FE	53.50
Hand Calculation	56.52

Note: Temperature refers to cylinder outer surface

Entegra-NNC

Stress Analysis – Case 1

HSE

- **The Stress analysis is being performed in 3 steps**
  - Step 1 – Prestressing Loads Applied
  - Step 2 – Raise model to temperatures associated with a liner temperature of 100°C (step 1 from HT)
  - Step 3 – Raise temperatures from step 2 of the heat transfer model and apply pressurisation to the inside of the concrete.
  - Analysis reached 1.3MPa and 195°C
  - TTC analysis achieved 0.9MPa only due to convergence problems in ABAQUS

Engineering Integrity and Performance

Entegra-NNC

Strain Results

HSE

- For consistency the strains are plotted as follows
- Hoop strain(Mechanical)= E11- THE11
- Axial strain(Mechanical)= E22- THE22

where

E11 and E22 are total strain

THE11 and THE22 are thermal strain

Engineering Integrity and Performance

Entegra-NNC

Deformation profiles at 0.84MPa and 179°C

HSE

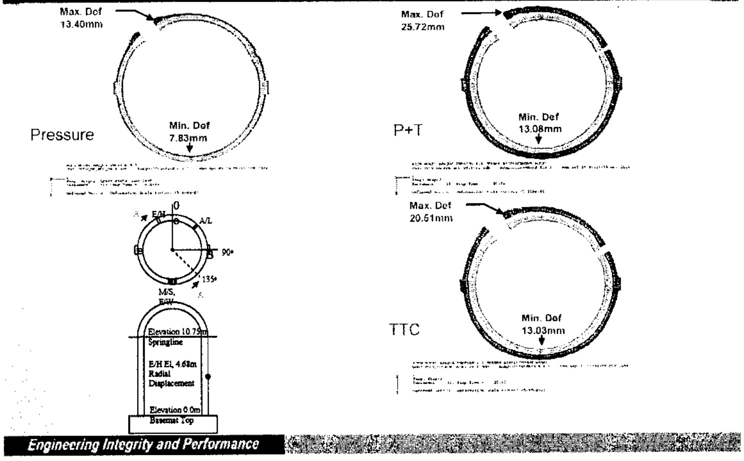

Max. Dof
13.40mm
Pressure
Min. Dof
7.83mm
Max. Dof
25.72mm
P+T
Min. Dof
13.08mm
0
E/H
A/L
90°
135°
M/S,
E/W
Elevation 10.75m
Springline
E/H El. 4.68m
Radial
Displacement
Elevation 0.0m
Basemat Top
Max. Def
20.51mm
TTC
Min. Dof
13.03mm

Engineering Integrity and Performance

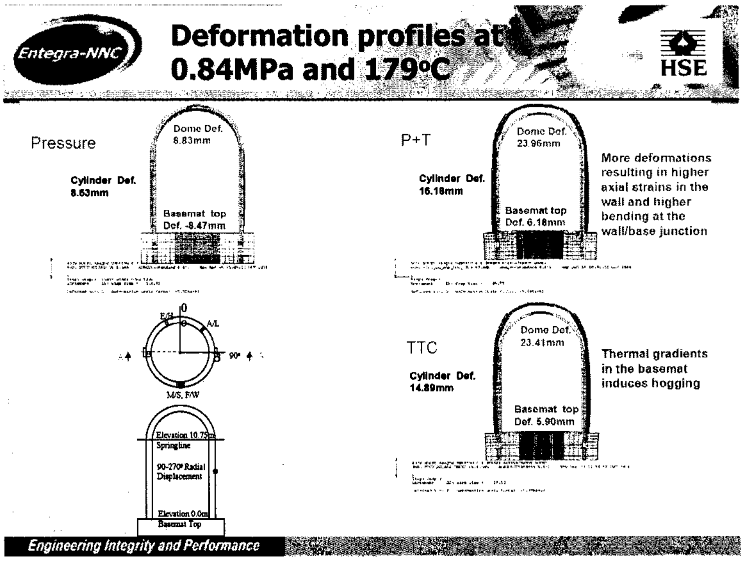

Deformation profiles at 0.84MPa and 179°C

Pressure

Dome Def. 8.83mm

Cylinder Def. 8.63mm

Basemat top Def. -8.47mm

P+T

Dome Def. 23.96mm

Cylinder Def. 16.18mm

Basemat top Def. 6.18mm

More deformations resulting in higher axial strains in the wall and higher bending at the wall/base junction

TTC

Dome Def. 23.41mm

Cylinder Def. 14.89mm

Basemat top Def. 5.90mm

Thermal gradients in the basemat induces hogging

0
E/H
A/L
90°
A
M/S, F/W
Elevation 10.75m
Springline
90-270° Radial Displacement
Elevation 0.0m
Basemat Top

Engineering Integrity and Performance

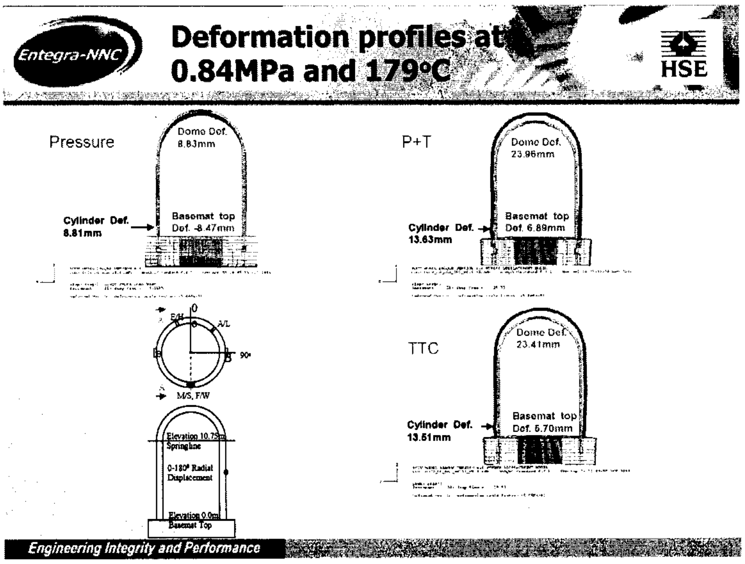

Deformation profiles at 0.84MPa and 179°C

Pressure

Dome Def. 8.83mm

Cylinder Def. 8.81mm

Basemat top Def. -8.47mm

P+T

Dome Def. 23.96mm

Cylinder Def. 13.63mm

Basemat top Def. 6.89mm

TTC

Dome Def. 23.41mm

Cylinder Def. 13.51mm

Basemat top Def. 5.70mm

0
E/H
A/L
90°
M/S, F/W
Elevation 10.75m
Springline
0-180° Radial Displacement
Elevation 0.0m
Basemat Top

Engineering Integrity and Performance

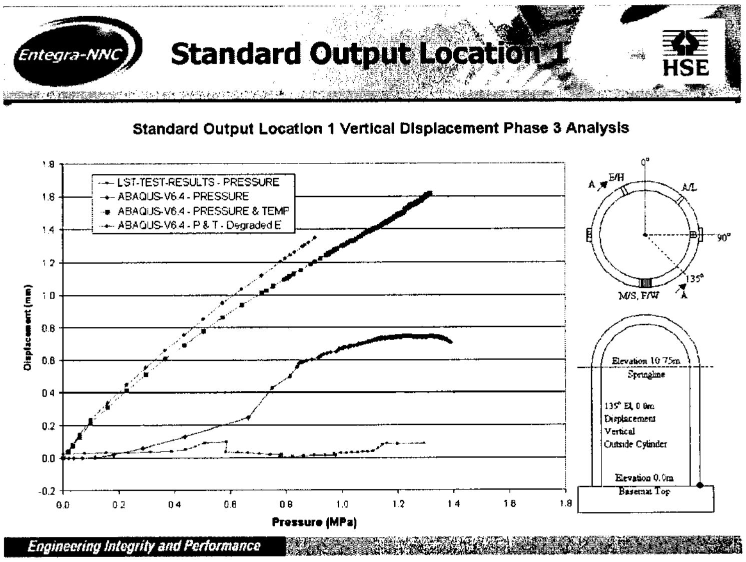

Standard Output Location 1

Standard Output Location 1 Vertical Displacement Phase 3 Analysis

Engineering Integrity and Performance

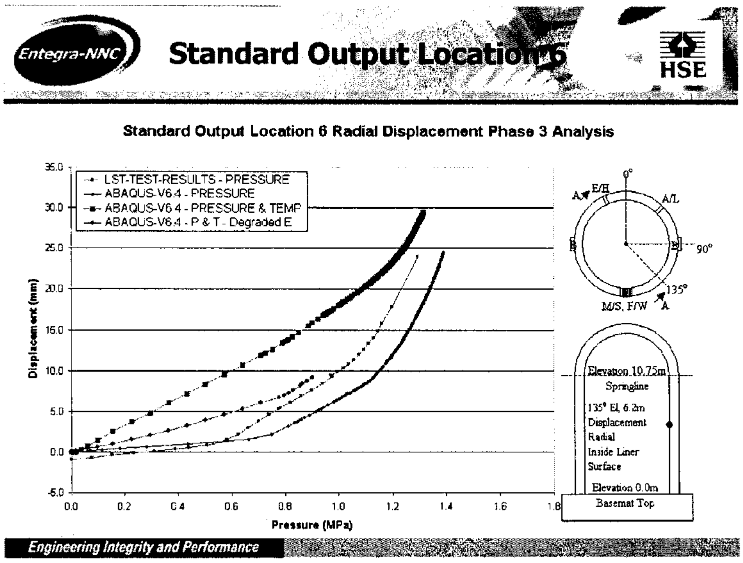

Standard Output Location 6

Standard Output Location 6 Radial Displacement Phase 3 Analysis

Engineering Integrity and Performance

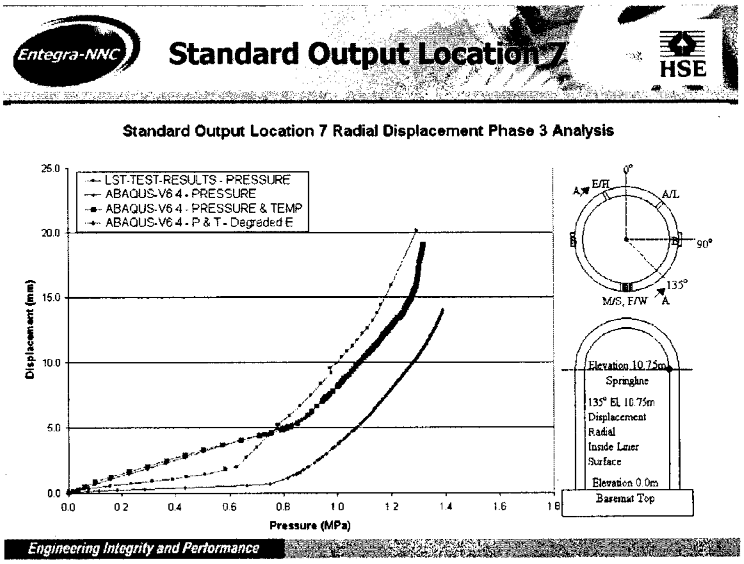

Standard Output Location 7

Standard Output Location 7 Radial Displacement Phase 3 Analysis

Engineering Integrity and Performance

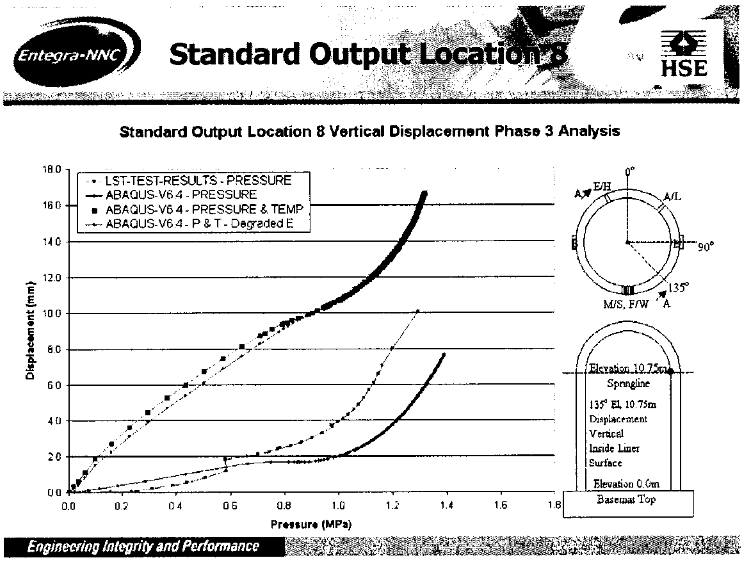

Standard Output Location 8

Standard Output Location 8 Vertical Displacement Phase 3 Analysis

Engineering Integrity and Performance

Standard Output Location 11

Standard Output Location 11 Vertical Displacement Phase 3 Analysis

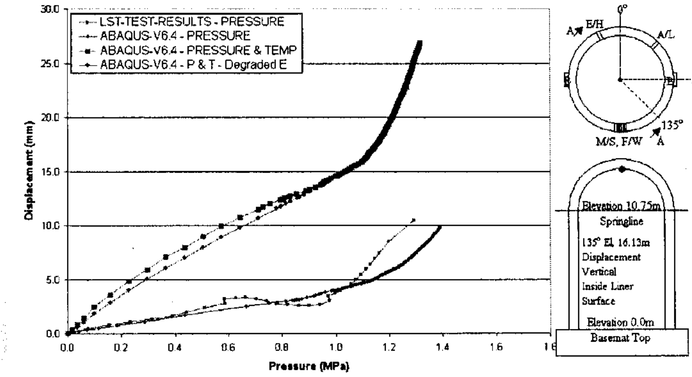

Engineering Integrity and Performance

Standard Output Location 12

Standard Output Location 12 Radial Displacement Phase 3 Analysis

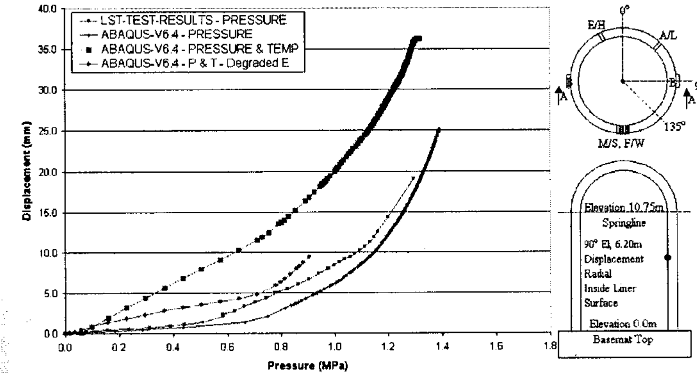

Engineering Integrity and Performance

Standard Output Location 13

Standard Output Location 13 Radial Displacement Phase 3 Analysis

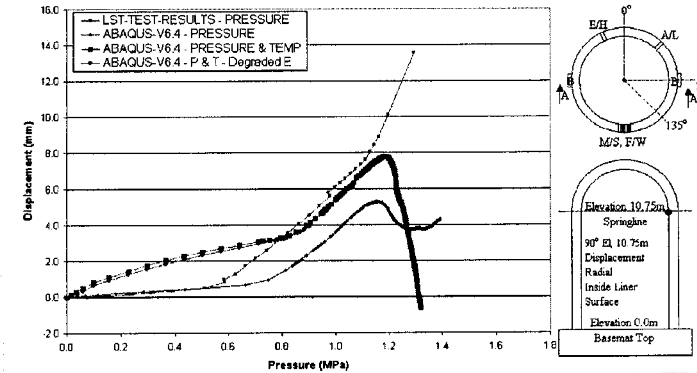

Engineering Integrity and Performance

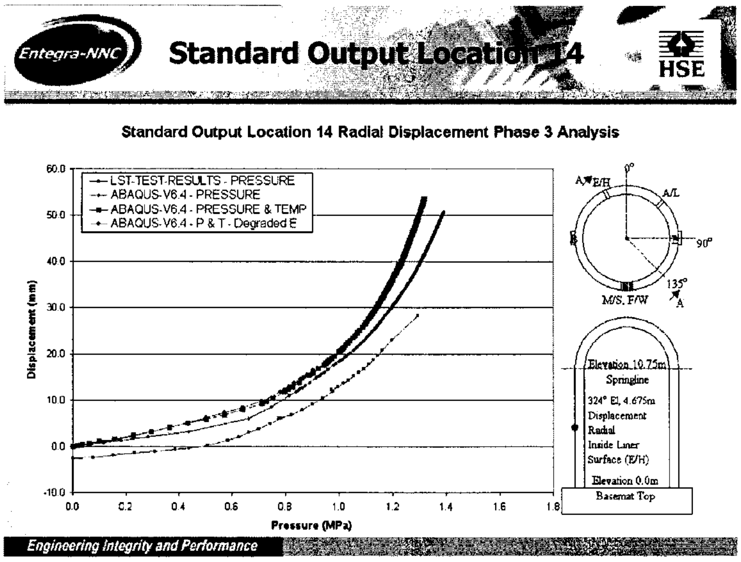

Standard Output Location 14

Standard Output Location 14 Radial Displacement Phase 3 Analysis

Engineering Integrity and Performance

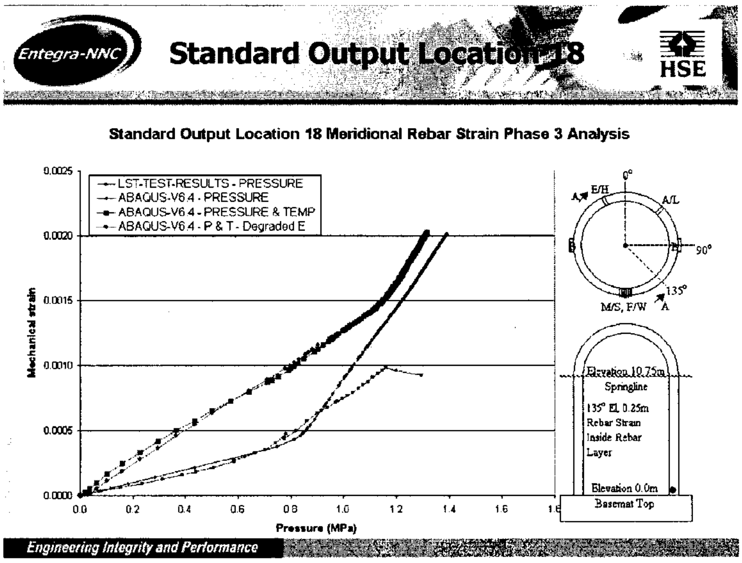

Standard Output Location 18

Standard Output Location 18 Meridional Rebar Strain Phase 3 Analysis

Engineering Integrity and Performance

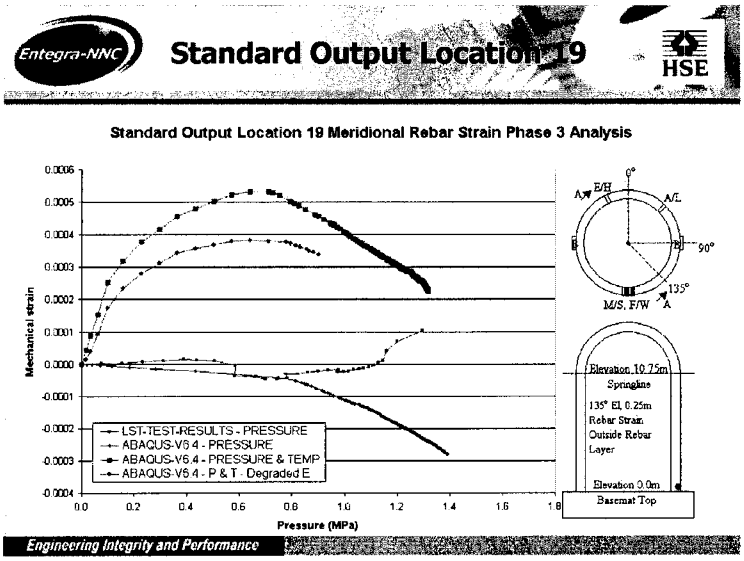

Standard Output Location 19

Standard Output Location 19 Meridional Rebar Strain Phase 3 Analysis

Engineering Integrity and Performance

Standard Output Location 22

Standard Output Location 22 Hoop Rebar Strain Phase 3 Analysis

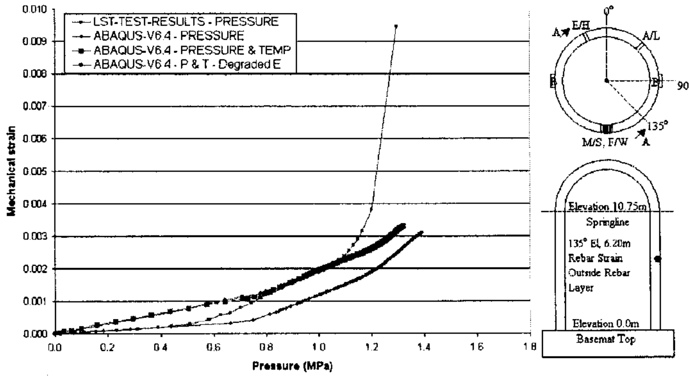

Engineering Integrity and Performance

Standard Output Location 23

Standard Output Location 23 Meridional Rebar Strain Phase 3 Analysis

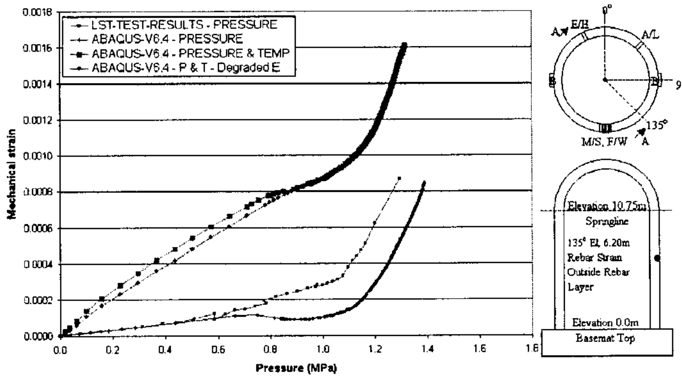

Engineering Integrity and Performance

Standard Output Location 32

Standard Output Location 32 Hoop Rebar Strain Phase 3 Analysis

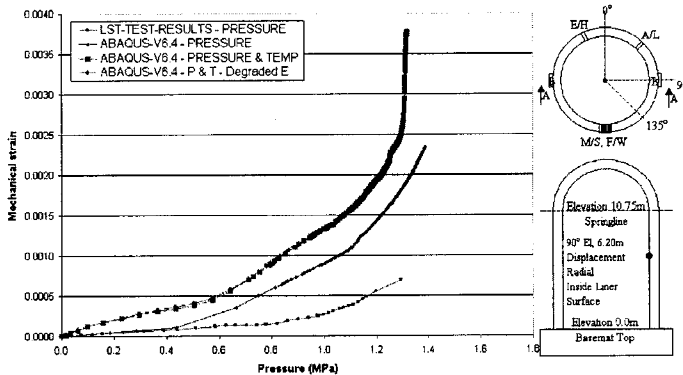

Engineering Integrity and Performance

Entegra-NNC

Standard Output Location 22

HSE

Standard Output Location 22 Hoop Rebar Strain Phase 3 Analysis

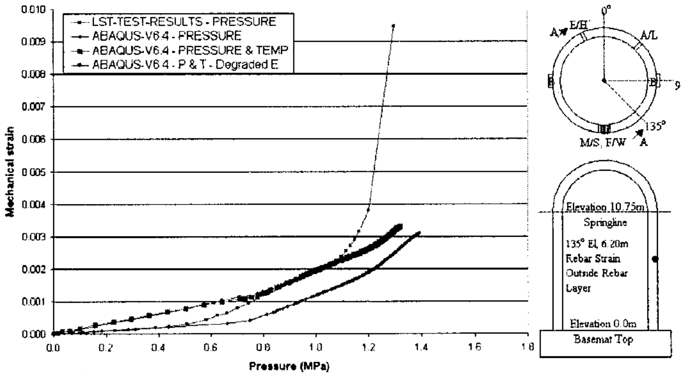

Engineering Integrity and Performance

Entegra-NNC

Standard Output Location 23

HSE

Standard Output Location 23 Meridional Rebar Strain Phase 3 Analysis

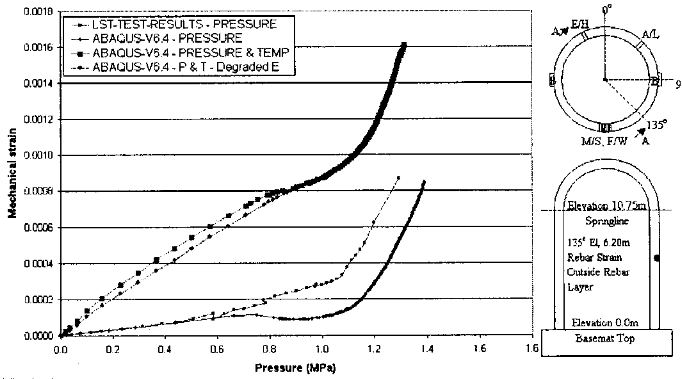

Engineering Integrity and Performance

Entegra-NNC

Standard Output Location 32

HSE

Standard Output Location 32 Hoop Rebar Strain Phase 3 Analysis

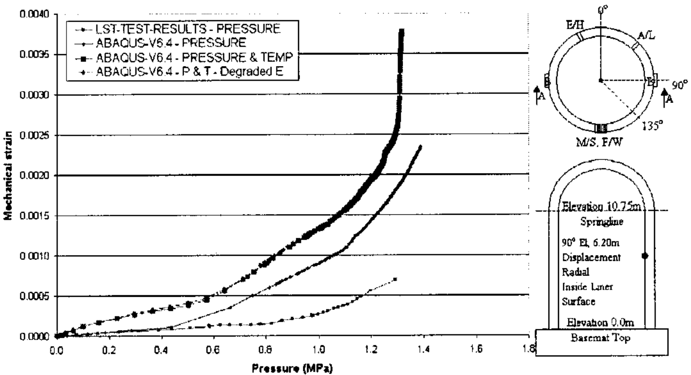

Engineering Integrity and Performance

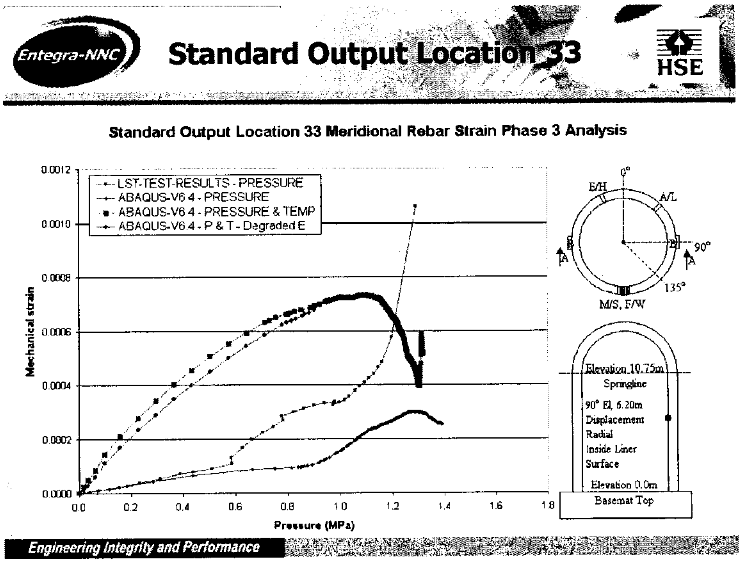

Entegra-NNC

Standard Output Location 33

HSE

Standard Output Location 33 Meridional Rebar Strain Phase 3 Analysis

Engineering Integrity and Performance

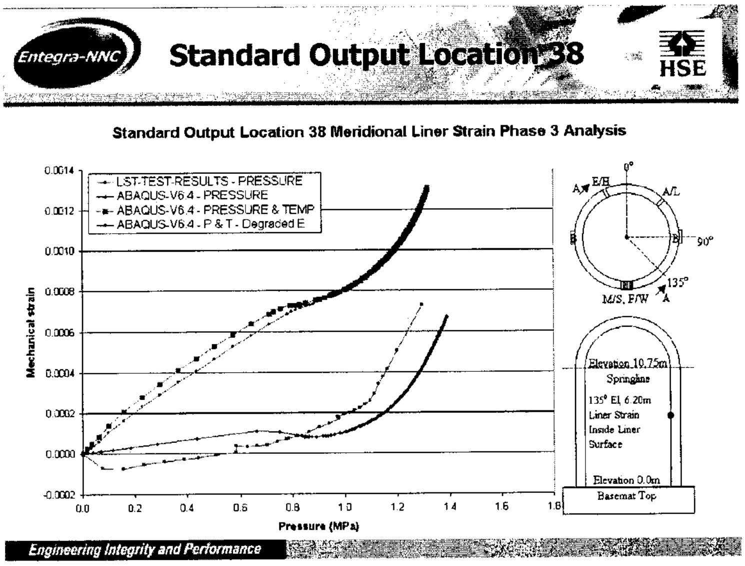

Entegra-NNC

Standard Output Location 38

HSE

Standard Output Location 38 Meridional Liner Strain Phase 3 Analysis

Engineering Integrity and Performance

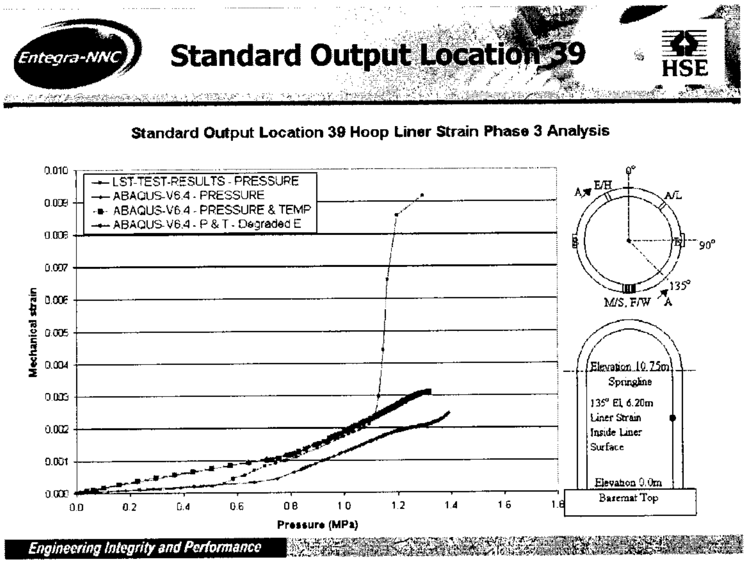

Entegra-NNC

Standard Output Location 39

HSE

Standard Output Location 39 Hoop Liner Strain Phase 3 Analysis

Engineering Integrity and Performance

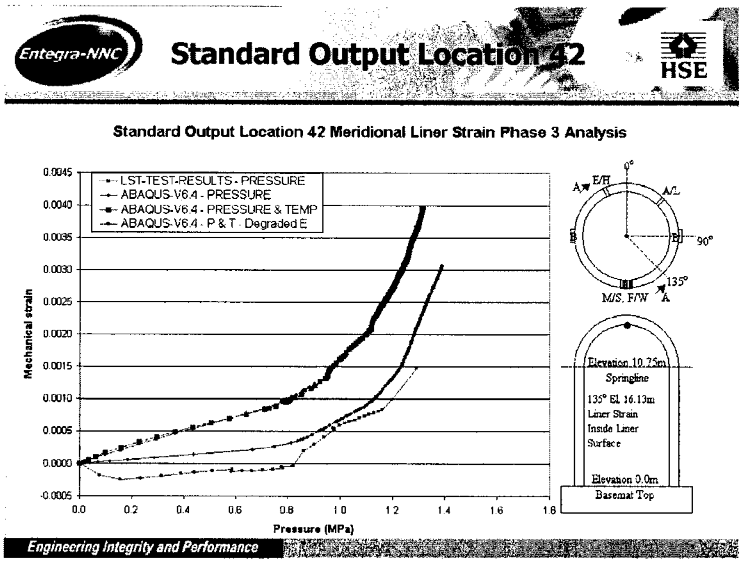

Standard Output Location 42

Standard Output Location 42 Meridional Liner Strain Phase 3 Analysis

Engineering Integrity and Performance

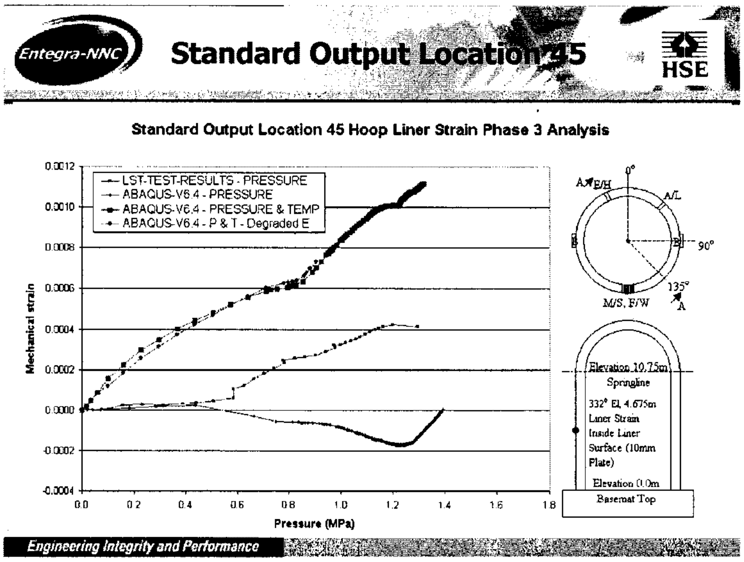

Standard Output Location 45

Standard Output Location 45 Hoop Liner Strain Phase 3 Analysis

Engineering Integrity and Performance

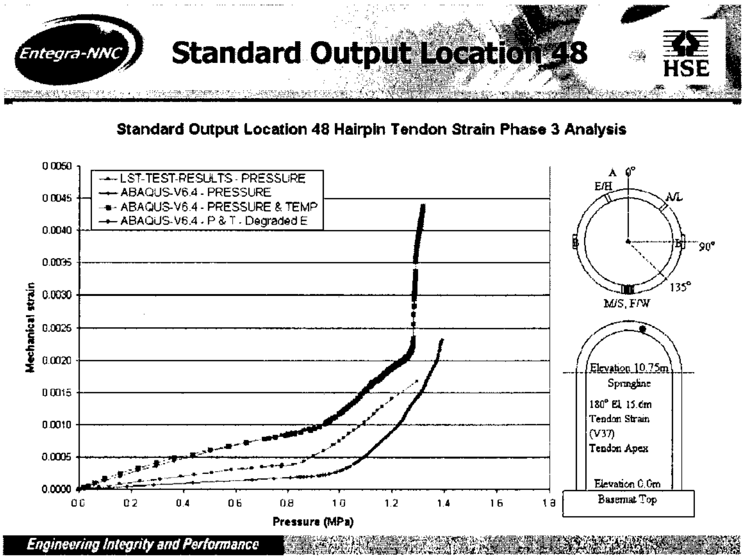

Standard Output Location 48

Standard Output Location 48 Hairpin Tendon Strain Phase 3 Analysis

Engineering Integrity and Performance

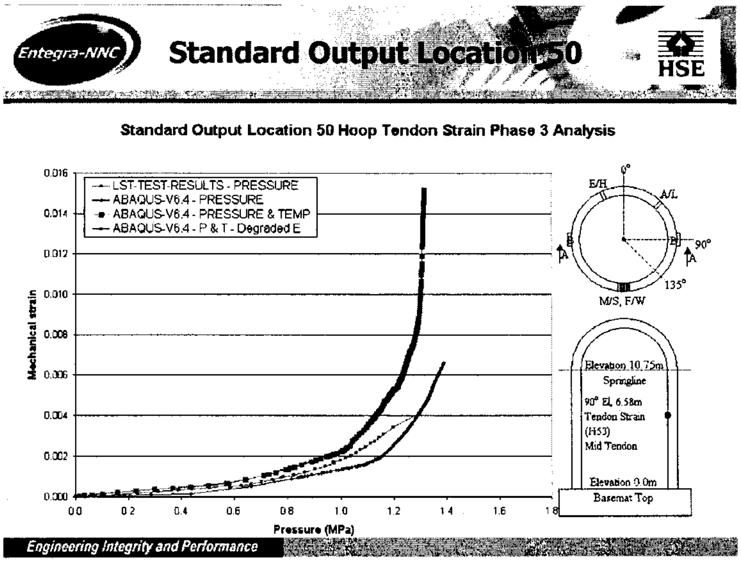

Standard Output Location 50

Standard Output Location 50 Hoop Tendon Strain Phase 3 Analysis

Engineering Integrity and Performance

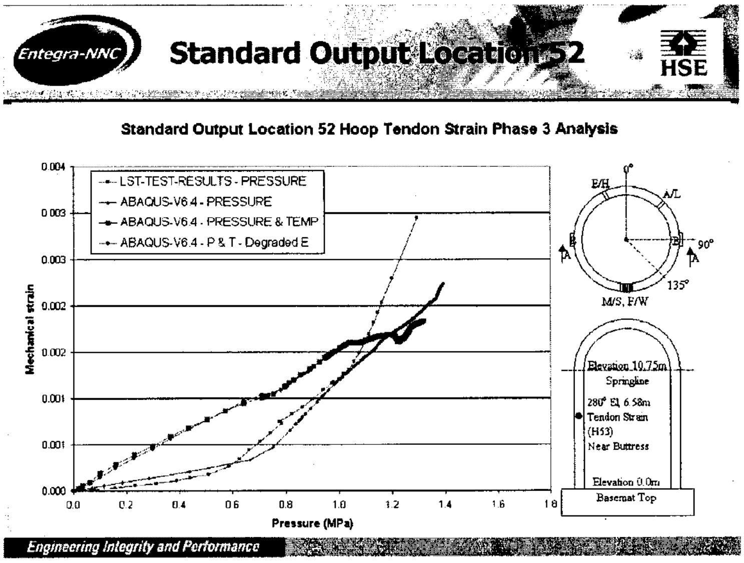

Standard Output Location 52

Standard Output Location 52 Hoop Tendon Strain Phase 3 Analysis

Engineering Integrity and Performance

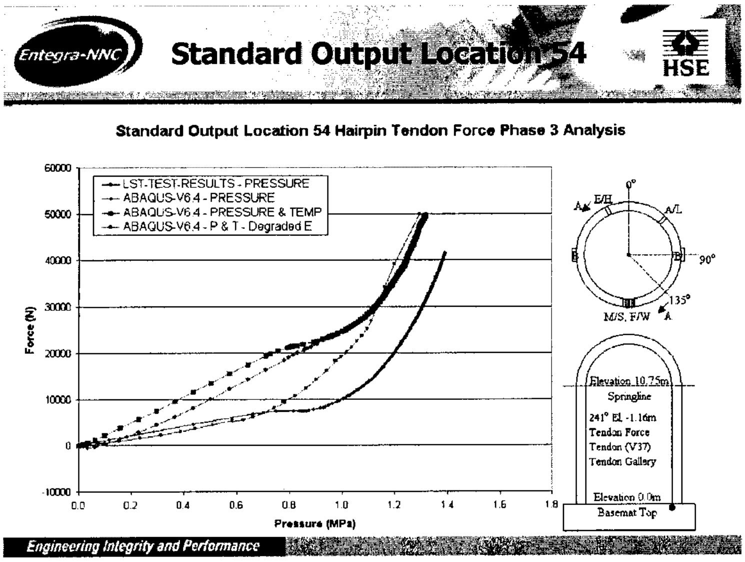

Standard Output Location 54

Standard Output Location 54 Hairpin Tendon Force Phase 3 Analysis

Engineering Integrity and Performance

Standard Output Location 55

Standard Output Location 55 Hoop Tendon Force Phase 3 Analysis

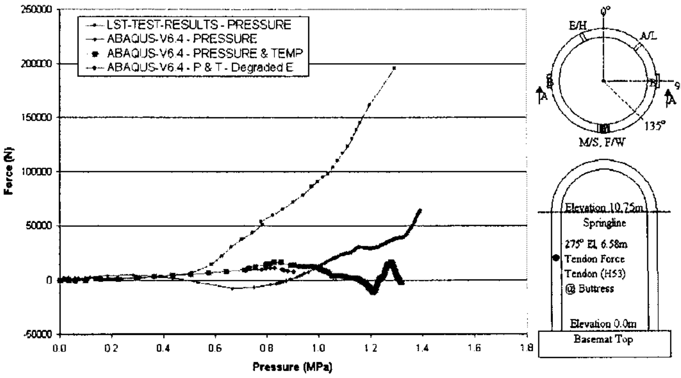

Engineering Integrity and Performance

Liner Rupture Pressure for Case 1 (Location 39)

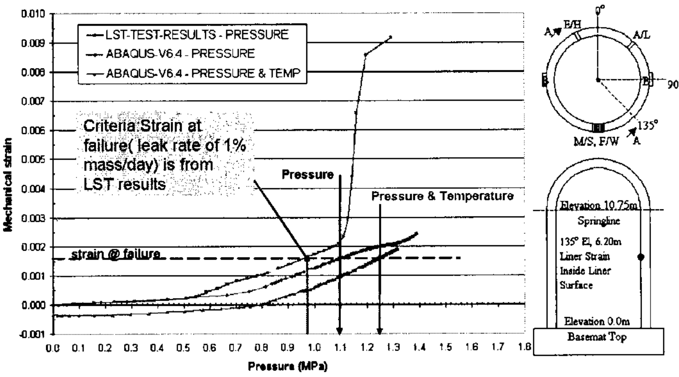

Engineering Integrity and Performance

Location 39 Hoop Stress

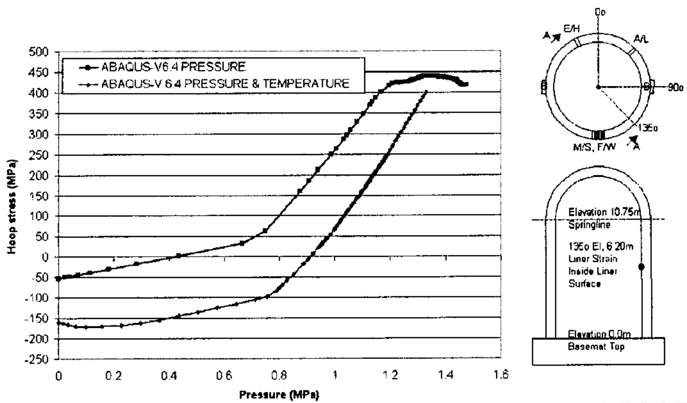

Engineering Integrity and Performance

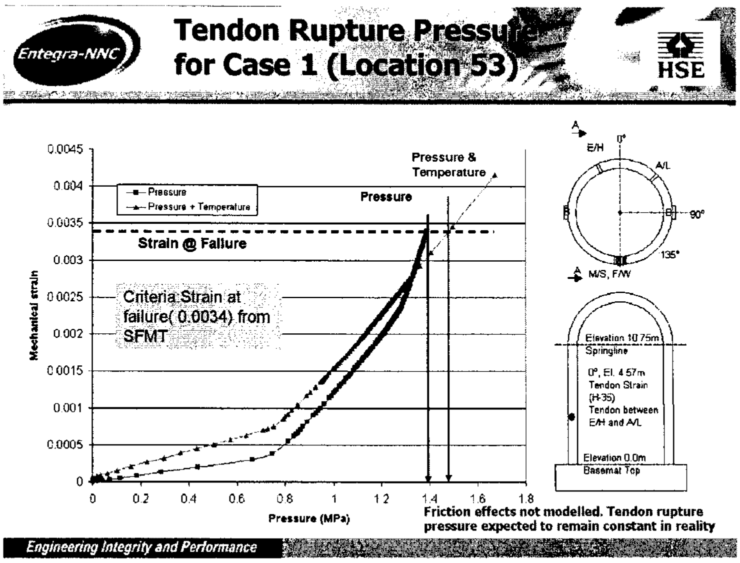

Tendon Rupture Pressure for Case 1 (Location 53)

Criteria:Strain at failure(0.0034) from SFMT

Friction effects not modelled. Tendon rupture pressure expected to remain constant in reality

Engineering Integrity and Performance

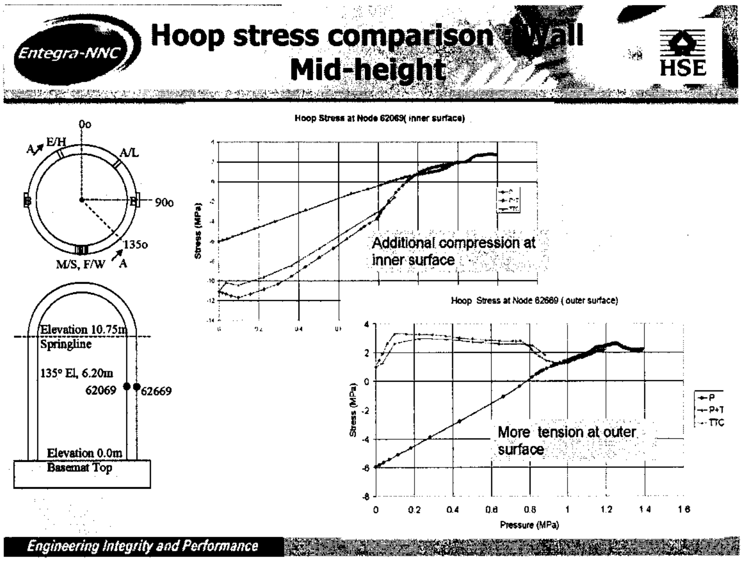

Hoop stress comparison : Wall Mid-height

Additional compression at inner surface

More tension at outer surface

Engineering Integrity and Performance

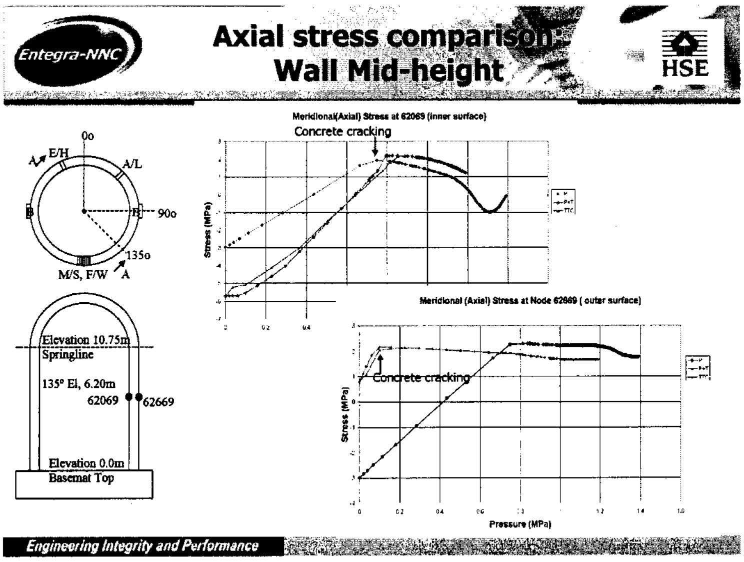

Axial stress comparison: Wall Mid-height

Concrete cracking

Concrete cracking

Engineering Integrity and Performance

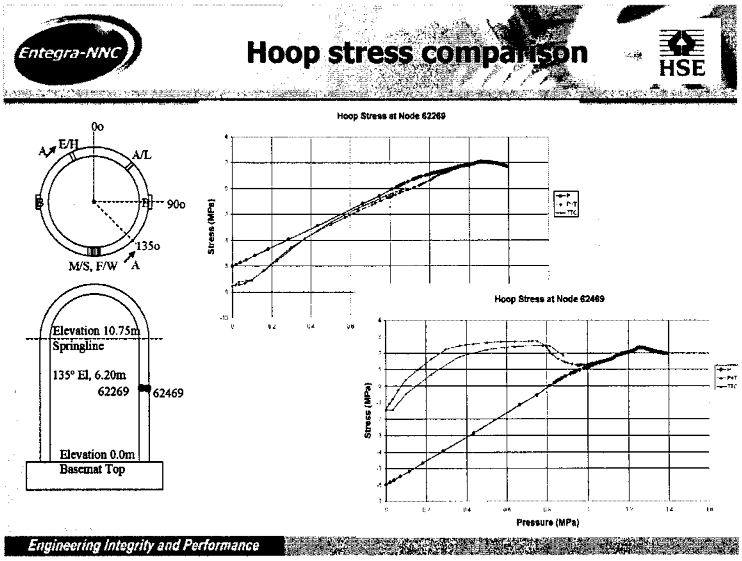

Hoop stress comparison

Engineering Integrity and Performance

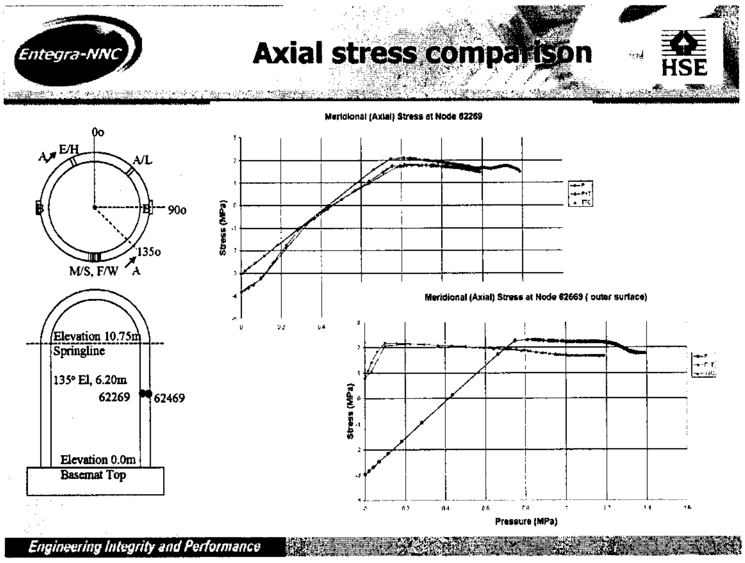

Axial stress comparison

Engineering Integrity and Performance

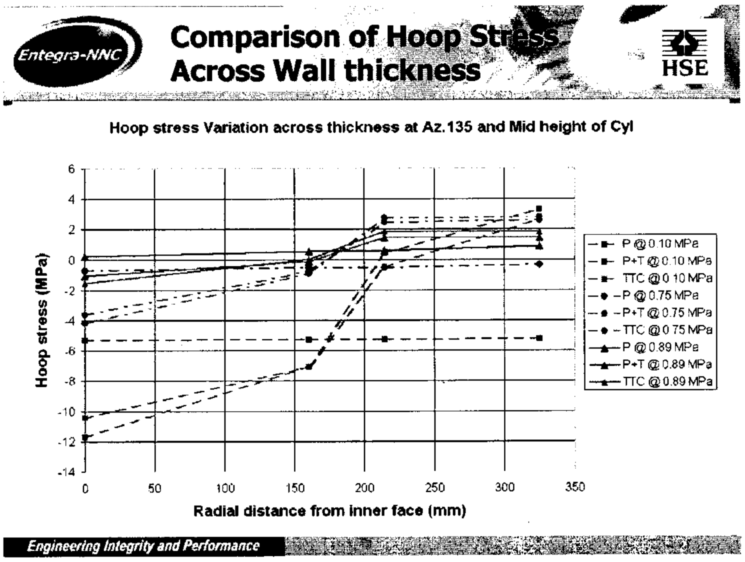

Comparison of Hoop Stress Across Wall thickness

Engineering Integrity and Performance

Comparison of Axial Stress Across Wall thickness

Meridional stress variation across thickness at Az.135 and Mid height of Cyl.

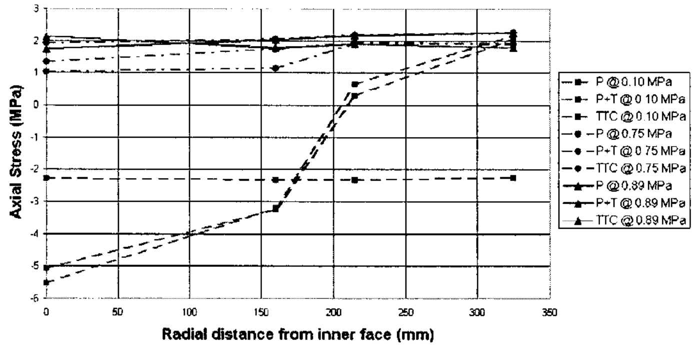

Engineering Integrity and Performance

Tendon Load Profile During Pressurization and Heat Up.

Heat Transfer & Pressure Tendon Load Profiles

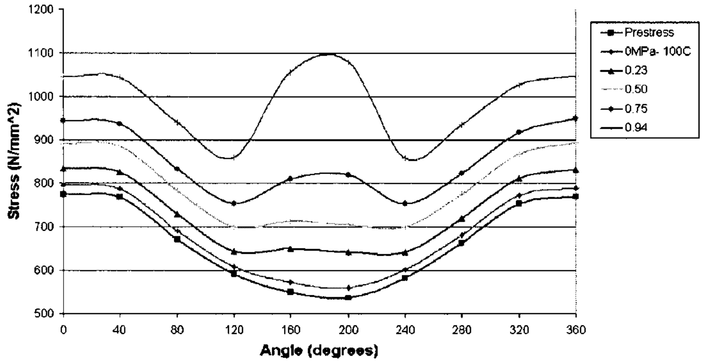

Engineering Integrity and Performance

Pressure + Temperature Analysis Vessel Displacement Profile at 135 Az.

Radial Displacement * 100

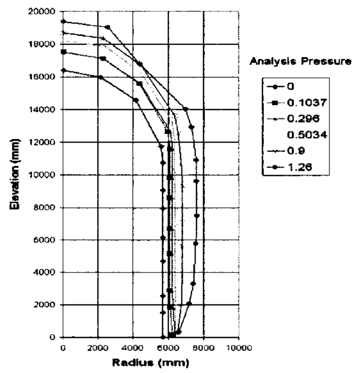

Engineering Integrity and Performance

Entegra-NNC

Comparison of Results: Calculated Pressures (MPa) & Strains (%)

HSE

Loading	Cracking		Liner Yield	Liner Rupture	Hoop Tendon Stress		Pressure @ Failure	Free Field Hoop Strain[ǀ]	Max Radial Displacement[+]	Mode
	Hoop	Meridional			Yield[**]	Rupture				
Pressure	0.6	0.6	0.76	1.1[*]	1.16	1.4[***]	1.4	0.12%	38.8mm	Liner tearing causing high leakage rates
Pressure + Temperature	0.6	0.6	0.83	1.25	0.96	1.5	1.25 1.50	0.18%	49.4mm	Liner tearing Hoop Tendon failure
Pressure + Temperature with TTC	0.6	0.6	0.82	> 0.9	-	-	-	-	-	
LST Test Results	**0.59**	-	-	**0.98**	**1.02**	-	**0.98** **1.295**	**0.17%** -	**28.30mm**	**Liner Tearing, 1% mass/day leak** **Max. Pressure @ 1000% mass/day leak**
SFMT Test Results	-	-	-	-	-	**1.4**	**1.4**	-	**88mm**	**Structural Collapse**

[*] Liner strain of 0.0017 reached at SOL39

[**] Assumed yield strain of 0.2% obtained from laboratory test on tendons at SOL50

[***] Hoop tendon strain of 0.0034 at the maximum SFMT pressure in tendon H53

[ǀ] Strains at SOL39 @0.98MPa

[+] Displacement at SOL 14 @1.295Mpa

Engineering Integrity and Performance

Entegra-NNC

Summary

HSE

- The thermal straining of the liner increases the rupture pressure
- Thermal effects delaying tendon failure due to modelling approximations
- Margin between liner rupture and tendon failure decreases
- Thermal effects cause higher compressive stresses at the inner concrete surface and causes cracking on the outer surface at lower internal pressure

Engineering Integrity and Performance

Entegra-NNC

Summary

HSE

- TTC is shown to have a small effect on PCCV strain distributions for the case analysed, but reduced vessel displacements are witnessed.

Engineering Integrity and Performance

Entegra-NNC

HSE

The End

Engineering Integrity and Performance

FE MODELLING OF REACTOR CONTAINMENTS - SOME RELEVANT TOPICS

- Modelling of thermal loading in load cases including both overpressure and temperature loads.
- Feasability study on FE modelling of local impact loads on concrete slabs.
- CONMOD - Combining non-destructive testing and finite element analysis as a part of an ageing management program.

Ola Jovall
Scanscot Technology, Sweden

Abstract

The design events for a reactor containment usually refers to accidental loading conditions for which leak-tightness and load-bearing capacity should be verified. This involves the containment to be loaded far into the non-linear range, putting high demands on the engineering simulations. Internal overpressurization and missile impact loads constitutes major load categories, for which the integrity of reactor containments has to be verified. In this paper, results from two different engineering simulation projects, including overpressurization and impact loads respectively, are evaluated against experimental test data. Another important issue is the long-time behaviour of reactor containments, and how to ensure that prescribed safety levels can be upheld during the lifetime of the plant. This is the topic of the third part of this paper, in which a project is presented where non-destructive testing and finite element analysis are combined as a part of an ageing management program.

Introduction

The design events for a reactor containment usually refers to accidental loading conditions for which leak-tightness and load-bearing capacity should be verified. This involves the containment to be loaded far into the non-linear range, putting high demands on the engineering simulations. It is therefore of vital importance to ensure that the methods applied for advanced structural analysis can be verified and validated. Internal overpressurization and missile impact loads constitutes major load categories, for which the integrity of reactor containments has to be verified.

In the ISP 48 project, the results from internal overpressurization simulations were studied and evaluated against experimental test data [1], [2]. In addition, analysis where also carried out for a combination of internal overpressurization and belonging temperature effects [3]. In another R&D project [4], two of the leading commercial computer codes for analysis of highly dynamic events have been evaluated against data from experimental tests of local impact of concrete.

Another important issue to be regarded is the long-time behaviour of reactor containments, and how to ensure that prescribed safety levels can be upheld during the lifetime of the plant. This issue is even more emphasized when licensees applies for extended operational lifetime of the plants, or when a power uprate of the plant is at hand. Within the frames of the CONMOD project [5], a feasibility study has been carried out regarding the application and understanding of Non-Destructive Testing (NDT) techniques for the assessment of conformity and condition of concrete reactor containments, and the integration of NDT with state-of-the-art Finite Element (FE) modelling techniques and analysis of structural behaviour. The NDT-methods and FEA-techniques has been tried and evaluated at the decommissioned Swedish reactor containment Barsebäck unit 1.

These topics will be further discusseed in the sections below.

Modelling of thermal loading in load cases including both overpressure and temperature loads

In the ISP 48 project internal overpressurization, in combination with belonging temperature effects, were studied. The modeling of the accidental temperature load inside the reactor containment was in the project stipulated to be applied as a temperature boundary condition [6]. Another possibility is to instead define the inside temperature, and specify the forced convection between the vapour and the containment structure. Both methods are specified in Figure 1.

For steady-state situations, or when the temperature changes slowly, the two methods will arrive at reasonably equal temperature fields in the structure. However, when studying accidental transient temperature events with fast temperature changes, such as for the "phase 3, case 2" analysis of the ISP 48 project (Figure 2), the temperature fields will be completely different, depending on the boundary condition assumed, see Figure 3. This difference in temperature field can, in some cases, have a large influence on the FE analysis results as is explained below.

When the concrete is uncracked, the mean temperature increase of the whole concrete section governs the radial deformation of the containment wall in the FE analysis. However, if the concrete is fully cracked, then it is the mean temperature increase of the embedded or attached steel parts that governs the radial deformation due to the fact that the cracked concrete to a great extent then have lost its stiffness, see Figure 4.

Figure 1. Application of temperature load. From [6], modified.

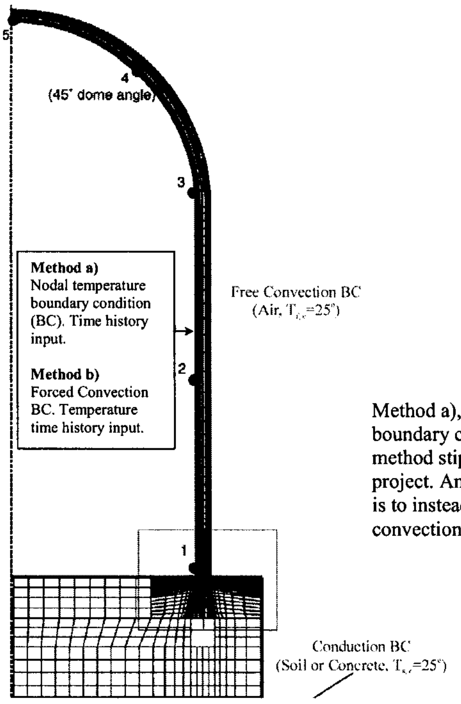
5
4
(45° dome angle)
3
Method a)
Nodal temperature boundary condition (BC). Time history input.
Method b)
Forced Convection BC. Temperature time history input.
2
1
Free Convection BC
(Air, T_{∞}=25°)
Conduction BC
(Soil or Concrete, T_{∞}=25°)

Method a), nodal temperature boundary condition, is the method stipulated in the ISP 48 project. An alternative method is to instead specify the forced convection, method b).

The mean temperature increase at maximum temperature for the ISP 48 “phase 3, case 2” analysis is for the whole concrete section 19 °C. The mean temperature increase if only the steel parts are considered, as for in an analysis of a fully cracked concrete section, is 135 °C, i.e. much larger than for an uncracked structure. This due to the fact that the steel liner at the inner wall surface is heated up to the temperature peak value. The mean temperature increase calculations are based on the wall section shown in Figure 5, and the temperature gradient “Temperature boundary condition shown” in Figure 3.

In Figure 6, the radial deformation for some different cases are shown; cracked or uncracked concrete combined with temperature boundary condition on the inner wall surface as well as for forced convection boundary conditions. As can be seen in the table in Figure 6, the radial deformation differs if the concrete is cracked or not.

To sum up, it is important how the transient temperature loads are applied in analysis of containment structures. If convection modeling is used, the structural response will be lower than if the temperature inside the containment is modeled as a temperature boundary condition. This difference is emphasized if the concrete cracks due to the combined loading of overpressure and temperature. In the ISP 48 “phase 3 case 2” analysis, the radial deformation at midheight of the containment wall can be somewhere between 3 and 16 mm (Figure 6) depending on which type of boundary conditions are applied for the temperature load on the inside of the containment, and whether the concrete is assumed to be cracked or not.

Figure 2. Transient temperature and pressure load applied inside the containment in ISP 48 phase 3, case 2 analysis.

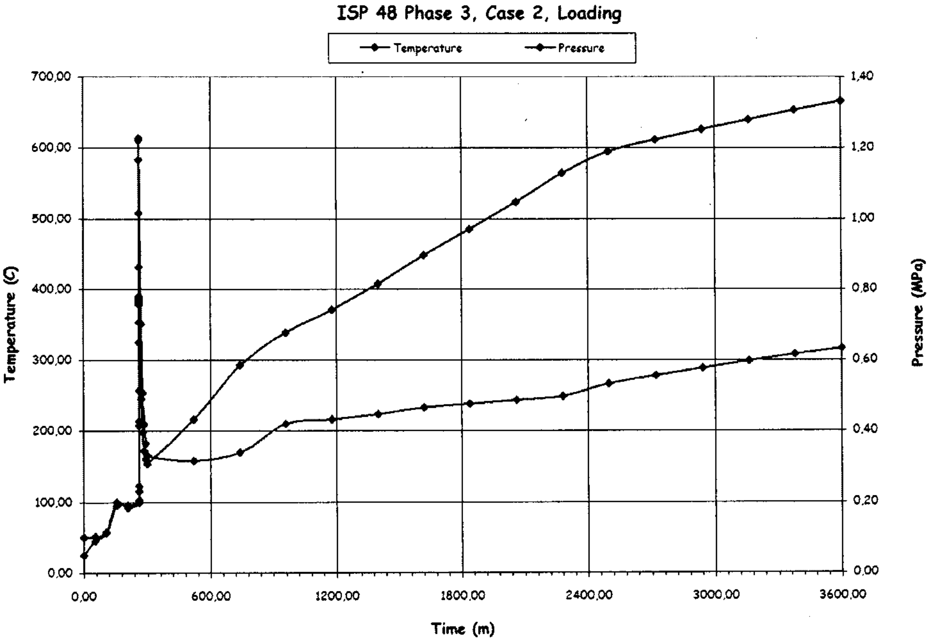

Figure 3. Temperature gradient through the containment wall at inside temperature peak, ISP 48 phase 3, case 2 analysis. Gradients are shown for different boundary condition assumptions on the inside of the containment.

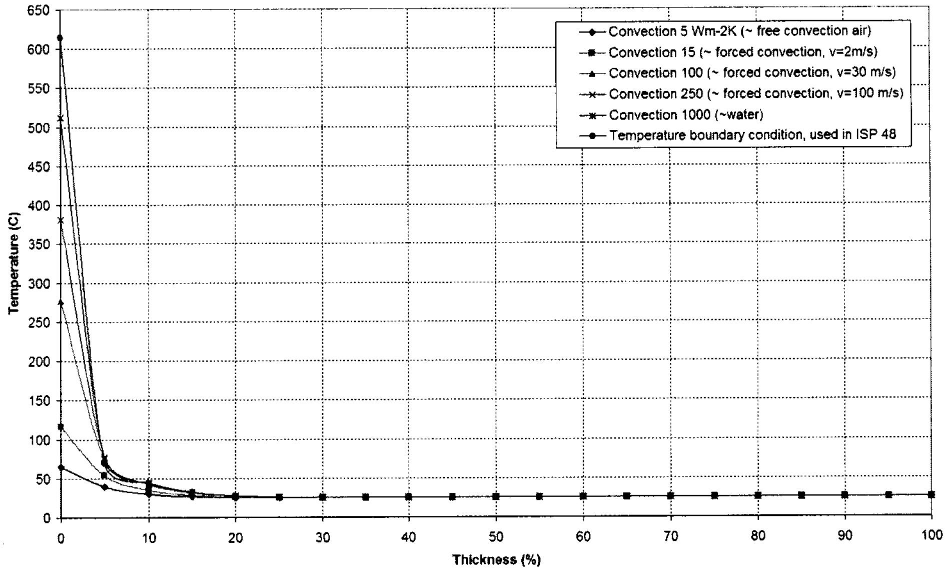

Figure 4. Stiffness of uncracked and cracked concrete in analysis.

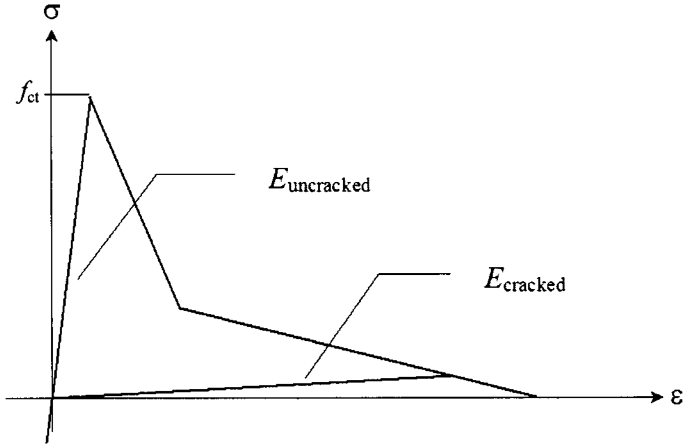
σ
f_{ct}
$E_{uncracked}$
$E_{cracked}$
ε

Figure 5. Cross section through the containment wall.

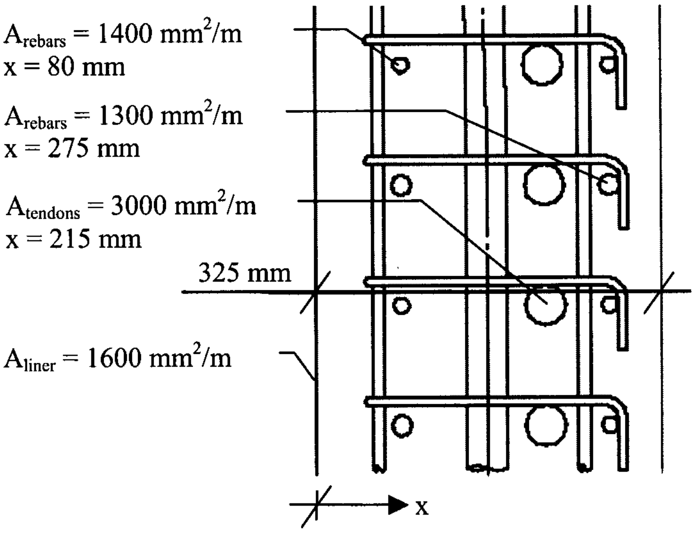
$A_{rebars} = 1400\ mm^2/m$
x = 80 mm
$A_{rebars} = 1300\ mm^2/m$
x = 275 mm
$A_{tendons} = 3000\ mm^2/m$
x = 215 mm
325 mm
$A_{liner} = 1600\ mm^2/m$
x

The liner constitutes appr. ¼ of the total steel area, and is heated up to the maximum peak temperature. This is the main reason why the mean temperature increase is much higher for the steel parts only than for the whole concrete section.

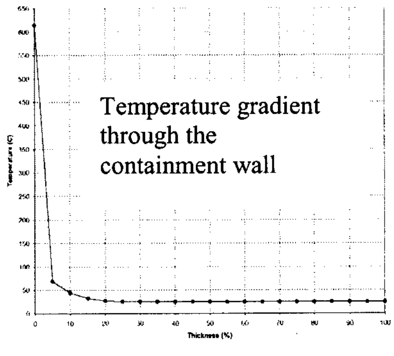

CSNI Workshop International Standard Problem 48

FE modelling of reactor containments – some relevant topics

---

1) **ISP 48 - Modelling of thermal loading in load cases including both overpressure and temperature loads**
2) **Feasability study on FE modelling of local impact loads on concrete slabs**
3) **CONMOD – Combining non-destructive testing of reactor containments with finite element analysis as a part of an ageing management program**

Ola Jovall – Scanscot Technology, Sweden

ISP 48 – Reactor containment

Pressure and temperature load analysis – some conclusions

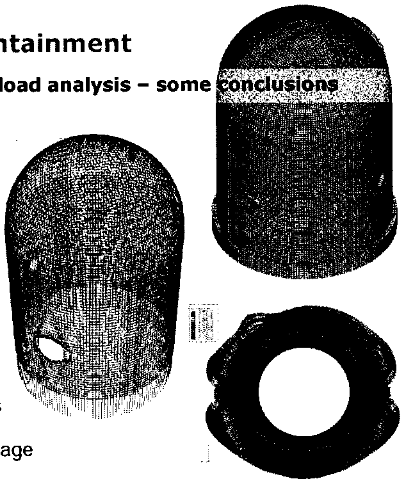

- 3D-model to capture the global structural behaviour
- Modeling of unbonded prestresssing tendons by contact formulation
- Modeling technique for combination of pressure and temperature load
- Analysis methods exists to carry out high quality non-linear numerical simulations
- Acceptance criterias for leakage (tearing of liner)

Local impact loads on concrete slabs

R&D project

- Feasability study using commercial FE software:
  - ABAQUS/Explicit
  - AUTODYN
- Numerical simulations evaluated against experimental test data

Local impact loads on concrete slabs

Experimental test data used for evaluation

- Test performed in Japan by:
  - Kobori Research Complex
  - Central Research Institute of the Electrical Power Industry
- Test results published in: Nuclear Engineering & Design
- Rigid and deformable missiles launched against reinforced concrete slabs
- Three missile velocities: 100, 150 and 215 m/s
- Several slab thicknesses

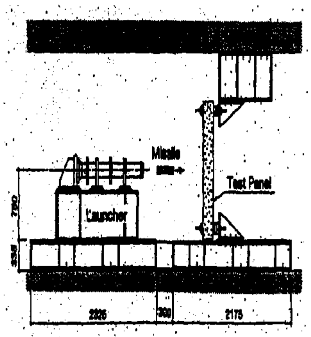

Local impact loads on concrete slabs

Local damage of impacted concrete

- Spalling
- Penetration
- Scabbing
- Normal perforation
- Punching cone failure

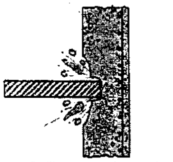
Spalling, crater and penetration

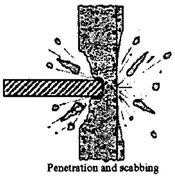
Penetration and scabbing

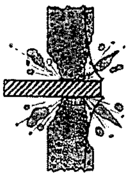
Perforation

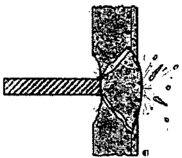
Punching out a concrete cone

Local impact loads on concrete slabs

FE modelling of test setup

- Axi-symmetrical model
- 3D-analysis for comparison

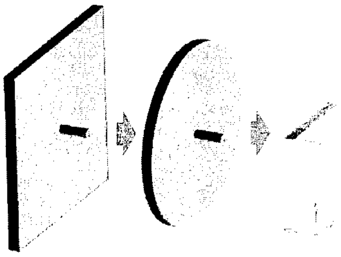

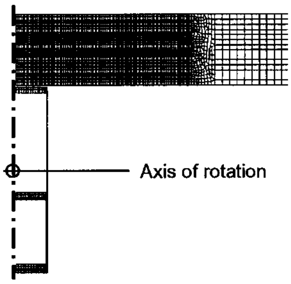

SCANSCOT Technology

Local impact loads on concrete slabs

Analysis results - Deformation of deformable missile

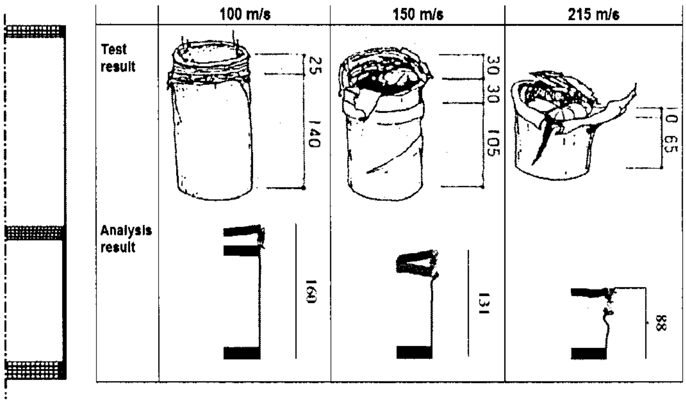
100 m/s
150 m/s
215 m/s
Test result
Analysis result
25
140
30
30
105
10
65
160
131
88

SCANSCOT Technology

Local impact loads on concrete slabs

Analysis results – Local damage of impacted concrete

- Penetration, deformable missile

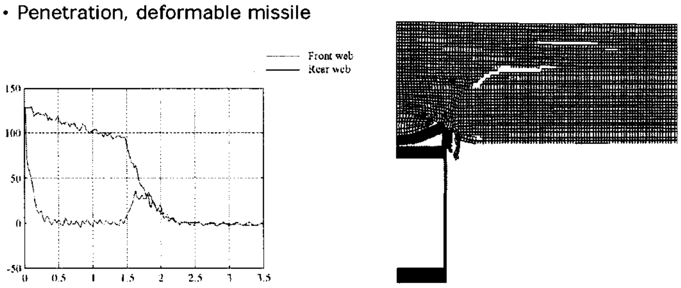

Penetration depth: test result = 12 mm, analysis rsult = 5-20 mm.

SCANSCOT Technology

Local impact loads on concrete slabs

Analysis results – Local damage of impacted concrete

- Perforation, deformable missile

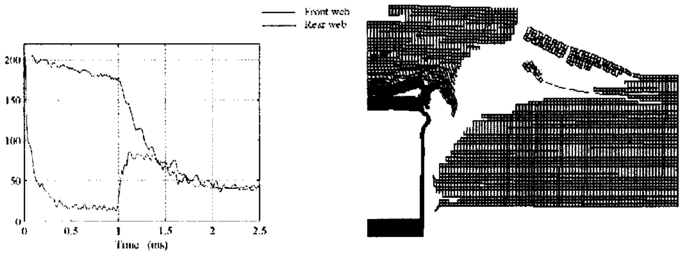

Perforation, residual velocity: test result = 55 m/s, analysis rsult = 40 m/s.

SCANSCOT technology

Local impact loads on concrete slabs

Analysis results – Local damage of impacted concrete

- Penetration and perforation, rigid missile

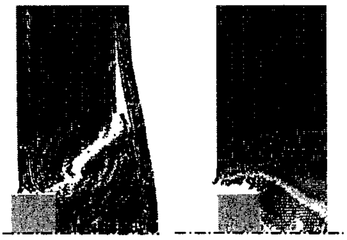

Missile velocity [m/s]	Slab thickness [mm]	Penetration depth	
		Test result [mm]	Analysis result [mm]
83	210	11	9
128	210	24	20
214	210	37	51
97	150	10	20
141	150	23	36
190	150	Perforation	103

SCANSCOT technology

Local impact loads on concrete slabs

Importance of deformability of the missile

The damage of the concrete slab is to a great extent dependent on if the missile is rigid or deformable.

- For the same missile velocity, and the same mass of the missile the penetration depth differ approximatly by a factor of 2.
- This is seen both in the experimental test results and in the analysis results.

Type of missile	Penetration depth [mm]		
	100 m/s	150 m/s	215 m/s
Rigid missile	10	23	Perforation
Deformable missile	4	12	Perforation

SCANSCOT technology

Local impact loads on concrete slabs

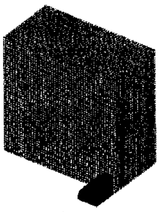

3D-model

Axi-symmetrical model
→ rebars modeled
as shell elements
3D-model
→ rebars modeled
as beam elements

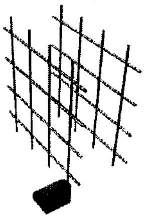

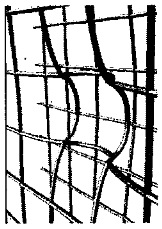

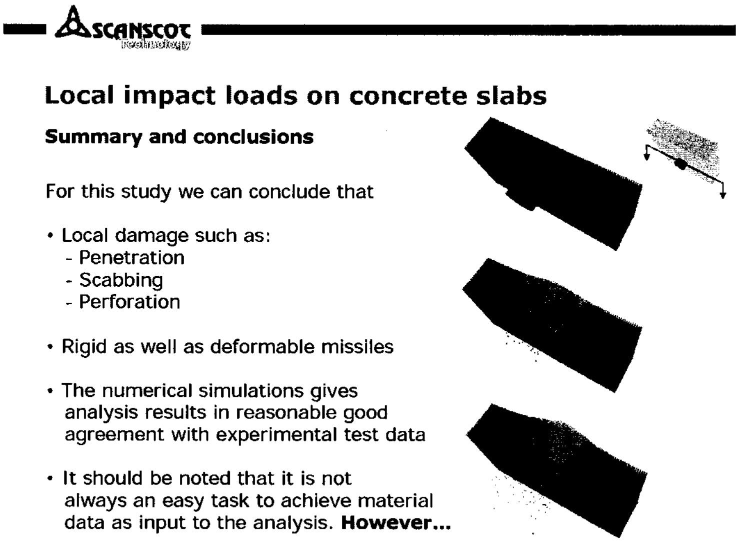

Local impact loads on concrete slabs

Summary and conclusions

For this study we can conclude that

- Local damage such as:
  - Penetration
  - Scabbing
  - Perforation
- Rigid as well as deformable missiles
- The numerical simulations gives analysis results in reasonable good agreement with experimental test data
- It should be noted that it is not always an easy task to achieve material data as input to the analysis. **However...**

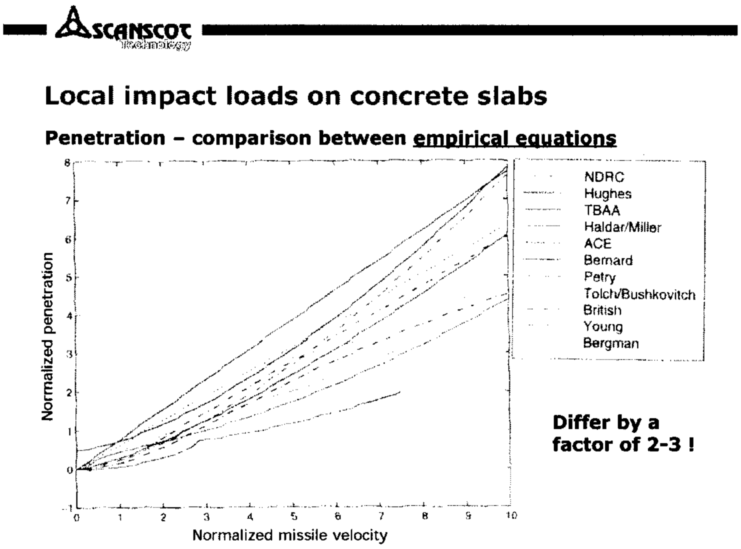

Local impact loads on concrete slabs

Penetration – comparison between empirical equations

Differ by a factor of 2-3 !

CONMOD – Combining NDT and FEA

Combining non-destructive testing (NDT) with finite element analysis (FEA) as a part of an ageing management program

- **Euratom 5th framework programme project**
- **Participants**
  - Electricité de France, EDF, France
  - Barsebäck NPP, Sweden
  - Force Technology, Denmark
  - Scanscot Technology, Sweden
- **Objectives**
  - Feasability study using NDT on concrete reactor containments
  - How to use FE analysis in combination with NDT as a part of a maintenance plan or ageing management program
- **Decommisioned Barsebäck Unit 1 containment to our disposal**
  - Nearly 30 years old reactor containment situated in Sweden

CONMOD – Combining NDT and FEA

Feasability study using non-destructive testing methods - 1

Investigate the possibilities to study or identify

- the as-built compliance with design (drawings)
- the condition and quality of the concrete
- the effect of time-dependent processes (deterioration)

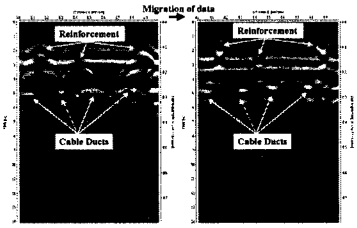

CONMOD – Combining NDT and FEA

Feasability study using non-destructive testing methods - 2

- NDT methods evaluated
  - several seismic methods
  - x-ray
  - radar
- The methods have been tested on
  - the decommissioned Barsebäck Unit 1 reactor containment
  - mock-ups with known defects
- NDT methods complemented with material testing of drilled cores from the containment to evaluate the predictions made by the NDT testing

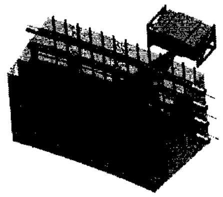

CONMOD – Combining NDT and FEA

How finite element analysis (FEA) can be utilized - 1

Finite element analysis could be utilized in several ways in combination with NDT examinations.

- Initial structural analysis of the containment based on nominal data
  - identify critical areas as a basis for planning of NDT investigations at site

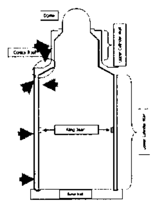

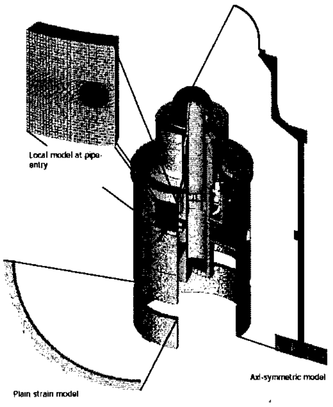

Barsebäck EDF FORCE SCANSCOT

CONMOD – Combining NDT and FEA

How finite element analysis (FEA) can be utilized - 2

- Structural analysis of the containment using updated input based on the information gained during the inspection of the structure
  - study the influence on leak-tightness and load-bearing capacity from identified deviations
- Inspections include monitoring of the structure, NDT methods, material testing of drilled cores, lift-off tests of unbonded tendons pressure tests combined with deformation measurements etc

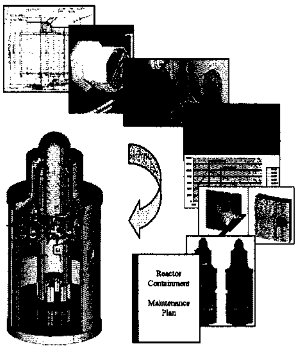
Reactor Containment Maintenance Plan

Barsebäck EDF FORCE SCANSCOT

CONMOD – Combining NDT and FEA

How finite element analysis (FEA) can be utilized - 3

- Simulate seismic NDT methods
  - predict or interpret testing response (site specific)
  - both for a healthy structure and for certain type of defect
  - sensitivity studies to determine the smallest defect possible to detect
  - help to chose the most efficient testing method to detect a certain type of deviation

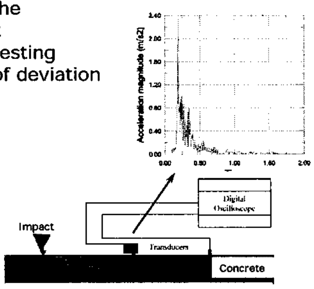
Acceleration magnitude (m/s2)
2.40
2.00
1.60
1.20
0.80
0.40
0.00
0.00
0.50
1.00
1.50
2.00
Digital Oscilloscope
Impact
Transducers
Concrete

Barsebäck EDF FORCE SCANSCOT

CONMOD – Combining NDT and FEA

Conclusions

- Non-destructive testing methods, together with monitoring systems and, if possible, core sampling, and other inspection methods can be a valuable tool in an ageing management program.
- However, testing methods need to be qualified.
- Finite element analysis can assist in to plan the NDT investigations, to interpret the NDT testing results and to understand the influence of identified deviations on the behavior of the containment

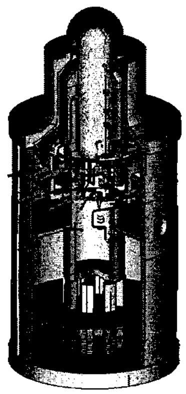

STATISTICAL ASSESSMENT OF THE PRESTRESS LEVEL BASED ON IN-SERVICE INSPECTIONS OF UNBONDED TENDONS

Patrick Anderson
Division of Structural Engineering, Lund University, Sweden

Abstract

For reactor containments, with unbonded tendons, the tendon force is measured at regular in-service inspections to secure that the prestress level is sufficient. It is not possible to achieve a complete assurance concerning the prestress level due to the limited sample size and the measuring error. A reliability-based model can be used to show if the measured force exceeds the minimum required prestress with adequate margins. Statistical assumptions about the non tested tendons have to be made to be able to evaluate the prestress level. The risk of one or several tendons being defected should also be considered to achieve a comprehensive evaluation.

Introduction

The prestressing system is essential to maintain high structural integrity of the reactor containment. To avoid through-wall cracks in the concrete the prestress shall counterbalance the tensile stresses expected at an internal accident. The effective prestress is decreased from its initial value due to different degradation mechanisms. The two most probable degradation mechanisms are time dependent deformation (longtime loss) and corrosion (causing defected tendons). Long-time losses arises from shrinkage and creep in the concrete and relaxation of the tendons. These mechanisms depend on several different environmental and material factors which make the loss difficult to predict. Corrosion which causes defected tendons could of course also cause an extensive loss of prestress.

To be able to measure the tendon force the tendon has to be unbonded, i.e. the space between the tendon and duct is not injected with cement grout. In Sweden six of the reactor containments are constructed with unbonded tendons. Instead of cement grout the unbonded tendons are protected from corrosion with injection of grease or by ventilation of dry air. For the containments with unbonded tendons regular in-service inspections are made to estimate the prestress level in the structure. The in-service inspections are made according to an American guide (Regulatory Guide 1.35, 1990). Fig. 1 and Fig. 2 shows measuring results from in-service inspections at different Swedish reactor containments. Both figures show tendon forces that are related to the original force at the tensioning. Fig. 1 shows vertical tendons, Fig. 2 horizontal tendons and every break point on the curves represents the mean value of the measured tendon forces of one inspection.

Fig 1, Vertical tendons

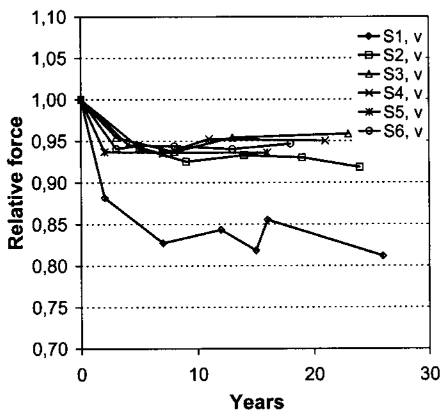

Fig 2, Horizontal tendons

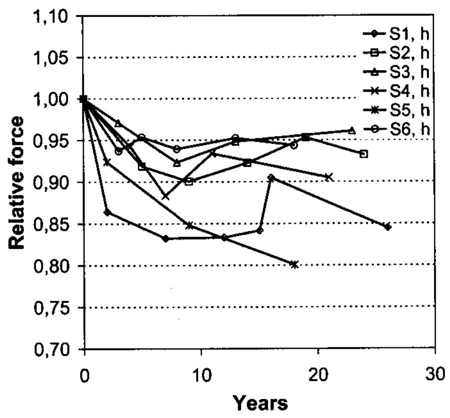

Apart from measuring the tendon force, one wire in two of the tendons shall also be removed and checked over its whole length to observe corrosion or other material defects. The prestressed system in reactor containments consists of hundreds of tendons, so it is not economically feasible to test all tendons. The guide recommends that between 2 and 4% of the tendons should be selected randomly at each inspection. In Regulatory Guide 1.35 (1990) the evaluation of the prestress level in principle is made according to two different approaches. 1) Each measured tendon force is compared with a lower limit for the *predicted force* at the time of the inspection. 2) The mean value of the measured tendon forces in one group (tendons under similar conditions) is compared with the *minimum required prestress level* (from design).

According to both the limited sample size and the measuring error, it is not possible to achieve a complete assurance concerning the prestress level. Some statistical assumptions about the non tested tendons have to be made to be able to rigorously evaluate the prestress level. A reliability-based model can show if the measured force exceeds the minimum required prestress level with adequate margins. The risk of one or several tendons being defected has to be considered to achieve a comprehensive model. Information concerning defected tendons (further referred to as *tendon dropout*) is limited. The small risk of tendon dropout makes it difficult to calculate the probability of dropout on the basis of in-service inspections. In this paper it is assumed that a general probability of tendon dropout is known. To fulfill the requirement of tightness at the internal design pressure the factor of interest is the prestress level in the concrete and not the force in individual tendons. Several tendons influence the prestress level in a specific part of the containment. This fact is important to consider both concerning the general level of prestress and in the case of tendon dropout.

Swedish concrete containments

Sweden has today eleven power-producing nuclear reactors located at four different sites. Eight of these reactors are of the type boiling water reactors (BWR) constructed by ASEA atom and three are of the type pressurized water reactors (PWR) constructed by Westinghouse. All Swedish reactors are constructed during the seventies and eighties and the operation of the first reactor was started in 1972.

All Swedish containments have a cylindrical concrete wall founded on a thick concrete plate. The top of the cylinders is either enclosed with a massive steel lid (BWR) or with a concrete dome (PWR). The wall consists from the outside of a bearing concrete shell, prestressed in two directions. Inside the concrete shell a steel liner is fixed to the outer concrete. On the inside of the steel liner a reinforced concrete shell is protecting the steel liner from missiles (e.g. from pipe pieces). Fig 3 and 4 shows examples of the containment outline for the two reactor types used in Sweden.

Fig. 3, BWR containment

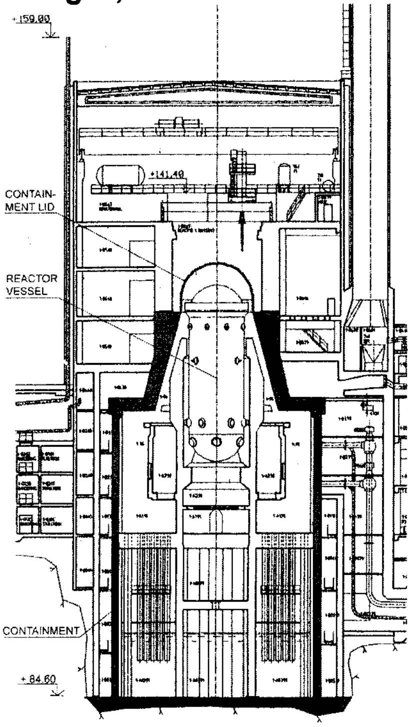

Fig. 4, PWR containment

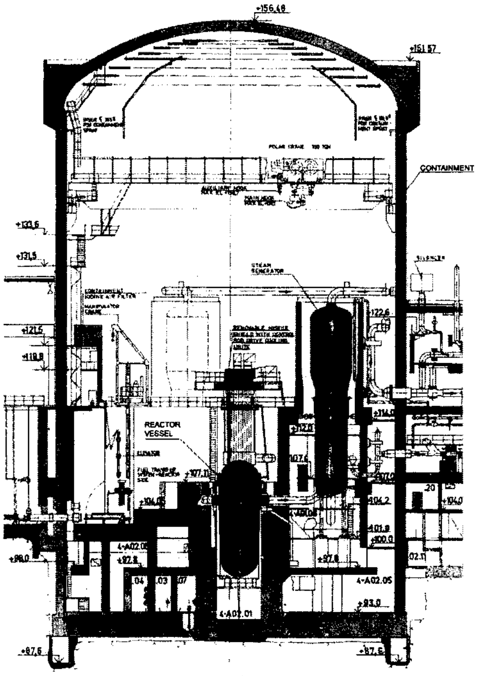

Swedish containments are designed for an overpressure of around 0.5 MPa (design pressure). It is prescribed that the concrete shall be in compressive state at the internal design pressure. This so called limit state of decompression can be seen as a conservative requirement, since the steel liner will maintain tightness even for loads that gives tensile stresses in the concrete. If the design pressure is increased with 50% it is also prescribed that the tensile yield limit for structural steel, reinforcement and tendons shall not be exceeded. This requirement will in general result in a lower accepted limit for the prestress, due to the generally high percentage of reinforcement in the containment.

Reliability model

The main requirement for the prestress level, which refer to the limit state of decompression, can be expressed by the limit state function,

$$g(\mathbf{X}) = q_R - q_s \qquad (1)$$

where q_R is the prestress and q_S is the tensile stress in the concrete from design pressure. X is a vector of random variables, $g(X)>0$ defines acceptance and $g(X)\leq 0$ a violation of the requirements. The event of violation of the requirement $g(X)\leq 0$ will further in this paper be denoted as event E. The presstress q_R is a random variable estimated from measurements and the tensile stress from design pressure q_S is assumed to be a deterministic value.

From the measurements at one in-service inspection the mean force μ_F and the standard deviation σ_F can be estimated for tendons with similar properties. It is assumed that the tendon force is independent and normally distributed.

The concrete in the containment can be assumed to be in compressive state (according to the limit state of decompression) and below the concrete compression strength. Linear elastic theory can therefore be used to express the influence from the tendons. The prestress in any point and direction of the structure depends on the remaining force in the influencing tendons. A structural part A_j is defined and represents a hypothetical part of the structure in which tendon j has the highest influence. The prestress $q_{R,j}$ in the structural part A_j can be calculated as

$$q_{R,j} = \sum_{i=1}^{N} F_i I_{i,j} \qquad (2)$$

where N is the total number of tendons, F_i is the remaining force in tendon i and $I_{i,j}$ is the influence factor describing the effect of tendon i on the structural part A_j. Fig 5 illustrates the influence for vertical tendons in the containment wall. The height of the containment is much larger than the distance between tendons (a) and therefore can the theory of a semi-infinite elastic shell be used to model the influence. The prestress is calculated at a chosen distance h_c from the edge and must be determined in accordance with the detailed design of the structure. It can for instance be taken as the thickness of the top or bottom slabs of the containment. The specific case of prestress from vertical tendons in the containment wall is discussed in the example.

Fig. 5, Special case of vertical tendons influencing the structural element A_j

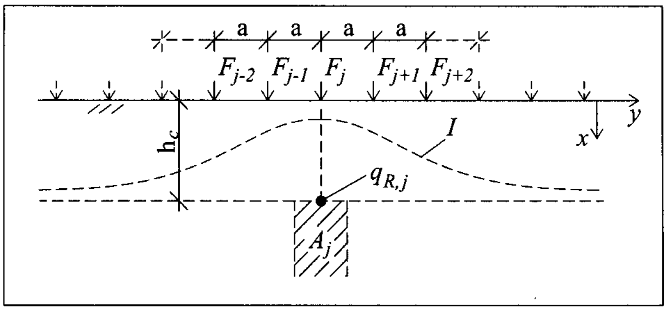

The tendons influencing A_j can be seen as a parallel system. Assuming that the tendon forces are independent and normally distributed the prestress $q_{R,j}$ will also be normally distributed with a mean $\mu_{q,j}$ and standard deviation $\sigma_{q,j}$ given by,

$$\mu_{q,j} = \mu_F \sum_{i=1}^{N} I_{i,j} \tag{3}$$

$$\sigma_{q,j} = \sigma_F \sqrt{\sum_{i=1}^{N} I_{i,j}^2} \tag{4}$$

The stress influence from the tendons represents the resistance and the tension stress in the wall, from internal design pressure, represents the load effect in the model. The probability of violation $P(E_j)$ for the structural part A_j is described in expression 5, where E_j expresses the event of decompression in A_j.

$$P(E_j) = \Phi(-\beta_j) \tag{5}$$

where Φ is the normal distribution function and $\beta_j = \dfrac{q_S - \mu_{q,j}}{\sigma_{q,j}}$.

According to the limit state of decompression the whole containment structure shall be in compressive state at a major internal accident. The requirement shall be fulfilled in all structural parts A_j, i.e. if the prestress is below the required stress in any section a violation of the requirements occurs. This means that the reliability model for the whole structure can be described as a series system of a number of the parallel systems, where each parallel system j represents the prestress level in the structural part A_j, one for each of N tendons.

The prestress in two adjacent structural parts are influenced by a number of the same individual tendons, i.e. the elements in the series system have some degree of correlation. The correlation between different parallel systems varies depending on the distance between the structural parts which they represent. This type of series system can be seen as unequally correlated and requires extensive numerical calculation to find the exact probability of violation (Thoft-Christensen, 1982). An upper bound probability of violation for the whole structure can be found if it is assumed that the elements in the series system are independent. The upperbound expression can be written as

$$P(E) = 1 - \prod_{j=1}^{N} \left(1 - P(E_j)\right) \tag{6}$$

where event E is the event that the limit state of decompression is violated in one or more structural parts. A fully correlated series system gives a lower bound probability of violation and is described in expression 7 (Thoft-Christensen, 1982).

$$P(E) = \max_{j=1}^{N}(P(E_j)) \tag{7}$$

More narrow limits can be found by using Ditlevsen bounds, see for example Melchers (1999). The mean correlation could be used to evaluate the effect of correlation (Toft-Christiansen, 1982). If the mean correlation is low, say less than 0.2, the probability of violation will be near the upper bound and if the correlation is high, say above 0.8, the probability of violation will be close to the lower bound. For containments which consist of a large number of tendons the mean correlation will in general be low.

It is also possible to calculate more exact values of the probability of violation by using numerical methods (Monte Carlo simulation), which is made in the example in this paper.

Tendon dropout

The possibility of tendon dropout due to corrosion or other material defects is included to get a more comprehensive model of reliability of the containment prestress. It is assume that the general probability of tendon dropout *P(TD)* is known and completely randomized, where *TD* is the event of a tendon being defected. Corrosion could be localised to some part of the containment due to cracks in the concrete wall or other conditions and therefore affect several of adjacent tendons. This type of correlation is not taken into consideration in this paper.

The probability of k defected tendons in a containment with totally N tendons can be calculated with the binominal distribution (expression 8), where D_k represents the event of k tendons being defected.

$$P(D_k) = \binom{N}{k} P(TD)^k (1 - P(TD))^{N-k} \tag{8}$$

The location of defected tendons in the structure will effect the probability of violation, especially for $k>1$ where the distance between defected tendons will be important. The event D_k is therefore divided into r possible sub-events, where each sub-event represents one combination of defected tendons. All sub-events have the same probability to occur. The probability of violation of the limit state given that k tendons are defected can therefore be calculated as

$$P(E_k) = \frac{1}{r}\sum_{i=1}^{r} P(E_{k,i}) \tag{9}$$

where E_k is the event of violation given that k tendons are defected, $r = \binom{N}{k}$ and $P(E_{k,i})$ is the probability of violation for the i:th combination of k defected tendons.

The event of violation given that k tendons are defected (E_k) and the event of k tendons being defected (D_k) can be seen as independent events. The total probability of violation can therefore be calculated as

$$P(E)=\sum_{k=0}^{N}P(E_k)P(D_k) \qquad (10)$$

In practice the number of combinations r will be extensive for large number of tendon dropouts *k*. With reasonable values on the general probability of tendon dropout (*P(TD)*), the probability of a large number of tendon dropouts (*P(D_k)*) will be low. Expression 10 can therefore be truncated at *k=b,* where P(D_b) is insignificant. The probability of tendon dropout is also included in the numerical calculation in the next chapter.

Example, PWR containment, vertical tendons

In this example the vertical prestress in a PWR containment is evaluated with the analytic method described above and with a numerical calculation (Monte Carlo simulation). The measured tendon force is chosen to fit this example.

The containment consists of totally 153 vertical tendons (N =153), which are located in the centre of the outer wall. The total height of the containment is around 65m and the radius (wall centre) is around 18m (see fig. 6). The measured tendon force from the last inspection has a mean value of 4.0MN and a standard deviation of 0.4MN. The distance between the tendons (*a*) is about 0.75m.

Fig. 6, Sketch of PWR containment

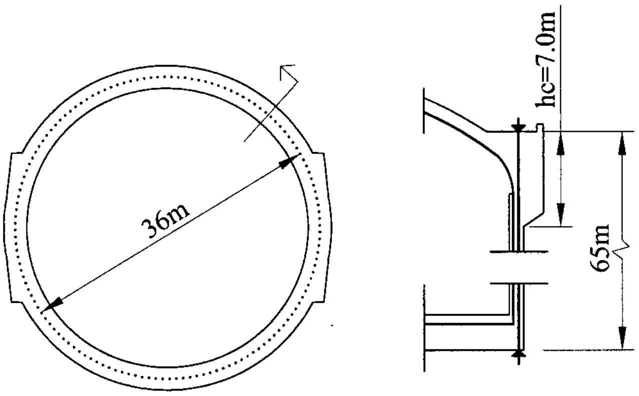

The critical level (h_c,) for the prestress is set as the lower edge of the buttress, 7m below the top anchorage of the tendons (see fig. 5). The prestress at this level is the sum of a number of influencing tendons according to expression 2. In this particular example it is reasonable to calculate the influence factors by expression 11 (solution by Boussinesq, see Timoshenko, 1970). This expression describes the stresses in a semi-infinite elastic shell with concentrated loads on the edge (see fig. 5).

$$I_i=\frac{2x^3}{\pi(x^2+y_i^{\,2})^2} \qquad (11)$$

x represents the depth (x = h_c = 7.0m) and y_i the horizontal distance to the load. Index i represents a tendon in relation to structural part *j*, e.i. i = 0 the influence from the tendon in the same section as structural part *j*, $i = \pm 1$ the tendons beside etc.. In this case the containment is assumed to be more or less rotary-symmetric, so the sum of influence factors is not varying between different structural parts A_j.

The required prestress per unit length of the containment wall q_S is calculated in expression 12, where the design pressure (p_{design}) for this containment is 0.50 MPa.

$$q_S = \frac{\pi R^2}{2\pi R} p_{design} = \frac{R}{2} p_{design} = 4.5 MN/m \tag{12}$$

To include the effects of tendon dropout an assumption of the general probability of tendon dropout ($P(TD)$) is required. In this example $P(TD)$ is assumed to be 10^{-3} at the time of the inspection. The probability of different fallouts $P(D_k)$ is calculated by expression 8 and shown in table 1 and 2.

Analytic calculation

The mean and standard deviation for the prestress (μ_q and σ_q) at the critical level h_c can be calculated by expressions 3 and 4. The 40 nearest tendons (on both sides of element j) are included in the calculation below. This gives sufficient accuracy in this example.

$$\mu_q = \mu_F (I_0 + 2\sum_{i=1}^{40} I_i) = 4.0 * 1.33 = 5.33 MN/m$$

$$\sigma_q = \sigma_F \sqrt{I_0^2 + 2\sum_{i=1}^{40} I_i^2} = 0.4 * 0.27 = 0.110 MN/m$$

Compared to influence from only one tendon the coefficient of variation (σ/μ) is in this case reduced with a factor 0.21.

The upper bound can be calculated with expression 6 and is shown in table 1. The mean correlation is calculated to 0.15 in this example. The probability of violation is therefore assumed to be quite close to the upper bound.

To find the total probability of violation the possibility of tendon dropout is included. To avoid extensive calculation work, expression 10 is truncated at 4 dropouts. Table 1 shows that the probability of 4 or more tendon dropouts is small in this example, $P(D_{k>4}) = 1 - P(D_{k\leq 4}) = 5.8*10^{-7}$. The maximum truncation error will therefore be $5.8*10^{-7}$, which can be considered as an insignificant error.

The upper bound of probability of violation for 1 to 4 tendon dropouts is calculated with expression 9 and the result is shown in table 1. The final upper bound for the probability of violation ($P(E)$) is calculated with expression 10 and shown in table 2.

Table 1, Result from analytic calculation

k	0	1	2	3	4	
$P(D_k)$	$8.58*10^{-1}$	$1.31*10^{-1}$	$1.0*10^{-2}$	$5.04*10^{-4}$	$1.89*10^{-5}$	
$P(E_k)^{1)}$	$3.86*10^{-12}$	$1.21*10^{-5}$	$1.77*10^{-2}$	$6.84*10^{-2}$	$1.59*10^{-1}$	$P(E)$
$P(D_k)P(E_k)$	$3.31*10^{-12}$	$1.60*10^{-6}$	$1.77*10^{-4}$	$3.45*10^{-5}$	$3.01*10^{-6}$	$2.16*10^{-4}$

1) Upper bound

Without considering the risk of tendon dropout the probability of violation is very low ($3.86*10^{-12}$). In the event of tendon dropout the probability of violation increases significantly. In the event of 4 dropouts (k = 4) the probability of violation of the limit state is about 16%

($P(E_k)$=1.59*10^{-1}). This increase of probability depends on the distribution of force influence. If the total influence on a structural part is distributed on many tendons the effect of dropout will be low. A well distributed influence will also have a positive effect on the standard deviation for the prestress σ_q. In this specific example the distribution of influence depends on h_c, where the influence increases with an increased h_c. $P(E)$ in Table 1 show the total probability of violation of the limit state with the assumption that 1 of 1000 tendons is defected (in general). Even if the assumption of defected tendons could be considered as low it increases the probability of violation significantly ($P(E)$ = 2.16*10^{-4}). The acceptance limit for $P(E)$ depends on the total required safety margins for the containment and failure modes not affected of the prestress level.

Numerical calculation

In the simulation the tendon forces in the structure are chosen randomly from the normal distribution with the mean and standard deviation (μ_F and σ_F) given for this example. To find the concrete prestress expression 2 together with the influence factors from expression 11 is used. The minimum prestress for all structural parts is then compared with q_S and if the prestress is below the limit a failure is recorded and added to a counter n_f. This procedure is repeated for a large number of samples (n) and the probability of violation $P(E)$ is finally calculated with expression 13.

$$P(E) = \frac{n_f}{n} \tag{13}$$

To include the effect of tendon dropout the probability of violation is calculated for each fallout of defected tendon. In the same procedure as described above k randomly select tendons is given zero force. The final probability of violation $P(E)$ is calculated with expression 10 and is shown in table 2.

Table 2, Results from numerical calculation,
1000 000 simulations (n)

k	0	1	2	3	4	
$P(D_k)$	8.58*10^{-1}	1.31*10^{-1}	1.0*10^{-2}	5.04*10^{-4}	1.89*10^{-5}	
$P(E_k)$	0	6.00*10^{-6}	5.89*10^{-3}	2.70*10^{-2}	7.08*10^{-2}	$P(E)$
$P(D_k)P(E_k)$	0	7.88*10^{-7}	5.88*10^{-5}	1.36*10^{-5}	1.34*10^{-6}	7.46*10^{-5}

The probability of violation is lower in the numerical calculation than the upper bound for the probability of violation in the analytical calculation. This is expected since the correlation between the different structural elements is included in the numerical calculation and therefore is closer to the actual probability. The upper bound can be considered as quite close to the numerical calculation in this example. In a case of a higher correlation the difference between the actual probability of violation and the upper bound will increase. The upper bound is however always on the "safe side".

Conclusions

Several tendons influence the prestress level in a specific part of the containment. This fact is important to consider both concerning the general level of prestress and for tendon dropouts. In the presented reliability model the total resistance is described as a series system with elements of parallel coupled components. The resistance for the individual components represents the remaining tendon force and the load in the model represents tensile stresses from the internal design pressure.

The elements in the series system are concluded to be unequally correlated. This makes it difficult to calculate the exact probability of violation. In the example it is concluded that the mean correlation is quite low. The actual probability of violation can therefore be assumed to be close to the value calculated with the upper bound expression. The upper bound is however always on the "safe side".

The effect of tendon dropout is calculated by assuming a general probability for a tendon being defected. This effect is in the example shown to be significant even with a low assumed general probability of tendon dropout. However, the detailed design for the containment will highly influence the effect of tendon dropout.

The structural integrity of the containment depends not only on the prestress level in the structure. The acceptable probability to fall below the minimum required prestress therefore both depends on the total required safety margins for the containment and the probability of failure modes not affected of the prestress level.

References

Regulatory Guide 1.35, 1990. Inservice Inspection of Ungrouted Tendons in Prestressed Concrete Containments, U.S. Nuclear Regulatory Commission (NRC), Revision 3.

Thoft-Christensen P, Baker M.J.,1982, Structural reliability theory and its applications, Springer

Melchers R.E., 1999, Structural reliability analysis and predictions, John Wiley & Sons Ltd

Timoshenko, S, Goodier, J N, 1970, Theory of elasticity, 3 revision, New York-Toronto-London.

Statistical assessment of the prestress level based on in-service inspections of unbonded tendons

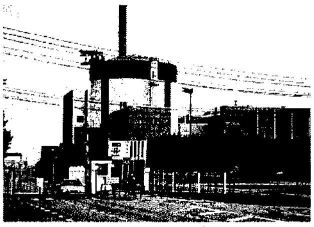

Presentation to the CSNI Workshop on International Standard Problem 48
Lyon, France - April 6-7, 2005
By
Patrick Anderson, University of Lund, Sweden

LUND INSTITUTE
OF TECHNOLOGY
Lund University

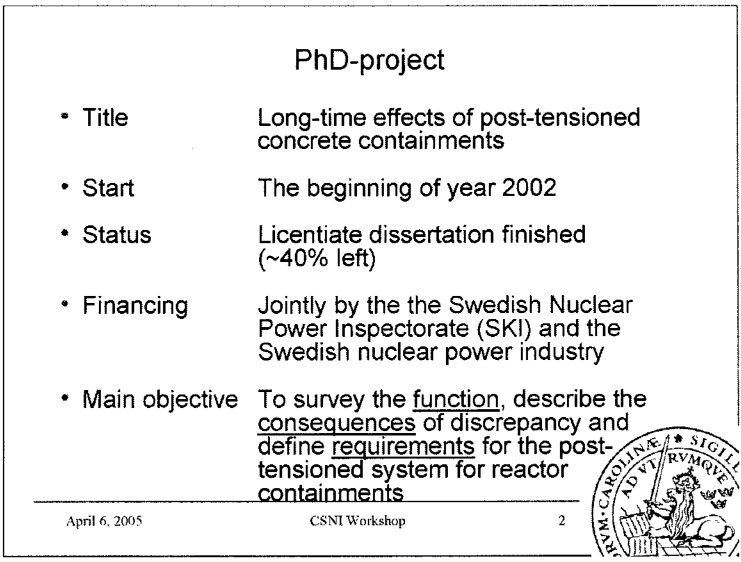

PhD-project

• Title	Long-time effects of post-tensioned concrete containments
• Start	The beginning of year 2002
• Status	Licentiate dissertation finished (~40% left)
• Financing	Jointly by the the Swedish Nuclear Power Inspectorate (SKI) and the Swedish nuclear power industry
• Main objective	To survey the function, describe the consequences of discrepancy and define requirements for the post-tensioned system for reactor containments

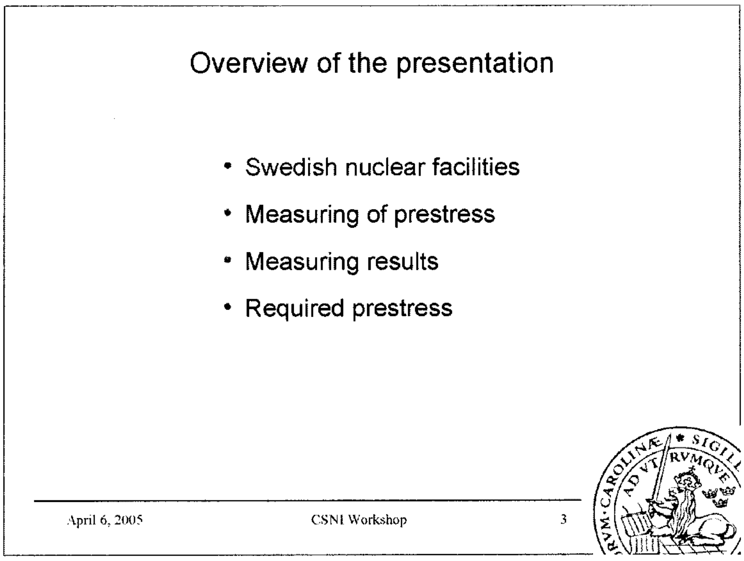

Overview of the presentation

- Swedish nuclear facilities
- Measuring of prestress
- Measuring results
- Required prestress

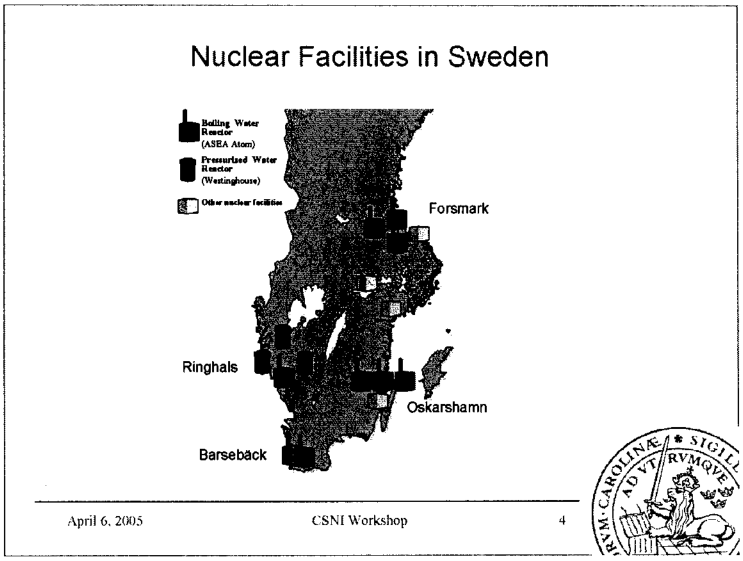

Nuclear Facilities in Sweden

Boiling Water Reactor (ASEA Atom)
Pressurized Water Reactor (Westinghouse)
Other nuclear facilities
Forsmark
Ringhals
Oskarshamn
Barsebäck

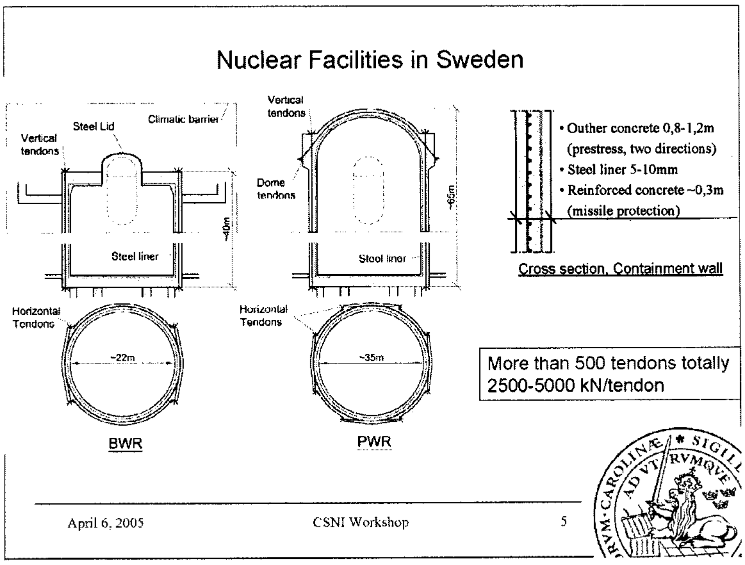

Nuclear Facilities in Sweden

Climatic barrier
Steel Lid
Vertical tendons
~40m
Steel liner
Horizontal Tendons
~22m
BWR
Vertical tendons
Dome tendons
~65m
Steel liner
Horizontal Tendons
~35m
PWR

- Outher concrete 0,8-1,2m (prestress, two directions)
- Steel liner 5-10mm
- Reinforced concrete ~0,3m (missile protection)

Cross section, Containment wall

More than 500 tendons totally
2500-5000 kN/tendon

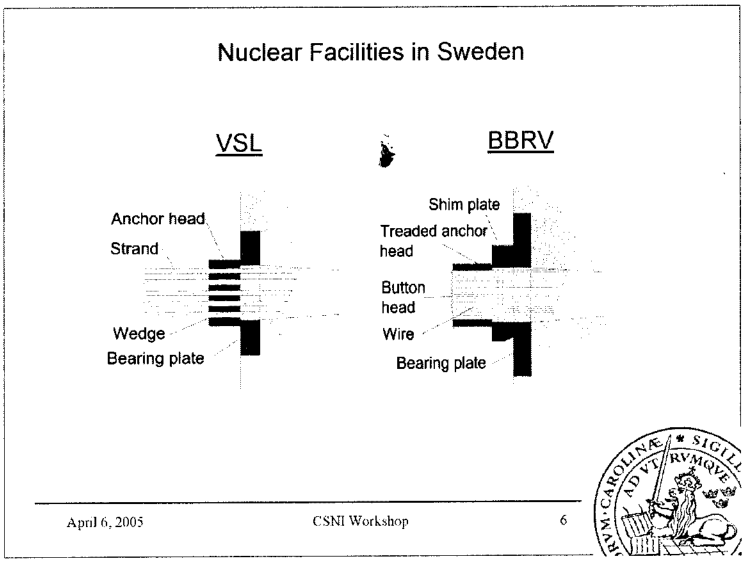

Nuclear Facilities in Sweden

VSL
Anchor head
Strand
Wedge
Bearing plate
BBRV
Shim plate
Treaded anchor head
Button head
Wire
Bearing plate

Measuring of tendon force

Measuring at the on going in-service inspection at Forsmark 3

Inspections acc. to NRC, Regulatory Guide 1.35

- 1, 3 and 5 years after ISIT and thereafter every 5th year
- The force is measured for 2-4 % of the tendons
- The tendon are selected randomly from each group
- One tendon from each group is detensioned

Measuring of tendon force

- The force is measured when the anchor lifts from the anchor plate (Lift-off technique)
- Measuring error 2-4% of the force
- Measuring error is assumed to be randomized
- The friction along the tendon (horizontal tendons) could give misleading results
- Measurements at Forsmark 2 indicate,

Loss of lift-off force (end force) > Loss of average force

nchor plate

Lift-off test in action (Forsmark 2, 03)

Jack measuring tendon force

(VSL-system)

Measuring results

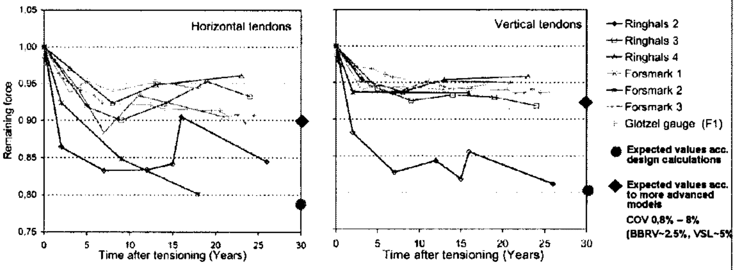

- Larger losses in Ringhals 2

  -Short time between tensioning and start of operation

  -Slow drying (heavy structure, one sided drying)

  (Start of operation => increased temperatur)

  -High concrete age at the initial tensioning

  (2 years between casting and tensioning)

Measuring results

Fixed gauges at Forsmark 1

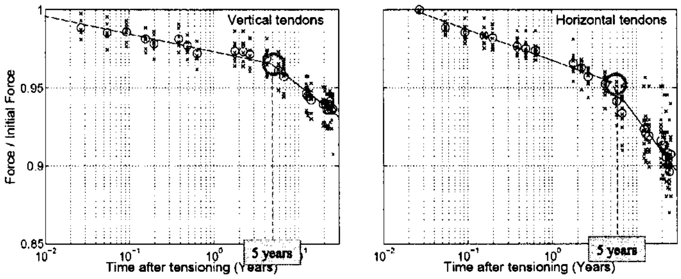

5 years ~ Start of operation

Required prestress

Do the measured forces meet the requirement?

Required prestress

Globally in the containment the concrete shall be in compressive state at the internal design pressure (p).

$\Rightarrow$ Horizontal $\boxed{q_S = pR}$ (force/unit lenght)

Vertical $\boxed{q_S = \frac{pR}{2}}$ (force/unit lenght)

$\boxed{0 \le q_R - q_S}$ (Limit state of decompression)

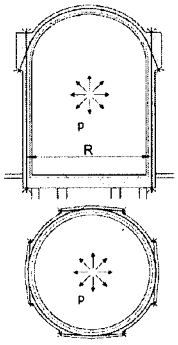

Required prestress

$$\boxed{q_{R,j}=\sum_{i=1}^{N}F_i I_{i,j}}$$

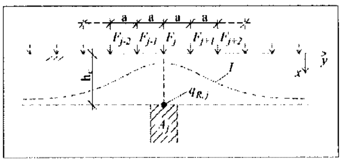
a
a
a
a
F_{j-2}
F_{j-1}
F_j
F_{j+1}
F_{j+2}
h_c
I
$q_{R,j}$
A_j
x
y

Influence from vertical tendons

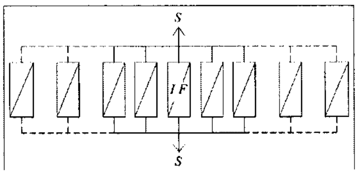

Reliability model for one structural part

Required prestress

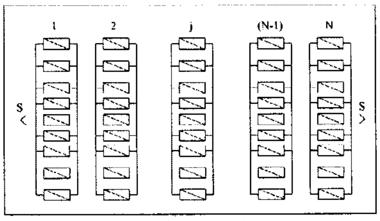

Reliability model for the whole structure

$$\boxed{p_f=1-\prod_{j=1}^{N}\left(1-P(E_j)\right)}$$

(Upper bound expression)

Required prestress

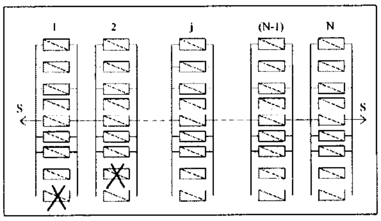

Tendon dropout

Required prestress

- Input
  - Measuring values => Mean and standard deviation (independent and normally distributed)
  - Influence from geometry, linear elastic model
  - Assumptions or estimations of the probability of tendon dropout
- Output
  - The probability of violation of the limit state of decompression, anywhere in the structure (p_f)
  - $p_f <$ accepted level

Licentiate report

Evaluation of the prestress level in nuclear reactor containments

- **Introduction**
- **Paper 1,** Average force along unbonded tendons; a field study at nuclear reactor containments in Sweden
  Nuclear Engineering and Design (2005)
- **Paper 2,** 30 years of measured prestress at Swedish nuclear reactor containments
  Submitted to Nuclear Engineering and Design
- **Paper 3,** Reliability-based evaluation of the prestress level in concrete containments with unbonded tendons
  Submitted to PCI Journal

PROBABILITY ANALYSIS OF REINFORCED CONCRETE STRUCTURE FAILURE OF NUCLEAR POWER PLANTS DUE TO LOSS OF COOLANT ACCIDENT

Juraj Králik
Faculty of Civil Engineering STU in Bratislava, Slovakia

Abstract

This paper presents the probability analysis of reinforced concrete containment structure of NPP with the reactor VVER V-230 under high internal overpressure. The probabilistic structural analysis (PSA) level 2 aims at an assessment of the probability of the concrete structure failure under excessive overpressure. In the non-linear analysis of the concrete structures a layered approximation of the shell elements with various material properties have been included. The uncertainties of longtime temperature and dead loads, material properties (concrete cracking and crushing, reinforcement, and liner) and model uncertainties were taken into account in the 10^6 direct MONTE CARLO simulations. The results of the probability analysis of the containment failure under excessive overpressure show that in the case of the LOCA accident at overpressure of 122,7kPa the probability is smaller than the required 10^{-4} for design resistance.

Introduction

The International Atomic Energy Agency set up a program to give guidance to its member states on the many aspects of the safety of nuclear power reactors. The resistance of the building structure has been checked for extreme steam pressure in the case of small or medium-sized accidents [9] and on the ground of these results the reconstruction of the structures and technological equipments was realized.

The concrete structures of hermetic zone were analyzed for number of situations, such as a LOCA (Loss of Coolant Accident) or a HELB (High Energy Line Break as steam line break) on the different primary loop piping system.

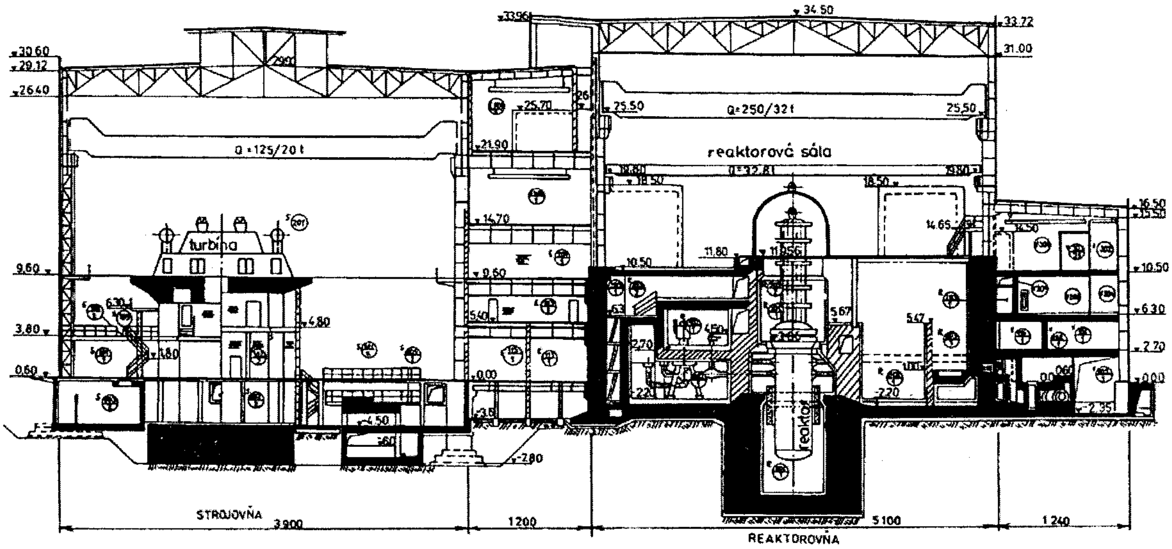
30.60
29.12
26.40
Q=125/20 t
turbína
9.60
3.80
0.60
STROJOVŇA
3900
1200
34.50
33.72
31.00
25.50
Q=250/32 t
reaktorová sála
10.50
6.30
2.70
0.00
5100
1240
REAKTOROVŇA

Figure 1. Cross section of NPP building V1 in Jaslovské Bohunice

In the case of the analysis PSA 2 level it's necessary to determine the probability of the concrete structure failure under higher overpressure. Consequently even in a case of a PSA project the objective was not to find the mean failure pressure, but rather the probability of failure under an internal overpressure of definite value.

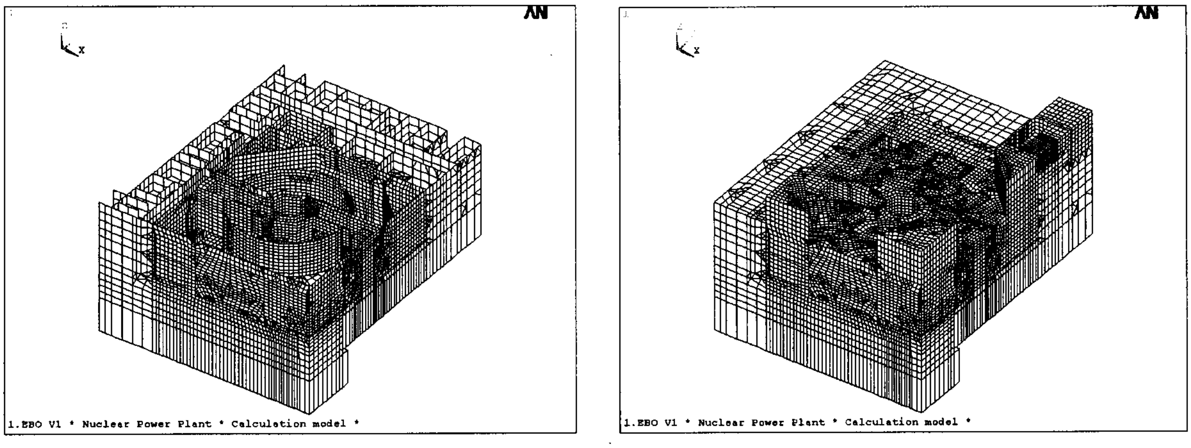
AN
1.EBO V1 * Nuclear Power Plant * Calculation model *
AN
1.EBO V1 * Nuclear Power Plant * Calculation model *

Figure 2. Calculation model of the NPP building with layered shell elements

The general purpose of the probability analysis of the containment integrity was to define the critical places of the structure elements and to estimate the structural collapse. In this paper the nonlinear analysis of the concrete containment resistance for mean values of loads, material properties and higher overpressure than BDBA (Beyond Design Basic Accident) is presented. Following these results the probability check of the structural integrity may be realized for the random value of the loads and material properties by MONTE CARLO method [15]. The probability check was considered in the critical places, which were defined from the previous nonlinear analysis for various loads (BDBA, DBA1 and DBA2) [8].

For a complex analysis of the load-bearing structure for different kind of loads, ANSYS 7.0 software and the program CRACK [8, 10] (created by Králik) were provided to solve this task. The building of the power block was idealized with a discrete model consisting of 26 923 elements with 325 036 DOF.

Scenario for LOCA loads

The accident scenario was defined by SIEMENS KWU, VÚEZ Tlmače and VÚJE Trnava within the Phare program and "The NPP V1 Reconstruction Project". The thermodynamic experimental analysis of the cooling pipe system and the numerical simulation were input data concerning the load behavior over time [18].

The original Design Basis Accident (DBA) defined as rupture of primary coolant circuit with equivalent diameter of 32mm and the Beyond DBA (BDBA) with a break of reactor coolant system main circulation line with double – end coolant discharge together with reconstructed Emergeny Core Cooling System were considered.

Concerning the small dynamic pressure load factor (versus 1.1) we used for BDBA (versus DBA), a load pressure of 120 kPa (versus 54 kPa) inside the containment and a 74 kPa (versus 51 kPa) inside 800m^3 EWST (Emergency Water Storage Tank).

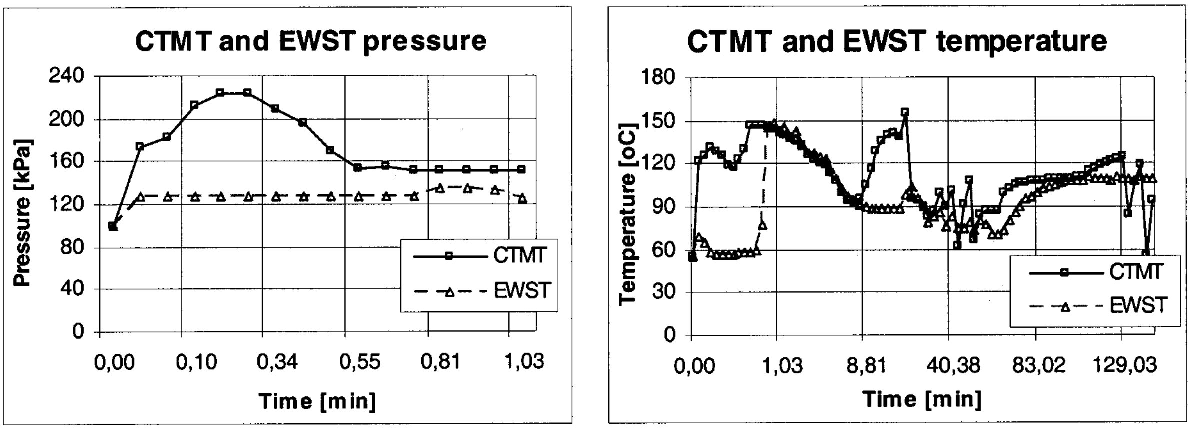

Figure 3. The peak of the pressure and temperature in CTMT and EWST for LOCA 2xØ500mm

The temperature in the hermetic zone increased during the LOCA accident. The ***peaks of the temperature*** are equal to 156°C in time 1707s (CTMT), or 149°C in time 57,75s (EWST) in accordance to thermodynamic analysis [18]. The effect of these temperature peaks is minimal during the accident and the acting of the overpressure loads. In the case of the harmonic amplitude of temperature the phase angle for concrete walls is superior to 24 hours. The strength of the concrete after LOCA accident increases about to 10% in consequence of the temperature loads during the accident.

The temperature in the hermetic zone and other rooms in the case of operating conditions was defined as the mean value certified by operator of NPP on the basis of experimental measurements, or as design temperature in the specified rooms. Actually the temperature is not constant but variable in the different places of rooms and it depends on affect of air-conditioning and the season, operating period and other factors. According to all that the operating temperature in containment HZ is equal to 50°C and more, it can be characterized by the heat transfer through the wall to rooms with lower temperature.

The long time effect of temperature (considering the concrete creep and shrinkage after 20 years), the dead loads from structures and technology were taken constant for nonlinear analysis. The overpressure loads in the tank 800m^3 was taken of value 33kPa and in the hermetic zone various from level 40kPa to 300kPa.

The total strain at any time t at a point in an element depends on elastic strain ε_{el}, creep strain ε_{cr}, temperature strain ε_{th} and shrinkage strain ε_{sh}

$$\varepsilon(t,\tau)=\varepsilon_{el}(t,\tau)+\varepsilon_{cr}(t,\tau)+\varepsilon_{th}(t,\tau)+\varepsilon_{sh}(t)=\frac{\sigma}{E(\tau)}+\frac{\sigma}{E(\tau)}\varphi(t,\tau)+\varepsilon_{th}(t,\tau)+\varepsilon_{sh}(t), \quad (1)$$

where τ is the time of load application, $E(\tau)$ is the elasticity modulus of the concrete and $\varphi(t,\tau)$ is the creep coefficient, defined as the ratio of creep strain at the time t to instantaneous elastic strain. To solve containment deformation we used a creep curve and shrinkage function according to STN 73 1201.

Nonlinear solution of concrete cracking and crushing

The constitutive model presented is a further extension of the smeared crack model, which was developed in reference [3, 4, 10] and later improved by many writers [16, 17]. Following the experimental results of Vecchio, Collins and Červenka [2, 3] and Kupfer [13] a new concrete cracking layered finite shell element was developed and incorporated into the ANSYS system. One concrete layer was considered as orthotropic material for which the direction of a crack is the same as the direction of a principal strain.

In this model the Kupfer's bidimensional failure criterion of concrete is considered (see Fig.5). The concrete compressive stress f_c, tensile concrete stress f_t and shear modulus G are reduced after the cracking of the concrete.

The stress-strain relation is defined following ENV 1992-1-1 (1991)

➲ Loading in compression region $\varepsilon_{cu} < \varepsilon^{eq} < 0$

$$\sigma_c^{ef} = f_c^{ef}.\frac{k.\eta-\eta^2}{1.+(k-2).\eta}, \quad \eta=\frac{\varepsilon^{eq}}{\varepsilon_c} \qquad (\varepsilon_c \doteq -0.0022, \quad \varepsilon_{cu} \doteq -0.0035) \qquad (2)$$

➲ Softening in compression region $\varepsilon_{cm} < \varepsilon^{eq} < \varepsilon_{cu}$

$$\sigma_c^{ef} = f_c^{ef}.\left(1-\frac{\varepsilon^{eq}-\varepsilon_c}{\varepsilon_{cm}-\varepsilon_{cu}}\right) \tag{3}$$

➲ Tension region $\varepsilon_t < \varepsilon^{eq} < \varepsilon_m$

$$\sigma_c^{ef} = f_t.\exp(-2.(\varepsilon^{eq}-\varepsilon_t)/\varepsilon_{tm}) \tag{4}$$

In the case of two dimension stress state the strength function in tension f_t and in compression f_c was considered as equivalent values f_t^{eq} and f_c^{eq}. In the plane of principal stresses can be defined the relation between the one and two stresses state due to plasticity function by Kupfer (see Fig.5).

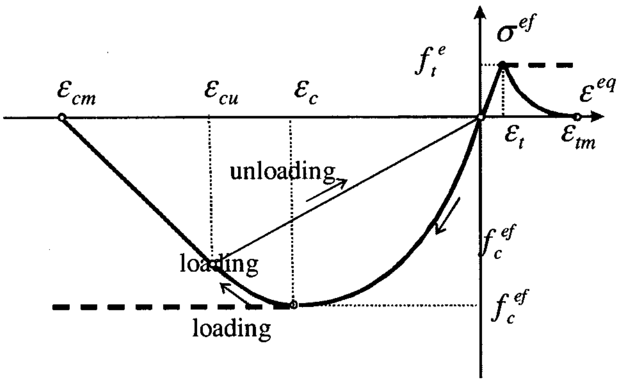

Figure 4. Stress-strain concrete diagram

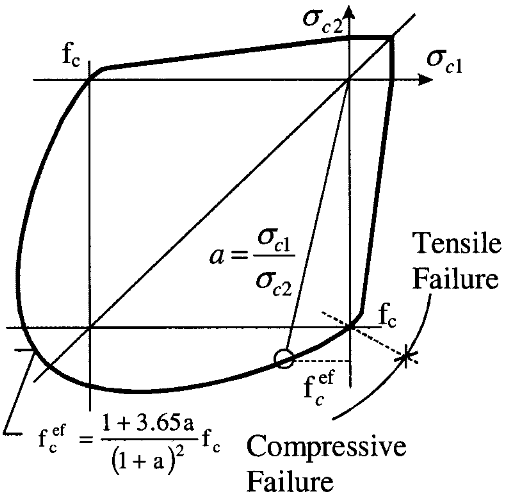

Figure 5. Kupfer's plasticity function

In the plane of principal stresses can be defined the relation between the one and two stresses state due to plasticity function by Kupfer (see Fig.5).

➲ Compression-compression

$$f_c^{ef} = \frac{1.+3.65.a}{(1.+a)^2}.f_c,\quad a=\frac{\sigma_{c1}}{\sigma_{c2}} \tag{5}$$

➲ Tension-compression

$$f_c^{ef} = f_c.r_{ec},\ r_{ec} = \left(1.+5.3278\frac{\sigma_{c1}}{f_c}\right),\ r_{ec} \geq 0{,}9 \tag{6}$$

➲ Tension-tension

$$f_t^{ef} = f_t.r_{et},\ r_{et} = \frac{A+(A-1).B}{A.B},\ B=K.x+A,\ x=\sigma_{c2}/f_c, \tag{7}$$

$$r_{et}=1.\Leftrightarrow x=0,\quad r_{et}=0{,}2 \Leftrightarrow x=1.$$

The shear concrete modulus G was defined for cracking concrete by Kolmar in the form

$$0<p<0{,}02$$

$$G=r_g.G_o,\ r_g=\frac{1}{c_2}\ln\left(\frac{\varepsilon_u}{c_1}\right),\quad c_1=7.+333(p-0{,}005),\quad c_2=10-167(p-0{,}005), \tag{8}$$

where G_o is initial shear modulus of concrete, ε_u is strain in the normal direction to crack, c_1 and c_2 are constants dependent on ratio of reinforcing, p is ratio of reinforcing transformed to the plane of rack.

Function of concrete failure (loss of integrity) can be defined in dependency to the components of the stresses in the crack plane of layer "l" by the function of failure surface F_u^l. The limit of damage at a point is controlled by the values of the so-called crushing or total damage function F_u. The modified Kupfer's condition is following

$$F_u^l = F_u^l\,(I_{\varepsilon 1};\, J_{\varepsilon 2};\, \varepsilon_u) = 0, \qquad F_u^l = \sqrt{\beta\left(3J_{\varepsilon 2}\right) + \alpha I_{\varepsilon 1}} - \varepsilon_u = 0\ , \tag{9}$$

where $I_{\varepsilon 1}$, $J_{\varepsilon 2}$ are strain invariants, and ε_u is an ultimate total strain extrapolated from uniaxial test results, α, β are material parameters determined from Kupfer's experiment results ($\beta = 1{,}355;\quad \alpha = 0{,}355\varepsilon_u$).

For the membrane and bending deformation of the reinforced concrete shell structure, we have chosen the SHELL91 layered shell element, on which we propose a plane state of stress on every single layer.

The stiffness matrix of reinforced concrete for the layer "l^{th}" can be written in the following form

$$\left[\mathbf{D}_{cr}^l\right] = \left[\mathbf{T}_c^l\right]^T \left[\mathbf{D}_c^l\right]\left[\mathbf{T}_c^l\right] + \sum_{j'=1}^{n} \left[\mathbf{T}_s^l\right]^T \left[\mathbf{D}_s^l\right]\left[\mathbf{T}_s^l\right],$$

where $\mathbf{T}_c$, $\mathbf{T}_s$ are the transformation matrices for concrete and reinforcement separately.

$$\left[\mathbf{D}^l\right] = \begin{bmatrix} B^l E_x^l & B^l \mu_{xy}^l E_x^l & 0 & 0 & 0 & 0 \\ B^l \mu_{xy}^l E_x^l & B^l E_y^l & 0 & 0 & 0 & 0 \\ 0 & 0 & 0 & 0 & 0 & 0 \\ 0 & 0 & 0 & G_{xy}^l & 0 & 0 \\ 0 & 0 & 0 & 0 & \dfrac{G_{yz}^l}{k_s} & 0 \\ 0 & 0 & 0 & 0 & 0 & \dfrac{G_{zx}^l}{k_s} \end{bmatrix}$$

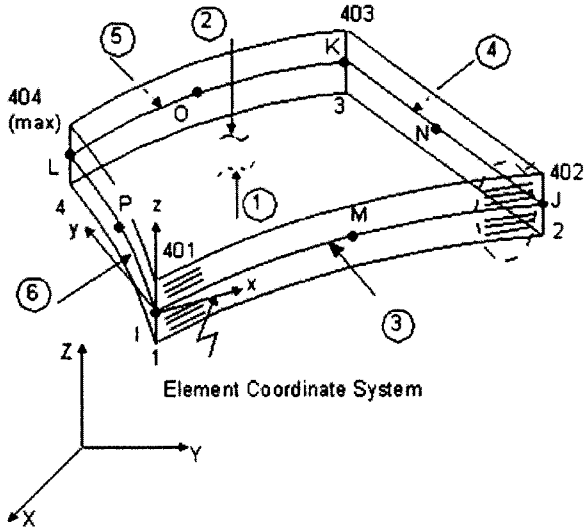

Figure 6. Layered shell element - SHELL91

$$B^l = \frac{E_y^l}{E_y^l - \left(\mu_{xy}^l\right)^2 E_x^l}, \tag{10}$$

where E_x^l (resp. E_y^l) is Young modulus l^{th} layer in the direction x (resp. y), G_{xy}^l, G_{yz}^l, G_{zx}^l are shear modulus l^{th} layer in plane xy, yz and zx ; k_s is coefficient of effective shear area ($k_s = 1 + 0{,}2\dfrac{A}{25t^2} \geq 1{,}2$), A is the element area, t is the element thickness.

The smeared crack model, used in this work, results from assumption, that the field of more micro cracks (not one local failure) brought to the concrete element will be created. A validity of this assumption is determined by size of finite element, hence its characteristic dimension $L_c = \sqrt{A}$, where A is the element area (versus integrated point area of element). For expansion of cracking is valid the assumption of constant failure energies G_f=*const*

$$G_f = \int_0^{\infty} \sigma_n(w)dw = A_G.L_c, \qquad w = \varepsilon_w.L_c, \tag{11}$$

where w is width of failure, σ_n is the stress in concrete in the normal direction, A_G is area under stress-strain diagram of concrete in tension. Concrete modulus for descend line of stress strain diagram in tension (crushing) can be described by Oliver in dependency to failure energies in the form

$$E_{c,s} = \frac{E_c}{1-\lambda_c}, \qquad \lambda_c = \frac{2G_f E_c}{L_c.\sigma_{\max}^2}, \tag{12}$$

where E_c is initial concrete modulus elasticity, σ_{max} is maximal stress in concrete tension. From the condition of real solution of relation (10) it follows, that the characteristic dimension of element must satisfy following condition

$$L_c \le \frac{2G_f E_c}{\sigma_{\max}^2}, \tag{13}$$

The characteristic dimension of element is determined by size of failure energy of element. A theory of concrete failure was implied and applied to the 2D layered shell elements SHELL91 and SHELL99. The program CRACK was checked and the results were compared with experimental results of Duddeck [4] and Hájek [6] in the work.

Červenka's model with strength degradation for 2D stresses, Kupfer's cond., degradation of shear modulus by Kalmár, stres-strain diagram by EC2 [5] were investigated in the work [12]. From the comparison of containment structure resistance follows that in case of concrete and steel liner jointed effect the damage of structure is attained at 260kPa and otherwise 220 kPa.

On base of non linear analysis providing the monotone increases of overpressure in CTMT the critical points in structure were defined.

These critical places correspond to concentration of singular tension forces after high bending deformation of wall at line "10" or "V" and the enfeeblement plate by hole of cell and near assembly cover. Figures 8 show the izosurface of principal deformations at TOP face of element (surface at positive face of element - normal element vector and global coordinate vector are identical).

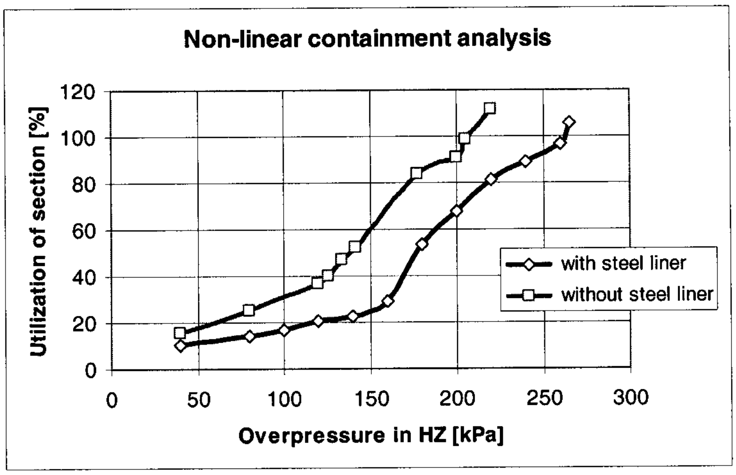

Figure 7. The Capacity of structure section over to overpressure load in HZ (CTMT)

Probabilistic analysis of containment structures

The methodology of probabilistic analysis of integrity of reinforced concrete structures of containment results from requirements [11, 14, 19] and experiences from their applications. In this report the direct simulation method MONTE CARLO [15] to solve the reliability considering the non linear behavior of reinforced concrete structures [10, 17, 19, 20] is used.

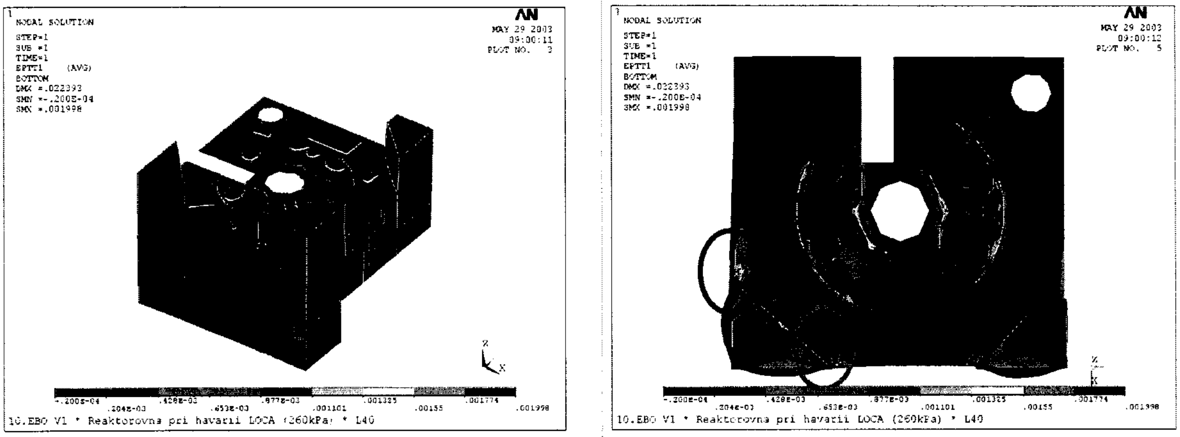

Figure 8. Critical point of containment structural loading at overpressure 260 kPa

The probability of loss integrity of reinforced concrete structure hence it will be calculated from the probability of no accomplishment condition of reliability *SF*,

$$P_f = P(SF < 0)\,, \tag{14}$$

where the reliability condition is defined by [15] in form

$$SF = R - E \geq 0, \qquad \text{various in the form relative} \qquad SF = R/E - 1 \geq 0 \tag{15}$$

where R is design capacity of structure, E design load effect. In the case of calculus the resistance of reinforced concrete structure leads off the condition of section integrity (3). The probabilistic analysis of the condition integrity of containment was realized by simulation of design check using the direct method MONTE CARLO under system ANSYS.

The probabilistic analysis of accident LOCA results from uncertainty of material properties, load level, non linear calculation and design condition. The deformation state of the structural elements was defined to reduce structural stiffness as complex of effects for level of load cases under accident LOCA for average load values and material properties. The total relative deformation for i - th load level can be defined as follows

$$\varepsilon^i_{var}(t,\tau) = \left\{\varepsilon^i_g(t,\tau).g_{var} + \varepsilon^i_{th}(t,\tau).T_{var} + \varepsilon^i_p(t,\tau).p_{var}\right\}e_{var}\,, \tag{16}$$

where ε^i_g, ε^i_{th} and ε^i_p are the vectors of relative deformations from dead and live loads (structural and technology weight), temperature and overpressure according to non linear solution of all structures for average load values; g_{var}, T_{var}, p_{var} and e_{var} are the variable defined by histograms (for normal and lognormal distribution) uncertainty of design conditions is expressed in the function of failure surface by (9), which is proposed as design value of reliability

$$E = \varepsilon_u \cdot f_{var}\,, \tag{17}$$

where ε_u is ultimate equivalent total deformation of concrete and f_{var} is variable defined by histogram (for normal and lognormal distribution).

The design structure reliability is defined depending on concrete failure condition (9) as follow

$$R = F_u(I_{\varepsilon 1};\, J_{\varepsilon 2};\, \varepsilon_u) + \varepsilon_u, \qquad F_u = \frac{1}{h}\cdot\int_0^h F^l_u\left(I_{\varepsilon 1}; J_{\varepsilon 2}; \varepsilon_u\right)dz \tag{18}$$

where h is the thickness of the plate.

The previous design analysis, calculations and additions include various uncertainties, which determine the results of probability bearing analysis of containment structural integrity is presented in the Table 2. On the base of mentioned inaccuracy of input dates for probabilistic analysis of loss integrity of reinforced concrete containment structures were determined their mean values and standard deviations, various the variable constant for normal and lognormal distribution.

Table 2 Variable constants of the input dates

	Variable constants			
	e_{var}	T_{var}	g_{var}	f_{var}
Mean value μ	1	1	1	1
Standard deviation [%]	11,1	10	10	15

Resulting from variability of input quantity 10^6 simulation in the MONTE CARLO's method under system ANSYS were realized, which determined the probability of loss containment structure integrity CTMT.

Table 3 Probability of loss containment structure integrity

	Load cases							
	LC36	LC37	LC38	LC39	LC40	LC41	LC42	LC43
Overpressure in CTMT [kPa]	180	200	220	240	260	265	280	300
Normal	$4,0.10^{-6}$	$9,3.10^{-4}$	0,01065	0,02878	0,06002	0,1763	0,5253	0,9999
Lognormal	0,00	2.210^{-5}	0,00426	0,02174	0,06424	0,1850	0,5474	0,8026

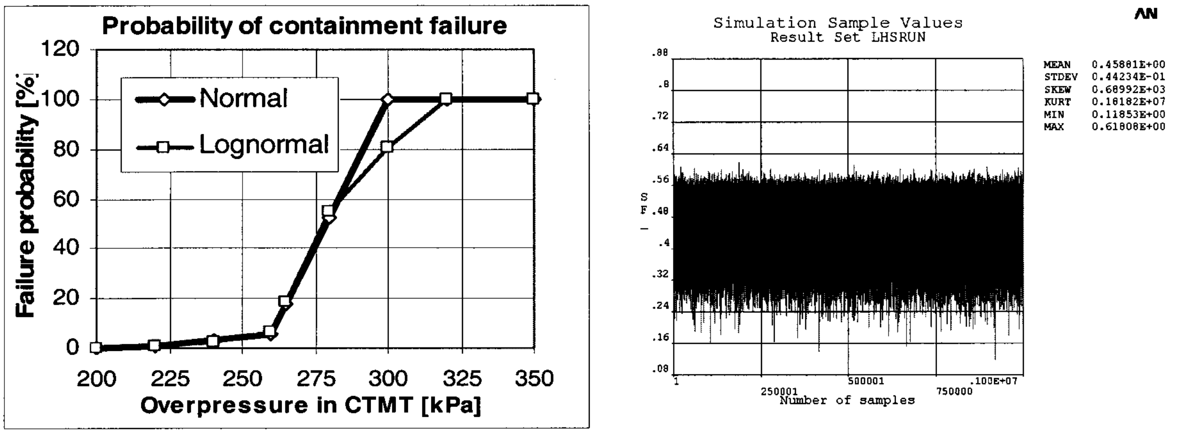

Figure 9. Probability of containment failure and Reliability function for 106 simulation

Some authors who deal with the probabilistic analysis of containment failure lead off the determination of the uncertainty design criteria (15% uncertainty is defined by Duke Power Company in analysis Oconee, chap.3), uncertainty of material properties (8% uncertainty is defined in Commonwealth Edison, 1981, appendix 4.4.1). Total uncertainty is presented with standard deviation value 8% and 17% using the normal probability distribution of containment failure.

The distribution function of containment failure probability for normal distribution of input data (see Fig.9) is obtained from non linear analysis with 2D failure criterion for mean properties values and overpressure 261,5kPa go out the presented consideration.

The curve of normal distribution corresponding to 8% of standard deviation is at very good agreement with failure function behavior achieved from the non linear calculation for different loading level (see Fig.9). For this case of probability distribution is the error factor equal to value 1,304.

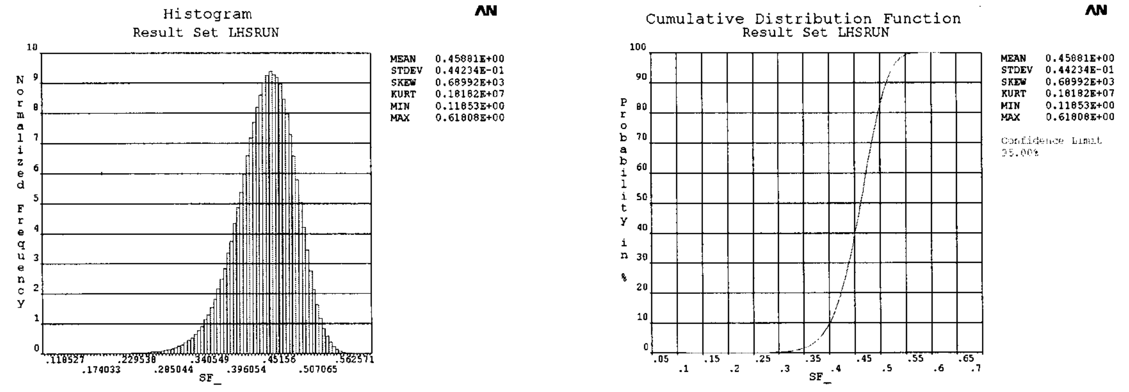

Figure 10. Histogram and reliability distribution function SF for 180kPa

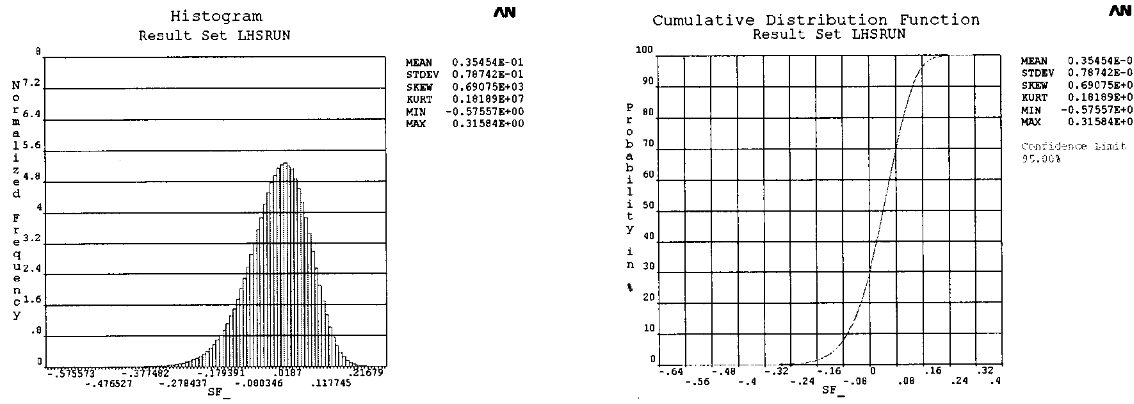

Figure 11. Histogram and reliability distribution function SF for 260kPa

Conclusion

The general purpose of the probability analysis of the containment integrity was to define the critical places of the structure elements and to estimate the structural collapse. The probability check of the structural integrity was realized for the critical places, which were defined from the previous nonlinear analysis for various loads (BDBA, DBA1 and DBA2) [10].

The previous nonlinear analysis and design check include various uncertainties, therefore the results of probability analysis of containment structural integrity are determined as follows:

- The initial items of the investigation of probability containment structural damage were the input values of structural material strength. In the case of reinforced concrete containment structure the strength of concrete was verified experimentally on 12 bore concrete samples. On the basis of these tests the quality of concrete after 20 years of operation was determined as concrete of class B40 ("best estimate") with standard deviation 11,1%.

- The basic starting points and the evaluation of mechanical properties correspond to assumptions and advances also used in the other projects [6], the deviations (differences) are in interval 8-12 % that can be determined by differences in the design of various nuclear power plants with reactor VVER V-230 . In some cases it might yield conservative values, other non conservative values.
- The model uncertainties of the nonlinear stress-strain relations of the reinforced concrete structures in consequence with the inaccuracy of numerical model were considered at 10-15%. The effect of concrete and steel liner joint can be included in this deviation.
- The inaccuracy in the estimation of the temperature values in the structures was determined at 10 %.
- The other computational assumptions, that neglect any influences (steel frame of the hinged door, holes,...) are ordinarily conservative. These effects affect no more than 3-5% error.

The nonlinear analysis of concrete structures was realized to take into account the concrete cracking and crushing, layered approximation of the shell elements with various material properties, orthotropic material depending on the direction of the rotated cracks and the orientation of reinforced steel, modified Kupfer's yield function, degradation of the shear modulus by Kolmar according to reinforcement properties.

The probability analysis of the concrete structure integrity was considered for the overpressure loads from 40kPa to 300kPa using the iterative stiffness of structure and mean properties of materials. The uncertainties of the loads level (longtime temperature and dead loads), the material properties (concrete cracking and crushing, reinforcement, and liner) and other influences following the inaccuracy of the calculated model and numerical methods were taken in the account in the 10^6 direct MONTE CARLO simulations statistically independent. The number of the simulations is determined by the number of input variable parameters [14] (the error decreases with factor $n^{-1/m}$, where n is the number of the simulations and m is the number of the input variable parameters).

The probability of the containment failure using the normal distribution of the input parameters is equal to 9, 31.10^{-4} for overpressure 200kPa taking the Kupfer's criteria of the structure failure (9).
The results of the probability analysis of the containment failure under high overpressure show that in the case of the LOCA accident at 122,7kPa is probability lesser than required 10^{-4}.

This paper was supported by Grant Agency ***MŠ SR VEGA 1/2136/05***.

References

[1] Bittnar,Z.-Šejnoha,J.: Numerical Methods in Structural Mechanics. Telford, London, 1996, 470 pp. ISBN 0-7277-2555-6.
[2] Collins,M.P.-Vecchio,F.-Mehlhorn,G.: An International Competition to Predict the Response of Reinforced Concrete Panels, Festschift Prof.Dr.Bruno Thürlimann zum 60.Geburtstag, ETH Zürich, 1983, pp.471-491.
[3] Červenka,V.: Constitutive Model for Cracked Reinforced Concrete, ACI Journal, pp. 877-882, Nov.1985.
[4] Duddeck,H.-Griebenow,G.-Schaper,G.: Material and Time Dependent Non-linear Behavior of Cracked Reinforced Slabs, Non-linear Behavior Reinforced Concrete Spatial Structures, Vol.1, IASS Symp.,Darmstadt, Werner-Verlag, Düsseldorf, 1978.
[5] Eurocode 2, Design of Concrete Structures, Part 1, CEC 1990.

[6] Hájek,J.-Fecko,L.-Nürnbergerová,T.: Pretvorenia železobetónových dosiek ohýbaných v dvoch smeroch pri dlhodobom zaťažení. Správa VÚ III-3-4/01.1, ÚSTARCH SAV Bratislava, 1983.

[7] IAEA : Guidelines for WWER 440/213 Containment Evaluation, Rep. IAEA, March 1995.

[8] Králik,J.: Experimental and Numerical Analysis of Reinforced Concrete Containment after Loss of Coolant Accident, In proc. The International Symposium on "Mechanics of Composites", October 14, 2002, Prague, Czech Republic, CTU in Prague, Klokner Institute, 2002, pp.91-98, ISBN 80-01-02621-3.

[9] Králik,J.-Cesnak,J.-Ivánková,O.-Jendželovský,N.-Prekop,Ľ.-Javorek,T: Dynamic Structural Soil Interaction Solution with Nonlinear Parameters. Upgraded of Safety and Reliability of Nuclear Power Plant Buildings under Extremal Loads. Seismic Resistant Analysis of Nuclear Power Plant Buildings.. VEGA 1/9355/02, 2002.

[10] Králik,J.-Cesnak,J.: Nonlinear Analysis of Power Plant Buildings with the VVER 230 Reactor after a Loss off Coolant Accident. In: Slovac Journal of Civil Engineering. Slovak University of Technology Bratislava, Vol. 2001/3, pp.18-32.

[11] Králik,J.: Probability Analysis of Reinforced Concrete Containmet Integrity due to High Internal Overpressure, In proc.: 21 CAD FEM User's Meeting 2003, Berlin-Potsdam, November 12-14, 2003, pp.1.4.5/1-11, ISBN-3-937523-00-6.

[12] Králik,J.: Probability Nonlinear Analysis of Reinforced Concrete Containment Damage due to High Internal Overpressure. Journal of Engineering mechanics, Brno January 2005. (in print).

[13] Kupfer,H.-Hilsdorf,H.K.-Ruesch,H.: Behavior of Concrete Under Biaxial Stresses, Journal ACI, Proc.V.66, No.8, Aug.1969, pp.656-666.

[14] Lenkei,P.-Györgyi,J.: Probabilistic Structural Analysis of Nuclear Containment under LB LOCA. Rep.JE Paks. N-Quad Ltd, Pécs, Hungary, 1999.

[15] Marek,P.-Brozzetti,J.-Guštar,M.: Probabilistic Assessment of Structures using Monte Carlo Simulation, Background, Exercises and Software, ITAM Academy of Sciences of the Czech Republic, GLOS s.r.o., Semily Czech Republic, Praha 2001.

[16] Meschke,G.-Mang,H.-Huemer,Th.: Inelastic material modelling of concrete and computer-aided retrofitting of a damaged RC shell. In proc.: Aspects in Modern Computational Structural Analysis, Meskouris&Wittek, ISBN 90 5410 927 0, Balkema, Rotterdam,1997, pp.231-245.

[17] Nilson,A.H.-Bažant,Z.-Chang,T.Y., et al: Finite Element Analysis of Reinforced Concrete, ASCE, New York, 1982.

[18] Rohár,M.: PSA level 2 for V-1 Bohunice NPP. 500mm LOCAs on cold leg with ECCS failure. VÚJE Trnava, Rep.no.2749/00/02/2002.

[19] Řeřicha P.-Šejnoha J.: Prediction of the lifetime of NPP containment considering various accident. In: Spolehlivost konstrukcí, Ostrava: Dům techniky, 2004, s. 7-10. ISBN 80-248-0573-1.

[20] Wittek,U.-Meiswinkel,R.: Non-linear structural analysis of RC structures eith reference to EC2 and DIN 1045 E2/97. In proc.: Aspects in Modern Computational Structural Analysis, Meskouris&Wittek, ISBN 9054109270, Balkema, Rotterdam, 1997, pp.199-213.

ANALYSIS OF 1:4 SCALE PRESTRESSED CONCRETE CONTAINMENT VESSEL (PCCV) MODEL SUBJECT TO PRESSURE AND THERMAL LOADING

Nam Ho Lee and Il Hwan Moon
Korea Power Engineering Company, Korea

Abstract

This paper describes the nonlinear analyses of a 1:4 scale model of a prestressed concrete containment vessel (PCCV) which incorporates both pressure and temperature effects. The analyses are performed using the results of the heat transfer analyses provided as time and/or pressure dependent thermal gradients at representative cross-sections in the model. This paper is focused on the behavior of the NUPEC/NRC 1:4-scale prestressed concrete containment vessel under pressure and temperature loading beyond the design basis.

In the nonlinear finite element analyses, the 1/4-scale PCCV including the axi-symmetric cylindrical vessel, the spherical dome and the concrete base slab are idealized as an axi-symmetric global model with axi-symmetric solid elements and shell elements. The temperature-dependent degradation properties of concrete and steel are considered. Both geometric and material nonlinearities including thermal effects are also addressed in the analyses. Menetrey-Willam concrete constitutive model with non-associated flow potential is adopted for this study. This study includes the results of the predicted thermal and mechanical behaviors of the PCCV subject to high temperature loading and internal pressure simultaneously.

In order to find the effect of accident high temperature on the ultimate capacity of each component, two kinds of analyses are performed; one for pressure only and the other for pressure with temperature. The results are compared with each other for the liner plate, reinforcement, prestressing tendon and concrete. The analysis results show that the temperature directly affects the behavior of the liner plate, but has a little impact on the ultimate pressure capacity of the PCCV.

Introduction

The purpose of the work contained herein is to describe the nonlinear analyses of a 1:4 scale model of prestressed concrete containment vessel (PCCV) that incorporates both internal pressure and thermal effects. The analyses are performed using the results of the heat transfer analyses provided as time and/or pressure-dependent thermal gradients at representative cross-section in the model.

This paper is focused on the behavior of the NUPEC/NRC 1:4-scale prestressed concrete containment vessel under pressure and temperature loading beyond design basis. In the nonlinear finite element analyses, the 1:4-scale PCCV including the axi-symmetric cylindrical vessel, the spherical dome and the concrete base slab are idealized as an axi-symmetric global model with axi-symmetric solid elements for concrete structure and shell elements for liner plate.

The temperature-dependent degradation properties of concrete and steel are incorporated in this analysis. Both geometric and material nonlinearities including thermal effects are also addressed in this analysis. Menetrey-Willam concrete constitutive model with non-associated flow potential is adopted for the analyses. This study includes the results of the thermal and mechanical behavior of the PCCV under high temperature loading and pressure simultaneously. Concrete material properties are modified in accordance with Dameron et al. Research [1], and rebar and tendon materials are adjusted in accordance with the formulas proposed by Dameron et al. [1] and Holmes [2], respectively. Variation in Liner Plate material property due to temperature was incorporated in accordance with Dameron et al. Research [1] and the ASME Section III, Division 1 – Appendix I.

In order to find the effect of accident high temperature on the ultimate capacity of each component, two kinds of analyses were performed; a combined thermal-mechanical analysis of the 1:4-scale PCCV model for saturated steam conditions (Case 1) and for a severe accident scenario (Case 2). The numerical results for each case were documented for a reduced set of Standard Output Locations and compared with the numerical results for mechanical (pressure) for liner plate, reinforcement, prestressing tendon and concrete. The computer program ABAQUS [3] was used to analyze the axi-symmetric finite element model of PCCV with nonlinear and temperature-dependent material properties of concrete, liner plate, reinforcing steel, and prestressing tendon.

Material Property and Modeling

To simulate the PCCV, the actual (tested) properties of concrete, reinforcing steel, post-tensioning tendon, liner plate and soil are used in the analysis. The properties for these materials given in Tables 1 through 3 are from test data provided by Sandia National Laboratories and used in the construction of the 1:4-scale PCCV [4] at Sandia. The strength reductions from increase of temperature are appropriately introduced to account for material degradation since high accident temperatures are introduced with accident pressure to the PCCV model.

The concrete is characterized by a materially nonlinear deformation behavior. The material non-linearity is assumed to occur due to cracking of concrete in tension and plasticity of concrete in compression. However, the material non-linearity due to the latter has relatively less influence than that due to the former on the failure mode of the containment structure under internal pressure. The Menetrey-Willam's failure model with a non-associated plastic flow that is known to be suitable to represent the tensile concrete cracking of the axi-symmtric finite element model is introduced in the numerical analysis [3].

Table 1 Concrete Material Property

Property	Basemat	Shell & Dome	Property	Basemat	Shell & Dome
Elastic Modulus(MPa)	27,950	26,970	Uniaxial Tensile Strength (MPa)	3.37	3.45
Uniaxial Compressive Strength (MPa)	39.16	47.30	Poisson's Ratio	0.18	0.18

Rebar materials are generally incompressible when they deform plastically and their yielding is independent of the pressure stress. The von Mises failure criterion is used for this steel material. Hsu noted that the stress-strain curves for bare steel bar and for steel bar embedded in concrete are quite different as shown in Figure 1(a) [5]. Therefore, the stress-strain relationship of rebar embedded in concrete has been used in reinforced concrete structure to simulate the realistic behavior of the rebar in concrete.

The stress-strain curve of the rebar for the numerical analysis is idealized by bilinear curve with a slope of E_s before yielding and a slope of E_p after yielding as illustrated in Figure 1(a). The equations of two lines are expressed at the stress level designated by f_y' at which the two straight lines intersect as shown in equation (1). The plastic modulus E_p' after yielding can be taken as a small fraction of the elastic modulus E_s.

$$f_s = E_s \varepsilon_s \quad \text{for } f_s \le f_y' \quad \text{and} \quad f_s = f_o' + E_p' \varepsilon_s \text{ for } f_s \succ f_y' \tag{1}$$

where f_o' is the vertical intercept of the post-yield straight line. The intersection stress level f_y' and the plastic modulus E_p' depend mainly on the level of the apparent yield stress f_y* illustrated in Figure 1(a). The values of f_y' and E_p' in the stress-strain relatinship used in the numerical analysis are calculated as equation (2) using the apparent yield stress f_y* and the strain-hardening modulus of the bare bar E_p from the actual material properties.

$$\frac{f_y'}{f_y} = 0.43 + 0.5\frac{f_y^*}{f_y} \quad \text{and} \quad \frac{E_p'}{E_p} = 3.3 - 2.5\frac{f_y^*}{f_y} \tag{2}$$

Table 2 Reinforcing Material Properties

	D6 (SD345)	D10 (SD390)	D13 (SD390)	D16 (SD390)	D19 (SD390)	D22 (SD390)	D19 (SD490)
Elastic Modulus (MPa)	1.69E5	1.83E5	1.83E5	1.83E5	1.84E5	1.91E5	1.86E5
Poisson's ratio	0.3	0.3	0.3	0.3	0.3	0.3	0.3
Yield Stress (MPa)	369.4	472.9	432.3	457.5	473.1	459.0	512.2
Tensile Stress (MPa)	489.4	665.9	610.6	616.5	658.3	680.8	709.7
Extension (%)	30.4	20.5	24.2	22.1	21.1	18.7	17.8

The stress-strain curve of a bare prestressing tendon comprised of two straight lines joined by a knee curve as shown in Figure 1(b) is used in the numerical analysis. The first part of the curve is a straight-line up to $0.7f_{pu}$ and the second part is expressed by Ramberg-Osgood equation(3) that meets the first part at the stress level of $0.7f_{pu}$.

$$f_p = E_{ps}'\varepsilon_p \Big/ \left[1 + \left(E_{ps}'\varepsilon_p / f_{pu}\right)^4\right]^{1/4} \tag{3}$$

where f_{pu}, f_p, E_p' and ε_p are the ultimate strength of the tendon, the strength in the tendon, the tangential modulus Ramberg-Osgood curve at zero load and the sum of strain in the tendon, respectively [5].

ABAQUS, the finite element program, has no function to incorporate the unbonded tendon. The prestressing tendons are modeled as rebar subelements in concrete using the embedded approach available in ABAQUS. The numerical modeling of tendons as rebar sub-elements implies that the tendons are assumed bonded to the concrete and slippage of the tendon in the tendon sheath is not considered in the numerical analysis.

The stress-strain behavior of the liner plate steel is modeled by using elasto-plastic model available in ABAQUS. The von Mises failure surface with kinematic hardening is used to represent the nonlinear behavior of the material.

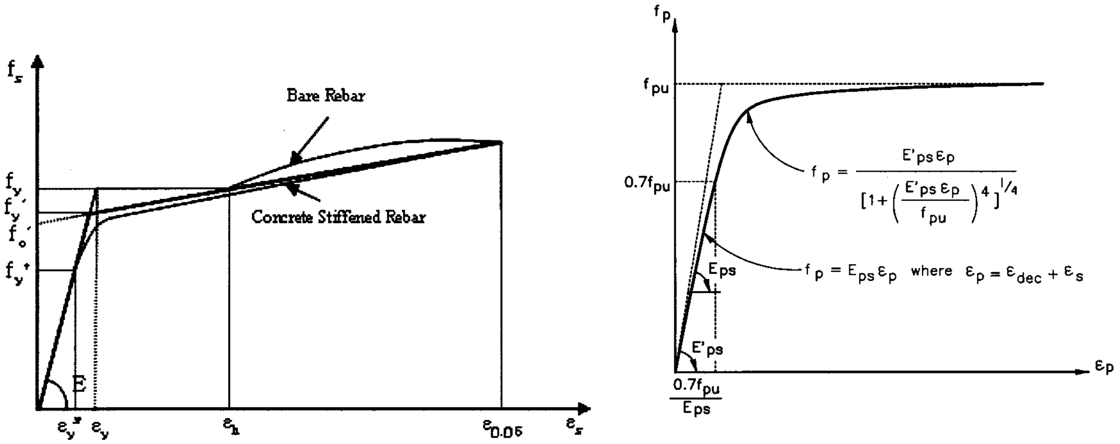

(a) Reinforcing Steel **(b) Prestessing Tendon**

Figure 1 Stress-Strain Relationships

Table 3 Material Properties (Tendon and Liner)

Property	Tendon	Liner	Property	Tendon	Liner
Elastic Modulus	191000 MPa	218,700 MPa	Poisson's Ratio	0.3	0.3
Elastic Limit Stress	1339 MPa	1339 MPa	Ultimate Strength	1912 MPa	499.158 MPa
Yield Strength	1691 MPa	375.595 MPa	Extension	4.5%	NA

A smooth curve for strength degradation versus temperature as estimated below (provided as a reference with temperature variation) is introduced into the finite element analysis model. Further, based on the literature, elastic modulus reduction is calculated by equation (1).

The thermal expansion coefficients of concrete is assumed to be constant at 1.18E-5 cm/cm/°C upto 260°C of temperature rise as shown in equation (4) and then gradually increases to 2.18E-5 cm/cm/°C at 430 °C and that of steels is assumed to be constant at 1.18E-5 cm/cm/°C upto 614°C of temperature rise as in equation (5) [6]. The thermal expansion coefficient of liner steel exposed to high temperature is calculated by ASME Section III, Division 1, Appendix-I [ASME, 1986].

$$S_{Rc} = \exp-(T/632)^{1.8} \text{ and } M_{Rc} = (S_{Rc})^{1/2} \quad \text{where T is in degree C} \qquad (4)$$

$$S_{Rs} = \exp-[(T-340)/300]^{1.9} \text{ and } S_{Rs} = 1.0 \;\; for \;\; T \le 340^\circ C \text{ where T is in degree C} \qquad (5)$$

Finite Element Model

General

The axi-symmetric finite element model which is utilized to predict the overall response of the 1:4 scale PCCV under internal pressurization and/or thermal loading is shown in Figure 2. This model consists of the axi-symmetric cylindrical vessel, a spherical dome and the concrete base slab. This model is intended to provide the overall behavior of the PCCV model taking into account of uplift. This model consists of axi-symmetric solid elements for concrete portions, nonlinear soil spring elements between basemat and foundation, and three-node shell elements connected to the axi-symmetric solid elements for concrete portions using rigid link elements as shown in Figure 2.

Model for Shell and Dome

The concrete portions of dome and cylindrical wall are modeled with the eight-node axi-symmtric solid elements. The liner steel on the inside surface of the PCCV is made up of three-node shell elements. The liner elements, which are offset from the prestressed concrete elements, are connected to the concrete solid elements by rigid link elements. All rebars and tendons are assumed to remain rigidly bonded to the concrete and thus modeled by using the rebar sub-element provided by ABAQUS computer program. Vertical liner anchors are modeled as a beam of rectangular cross-section dimension. The cross-sections of liner anchors are computed based on the area and the bending stiffness of the embedment. Prestressing is induced in the tendons with a function through the *INITIAL CONDITIONS option in ABAQUS.

Model for Base Slab

The base slab is included in the finite element model to simulate the possible vertical uplift of the base during internal pressurization and to estimate the effect of the base slab on the failure mode. The previously described shell and dome model is connected to the base slab model consisting of eight-node solid elements with considering tendon gallery.

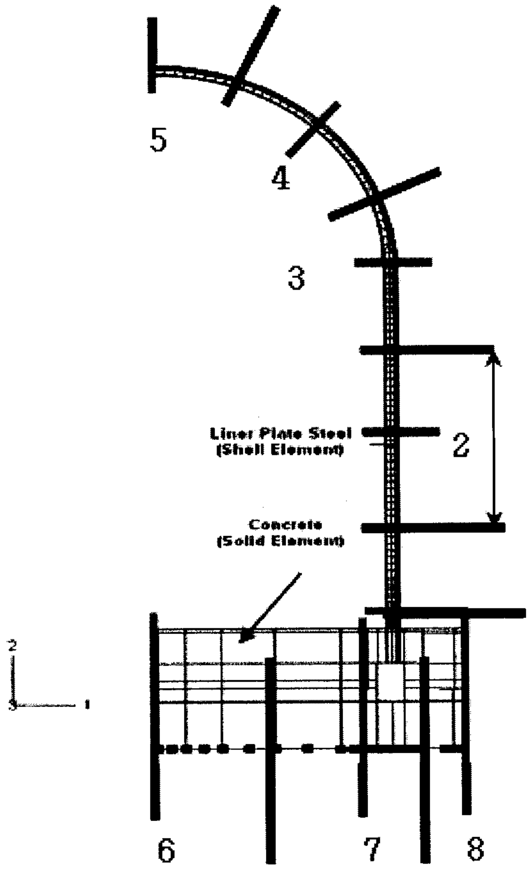

Figure 3 Axi-symmetric Finite Element Model of PCCV

The liner plate simulated by three-node shell elements is assumed rigidly connected to the eight-node concrete solid elements unlike those for cylindrical shell since the interaction effect of liner steel and concrete during the flexural deformation of the slab is not significant in the thick base slab of PCCV.

Reinforcements in the base slab are estimated from the provided structural drawings and are included in the analysis model. All rebars in the base slab are modeled as those of shell portion by using the rebar subelement of ABAQUS.

The bottom of the slab rests on a soil foundation modeled by nonlinear soil springs with tension cut-off. Since the soil properties were not provided by Sandia National Laboratories, an appropriate elastic modulus was used only to simulate the uplift by using the nonlinear spring with tension cut-off.

Prestressing Forces in Tendon

The meridional stress and hoop stress along the length of the tendon in the concrete are estimated with the prestressing losses at the time of testing. The prestressing force was introduced prior to applying the internal pressure and/or thermal loadings to the numerical model. The four types of losses given specific modeling consideration are (1) the friction between the tendon and the concrete, (2) the elastic shortening of the concrete, (3) the creep and shrinkage of the concrete, and (4) the stress relaxation in the prestressed tendons.

The vertical prestressing forces of 106.27kips before anchoring and 96.04kips after anchoring are introduced from the PCCV Model-General Arrangement. Based on the prestressing forces at anchorage, the magnitudes of the vertical tendon stress are calculated along the length of the vertical tendon and considered in the finite element analysis model using the losses shown in Table 4. Similarly, the hoop tendon forces of 95.27kips before anchoring and 73.52kips after anchoring are used in the calculation of hoop tendon stress.

Table 4 Prestressing Losses

	Vertical Tendon Loss MPa (ksi)	Hoop Tendon Loss MPa (ksi)
Elastic shortening of concrete	31.855 (4.620)	31.855 (4.620)
Creep of concrete	66.999 (9.717)	83.829 (12.158)
Shrinkage of concrete	129.309 (18.754)	129.309 (18.754)
Steel relaxation	19.747 (2.864)	14.473 (2.099)
Total losses	247.910 (35.955)	259.473 (37.632)

Self-weight, Internal Pressure and Thermal Loading

Because of the elastic support below the bottom slab, the effect of the weight of the structure had to be initially considered prior to internal pressurization and/or thermal loading. This is accomplished by specifying a mass proportional load for each material included in the 1:4 scale PCCV model prior to initiating the internal pressure and/or thermal loading. The weights of each material are considered in the numerical model by using the GRAVITY parameter of *DEAD LOAD option of ABAQUS. The loading histories of internal pressure and thermal loading are shown in Figures 3 and 4. The heat distribution result through thickness of wall and base slab provided by the Sandia National Laboratories are considered for thermal loading analyses.

Thermal gradients at eight sections including dome apex, 45° dome angle, spring line, mid-height, wall-mat junction, center of base slab, near wall-mat junction of base slab and edge of base slab are provided by Sandia National Lab. Thermal gradient specified at each thermal gradient section is identically applied to both halves of each thermal gradient section (mid-points of neighboring sections centering the section) as the thermal gradients of each neighboring thermal gradient section are not much different from those for each section. The temperature time history and pressure time history (shown in Figures 3 and 4) are applied at nodes of finite element model.

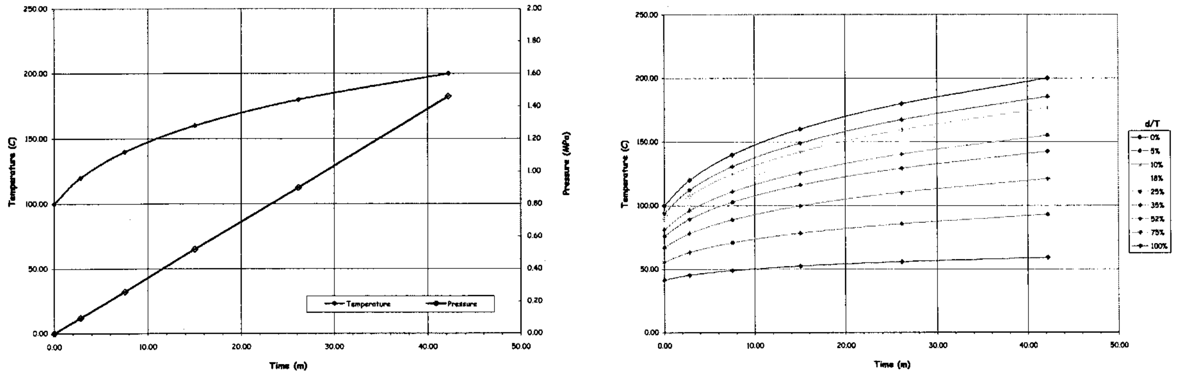

(a) Temperature and Pressure (b) Typical Temperature Distribution at Section 1
Figure 3 Loading History for Steamed Saturated Condition (Case 1)

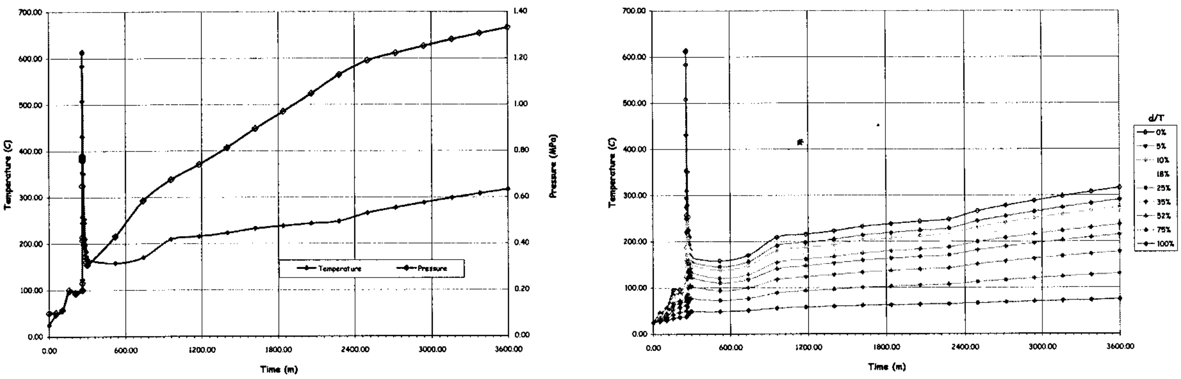

(a) Temperature and Pressure (b) Typical Temperature Distribution at Section 1
Figure 4 Loading History for Severe Accident Scenario (Case 2)

Analysis Results and Discussion

Results at Standard Output Locations

The ISP-48 phase 2 analysis results at standard outputs locations (limited to azimuth 135 degrees) from three-dimensional analysis were officially submitted to the OECD/NEA and compared with the SFMT (Structural Failure Mechanism Test) results. However, axi-symmetric analysis results were also performed at the ISP-48 phase 2 and the analysis results from the finite element analysis for temperature and pressure loading histories provided by Sandia National Laboratories (see Appendix-A) and are basically submitted for ISP-48 phase 3.

The rebars are assumed yielded when the stresses in the rebars exceed the nominal yield stresses defined for each rebar type. The computer program ABAQUS tracks the yielding of each rebar included in the finite element model automatically and allows the corresponding pressure level to be computed. The behavior of concrete up to the tensile strength is characterized by the theory of linear elasticity and a crack is initiated at tensile strength. In ABAQUS, cracking is assumed to occur when stress reaches a failure surface, which is called the "crack detection surface", and the program indicates the cracking automatically.

Based on the above, the pressure levels corresponding to the event milestones requested by Sandia National Laboratories are shown in Table 5. Also, the behavior under high temperature and pressure loading histories are compared with SFMT test results and the pressure-dependent behavior as shown in Figures 7 through 15. The liners are yielded and/or ruptured at higher pressure when both temperature and pressure were simultaneously applied than when subjected to pressure only.

Table 5 Comparisons of Pressure Levels (MPa) Corresponding to Events Milestone

	Pressure Only	Case 1	Case 2
First cracking of concrete due to hoop stress (mid-height)	0.64	0.64	0.64
First cracking of concrete due to meridional stresses (mid-height)	0.60	0.60	0.60
First yield of hoop rebar (mid-height)	1.16	0.88	0.78
First yield of meridional rebar (above dome 45°)	1.42	1.03	1.03
Liner yield due to hoop stresses (mid-height)	0.75	1.03	0.49
Liner rupture due to hoop stresses (mid-height)	0.97	1.20	1.19
Liner yield due to meridional stresses (wall base, El. 0.25m)	1.42	1.46	0.49
Liner rupture due to meridional stresses (wall base, El. 0.25m)	-	-	0.46
Liner yield due to hoop stresses (splingline, El. 10.75m)	1.03	1.20	0.48
Liner plate rupture due to hoop stresses (springline, El.10.75m)	1.46	1.47	0.46
Liner yield due to meridional stresses (dome, El.16.13m)	1.10	1.35	0.48
Liner plate rupture due to meridional stresses (dome, El.16.13m)	-	1.47	-
Hoop tendons reaching 1% strain (mid-height)	1.43	1.41	-
Hoop tendons reaching 2% strain (mid-height)	1.48	1.46	-
Hoop tendons reaching 3% strain (mid-height)	1.51	1.47	-

Displacements

The displacement transducers were 'zeroed' prior to the start of the SFMT before filling the vessel with water and the measured displacements reflect only the response to pressure (including the hydrostatic pressure). That is, the measured displacements in the SFMT did not include the effects of prestressing, nor any other previous loading [4]. Therefore, the displacements due to prestressing and dead load were subtracted from those of numerical analyses for comparison with the corresponding measured displacements.

Figures 7 through 10 show direct comparisons of analysis results and measured radial displacements versus pressure at various locations under pressure only and/or with thermal loading. To confirm whether the numerical model established at Phase 2 is appropriate for Phase 3, the results under pressure history alone are directly compared with those from SFMT. The additional hydraulic effects on the radial displacements are negligible relative to those from the ultimate internal pressure and therefore the hydraulic effects are not considered in the numerical analysis in Phase 3.

As shown in Figures 7 through 10, the radial displacements under pressure only correspond well with the numerical results and the measured displacements from SFMT, except for the displacement at Standard Location #7 (Az 135°, El. 10.75m Spring Line). A combined mechanical-thermal analysis simulating a saturated steam condition (Case 1) shows that the temperature history starting with 100°C created a sudden increase in displacements at initial stage, but the slopes expressing the pressure-displacement relationship with increasing temperature and pressure appeared very similar to the trend for the pressure only case.

In Case 2 for a severe accident scenario, the pressures were changed suddenly from 0.2 MPa to 0.78 MPa and back to 0.31 MPa for short periods between 260 through 300 minutes, and then increased to 1.33Mpa. The temperatures were also changed from 100°C to 615°C and then to 165°C at the same short intervals as those for the pressure history and then increased gradually to 316°C at 3600 minute (see Figure 4).

The analysis results for Case 2 show that the displacements due to the sudden increase in temperature and pressure for a very short time period were not fully recovered when returned to the starting temperature and pressure. This can be interpreted as sort of residual deformation from damage to the liner plate and/or concrete portion due to instantaneous high temperature and pressure loading. Unfortunately, the analysis for Case 2 was stopped at 1.1974 MPa due to divergence and the behaviors could not be investigated beyond 1.1974 MPa. The ultimate capacity may drop rapidly with a sudden increase in deformation which in turn will induce divergence (see Figure 7 through Figure 10).

To evaluate the effects of the liner expansion caused by high temperature during very short periods on the structural behavior, a case (Case 3) of analysis was additionally performed with high temperature (Case 2 temperature history) applied only to the liner under pressure loading assuming no transfer of temperature to the concrete portion. The analysis results show that the displacements due to liner expansion do not increase significantly in comparison with those due to the pressure loading only, except for the vertical displacements in the dome portion.

Strains in Reinforcements

The strain gages were not reset after the LST (Limit State Tests). The residual strain was the base strain for the SFMT. To confirm the numerical model for rebars, the recorded residual strain at the beginning of SFMT was subtracted from the measured strains and compared with those from numerical analysis under pressure only (see Figures 11 through 13).

Figures 11 through 13 show that the strains in the reinforcements under pressure only compare well with the numerical results and the measured displacements from SFMT except for the strain at Standard Location #24 (Az 135°, El. 10.75m Hoop Outer Rebar Layer at Spring Line).

A combined mechanical-thermal analysis simulating a saturated steam condition (Case 1) shows that the thermal loading history starting with 100°C created abrupt increase in strains at initial stage similar to the displacements, but the slopes expressing the pressure-displacement relationships with increasing temperature and pressure appeared closer to the trend for pressure only.

The strains in the outer hoop rebar (D18) at mid-height of the cylinder (135°, EL. 6.20m) are typically 0.5%, 0.45%, 1.5% at 1.4 MPa for Case 1, Case 2 and pressure only, respectively. Considering a yield strain 0.25% calculated from a yield stress 457.5 MPa and elastic modulus 1.83E+05 provided by Sandia Lab in Table 2 [4], the pressures corresponding to 0.25% of yield strain for bare bar are 0.81MPa, 0.77MPa and 1.42 MPa, respectively.

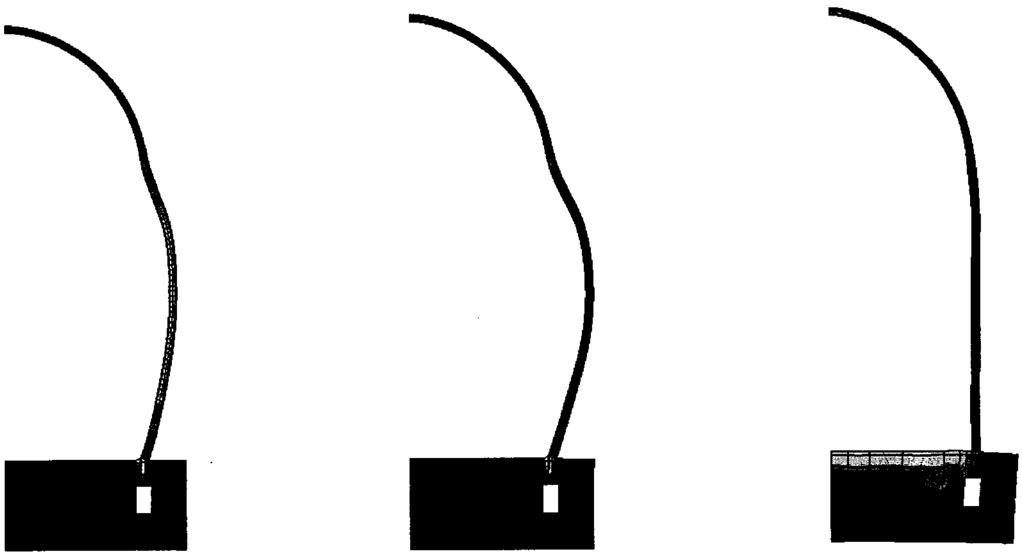

(a) Pressure Only (at P= 1.46 MPa) (b) Case 1(at P=1.46 MPa) (c) Case 2(at P=1.197 MPa)

Figure 5 Deformed Configuration of Axi-symmetric Finite Element Model

The analysis results for Case 2 shows that the rebar strains due to the sudden increase of temperature and pressure for short durations, do not fully recover back to the strains at initial pressure and temperature. This can be interpreted as sort of residual deformations from damage to liner plate and/or concrete portion due to instantaneous high temperature and pressure loading. Unfortunately, the analysis for Case 2 was stopped at 1.1974Mpa due to divergence and the behaviors could not be investigated.

Figure 11 and Figure 12 show that the strains in the merdional outer rebar near wall-mat junction were not high and the residual strains are almost negligible. The residual strains remained in the inner layer of rebar around wall-mat junction during abrupt change of temperature.

Liner Strains and Stress

The recorded results of the liner from the SFMT were not meaningful to compare with the analysis results at Phase 2 since the liner was already torn partially during LST and the recorded data for the liner plate including strains could not be compared with those from the numerical analysis under pressure only. The strains in the liner from the numerical analyses for pressure only, saturated steam condition (Case 1) and severe accident scenario (Case 2) were compared with each other.

Maximum compressive stresses in the liner versus the corresponding pressure loadings are illustrated in Table 6 at some typical locations. Case 2 shows that the stresses in liner were under compressive behavior at pressures between 0.2 MPa and 0.78 MPa and temperature between 100°C and 615°C for short periods of around 260 through 300 minutes.

The buckling stress considering the horizontal spacing of liner anchor (150.15mm) is calculated to 122.2Mpa and thus most of stresses of Case 1 and Case 2 shown in Table 6 are beyond the calculated buckling stress.

Table 6 Max. Compressive Stress in Liner Surface with Pressure and Temperature

Location	Case 1			Case 2			Remark
	Pressure (MPa)	Temperature (°C)	Stress (MPa)	Pressure (MPa)	Temperature (°C)	Stress (MPa)	
#36(El. 0.25m)	0.138	106.6	-86	0.42	353	-314	Merid.
#37 (El. 0.25m)	0.14	106.6	-214	0.42	353	-417	Hoop
#38 (El. 6.20m)	0.14	106.6	-181	0.42	353	-365	Merid.
#39 (El. 6.20m)	0.14	106.6	-164	0.42	353	-375	Hoop
#40 (El. 10.75m)	0	100.0	-58	0.42	353	-252	Merid.
#41 (El. 10.75m)	0.14	106.6	-132	0.46	365	-424	Hoop
#42 (El. 16.13m)	0.10	104.5	-146	0.46	365	-368	Merid.

Tendon Stress and Concrete Cracking

Tendon strains gages were 're-zeroed' before the SFMT [4] and thus the analysis tendon strains prior to the start of pressurization were deducted from the tendon strains during pressure to directly compare with the measured tendon strain. Tendon strains under both temperature and pressure are increased in comparison with those under pressure only. Temperature has definitely an effect on the ultimate pressure capacity of PCCV. The finite element analysis under internal pressure only results show that the first concrete cracking in the numerical model occurs at a pressure level of 0.60 MPa and is located at the surface of cylindrical wall at the wall and basemat joint. At the pressure level of 0.64 MPa, the elements at mid-height of wall cylinder are cracked in both the hoop and meridional directions.

Conclusions

The liners are yielded and/or ruptured at higher pressure when both temperature and pressure were simultaneously applied than when subjected to pressure only. However, the reinforcements are yielded at lower pressure when both temperature and pressure were simultaneously applied than when subjected to pressure only.

The first concrete cracking is occurred at similar pressure for both pressure only and pressure with temperature. The tendon strains reaching 1%, 2% and 3% are occurred at similar pressure for both cases considering pressure only and pressure with temperature.

Case 2 shows that the stresses in liner were under compressive behavior at pressures between 0.2 MPa and 0.78 MPa and temperature between 100°C and 615°C. Thus, the compressive stresses due to temperature and the restraints of concrete may cause liner buckling and geometric nonlinear need to be considered in the analysis.

References

[1] Dameron, R.A., Hansen, B.E., Parker, D.R. and Rashid, Y.R., *Posttest Analysis of NUPEC/NRC 1:4 Scale Prestresssed Concrete Containment Vessel Model*, NUREG/CR-6809 SAND2003-0839P ANA-01-0330, Sandia National Laboratories, Albuquerque, NM, March 2003.

[2] Holmes, M., Anchor, R.D., Cook, M.D. and Crook, R.N., *The Effects of Elevated Temperatures on the Strength Properties of Reinforcing and Prestressing Steels*, The Structural Engineer, Vol. 60B, No. 1, March 1982

[3] ABAQUS User's Manual, Version 6.4, 2003. ABAQUS Inc.

[4] Hessheimer, M.F., Klamerus, E.W., Lambert, L.D. and Rightley, G.S., *Overpressurization Test of a 1:4-Scale Prestressed Concrete Containment Vessel Model*, NUREG/CR-6810, SAND2003-0840P, Sandia National Laboratories, Albuquerque, March 2003.

[5] Hsu, T. T.C., *Unified Theory of Reinforced Concrete*, CRC Press 1993, 205-218 pp.

[6] Mazars J., Dube J.F., Flejou J.L. and Ghavamian Sh., *A Damage Multi-layered F.E. Model for the Seismic Response of R.C. Structures – A Tool for Understanding the Real Behaviour*, Proceeding 10th EAEE, 1994.

[7] Neville, A.M., Properties of Concrete, The Pitman Press, 1981, pp. 433-528

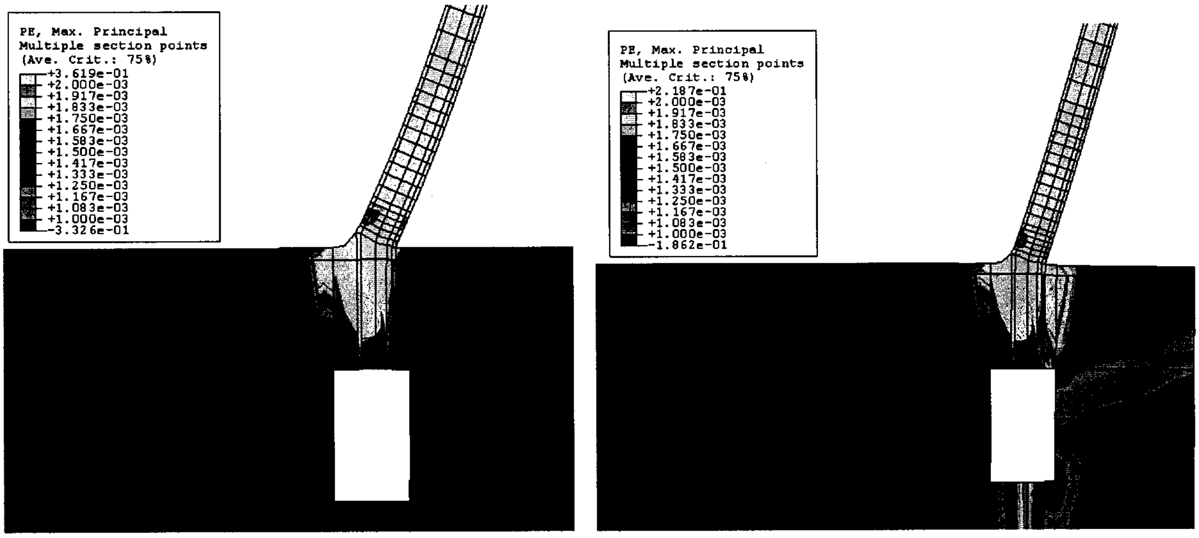
PE, Max. Principal
Multiple section points
(Ave. Crit.: 75%)
+3.619e-01
+2.000e-03
+1.917e-03
+1.833e-03
+1.750e-03
+1.667e-03
+1.583e-03
+1.500e-03
+1.417e-03
+1.333e-03
+1.250e-03
+1.167e-03
+1.083e-03
+1.000e-03
-3.326e-01
PE, Max. Principal
Multiple section points
(Ave. Crit.: 75%)
+2.187e-01
+2.000e-03
+1.917e-03
+1.833e-03
+1.750e-03
+1.667e-03
+1.583e-03
+1.500e-03
+1.417e-03
+1.333e-03
+1.250e-03
+1.167e-03
+1.083e-03
+1.000e-03
-1.862e-01

(a) Under Pressure Only (at P=1.46 MPa) (b) Case 1(at P=1.46 MPa, T=200°C)

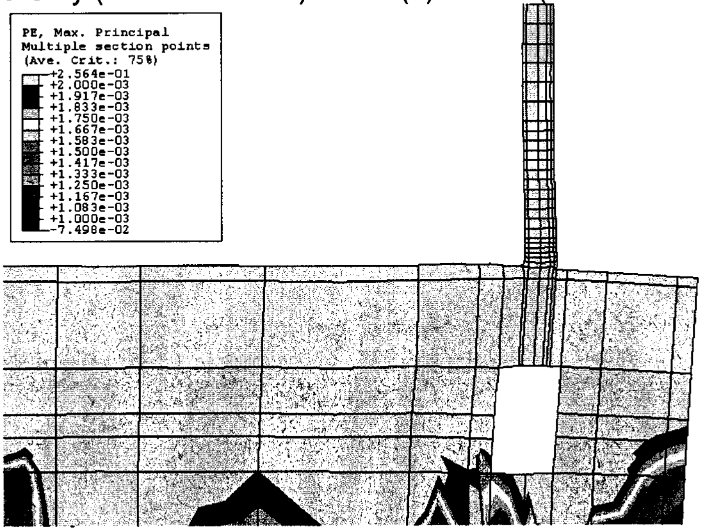
PE, Max. Principal
Multiple section points
(Ave. Crit.: 75%)
+2.564e-01
+2.000e-03
+1.917e-03
+1.833e-03
+1.750e-03
+1.667e-03
+1.583e-03
+1.500e-03
+1.417e-03
+1.333e-03
+1.250e-03
+1.167e-03
+1.083e-03
+1.000e-03
-7.498e-02

(c) Case 2(at P=1.197 MPa, T= 265°C)

Figure 6 Principal Stress (Crack Patterns) around Wall-Mat Junction (cont'd)

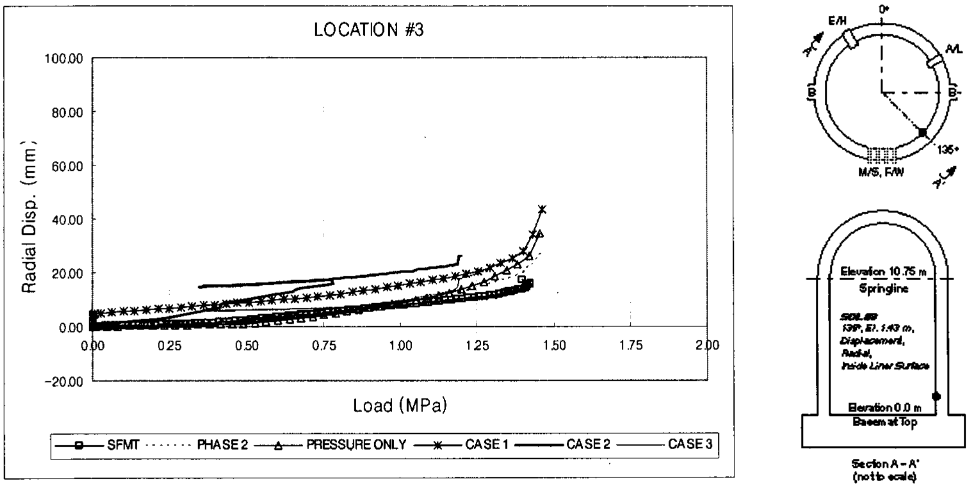

Figure 7 Load-Displacement (# 3, 135°, El. 1.43m, Radial, Inside Liner Surface)

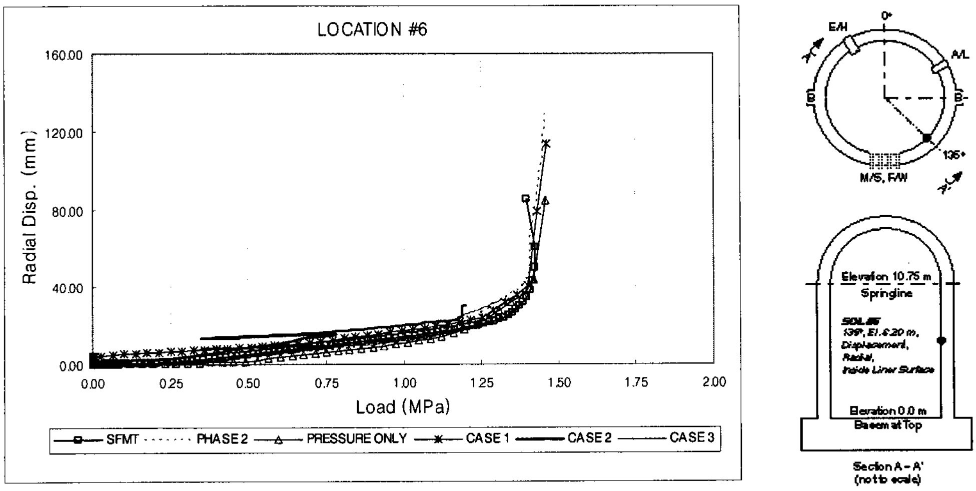

Figure 8 Load-Displacement (# 6, 135°, El. 6.20m, Radial, Inside Liner Surface)

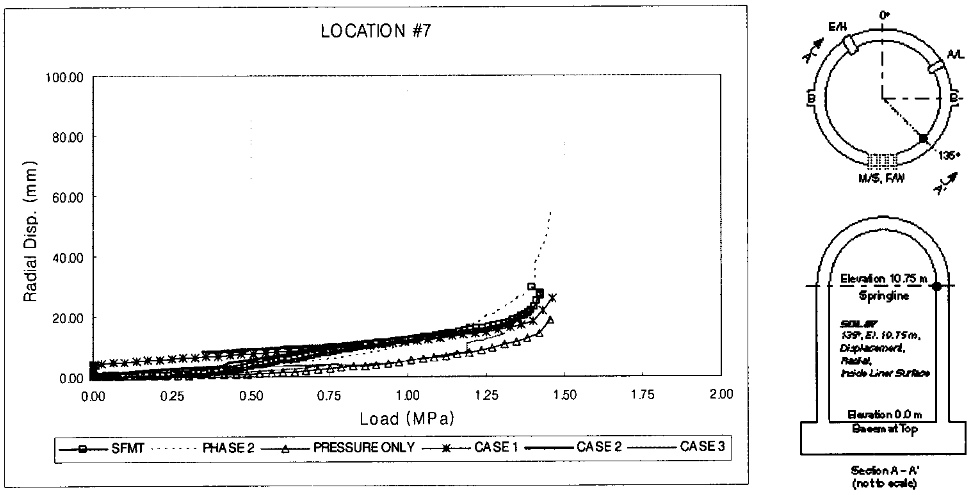

Figure 9 Load-Displacement (# 7, 135°, El. 10.75m, Radial, Inside Liner Surface)

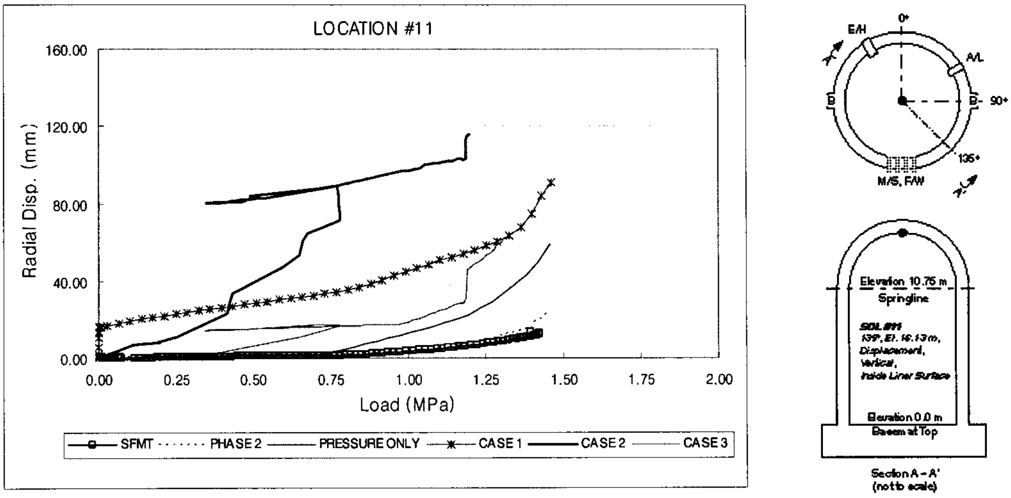

Figure 10 Load-Displacement (# 11, 135°, El.16.13m, Vertical, Inside Liner Surface)

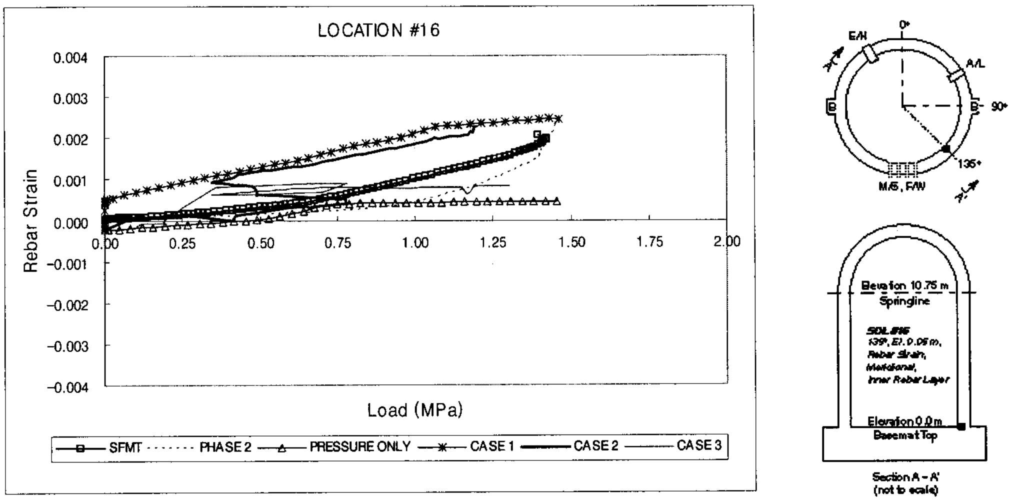

Figure 11 Load-Rebar Strain (# 16, 135°, El. 0.05m, Meridional Inner Rebar Layer)

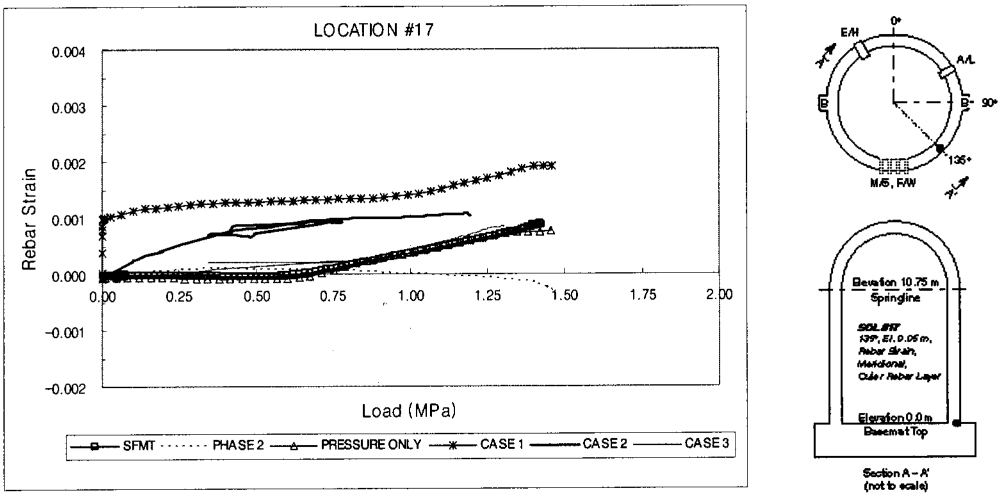

Figure 12 Load-Rebar Strain (# 17, 135°, El. 0.05m, Meridional Outer Rebar Layer)

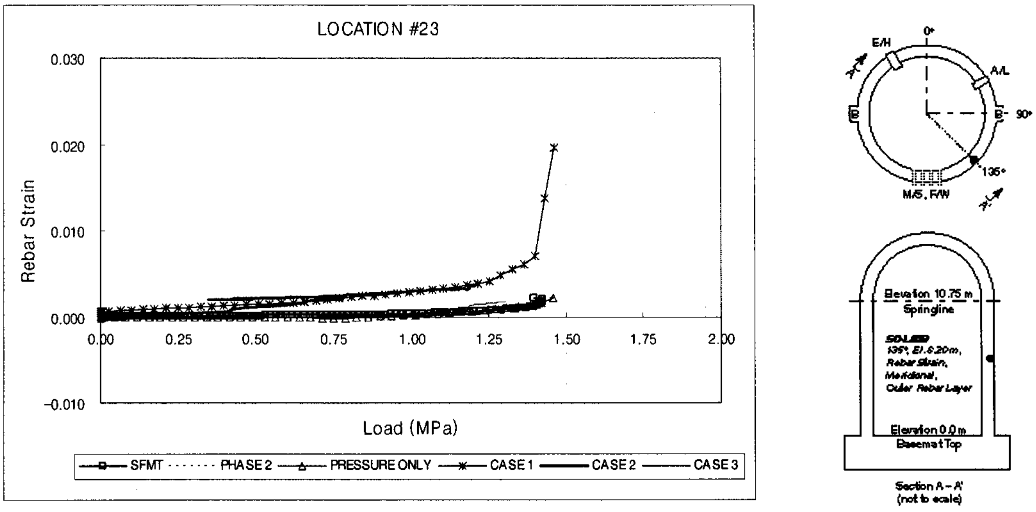

Figure 13 Load-Rebar Strain (# 23, 135°, El. 6.20m, Meridional Outer Rebar Layer)

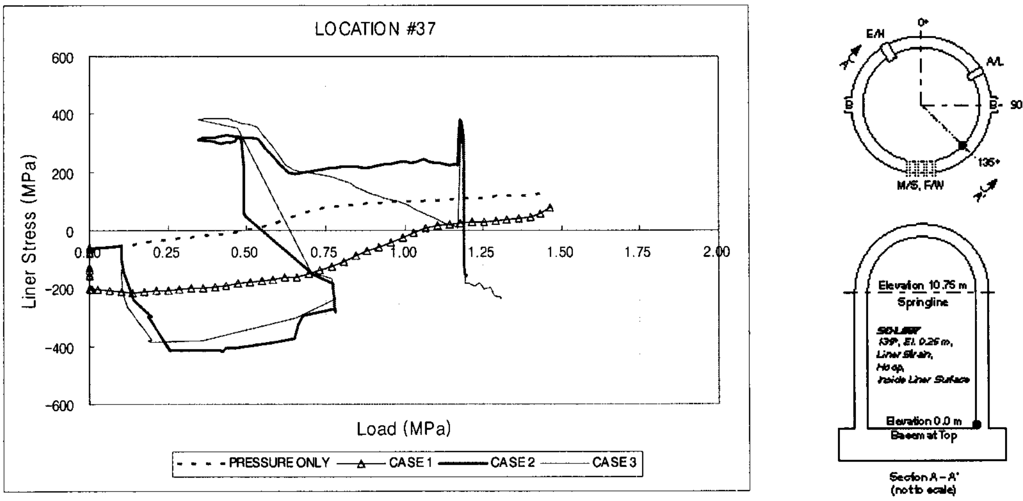

Figure 14 Load-Liner Stress (# 37, 135°, El. 0.25m, Hoop Inside Liner Surface)

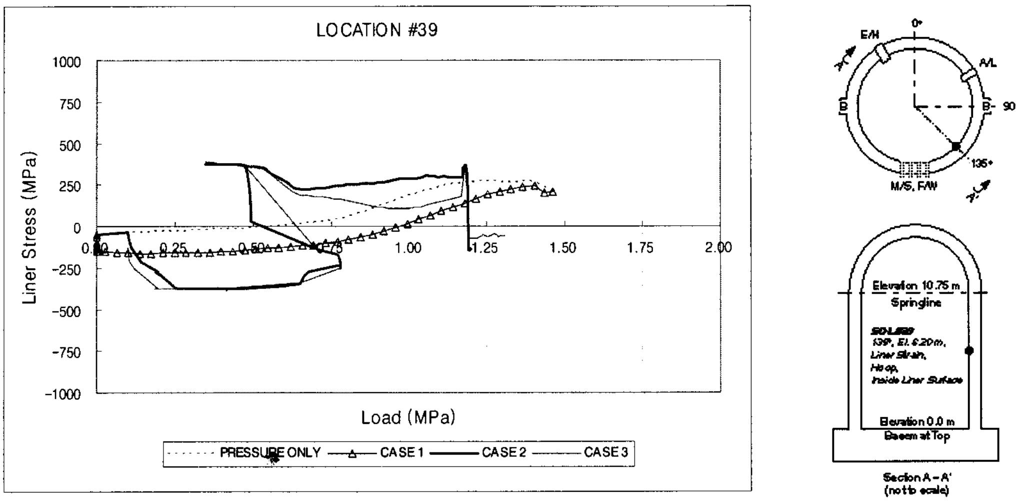

Figure 15 Load-Liner Stress (# 39, 135°, El. 6.2m, Hoop Inside Liner Surface)

CSNI Workshop - International Standard Problem 48

NONLINEAR FINITE ELEMENT ANALYSIS OF 1:4-SCALE PCCV MODEL WITH THERMAL LOADING

(April 4-7, 2005)

Nam Ho Lee & Il-Hwan Moon

KOPEC 한국전력기술주식회사
Korea Power Engineering Company, Inc

Table of Contents

- Introduction
- Material Property and Model
- Finite Element Model
- Loading Condition
- Analysis Results

Introduction

- Finite Element Model
  - Axi-symmetric Solid Element for Concrete Model
  - Model using Axi-symmetric Shell Element for Liner
  - Nonlinear Soil-spring Simulating Base Slab Uplift
  - Bonded Type Rebar and Prestressing Tendon Model
- Material Models & Material Properties
  - Menetrey-Willam Concrete Model (with Elliptic Function of 0.52)
  - Concrete Stiffened Rebar Model (Hsu's Model)
  - Material Test Results by SNL
  - Temperature-dependent Degradation Properties (Concrete and Steel)
- Loadings
  - Dead Weight & Prestressing Force (Loss Considered)
  - Internal Pressure (Surface Pressure)
  - Thermal Loadings
    - Case 1 : Loading History for Steamed Saturated Condition
    - Case 2 : Loading History for Severe Accident Scenario
    - Case 3 : Liner Extension Only due to Severe Temperature

Material Properties and Models - Concrete

- **Menetrey-Willam Concrete Failure Criteria**
  - **Model Parameters**
    - Elliptic function(K) : 0.52
      (good agreement with Kuper's Biaxial Test)
    - Friction angle : 71.32828
    - Dilation angle : 56.97448

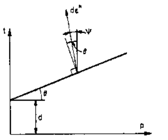

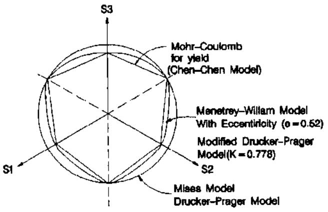
S3
Mohr-Coulomb for yield (Chen-Chen Model)
Menetrey-Willam Model With Eccentricity (e=0.52)
Modified Drucker-Prager Model(K=0.778)
S2
S1
Mises Model
Drucker-Prager Model

(Menetrey-Willam's yield surface)

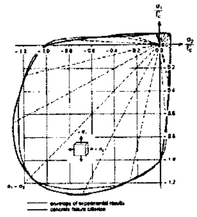

Biaxial Failure
(Comparison with Kuper's Test)

Material Properties and Models - Concrete

- **Postfailure Stress-Strain Relation (Tension Stiffening)**
  - **Stress is provided as a function of cracking strain**

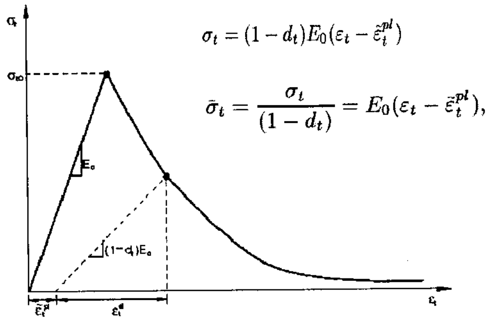

$$\sigma_t = (1 - d_t)E_0(\varepsilon_t - \tilde{\varepsilon}_t^{pl})$$

$$\bar{\sigma}_t = \frac{\sigma_t}{(1 - d_t)} = E_0(\varepsilon_t - \tilde{\varepsilon}_t^{pl}),$$

Material Properties and Models - Concrete

- **Material Properties (Test Data for Trial Mix Concrete)**
- **Comparisons of Concrete Models in ABAQUS**
- **Temperature-Dependant Degradation (Dameron et. al)**

  - **Strength Degradation**

    $$S_{Rc} = \exp{-(T/632)^{1.8}}$$

  - **Elastic Modulus Degradation**

    $$M_{Rc} = (S_{Rc})^{1/2}$$

  - **Thermal Expansion (Neville)**

    1.18E-5 cm/cm/°C up to 260°C

    2.18E-5 cm/cm/°C at 430°C

Material Properties and Models - Rebar

- **Modeling methods for Rebar**
  - **Stress-Strain Relationship - Hsu's Model**
  - **Material Properties (Test Data)**
  - **Temperature-Dependant Degradation (Dameron et. al)**

• **Strength Degradation**

$$S_{Rs} = \exp-[(T-340)/300]^{1.9}$$

$$S_{Rs} = 1.0 \quad for \quad T \leq C340^{\circ}C$$

• **Elastic Modulus Degradation**

$$M_{Rc} = (S_{Rc})^{1/2}$$

• **Thermal Expansion (Neville)**

☞ **1.18E-5 cm/cm/°C up to 614°C**

Material Properties and Models - Prestressing Tendon

- **Modeling Methods for Pre-stressing Tendon**
  - **Use rebar subelement in ABAQUS with prestressing**
  - **Ungrouted condition was not considered(assume bonded tendon)**
  - **Stress-Strain Relations - Hsu's Model**
  - **Temperature-Dependant Degradation (Dameron et. al)**

Material Properties (Test Data)

Property	Values
Elastic Modulus	191000 MPa
Elatic Limit Stress	1339 Mpa
Yield Strength	1691 Mpa
Poisson's Ratio	0.3
Ultimate Strength	1912 MPa
Extension	4.5%

Material Properties and Models – Liner Plate Steel

- **Material Properties (Test Data)**
- **Temperature-Dependant Degradation (Dameron et. al.)**

  ☞ **Use the same degradation formula as those for rebar**
- **Thermal Expansion [ASME Section III, Division 1, Appendix-I)]**

Temp. (°C)	**38**	**93**	**149**	**204**	**260**	**316**	**371**	**427**	**538**	**593**	**621**
Expansion (10^{-5}/°C)	**1.17**	**1.24**	**1.31**	**1.39**	**1.44**	**1.51**	**1.55**	**1.60**	**1.67**	**1.71**	**1.71**

FINITE ELEMENT MODEL - AXISYMMETRIC MODEL

- Concrete : 8-Node Axi-symmtric Solid Element
- Liner plate : 3-Node Axi-symmtric Shell Element
- Vertical liner anchor : Beam Element
  (Rectangular Cross-section)
- Foundation : Compressive spring (Tension cut-off)
- Tendon : Prestressing induced by the initial condition
- Consider Geometric Nonlinear

FINITE ELEMENT MODEL - AXISYMMETRIC MODEL

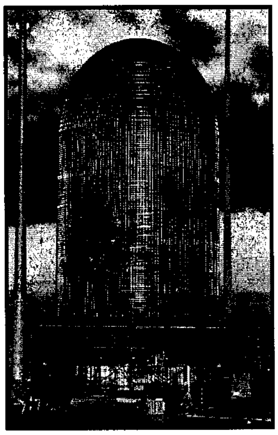

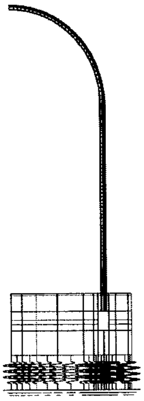

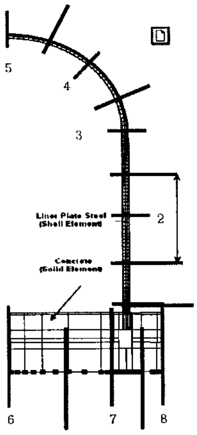

FINITE ELEMENT MODEL - LOADING CONDITIONS

- Dead Weight & Prestressing
- Loading Histories □
  - Internal pressure (element surface load)
  - Temperature distribution through wall thickness (nodal load, SNL)

ANALYSIS RESULTS - DEFORMED SHAPES

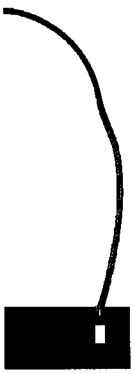

Pressure Only(1.46 MPa)

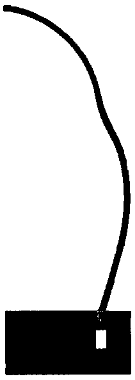

Case 1(1.46 MPa)

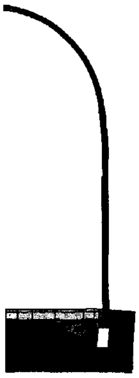

Case 2(1.197 MPa)

DEFORMED SHAPES (PRESSURE ONLY vs CASE 1)

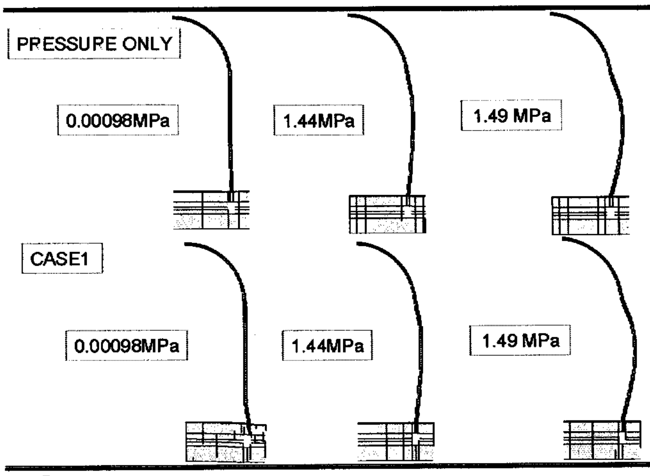
PRESSUPE ONLY
0.00098MPa
1.44MPa
1.49 MPa
CASE1
0.00098MPa
1.44MPa
1.49 MPa

DEFORMED SHAPES AT TYPICAL STEPS FOR CASE 2

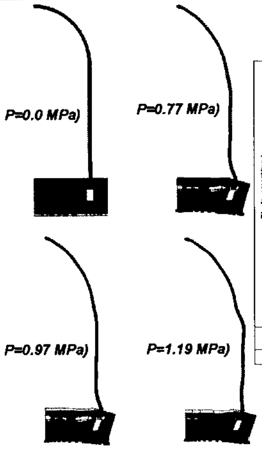
P=0.0 MPa)
P=0.77 MPa)
P=0.97 MPa)
P=1.19 MPa)

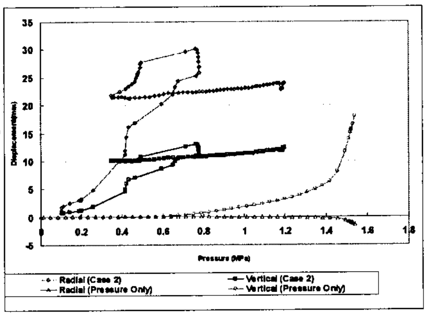

ANALYSIS RESULTS - DISPLACEMENT

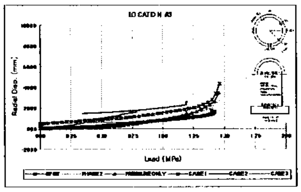

Base of Cylinder (Radial)

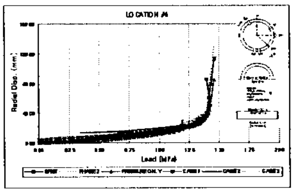

Midheight (Radial)

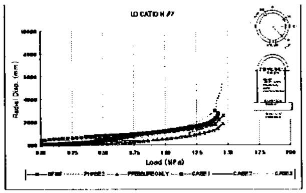

Springline (Radial)

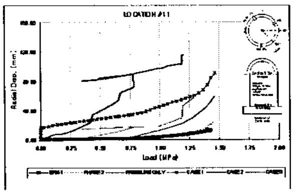

Dome Apex (Vertical)

ANALYSIS RESULTS - STRAIN OF REBAR AND TENDON

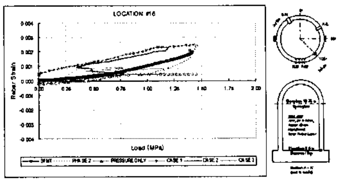

Base of Cylinder (Meridional, Inner)

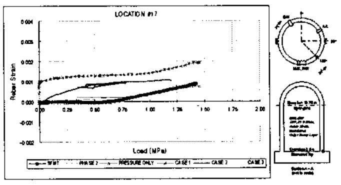

Base of Cylinder (Meridional, Outer)

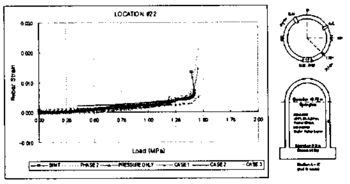

Midheight (Hoop, Outer)

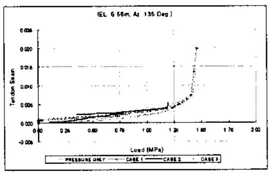

Tendon Strain (Midheight, Hoop)

ANALYSIS RESULTS - LINER STRESS AND STRAIN

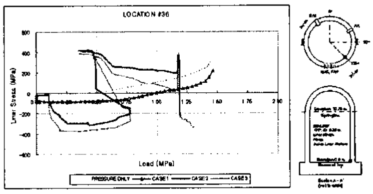

Base of Cylinder (Meridional, Stress)

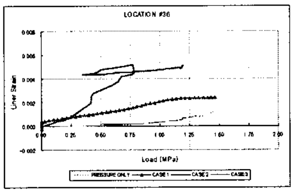

Base of Cylinder (Meridional, Strain)

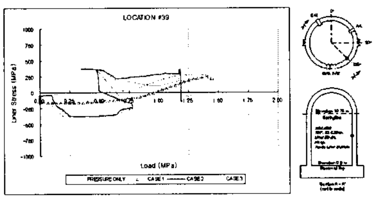

Midheight (Hoop, Stress)

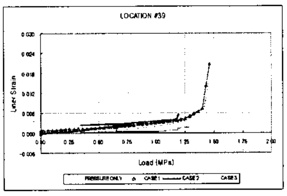

Midheight (Hoop, Strain)

ANALYSIS RESULT SUMMARY- EVENT MILESTONES

Event Milestones	Pressure Only	Case 1	Case 2
First cracking of concrete due to hoop stress (mid-height)	0.64	0.64	0.64
First cracking of concrete due to meridional stresses (mid-height)	0.60	0.60	0.60
First yield of hoop rebar (mid-height)	1.16	0.88	0.78
First yield of meridional rebar (above dome 45°)	1.42	1.03	1.03
Liner yield due to hoop stresses (mid-height)	0.75	1.03	0.49
Liner rupture due to hoop stresses (mid-height)	0.97	1.20	1.19
Liner yield due to meridional stresses (wall base, El. 0.25m)	1.42	1.46	0.49
Liner rupture due to meridional stresses (wall base, El. 0.25m)	-	-	0.46
Liner yield due to hoop stresses (splingline, El. 10.75m)	1.03	1.20	0.48
Liner plate rupture due to hoop stresses (springline, El.10.75m)	1.46	1.47	0.46
Liner yield due to meridional stresses (dome, El.16.13m)	1.10	1.35	0.48
Liner plate rupture due to meridional stresses (dome, El.16.13m)	-	1.47	-
Hoop tendons reaching 1% strain (mid-height)	1.43	1.41	-
Hoop tendons reaching 2% strain (mid-height)	1.48	1.46	-
Hoop tendons reaching 3% strain (mid-height)	1.51	1.47	-

ANALYSIS RESULT SUMMARY- STRESS IN LINER

Location	Case 1			Case 2			Remark
	Pressure (MPa)	Tempera-ture (°C)	Stress (MPa)	Pressure (MPa)	Tempera-ture (°C)	Stress (MPa)	
#36	0.138	106.6	-86	0.42	353	-314	Merid. El. 0.25m
#37	0.14	106.6	-214	0.42	353	-417	Hoop El. 0.25m
#38	0.14	106.6	-181	0.42	353	-365	Merid. El. 6.20m
#39	0.14	106.6	-164	0.42	353	-375	Hoop El. 6.20m
#40	0	100.0	-58	0.42	353	-252	Merid. El. 10.75m
#41	0.14	106.6	-132	0.46	365	-424	Hoop El. 10.75m
#42	0.10	104.5	-146	0.46	365	-368	Merid. El. 16.13m

Note : The buckling stress considering the horizontal spacing of liner anchor (150.15mm) is calculated to -122.2MPa

DISCUSSIONS

- The liners are yielded and/or ruptured at higher pressure when both temperature and pressure were simultaneously applied than when subjected to pressure only.
- However, the reinforcements are yielded at lower pressure when both temperature and pressure were simultaneously applied than when subjected to pressure only.
- The first concrete cracking is occurred at similar pressure for both pressure only and pressure with temperature.
- The tendon strains reaching 1%, 2% and 3% are occurred at similar pressure for both cases considering pressure only and pressure with temperature.
- The stresses in liner were under compressive behavior at pressures between 0.2 MPa and 0.78 MPa and temperature between 100°C and 615°C.
- Thus, the compressive stresses due to temperature and the restraints of concrete may cause liner buckling and geometric nonlinear need to be considered in the analysis.

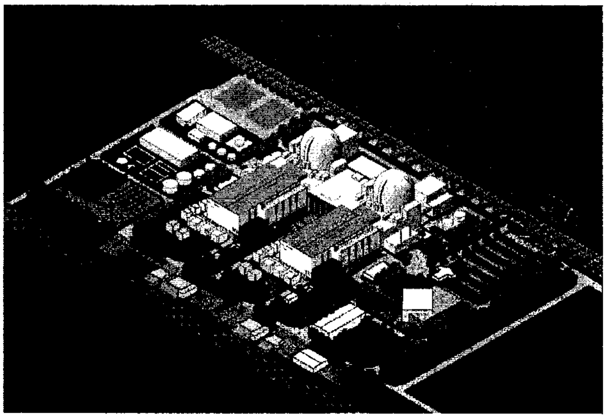

SEVERE ACCIDENT LOAD IN DESIGN

- Required at Design Stage Meeting with Design Code?
  - Consider severe accident load in load combination?
  - Just check the ultimate capacity with nonlinear analysis?
- SRP 3.8.1 (USNRC NUREG 0800, DRAFT Rev. 2 1996)
  - Required to consider in the design
- Are there requirements in Europe and Others?

SEVERE ACCIDENT LOAD COMBINATION IN SRP 3.8.1

The requirements of Sub-article CC-3720 of the ASME Code shall be met for the following loading conditions.

Factored Load Category

① Dead Load + Pg1 + Pg2

② Dead Load + Pg1 + Pg3

Service Load Category

① Dead Load + Pg3

Pg1= Pressure resulting from an accident that releases hydrogen generated from 100% fuel clad metal-water reaction

Pg2= Pressure resulting uncontrolled hydrogen burning

Pg3= Pressure resulting from post-accident inerting assuming carbon dioxide is the inerting agent

Factored Load Category

Membrane compression strain : 0.005in/in

Membrane tension strain : 0.003in/in

Combined membrane and bending (Compression : 0.014in/in, Tension : 0.010in/in)

Service Load Category

Membrane compression/ tension strain : 0.002in/in

Combined membrane and bending : 0.004in/in

SAFETY ASSESSMENT OF PCCV UNDER SEVERE ACCIDENT CONDITIONS

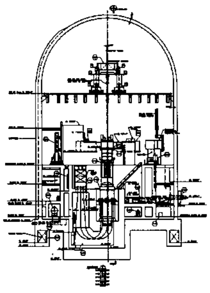

Dimension of Korean PCCV

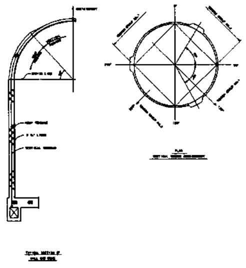

Tendon Layout

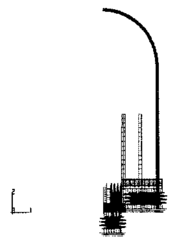

Finite Element Model

SAFETY ASSESSMENT OF PCCV UNDER SEVERE ACCIDENT CONDITIONS

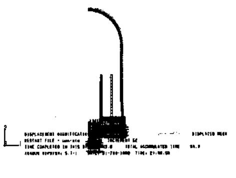

Prestresing

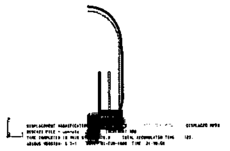

Internal Pressure Only

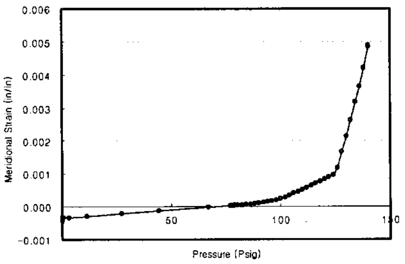

Functional pressure limit of PCCV is 134psig in accordance with the allowable strain in ASME CC-3720.

Discussion

Appropriate Analysis and Design

- **Check only a requirement for liner plate (allowable strain) ?**
- **No need to design limits required by Design Code (ASME CC-3420) for tendon, concrete, reinforcements ?**
- **Liner strain for design limits required by Design Code (ASME CC-3720)**
  - **acceptable to derive from nonlinear analysis such as ISP-48 analysis ?**

Applicability of Severe Accident Load to MC Component (e.g. Equipment Hatch)

- **SRP 3.8.2 Requirements : Subarticle NE-3220 of ASME shall met for "Level C service Limits" - Dead Load + Pg1 + Pg2 (or Pg3)**
  - **Class MC components are required to certify (design & fabricate) to maintain leak-tightness under severe accident load conditions?**
  - **What about test pressure – DBA pressure and/or Severe Accident pressure ?**

Applicability of Severe Accident Load to SIT (Structural Integrity Test)

- **Does the containment have the capability to safely withstand pressure tests at 1.10 (steel containment) and 1.15 times (concrete containment) the severe accident pressure?**

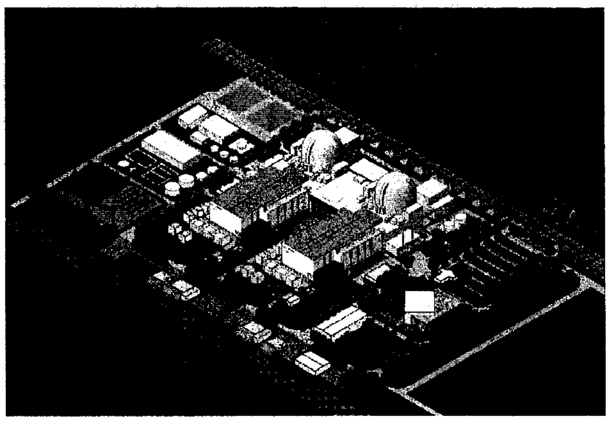

Material Properties and Models - Concrete

Material Properties

Property	Value for basemat	Value for shell & dome
Elastic Modulus	27950 MPa	26970 Mpa
Uniaxial Compressive Strength	39.16 Mpa	47.30 MPa
Uniaxial Tensile Strength	3.37MPa	3.46 Mpa
Poisson's Ratio	0.18	0.18

Radial Displacement Depending on the Concrete Model

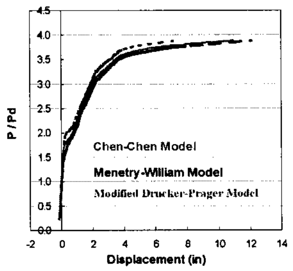

Material Properties and Models - Rebar

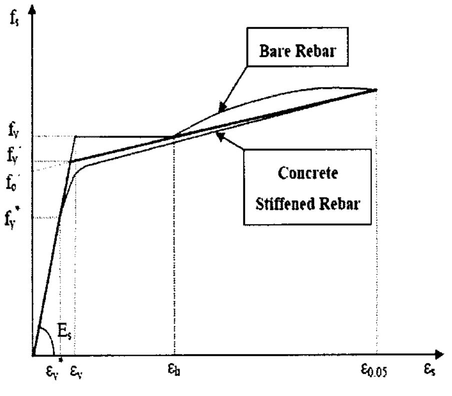
f_s
Bare Rebar
Concrete Stiffened Rebar
f_y
f_y'
f_o'
f_y*
E_s
ε_y*
ε_y'
ε_n
ε_{0.05}
ε_s

Stress-Strain for Rebar (Hsu)

Material Properties and Models - Prestressing Tendon

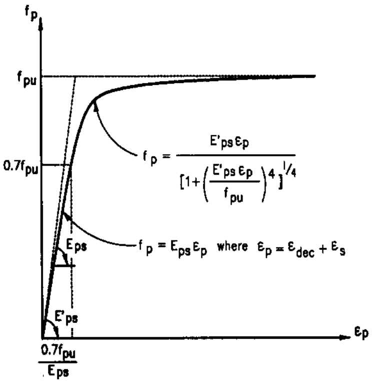
f_p
f_{pu}
$0.7f_{pu}$
$f_p = \frac{E'_{ps}\varepsilon_p}{\left[1+\left(\frac{E'_{ps}\varepsilon_p}{f_{pu}}\right)^4\right]^{1/4}}$
E_{ps}
$f_p = E_{ps}\varepsilon_p$ where $\varepsilon_p = \varepsilon_{dec} + \varepsilon_s$
E'_{ps}
ε_p
$\frac{0.7f_{pu}}{E_{ps}}$

Stress-Strain for Tendon (Hsu)

FINITE ELEMENT MODEL - LOADING CONDITIONS

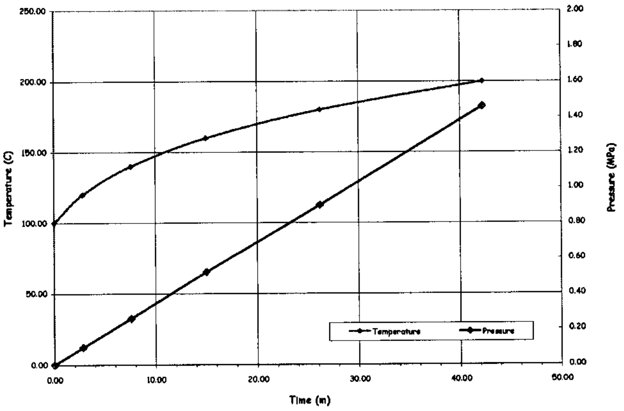

Steamed Saturated Condition

FINITE ELEMENT MODEL - LOADING CONDITIONS

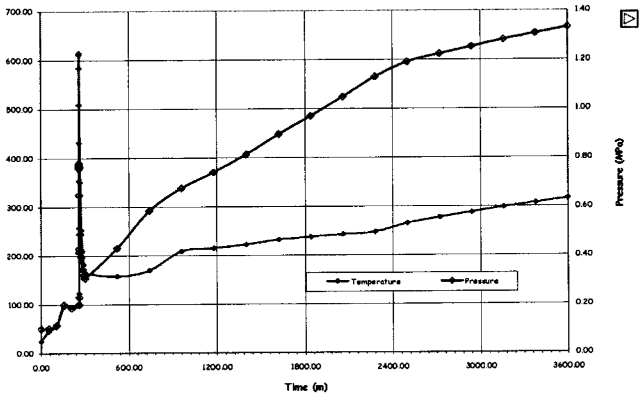

Severe Accident Scenario

Loading History for Steamed Saturated Condition

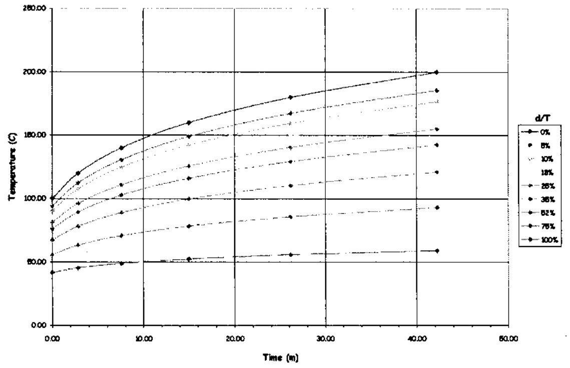

Typical Temperature Distribution at Section 1 (Case 1)

Loading History for Severe Accident Scenario

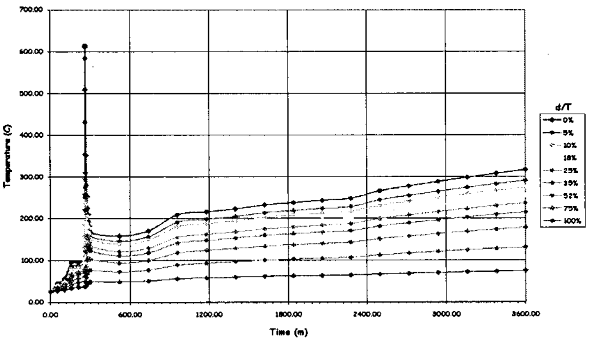

Typical Temperature Distribution at Section 1 (Case 2)

ANALYSIS RESULTS – DISPLACEMENT (Wall-Mat Junction)

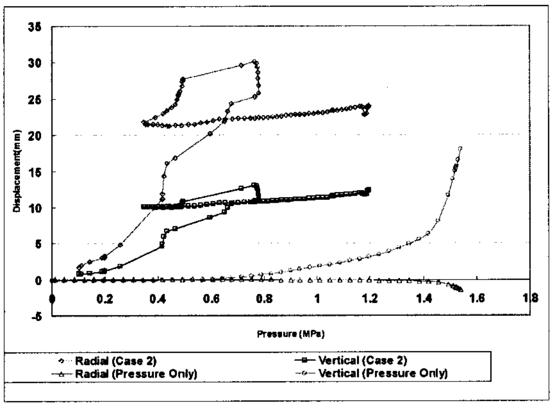

ANALYSIS RESULTS – DISPLACEMENT (Dome Apex)

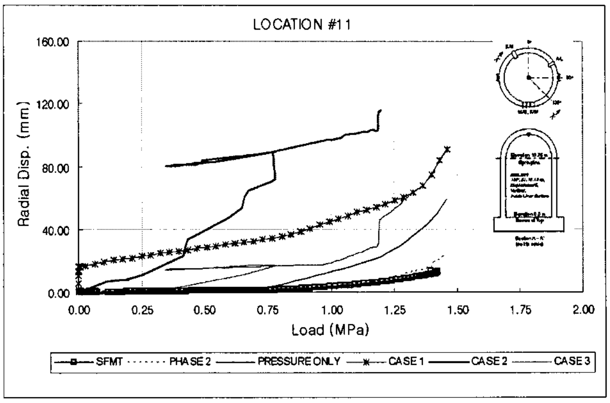

ANALYSIS RESULTS – DISPLACEMENT (Mid-Height Radial)

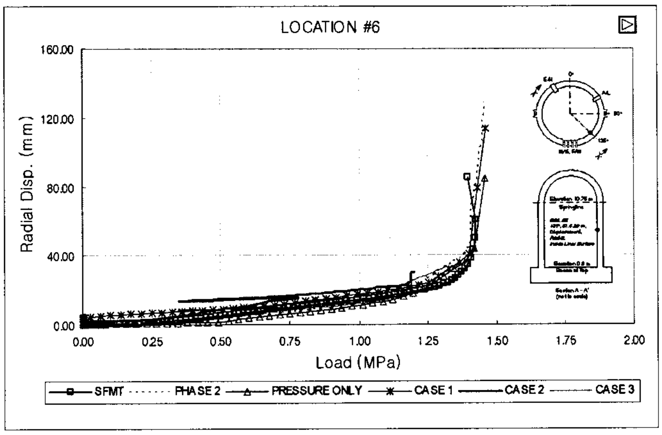

CONCRETE CRACKING AROUND WALL-MAT JUNCTION

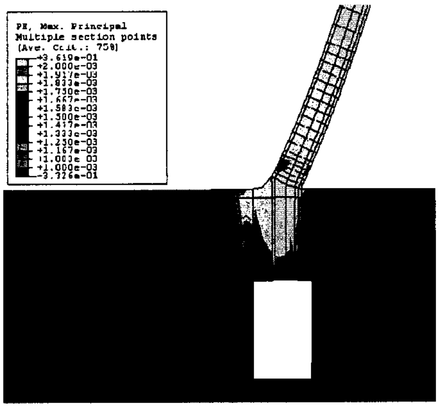
PE, Max. Principal
Multiple section points
(Ave. Crit.: 75%)
+3.619e-01
+2.000e-03
+1.917e-03
+1.833e-03
+1.750e-03
+1.667e-03
+1.583e-03
+1.500e-03
+1.417e-03
+1.333e-03
+1.250e-03
+1.167e-03
+1.083e-03
+1.000e-03
-3.326e-01

Under Pressure Only (at P=1.46 Mpa)

CONCRETE CRACKING AROUND WALL-MAT JUNCTION

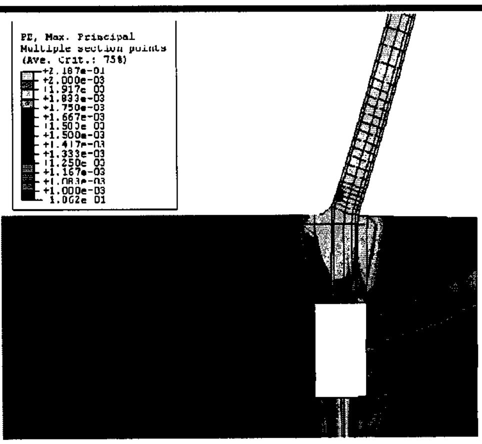

Case 1(at P=1.46 MPa, T=200°C)

INDIRECT CONSIDERATION OF UNBONDED TENDONS IN 1/4 PCCV MODEL

Hyo-Gyoung Kwak *, Jae Hong Kim *, Sun-Hoon Kim **, and Yun-Suk Chung ***
* Korea Advanced Institute of Science and Technology, Republic of Korea
** Youngdong University, Republic of Korea
*** Korea Institute of Nuclear Safety, Republic of Korea

Abstract

This paper concentrates on the development of a tendon model which can simulate slip behavior between unbonded tendons and concrete for finite element modeling of 1/4 PCCV (1:4-scale prestressed concrete containment vessel) model. Differently from the bonded tendon depended on structural section, a stress increase beyond the effective value of initial prestress in the unbonded tendon is mainly depended on the structural member. Therefore, the tendon stress in the unbonded tendon can be represented as having uniform distribution along the length of the member if the friction loss is not included. To trace the structural response of prestressed concrete structures, accordingly, a modified stress-strain curve for the unbonded tendon can be derived through performing the successive iterations. This indirect tendon model can take into account the slip effect between unbonded tendon and concrete, and then it is incorporated into commercialized programs such as DIANA and ABAQUS which have the fundamental limitation in simulating the unbonded tendon. Finally, the ultimate pressure capacity analyses of 1/4 PCCV model are carried out to evaluate the efficiency and applicability of this tendon model. The numerical results show that 1/4 PCCV represents the ultimate resisting capacity larger than 3 times of the design pressure.

Introduction

Differently from the structural damages in most infra-structures such as bridges, buildings, tunnels, and storage tanks, which can be repaired or strengthened with time and cause no additional serious problem, the occurrence of damages in the nuclear power plant (NPP) may cause many serious problems for long time. Accordingly, the design and construction of NPP are strictly guided by the related design codes, and a containment is also placed out side of NPP to cope with an internal accident such as LOCA (loss of coolant accident with pressure and temperature increase in the containment) or an external event such as aircraft crash, explosions, and earthquakes and, in advance, to constitute the ultimate barrier against the dissemination of fissile products towards the general public (fib, 2001).

In this study, to conduct the numerical analysis for the structural safety of a containment structure, loss of coolant accident (LOCA) is considered as the basic accidental load, and pressurized water reactor (PWR) containment structure used in Kori, Uljin, and Younggwang in Korea is considered as a target structure. The PWR containment structure is a prestressed concrete shell structure which has hemisphere dome and is reinforced with unbonded internal tendons. The structure analyzed in this study is the 1/4 scale prestressed concrete containment vessel (PCCV) which consists of wall, continuous dome, and base (Hessheimer et al., 1997), and it was tested by Sandia National Laboratories (2000).

The target structure, 1/4 PCCV, has unbonded tendons for the prestressing system. The structural behavior of prestressed concrete structure (PSC) structures with unbonded tendons is member-dependent instead of section-dependent, and the stress in unbonded tendons depends on the deformation of the entire member and is assumed to be uniform at all sections along the span length. This means that the stress cannot be directly determined from a cross-section analysis with the conventional strain compatibility condition as in the case of bonded tendons. To determine the resisting capacity of PSC structures with unbonded internal tendons, accordingly, an exact prediction of the tendon force must be preceded, and consideration of the slip effect along the tendon sheath as well as the stress relaxation with time is emphasized.

Analysis

Since tendon arrangement and buttress of the containment structure is not axisymmetric, 3-dimensional finite element analysis is accomplished with DIANA 8.1 which is one of commercialized programs (DeWitte and Kikstra, 2002). The purpose of this analysis is focused on material nonlinear analysis to predict ultimate pressure capacity (UPC) of the 1/4 PCCV containment structure, when it is subjected to internal pressure loading. Table 1 shows generals from the geometry to the material properties for 1/4 PCCV (Sandia National Laboratories, 2000).

Table 1. Details for 1/4 PCCV

Properties	Dome	Wall	Base
Geometry	325㎜+1.6㎜ Shell $\rho_{s,\text{in}}=0.29\%$ $\rho_{s,\text{out}}=0.28\%$	275㎜+1.6㎜ Shell $\rho_{s,\text{in}}=0.80\%$ $\rho_{s,\text{out}}=0.64\%$	Solid
Concrete	$f_c'=53.4$㎫ $f_{cr}=2.21$㎫		$f_c'=45.6$㎫ $f_{cr}=2.21$㎫
Re-bar	$f_y=480$㎫ $f_u=629$㎫		
Liner	$f_{ly1}=375$㎫ $\varepsilon_{ly1}=0.18\%$ $f_{ly2}=447$㎫ $\varepsilon_{ly2}=5.08\%$ $f_{lu}=488$㎫ $\varepsilon_{lu}=33.2\%$		
Tendon	Three 13.7㎜ seven-wire strand($A_p=339$㎟) with $f_{pu}=1886$㎫ $\varepsilon_{pu}=3.37\%$		

Finite Element Model

Suitable finite element idealizations for the representative members are conducted. The outer part of base is modeled with 1584 20-node hexahedral solid elements, and the inner part of base with 264 15-node tetrahedral solid elements. Wall and the lower part of dome are composed with 1144 8-node quadratic layered shell elements, and the upper part of dome with 180 6-node triangular layered shell elements. Different material properties of concrete and reinforcing steel across the depth are represented by using the layered section approach. On the other hand, the tendon is simulated by an embedded truss element and its contribution to the global stiffness is superposed to the concrete element.

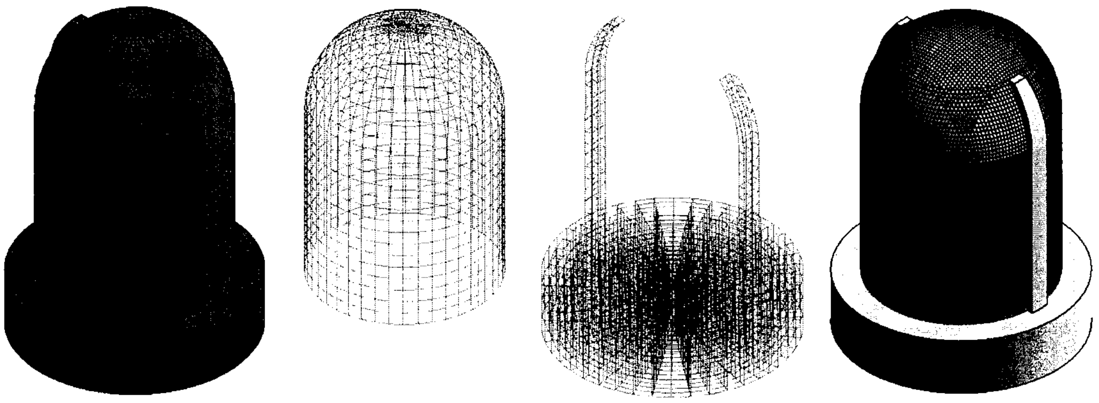

Figure 1. Finite Element Model

Material Model

Material nonlinear models for steel and concrete are constructed on the basis of the CEB-FIP MC90. Especially to simulate the cracking behavior of concrete, smeared crack model considering the rotation of crack angle is adopted, and the tension stiffening effect and their interaction are also taken into consideration. The nonlinear behavior of concrete is described by the stress-strain relation introduced by Hognestad, and the reinforcing steel is assumed to be a linear elasto-plastic material. On the other hand, the tendon is approximated by a series of straight pre-stressing steel segments maintaining a constant force and sectional area.

Indirect Consideration of Unbonded Tendons

Differently from the bonded tendon and reinforcing steel in a usual concrete structure, the internal tendon used in PCCV represents no bond characteristic. A stress increase beyond the effective prestress in an unbonded tendon, therefore, requires the introduction of a different numerical algorithm (Yonezawa et al., 2002) because the slip behavior is not section-dependent but member-dependent and cannot be considered at the classical approach in which the influence of tendon is transformed into an equivalent lateral load.

A new model is based on the slip behavior of unbonded tendons. Focusing on the tendon stress representing a uniform distribution along the length when the friction loss between concrete and tendon is excluded, the maximum strain level determined in the analysis of the same structure with bonded tendon has been averaged as shown in Figure 2(a). In advance, using a strain reduction factor which means a ratio of the maximum strain to the average strain, the modified stress-strain curve of an unbonded tendon can be derived thorough successive iterations. These calculation procedures can be expressed by

$$\varepsilon_{j,\mathrm{ave}}(p)=\frac{1}{L}\int_0^L \varepsilon_j(x,p)\,dx\ ,\quad \sigma_{j,\mathrm{ave}}(p)=f\left(\varepsilon_{j,\mathrm{ave}}(p)\right) \qquad (1)$$

$$\varepsilon_{j,\max}(p)=\max[\varepsilon_j(x,p)]\ ,\quad \sigma_{j,\max}(p)=f\left(\varepsilon_{j,\max}(p)\right) \qquad (2)$$

where *f* is the stress-strain relationship of a bonded tendon.

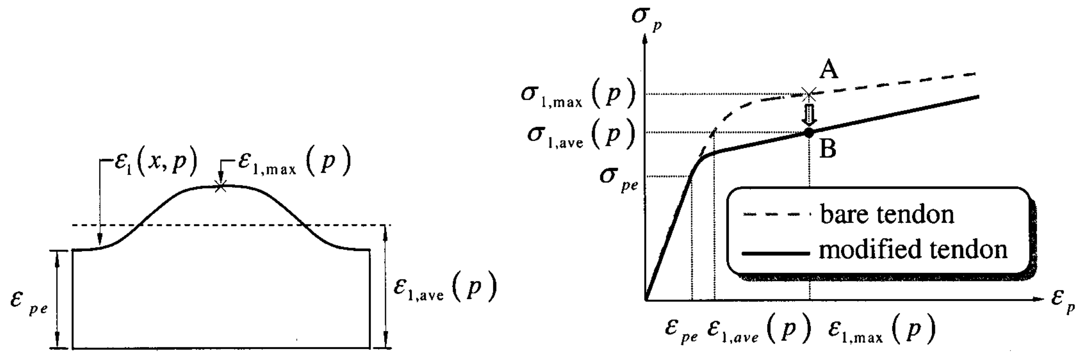
$\varepsilon_1(x,p)$
$\varepsilon_{1,\max}(p)$
ε_{pe}
$\varepsilon_{1,\text{ave}}(p)$
σ_p
A
$\sigma_{1,\max}(p)$
$\sigma_{1,\text{ave}}(p)$
σ_{pe}
B
bare tendon
modified tendon
ε_{pe} $\varepsilon_{1,ave}(p)$ $\varepsilon_{1,\max}(p)$
ε_p

(a) strain distribution

(b) Modified stress-strain curve

Figure 2. Unbonded tendon model

Finally, the modified stress-strain relationship g_j of an unbonded tendon can be derived by taking $\sigma_{j,\text{ave}}(p)$ corresponding to the strain $\varepsilon_{j,\text{ave}}(p)$ at a bonded tendon as the stress corresponding to the strain $\varepsilon_{j,\max}(p)$ at an unbonded tendon, as shown in Figure 2(b), where p_i is an arbitrary tendon force between effective tendon force $(A_p\sigma_{pe})$ and ultimate tendon force $(A_p\sigma_{pu})$. That is,

$$g_j^{-1}\left(\sigma_{j,\text{ave}}(p_i)\right) = f^{-1}\left(\sigma_{j,\max}(p_i)\right) \qquad (3)$$

To completely define the unbonded tendon model, a lot of iterations for correction of the primary tendon stress calculated at a structure with bonded tendons should be accomplished at the pre-analysis stage. Figure 3 shows the flow chart for the pre-analysis conducted in this paper, and the structure with unbonded tendons can be effectively analyzed by using this derived tendon model.

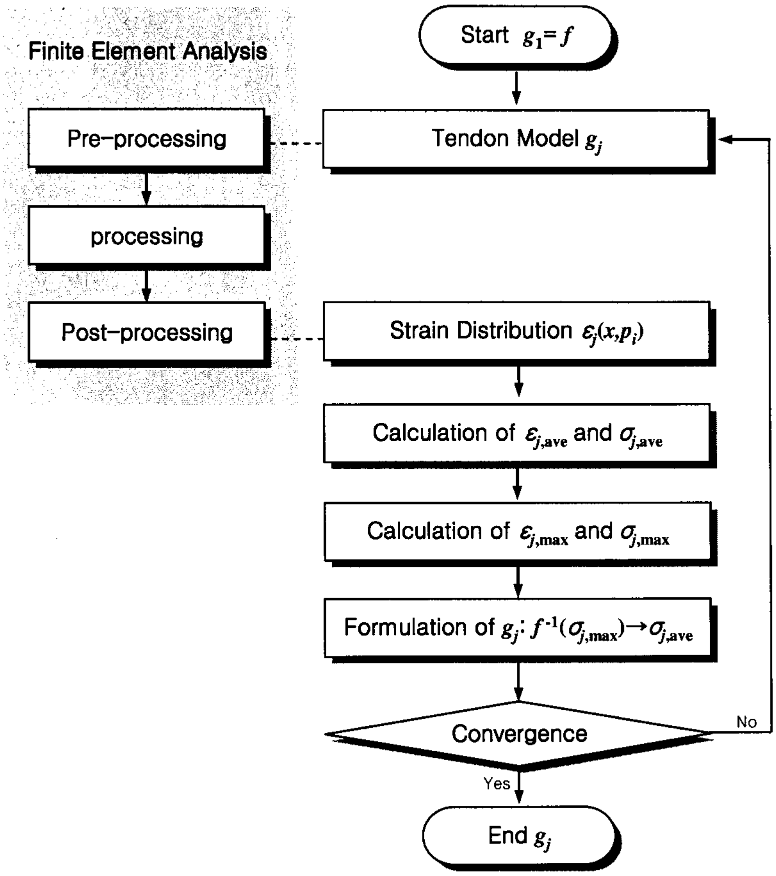
Finite Element Analysis
Pre-processing
processing
Post-processing
Start $g_1=f$
Tendon Model g_j
Strain Distribution $\varepsilon_j(x,p_i)$
Calculation of $\varepsilon_{j,\mathrm{ave}}$ and $\sigma_{j,\mathrm{ave}}$
Calculation of $\varepsilon_{j,\mathrm{max}}$ and $\sigma_{j,\mathrm{max}}$
Formulation of g_j: $f^{-1}(\sigma_{j,\mathrm{max}})\rightarrow\sigma_{j,\mathrm{ave}}$
Convergence
No
Yes
End g_j

Figure 3. Derivation procedure for deriving unbonded tendon model

Results

To establish the validity of the introduced model, correlation studies between analytical results and experimental data are conducted. Nonlinear analysis of 1/4 PCCV is accomplished, and Newton-Raphson algorithm is adopted to trace the nonlinear behavior of this example structure.

Figure 5 shows deformed shape of 1/4 PCCV according to an increase of internal pressure, and Figure 6 shows the corresponding normal strain measured at the outer reinforcing bar. The analytical results predicted show good agreement with the measured values.

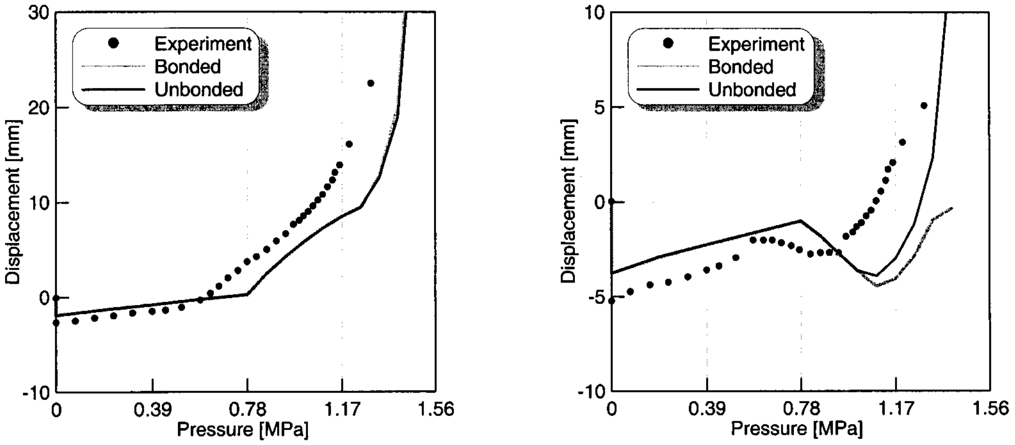

(a) radial at mid-height **(b) vertical at dome-apex**

Figure 5. Deformation

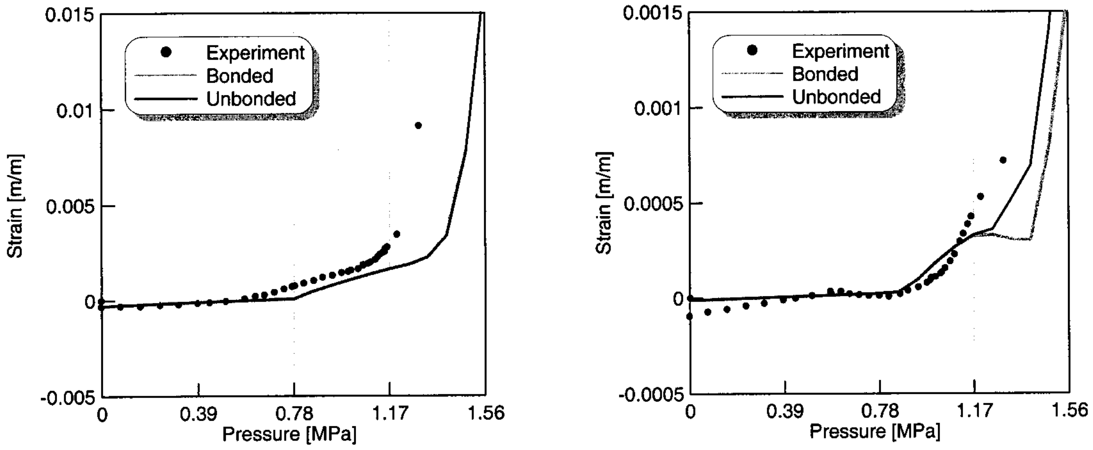

(a) hoop at mid-height **(b) meridional at spring-line**

Figure 6. Strain at outer reinforcing bar

From above two figures, it is convinced that a PSC structure with unbonded tendons present more brittle failure than that with bonded tendons. And figure 7 shows the structural behavior when PCCV is structurally collapsed. At the internal pressure is 1.170MPa, the crack of concrete is fully developed and the deformed shape is figure 7(a). At 1.248MPa, the outer reinforcing bar present some yield behavior such as figure 7(b). And at 1.326MPa, the tendon strain in part reaches about 0.01 that could be a yielding point of a tendon, figure 7(c).

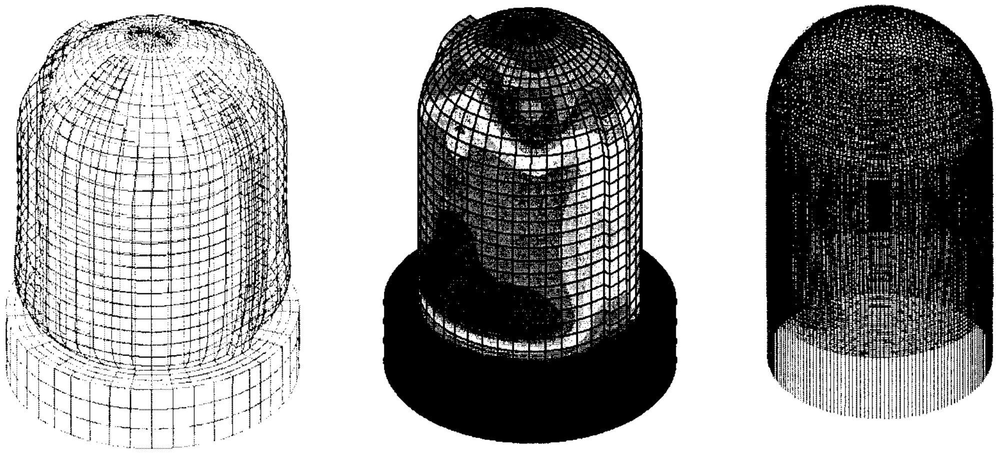

(a) deformed shape (b) outer re-bar strain (c) tendon strain

Figure 7. Behavior at the failure

Conclusion

This paper introduces an improved tendon model for the nonlinear analysis of prestressed concrete containment structures with unbonded tendons. Correlation studies show that the introduced numerical algorithm can effectively consider the slip effect dominant in the case of unbonded tendons, and makes it possible to implement the slip effect while modeling a structure with commercialized programs such as DIANA, NASTRAN, and ABAQUS.

The obtained numerical results show that the ultimate pressure capacity of 1/4 PCCV reserves about 3 times of design internal pressure (0.39MPa). If the ultimate pressure capacity (UPC) is defined the tendon yield point, it is 3.4 times of design pressure. And the other surveyed fact is that the slip behavior of unbonded tendons is dominant in vertical tendons because of their varying strain level along the length.

Acknowledgements

The research reported in this paper was made possible by the financial support from the Korea Institute of Nuclear Safety (KINS). The authors would like to express their gratitude to this organization for the financial support.

References

Comite Euro-International du Beton, *CEB-FIP Model Code for Concrete Structures*, Thomas Telford, 1990.

De Witte, F. C., and Kikstra, W. P., *DIANA-8.1 User's Manual – Element Library, Material Library, Analysis Procedures*, TNO Building and Construction Research, 2002.

fib Task Group on Containment Structures, *Nuclear Containments*, International Federation for Structural Concrete (*fib*), 2001.

Hessheimer, M. F., Pace, D. W., Klamerus, E. W., Matsumoto, T., and Costello, J. F., "Instrumentation and Testing of a Prestressed Concrete Containment Vessel Model", *Transactions of the 14th International Conference on Structural Mechanics in Reactor Technology (SMiRT 14)*, Lyon, France, 1997, H03-4, pp. 97-103.

Naaman, A. E., Burns, N., French, C., Gamble, W. L., and Mattock, A. H., "Stress in Unbonded Prestressing Tendons at Ultimate: Recommendation", *ACI Structural Journal*, Vol. 99, No. 4, 2002, pp. 518-529.

Sandia National Laboratories, *Pretest Round Robin Analysis of a Prestressed Concrete Containment Vessel Model*, U. S. Nuclear Regulatory Commission (NRC) and Nuclear Power Engineering Corporation (NUPEC), NUREG/CR-6678, 2000.

Yonezawa, K., Imoto, K., Watanabe, Y. and Akimoto, M., "Ultimate capacity analysis of 1/4 PCCV model subjected to internal pressure", *Nuclear Engineering and Design*, Vol. 212, 2002, pp. 357-379.

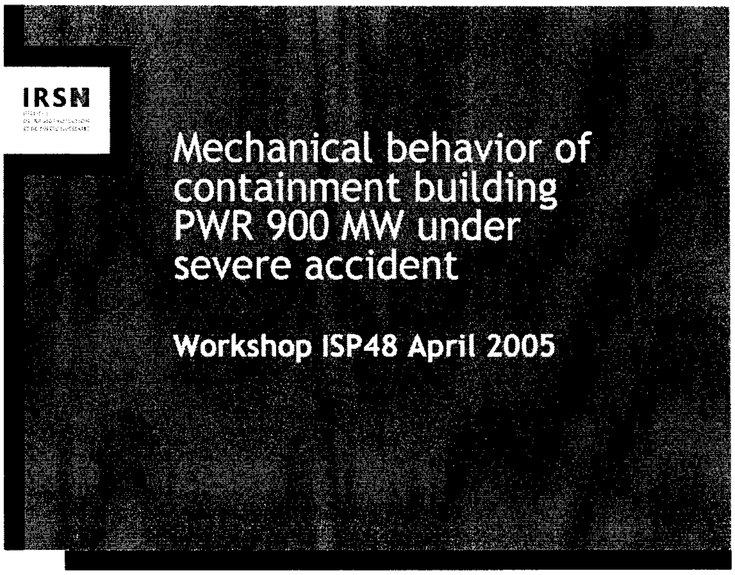

IRSN

Mechanical behavior of containment building PWR 900 MW under severe accident

Workshop ISP48 April 2005

Mechanical behavior of containment building PWR 900MW under severe accident « global model »

SUMMARY

1. Introduction.
2. Initial state of the containment building before the accident.
3. Results of nonlinear calculations of the structure under accidental loading.
4. Use the Experience feedback to define a criterion of tear of the liner with the assistance of a experts group.
5. Conclusions on the global mechanical behavior of the containment building.

INTRODUCTION

- The mechanical behavior of the containment building was studied within the framework of "Probabilistic Safety Assessment level 2" project carried out by the IRSN on the PWR 900 MW, in order to quantify the possible leak of these building in the event of severe accidents.
- The deterministic three dimensional calculations use a multi-scale method aiming to apprehend the behavior of the structure with successive levels of detail, by distinguishing the current zone from the containment building, the equipment hatch area and finally its closing device.
- These calculations use the finite elements method and CAST3M code developed by the CEA.

MULTI-SCALE METHOD

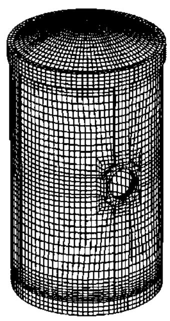

Global model 360°

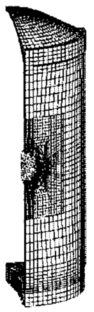

Global model 90°

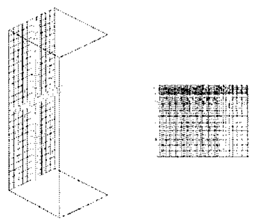

Finer models for liner

INTRODUCTION

- The first part of exposed comprises the presentation:
  - global model to define the mechanical state of the containment building before the accident, after setting of prestressing and ageing.
  - model of quarter of the containment building in order to classify the most penalizing scenarios of severe accidents, to locate the sensitive area of the structure and to determine the boundary conditions to impose on more refined containment models.

INITIAL STATE OF THE CONTAINMENT BUILDING BEFORE THE ACCIDENT

- The objective is to evaluate the state of the structure at 30 years, under loading of deadweight and prestressing.

- Use of a global model 3D-360° with exact geometry with different materials : concrete, rebar, tendons, liner, ground, internal structures, metal sleeve, ring and cover of the equipment hatch.

INITIAL STATE OF THE CONTAINMENT BUILDING BEFORE THE ACCIDENT

- Assumptions taken in modeling :
  - Use of the realistic mechanical characteristics resulting from construction and pressure tests of Blayais 3.
  - Use of BPEL 1999 formulas to evaluate the differed concrete deformation (shrinkage and creep) and the instantaneous and differed losses of tension in the tendon.
  - Taking into consideration the deviations of the tendon around the equipment hatch and personal airlocks.
  - Taking into consideration the losses by linear and angular friction as well as the instantaneous losses due to tendon anchoring shift.

INITIAL STATE OF THE CONTAINMENT BUILDING BEFORE THE ACCIDENT

- Taking into consideration the phase of setting in prestressed into nine phases (Vertical tensioned per thirds, horizontal tensioned by fifth).

- Taking into consideration the losses by relaxation (creep) of steel (2.5%)

- Taking into consideration the concrete drying and the successive moments of concreting along vertical axis.

INITIAL STATE OF THE CONTAINMENT BUILDING BEFORE THE ACCIDENT

Dome tendons

Vertical and Horizontal tendons of containment

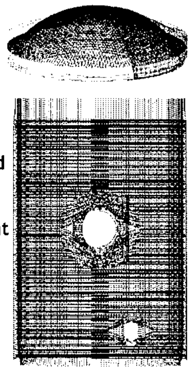

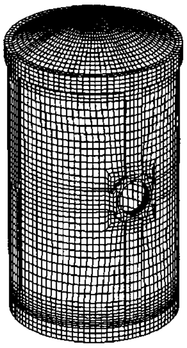

General view of 3D-360° model

INITIAL STATE OF THE CONTAINMENT BUILDING BEFORE THE ACCIDENT

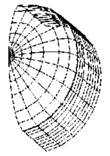

Equipment hatch
Sleeve and cover

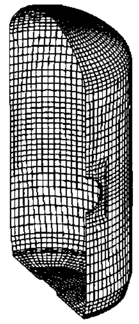

Liner mesh

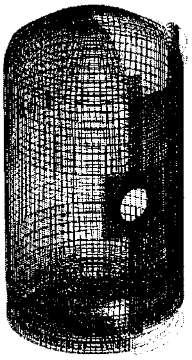

Rebar

INITIAL STATE OF THE CONTAINMENT BUILDING BEFORE THE ACCIDENT

- Comparison of shrinkage and creep deformation with respect to the average values measured on the PWR 900 MW at 20 years.
- Under estimate of differed losses compared to the values measured on the PWR 900 MW.
- Study of sensitivity of the results according to the kinetics of creep:
  - +50% of differed losses (equivalent of the actual state measured).
  - +100% of differed losses (equivalent with an extrapolation at 40 years).

NONLINEAR CALCULATIONS OF THE CONTAINMENT UNDER ACCIDENTAL LOADING

- The aim is to study the nonlinear behavior of the structure under accidental loading in temperature and/or pressure. These calculations will provide also the boundary conditions for the local model.
- Use of a global model 3D-90° with exact geometry, with different materials : concrete, rebar, tendons, liner, ground, internal structures, metal sleeve, ring and cover of the equipment hatch.

Three dimensional global model of the containment

Model includes :

1. **Dome**
2. **Cylinder**
3. **Basemat**
4. **Equipment hatch**
5. **Effect of the ground**

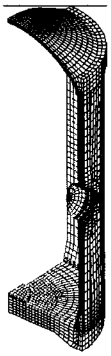

NONLINEAR CALCULATIONS OF THE CONTAINMENT UNDER ACCIDENTAL LOADING

- Assumptions taken in modeling :
  - Use of an elastoplastic law of behavior for the tendons, the rebar and the liner.
  - Use of the traction diagram of the liner for a temperature of 100C°.
  - Use for the concrete the Ottosen constitutive model with smeared cracks.
  - Use of the best estimate mechanical characteristics carried out by EDF.

NONLINEAR CALCULATIONS OF THE CONTAINMENT UNDER ACCIDENTAL LOADING

- The accident scenario studied is a slow rise in pressure without dynamic effect until a pressure of 11 absolute bar.
- Two other thermomechanical scenarios were also studied:
  - ✓ Scenario AF comprises a rise in pressure and in temperature corresponding to a hydrogen combustion followed by a slow rise for the phase Melt-Corium Concrete Interaction (MCCI)
  - ✓ Scenario AS comprises a slow rise in pressure and temperature.
- The definition of the thermal loadings of the building under the effect of the transient of scenarios AF and AS were carried out with a finer 3D-90° model.

AF Scenario

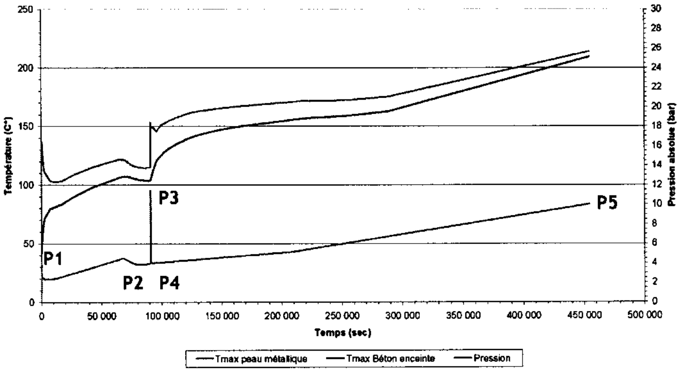

NONLINEAR CALCULATIONS OF THE CONTAINMENT UNDER ACCIDENTAL LOADING

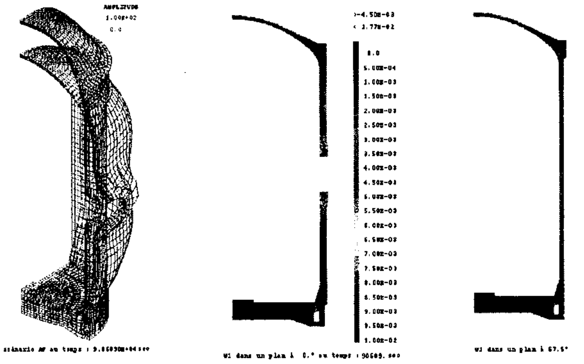
AMPLITUDE
1.00E+02
0.0
scénario AF au temps : 9.06090E+04 sec
>-4.50E-03
< 1.77E-02
0.0
5.00E-04
1.00E-03
1.50E-03
2.00E-03
2.50E-03
3.00E-03
3.50E-03
4.00E-03
4.50E-03
5.00E-03
5.50E-03
6.00E-03
6.50E-03
7.00E-03
7.50E-03
8.00E-03
8.50E-03
9.00E-03
9.50E-03
1.00E-02
W1 dans un plan à 0.° au temps : 90609. sec
W1 dans un plan à 67.5°

Radial displacement level +22,9 m azimuth 67,5°

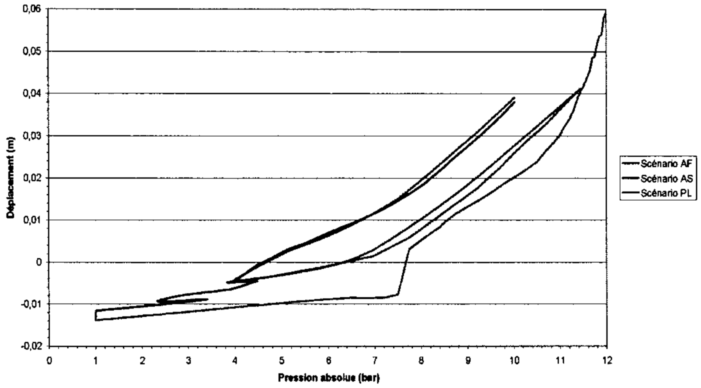

ϵ^{Eq} plastic in the liner level +22,9 azimuth 67,5°

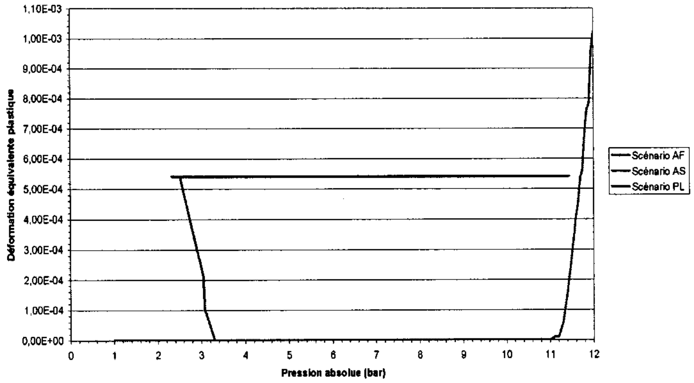

ϵ^{Eq} plastic MAX in the liner

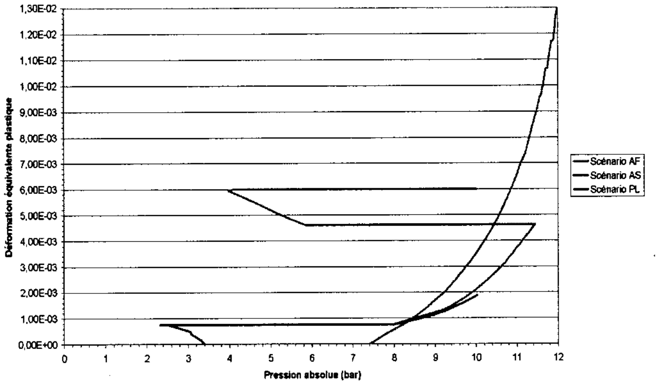

ANALYSIS OF THE CALCULATIONS RESULTS

- Confirmation of sensitive areas of containment building, in particular the zone of equipment hatch and the zone of gusset with cracks crossing of this areas towards the prestressing gallery.
- Comparison of the computation results of the three studied scenarios (PL, AF and AS) makes it possible to evaluate the temperature effect in the accidental loading.
- The plastic equivalent strain obtained in scenario AF after the peak pressure (mark P4) is more significant than the on obtained with the peak (mark P3), effect of the thermal loading.

ANALYSIS OF THE CALCULATIONS RESULTS

- The leakage through the possible tears of the liner and the cracks in the prestressed concrete wall of the containment.
- The calculated strain of the liner remain much lower than the values of the yield strain of material : theoretically, there should not be tearing of the liner, (and the confinement should be preserved!!!)
- Need for defining a criterion of tearing of the liner made from the Experience feedback.

USE THE EXPERIENCE FEEDBACK TO DEFINE A CRITERION OF TEAR OF THE LINER

- Use of the mock-up tests to define a criterion of tear of the liner and particularly the tests on PCCV (NUPEC-NRC-SANDIA) with the assistance of a group of experts.
- RCCV and PCCV represent respectively mock-ups of containment building on 1/6 and 1/4 scale made of reinforced concrete and prestressed with liner.
- Tests in dry air at ambient temperature then failure mode test with water for PCCV.

PCCV (NUPEC - NRC - SANDIA)

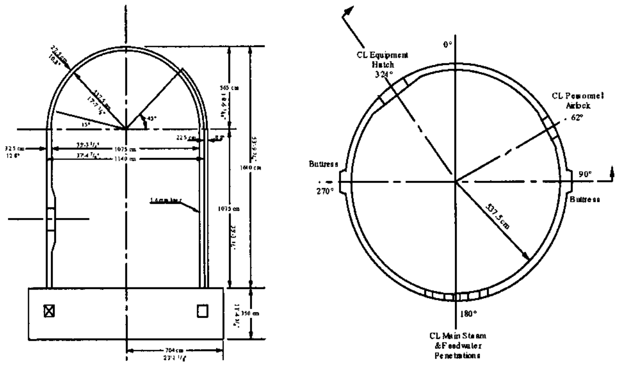
22.5 cm
10.8"
512.5 cm
17'-7 5/8"
15°
45°
22.5 cm
8.8"
32.5 cm
12.8"
39-3 1/4"
1075 cm
37-4 7/8"
1140 cm
565 cm
1610 cm
1.6 mm liner
1075 cm
350 cm
704 cm
0°
CL Equipment Hatch 324°
CL Personnel Airlock 62°
Buttress
270°
90°
Buttress
537.5 cm
180°
CL Main Steam &Feedwater Penetrations

PCCV (NUPEC - NRC - SANDIA)

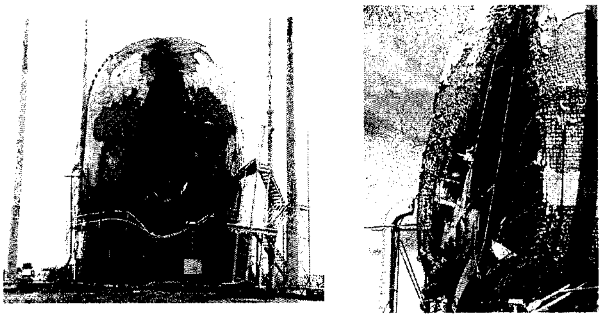

Failure Mode Test

PCCV (NUPEC - NRC - SANDIA) Estimated Leak Rates

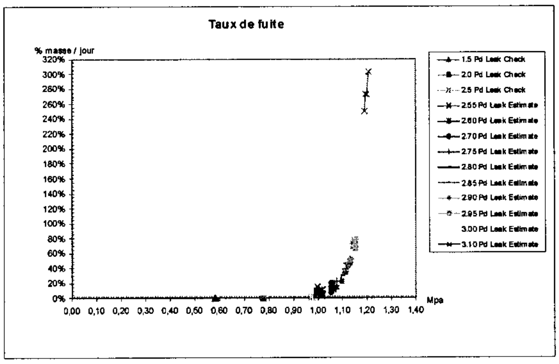

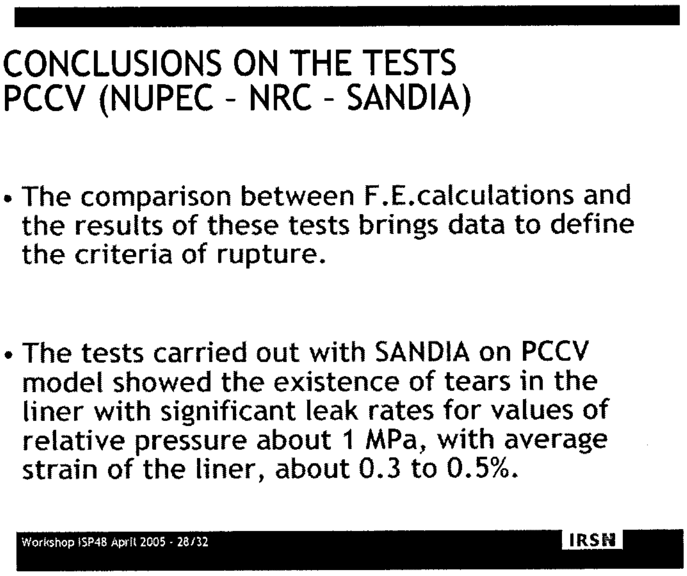

CONCLUSIONS ON THE TESTS PCCV (NUPEC - NRC - SANDIA)

- The comparison between F.E.calculations and the results of these tests brings data to define the criteria of rupture.

- The tests carried out with SANDIA on PCCV model showed the existence of tears in the liner with significant leak rates for values of relative pressure about 1 MPa, with average strain of the liner, about 0.3 to 0.5%.

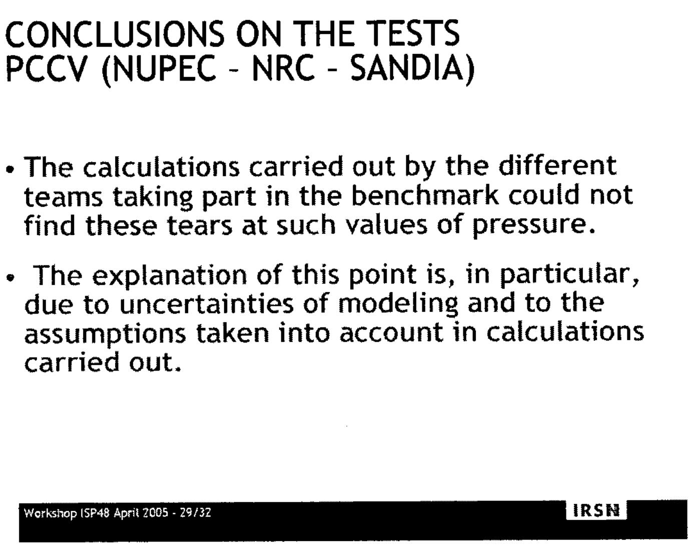

CONCLUSIONS ON THE TESTS PCCV (NUPEC - NRC - SANDIA)

- The calculations carried out by the different teams taking part in the benchmark could not find these tears at such values of pressure.
- The explanation of this point is, in particular, due to uncertainties of modeling and to the assumptions taken into account in calculations carried out.

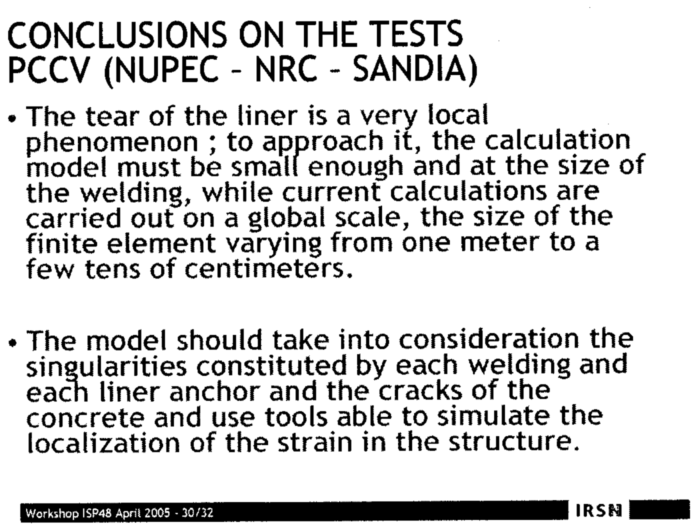

CONCLUSIONS ON THE TESTS PCCV (NUPEC - NRC - SANDIA)

- The tear of the liner is a very local phenomenon ; to approach it, the calculation model must be small enough and at the size of the welding, while current calculations are carried out on a global scale, the size of the finite element varying from one meter to a few tens of centimeters.

- The model should take into consideration the singularities constituted by each welding and each liner anchor and the cracks of the concrete and use tools able to simulate the localization of the strain in the structure.

CONCLUSIONS ON THE TESTS PCCV (NUPEC - NRC - SANDIA)

- The transposition of the results of RCCV and PCCV tests to the calculations of the containments building led to the following global criterion: the maximum plastic strain obtained by nonlinear calculations in the current zone must be lower than a value of 0.30 % ± 0.15 %
- Beyond this value a risk of tear of the liner is very probable by localization.
- This criterion takes into account the assumptions and uncertainties of modeling (size of the F.E. and liner homogenized)

CONCLUSIONS ON THE GLOBAL MECHANICAL BEHAVIOR OF THE CONTAINMENT BUILDING

- Confirm the stability and the confinement of the containment building for at least 0,8 MPa (absolute pressure). Mechanical behavior is quasi-reversible.
- Value of the rupture strain of 0.3 % for the liner, recommended by the group of experts and in conformity with French RCC-M code, corresponds to a pressure in the containment about 0.975 MPa for slow rise pressure scenario and 1.05 MPa for AF scenario (absolute pressure)
- Need to check the liner, in particular, defects of welding, corrosion...

Mechanical behavior of containment building PWR 900MW under severe accident « local model »

SUMMARY

1. Local model:
   the equipment hatch
2. Restricted model : ring,
   flanges and hemispherical head
3. Some results of mechanical
   studies
4. Conclusions

Local model: the equipment hatch

multi-scale step

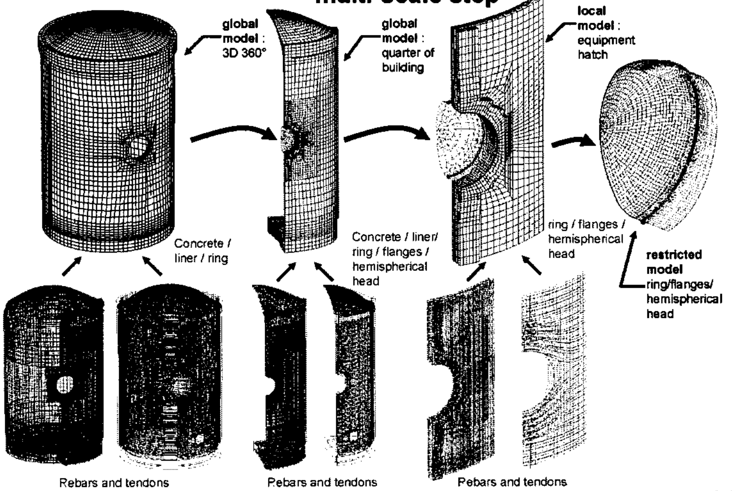

global model : 3D 360°

global model : quarter of building

local model : equipment hatch

Concrete / liner / ring

Concrete / liner/ ring / flanges / hemispherical head

ring / flanges / hemispherical head

restricted model ring/flanges/ hemispherical head

Rebars and tendons

Pebars and tendons

Pebars and tendons

Geometry of the local model and of the restricted model

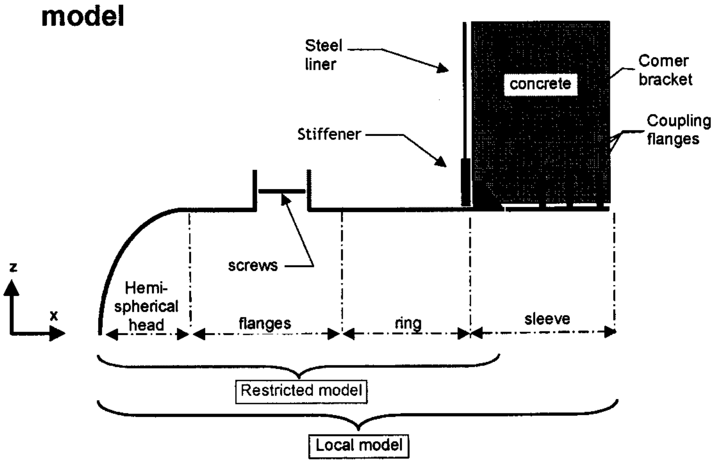

Steel liner

concrete

Corner bracket

Coupling flanges

Stiffener

screws

z

x

Hemi-spherical head

flanges

ring

sleeve

Restricted model

Local model

The local model of the equipment hatch

Finite-elements model

- **Composition : concrete, steel liner, sleeve, ring, hemispherical head, flanges,** screws, rebars and prestressing tendons, coupling flanges and corner brackets, stiffener

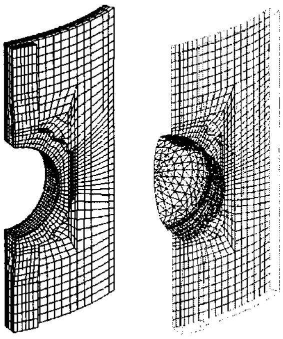

Le modèle local de la traversée

Finite-elements model

Composition: concrete, steel liner, sleeve, ring, hemispherical head, **flanges, screws**, rebars and prestressing tendons, **coupling flanges and corner brackets of anchoring to the concrete, stiffener**

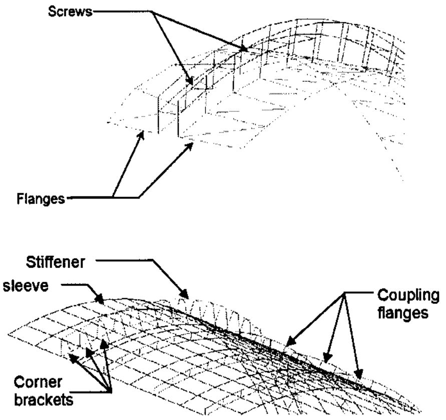

Le modèle local de la traversée

Finite-elements model

- **Composition:** concrete, steel liner, sleeve, ring, hemispherical head, flanges, screws, **rebars and prestressing tendons**, coupling flanges and corner brackets, stiffener

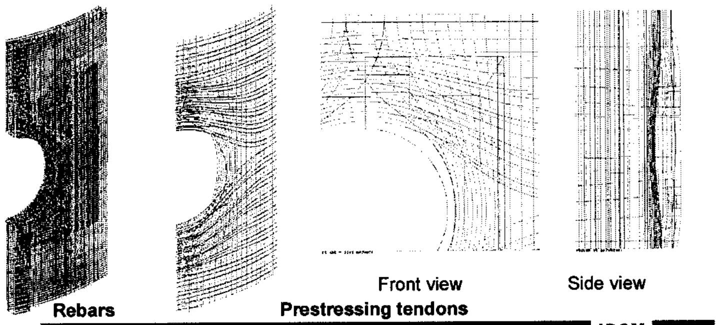

The local model: methodology for calculations

Initial state

- Projection of the deferred deformations fields (shrinkage and creep)
- Projection of the prestressing of the tendons from the global model onto the local model with an iterative re-adjustment in order to compensate the elastic contraction
- Screws prestressed with tightening value

Implementation of the calculation of the loading

- Projection of the displacements fields from the global model onto the limits of the local model at each time step
- Nonlinear thermal calculation specific to the local model
- Application of the internal pressure and own weight

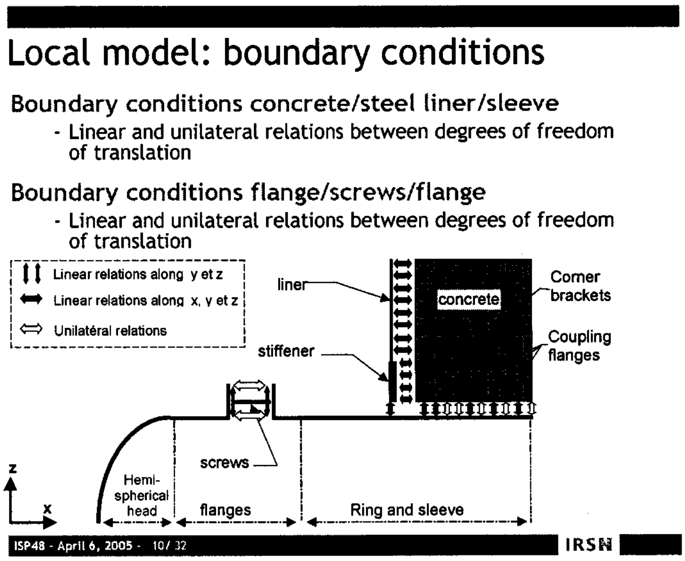

Local model: boundary conditions

Boundary conditions concrete/steel liner/sleeve
- Linear and unilateral relations between degrees of freedom of translation

Boundary conditions flange/screws/flange
- Linear and unilateral relations between degrees of freedom of translation

Linear relations along y et z
Linear relations along x, y et z
Unilatéral relations
liner
stiffener
concrete
Corner brackets
Coupling flanges
screws
z
x
Hemi-spherical head
flanges
Ring and sleeve

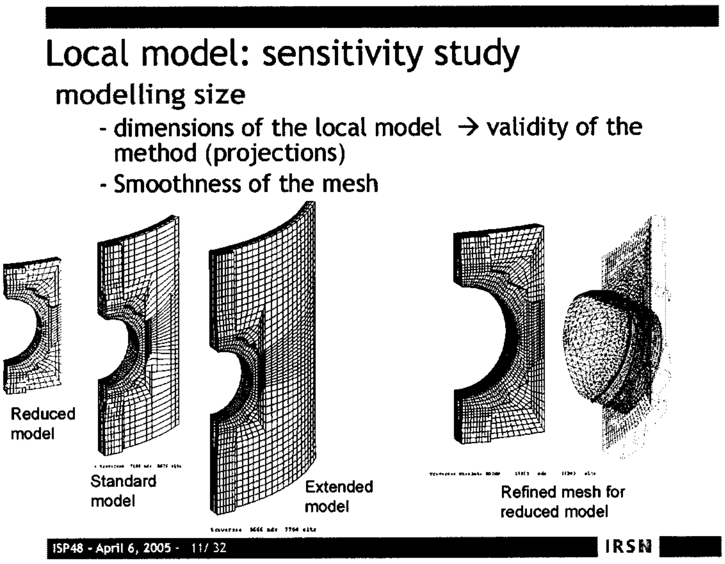

Local model: sensitivity study

modelling size
- dimensions of the local model → validity of the method (projections)
- Smoothness of the mesh

Reduced model
Standard model
Extended model
Refined mesh for reduced model

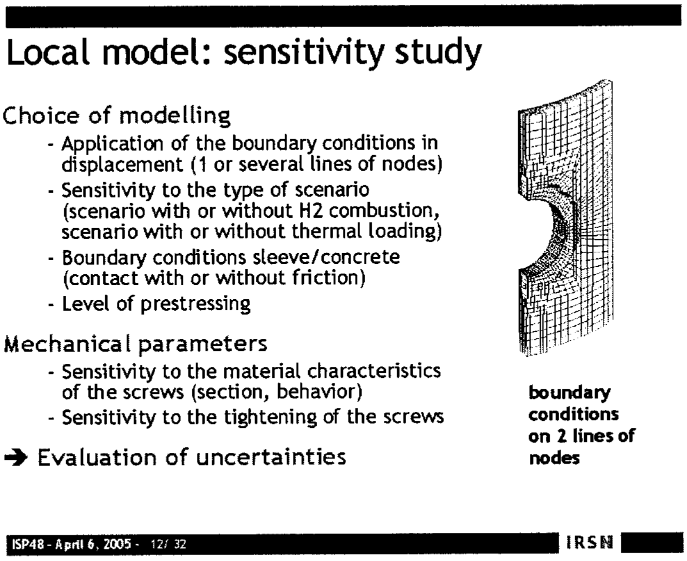

Local model: sensitivity study

Choice of modelling
- Application of the boundary conditions in displacement (1 or several lines of nodes)
- Sensitivity to the type of scenario (scenario with or without H2 combustion, scenario with or without thermal loading)
- Boundary conditions sleeve/concrete (contact with or without friction)
- Level of prestressing

Mechanical parameters
- Sensitivity to the material characteristics of the screws (section, behavior)
- Sensitivity to the tightening of the screws

➔ Evaluation of uncertainties

boundary conditions on 2 lines of nodes

The insufficiencies of the local model

sleeve/flanges modeled by shell elements

- Structure represented by shells → distance between the shells equal to the length of the screws
- No spacers, no surface of friction
- Relative sliding of the flanges blocked

screws modeled by truss elements

- No shear force, work only in traction
- No lateral contact between the flange and the screws with or without free lateral space

→ restricted model in mass elements even for screws

The restricted model :
ring, flanges and hemispherical head

The restricted model ring/flanges/head

Description of the geometry

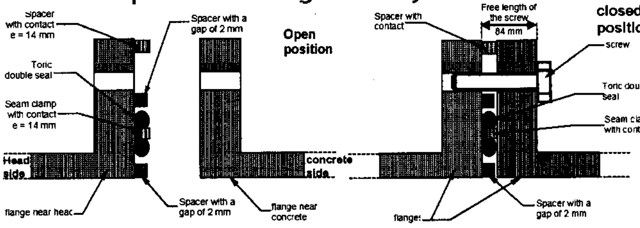
Spacer with contact e = 14 mm
Toric double seal
Seam clamp with contact e = 14 mm
Head side
flange near head
Spacer with a gap of 2 mm
Spacer with a gap of 2 mm
Open position
flange near concrete
concrete side
Spacer with contact
Free length of the screw
84 mm
closed position
screw
Toric double seal
Seam clamp with contact
flanges
Spacer with a gap of 2 mm

Sectional drawing of the flanges oppened and closed

Pictures of the flanges near concrete

The restricted model ring/flanges/bottom

Finite-elements model

- Composition: ring and hemispherical head, flanges and screws

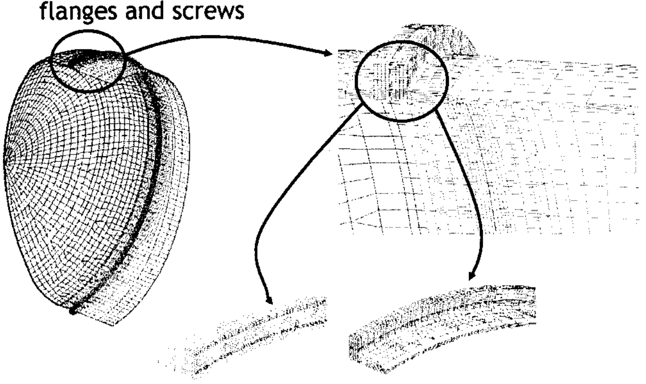

The restricted model: methodology for calculations

Initial state

- Determination of a longitudinal gap and a lateral gap between each screw and the flange to simulate a tightening after the setting into prestressing of the containment building (drilling of the holes and borings after containment prestressing)
  → Suppression of initial shearing of the screws at the beginning of the loading
  → Prestressed screws with the value of tightening

Implementation of the calculation of the loading

- Projection of the displacements fields from the local model onto the limits of the restricted model at each time step
- Nonlinear thermal calculation specific to the restricted model
- Application of the internal pressure and own weight

The restricted model: Boundary conditions

Tightening of the flanges

- Longitudinal unilateral relation (according to OX)
  - between the head of the screw and the flange
  - between the holds or screw clamp and the flange (contact with or without friction)

Fixing of the screw in the loose flange

- Linear or unilateral relation in the plane of the flanges (according to OY and OZ)
  - between the shank of the screw and the flange

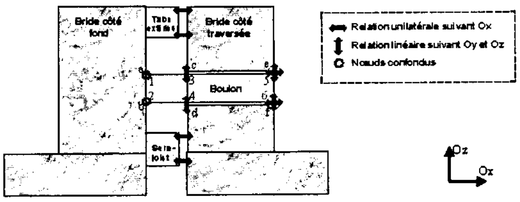
Bride côté fond
Tabl extérieur
Bride côté traversée
Boulon
Serre-joint
c
e
1
3
5
2
4
6
d
f
Relation unilatérale suivant Ox
Relation linéaire suivant Oy et Oz
Noeuds confondus
Oz
Ox

Three types of considered screws

E24 steel (mild steel)
- yield stress of about 240/210 MPa at 20°C/100°C
- Diameter 33 mm (furrow of a screw 3,5 mm)

Z6 CNU 17.4 Steel
- yield stress of about 790/730 MPa at 20°C/100°C
- Diameter 33 mm (furrow of a screw 1,5 or 3,5 mm)

40 CNDV 07.03 Steel
- yield stress of about 900/850 MPa at 20°C/100°C
- Diameter 24 mm (furrow of a screw 3,5 mm)

Some results of the mechanical studies

Risk of loss of containment

Two complementary ways of loss of containment according to the possibility of relative sliding of the flanges

Local model
- Rupture of the screws in traction
- Spacing of the flanges → risk of direct leakage in the atmosphere
- No relative sliding of the flanges

Restricted model
- Partial blocking of the relative sliding of the flanges caused by friction and by the screws
- No significant spacing of the flanges
- Important shearing of the screws → risk of break of the screws on the 2/3 of the circumference

Reality ranges between these two phenomena according to the real conditions of contact and friction between the two flanges

Deformation of the screws with pressurization

The plastic deformation, variable according to the type of screws, is responsible for an irreversible spacing of the flanges

- Spacing of the flanges and beginning of plastification
  - delayed by a high yield stress
  - advanced with a small section
- Residual spacing of the flanges in the event of hydrogen combustion

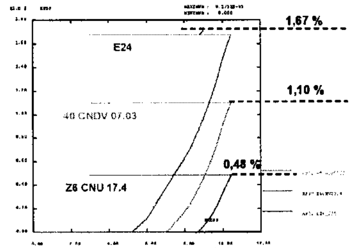

Maximal plastic deformations of screws in function of the pressure

Spacing of the flanges

The spacing, variable according to the type of screws, generates a potential leakage according to the seal shape recovery

- plastic deformation of the screws = irreversible spacing of the flanges = residual spacing post-peak
  - Weaker for a high yield stress
  - More important with a weaker section
- Residual spacing of the flanges in the event of hydrogen combustion

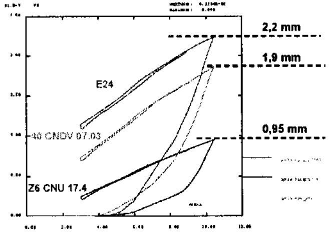

Maximal spacing of the flanges in function of the pressure

Pressure of spacing of the flanges and potential surfaces of escape (absolute bars)

Pressure in bar (abs.)	Leakage surface area 1 cm²	Leakage surface area 10 cm²	Leakage surface area 50 cm²
E24 Ø 33 mm	6,03	7,26	9,57
Z6 CNU 17.4 Ø 33 mm	6,64	9,36	> 12,00
40 CNDV 07.03 Ø 24 mm	5,50	7,20	10,19
spacing max. of the flanges	33~41 µm	264~288 µm	1066~1103 µm

Opening of the flanges

Opening on larger radius spacer

- **No opening to the right of the seals**
- **Re-closing of the set of 2 mm at the smaller radius spacer**

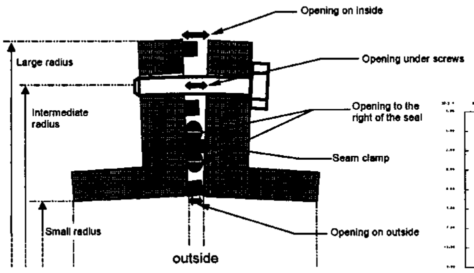
Opening on inside
Opening under screws
Large radius
Intermediate radius
Opening to the right of the seal
Seam clamp
Small radius
Opening on outside
outside

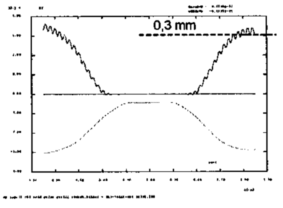

opening profile of the flanges

Deformation of the flange

The differential displacement of the various generating lines of the ring, imposed by the concrete, causes a warping and an ovalization of the flange near the ring which are opposed to the deformations of the flange near the hemispherical head

- **The differential warping of the flanges is responsible for the flanges opening**
- **The differential ovalization of the flanges is responsible for the screws shearing**
- **The contact forces are not uniform under the seam clamp and low under the external spacer (weaker friction is not opposed any more to the differential ovalization of the flanges)**
- **Consequently, the screws plasticize at low pressure by shearing on almost all the circumference**

Differential ovalization of the flanges according to type of screw

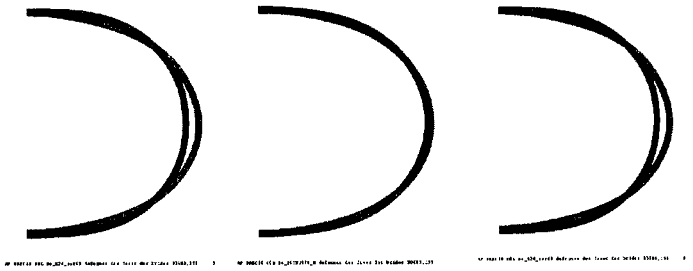

Screws E24 (Ø=33mm) **Screws Z6CNU17.4 (Ø =33mm)** **Screws 40CNDV07.03 (Ø =24mm)**

Deformations of the flanges at 10 bar, amplification : 100 times

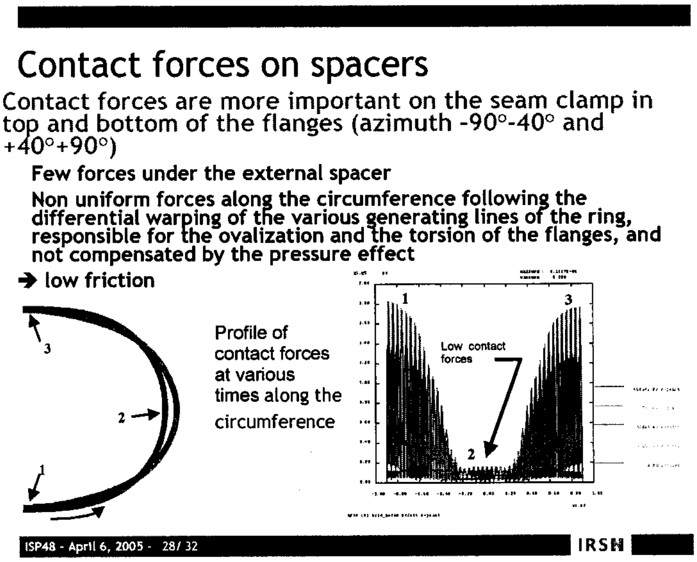

Contact forces on spacers

Contact forces are more important on the seam clamp in top and bottom of the flanges (azimuth -90°-40° and +40°+90°)

- **Few forces under the external spacer**
- **Non uniform forces along the circumference following the differential warping of the various generating lines of the ring, responsible for the ovalization and the torsion of the flanges, and not compensated by the pressure effect**

➔ low friction

Profile of contact forces at various times along the circumference

ISP48 - April 6, 2005 - 28/ 32

IRSN

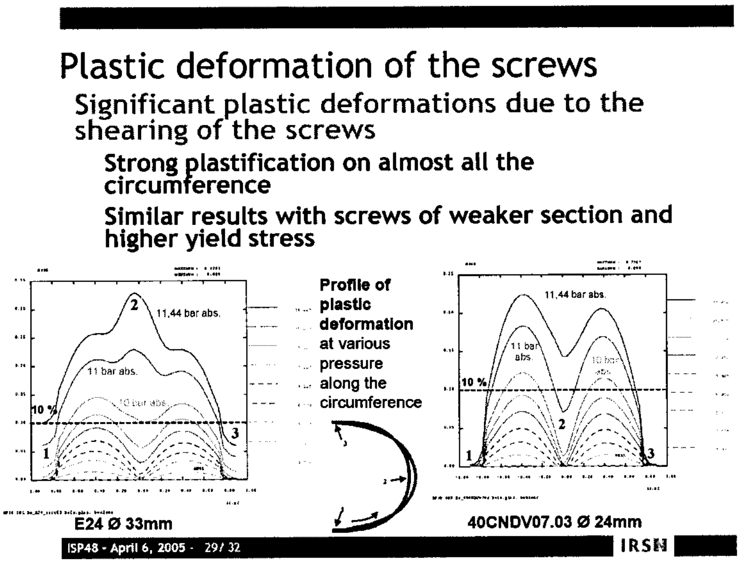

Plastic deformation of the screws

Significant plastic deformations due to the shearing of the screws

- **Strong plastification on almost all the circumference**
- **Similar results with screws of weaker section and higher yield stress**

Profile of plastic deformation at various pressure along the circumference

E24 Ø 33mm

40CNDV07.03 Ø 24mm

ISP48 - April 6, 2005 - 29/ 32

IRSN

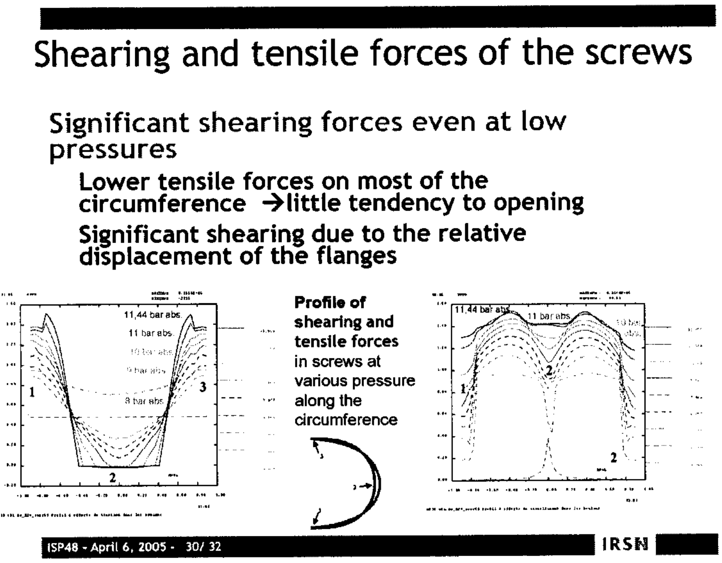

Shearing and tensile forces of the screws

Significant shearing forces even at low pressures

- **Lower tensile forces on most of the circumference ➔little tendency to opening**
- **Significant shearing due to the relative displacement of the flanges**

Profile of shearing and tensile forces in screws at various pressure along the circumference

ISP48 - April 6, 2005 - 30/ 32

IRSN

Gap between screws and flanges and plastic deformation of the screws

Taking into account the lateral gap between screws and flanges and modification of tightening

Little effect of tightening of the screws

Significant gain brought by the gap flanges/screws (3mm for the screws of 33mm in E24 steel)

maximum of the plastic deformation of screws in function of the pressure

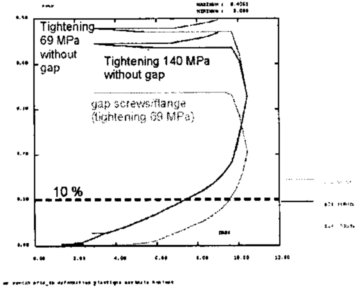

Conclusions

Detail modellings

- confirm the results of the global model (stability, leaktighness)
- Allow the taking into account of contact/friction between flanges
- Allow a modelling of tightening after the setting of the containment building in prestressing
- ➔ realistic analysis of screws shearing
- Underline the role of the gap between flanges and screws

These detail modellings indicate

- the weakness of the screws out of E24 steel of 33mm of diameter in the event of severe accident
- Moderate profit brought by screws of high grade of steel but of weaker section

THE CREEP OF CONFINEMENT BUILDING'S ELEMENTS, FINITE ELEMENT ANALISYS ON CONFINEMENT AGEING PROGRAM

Csaba Nyárádi
Senior engineer
Nuclear Power Plant Paks Hungary

Abstract

1. The creep of confinement building's elements.

Measuring the crab of different parts confinement building at the time during installation, future activity designed.

2. Finite element analysis on confinement.

Informative description: last and newest activity on FEM, selection of critical elements, finite element analysis, limits and results.

3. Ageing program.

There is some short information about ageing program at NPP Paks.

Introduction

The NPP PAKS is first of nuclear power plant type VVER-440-213 built with condenser tower to decrease pressure under severe accident in the hermetic space. NPP has four units, each unit power output is 460 [MWe]. Designed pressure during designed accident in confinement is 0,25 [MPa] absolute.

During the time putting NPP to commission we made a mechanical and leakage test on designed pressure level. Meantime this process we made a measuring program to measure the maximal crab of pointed elements on the largest face of confinement.

Our factory's board decided – based on international experiences in last 10 years – launching a license renewing program. Ageing is a part of these program. I will talk about some actions on hermetic liner.

1. The crab of confinement building's elements.

In years, when the first semicontainment nuclear power plants was build, it was a very exiting question self-righting of building. One of commensurable parameters is the crab of building's element.

During the time putting NPP to commission we made a mechanical and leakage test on designed pressure level. Meantime this process we made a measuring program to measure the maximal crab of pointed elements on the largest face of confinement.

The work was examined by Institute of Geodetic of University of Technology Budapest, entrusted by Power Engineering and Contractor Co.

Measuring program was perform during first integrated leakage test on designed pressure – 0,25 [MPa] absolute – on hermetic volume (picture – 1.).

I would foreshow the mean activities and results.

The most sore points on building are on western side of localization tower, vertical walls of air traps.(picture – 2.), size is about 40 m x 50 m.

First measurement was achieved in 8÷13, September 1982. at unit 1.
There was fixing up27 measuring points on the wall. There was spot marked K6 had extreme shifting; 4 ± 0,88[mm] (picture - 3.). Calculated average middle error was ± 0,70 [mm]. Representative shifting is between 1,0 ÷ 4,0 [mm].

In July 1986. measuring was executed on 3. unit. There was fixing up 25 measuring spots on the wall. (picture 4.) There was spot marked 35 had maximal shifting 5,7 [mm]. Calculated average middle error was ± 0,65 [mm]. In this case real extreme shifting is 5,7 – 1.02= 4.68 [mm]. Representative deformation is between 1,7 ÷ 4,4 [mm].

In June 1987. measuring was executed on 4. unit. There was fixing up25 measuring spots on the wall.(picture 5.). There was spot marked 43 had maximal shifting 3,2 [mm]. Calculated average middle error was ± 0,60 [mm]. In this case real extreme shifting is 3,2 – 0.6= 2.6 [mm]. Representative deformation is between 0,3 ÷ 2,6 [mm].

Our management decided to execute the measuring program in next years, connected to ageing, periodical safety assessment and lifetime expansion programs.

2. Finite element analysis on confinement

In 1998 we initiated an analysis to investigate adequacy of critical elements of hermetic wall. In frame this work it was perform a finite element analysis. Calculation was executed with COSMOS/M v. 2.0 and AXIS-3D v. 2.55 software.

In this presentation will be shown the mean results only.

Construction of hermetic space is different as usual, VVER-440/213 type has a rectangular shape, then again general construction is cylindrical.

According this fact it was appointed definite parts of this area:

No	DESIGNATION	PIECES / UNIT
1.	liner	
2.	pipe penetrations	929
3.	pipe penetrations – spare part	156
4.	hermetic cover for mounting holes – rectangular and cylindrical	20. – total amount
5.	hermetic doors	27
6.	reactor cupola	1
7.	hermetic air flaps	12

Calculated feasibility of failures you can study in table below:

No.	Part of construction	feasibility of failure
1.	Connection between liner and reinforced concrete	$5{,}8*10^{-8} \div 10^{-10}$
2.	Hermetic pipe penetration	10^{-8}
3.	Hermetic cover (3500 * 1400 [mm])	$6{,}94 * 10^{-5}$
4.	Hermetic cover (∅ 3400 [mm])	$1{,}53 * 10^{-3}$
5.	Hermetic door	$5{,}67 * 10^{-5}$
6.	Reactor cupola	$<10^{-9}$
7.	Pipe penetration – spare (blind)	$5{,}1 * 10^{-4} \div 10^{-9}$
8.	Hermetic air flap	

Final conclusion of study is:
Feasibility of hermetic area's leakage caused by failure of parts of construction to be more than limited by authority is no more than 0,015.

Decree No 108/1997, Nuclear Safety Regulation ordered by Hungarian Government contains three main tasks to do:

1 – license renewal

2 – periodical safety assessment

3 – annual updating of the final safety report

Paks NPP Co. executed a large-scale safety enhancement program between 1996 and 2002.

In frame of level 2 PSA evaluation NPP had made an analysis trusted Atomic Energy Research Institute (AEKI) and Institute for Electric Power Research (VEIKI). The evaluation containment performance was carried out by the ABS Consulting Inc. (formerly EQE). Consistent with the nature of the PSA, the evaluation methodology is based on estimating the capacity of the containment structure in terms of probabilistic parameters for a number of possible failure modes.

A Level 2 probabilistic safety assessment (PSA) is being conducted for the Paks Nuclear Power Plant to estimate the probability of radioactive release from the containment structure during a hypothetical beyond-design-basis accident. As part of this PSA, an evaluation of the capacity of the containment structure for elevated pressure and temperature loadings is required.

The calculated capacities are dependent on several factors, including the material properties, modeling assumptions, and the postulated failure criteria. Obviously, uncertainty in modeling and criteria and variability of material properties introduce considerable uncertainty/variability in the calculated capacity estimates. In view this, the pressure capacity for any failure mode is considered to be a random variable.

The items on the pressure boundary can be divided to two main categories:
(1) The reinforced concrete structural components, i.e., the walls and slabs (and a relatively small number of structural beams and columns
(2) various penetrations through the reinforced concrete elements, such as doors, equipment hatches, electrical and piping penetrations, etc.

Accordingly, the evaluations were divided to two main tasks:
Evaluation of the reinforced concrete pressure boundary
evaluation of penetrations.

The mean overall containment capacity was computed to be 0.35 [MPa], and the "high confidence of low probability of the failure" capacity as 0.235 [MPa]. The mean and 95% confidence containment fragility curves are shown in the picture – 6.

3. Ageing program.

Outline of monitoring program on confinement's reinforced concrete structure - short description, tests of samples, monitoring results, steps need to do to times to come.

Monitoring programs:
a/- control of building movement
b/- control cracks in concrete
c/- control of the reinforced concrete behavior in boric acid environment
d/- control of the liner's corrosion

Results:
a/-settlement is consolidated at all buildings
b/- mapping is executed, periodic control needs to continue,
c/- pools reconstruction –stopped leakage, based on laboratory tests : no significant effects of boric acid

d/- at the hidden side is a live problem, found places are changed and repaired, it have to listen to continuously.

You can find a detailed composition about this topic at issues of SALTO 1st meeting of WG 4 03-05 March Vienna, IAEA, (**LICENCE RENEWAL and CONDITION MONITORING PRACTICE at Paks NPP** Structures and Structural Components)

BIOGRAPHY:

1. Creep monitoring of localization tower – bulletin outline NPP's unit 1.08 13.September.1982.

   Elaborated by: Technological University Budapest, Geological Institute,

   Geometer and Analyzer of soil Engineering Company.

2. Deformation monitoring of localization tower of NPP's unit 3. during it's ILRT. July 1986

   Elaborated by: Technological University Budapest, Geological Institute

   Geometer and Analyzer of soil Engineering Company.

3. Deformation monitoring of localization tower of NPP's unit 4. during it's ILRT. Jun. 1987

   Elaborated by: Technological University Budapest, Geological Institute,

   Geometer and Analyzer of soil Engineering Company.

4. LEVEL 2 PROBABILISTIC SAFETY ASSESSMENT OF THE PAKS NUCLEAR POWER PLANT FINAL REPORT August 2000 – December 2003

5. LICENCE RENEWAL and CONDITION MONITORING PRACTICE at Paks NPP

   Structures and Structural Components SALTO 1st Meeting of WG4 03-March-2005Vienna, IAEA

Picture – 1.

Shape of hermetic boundary Unit 2.

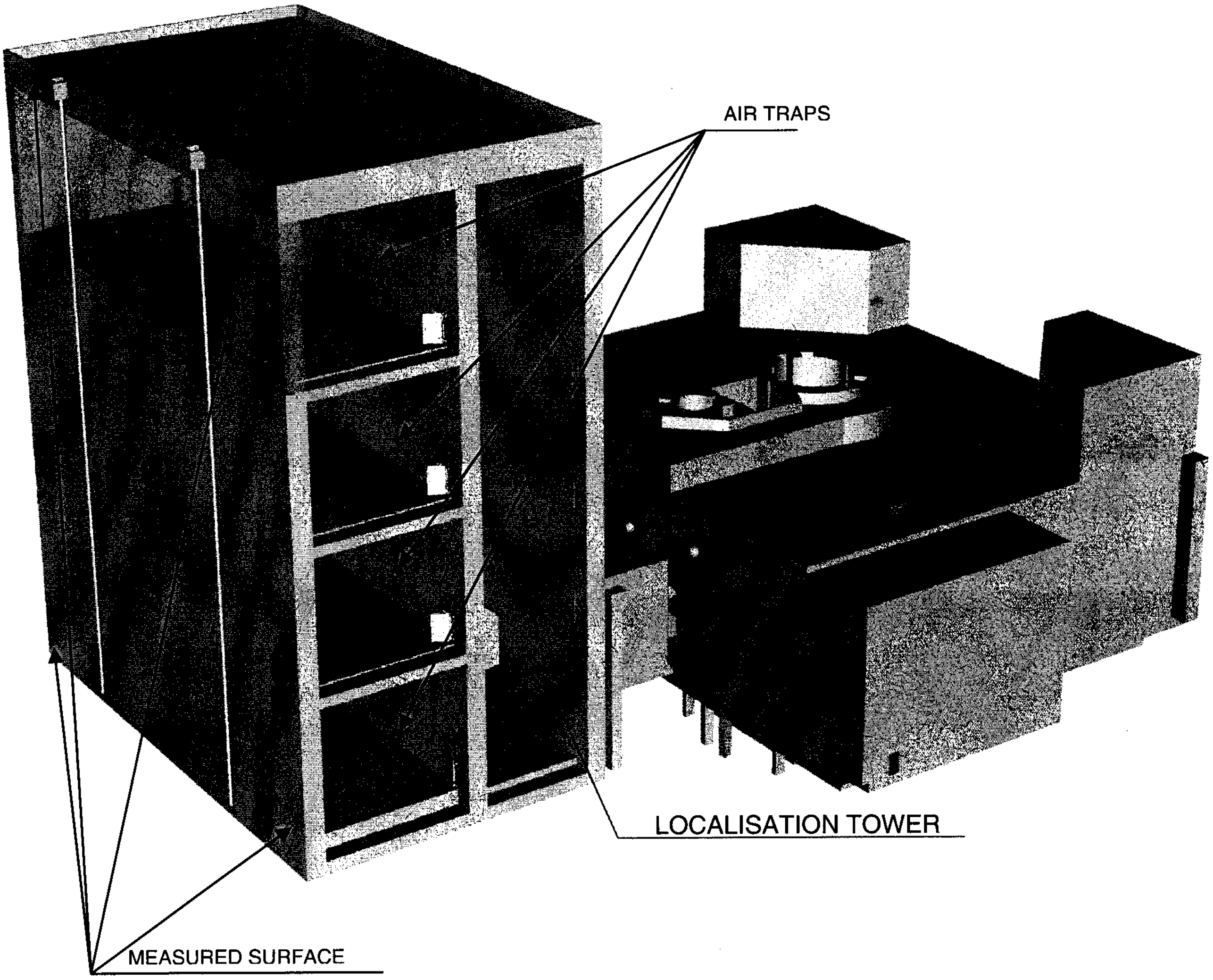
AIR TRAPS
LOCALISATION TOWER
MEASURED SURFACE

Picture- 2.

scheme of vertical wall of localization tower of unit 1. NPP Paks Hungary
note: B – left side of wall
J – right side of wall
K – middle side of wall numbers – height of spots

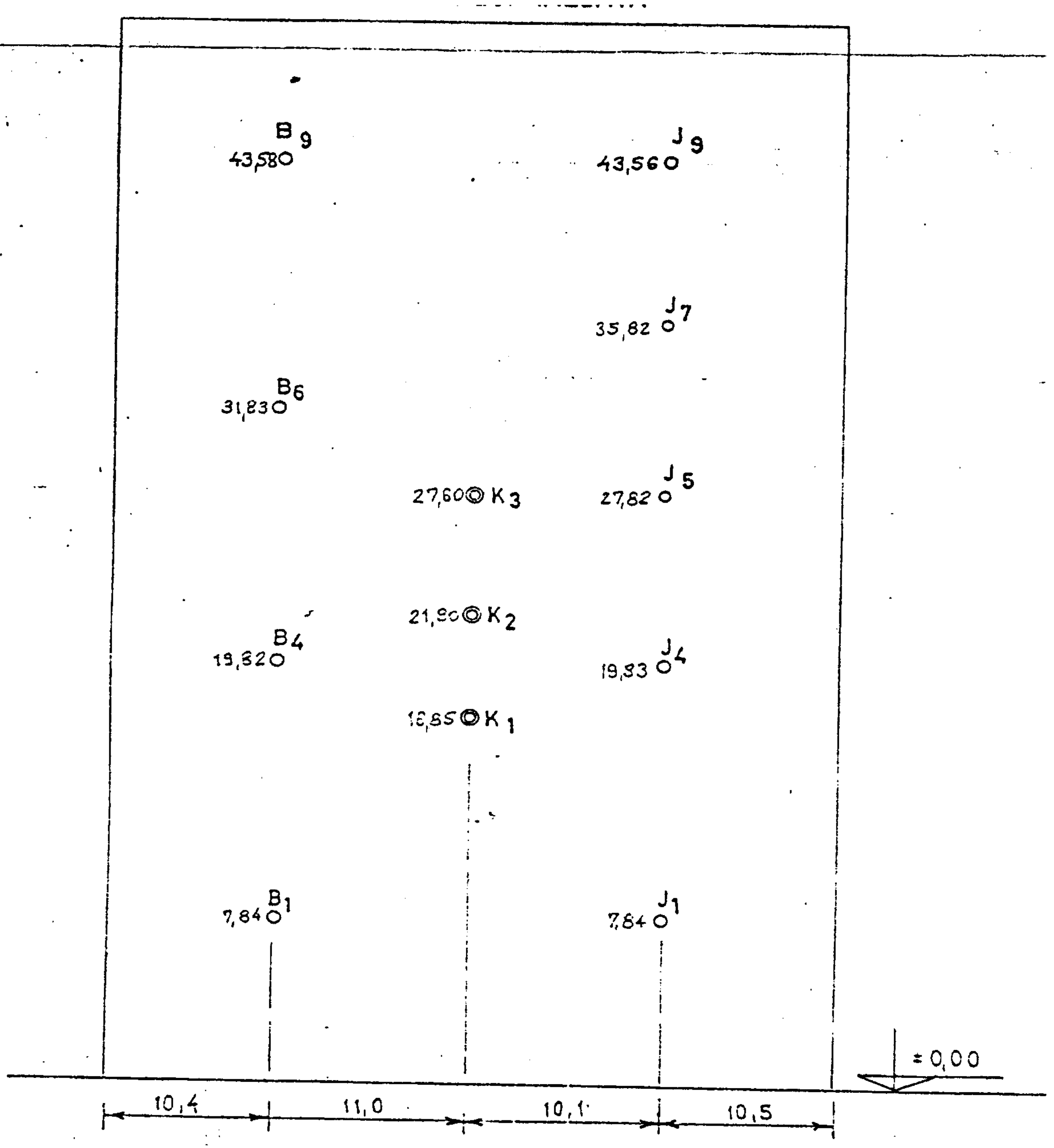
B9
43,580
J9
43,560
J7
35,82
B6
31,830
27,60 K3
J5
27,82
21,80 K2
B4
19,820
J4
19,33
16,85 K1
B1
7,84
J1
7,84
±0,00
10,4
11,0
10,1
10,5

picture – 3.

Scheme of vertical wall of localization tower of unit 3. NPP Paks Hungary

note: numbers – identification of spots

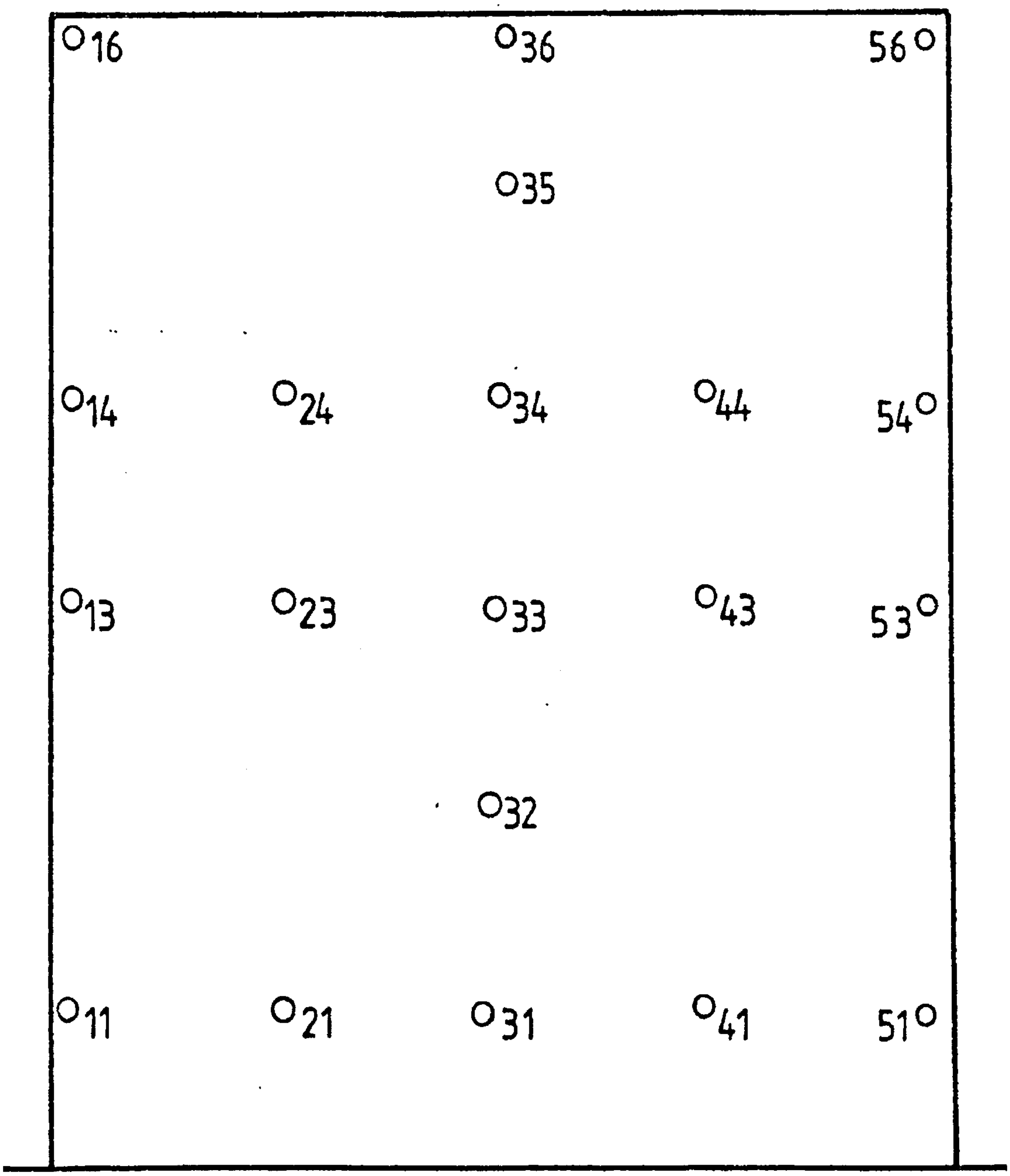
16
36
56
35
14
24
34
44
54
13
23
33
43
53
32
11
21
31
41
51

Picture – 4.

Scheme of vertical wall of localization tower of unit 4. NPP Paks Hungary

note:

numbers:– identification of spots – first number – rows (vertical position)
– second number – columns (horizontal position)

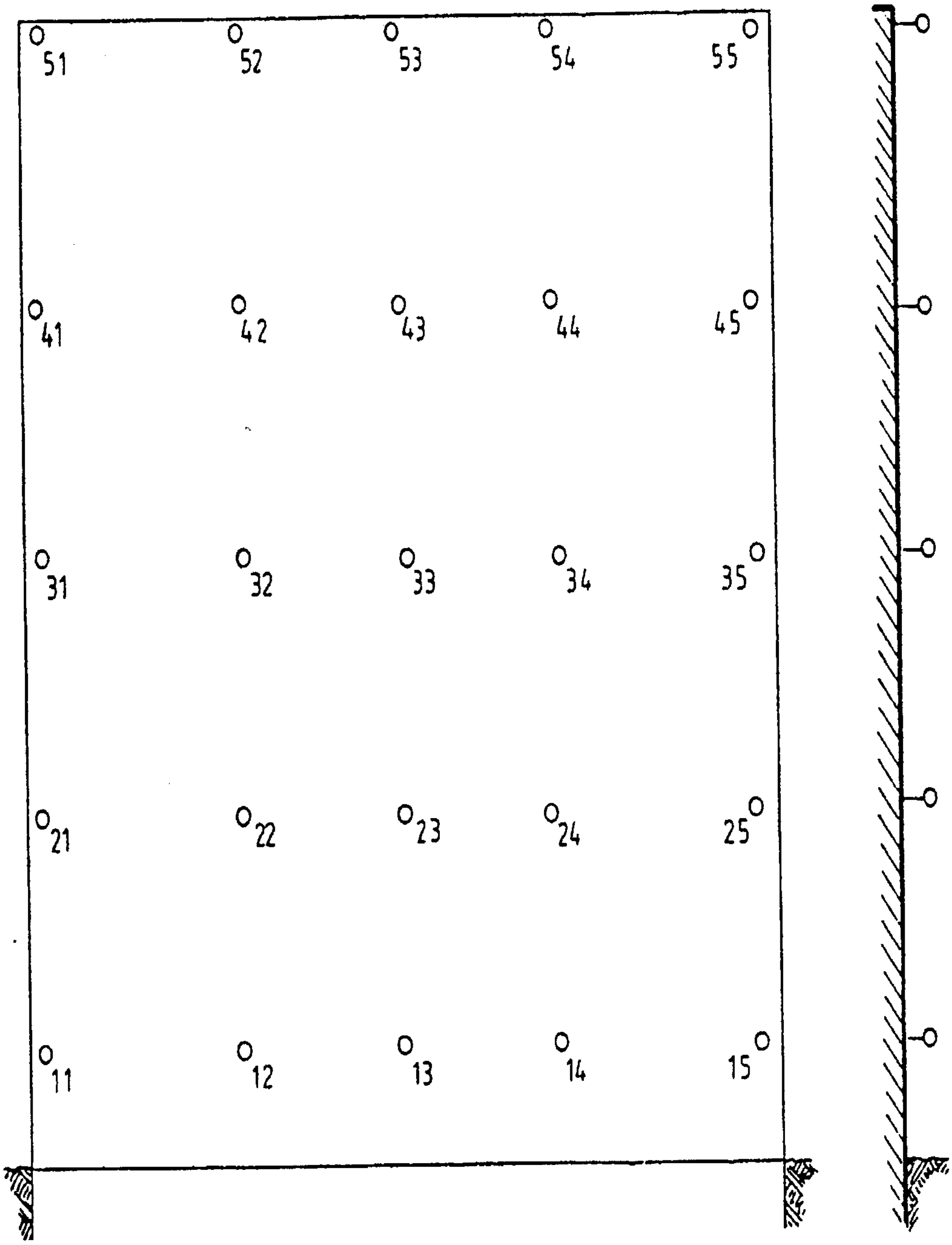
51
52
53
54
55
41
42
43
44
45
31
32
33
34
35
21
22
23
24
25
11
12
13
14
15

Picture – 5.

Paks NPP Unit 3 finite element model, looking South-West.

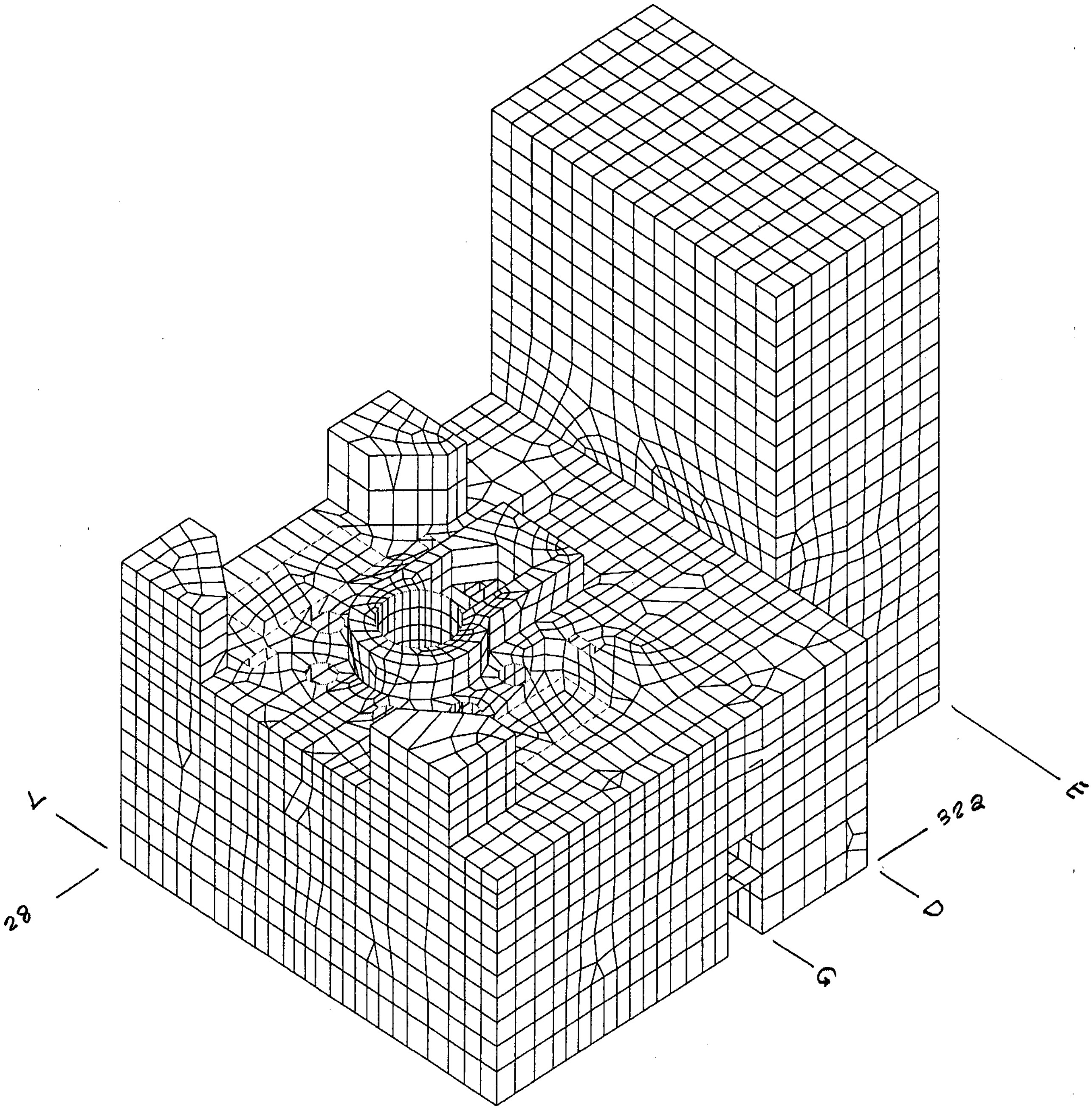

Picture – 6.

The mean and 95% confidence containment fragility curves.

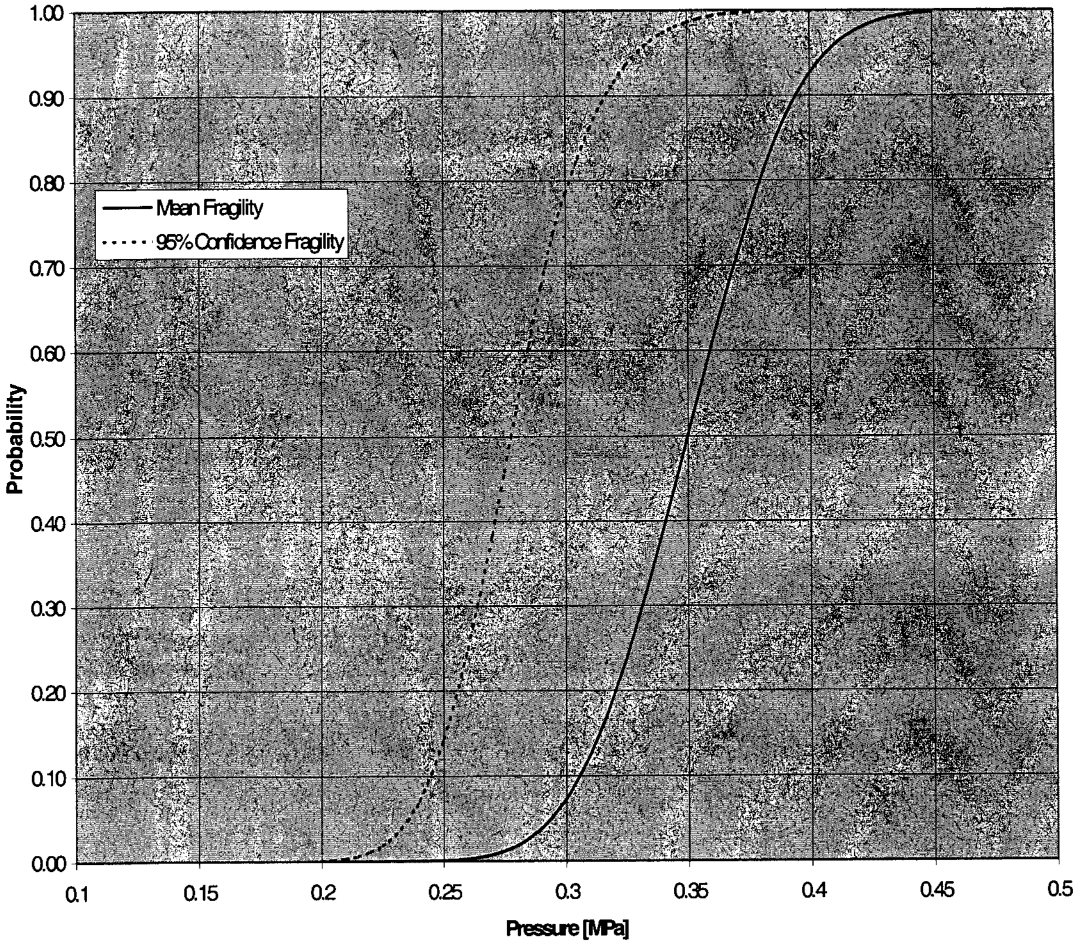

OECD NEA ISP 48 LYON FRANCE 6-7 APRIL 2005

The creep of confinement building's elements, Finite element analisys on confinement Ageing program

CSABA NYÁRÁDI
senior engineer
Paks Nuclear Power Plant Ltd.
P.O.B 71. 7031 Paks,
Hungary
nyaradi@npp.hu

OECD NEA ISP 48 LYON FRANCE 6-7 APRIL 2005

ABSTRACT

The creep of confinement building's elements.

Measuring the crab of different parts of confinement building at the time during installation, designed future activity.

Finite element analisys on confinement.

Informative description: last and newest activity on FEA, selection of critical elements, fnite element analisys, limits and results.

Ageing program.

Short information about ageing program at NPP Paks.

OECD NEA ISP 48 LYON FRANCE 6-7 APRIL 2005

Content of presentation

1. Introduction
2. The construction and structure of hermetic space (confinement.)
3. The crab of confinement building's elements.
4. Finite element analisys on confinement.
5. Ageing program.

OECD NEA ISP 48 LYON FRANCE 6-7 APRIL 2005

Introduction

Paks Nuclear Power Plant is the only commercial nuclear facility in Hungary, which has been operational since 1982.

Declaring the lifetime extension program, Paks NPP pays distinguished attention on confinement integrity.

In view of future and assuring longterm safety factory NPP Paks have been doing a decision a wide range of program surveying and reconstruction.

OECD NEA ISP 48 LYON FRANCE 6-7 APRIL 2005

The panorama of NPP Paks

OECD NEA ISP 48 LYON FRANCE 6-7 APRIL 2005

The construction and structure of hermetic space (vertical cut.)

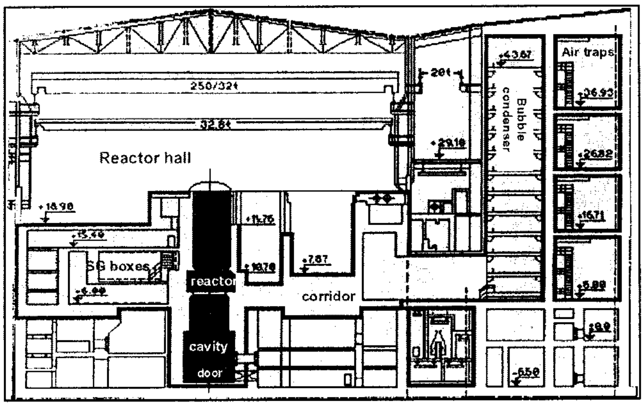
250/32t
32,8t
201
+43.67
Air traps
+36.93
Bubble condenser
+29.10
+26.82
Reactor hall
+18.90
+15.40
+11.76
+16.71
SG boxes
+10.70
+7.87
reactor
+6.90
corridor
+5.80
cavity
door
+0.0
-6.50

OECD NEA ISP 48 LYON FRANCE 6-7 APRIL 2005

The construction and structure of hermetic space (3 d sight.)

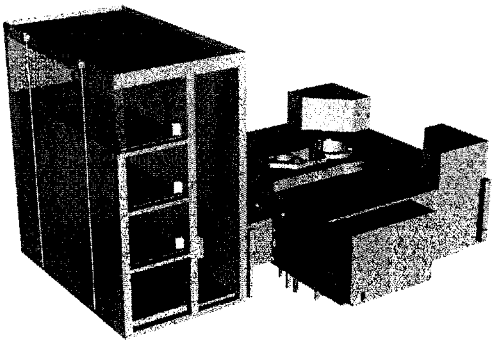

OECD NEA ISP 48 LYON FRANCE 6-7 APRIL 2005

Position of measuring points at unit 1.

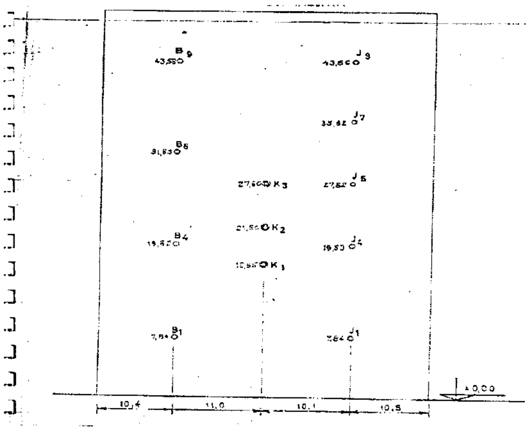
B9
43,580
J9
J7
B6
K3
J5
K2
B4
J4
K1
B1
J1
10,4
11,0
10,1
10,5
±0,00

OECD NEA ISP 48 LYON FRANCE 6-7 APRIL 2005

There was point marked K6 had extreme shifting;

4 ± 0,88[mm]

Calculated average middle error was: ± 0,70 [mm].

Representative shifting is between
1,0 ÷ 4,0 [mm]

OECD NEA ISP 48 LYON FRANCE 6-7 APRIL 2005

Position of measuring points at unit 3.

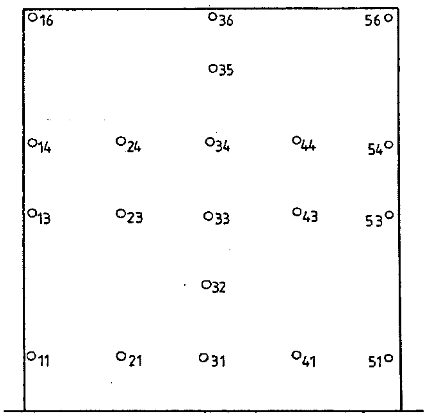
16
36
56
35
14
24
34
44
54
13
23
33
43
53
32
11
21
31
41
51

OECD NEA ISP 48 LYON FRANCE 6-7 APRIL 2005

There was point marked 35 had maximal shifting 5,7 [mm].
Calculated average middle error was ± 0,65 [mm].

In this case real extreme shifting is:

5,7 - 1.02= 4.68 [mm].

Representative deformation is between :

1,7 ÷ 4,4 [mm].

OECD NEA ISP 48 LYON FRANCE 6-7 APRIL 2005

Position of measuring points at unit 4.

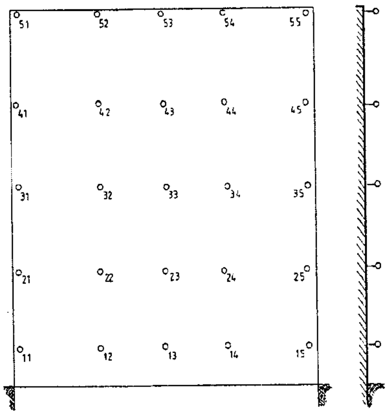
51
52
53
54
55
41
42
43
44
45
31
32
33
34
35
21
22
23
24
25
11
12
13
14
15

OECD NEA ISP 48 LYON FRANCE 6-7 APRIL 2005

There was spot marked 43 had maximal shifting 3,2 [mm].
Calculated average middle error was ± 0,60 [mm].

In this case real extreme shifting is:

3,2 – 0.6= 2.6 [mm].

Representative deformation is between:

0,3 ÷ 2,6 [mm].

OECD NEA ISP 48 LYON FRANCE 6-7 APRIL 2005

Finite element analisys on confinement - A

In 1998 we initiated an analysis to investigate adequacy of critical elements of hermetic wall.

In frame this work it was perform a finite element analysis.

Calculation was executed with

COSMOS/M v. 2.0 and AXIS-3D v. 2.55 software.

OECD NEA ISP 48 LYON FRANCE 6-7 APRIL 2005

Finite element analisys on confinement - A

VVER-440/213 type has a rectangular shape, then again general construction is cylindrical.

Appointed parts of hermetic boundary:

No.	DESIGNATION	PIECES / UNIT
1.	LINER	
2.	PIPE PENETRATIONS	929
3.	PIPE OENETRATIONS – SPARE	156
4.	HERMETIC LOCKS – RECTANGULAR AND CYLINDRICAL	20 – TOTAL AMOUNT
5.	HERMETIC DOORS	27
6.	REACTOR SHAFT DOME	1
7.	HERMETIC AIR FLAPS	12

OECD NEA ISP 48 LYON FRANCE 6-7 APRIL 2005

Finite element analisys on confinement - A

Calculated feasibility of failures you can study in table below:

No.	PART OF CONSTRUCTION	FEASIBILITY OF FAILURE
1.	Connection between liner and r.c.	$5{,}8 * 10^{-8} \div 10^{-10}$
2.	Hermetic pipe penetration	10^{-8}
3.	Hermetic pipe penetrations – spare, blinded	$5{,}1 * 10^{-4} \div 10^{-9}$
4.	Hermetic lock (3500 * 1400 [mm])	$6{,}94 * 10^{-5}$
5.	Hermetic lock (ND 3400 [mm])	$1{,}53 * 10^{-3}$
6.	Hermetic door	$5{,}67 * 10^{-5}$
7.	Reactor shaft dome	$< 10^{-9}$
8.	Hermetic air flap	$< 10^{-9}$

OECD NEA ISP 48 LYON FRANCE 6-7 APRIL 2005

Finite element analisys on confinement - A

Final conclusion of study:

Feasibility of hermetic area's leakage

caused by failure of parts of construction depending on overpressure to be more than limited by authority

is no more than 0,015 .

OECD NEA ISP 48 LYON FRANCE 6-7 APRIL 2005

Finite element analisys on confinement - B

As part of Level 2 PSA, an evaluation of the capacity of the containment structure for elevated pressure and temperature loadings was executed.

The items on the pressure boundary can be divided to two main categories:

(1) The reinforced concrete structural components, i.e., the walls and slabs (and a relatively small number of structural beams and columns)

(2) various penetrations through the reinforced concrete elements, such as doors, equipment hatches, electrical and piping penetrations, etc

OECD NEA ISP 48 LYON FRANCE 6-7 APRIL 2005

Finite element analisys on confinement - B

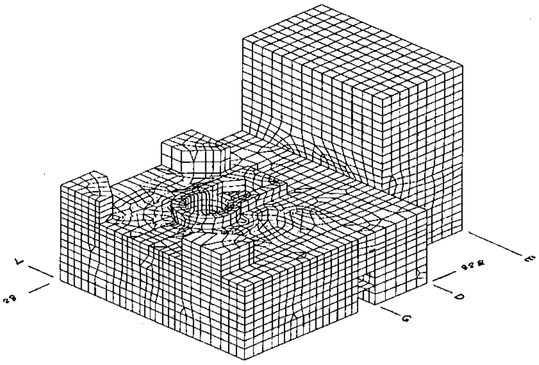

Paks NPP Unit 3 finite element model, looking South-West

OECD NEA ISP 48 LYON FRANCE 6-7 APRIL 2005

Finite element analisys on confinement - B

The mean overall containment capacity was computed to be
0.35 [MPa]
, and the “high confidence of low probability of the failure” capacity as
0.235 [MPa].

The mean and 95% confidence containment fragility curves are shown on next page

---

OECD NEA ISP 48 LYON FRANCE 6-7 APRIL 2005

Finite element analisys on confinement - B

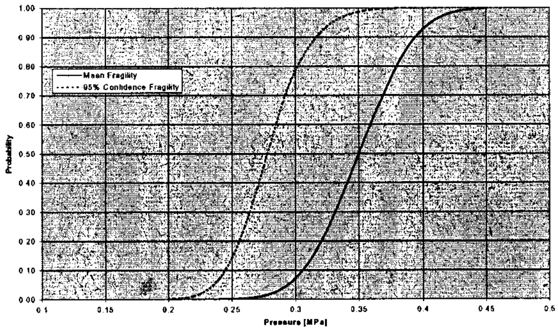

The mean and 95% confidence containment fragility curves.

OECD NEA ISP 48 LYON FRANCE 6-7 APRIL 2005

Temperature Effects

Temperature effects within the range of temperatures specified for the study have negligible effect on Paks containment overpressure study results.

The effect to concrete and reinforcing steel strength due to the about 90[°C] temperature rise on the interior surface is negligible

---

OECD NEA ISP 48 LYON FRANCE 6-7 APRIL 2005

Temperature Effects

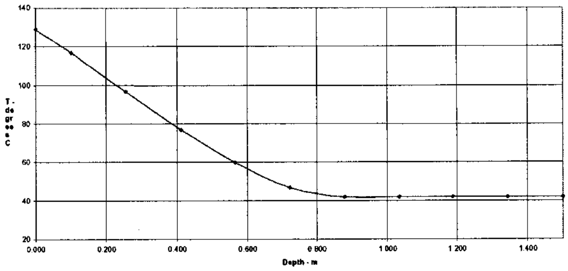

Typical temperature distribution through a steam generator compartment wall at about 48 hours after event

GRS CALCULATIONS IN THE FRAMEWORK OF ISP48 ON SANDIA PRE-STRESSED CONCRETE CONTAINMENT MODEL

Hans Grebner, Jürgen Sievers
Gesellschaft für Anlagen- und Reaktorsicherheit (GRS) mbH, Köln, Germany

Abstract

Large scale tests of the failure behaviour of a 1:4 scaled pre-stressed concrete containment vessel with metallic liner were performed at Sandia National Laboratories (Albuquerque, New Mexico) in the years 2000 and 2001.

The tests were basis for the International Standard Problem ISP 48, defined to perform an international comparative study on the present state of analysis methods used for the assessment of pre-stressed concrete containments concerning load-carrying capacity. The tasks within ISP48 include loading of the containment model by internal pressure or by superposition of pressure and temperature gradients in the wall. Especially the failure behaviour as well as the cracking and the formation of leaks through cracks in the steel liner and the concrete are of interest. In the paper selected results of GRS analyses are summarized.

Introduction

At SANDIA National Laboratories (Albuquerque, New Mexico) a series of large scale tests with model containments have been performed during the last 15 years. First a 1:6 scaled reinforced concrete model was investigated [1]. GRS has performed pre- and post-calculations of the structural behaviour of that model containment [2]. Then the failure behaviour of a mixed scale steel containment was studied [3].

Recently large scale tests of the failure behaviour of a 1:4 scaled pre-stressed concrete containment vessel were performed [4]. **Fig. 1** gives a schematic view of the containment model, which includes a thin metallic liner at the inner surface. A view of the completed model before the start of the experiments is shown in **Fig. 2**.

In combination with the tests calculations were carried out by several institutions. After completion of the tests the International Standard Problem (ISP) No. 48, supported by CSNI-IAGE working group, was defined to perform an international comparative study on the present state of analysis methods used for the assessment of pre-stressed concrete containments concerning load-carrying capacity. Especially the failure behaviour in the steel liner and the concrete are of interest. GRS participates in ISP 48 [5,6]. In the following exemplary analysis results are summarized.

Basis of the standard problem is the so-called Limit State Test [4] which is characterized by an increase of internal pressure up to 1.29 MPa (about 3.3 times design pressure). At this pressure the leak rate through leaks in the steel liner and the concrete was higher than the amount which could be compensated by the nitrogen supply system.

After repair of the liner a further test (called Structural Failure Mode Test) was performed. Before this test the model was nearly completely filled with water. The internal pressure was generated by a small amount of nitrogen. At about 1.33 MPa single circumferential tendons broke. The test ended with a catastrophic failure of the containment model, as described in [4]. A maximum pressure value of 1.42 MPa (about 3.63 times design pressure) was reached in this case.

Analysis - models

First axisymmetric finite element models of the 1:4 containment vessel were developed to simulate the structural behaviour without consideration of geometric inhomogenities due to penetrations in the wall. **Fig. 3** shows the analysis model and its main components.The steel liner at the inner surface and the concrete parts are represented by 8-node isoparametric elements with 4 integration points, while the rebars and tendons are modelled as truss elements (with 3 nodes for the meridional and radial ones and one node for those in hoop direction). At the present stage a stiff coupling between steel and concrete is simulated. Dimensions and material data are taken from [4].

During performance of the calculations with the axisymmetric model it became obvious that the dome behaviour could not be simulated well. Therefore a full three-dimensional model of a 90°-section of the containment model was developed additionally. The complete finite element model and some details are shown in **Fig. 4**. Here the position of the tendons in the dome part fully coincides with the SANDIA containment model. Again rebars and tendons are simulated by truss elements. For the concrete parts 8-node isoparametric 3d-elements are used and the liner is simulated by shell elements.

While studying the second case of Phase 3 of the ISP numerical problems showed up in calculations with the global models shown in Fig. 3 and Fig.4. To get some local information a very simple axisymmetric model consisting of a section (slice) of the cylindrical part of the containment was considered. The model is shown in **Fig. 5**. It contains all rebar and tendon elements located in the slice.

For the liner, the rebar elements and the tendons elastic-plastic material models with temperature dependent data are used. The concrete material model includes the formation of micro-cracks for tensile stresses exceeding a critical value as well as crushing for high compressive stresses. **Figs. 6** and **7** show the uniaxial stress-strain curves for steel components and concrete at room temperature used in the material models. The temperature dependence of some data is shown in **Figs. 8** and **9.** Here as example the behaviour of the yield stress of the steel components and of Young's modulus and the maximum tensile strenght of concrete as function of temperature is shown.

The pre-stressing of the tendons is simulated by initial strains in the respective truss elements. The containment model is loaded by increasing internal pressure or by a combination of pressure and temperature loading. For the calculations the finite element program system ADINA [7] was used.

Loading

As described before calculations were performed on the so-called Limit State Test with internal pressure loading (Phase 2 of ISP 48). Additionally two fictitious loading cases with a combination of internal pressure and temperature loading were considered (Phase 3 of ISP 48). In case 1 a simultaneous increase of pressure and temperature (as for saturated steam) was considered, while in case 2 a station blackout scenario is simulated. The time dependence of internal pressure and temperature at the inner surface of the containment for the two cases is shown in **Figs. 10** and **11.** Resulting temperature distributions in a typical cross section of the containment model are shown in **Figs. 12** and **13**. The temperature values were gained by heat conduction calculations with an axisymmetric model performed by David Evans and Associates (DEA) [8] with the temperatures of Figs. 10 and 11 as boundary conditions and were made available to the ISP participants [9]. The temperatures given at several cross sections as well as interpolated values were used as loading in the GRS calculations of the respective cases. From Figs. 8 and 9 it can be seen that for case 1 (temperatures up to 200°C) the temperature dependence of the material data is of little influence.

Analysis results on pressure loading

Some typical results of the different calculations of the pressure only case (Phase 2) are summarized in the **Figs. 14** to **23**.
If possible numerical results are compared to experimental results of the Limit State Test.

Figs. 14 to **17** show the deformation of the complete axisymmetric model for different values of internal pressure.

Figs. 18 and **19** present the radial displacements at 6.2 m from the basemat and the vertical displacements at the top of the dome (16.2 m) as function of internal pressure. For the vertical displacement of the top of the dome the axisymmetric model shows larger deviations to the experiment at pressure values above 0.75 MPa, while the 3d-results show a much better coincidence. This is mostly due to the more realistic modelling of the tendons in the 3d-model especially in the dome region. The axisymmetric model can not provide an adequate modelling of the hairpin tendons in the upper dome part. Furthermore the formation of micro-cracks and the post-cracking stiffening behaviour have influence on the vertical deformation of the dome. Further investigations are in progress.

Figs. 20 to **23** give further examples of comparisons between calculations (axisymmetric and 3d) and measurement, especially strains in the concrete, of the liner, rebars and tendons at typical locations in the cylindrical part of the model. Due to numerical problems at present for the 3d-calculation only results up to 1.1 MPa internal pressure are available.

For pressure loading up to 0.6 MPa (about 1.5 times design pressure) the calculated results of displacements and strain in the concrete, the liner, the rebars and the tendons agree very well with measured data. Major differences between experiment and analysis are found in the pressure region of about 0.6 to 0.74 MPa in which the crack formation in the concrete starts. The extension of micro-cracks in the slice model is presented in **Fig. 24**. The orientation of these micro-cracks is perpendicular to crack opening stresses in circumferential and axial direction. In this pressure region the deviations may be due to a too stiff coupling of concrete and steel in our finite element models, which will be investigated by further studies.

For the pressure region 0.75 to 1.0 MPa mostly a good coincidence of calculation and measurement is found. Above 1.0 MPa plastification starts in the hoop rebars and again larger differences between experiment and calculation are found. At the maximum load of the limit state test (1.29 MPa) hoop tendon strains of nearly 1% are calculated with the models, which is about 30% of the uniaxial rupture strain. The maximum strain values in the rebars and the liner range below 1%. Thus a larger difference to the uniaxial rupture strain is found in this case. The structure behaviour of the cylindrical section for pressures above 1.3 MPa could be simulated only with the axisymmetric slice model. It shows increase of deformation and strains with much greater gradients due to strong plastification of the steel components. All in all it is expected that the failure of the model containment in the Structural Failure Mode Test which started with breaks of single circumferential tendons at 1.33 MPa can only be predicted by consideration of the geometric inhomogenities due to penetrations.

Analysis results on pressure and temperature loading

The next results presented are for the calculations with combined pressure and temperature loading (Phase 3, case 1 and 2), starting with case 1.

Curves of the radial displacement are shown in **Fig. 25** for the slice model and the axisymmetric complete model (height position 6.2 m above basemat) for the case 1 temperature load compared to pressure only results for the axisymmetric complete model. The coincidence between the two models is very good, while a significant difference is found for the two load cases. **Figs. 26** and **27** present hoop stresses and strains in the concrete for integration points near inner and outer wall for the slice model. The figures show that the pre-stressing of the concrete near the outer surface disappears due to the temperature gradient only, i.e. in case 1 even with internal pressure equal to zero. Due to the thermal gradient near the outside of the wall axial micro-cracks are initiated at very low pressure values, while near the inside the micro-cracks start at pressure values of about 0.7 MPa. **Fig. 28** shows hoop and meridional strains in the liner. **Fig. 29** presents a comparison of the inner and outer hoop rebar strain (for the slice model). The influence of the thermal gradient in the wall causes compressive strains for the inner rebar up to about 0.6 MPa while the outer rebar starts directly with tensile strains. Furthermore the behaviour of the tendons is presented in **Fig. 30**. While the meridional tendon remains elastic, the plastification in the hoop tendon starts at about 1.3 MPa. At the end of the transient a strain value of about 2.7% is reached which is not very far away from the rupture strain.

Finally some exemplary results for case 2 are given. Due to numerical problems this load case was calculated with the slice model only, i.e. the results shown are representative for a cylindrical section at 6.2 m above the basmat. **Fig. 31** shows the time dependence of the radial displacement at the inner surface of the model. Comparisons of hoop strains of concrete positions near inside or outside of the wall are shown in **Fig. 32**. As at the inside integration point in the concrete high temperatures occur, in the first 30 hours of the transient compressive strains are found in this case. The differences between inside and outside at the end of the transient are again due to the thermal gradient through the wall. **Fig. 33** shows the behaviour of hoop and meridional liner strains, where mainly compressive strains are found. Hoop rebar strains for inner and outer rebars are given in **Fig. 34**. Furthermore the tendon strains are presented in **Fig. 35**. Although for short times the inner surface experiences temperature values up to 600°C, at the position of the tendons (at about 58% of the wall thickness) the temperature values remain below 80°C during the whole transient (compare Fig. 13). Therefore the tendons remain elastic until the end of the transient, where the hoop tendon just reaches the beginning of plastification.

As in the pressure only case the calculations with temperature loading (case 1 and case 2) show regions with plastification (even at smaller pressure values). Again the maximum strain values are below the critical ones in both cases, but in case 1 the hoop tendon strains show only a small margin to the rupture strain.

Crack opening displacements

If the maximum principal stress in an integration point of a concrete element reaches the maximum tensile stress in the concrete $\square_t$ (see Fig. 7), a micro-crack is formed at this point according to the smeared crack approach [7]. The stress normal to the crack surface at this point gradually decreases to zero, while the normal strain $\square$ may be related to the crack opening displacement $\square$ by the equation [10]:

$$\delta = (\varepsilon - \varepsilon_t) \cdot l_e$$

Here $\square_t$ is the strain-value corresponding to the maximum tensile stress $\square_t$ and l_e is a characteristic length of the finite elements considered. If the fracture energy G_f of concrete is used as input to ADINA, l_e may be evaluated by the relation [7]:

$$l_e = \frac{2 \cdot E_0 \cdot G_f}{\sigma_t^2 \cdot \xi}$$

E_0 is the initial Young's modulus. $\square$ describes the normal strain value ($\square \cdot \square_t$), where the normal stress reaches zero. **Fig. 36** shows a typical example of the circumferential stress versus strain behaviour, calculated for the pressure only case at a concrete integration point of the slice model. If one considers a line of integration points through the containment wall, for different pressure values crack opening profiles can be evaluated as presented in **Fig. 37**. At the internal pressure 1.4 MPa a crack opening displacement of about 0.3 mm is calculated through the wall.

To use this result for a leak rate evaluation it must be taken into account that an axisymmetric finite element model simulates only one radian i.e. about 60° in circumferential direction. In the SANDIA containment model a large number of axial cracks was found for the complete circumference (see [4]), but there is no information available about measured crack widths. Further work is necessary on that topic.

Summary

The SANDIA tests of the 1:4 pre-stressed containment model of a PWR are used as basis for analyses performed in the framework of the International Standard Problem ISP48. GRS participates in this ISP with finite element calculations. For this purpose axisymmetric and 3d models were developed. The concrete parts are simulated by 8-node elements, while for rebar steels and tendons truss elements are used. The metallic liner at the inside of the containment is model either by 8-node or by shell elements. The necessary input data for the non-linear material models used were deduced from data made available by SANDIA. The models are loaded by the pre-stressing of the tendons and by increasing internal pressure (up to about 1.3 MPa) as well as by additional thermal loads.

The analyses for the pressure only case show that first axial micro-cracks in the concrete are found at about 0.75 MPa and above about 0.9 MPa micro-cracks in the other directions are found. At the maximum load (1.3 MPa) almost all concrete parts of the model have micro-cracks which may cause leaks.

Nevertheless the failure of the containment model is not expected for loads up to 1.3 MPa without consideration of geometric inhomogenities due to penetrations in the wall. Although the calculated strains in liner, rebars and tendons show some plastification, the maximum values are below the critical ones.

The studies of the cases with temperature loading indicate that a failure of the model containment due to the combined pressure and temperature load is not expected in the regions far away from penetrations in the wall although the safety margins concerning the hoop tendon strain are relatively small.

Finally a first attempt to estimate crack opening displacements in the concrete from the finite element results is presented.

Acknowledgement

The work described in this paper is sponsored by the German Ministry of Economics and Labor.

References

[1] Horschel, D. S., Jung, J. (1986), Construction and Analysis of a 1/6th-scale Concrete Containment Model. SAND 86- 1089 C.
[2] Bachmann, P., et al. (1988), Analyse zur Bestimmung des Versagensdruckes und des Versagensverhaltens eines Stahlbetoncontainments im Maßstab 1:6 (Vorausberechnungen). GRS-A-1415.
[3] Luk, V. K., et al. (2000), Design, Instrumentation and Testing of a Steel Containment Vessel Model. NUREG/CR -5679 .
[4] Hessheimer, M. F., et al. (2003), Overpressurization Test of a 1:4 Scale Pre-stressed Concrete Containment Model. NUREG/CR-6810.
[5] ADINA (2003), A Finite-Element-Program for Automatic Dynamic Incremental Nonlinear Analysis, Version 8.1 – Theory and Modeling Guide, Volume I: ADINA. ADINA R&D, Inc., Watertown, Massachusetts.
[6] Grebner, H., Sievers, J. (2004), Structure Mechanics Analysis of the Pres-stressed Concrete Model Containment Tested at Sandia National Laboratories- Contribution to International Standard Problem (ISP) 48. NEA/CSNI/R(2004)11, 213-233.
[7] Grebner, H., Sievers, J. (2005), Structure Mechanics Analysis of the Pres-stressed Concrete Model Containment Tested at Sandia National Laboratories- Contribution to International Standard Problem (ISP) 48, Phase 3. To appear in ISP 48 phase 3 report.
[8] Dameron, R., et al. (2004), Analysis of Axisymmetric Prestressed Concrete Containment Vessel (PCCV) Including Thermal Effects. Report David Evans and Associates, Inc., San Diego, California.

[9] Hessheimer, M. F. (2004), E-Mail on Temperature Gradients dated August 24, 2004.
[10] Curbach, M. (1987), Festigkeitssteigerung von Beton bei hohen Belastungsgeschwindigkeiten. Doctor-Thesis, Karlsruhe.

Figure 1. **Major dimensions of the pre-stressed containment model (the wall includes hoop, meridional and radial rebars as well as hoop and meridional tendons)**

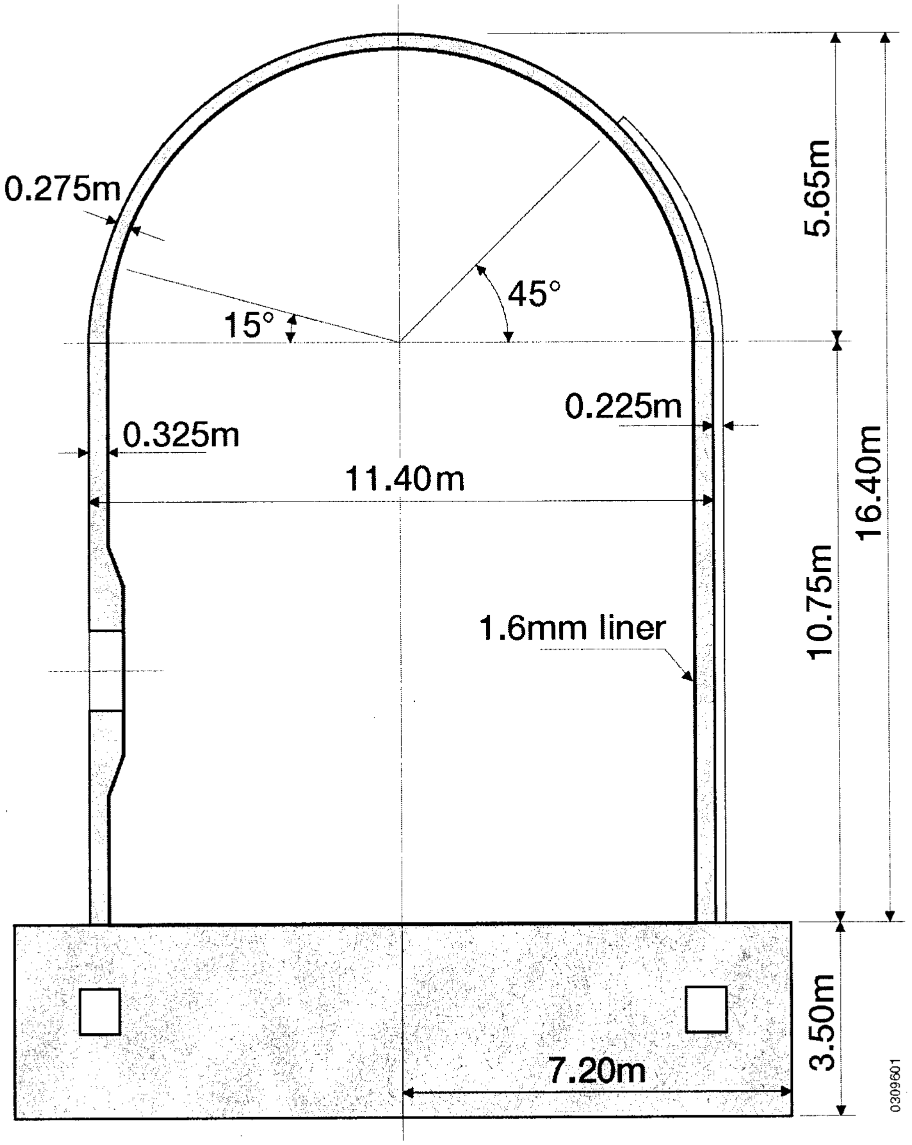
0.275m
15°
45°
0.225m
0.325m
11.40m
1.6mm liner
7.20m
5.65m
10.75m
16.40m
3.50m
0309601

Figure 2. View of the completed Sandia containment model (from [4])

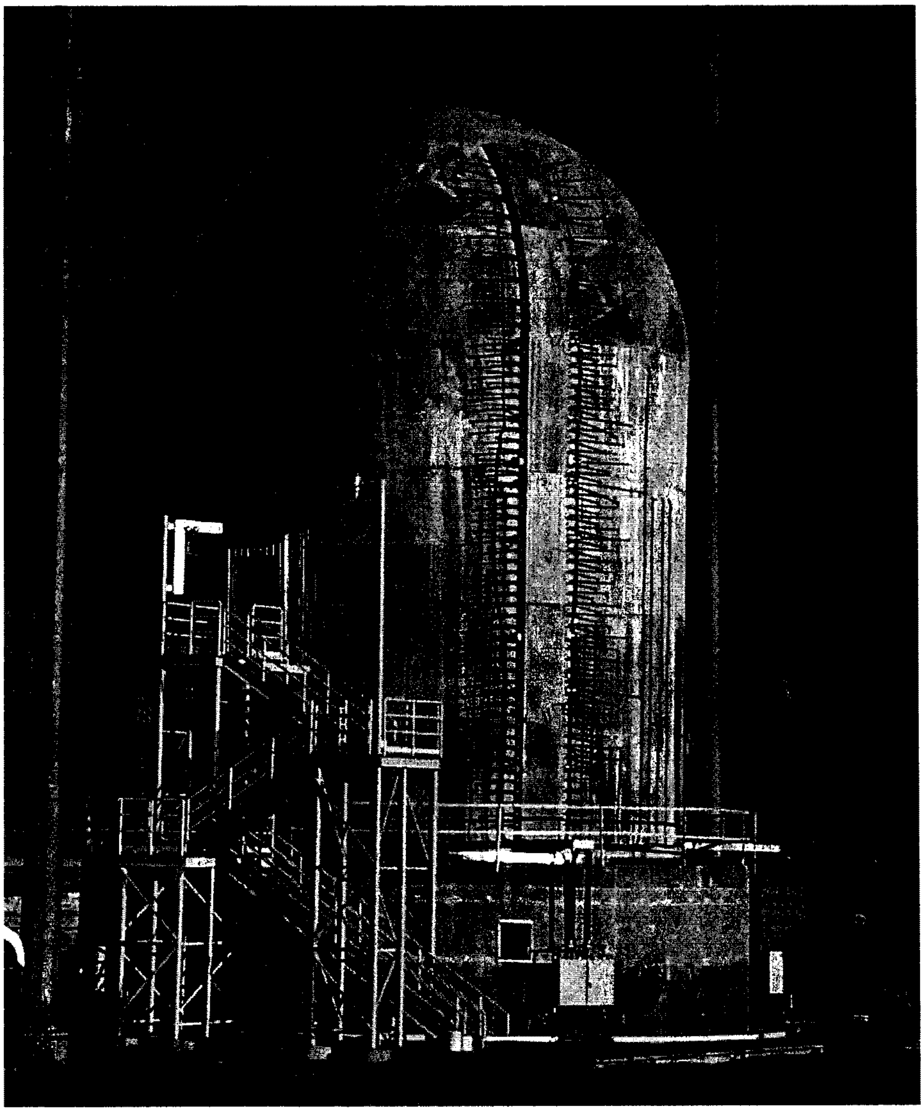

Figure 3. Axisymmetric finite element model

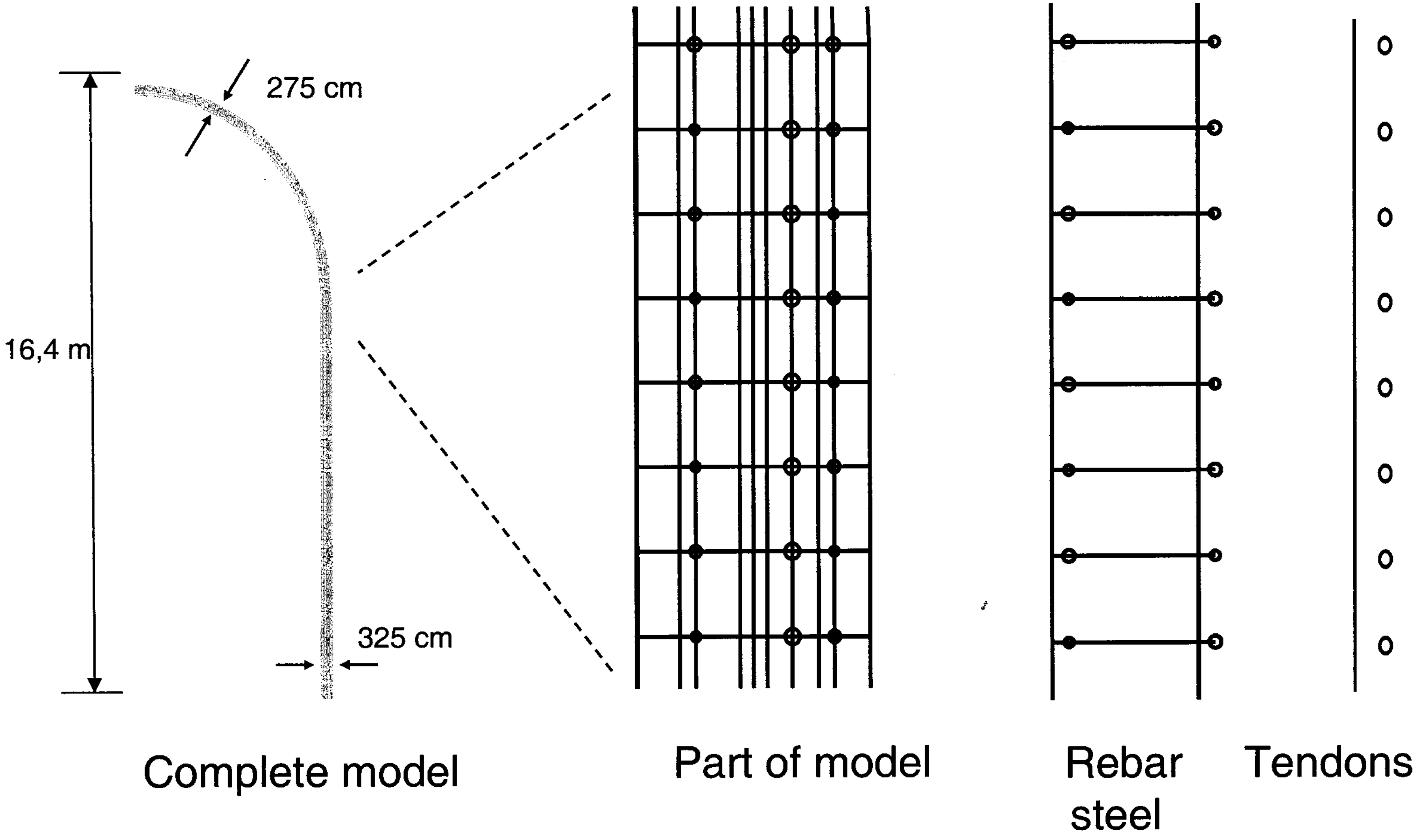
275 cm
16,4 m
325 cm
Complete model
Part of model
Rebar steel
Tendons

Figure 4. **3d finite element model of a 90°-section**

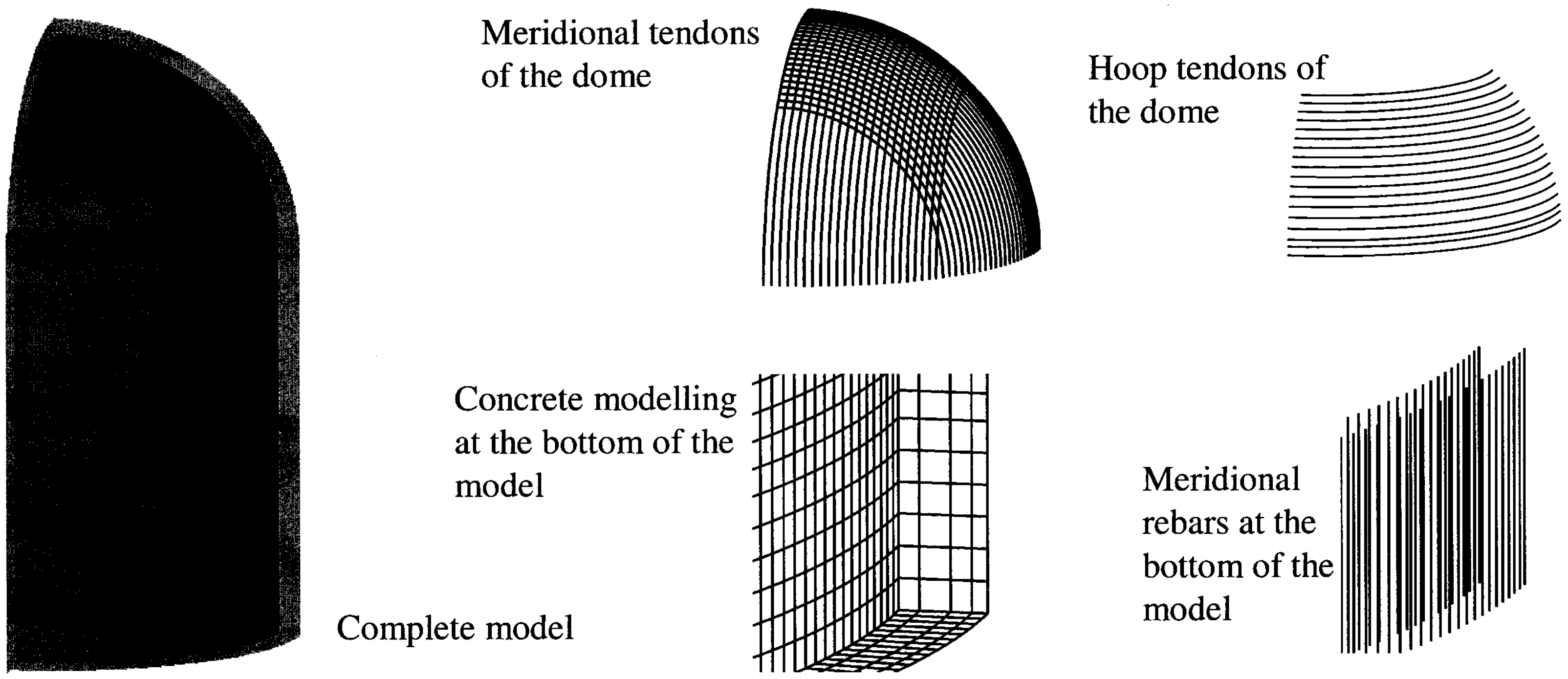
Meridional tendons of the dome
Hoop tendons of the dome
Concrete modelling at the bottom of the model
Meridional rebars at the bottom of the model
Complete model

Figure 5. Axisymmetric finite element model of a cylindrical section (slice model)

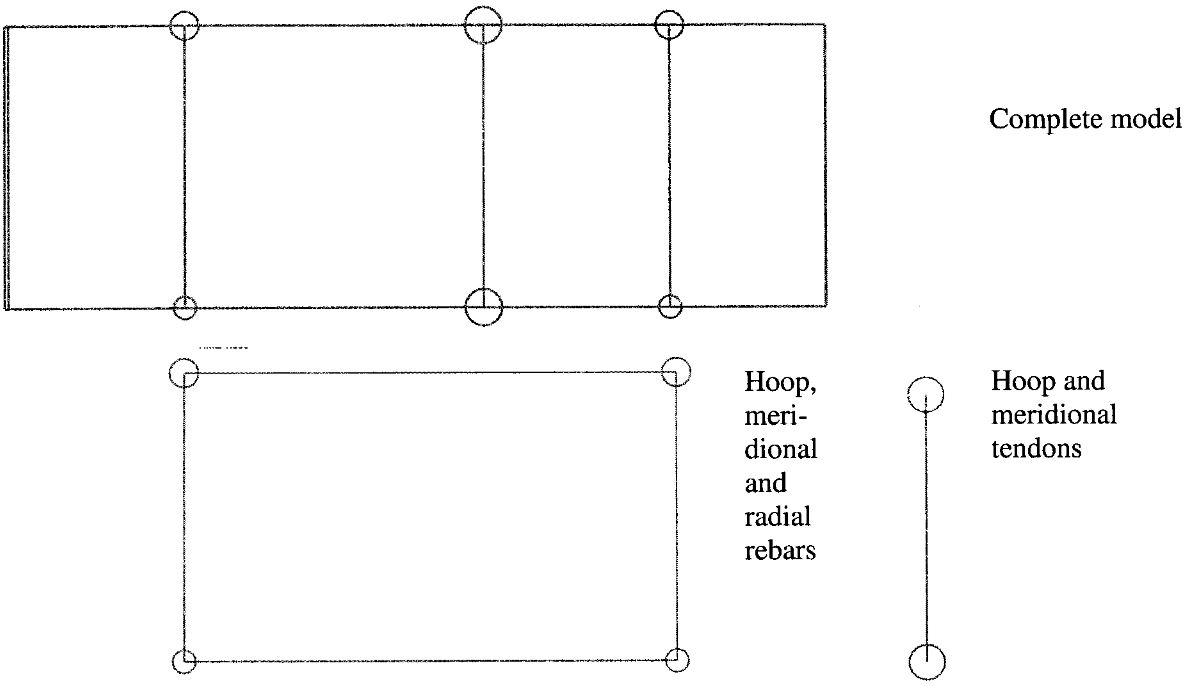
Complete model
Hoop, meridional and radial rebars
Hoop and meridional tendons

Figure 6. Uniaxial stress-strain curves used in the steel components (at 24°C)

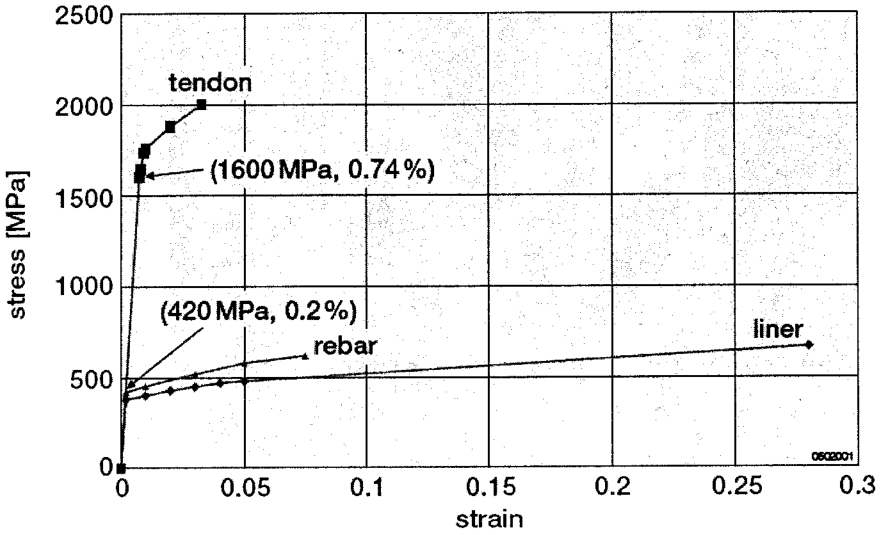

Figure 7. Uniaxial stress-strain curve used in the concrete model (schematically)

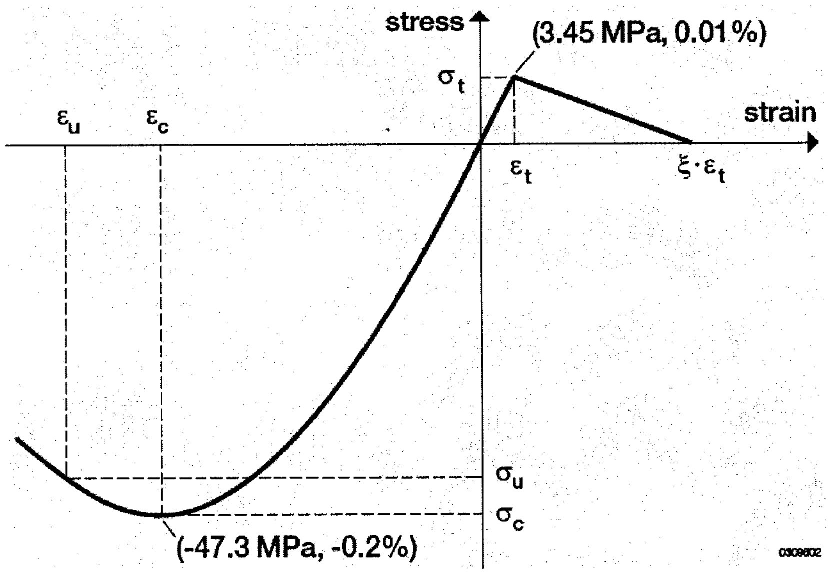
stress
(3.45 MPa, 0.01 %)
σ_t
strain
ε_u
ε_c
ε_t
$\xi \cdot \varepsilon_t$
σ_u
σ_c
(-47.3 MPa, -0.2%)

Figure 8. Temperature dependence of the yield stress for the steel components

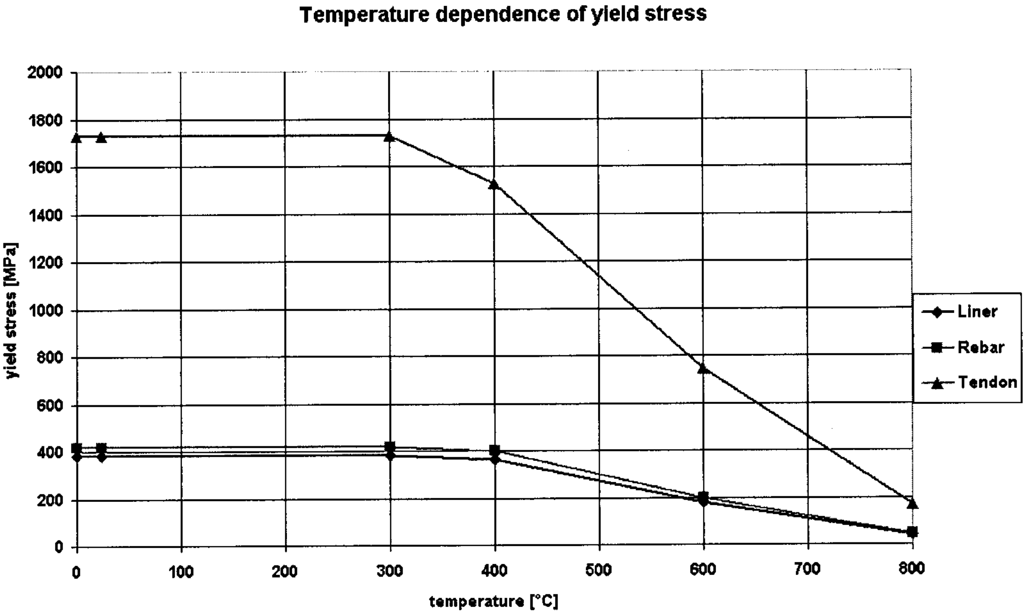

Figure 9. Temperature dependence of Young's modulus and maximum tensile stress for concrete

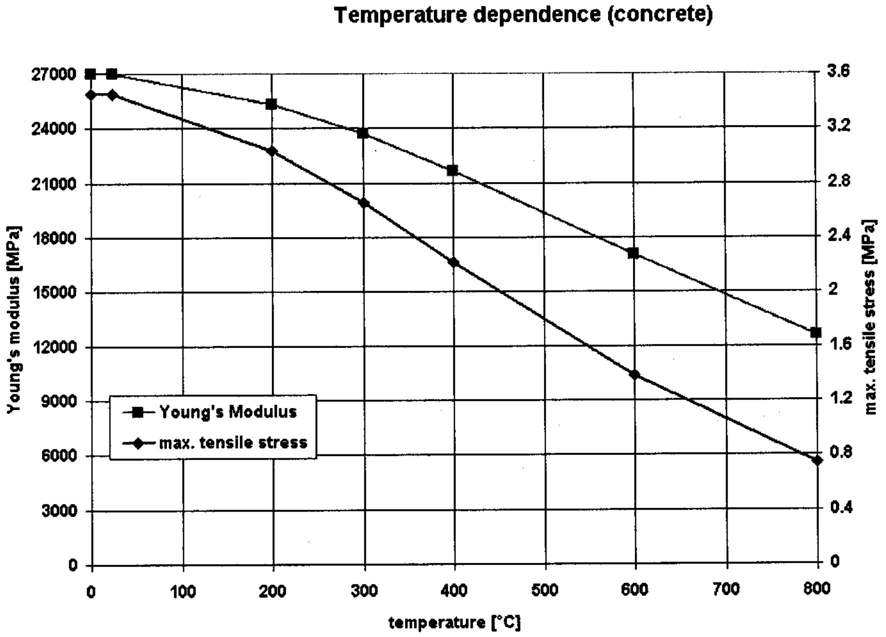

Figure 10. Time functions for pressure and temperature at inner surface ISP Phase 3, case 1 (from [9])

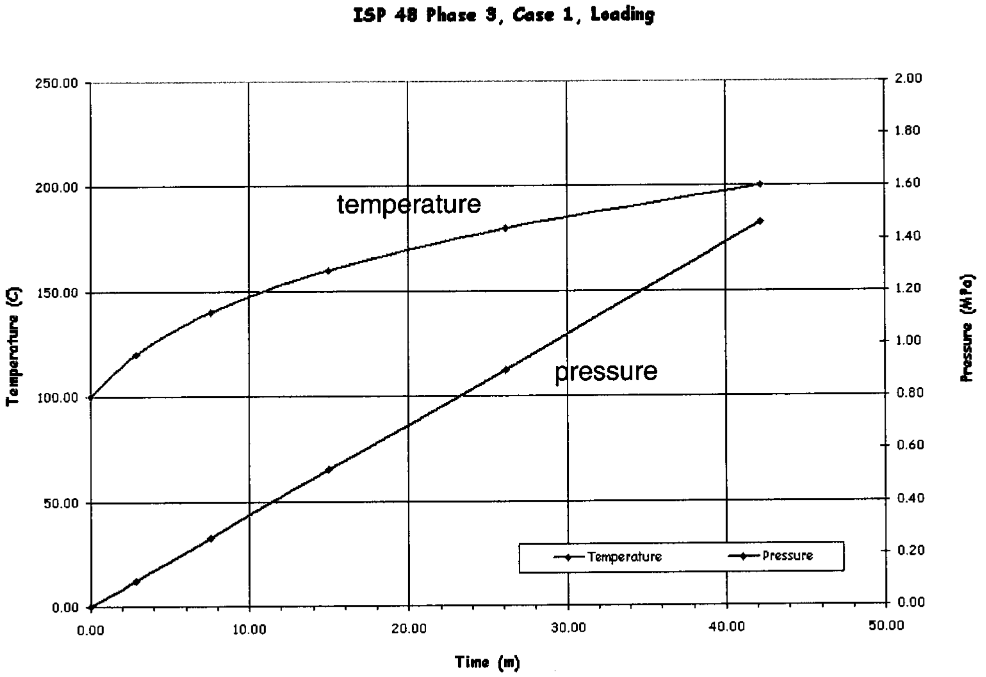

Figure 11. Time functions for pressure and temperature at inner surface ISP Phase 3, case 2 (from [9])

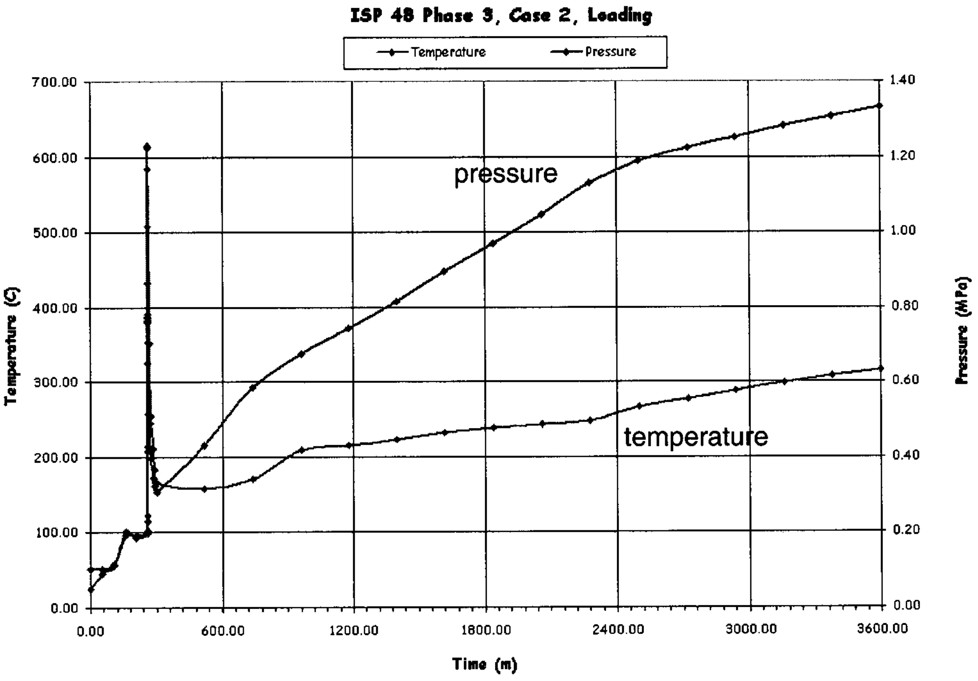

Figure 12. Time functions for temperature at different positions in the wall ISP Phase 3, case 1 (from [9])

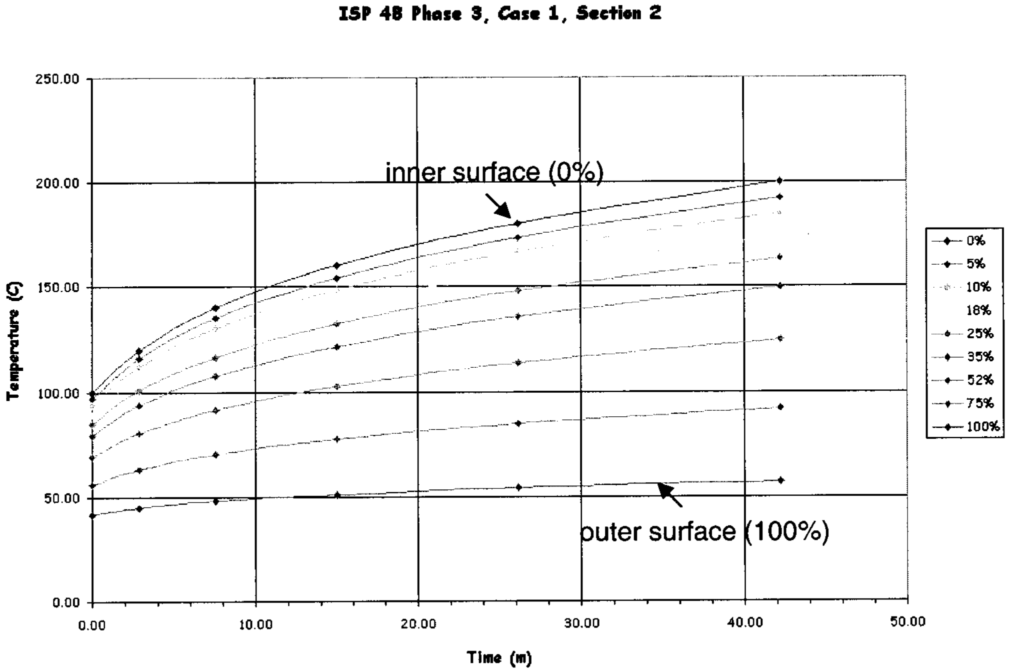

Figure 13. Time functions for temperature at different positions in the wall ISP Phase 3, case 2 (from [9])

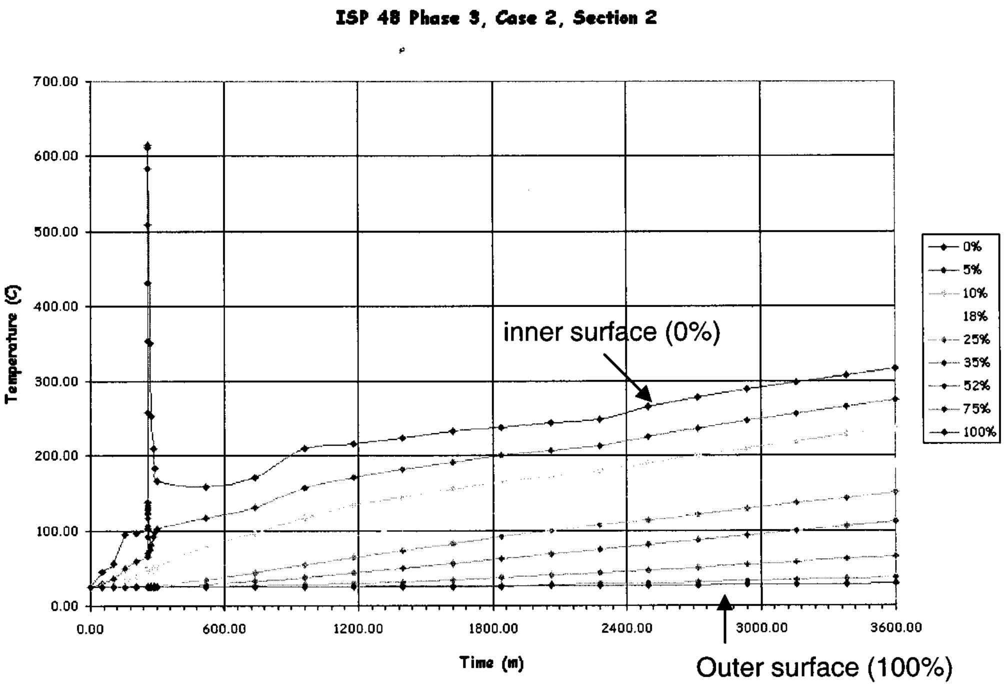

Figure 14. Deformation of axisym-metric model at 0.7 MPa (magnification of displacements = 50), pressure only case

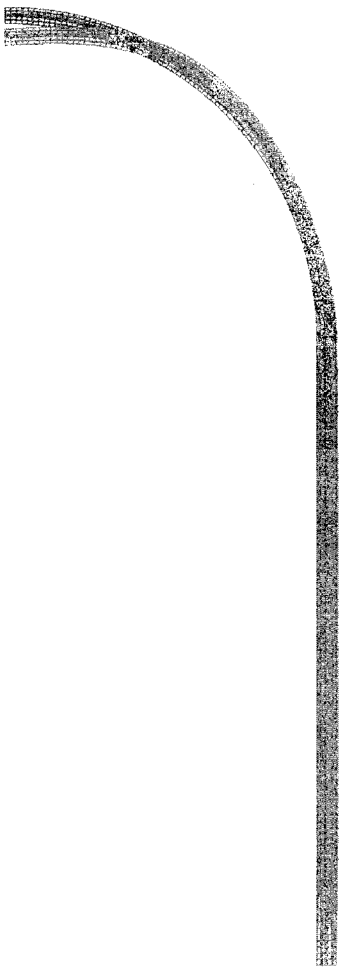

Figure 15. Deformation of axisym-metric model at 1.0 MPa (magnification of displacements = 50), pressure only case

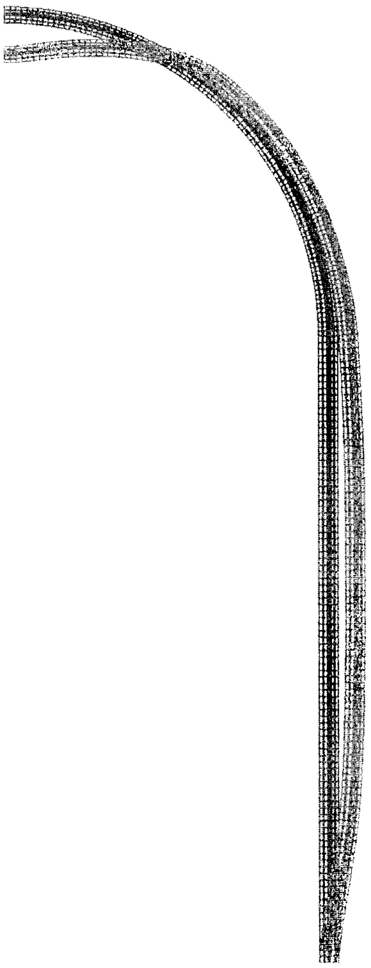

Figure 16. Deformation of axisym-metric model at 1.3 MPa (magnification of displacements = 10), pressure only case

Figure 17. Deformation of axisym-metric model at 1.4 MPa (only in calcu-lation, magnification of displacement = 10), pressure only case

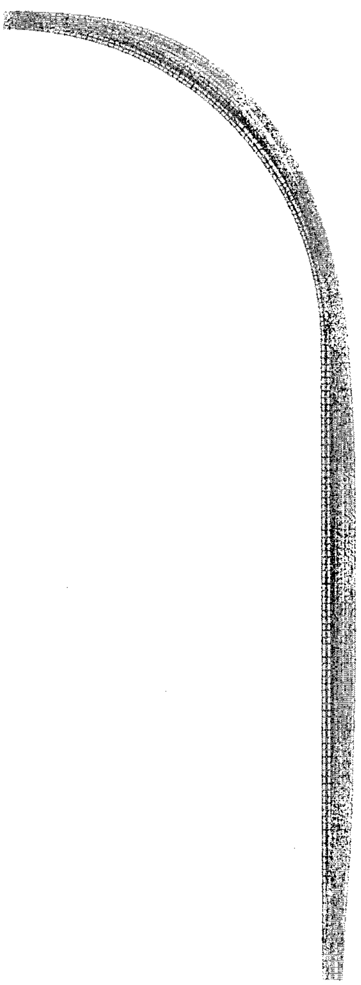

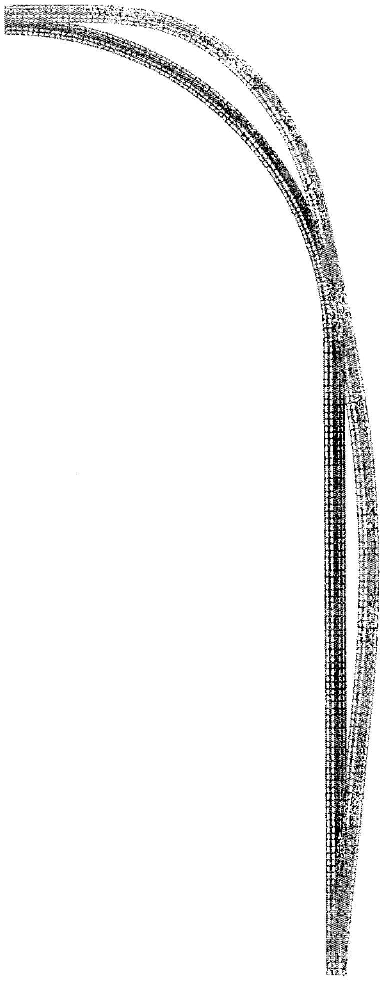

Figure 18. Radial displacements in cylindrical containment part (position 6.2 m above basemat), pressure only – experimental values and calculated results

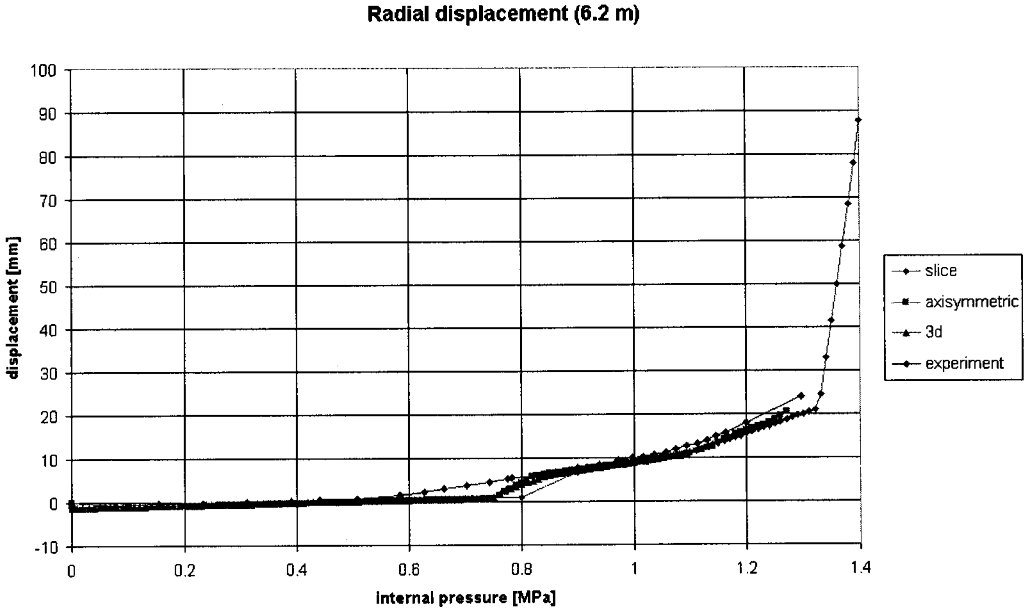

Figure 19. Vertical displacements at top of containment (position 16.12 m above basemat), pressure only – experimental values and calculated results

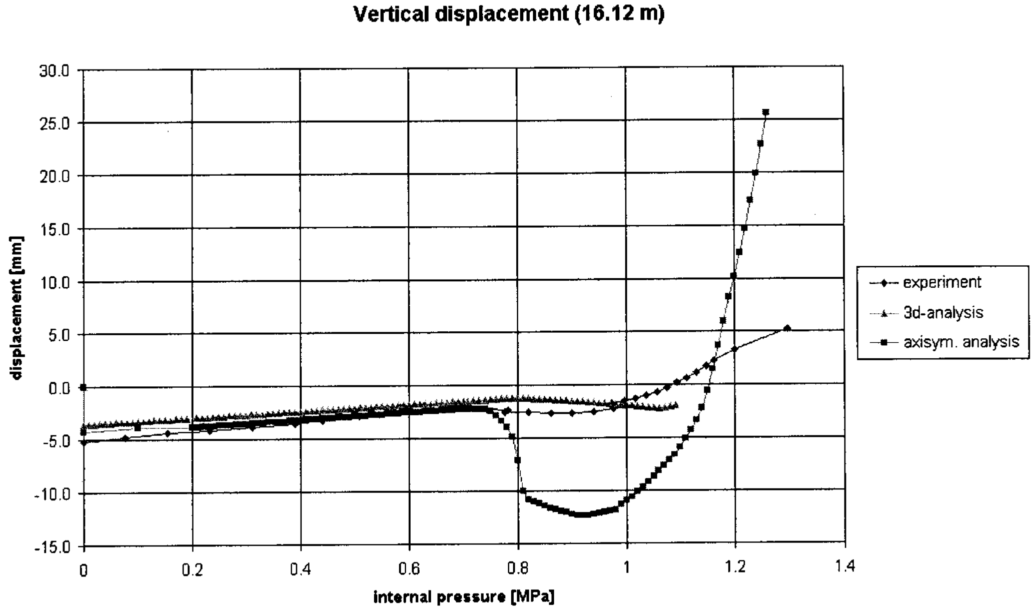

Figure 20. Concrete hoop strains in the cylindrical part of the containment (position 6.2 m above basemat), pressure only – experimental values and calculated results

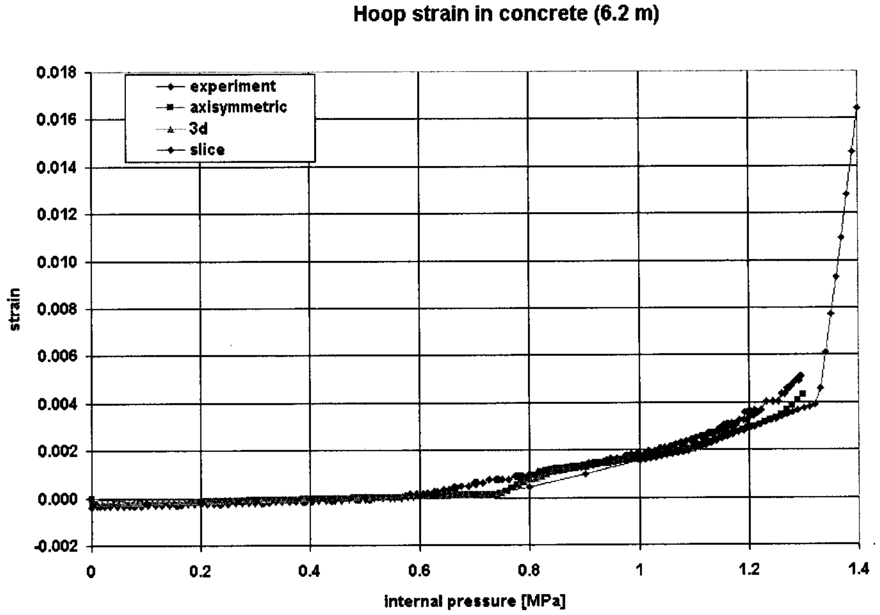

Figure 21. Liner hoop strains in the cylindrical part of the containment (position 6.2 m above basemat), pressure only – experimental values and calculated results

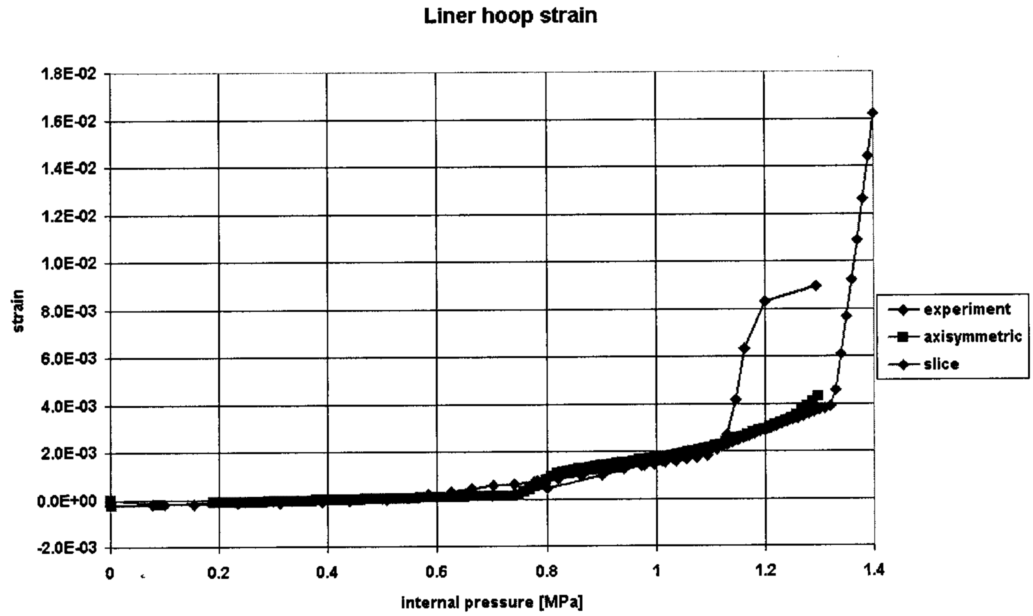

Figure 22. Rebar hoop strains in the cylindrical part of the containment (position 6.2 m above basemat), pressure only – experimental values and calculated results

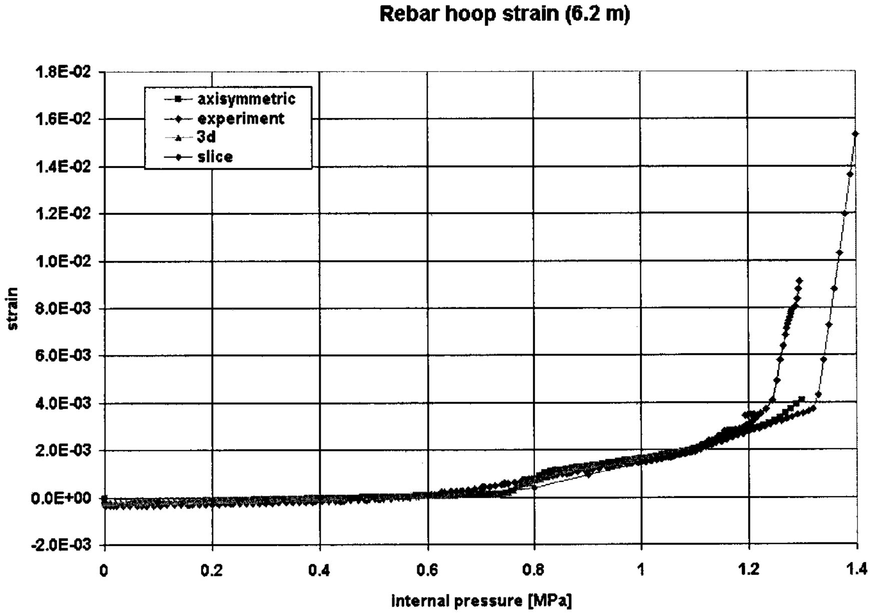

Figure 23. Hoop tendon strains in the cylindrical part of the containment (position 6.2 m above basemat), pressure only – experimental values and calculated results

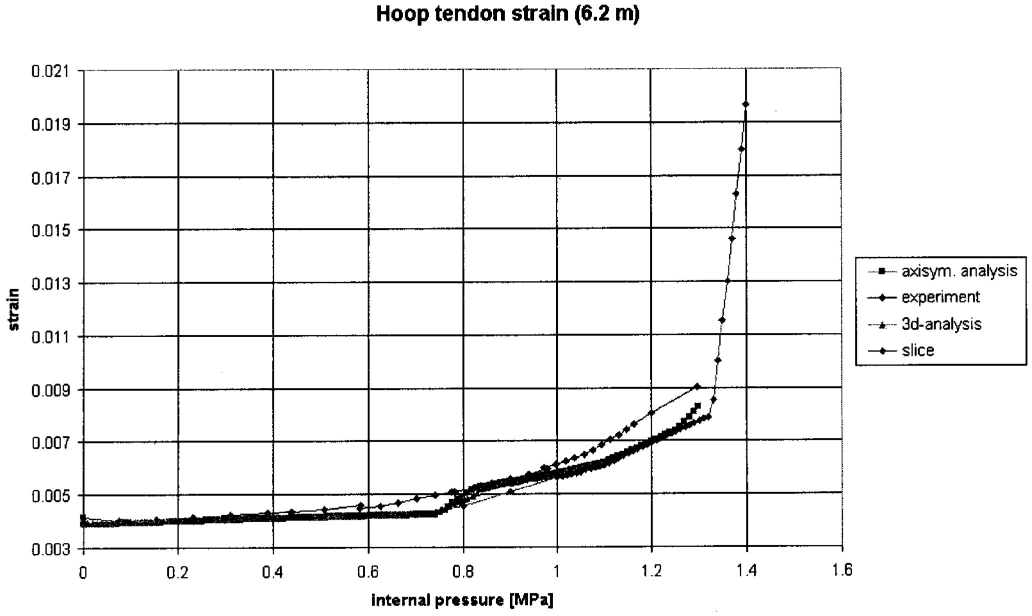

Figure 24. Formation of axial and radial micro-cracks at internal pressure 0.8 and 1.4 MPa (axisymmetric slice model)

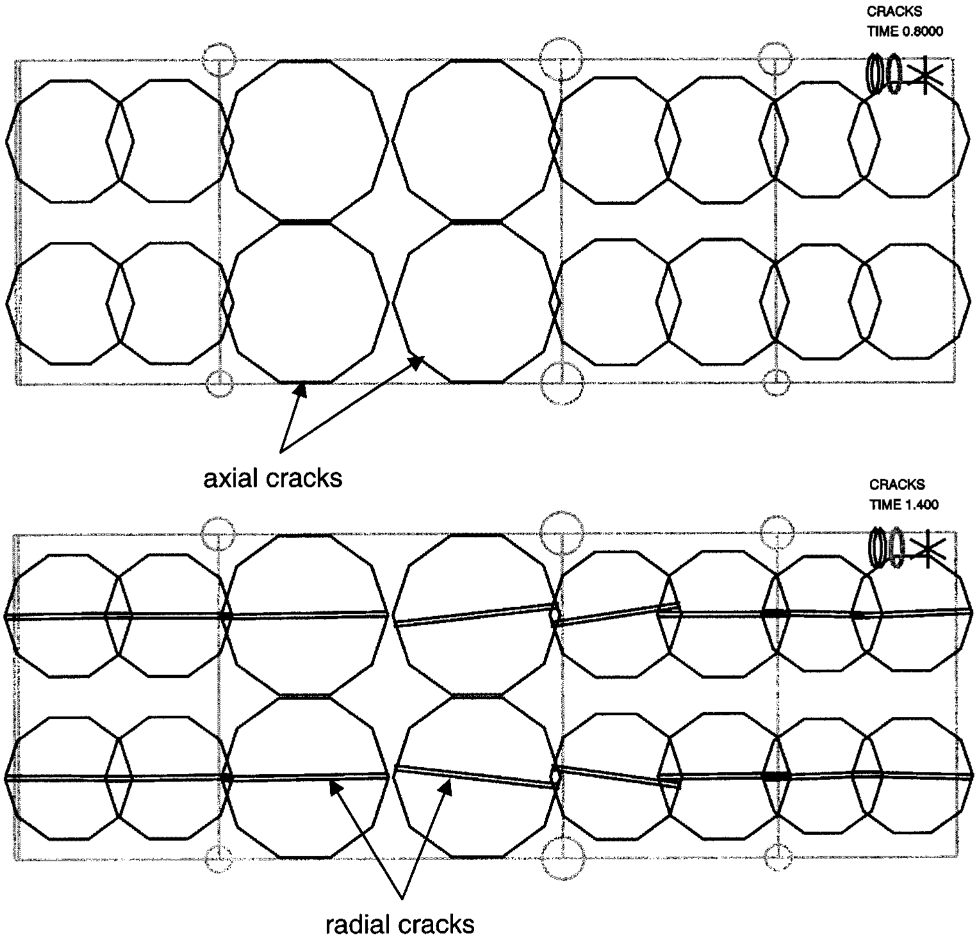
CRACKS
TIME 0.8000
axial cracks
CRACKS
TIME 1.400
radial cracks

Figure 25. Radial displacement in the cylindrical part of the containment, pressure only and temperature case 1 (complete axisymmetric and slice model)

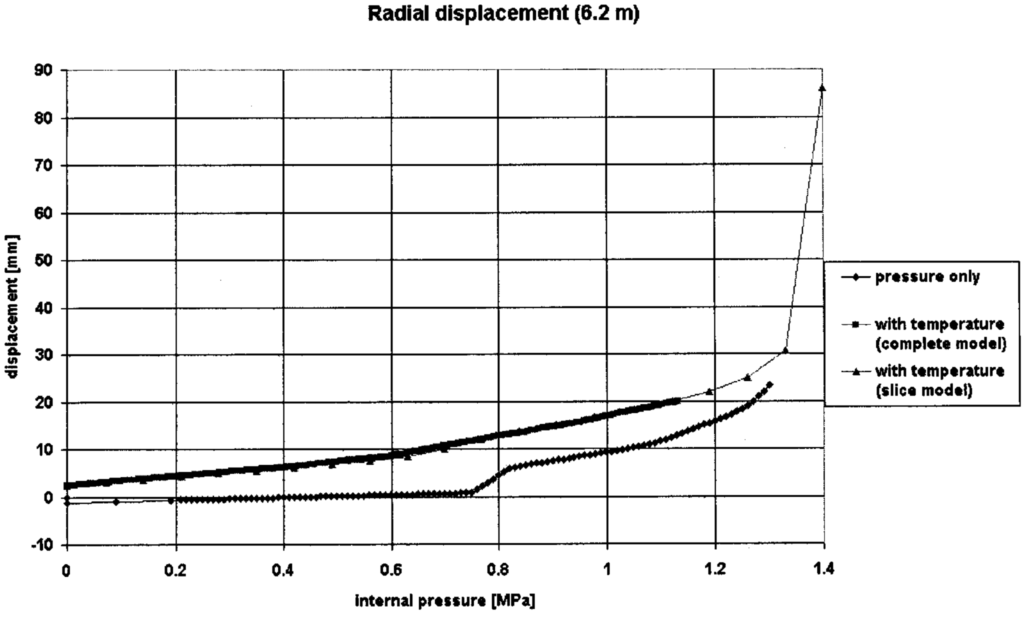

Figure 26. Hoop stress in concrete for points near inner and outer surface, pressure and temperature case 1 (axisymmetric slice model)

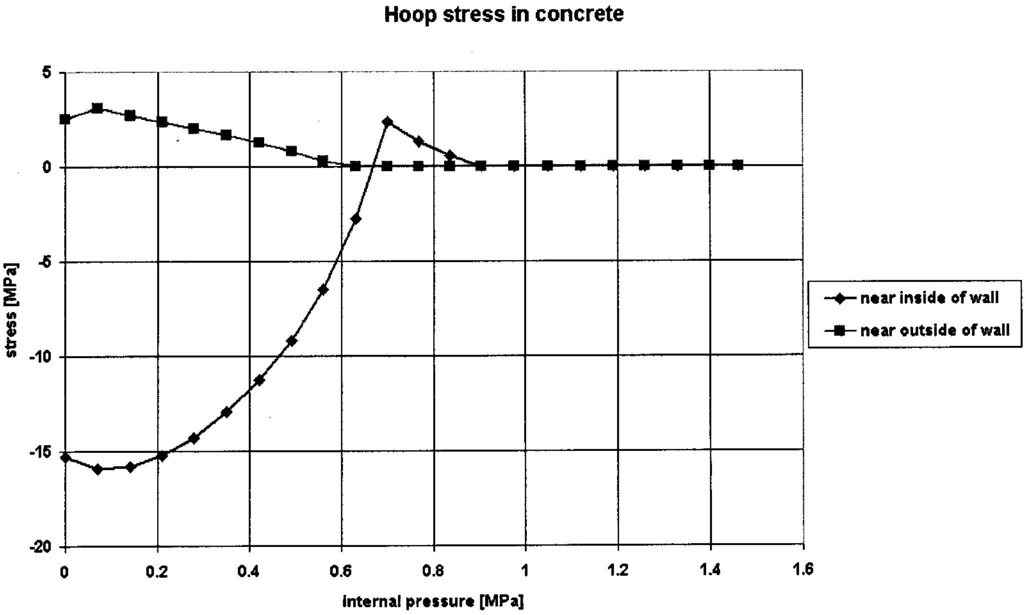

Figure 27. Hoop strain in concrete for points near inner and outer surface, pressure and temperature case 1 (axisymmetric slice model)

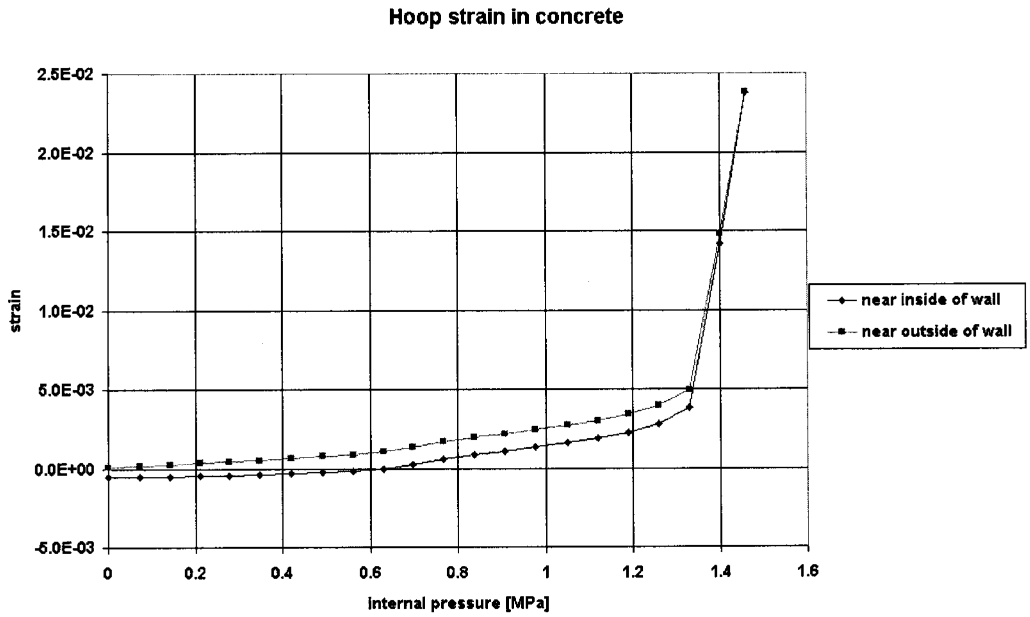

Figure 28. Liner strains (hoop and circumferential), pressure and temperature case 1 (axisymmetric slice model)

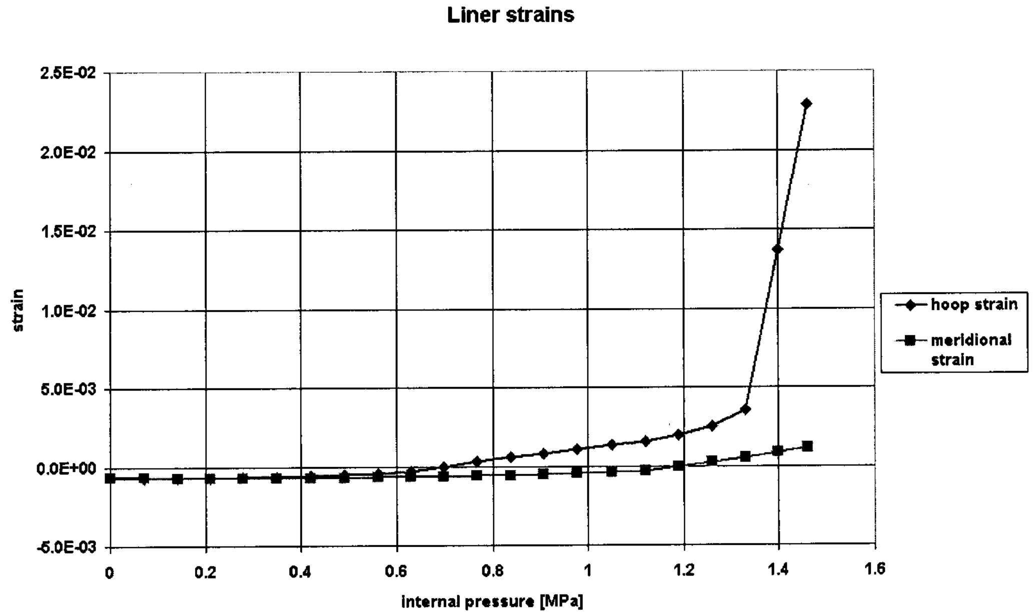

Figure 29. Hoop rebar strain for inner and outer rebar, pressure and temperature case 1 (axisymmetric slice model)

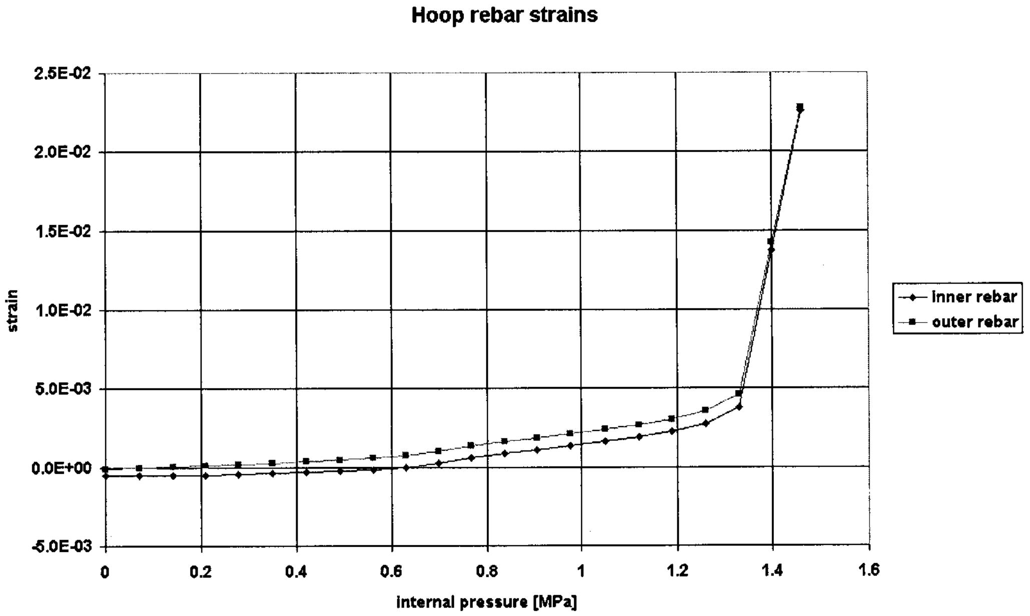

Figure 30. Tendon strains, pressure and temperature case 1 (axisymmetric slice model)

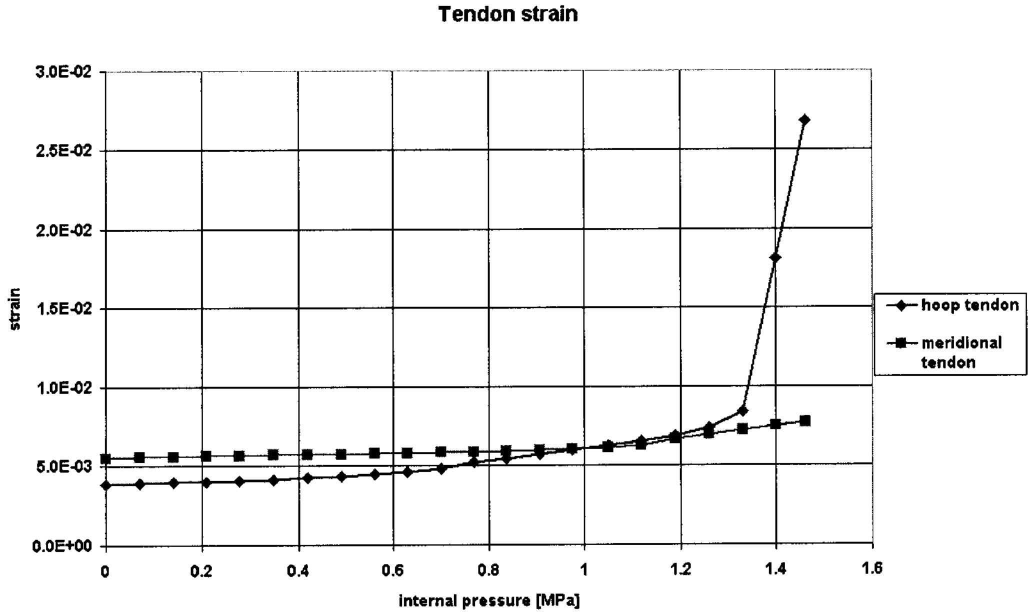

Figure 31. Radial displacement, pressure and temperature case 2 (slice model)

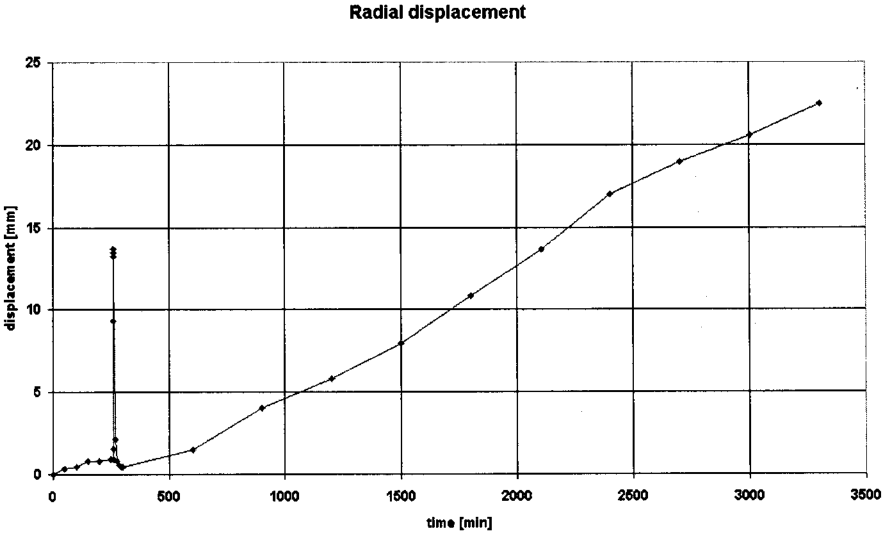

Figure 32. Hoop strains in concrete for points near inner and outer surface, pressure and temperature case 2 (slice model)

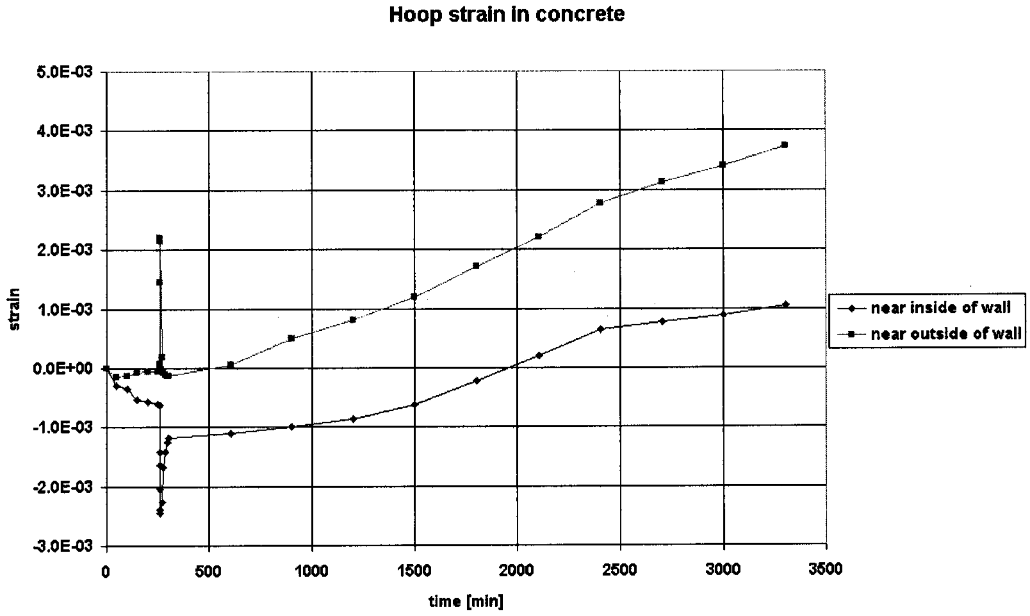

Figure 33. Liner strains, pressure and temperature case 2 (slice model)

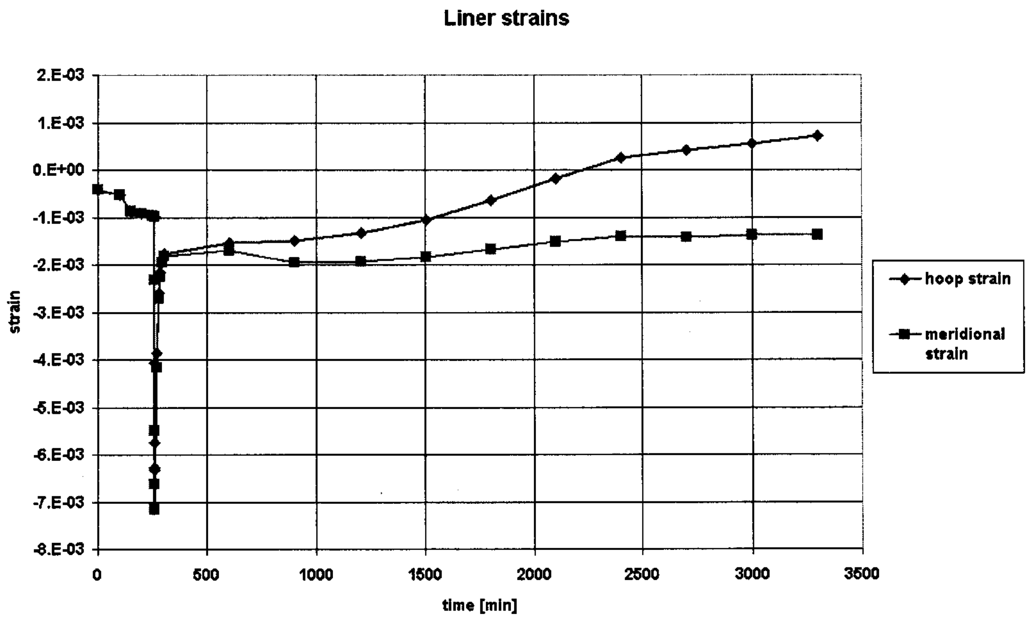

Figure 34. Hoop rebar strains for inner and outer rebar, pressure and temperature case 2 (slice model)

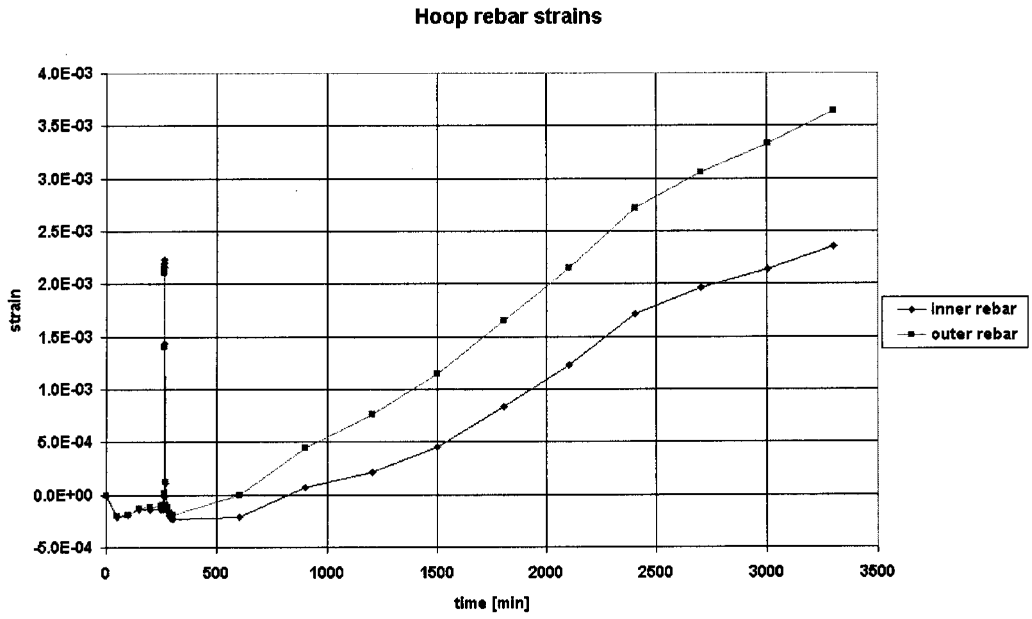

Figure 35. Tendon strains, pressure and temperature case 2 (slice model)

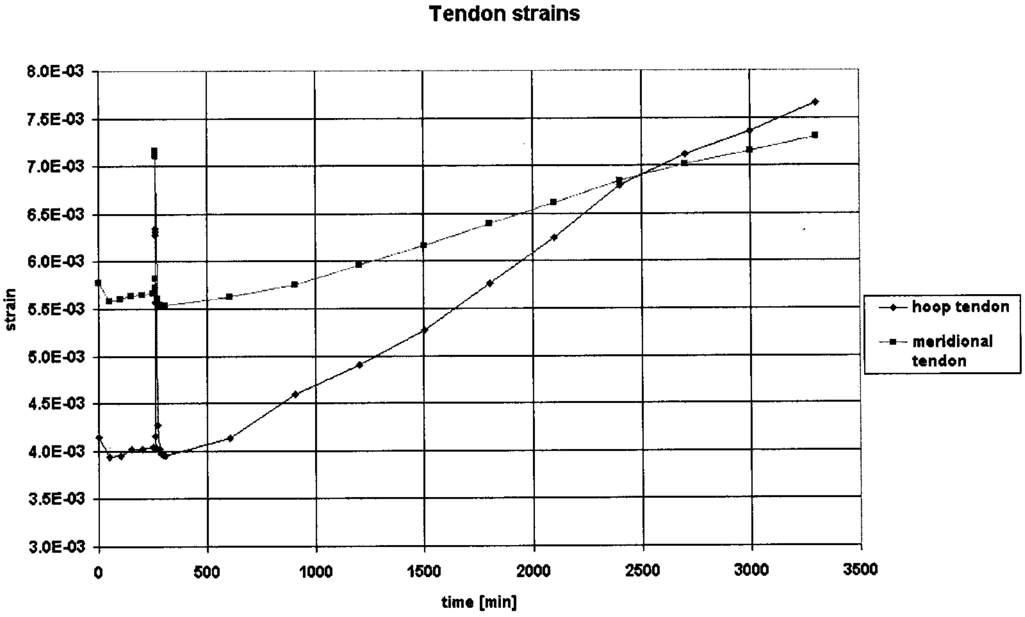

Figure 36. Part of a typical stress-strain curve for a integration point in concrete, components normal to crack face, slice model, pressure only case

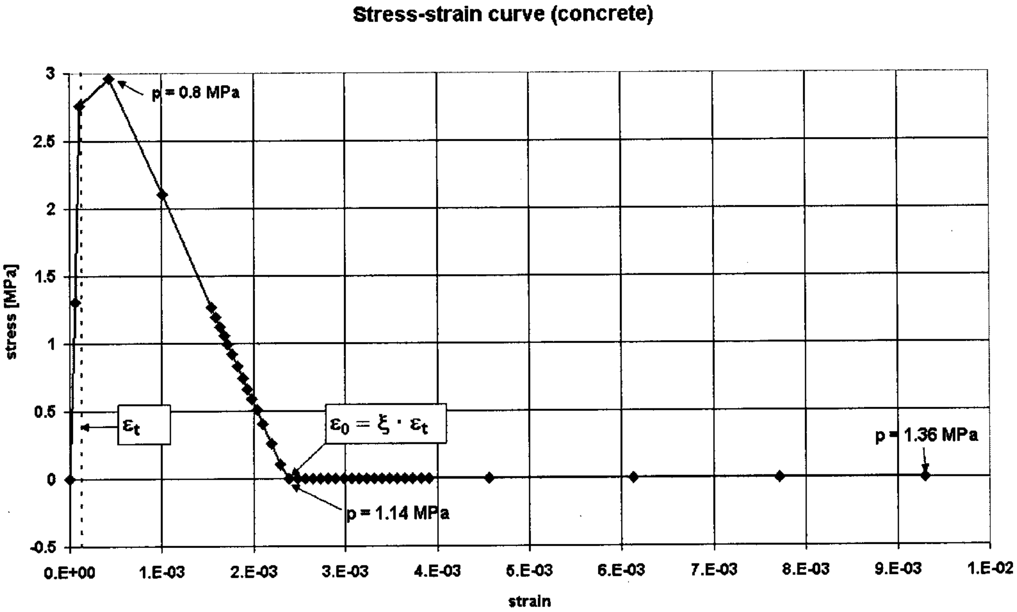

Figure 37. Crack opening displacements for a line of integration points (in concrete) through the wall, slice model, pressure only case

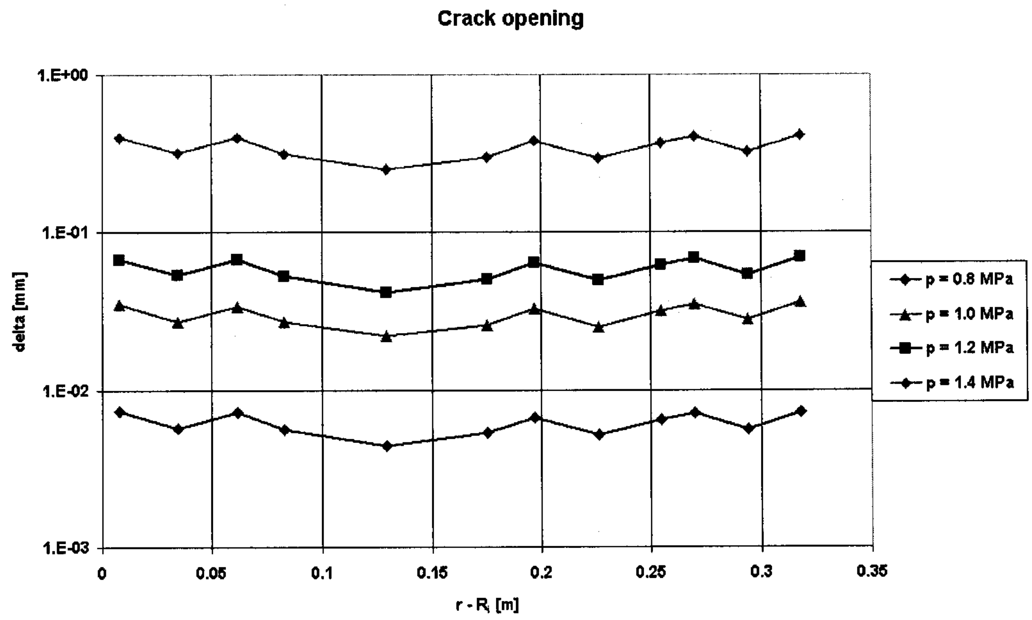
Crack opening
1.E+00
1.E-01
1.E-02
1.E-03
delta [mm]
0
0.05
0.1
0.15
0.2
0.25
0.3
0.35
r - Ri [m]
p = 0.8 MPa
p = 1.0 MPa
p = 1.2 MPa
p = 1.4 MPa

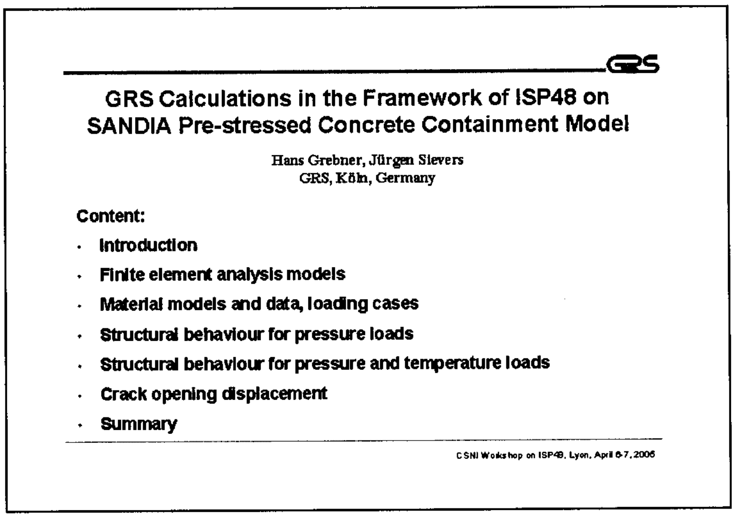

GRS Calculations in the Framework of ISP48 on SANDIA Pre-stressed Concrete Containment Model

Hans Grebner, Jürgen Sievers
GRS, Köln, Germany

Content:

- **Introduction**
- **Finite element analysis models**
- **Material models and data, loading cases**
- **Structural behaviour for pressure loads**
- **Structural behaviour for pressure and temperature loads**
- **Crack opening displacement**
- **Summary**

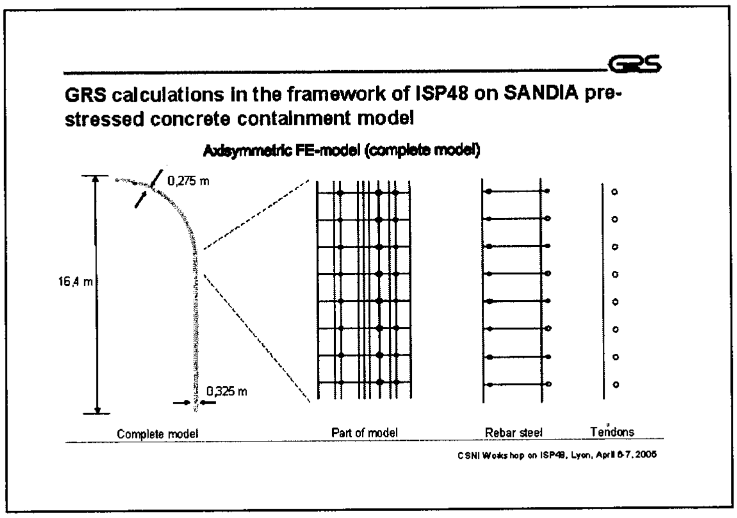

GRS calculations in the framework of ISP48 on SANDIA pre-stressed concrete containment model

Axisymmetric FE-model (complete model)

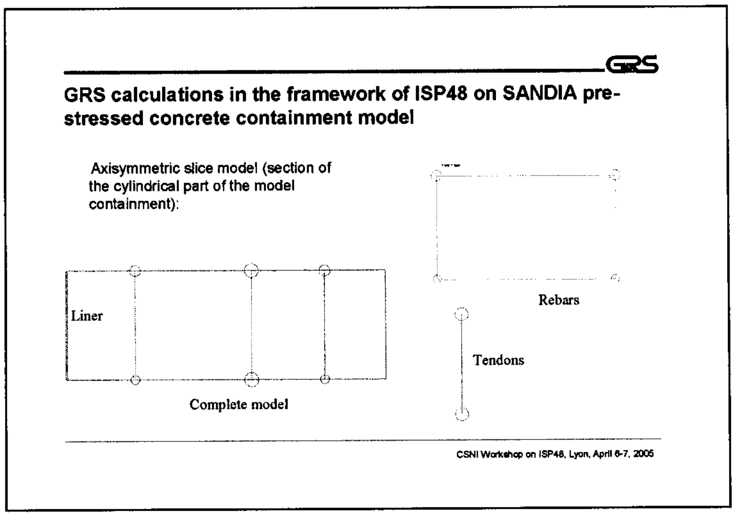

GRS calculations in the framework of ISP48 on SANDIA pre-stressed concrete containment model

Axisymmetric slice model (section of the cylindrical part of the model containment):

Liner
Complete model
Rebars
Tendons

CSNI Workshop on ISP48, Lyon, April 6-7, 2005

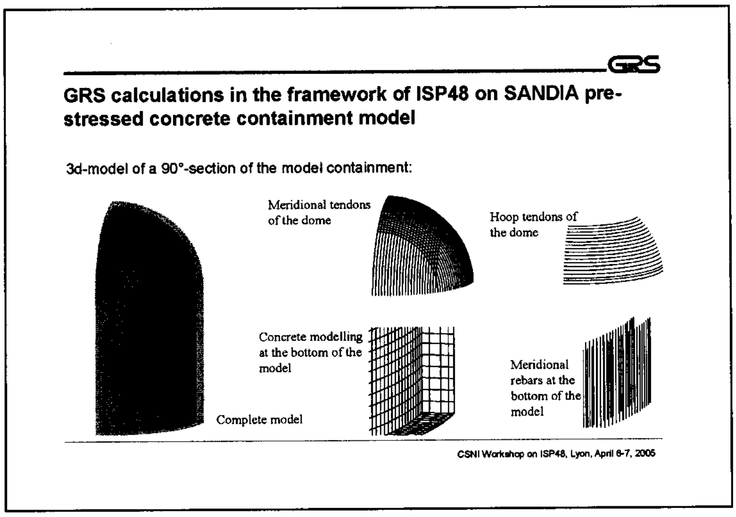

GRS calculations in the framework of ISP48 on SANDIA pre-stressed concrete containment model

3d-model of a 90°-section of the model containment:

Meridional tendons of the dome
Hoop tendons of the dome
Concrete modelling at the bottom of the model
Meridional rebars at the bottom of the model
Complete model

CSNI Workshop on ISP48, Lyon, April 6-7, 2005

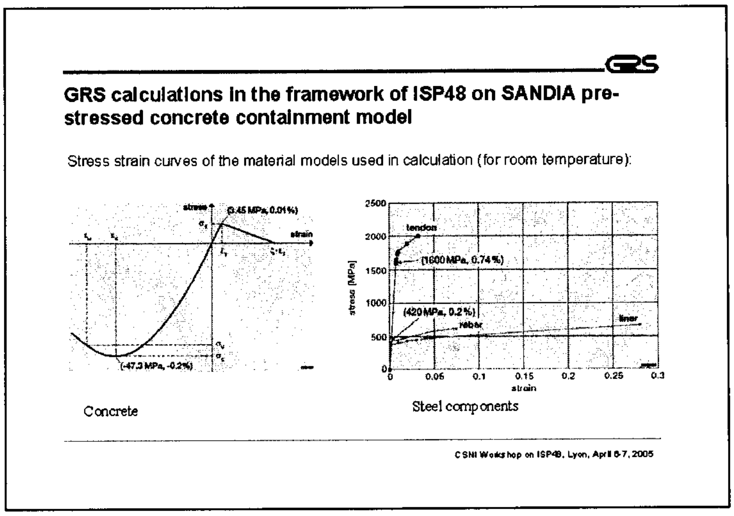

GRS calculations in the framework of ISP48 on SANDIA pre-stressed concrete containment model

Stress strain curves of the material models used in calculation (for room temperature):

Concrete

Steel components

CSNI Workshop on ISP48, Lyon, April 6-7, 2005

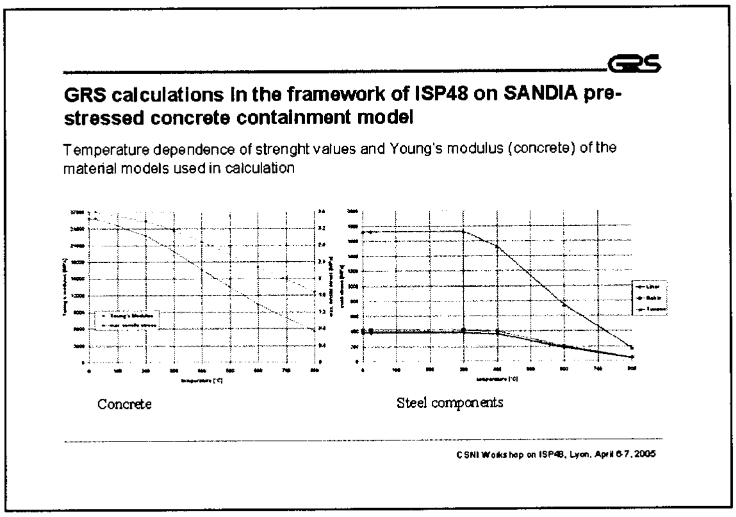

GRS calculations in the framework of ISP48 on SANDIA pre-stressed concrete containment model

Temperature dependence of strenght values and Young's modulus (concrete) of the material models used in calculation

Concrete

Steel components

CSNI Workshop on ISP48, Lyon, April 6-7, 2005

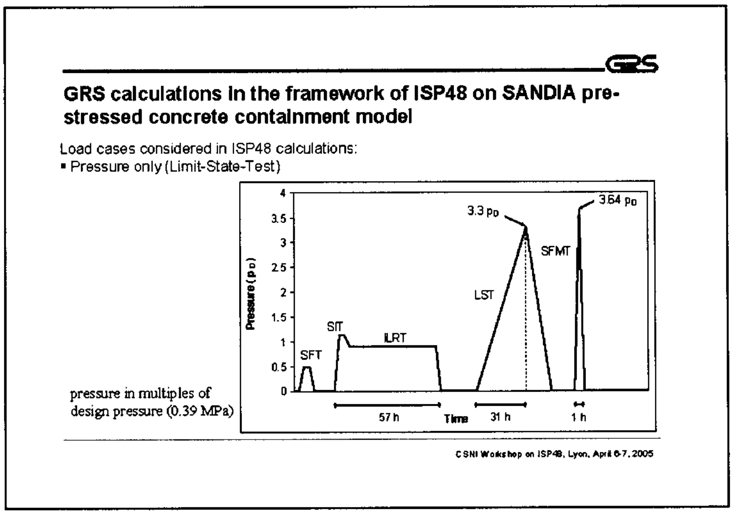

GRS calculations in the framework of ISP48 on SANDIA pre-stressed concrete containment model

Load cases considered in ISP48 calculations:

- Pressure only (Limit-State-Test)

pressure in multiples of design pressure (0.39 MPa)

CSNI Workshop on ISP48, Lyon, April 6-7, 2005

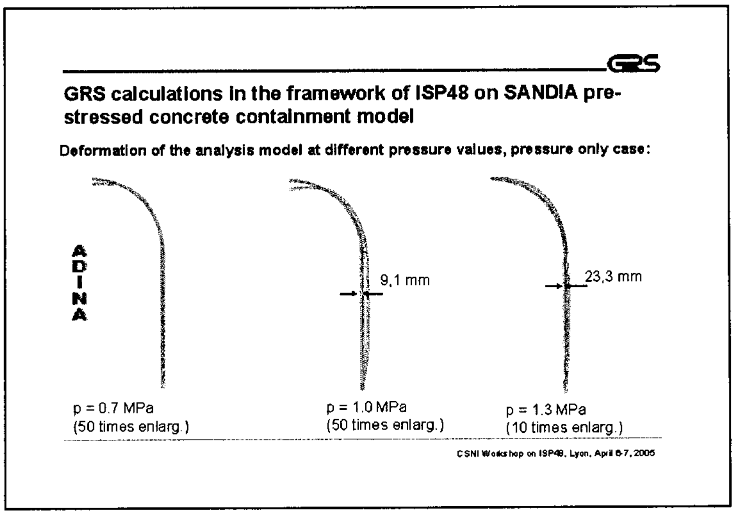

GRS calculations in the framework of ISP48 on SANDIA pre-stressed concrete containment model

Deformation of the analysis model at different pressure values, pressure only case:

p = 0.7 MPa
(50 times enlarg.)

p = 1.0 MPa
(50 times enlarg.)

p = 1.3 MPa
(10 times enlarg.)

CSNI Workshop on ISP48, Lyon, April 6-7, 2005

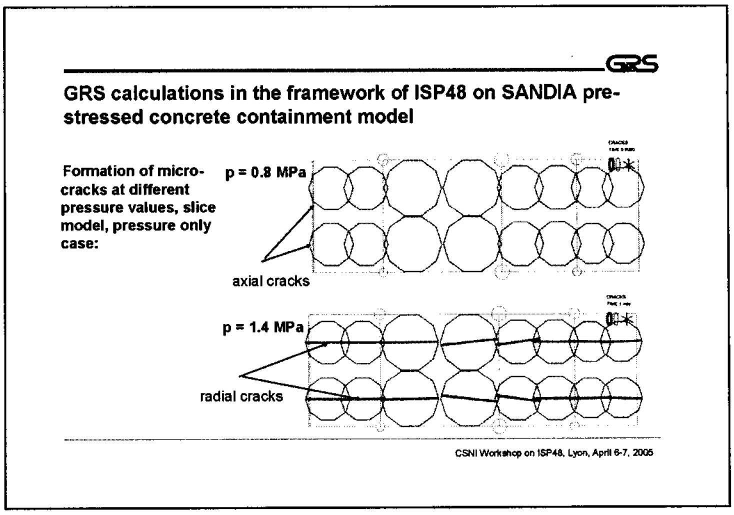

GRS calculations in the framework of ISP48 on SANDIA pre-stressed concrete containment model

Formation of micro-cracks at different pressure values, slice model, pressure only case:

CSNI Workshop on ISP48, Lyon, April 6-7, 2005

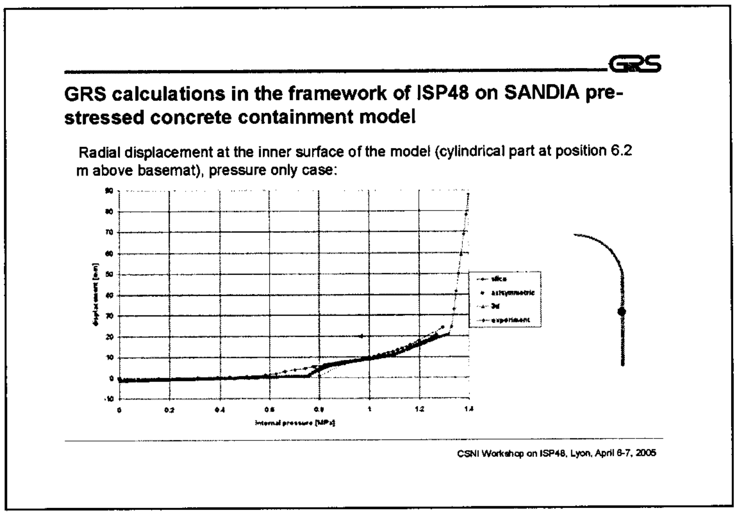

GRS calculations in the framework of ISP48 on SANDIA pre-stressed concrete containment model

Radial displacement at the inner surface of the model (cylindrical part at position 6.2 m above basemat), pressure only case:

CSNI Workshop on ISP48, Lyon, April 6-7, 2005

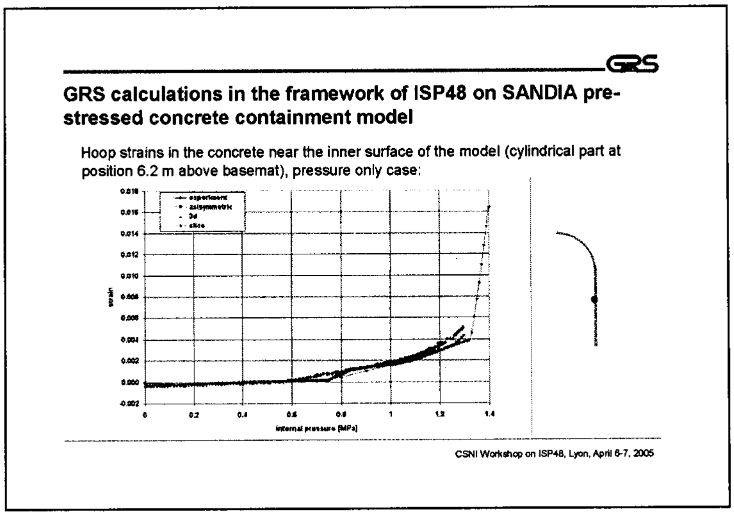

GRS

GRS calculations in the framework of ISP48 on SANDIA pre-stressed concrete containment model

Hoop strains in the concrete near the inner surface of the model (cylindrical part at position 6.2 m above basemat), pressure only case:

CSNI Workshop on ISP48, Lyon, April 6-7, 2005

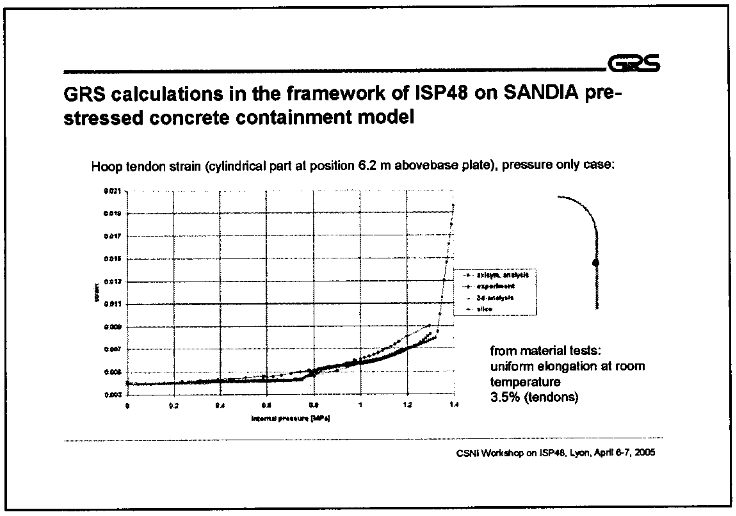

GRS

GRS calculations in the framework of ISP48 on SANDIA pre-stressed concrete containment model

Hoop tendon strain (cylindrical part at position 6.2 m abovebase plate), pressure only case:

from material tests:
uniform elongation at room temperature
3.5% (tendons)

CSNI Workshop on ISP48, Lyon, April 6-7, 2005

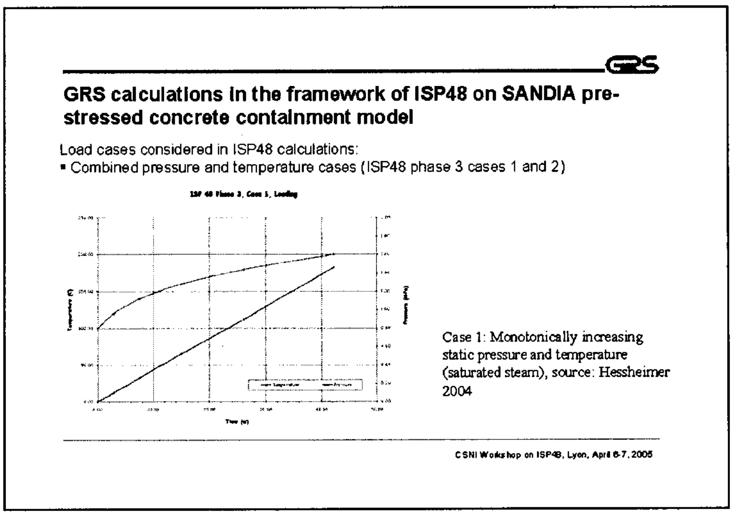

GRS calculations in the framework of ISP48 on SANDIA pre-stressed concrete containment model

Load cases considered in ISP48 calculations:
- Combined pressure and temperature cases (ISP48 phase 3 cases 1 and 2)

Case 1: Monotonically increasing static pressure and temperature (saturated steam), source: Hessheimer 2004

CSNI Workshop on ISP48, Lyon, April 6-7, 2005

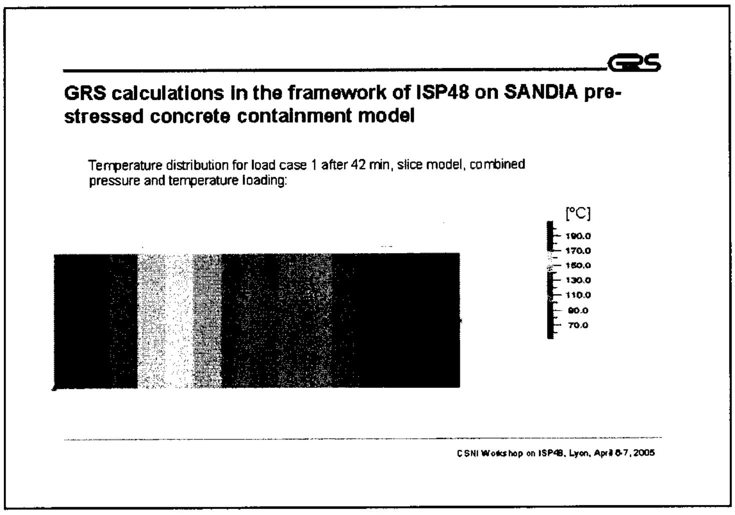

GRS calculations in the framework of ISP48 on SANDIA pre-stressed concrete containment model

Temperature distribution for load case 1 after 42 min, slice model, combined pressure and temperature loading:

CSNI Workshop on ISP48, Lyon, April 6-7, 2005

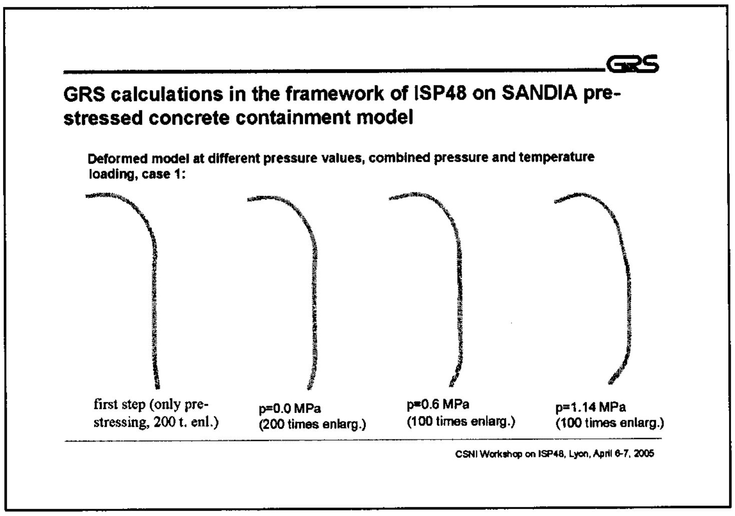

GRS calculations in the framework of ISP48 on SANDIA pre-stressed concrete containment model

Deformed model at different pressure values, combined pressure and temperature loading, case 1:

first step (only pre-stressing, 200 t. enl.)

p=0.0 MPa (200 times enlarg.)

p=0.6 MPa (100 times enlarg.)

p=1.14 MPa (100 times enlarg.)

CSNI Workshop on ISP48, Lyon, April 6-7, 2005

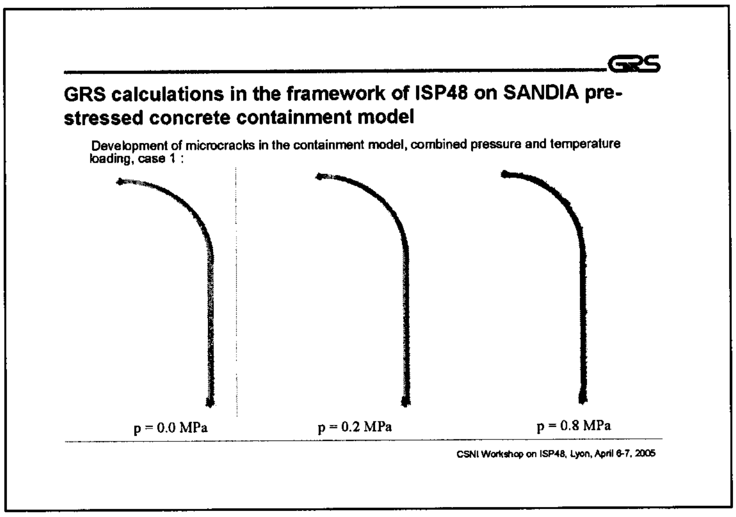

GRS calculations in the framework of ISP48 on SANDIA pre-stressed concrete containment model

Development of microcracks in the containment model, combined pressure and temperature loading, case 1 :

p = 0.0 MPa

p = 0.2 MPa

p = 0.8 MPa

CSNI Workshop on ISP48, Lyon, April 6-7, 2005

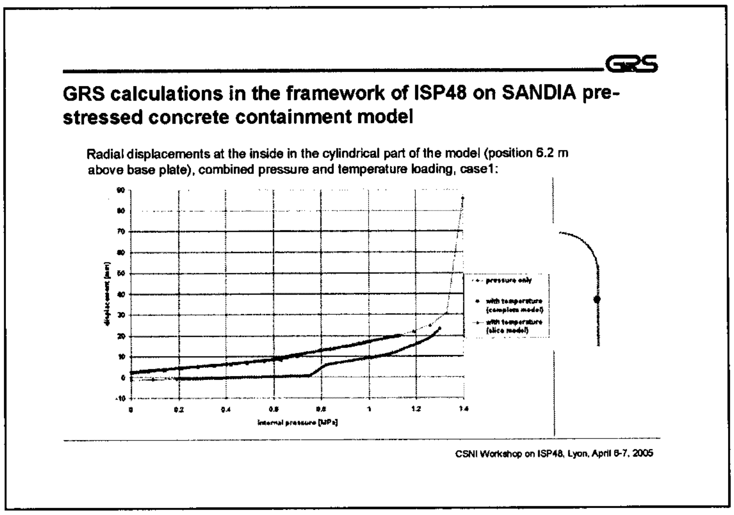

GRS calculations in the framework of ISP48 on SANDIA pre-stressed concrete containment model

Radial displacements at the inside in the cylindrical part of the model (position 6.2 m above base plate), combined pressure and temperature loading, case1:

CSNI Workshop on ISP48, Lyon, April 6-7, 2005

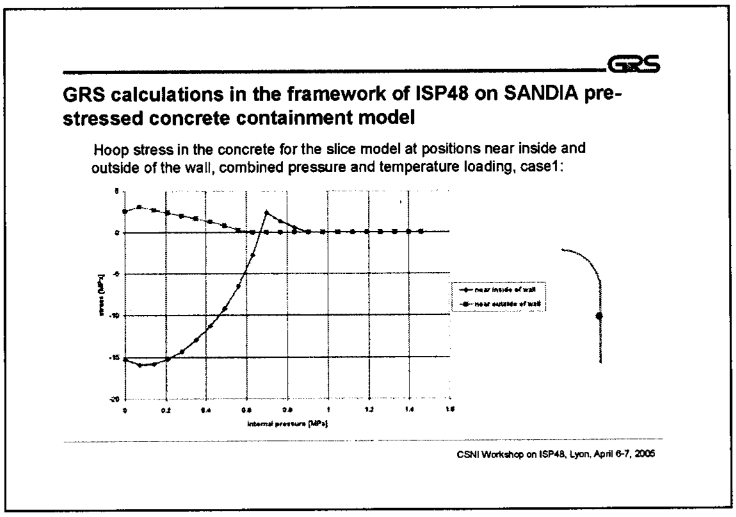

GRS calculations in the framework of ISP48 on SANDIA pre-stressed concrete containment model

Hoop stress in the concrete for the slice model at positions near inside and outside of the wall, combined pressure and temperature loading, case1:

CSNI Workshop on ISP48, Lyon, April 6-7, 2005

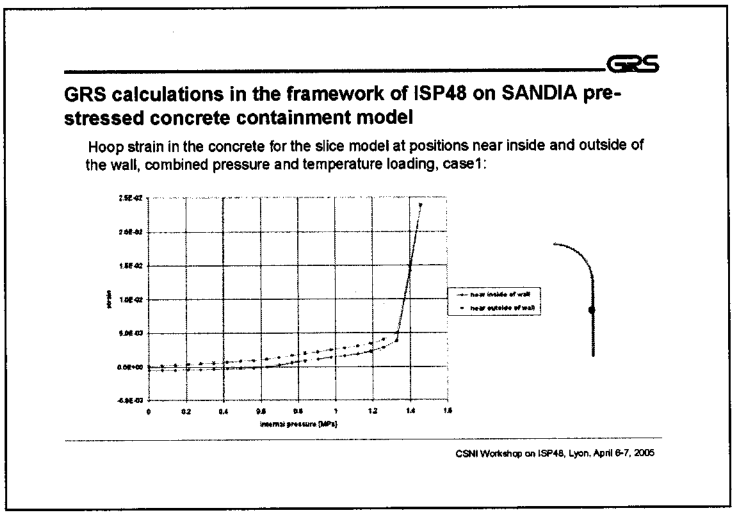

GRS calculations in the framework of ISP48 on SANDIA pre-stressed concrete containment model

Hoop strain in the concrete for the slice model at positions near inside and outside of the wall, combined pressure and temperature loading, case1:

CSNI Workshop on ISP48, Lyon, April 6-7, 2005

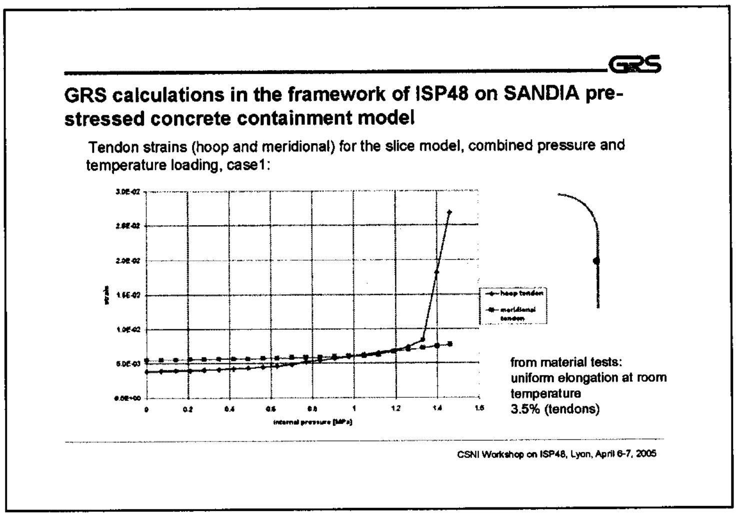

GRS calculations in the framework of ISP48 on SANDIA pre-stressed concrete containment model

Tendon strains (hoop and meridional) for the slice model, combined pressure and temperature loading, case1:

from material tests:
uniform elongation at room temperature
3.5% (tendons)

CSNI Workshop on ISP48, Lyon, April 6-7, 2005

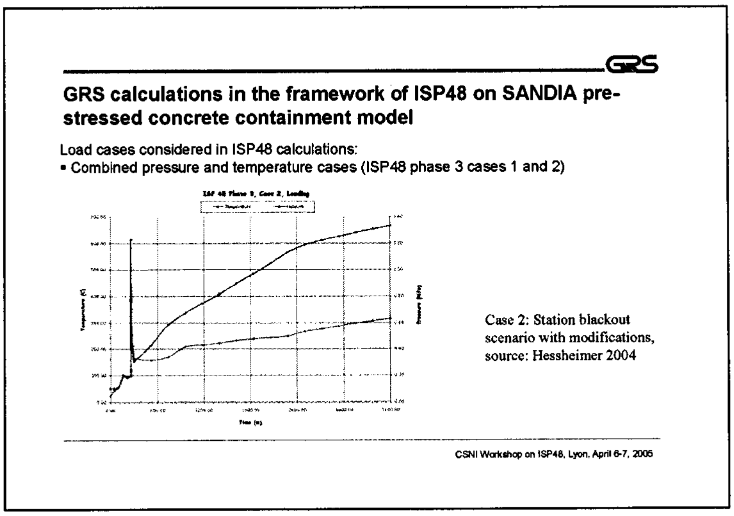

GRS calculations in the framework of ISP48 on SANDIA pre-stressed concrete containment model

Load cases considered in ISP48 calculations:
- Combined pressure and temperature cases (ISP48 phase 3 cases 1 and 2)

Case 2: Station blackout scenario with modifications, source: Hessheimer 2004

CSNI Workshop on ISP48, Lyon, April 6-7, 2005

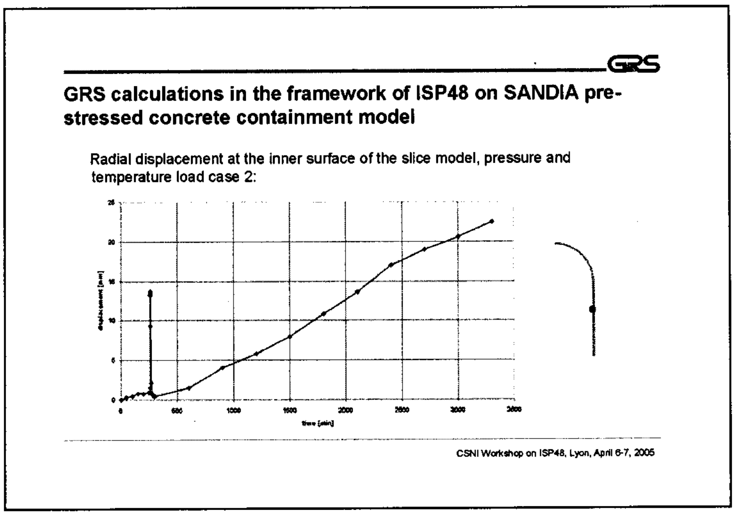

GRS calculations in the framework of ISP48 on SANDIA pre-stressed concrete containment model

Radial displacement at the inner surface of the slice model, pressure and temperature load case 2:

CSNI Workshop on ISP48, Lyon, April 6-7, 2005

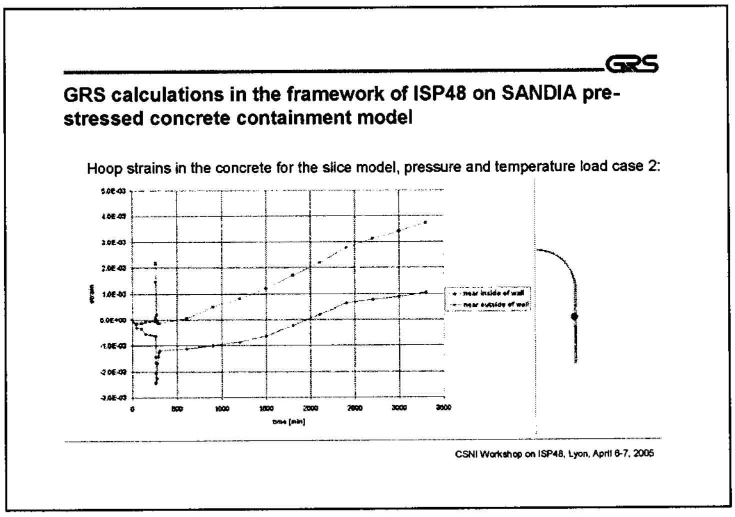

GRS calculations in the framework of ISP48 on SANDIA pre-stressed concrete containment model

Hoop strains in the concrete for the slice model, pressure and temperature load case 2:

CSNI Workshop on ISP48, Lyon, April 6-7, 2005

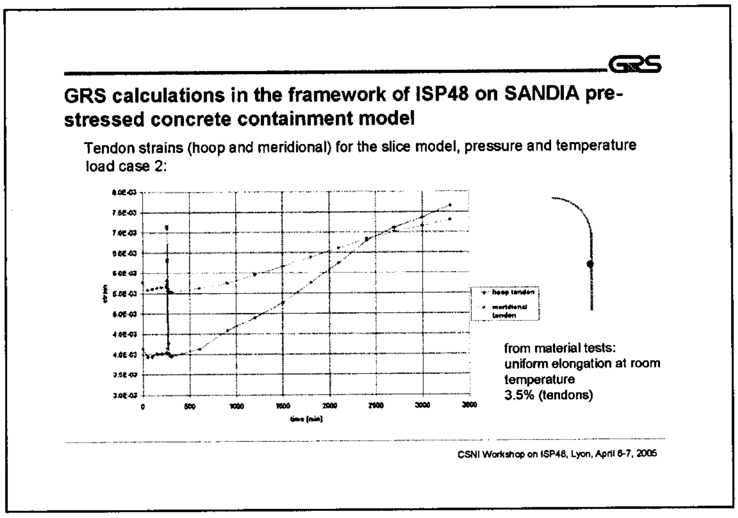

GRS calculations in the framework of ISP48 on SANDIA pre-stressed concrete containment model

Tendon strains (hoop and meridional) for the slice model, pressure and temperature load case 2:

from material tests:
uniform elongation at room temperature
3.5% (tendons)

CSNI Workshop on ISP48, Lyon, April 6-7, 2005

GRS calculations in the framework of ISP48 on SANDIA pre-stressed concrete containment model

Crack opening displacement in the concrete:

If the maximum tensile stress in the concrete is reached in an integration point of a concrete element, according to the smeared crack approach a micro-crack is formed at this point. The normal stress at this point gradually decreases to zero, while the normal strain e may be related to the crack opening displacement d by the equation:

$$d = (e - e_t) \cdot l_c$$

Here e_t is the strain-value corresponding to the maximum tensile stress s_t and l_c is a characteristic length of the element considered. If the fracture energy G_f of concrete is used as input to ADINA, l_c may be evaluated by the relation:

$$l_c = \frac{2\,E_0\,G_f}{s_t^2\,x}$$

E_0 is the initial Young's modulus and x is described later.

CSNI Workshop on ISP48, Lyon, April 6-7, 2005

GRS calculations in the framework of ISP48 on SANDIA pre-stressed concrete containment model

Stress strain curve in an integration point in the concrete (slice model, pressure only, integration point near inner surface):

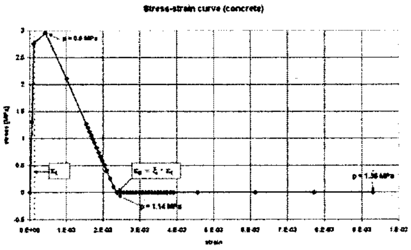

CSNI Workshop on ISP48, Lyon, April 6-7, 2005

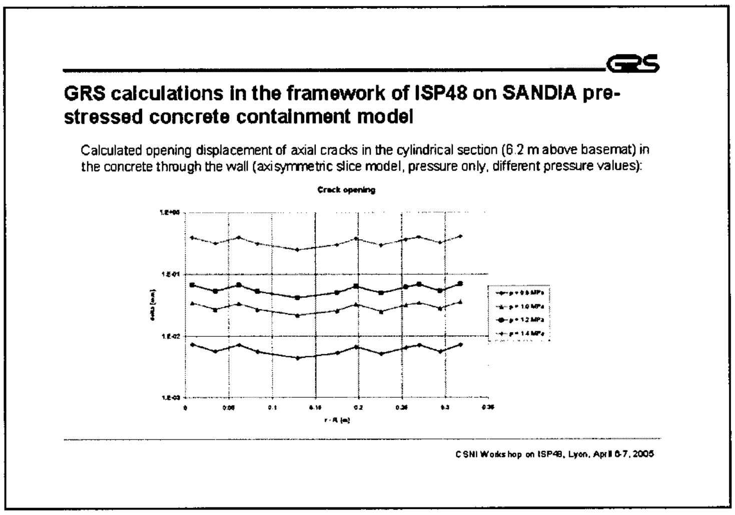

GRS calculations in the framework of ISP48 on SANDIA pre-stressed concrete containment model

Calculated opening displacement of axial cracks in the cylindrical section (6.2 m above basemat) in the concrete through the wall (axisymmetric slice model, pressure only, different pressure values):

CSNI Workshop on ISP48, Lyon, April 6-7, 2005

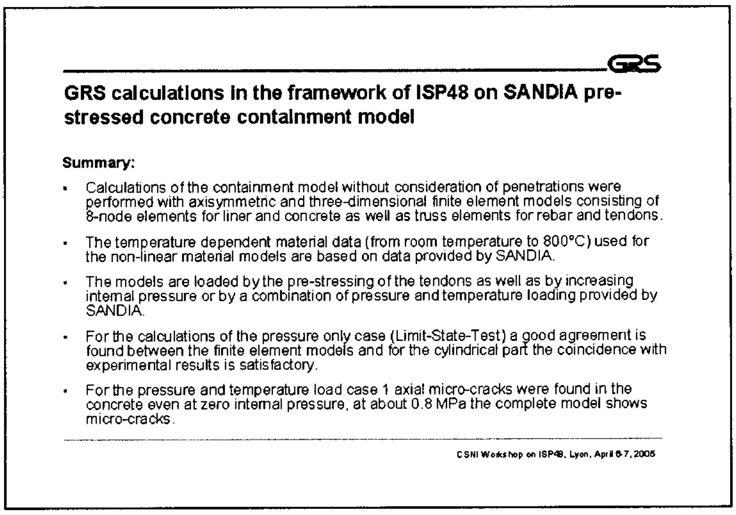

GRS calculations in the framework of ISP48 on SANDIA pre-stressed concrete containment model

Summary:

- Calculations of the containment model without consideration of penetrations were performed with axisymmetric and three-dimensional finite element models consisting of 8-node elements for liner and concrete as well as truss elements for rebar and tendons.
- The temperature dependent material data (from room temperature to 800°C) used for the non-linear material models are based on data provided by SANDIA.
- The models are loaded by the pre-stressing of the tendons as well as by increasing internal pressure or by a combination of pressure and temperature loading provided by SANDIA.
- For the calculations of the pressure only case (Limit-State-Test) a good agreement is found between the finite element models and for the cylindrical part the coincidence with experimental results is satisfactory.
- For the pressure and temperature load case 1 axial micro-cracks were found in the concrete even at zero internal pressure, at about 0.8 MPa the complete model shows micro-cracks.

CSNI Workshop on ISP48, Lyon, April 6-7, 2005

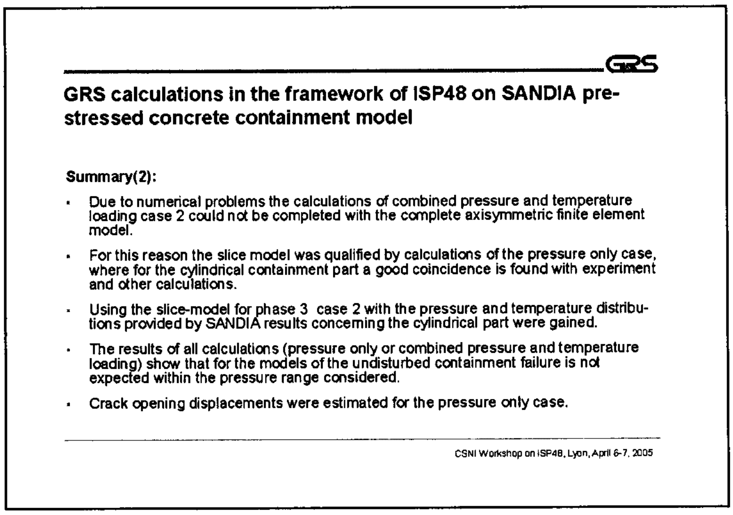

GRS calculations in the framework of ISP48 on SANDIA pre-stressed concrete containment model

Summary(2):

- Due to numerical problems the calculations of combined pressure and temperature loading case 2 could not be completed with the complete axisymmetric finite element model.
- For this reason the slice model was qualified by calculations of the pressure only case, where for the cylindrical containment part a good coincidence is found with experiment and other calculations.
- Using the slice-model for phase 3 case 2 with the pressure and temperature distributions provided by SANDIA results concerning the cylindrical part were gained.
- The results of all calculations (pressure only or combined pressure and temperature loading) show that for the models of the undisturbed containment failure is not expected within the pressure range considered.
- Crack opening displacements were estimated for the pressure only case.

CSNI Workshop on ISP48, Lyon, April 6-7, 2005

POSTTEST ANALYSIS OF A 1:4 SCALE PCCV MODEL – EFFECTS OF PRESSURE AND TEMPERATURE LOADINGS

Jan Stepan
Nuclear Research Institute Rez, div. Energoprojekt Praha, Prague, Czech republic

ABSTRACT

The paper deals with the analysis of a 1:4 scale prestressed concrete containment vessel (PCCV) model under both pressure and temperature loadings. The model corresponds to the PCCV of PWR plants in Japan and was constructed by NUPEC at Sandia National Laboratories. Tests of the model were addressed at ultimate behavior of structure under pressure loading. The first part of analyses presented in this paper simulated behaviour of the model during limit state test and there is emphasis on comparison of the test and analysis results. The next part of analysis is addressed at effects of combination of pressure and temperature loadings. The calculations were made for two characteristic pressure and temperature histories and the results were compared with the response of structure under pressure loading without temperature effects.

Analysis model

The analysis model is created in Abaqus general-purpose finite element program. The principal objective was to model behaviour of the whole structure including openings. The concrete is basic part of the model and is modeled by brick elements. Rod elements model rebars and prestressing tendons and they are embedded into concrete elements. Liner is modeled by plate elements connected on inner surface with concrete elements. Model includes EH and AL openings including change of wall thickness and changes in rebar and prestressing tendons. M/S openings weren't modeled because they have small impact on global response of structure and only added rebar rods were considered in model.

Basics characteristics and simplifications are abstracted into next points:

- The model includes concrete wall of cylindrical and dome part of structure. Basement wasn't modeled, its stiffness was neglected and connection between cylindrical wall and basement is modeled by external fix support, which eliminates displacements and rotations (effect of this simplification is small because the stiffness of basement is much more higher in comparison with the stiffness of remaining parts of structure).
- Rebar and prestressing tendons were modeled by rod elements considering actual geometry around openings. Two simplifications were applied – the radial rebar wasn't modeled due to size limit of model and anchors of hoop cables were replaced by continual connections of elements due to elimination of cracks and instabilities in anchor area at buttress.
- Prestressing tendons were modeled as bonded tendons. Prestressing force along tendons was considered as uniform by mean value of measured force.
- Connection of liner and concrete doesn't respect actual design and is performed by common nodes of liner and concrete elements. So, results in liner corresponding to global behavior but there could be differences in places with local peak of stress (connection of liner to frame of openings, connection with basement).
- Starting state of analysis was unbroken structure. Cracking due to shrinkage was modeled by decreasing of modulus of elasticity along with lower tensile strength of concrete in tension.

Material characteristics were sets pursuant to results of tests. Abaqus Concrete damage plasticity model was used for modeling of non-linear behavior of concrete. The behavior of concrete in compression was assigned by Euro code 2, the behavior in tension was assigned by tensile strength and fracture energy. The non-linear behavior of rebar, presstresing tendons and liner was modeled by Abaqus Iron plasticity model. As indicated above, the prestressing tendons were modeled as bonded cables and their prestressing force was set by mean value of measured force. The prestressing force of hoop tendons is 30t, the prestressing force of vertical tendons is 41t.

Each analysis was performed in two steps. The firs step was application of prestressing and dead load. The second step was application of internal overpressure and optionally temperature. The presstresing was applied by initial conditions type stress. The internal overpressure was applied at liner elements. Forces in nodes at border of openings replaced the effect of internal ovepressure at locks.

The analysis model was the same in both Phase II and Phase III analysis. In Phase II (only pressure loading) the Abaqus/Explicit quasi-static analysis was used. Change of overpressure in time was defined by linear function with the end at 1.6 MPa. In Phase III the response of structure was solved by Abaqus/Standard. The change of the analysis type was forced by properties of Abaqus/Explicit which is not able to read temperature data along with restart from initial conditions. Using of Abaqus/Standard enabled to do analysis in the real time but due to higher sensitivity of calculation to the solving instabilities it is more difficult to solve the final failure mode of the structure.

Loadings

ISP 48 Phase II solves response of the structure under only pressure loading, history of the pressure loading corresponds to the Phase III case 1 loading. Phase III loadings includes pressure and temperature loadings. Case 1 represents time independent loading with continually increasing pressure and temperature corresponding to the saturated steam temperature. Case 2 corresponds to the simplified existing Station Blackout scenario including hydrogen detonation, there is real-time pressure and temperature loading history. The basic difference between these two cases is in the character of the temperature gradient across the wall section. In the case 1 loading, the temperature gradient corresponds with the steady state heat transfer – temperature gradient is closed to linear at every time step. In the case 2 loading, the temperature gradient corresponds to the time history of the thermal loading and material properties – temperature gradient isn't linear and is changing in time. This difference of loadings characters is evident in the tendon forces. During the case 1 loading the change of tendon temperature is similar to the change of concrete temperature and the impact of temperature changes to the tendon forces is small. On the contrary, during the case 2 loading there is considerable difference between the temperature of concrete and tendons and the tendon force history shows rise due to temperature loading.

Temperature degradation of concrete and steel (strength and modulus) could be considered in case of higher temperature loadings. For steel, there are interesting temperatures above 300°C, for concrete the boundary temperature is about 100°C. Due to parallel pressure loading, the PCCV structure acted mainly in tension and resistance is driven by properties of tendons and rebars. So, the temperature degradation is interesting especially for steel parts of structure. The case 1 temperature history shows that the temperature is under 300°C and therefore there is no need to consider temperature degradation of steel properties in this load case. In case 2 loading there is the temperature above 300°C twice. At first it is during hydrogen detonation when temperature rises above 600°C. Due to short time period of this loading the depth of wall temperature is above 300°C aprox. 5% of total wall thickness and only liner is hit by temperature degradation. The second exceeding of temperature 300°C is at time aprox. 50 hours and then the temperature is continuously raising. In this case the increasing of temperature is long term and temperature degradation could affect rebar and tendon but due to higher pressure (close to the bearing capacity of the structure) the temperature couldn't be critical reason of structure failure. Following assumptions were considered in presented analysis: in case 1 analysis no temperature degradation was applied, in case 2 analysis the temperature degradation was applied only for liner.

Analysis results

Comparison of global deformation for pressure and pressure+temperature loadings is in Figure 6 to Figure 9 for case 1 and in Figure 20 to Figure 23 for case 2. Figure 14 and Figure 15 show comparison of case 1 deformation history at 135°, 90° and at openings. Comparison for case 2 is in Figure 24 and Figure 25. For case 1 there is a comparison for test, results of phase II analysis (Explicit), results of analysis for pressure loading and results of analysis for pressure and temperature loadings. For case 2 there is only a comparison for pressure loading and pressure+temperature loadings. The comparison of analysis results for only pressure loading (Explicit x Standard) shows that the results are very close to the pressure until the concrete cracking. At higher pressures there is a lower increase of deformation for Standard analysis due to an added small permanent stiffness of concrete elements which helps increase a stability of solution (this stiffness is imposed by duplicating of concrete elements - there is always one nonlinear concrete element along with one linear element with small stiffness at aprox. 1/10 of the original concrete stiffness). The influence of temperature loading on deformation of structure is favorable – increasing of inner temperature suppresses differences of deformation around openings (comparison of deformation history at elevation 4.68 for different azimuths is in Figure 16 and Figure 26).

The global failure of structure and maximum internal overpressure is determined by bearing capacity of prestressing tendons. History of deformation shows rapid increasing after 1.3MPa. It corresponds to reaching of yield stress in tendons at 1.25MPa. Figure 12 and Figure 13 show tendon strain at 1.25MPa (stress in tendons reaches the yield stress) and at 1.52MPa (strain in tendons reaches 2%). Especially at overpressure 1.52MPa there is the expressive difference in distribution of strain along tendons due to rigid connection between tendon nodes and nodes of concrete wall. This type of connection doesn't make possible to correctly simulate tendon failure in case of structures prestressed by unbonded tendons. Despite it, the final failure mode during SFMT corresponds to state of stress detected by analysis. The comparison of tendons strain history in Figure 17 shows, that the collapse of structure happened when started the rapid increasing of tendons strain after reaching of the yield point. Figure 10 shows liner strain in circumferential direction at 1.0MPa (stress in liner reaches the yield stress). The peak of strain is between openings next to E/H (approximately at 0°) due to change of curvature of the concrete wall. Additional concentrations of strain are at buttresses and at ending of additional rebar around openings.

Question is how to set the limits of plastic strain of liner and tendons. Theoretically, due to plastic capacity of liner, the tightness could be preserved till global failure. The results of real structure test show that the tears of liner appear before the failure of structure (detailed inspections after LST revealed 26 discrete tears in the liner, all located at vertical field welds, and fabrication defects contributed to nearly all of the liner tears). Analogous, the breaking of tendons started at hoop strain approximately 1% although the tests of cables assign the breaking at strain 3.5%. For purpose of this analysis the strain at breaking of tendon and at liner tearing was set at reaching of yield stress.

The basic milestones of structure behaviour during overpressuration are summarized in the following table:

Pressure	Event
0.44 MPa	Beginning of cracking around E/H
0.60 MPa	Beginning of cracking of cylinder in circumferential direction
0.96 MPa	Continual horizontal cracks in cylinder
1.15 MPa	Yielding stress in liner
1.25 MPa	Yielding stress in tendons
1.25-1.30 MPa	Collapse of structure after breaking some tendons

The influence of heat rate on the structure state of stress is well demonstrated by force in tendons. The history of tendon forces is in Figure 17 for case 1 and Figure 27 for case 2. For case 1 loading, the force history for pressure and temperature loading is close to the force history for only pressure loading. On the other hand, there is big difference of tendon forces between pressure and pressure+temperature loading in case 2. Similar results are for the liner and rebar (Figure 18 and Figure 19 for case 1, Figure 28 and Figure 29 for case 2). In case of rebar and liner, when we compare strains, there is next curve added into the charts – due to temperature loading it is necessary to differentiate the strain corresponding to the deformation and the strain corresponding to the stress (this strain is marked as "true" in the charts). Especially in case 2 there is the strong dependence of strain in rebar and liner on the depth of elements in the wall from the inner surface. The extreme case is liner which temperature responses to the inner temperature of containment with no delay and in case of fast changes of temperature the strain reaches high values.

Results discussion

Commentary on model:

- the model used for the analysis describes global behaviour of the structure altogether well especially for case 1 loading. For the case 2 loading analysis there would be better to change the element mesh and use more elements across the wall thickness. The four linear elements used in current model are too coarse considering temperature gradient across the wall thickness.
- a global model is able to simulate beaviour of the structure from strength point of view. But there is need to create detail models to analyze liner behaviour and its tightness ability along with the liner anchors.

Commentary on results and results evaluation:

- In the Case 1 pressure loading, comparison of the analysis results and test results shows relatively good mutual equality. The results at the lower pressures are close to the real structure response. At the higher pressures there are effects of tendon modeling (instead of unbonded tendons there is rigid connection between tendons nodes and nodes of concrete wall in the model) and added stiffness of concrete elements. Used type of tendon-wall connection doesn't make possible to correctly simulate ultimate tendon failure in case of structures prestressed by unbonded tendons but up to the tendon yielding stress, the results of analysis are suitable.
- comparison of the results of temperature-pressure loading analysis with the results of pressure loading analysis shows that temperature loading with the temperature gradient across the wall

close to uniform is more favorable. On the other hand, long term high temperature loading causes temperature degradation into higher depth of wall. Rapid changes of temperature in containment are the most dangerous for liner, response of the rest of structure is suppressed by thermal capacity of structure material.

- the temperature degradation effects weren't too important in analyzed loading cases. Degradation of concrete has low effect due to tensile stress of concrete - pressure loading history corresponds to temperature loading history so there is high pressure at higher temperatures. Temperature degradation of steel has no effect in the case 1 loading due to low temperature. In case 2, there is considerable effect on liner during hydrogen detonation but due to relatively short time period of this loading there is no temperature degradation of rebar or tendons. Temperature degradation at final part of case 2 loading history could affect inner rebar row but the corresponding pressure loading is at the bearing capacity of the structure and likely there will be the structure failure before the temperature degradation could affect the rebar.
- beyond the direct influence of the temperature on degradation of material properties there are additional effects, e.g. thermal spalling of concrete at higher heating rates or redistribution and decrease of thermal stress in concrete. Simulation of these effects is more complicated (in global models) so it is difficult to include them directly into analysis. On the other hand, influence of thermal spalling of concrete can be decreased for example by applications of polypropylene fibres – higher temperature destroy the fibres and porosity of the concrete increases.
- the analysis results show that the temperature couldn't change the failure mode of the structure significantly and, especially for long term thermal loading, the pressure will be the critical loading. On the other hand, thermal loading with fast changes of inner temperature is the critical loading for liner.

Conclusion

Analysis performed during Phase II and Phase III of ISP48 showed the ability of actual analytical tools to simulate a behaviour of a such complex concrete structure as the PCCV is. Solving of the same problem by a number of groups from several countries enabled to compare different approach and ways how to analyze this problem. Acquired knowledge can be summarized into the following points:

- actual analytical tools based on FEM enable to analyze the structure in very complex way including a nonlinear behaviour. But this approach needs more detailed information about material properties and corresponding material testing.
- the test results showed differences of ultimate failure stress/strain between the individual material tests and the behaviour of the same material in the structure. For example, due to plastic capacity of liner, the tightness could be preserved till global failure but the results of real structure test show that the tears of liner appear before the failure of structure. Similarly, the breaking of tendons started at hoop strain approximately 1% although the tests of cables assign the breaking at strain 3.5%.
  Comparison of analysis and test results shows that conservatively it is possible to use the yield stress/strain of the material, i.e. conservatively it is possible to expect the liner tearing at the point of reaching of the yield strain and expect the failure of the structure after reaching of the yield strain in the first tendon.
- temperature effects weren't too considerable in analyzed load cases (except liner there was no temperature degradation of material). Concerning material input data, the temperature

degradation is in detail described by standards for design of buildings against fire and number of tests have been accomplished. Difference of the PCCV structures is in the more solid and compact structure and corresponding higher sensitivity of the structure to the fast temperature changing. Changes of temperature are critical for design of liner. There is need to analyze the liner not only as part of global model but also in detail models.

- concurrent expansion of a computing technology and capabilities of analytical tools enable to analyze the structure not only in single deterministic step but also with considering of uncertainties of the input data as a sensitivity or fully probabilistic analysis. Importance of this type of analysis increases in case when the variability of parameters in time have to be considered. Typical example is determination of presstresing force after several decades - only for creep of concrete, there are number of uncertainties (concrete strength, water/cement and aggregate/cement rations, humidity time history, temperature time history).

References

[1] NEA/CSNI/R(2004)11, International Standard Problem No.48 Containment Capacity - Phase 2 Report Results of Pressure Loading Analysis.

[2] R. Dameron, M. Wolohan, B. Hansen, E. Kelley, M. Hessheimer (2004), Analysis of Axisymmetric Prestressed Concrete Containment Vessel (PCCV) Including Thermal Effects - A Summary of Temperature Section Results, Analytical Assumptions and Technical Approach for use by the ISP48 Analysis Exercise Participants.

[3] CSN P ENV 1992-1-1 (1996) Design of concrete structures (European prestandard), Český normalizační institut, Prague.

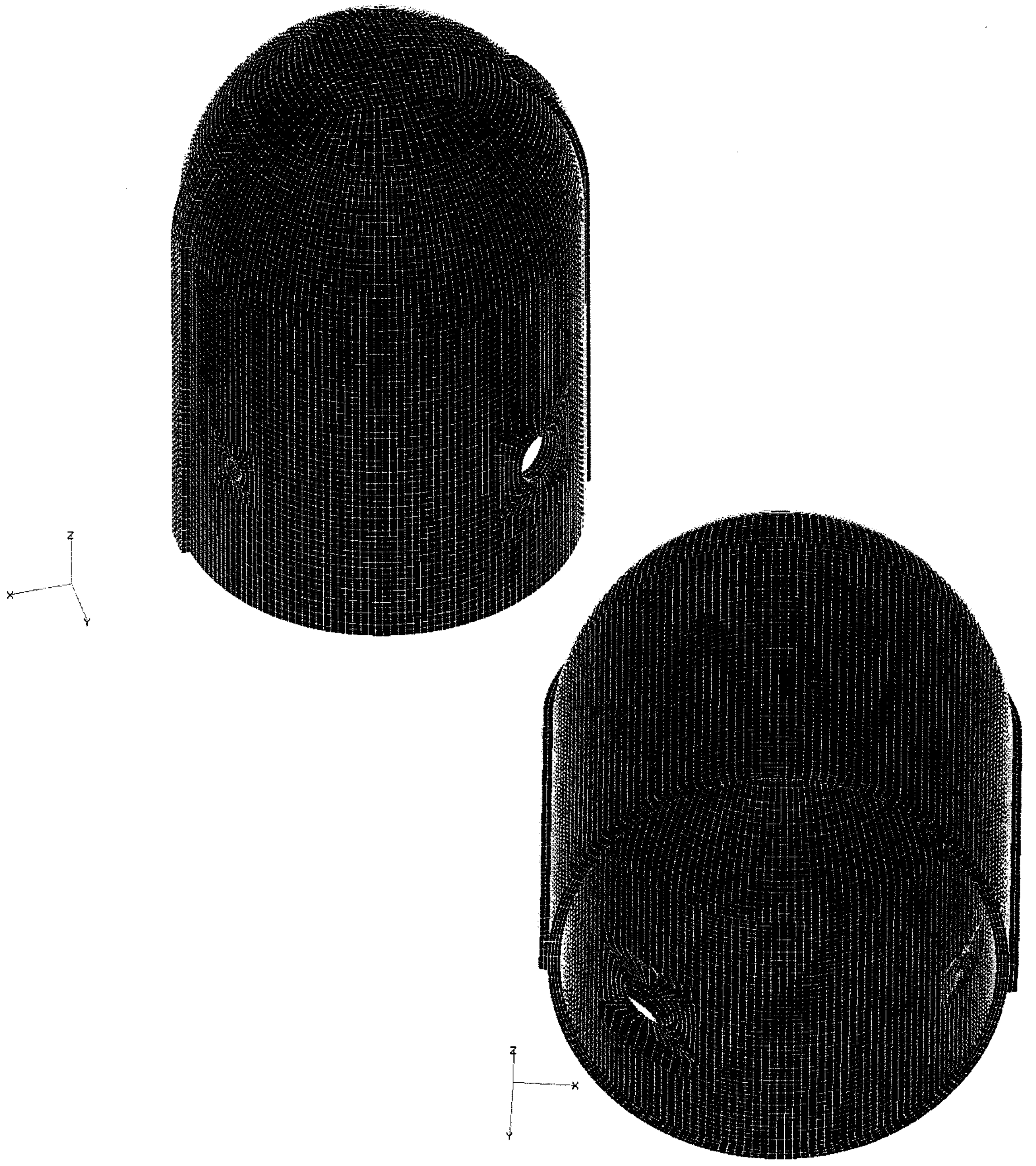

Figure 1 FEM model

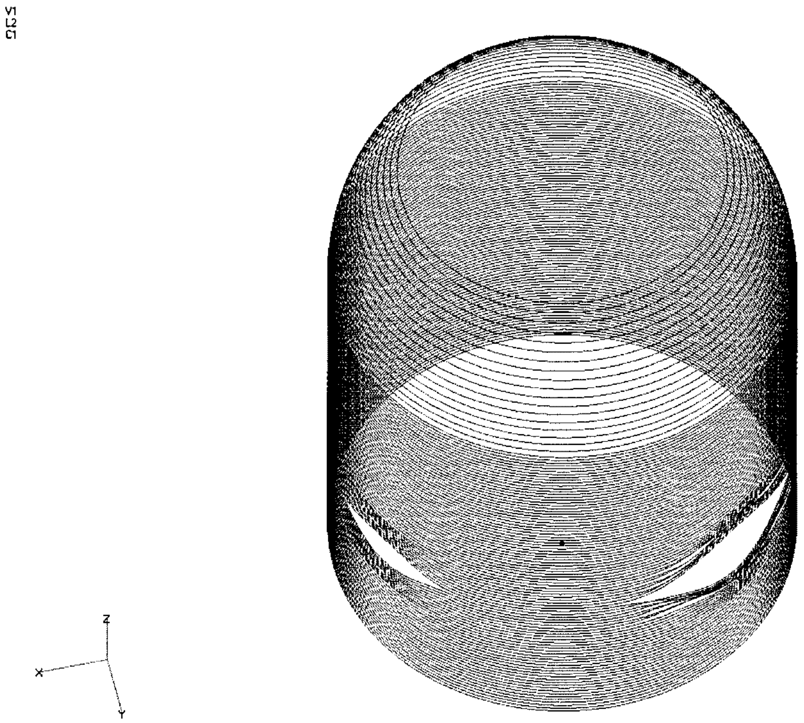

Figure 2 Prestressed tendon elements – hoop tendons

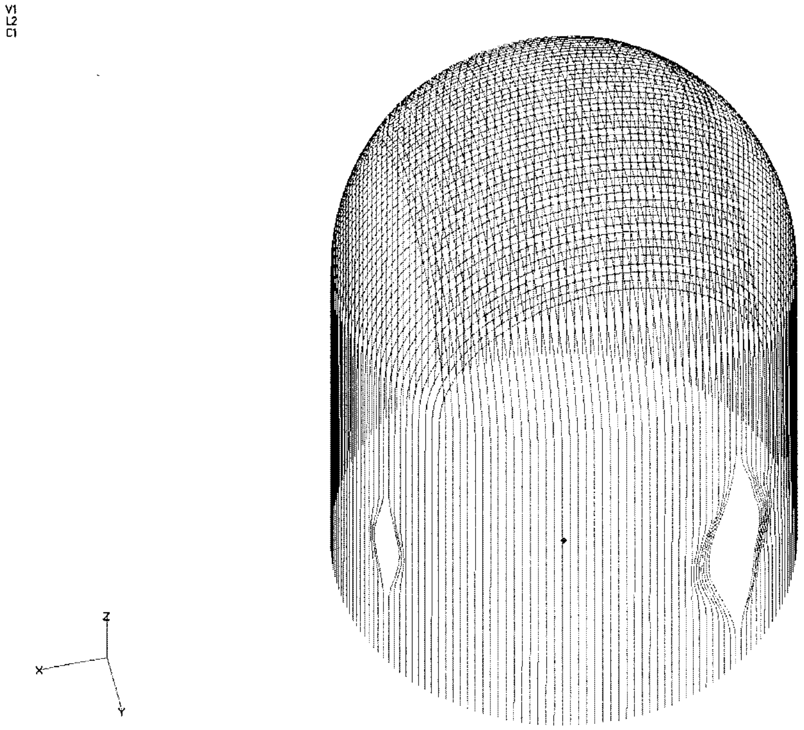

Figure 3 Prestressed tendon elements – vertical tendons

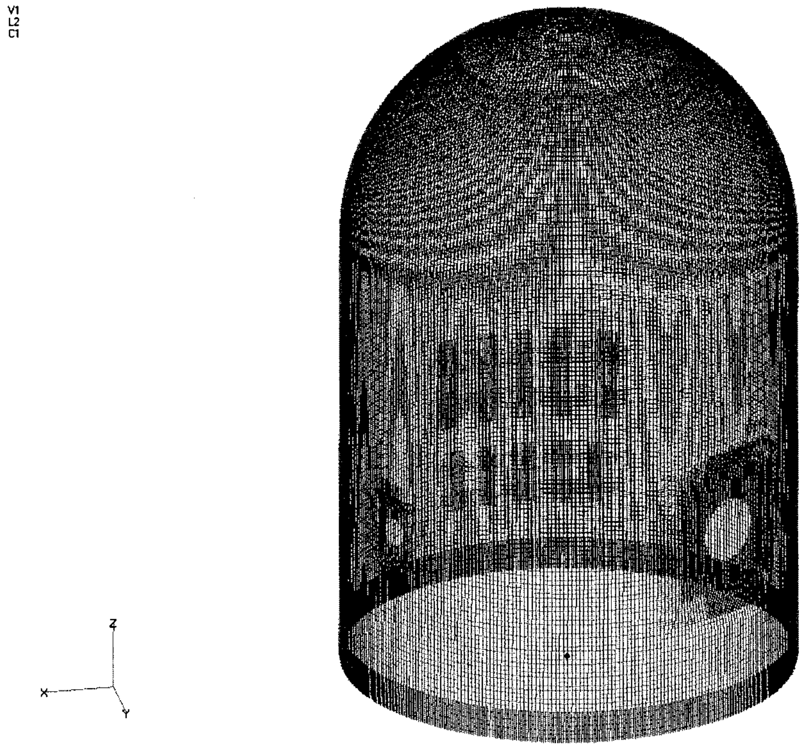

Figure 4 Rebar elements – inner row

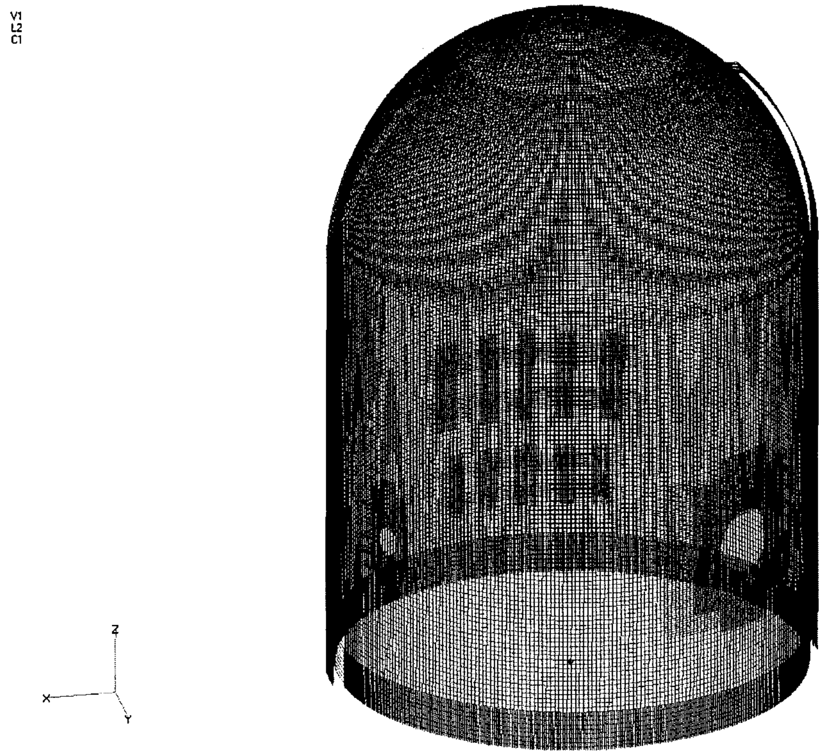

Figure 5 Rebar elements – outer row

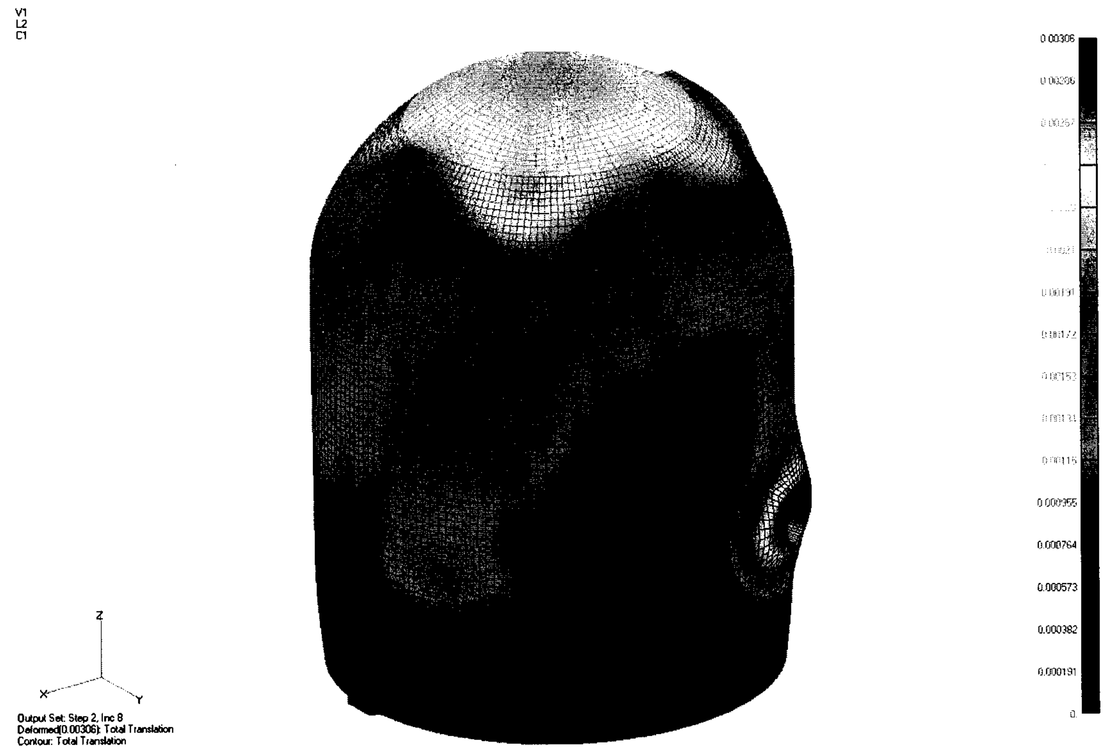
V1
L2
C1
0.00306
0.000955
0.000764
0.000573
0.000382
0.000191
0
Z
X
Y
Output Set: Step 2, Inc 8
Deformed(0.00306): Total Translation
Contour: Total Translation

Figure 6 Case 1: Total deformation at 0.6MPa – loading by pressure

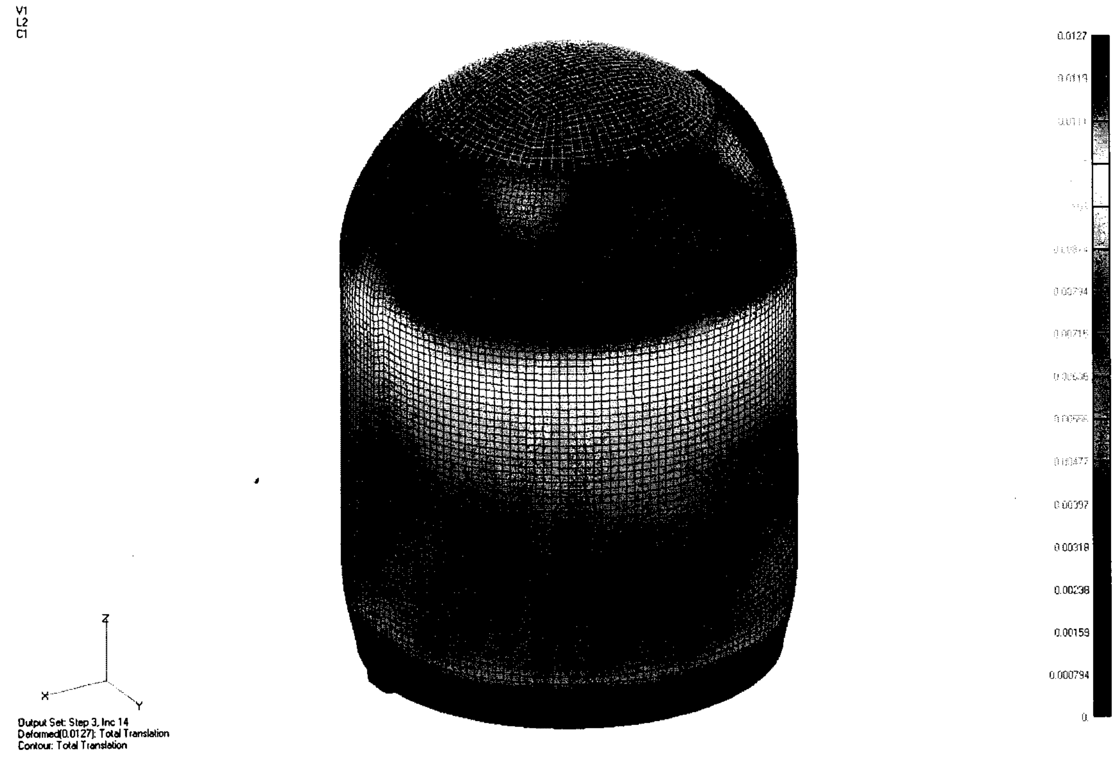
V1
L2
C1
0.0127
0.00397
0.00318
0.00238
0.00159
0.000794
0
Z
X
Y
Output Set: Step 3, Inc 14
Deformed(0.0127): Total Translation
Contour: Total Translation

Figure 7 Case 1:Total deformation at 0.6MPa – loading by pressure and temperature

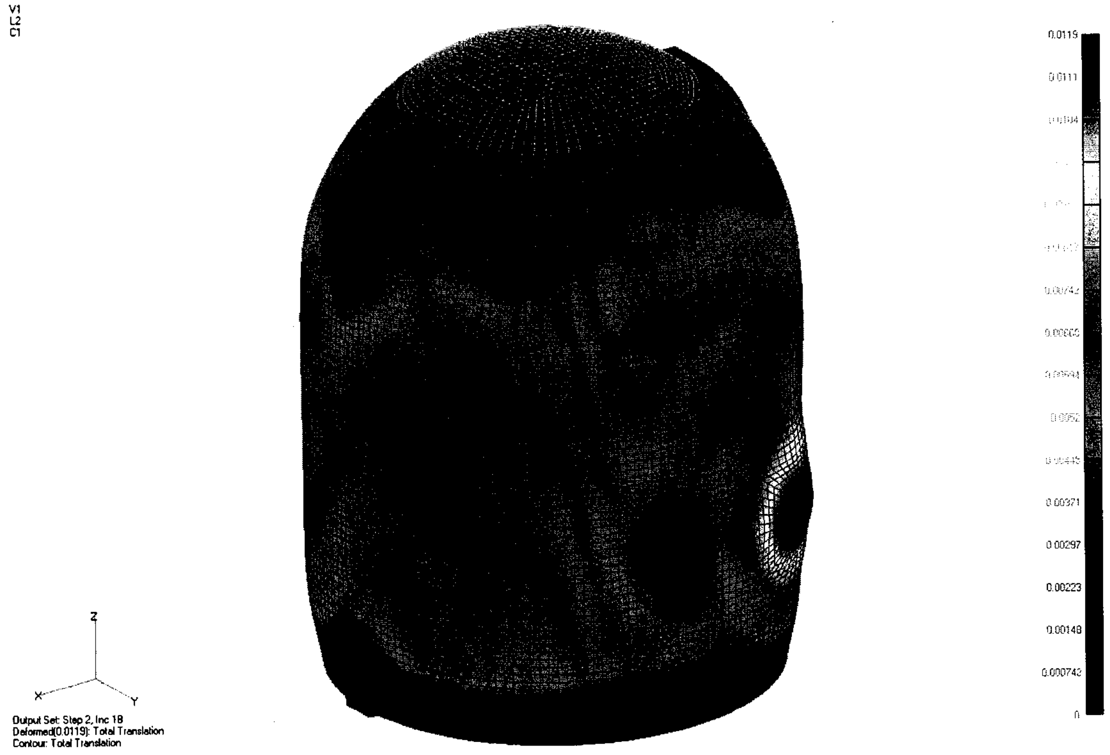
V1
L2
C1
0.0119
0.0111
0.0104
0.00742
0.00668
0.00594
0.0052
0.00445
0.00371
0.00297
0.00223
0.00148
0.000742
0
Z
X
Y
Output Set: Step 2, Inc 18
Deformed(0.0119): Total Translation
Contour: Total Translation

Figure 8 Case 1:Total deformation at 1.0MPa – loading by pressure

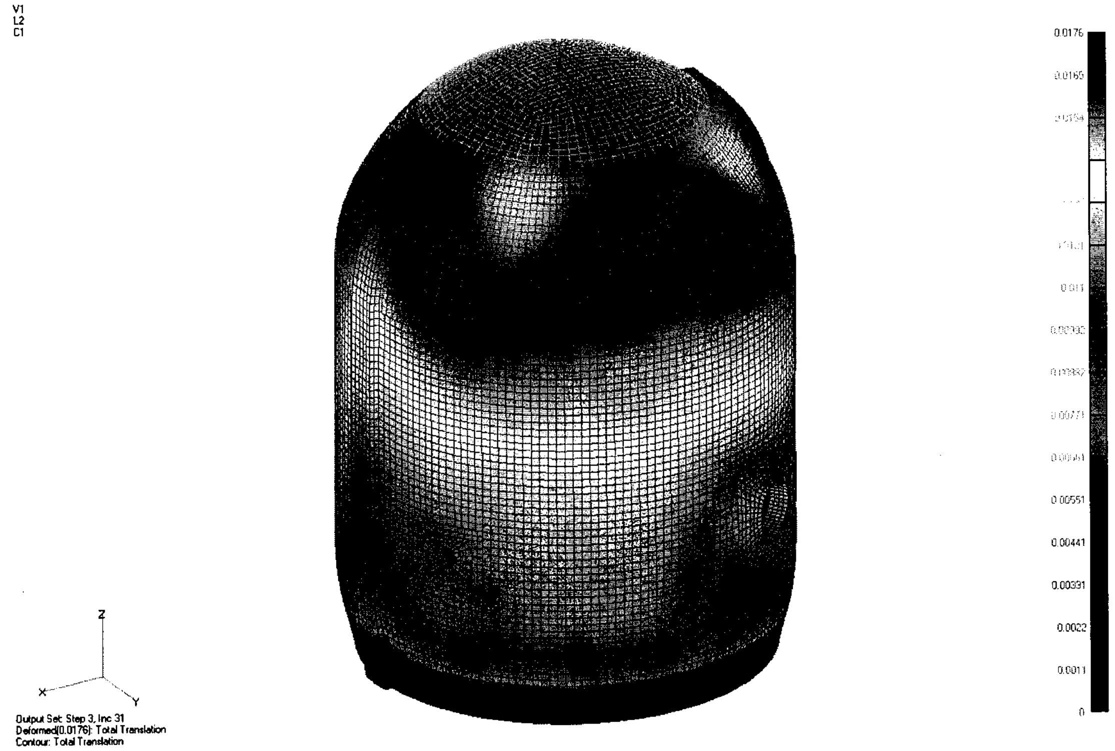
V1
L2
C1
0.0176
0.0165
0.0154
0.0121
0.011
0.00992
0.00882
0.00771
0.00661
0.00551
0.00441
0.00331
0.0022
0.0011
0
Z
X
Y
Output Set: Step 3, Inc 31
Deformed(0.0176): Total Translation
Contour: Total Translation

Figure 9 Case 1:Total deformation at 1.0MPa – loading by pressure and temperature

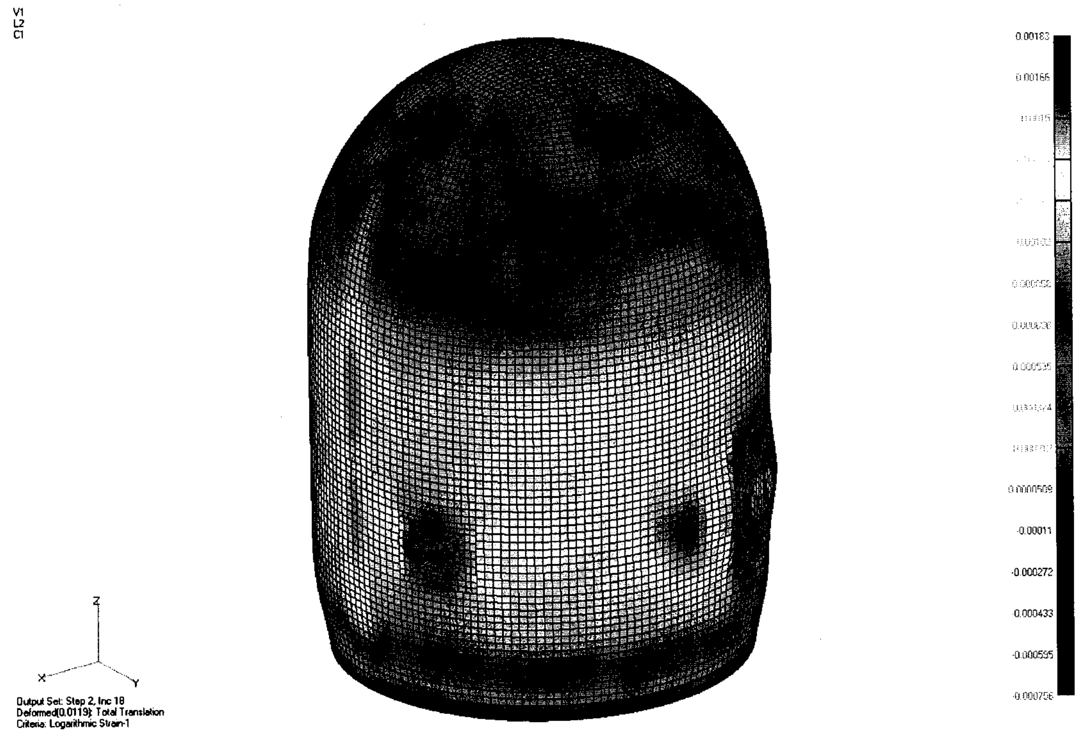
V1
L2
C1
0.00183
0.00166
0.0000509
-0.00011
-0.000272
-0.000433
-0.000595
-0.000756
Z
X
Y
Output Set: Step 2, Inc 18
Deformed(0.0119): Total Translation
Criteria: Logarithmic Strain-1

Figure 10 Case 1:Liner strain in circumferential direction at 1.0MPa – loading by pressure

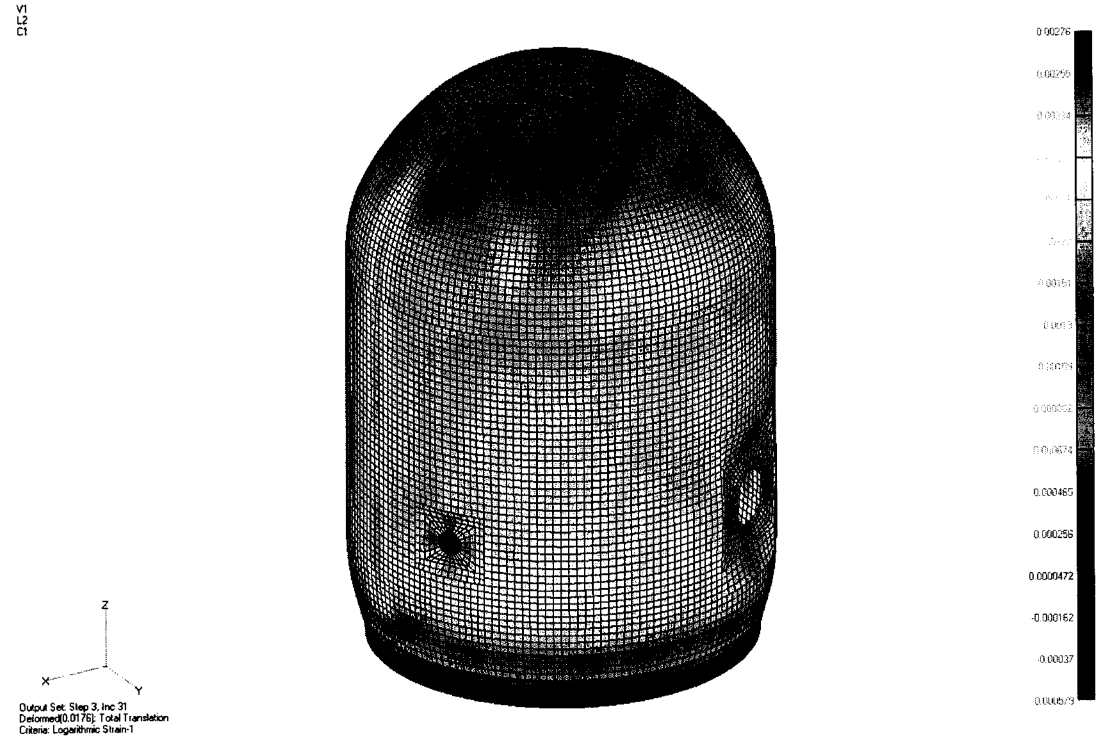
V1
L2
C1
0.00276
0.00255
0.000465
0.000256
0.0000472
-0.000162
-0.00037
Z
X
Y
Output Set: Step 3, Inc 31
Deformed(0.0176): Total Translation
Criteria: Logarithmic Strain-1

Figure 11 Case 1:Liner strain in circumferential direction at 1.0MPa – loading by pressure and temperature

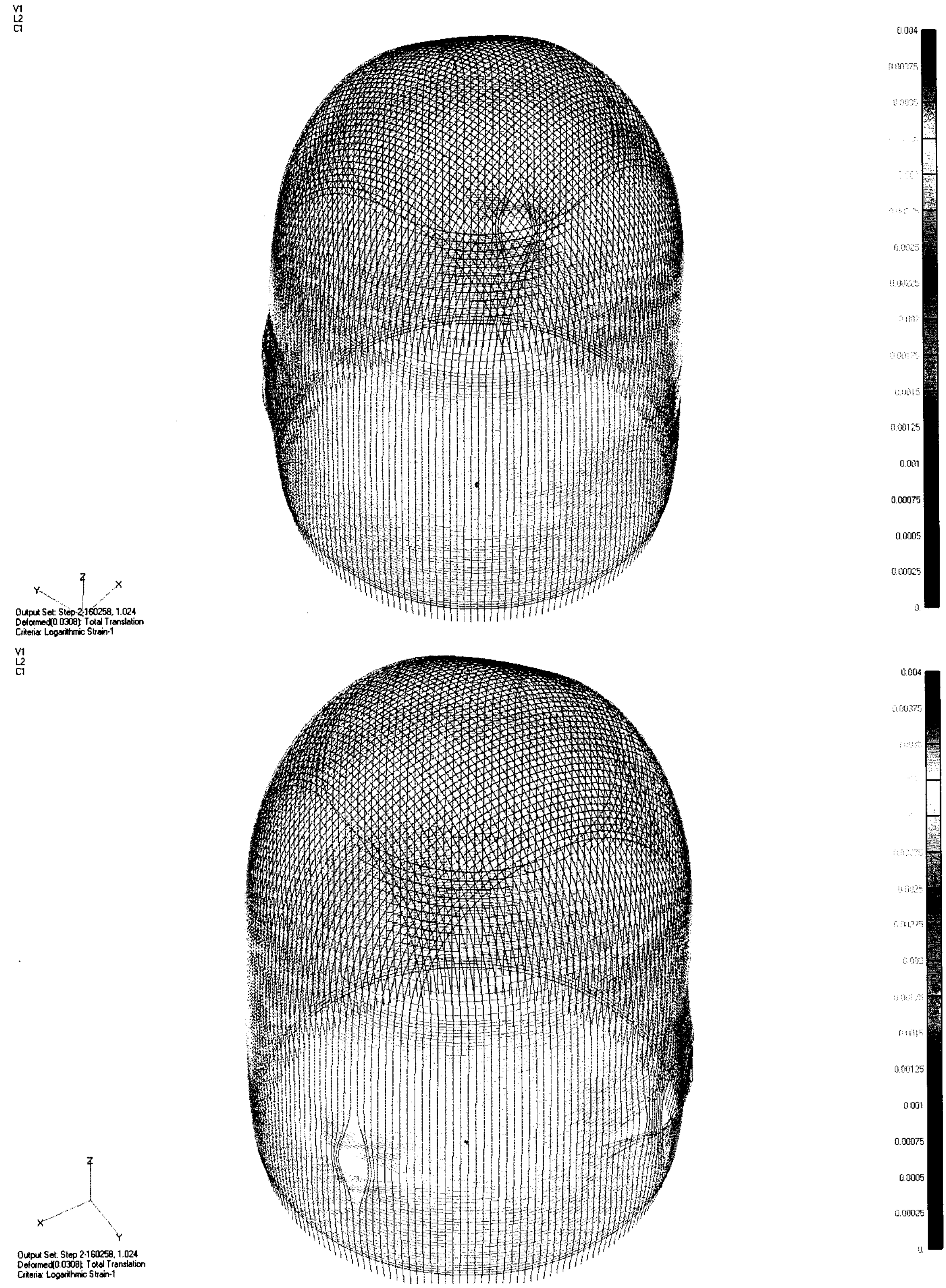
V1
L2
C1
0.004
0.00375
0.0025
0.00225
0.00125
0.001
0.00075
0.0005
0.00025
0.
Z
Y
X
Output Set: Step 2-160258, 1.024
Deformed(0.0308): Total Translation
Criteria: Logarithmic Strain-1
V1
L2
C1
0.004
0.00375
0.00125
0.001
0.00075
0.0005
0.00025
0.
Z
X
Y
Output Set: Step 2-160258, 1.024
Deformed(0.0308): Total Translation
Criteria: Logarithmic Strain-1

Figure 12 Tendon strain at 1.25MPa – loading by pressure , stress in tendons reaches yield stress

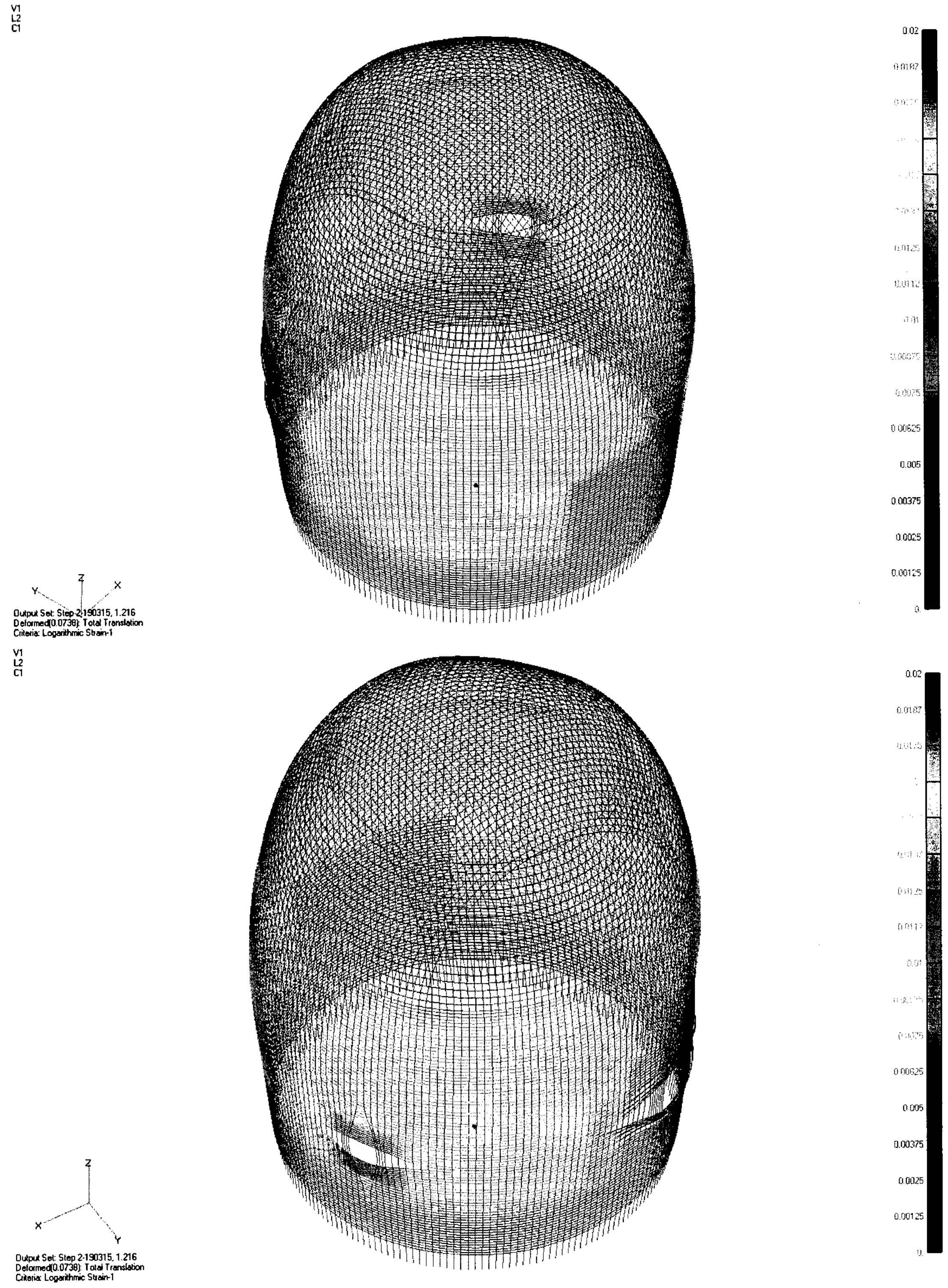

Figure 13 Tendon strain at 1.52MPa – loading by pressure, strain in tendons reaches 2%

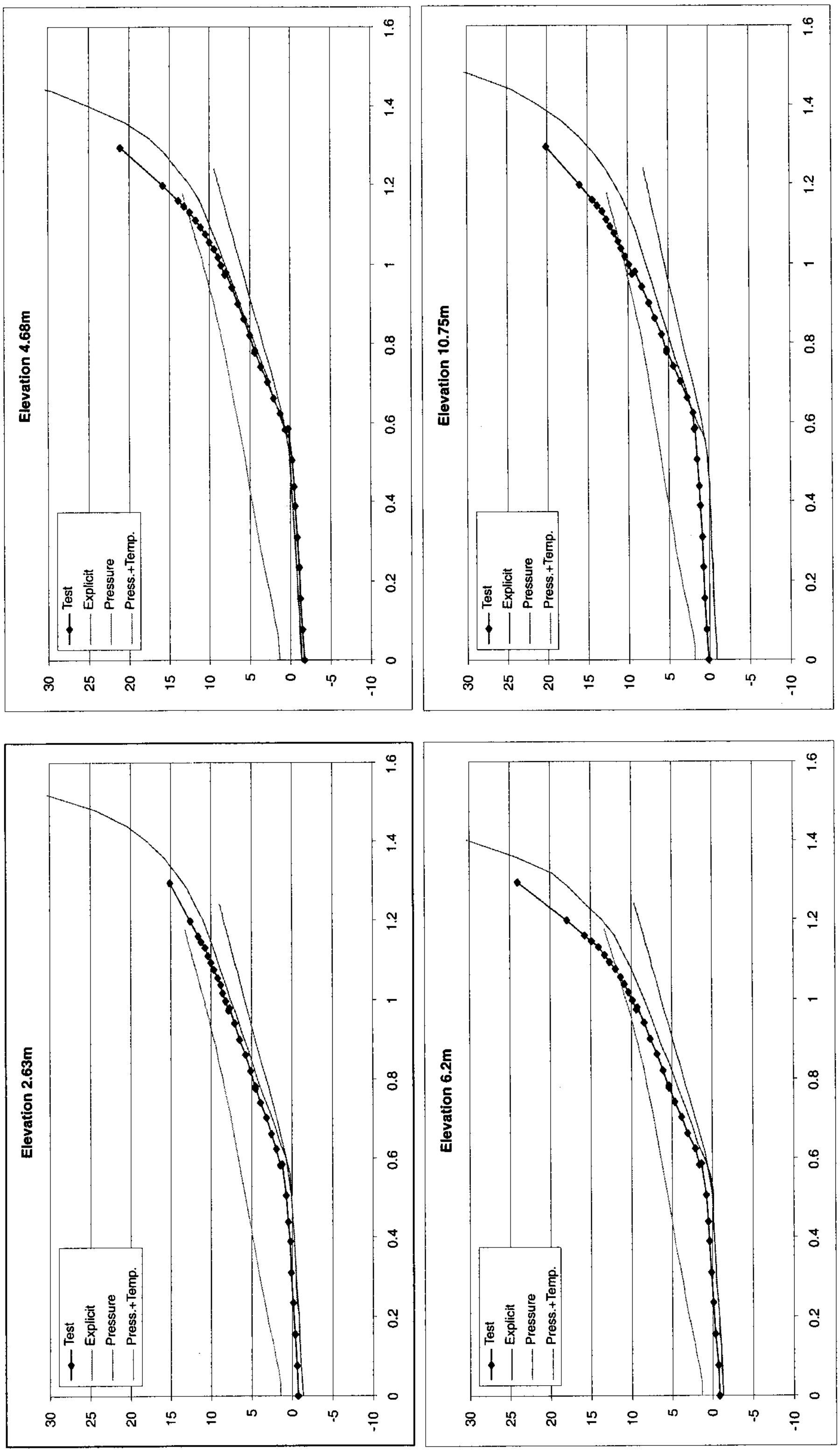

Figure 14 Case 1:Comparison of radial displacements at 135 degrees (mm, MPa)

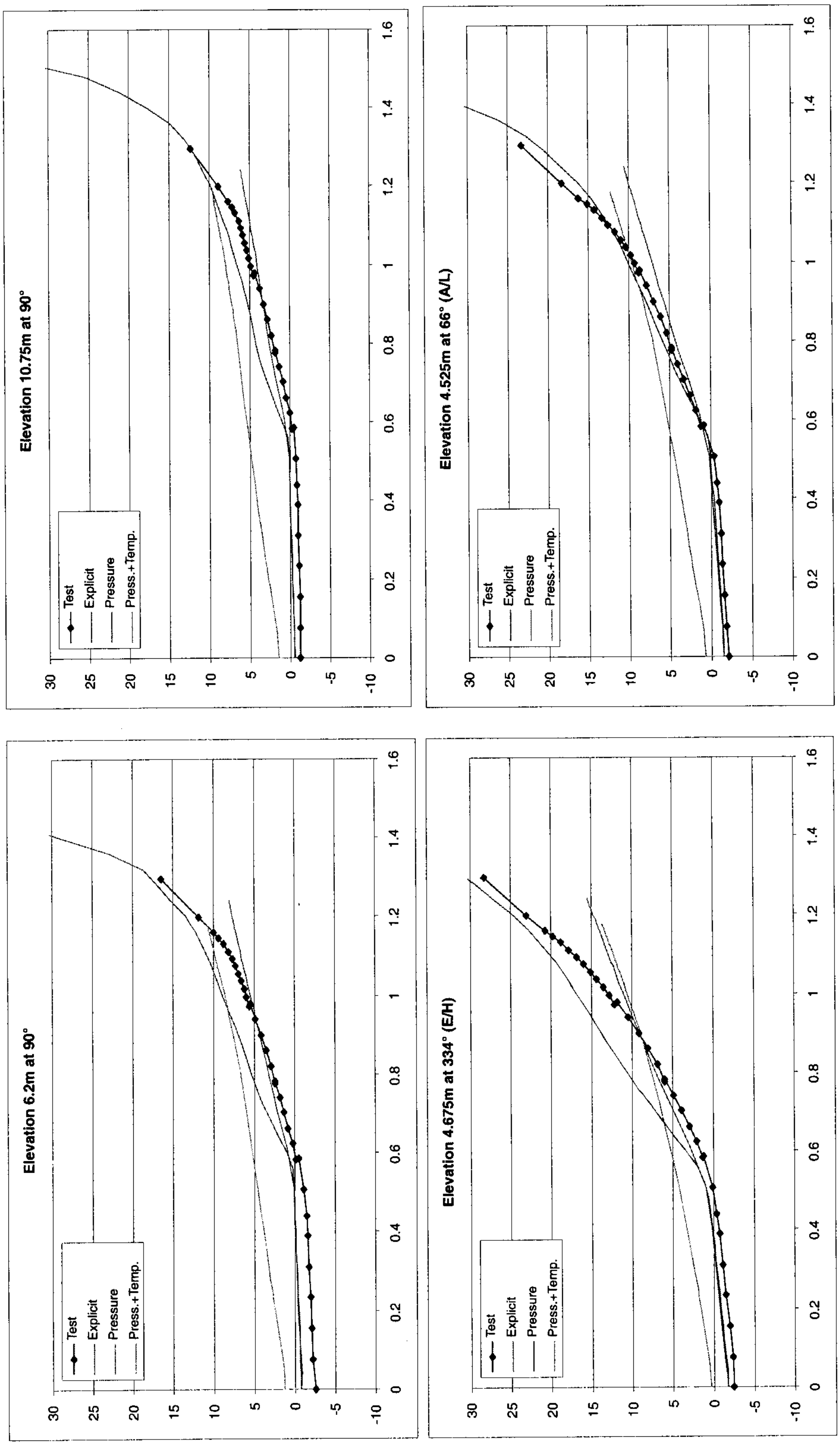

Figure 15 Case 1:Comparison of radial displacements at 90 degrees and openings (mm, MPa)

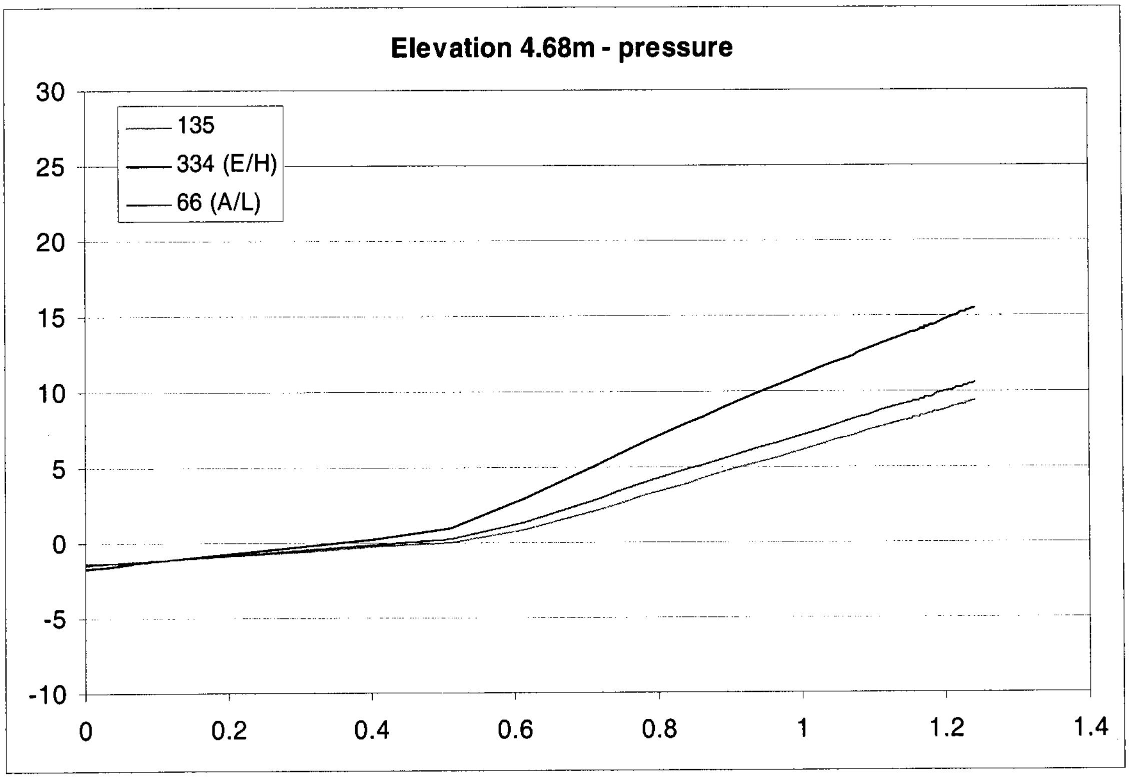

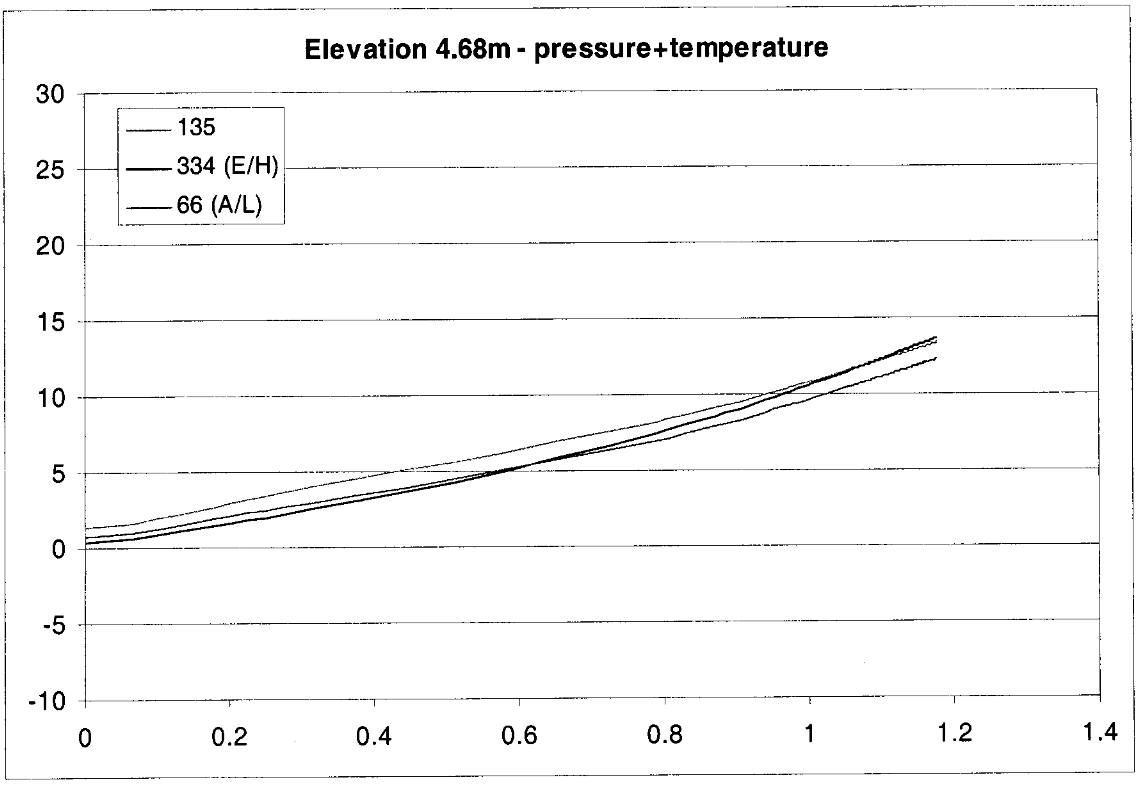

Figure 16 Case 1:Comparison of radial displacements at elevation 4.68 for different azimuths (mm, MPa)

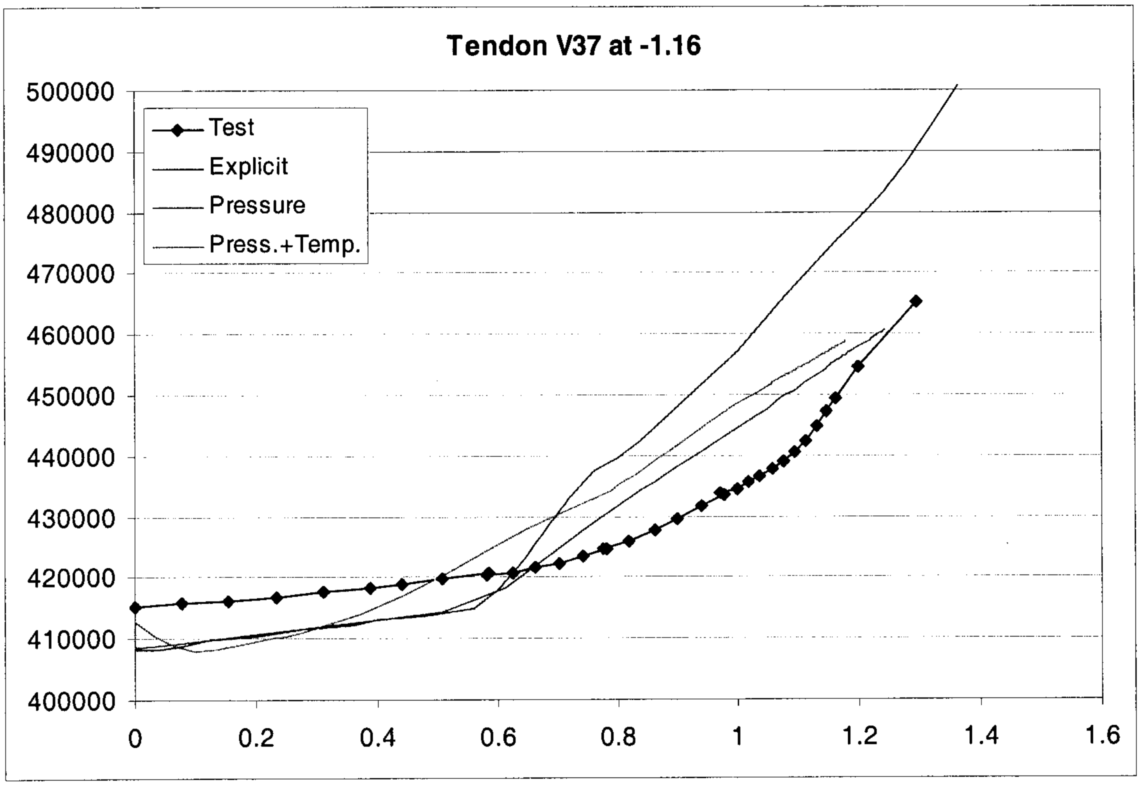

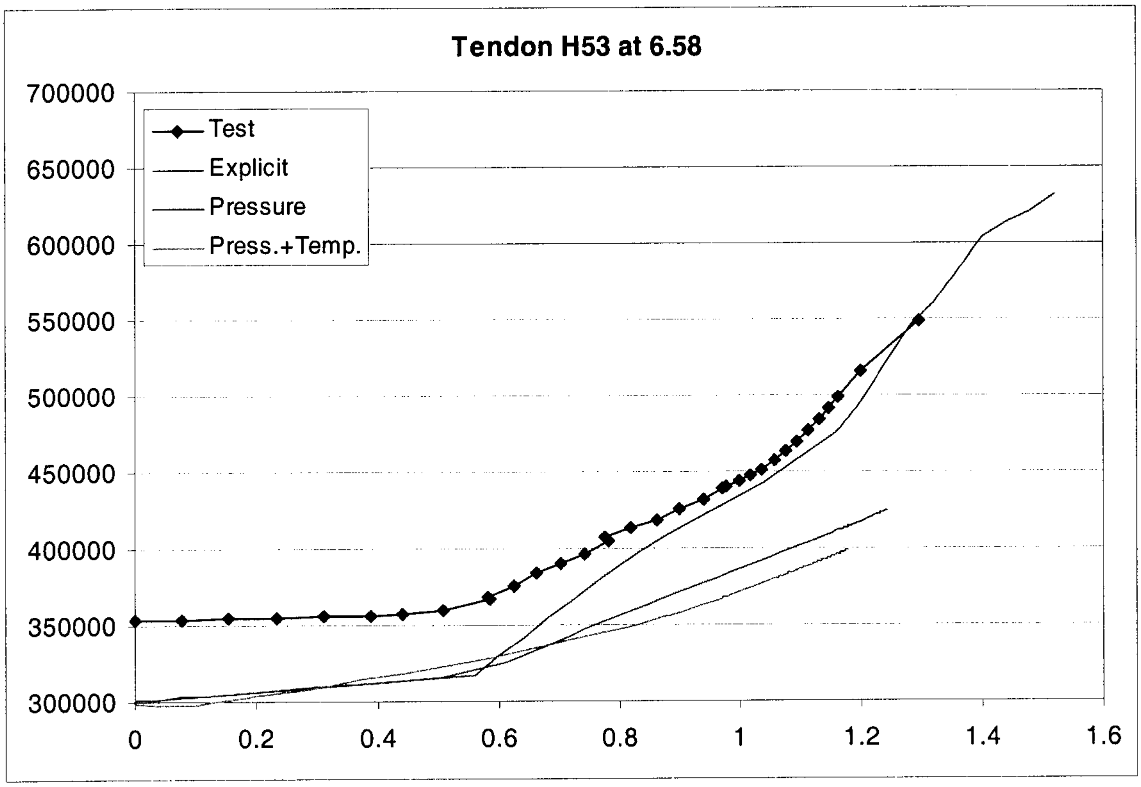

Figure 17 Case 1:Comparison of tendons strain and force (m/m or N, MPa)

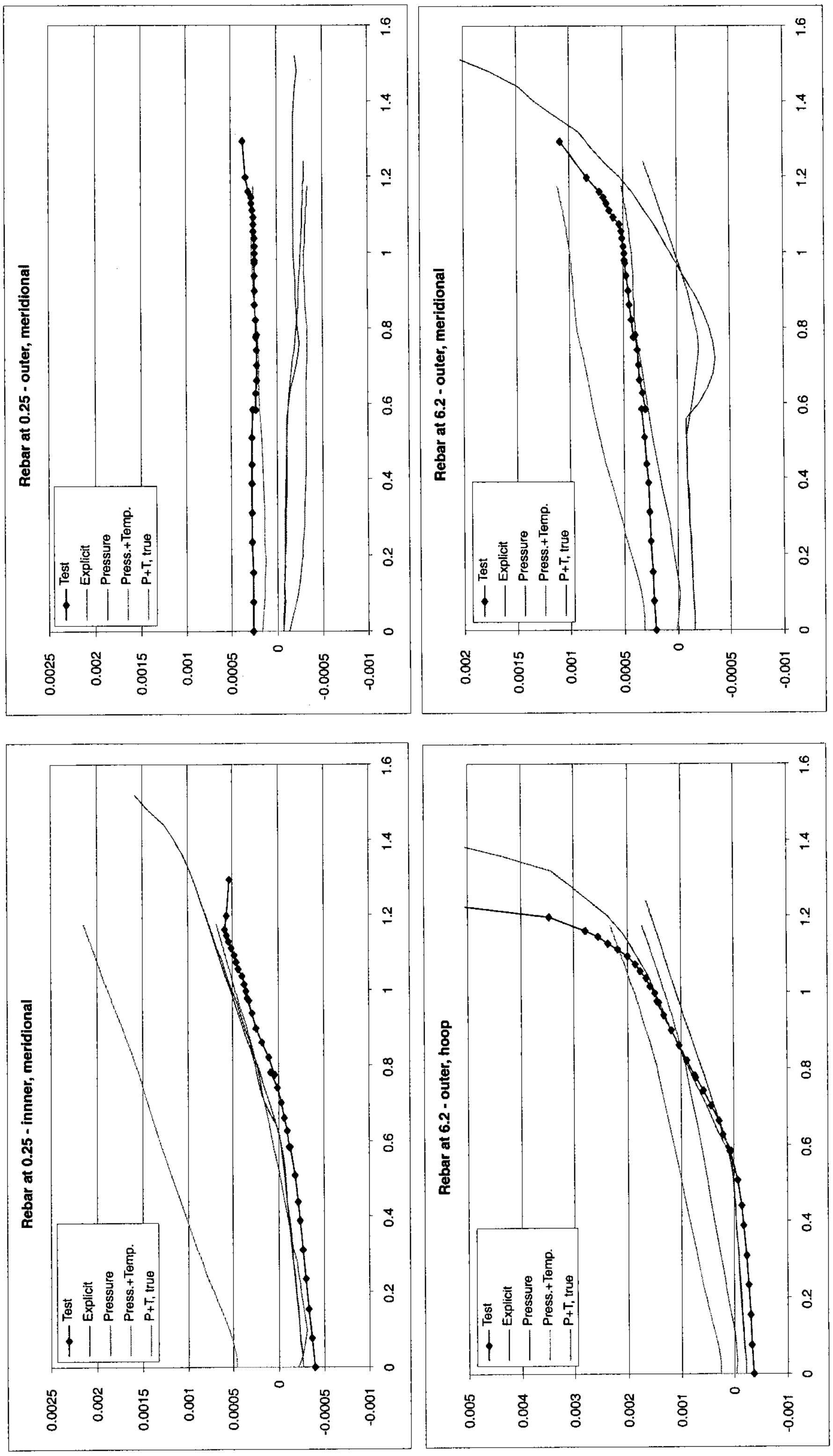

Figure 18 Case 1:Comparison of rebar strain (m/m, MPa)

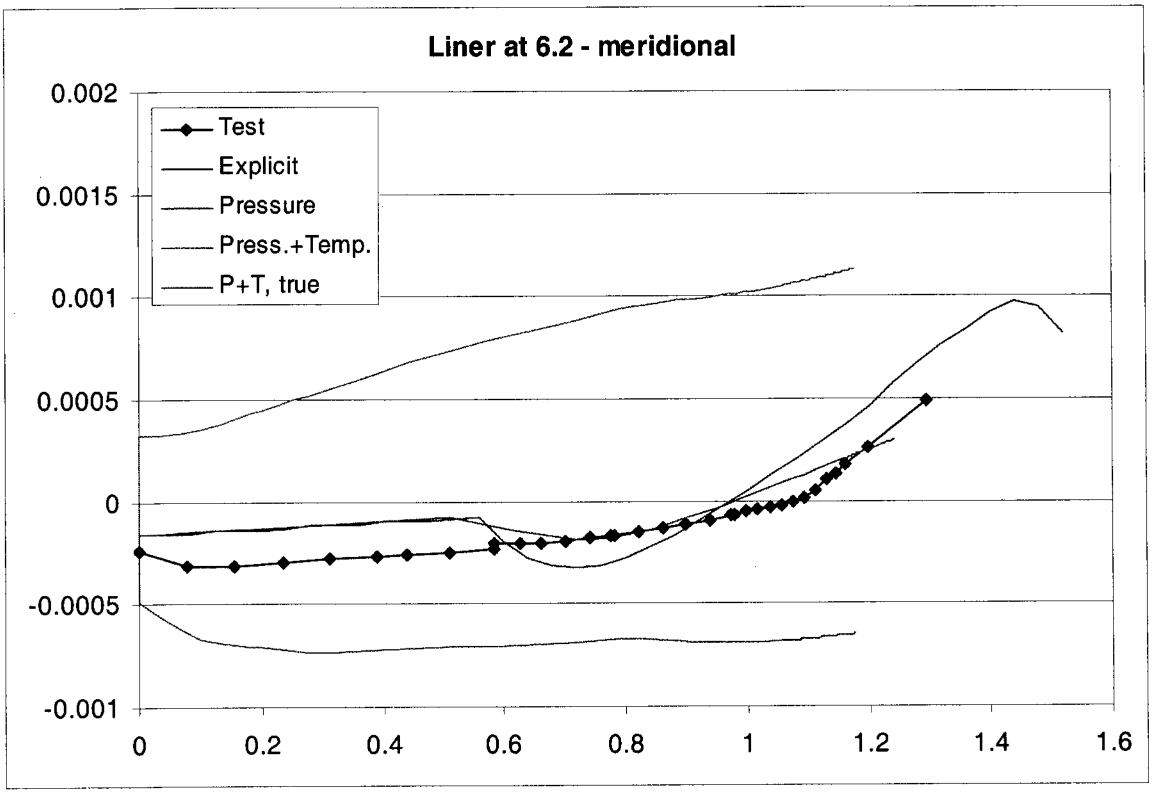

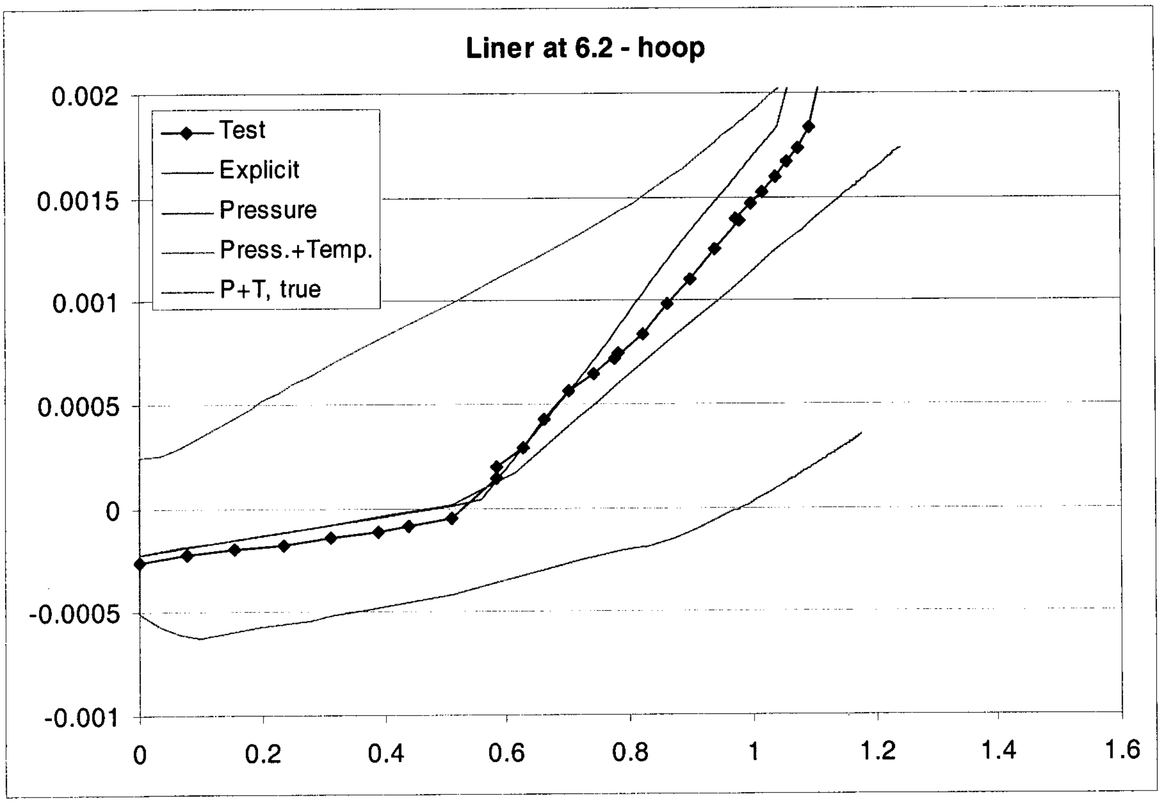

Figure 19 Case 1:Comparison of liner strain at 135° (m/m, MPa)

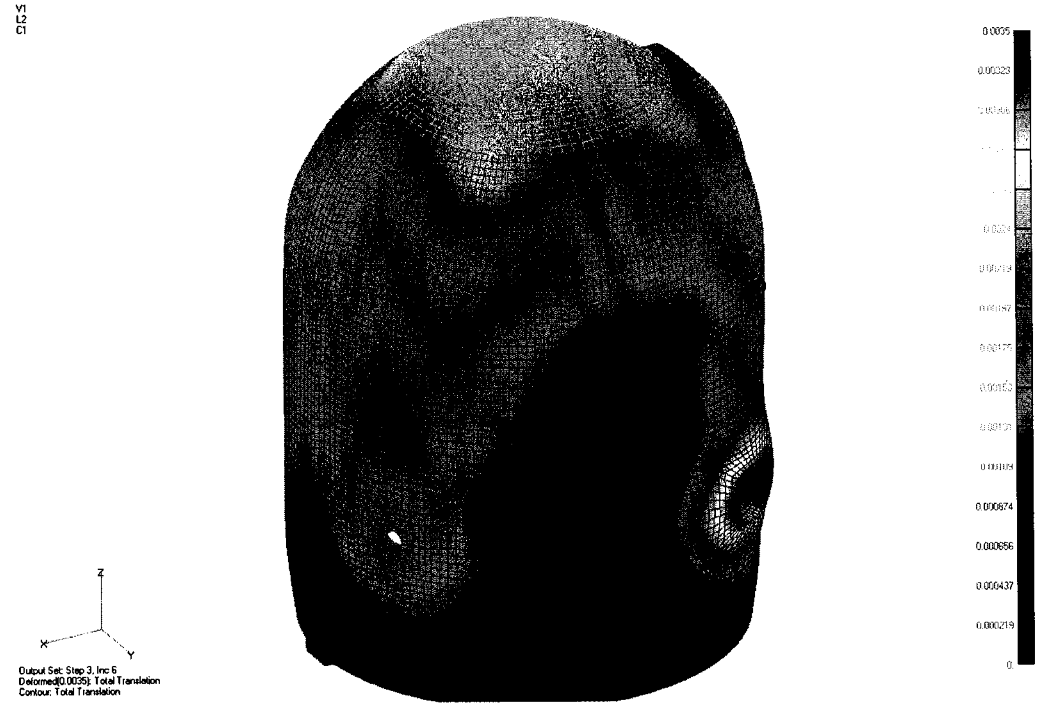
V1
L2
C1
0.0035
0.000874
0.000656
0.000437
0.000219
0.
Z
X
Y
Output Set: Step 3, Inc 6
Deformed(0.0035): Total Translation
Contour: Total Translation

Figure 20 Case 2:Total deformation at time of hydrogen detonation – loading by pressure

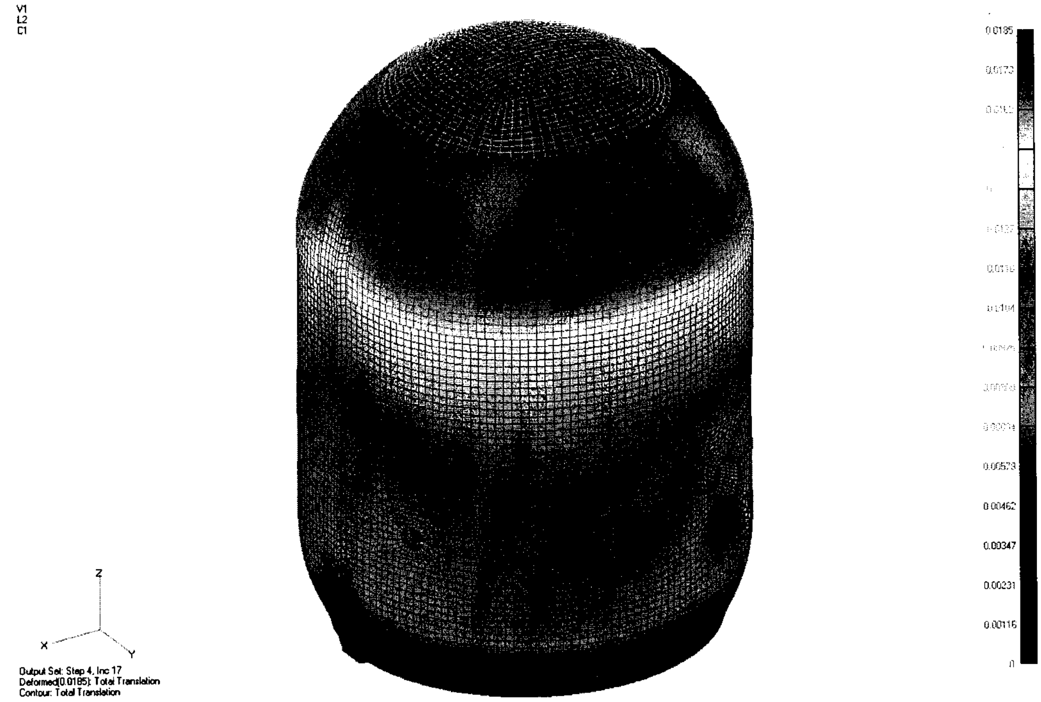
V1
L2
C1
0.0185
0.0173
0.00573
0.00462
0.00347
0.00231
0.00116
0
Z
X
Y
Output Set: Step 4, Inc 17
Deformed(0.0185): Total Translation
Contour: Total Translation

Figure 21 Case 2:Total deformation at time of hydrogen detonation – loading by pressure and temperature

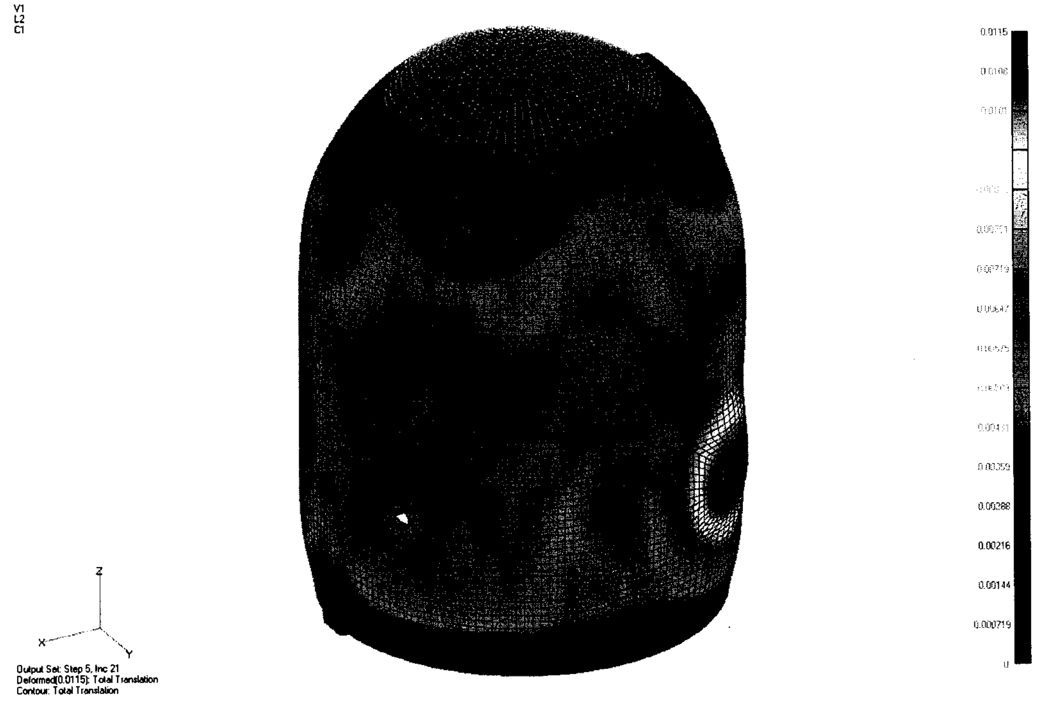
V1
L2
C1
0.0115
0.0108
0.0101
0.00791
0.00719
0.00647
0.00575
0.00503
0.00431
0.00359
0.00288
0.00216
0.00144
0.000719
0.
Z
X
Y
Output Set: Step 5, Inc 21
Deformed(0.0115): Total Translation
Contour: Total Translation

Figure 22 Case 2:Total deformation at time 3600 min. – loading by pressure

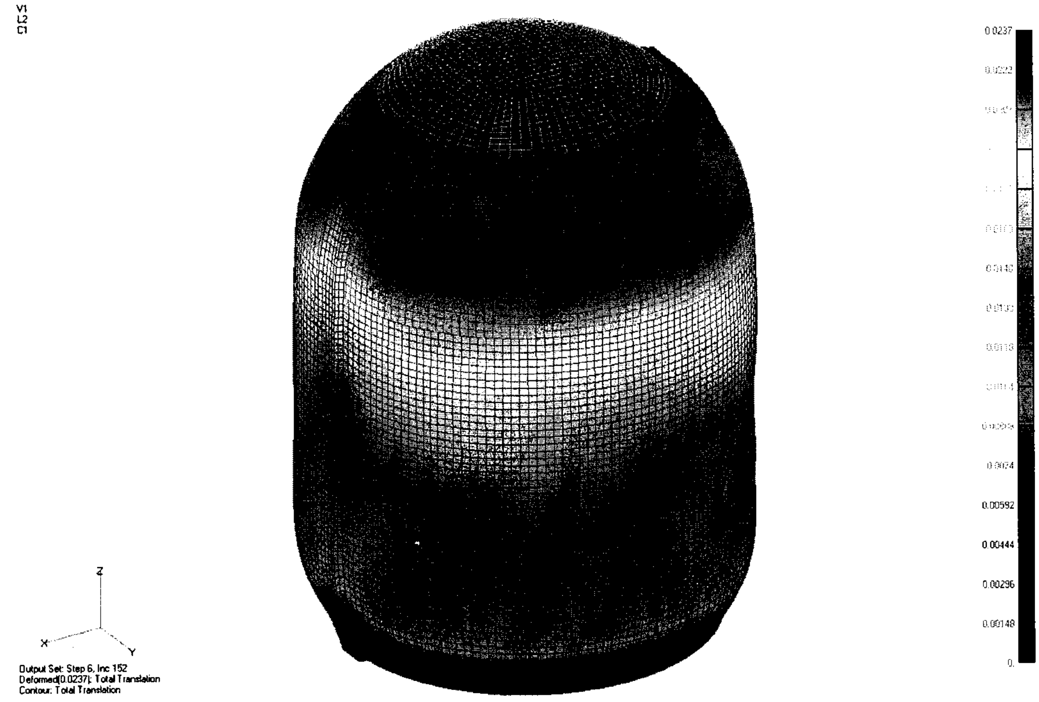
V1
L2
C1
0.0237
0.0222
0.0148
0.0133
0.0118
0.0074
0.00592
0.00444
0.00296
0.00148
0.
Z
X
Y
Output Set: Step 6, Inc 152
Deformed(0.0237): Total Translation
Contour: Total Translation

Figure 23 Case 2:Total deformation at time 3600 min. – loading by pressure and temperature

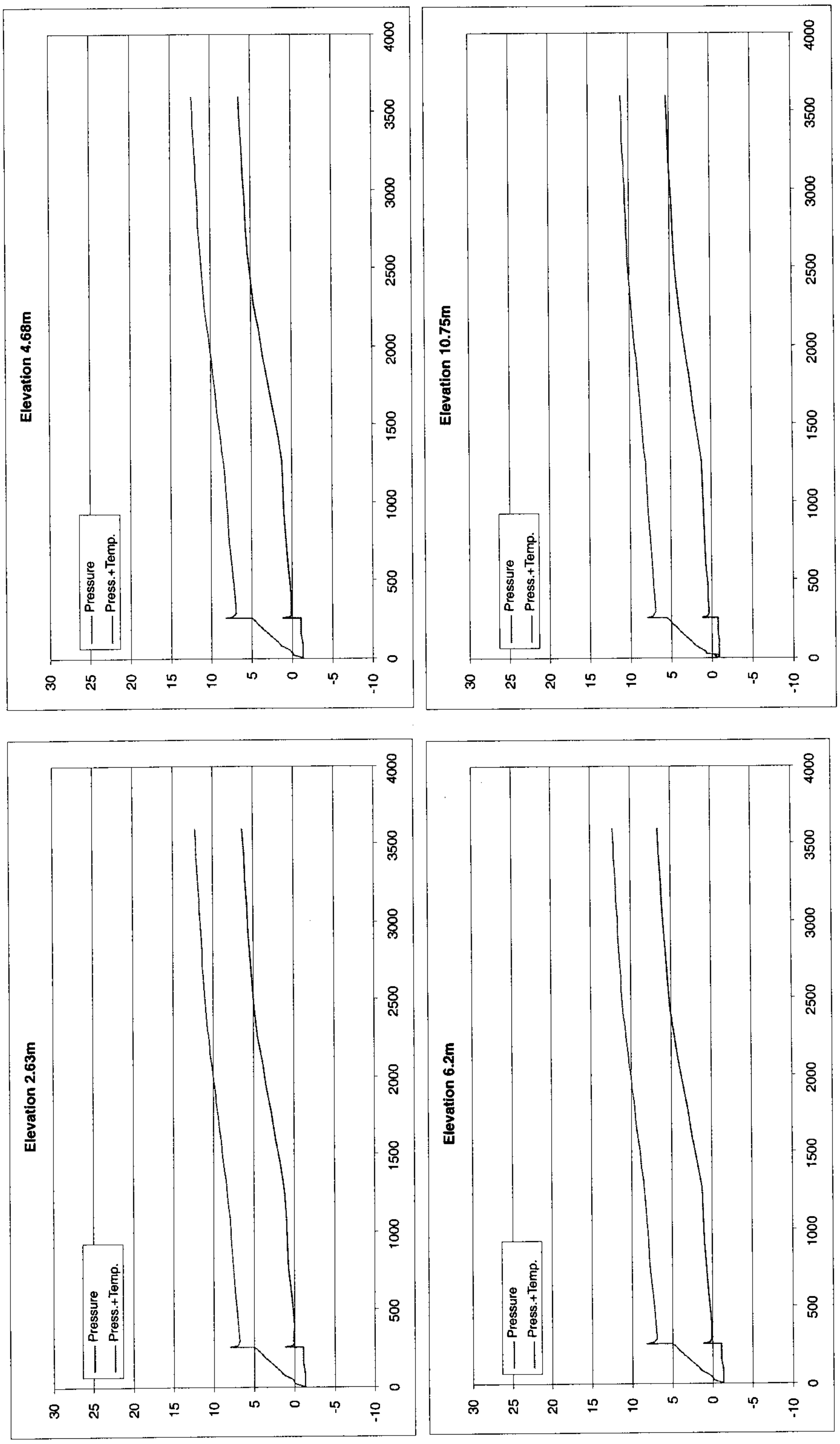

Figure 24 Case 2:Comparison of radial displacements at 135 degrees (mm, MPa)

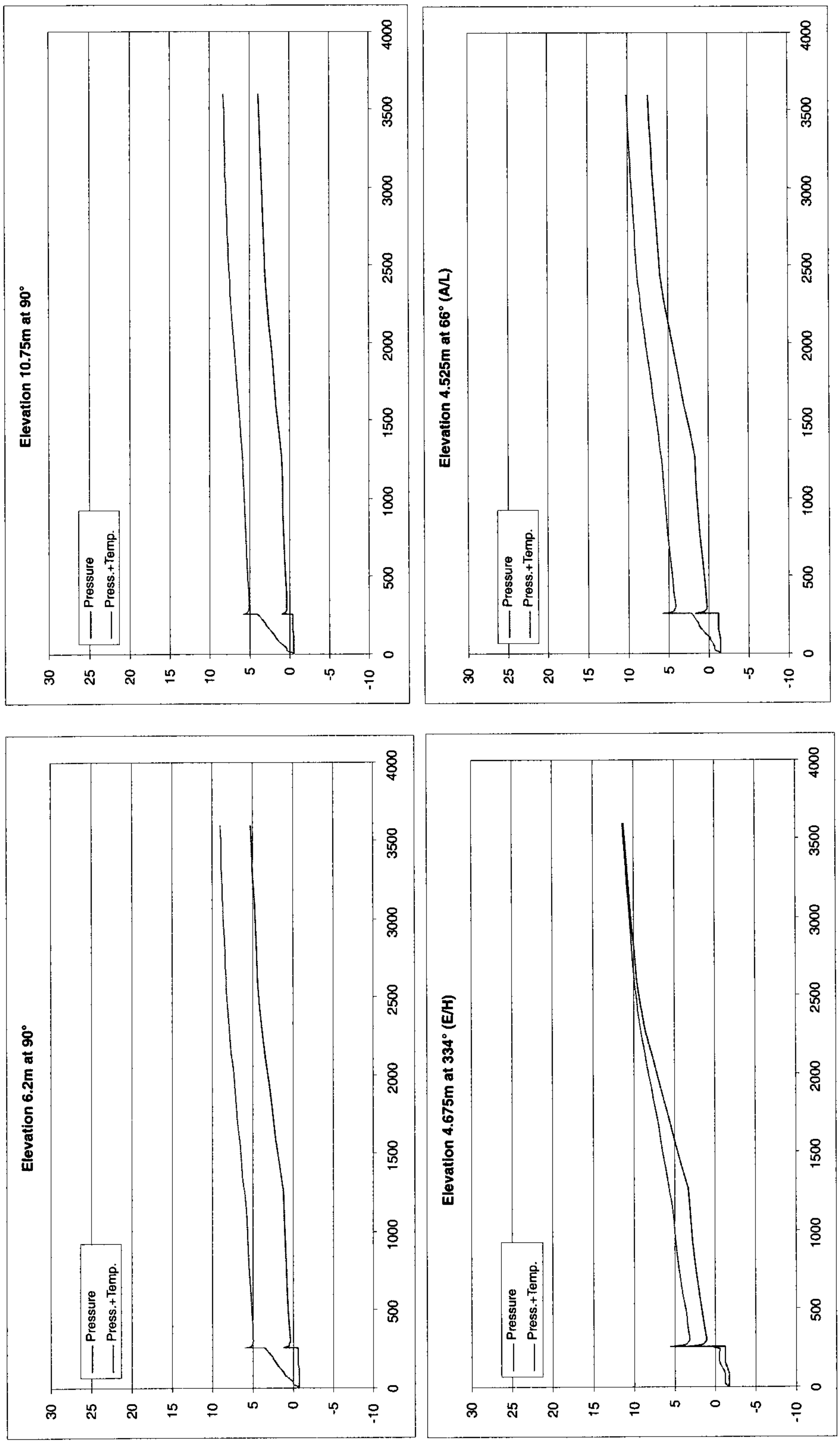

Figure 25 Case 2:Comparison of radial displacements at 90 degrees and openings (mm, MPa)

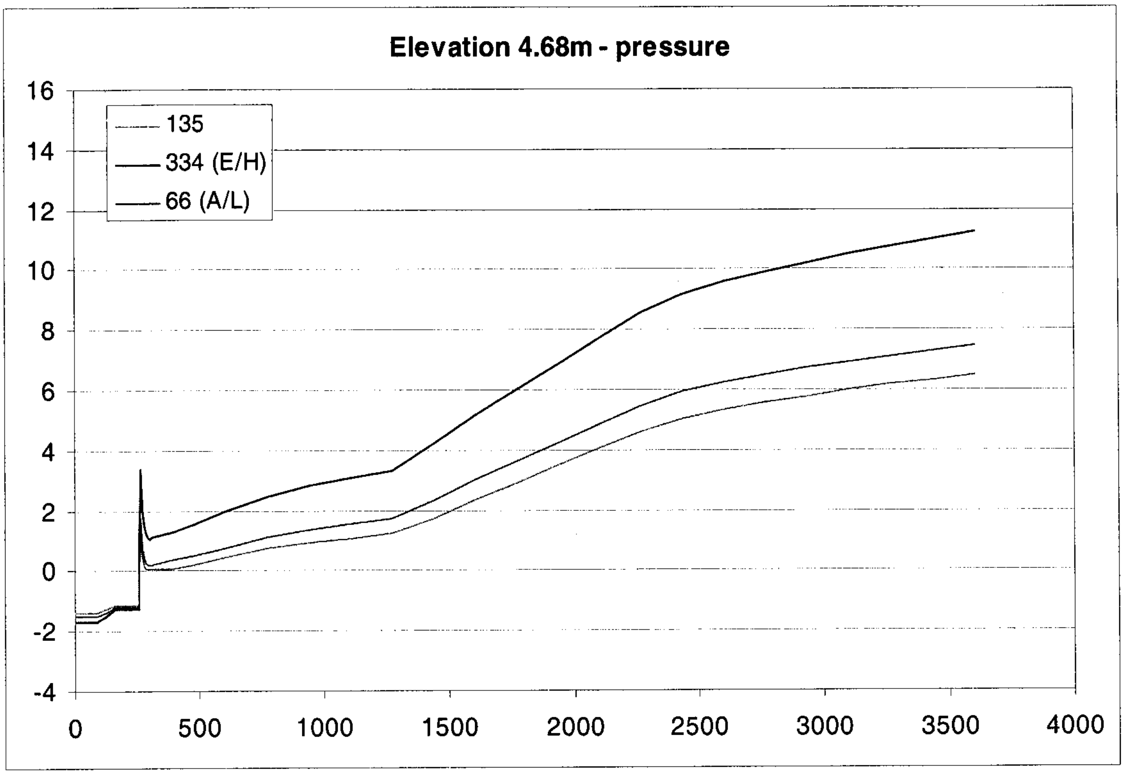

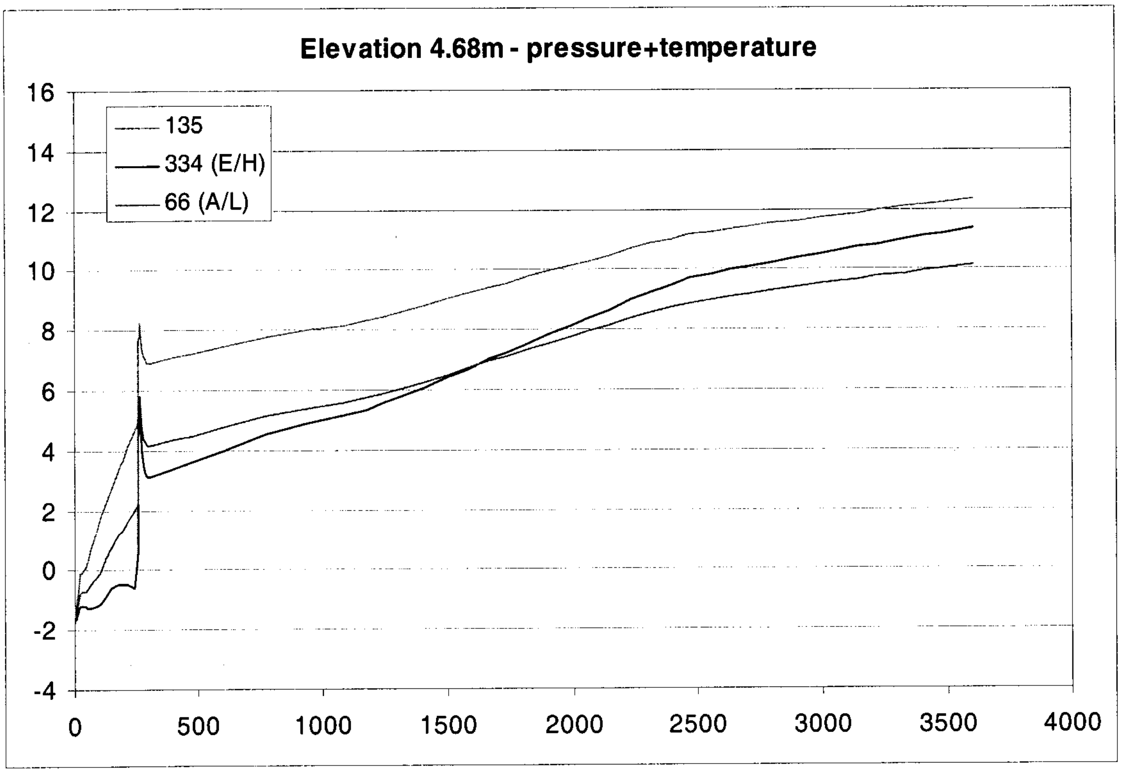

Figure 26 Case 2:Comparison of radial displacements at elevation 4.68 for different azimuths (mm, MPa)

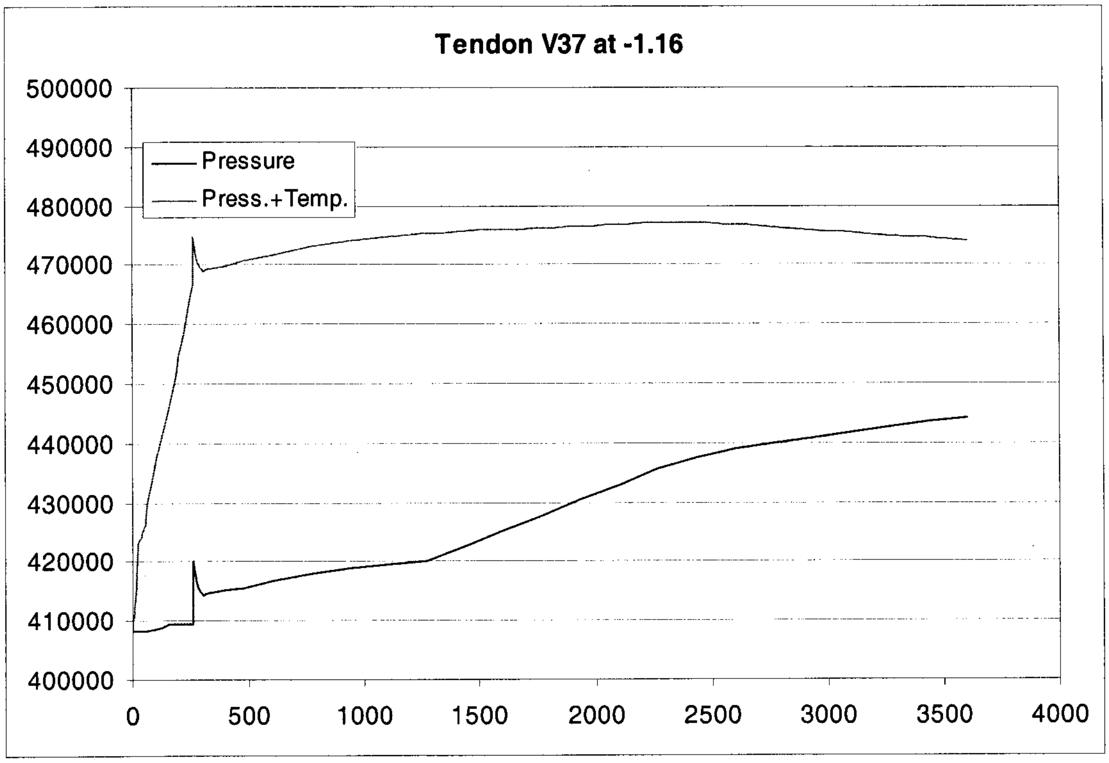

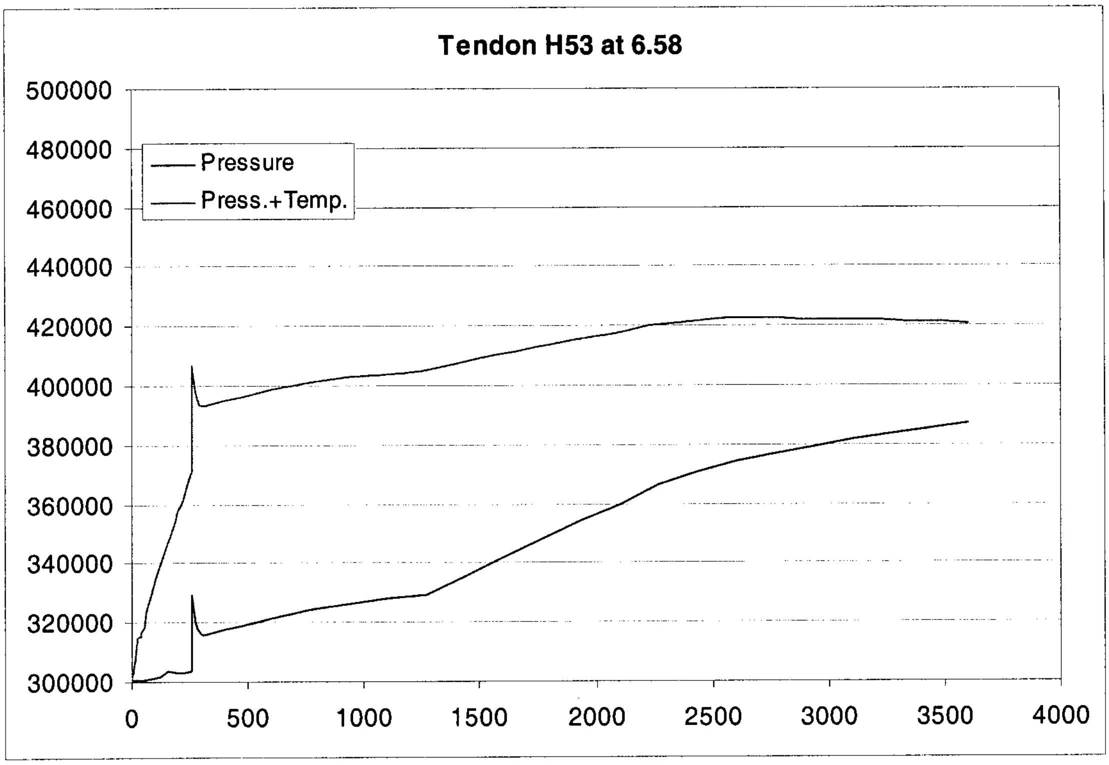

Figure 27 Case 2:Comparison of tendons strain and force (m/m or N, MPa)

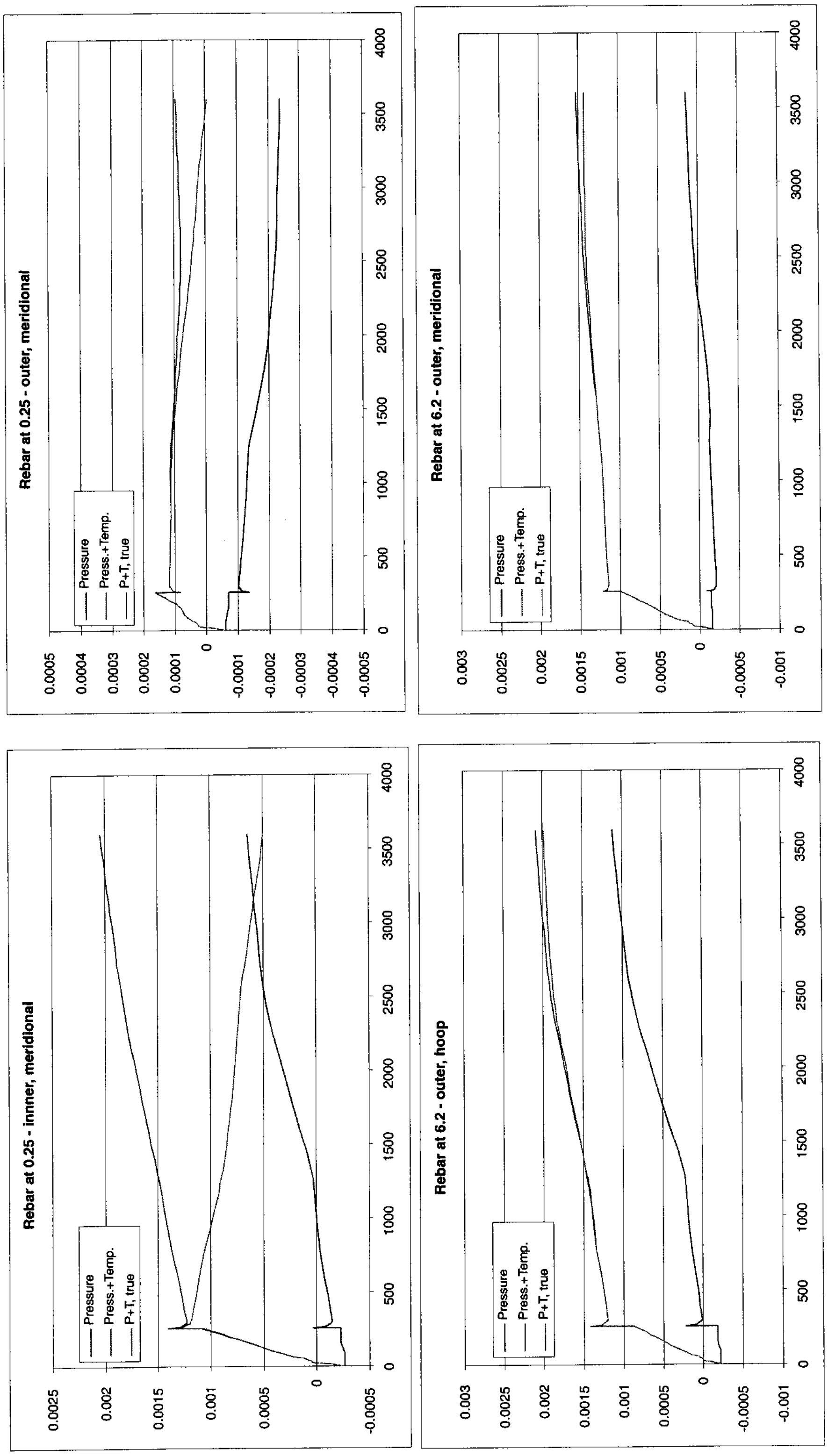

Figure 28 Case 2:Comparison of rebar strain (m/m, MPa)

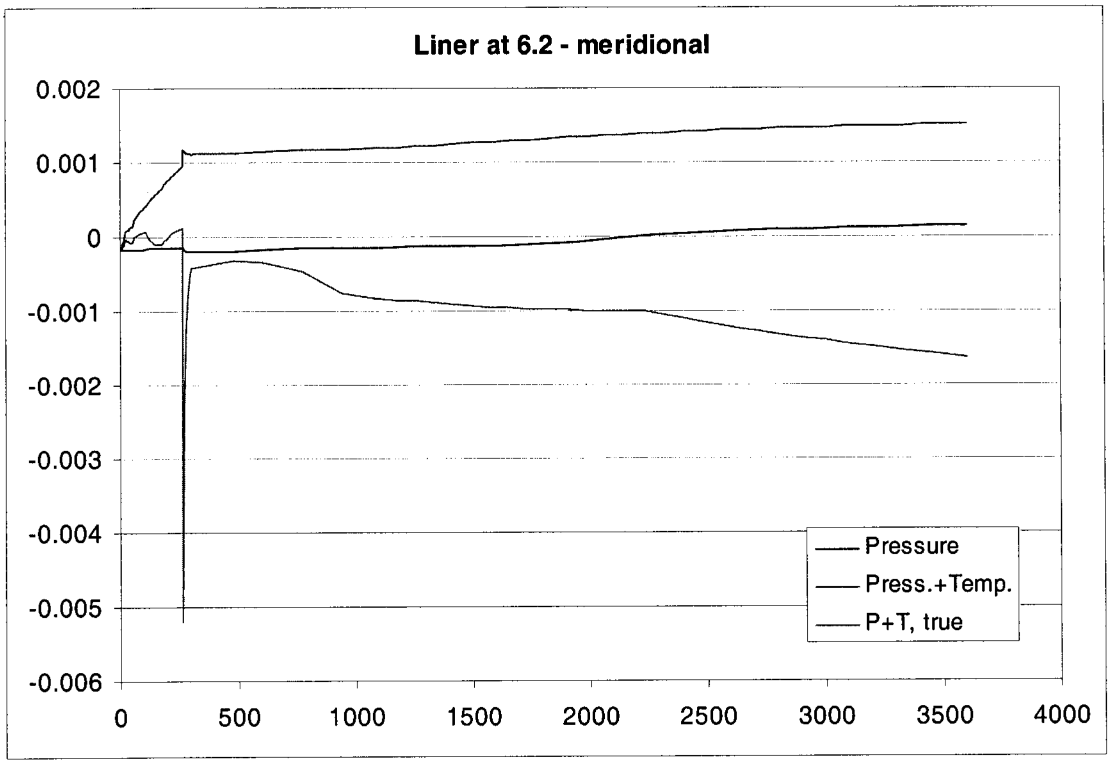

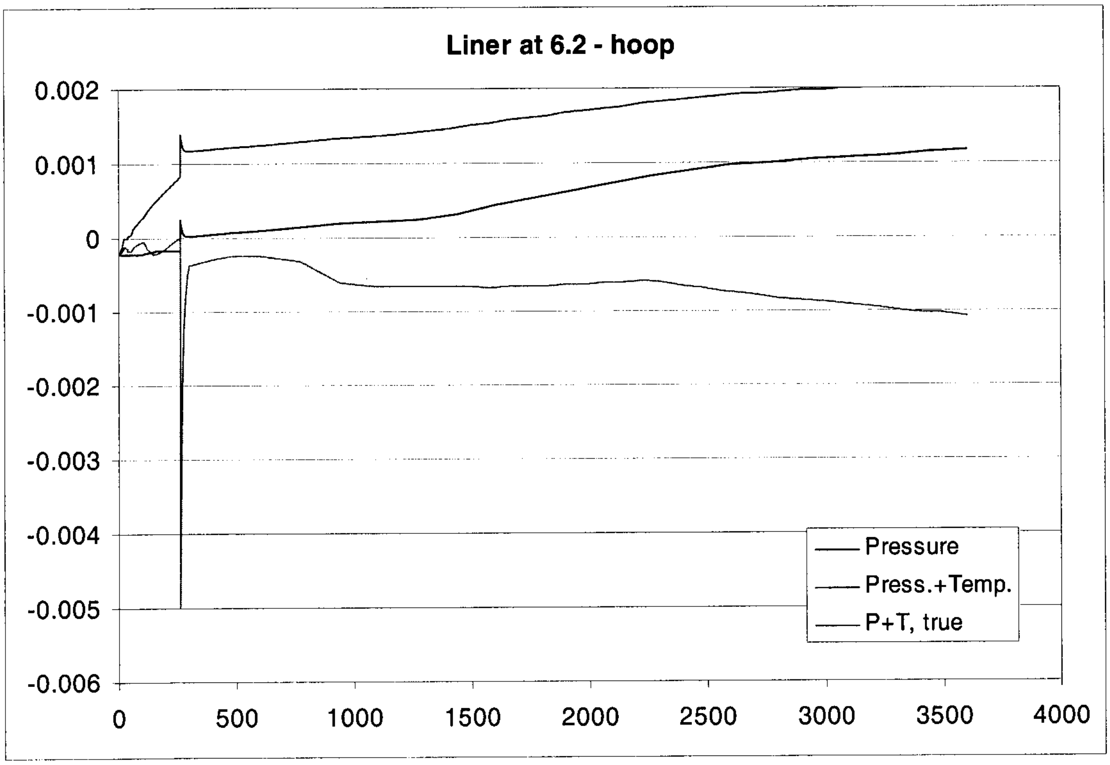

Figure 29 Case 2:Comparison of liner strain at 135° (m/m, MPa)

ISP 48
CSNI Workshop

POSTTEST ANALYSIS OF A 1:4 SCALE PCCV MODEL

Jan Štěpán

Basic characteristics and simplifications

- The model includes only concrete wall of cylindrical and dome part of structure, the wall was modeled by brick elements. The model includes EH and AL openings including change of wall thickness.
- Liner was modeled by plate elements connected with inner surface of concrete elements.
- Rebar and prestressing tendons were modeled by rod elements considering actual geometry around openings. Prestressing tendons were modeled as bonded tendons. Prestressing force along tendons was considered as uniform by mean value of measured force.

FE model of containment structure

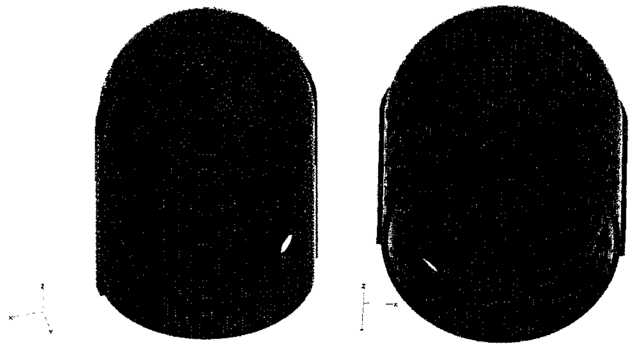

Prestressed tendon elements

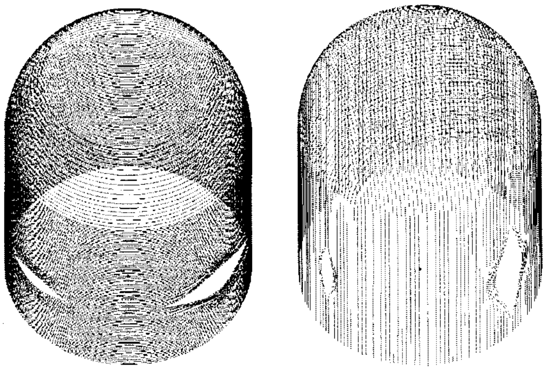

Rebar elements – inner and outer row

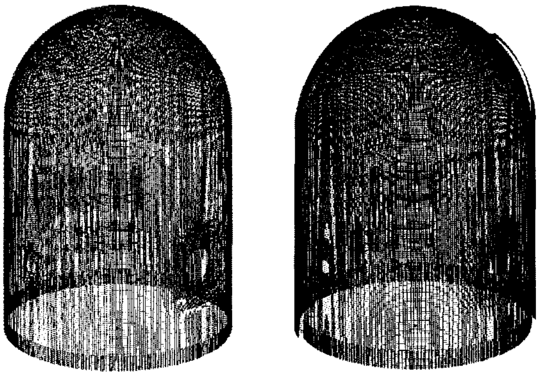

Modeling of non-linear material

- Concrete –Abaqus Concrete damage plasticity model - in compression by Eurocode 2 (stress/strain diagram), in tension by tensile strength and fracture energy.
- Rebar, presstresing tendons and liner - Abaqus Iron plasticity model - material characteristics were sets according results of material tests (stress/strain diagrams).
- Failure criteria / ultimate strain = ?

Section - hoop direction

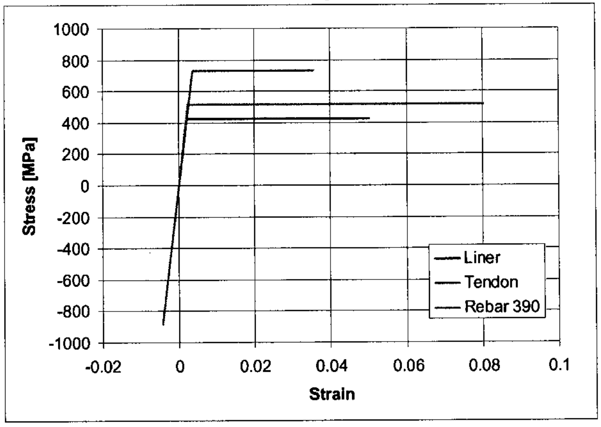

Analysis steps

- Starting state of analysis was unbroken structure. Cracking due to shrinkage was modeled by decreasing of modulus of elasticity along with lower tensile strength of concrete.
- Analysis was performed in two steps. The first step was application of prestressing and dead load. The second step was application of internal overpressure and optionally temperature.
- Phase II (pressure only) – prestressing by Abaqus/Standard, internal pressure by Abaqus/Explicit
- Phase III (pressure + temperature) – Abaqus/Standard

Temperature degradation

- Concrete –boundary temperature is aprox. 100°C but due to parallel pressure loading, the PCCV structure acted mainly in tension and resistance is driven by properties of tendons and rebars, the degradation of concrete properties has low effect.
- Steel - there are interesting temperatures above 300°C
- Case 1 - temperature is under 300°C => there is no need to consider temperature degradation
- Case 2 - the temperature above 300°C is twice, effective impact only for liner

Case 1 loading

ISP 48, Phase 3, Case 1, Section 2

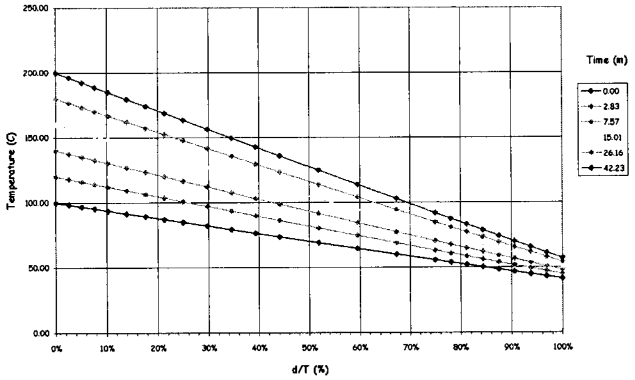

Case 2 loading

ISP 48, Phase 3, Case 2, Section 2

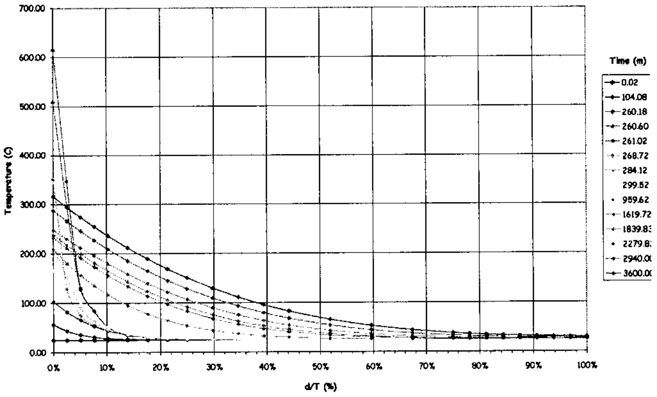

Case 1 loading

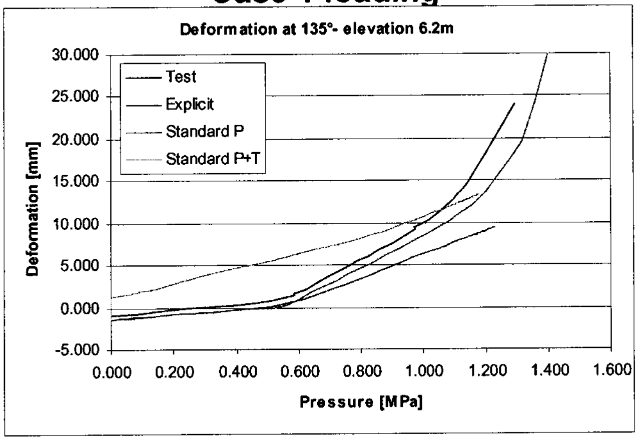

Case 1 – deformation at 0.6MPa

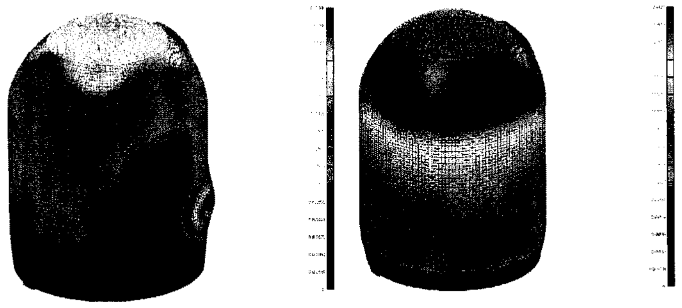

Case 1 – Comparison of radial displ.

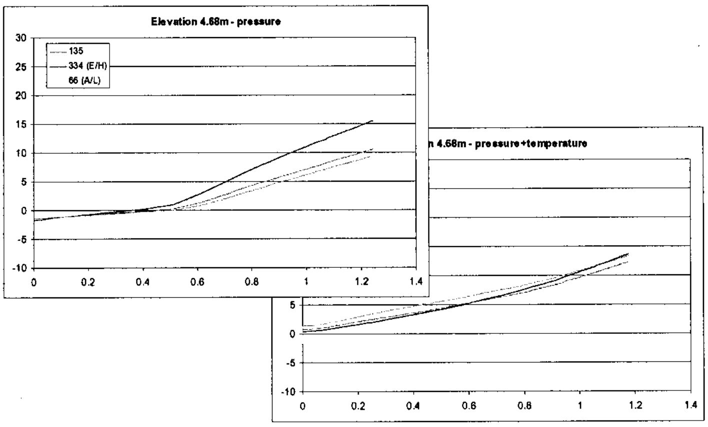

Case 2 – Comparison of radial displ.

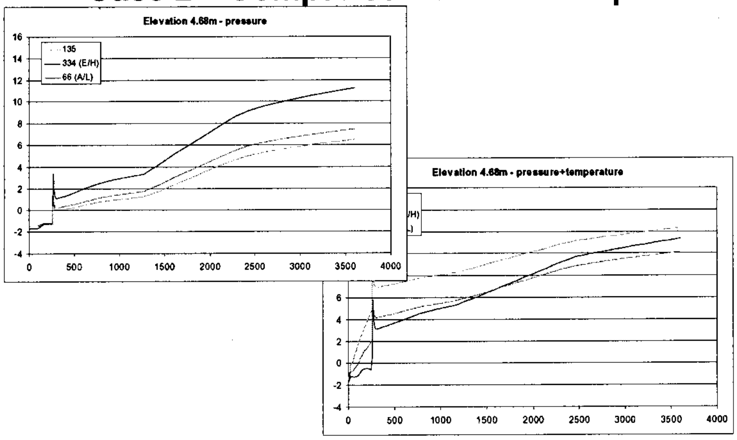

Nuclear Research Institute Řež, div. Energoprojekt, Prague, Czech republic

Case 1 – Comparison of tendon forces

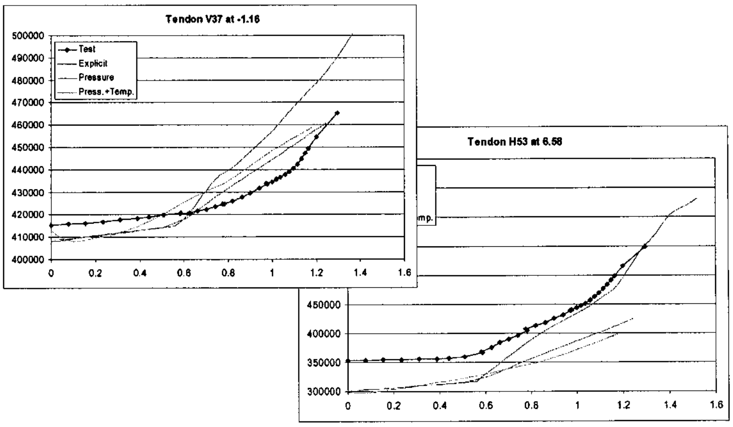

Nuclear Research Institute Řež, div. Energoprojekt, Prague, Czech republic

Case 2 – Comparison of tendon forces

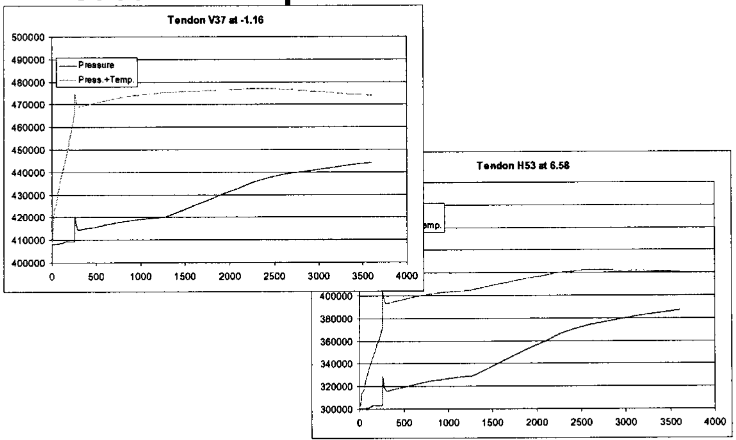

Nuclear Research Institute Řež, div. Energoprojekt, Prague, Czech republic

Case 1 – Comparison of liner strain

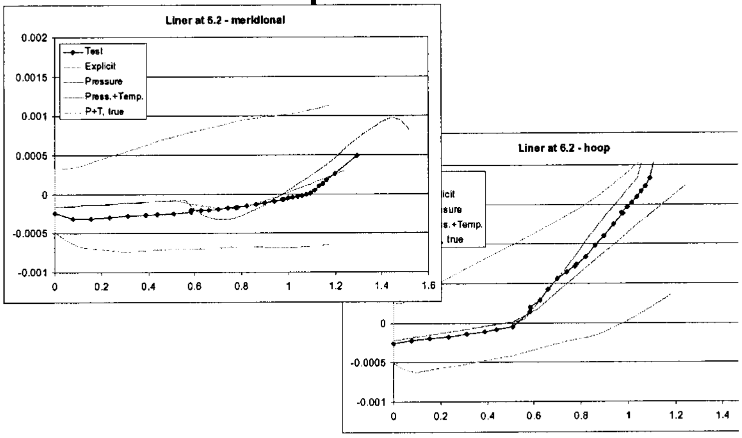

Case 2 – Comparison of liner strain

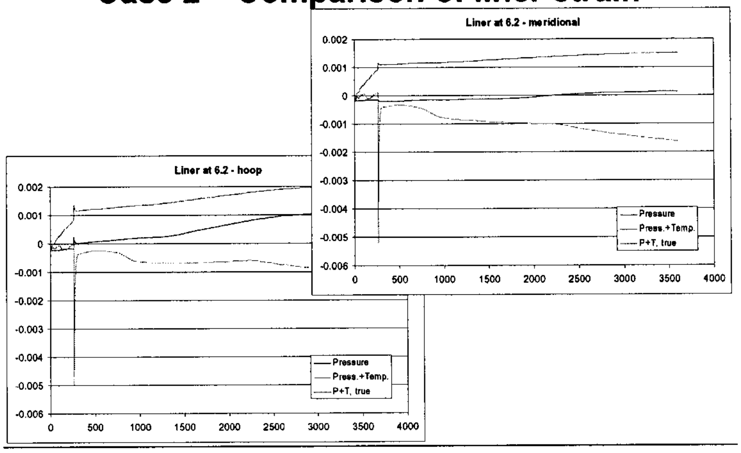

Milestones during overpressuration

Pressure	Event
0.44 MPa	Beginning of cracking around E/H
0.60 MPa	Beginning of cracking of cylinder in circumferential direction
0.96 MPa	Continual horizontal cracks in cylinder
1.15 MPa	Yielding stress in liner
1.25 MPa	Yielding stress in tendons
1.25-1.30 MPa	Collapse of structure after breaking some tendons

Summary of ISP 48

- **actual analytical tools based on FEM enable to analyze the structure in very complex way including a nonlinear behaviour. But this approach needs more detailed information about material properties and corresponding material testing.**
- **the test results showed differences of ultimate failure stress/strain between the individual material tests and the behaviour of the same material in the structure.**
- **the temperature degradation is in detail described by standards for design of buildings against fire and number of tests have been accomplished.**

Summary of ISP 48

- the temperature didn't change the failure mode of the structure significantly but changes of temperature are critical for design of liner. There is need to analyze the liner not only as part of global model but also in detail models.
- concurrent expansion of a computing technology and capabilities of analytical tools enable to analyze the structure not only in single deterministic step but also with considering of uncertainties of the input data as a sensitivity or fully probabilistic analysis. Importance of this type of analysis increases in case when the variability of parameters in time have to be considered.

EXPERIMENTAL STUDIES ON THE FAILURE BEHAVIORS OF A PRESTRESSED CONCRETE CONTAINMENT BUILDING

Young-Sun Choun^{1)}, **Nam-So Cho**^{2)}, **and Jeong-Moon Seo**^{3)}

1) Integrated Safety Assessment Division, Korea Atomic Energy Research Institute, Korea
2) Hyundai Institute of Construction Technology Development, Korea
3) Advanced Reactor Technology Development, Korea Atomic Energy Research Institute, Korea

Abstract

This paper summarizes the containment wall panel tests for the evaluation of a nonlinear behavior of a containment building and the estimation of the air flow rate through cracks under a severe accident condition. Test specimens were designed to represent a wall segment of a prestressed concrete containment building, and the test apparatus were set up to simulate the stress conditions of the segment. Panel tests investigate the followings; a) the cracking behavior of a concrete containment building, b) a constitutive model of the concrete used for the containment in the KSNP (Korean Standard Nuclear Plants), c) the effects of a liner on the cracking behavior of a containment wall, and d) the air leakage characteristics through the cracks of a containment wall. Test results will be used for the evaluation of the structural and functional integrity of containment buildings and the development of a nonlinear finite element software NUCAS (Nuclear Containment Analysis System).

Introduction

Many engineers and researchers have investigated the structural behavior of a reinforced or prestressed concrete containment building through an analytical or experimental study. Since the structural nonlinear behaviors of concrete containment buildings are complicated, it is not easy to make precise predictions of their structural behaviors with analytical methods. To overcome the limitations of the analytical methods, therefore, experimental studies have been conducted since the 1970s. The University of Alberta conducted containment wall segments tests [1,2,3] and EPRI (Electric Power Research Institute) carried out half-thickness element tests [4,5]. Recently, SNL (Sandia National Laboratories) performed RCCV (Reinforced Concrete Containment Vessel) and PCCV (Prestressed Concrete Containment Vessel) model tests [6,7].

In Korea, KAERI (Korea Atomic Energy Research Institute) has conducted RC panel tests since 2001 [8,9]. Through the RC panel tests, the cracking behaviors of a concrete containment building were investigated, and a constitutive model of the concrete used for the containment in the KSNP (Korean Standard Nuclear Plants) was developed. In addition, the effects of a liner on the cracking behavior of a containment wall were evaluated and the air leakage characteristics through the cracks of a containment wall were examined. The results of the experimental study are introduced in this paper.

Cracking behavior of a containment building

Uniaxial and biaxial tension tests for the reinforced concrete panels were conducted in order to investigate the crack patterns occurred in the wall of a prestressed concrete containment building due to the high pressure under a severe accident [10].

Test specimen

Test specimen was designed to correspond to the midheight region of the containment wall, because the failure of the midheight region of the containment building is one of the major failure modes. Considering the loading capability of the actuator systems, a half-thickness panel model as shown in Figure 1 was used for the test. Tendon ducts were embedded in the specimen to consider the unbonded tendon.

While the design compressive strength of the concrete for the nuclear power plant containment is

40 MPa, strengths actually achieved are found to be around 60 MPa. Therefore, two compressive strengths of the concrete were considered as the test variables. Six specimens were classified into two groups according to the compressive strength of the concrete, and in each group, one specimen was used in a uniaxial tension test and the other two specimens were used in the biaxial tension tests.

Figure 1. Specimen for the crack test (unit:mm)

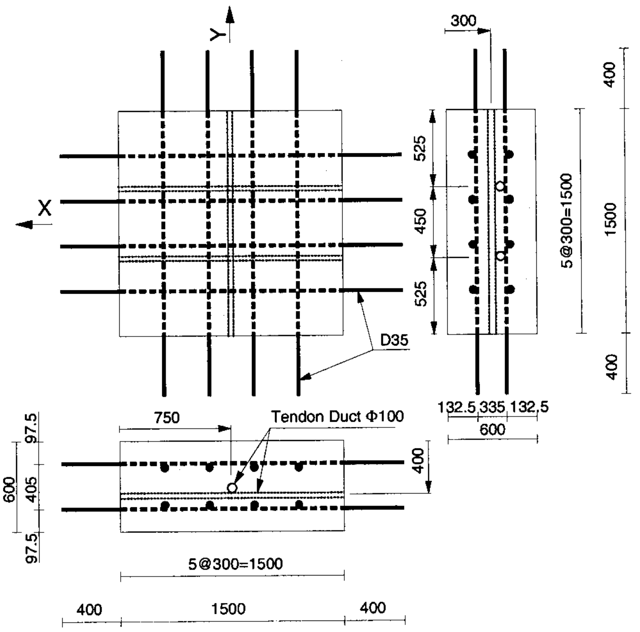

Test setup

The target region in a whole containment structure corresponds to the midheight location of the containment wall, where the biaxial tension loads act at a ratio of 2:1 in the hoop and meridional directions. Therefore, the loading system was equipped to make it possible to simultaneously apply loads in both directions, thus ensuring a target load ratio. The loading system consisted of three hydraulic jacks of a 2,000 kN capacity for the hoop direction and three hydraulic jacks of a 1,000 kN capacity for the meridional direction (Figure 2).

The loading rate was 60 kN/min in the hoop direction and various measurement data was acquired from the loadcell, strain gage, and LVDT(linear variable differential transformer) at intervals of 5 sec using an automatic data acquisition system.

Figure 2. Layout of the test setup for the crack test

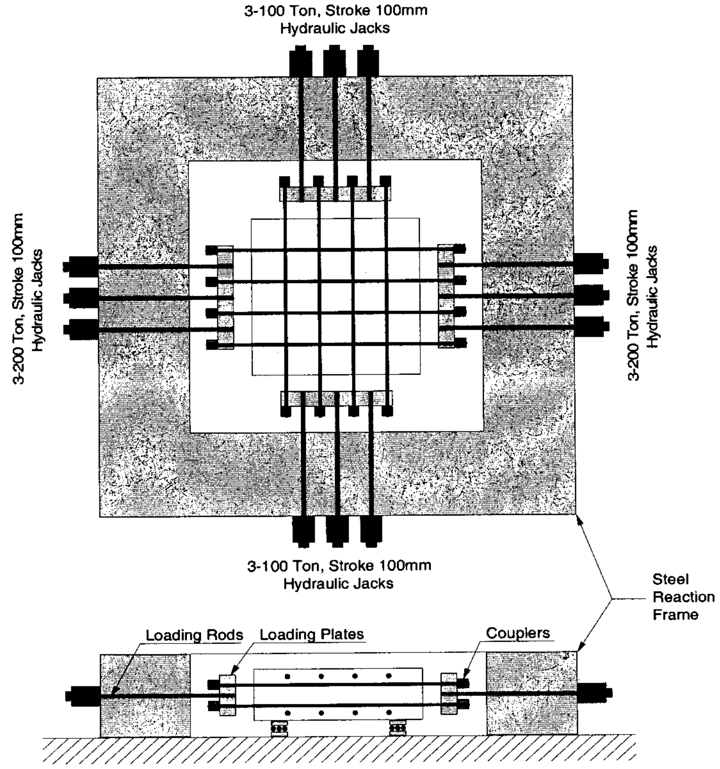
3-100 Ton, Stroke 100mm
Hydraulic Jacks
3-200 Ton, Stroke 100mm
Hydraulic Jacks
3-200 Ton, Stroke 100mm
Hydraulic Jacks
3-100 Ton, Stroke 100mm
Hydraulic Jacks
Steel
Reaction
Frame
Loading Rods
Loading Plates
Couplers

Test results

Cracking behavior

The first crack occurred at the center of the specimen in the meridional direction along the line where a tendon duct had been embedded. This crack propagated into a through-crack such that it dominated the behavior of the reinforced concrete panels. These results coincide with the anticipation that cracks would occur at the region that has the largest loss of a cross section. Figure 3 shows the typical crack patterns of the specimens, and Table 1 shows the cracking forces and stresses at an initial crack. In Table 1, S40 and S60 indicate the compressive strengths of concrete 40 MPa and 60 MPa, and U and B indicate the uniaxial and biaxial tests, respectively.

Successive cracks occurred on the surface right above the meridional directional reinforcements. For the most part, these cracks were detected above the farthest outside reinforcement and were followed by an additional crack above the reinforcements 150 mm away from the center.

While most cracks took the form of a straight line in the uniaxial tests, the biaxial tests changed their shapes into somewhat meandering formations due to the variation of the principal stress.

In a comparison for the compressive strength of concrete, the higher the compressive strength, the greater the number of cracks but the smaller the crack width.

Figure 3. Crack pattern after the uniaxial and biaxial tension tests

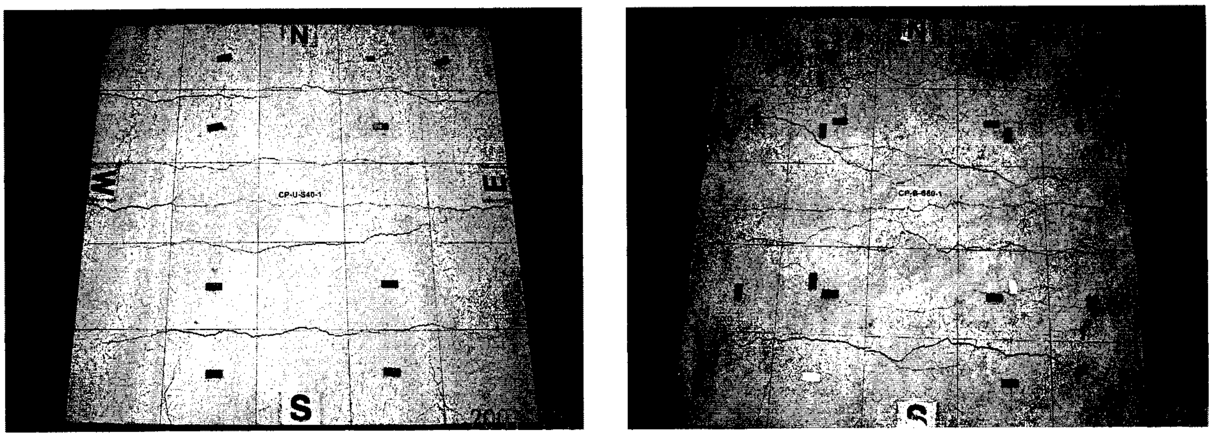

(a) U-S40 **(b) B-S60**

Table 1. Load and stress at an initial crack occurrence

Specimen	Results of material tests		Load at initial crack			Stress at initial crack	
	$f_{ck}^{(1)}$, MPa	$f_{sp}^{(2)}$, MPa	$P^{(3)}$, kN	$P_c^{(4)}$, kN	$P_s^{(5)}$, kN	$f_c^{(6)}$, MPa	$f_s^{(7)}$, MPa
S40-U	41.2	4.09	1480	1399	81	1.88	193
S40-B1	41.9	2.87	1541	1451	90	1.96	201
S40-B2	41.9	2.87	1598	1505	93	2.03	208
S60-U	61.4	5.00	1612	1520	92	2.05	211
S60-B1	54.5	5.00	1532	1446	86	1.95	200
S60-B2	54.0	5.00	1634	1542	92	2.08	214

(1) f_{ck} : cylinder compressive strength of concrete
(2) f_{sp} : splitting tensile strength of concrete
(3) P : total external tensile force
(4) P_c : force sustained by concrete
(5) P_s : force sustained by reinforcements
(6) f_c : stress of concrete
(7) f_s : stress of reinforcements

Cracking loads and stresses

The cracking load was observed at the very point where the slope of the stress-strain curve abruptly changes. As shown in Table 1, the cracking load dose not show a distinctive difference between specimen S40 and S60. Taking into account that the concrete compressive strengths resulting from the material tests were less than 40 MPa, however, the specimen made of a higher strength concrete could have shown a higher cracking load. In the case of a high-strength concrete, on the whole, the cracking load was not really affected by the compressive strength of the concrete. In a comparison with the split tensile strength of concrete, the stress of the concrete at the point of the first crack occurrence did not reach 50% of the tensile strength of the concrete in either the uniaxial or biaxial tests.

Constitutive model of concrete used in the KSNP

Uniaxial and biaxial tension tests for the three different reinforced concrete panels with different reinforcement ratios were conducted for developing a constitutive model of the concrete used in the Korean Standard Nuclear Plants [11].

Test specimen

Test variables were the reinforcement ratio and the applied load ratio in two directions. The reinforcement ratio was chosen as 0.009, 0.0135, and 0.0188, because the minimum reinforcement ratio of the existing containment buildings in Korea is approximately 0.008. These values correspond to a higher region within the range of the reinforcement ratios of the existing containment walls of nuclear power plants. The design strength of the concrete used in all the specimens was 40 MPa. Table 2 shows the design configuration of the test specimen according to the reinforcement ratio, where c and d_b are the cover depth of the concrete and the diameter of the reinforcement, respectively. The details of the specimen are shown in Figure 4.

Three types of biaxial tension loads, 1:1, 1:0.577, and 1:0.268, were considered. These applied load ratios are 45, 60, and 75 degrees, expressed by an angle in the first quadrant of the tension-tension region, respectively.

Table 2. Specimen details according to reinforcement ratio

Reinforcement ratio	Reinforcement details	Specimen size [mm]	Cover depth [mm]	c/d_b	Reinforcement spacing [mm]
R1 = 0.0090	8-D29	1500x1500x380	80	2.8	300
R2 = 0.0135	8-D29	1000x1000x380	80	2.8	200
R3 = 0.0188	10-D29	900x900x380	80	2.8	150

Figure 4. Specimen configurations and dimensions (unit:mm)

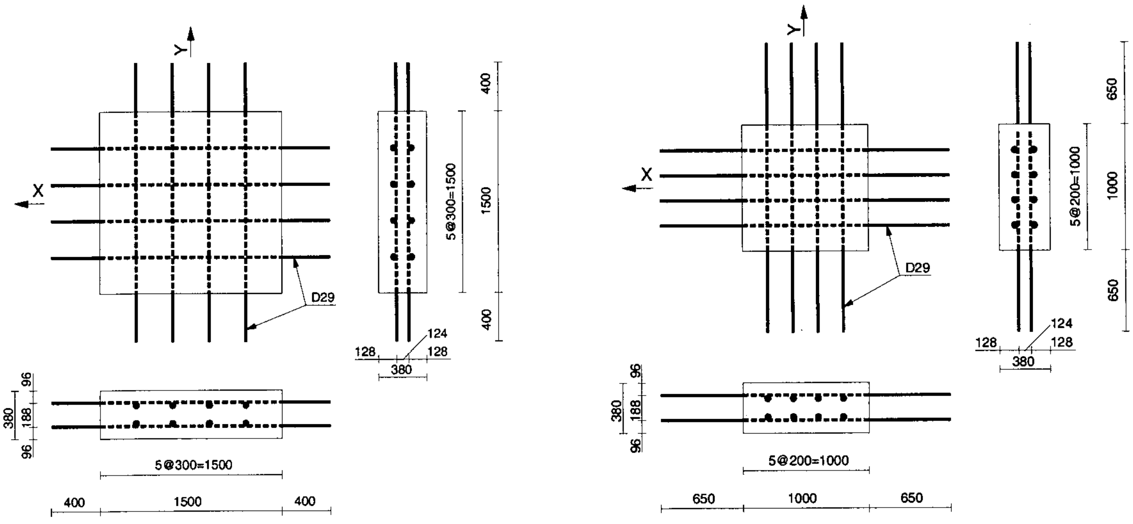
Y
X
D29
400
1500
400
5@300=1500
124
128
128
380
96
188
96
380
5@300=1500
400
1500
400
Y
X
D29
650
1000
650
5@200=1000
124
128
128
380
96
188
96
380
5@200=1000
650
1000
650

(a) R1 series

(b) R2 series

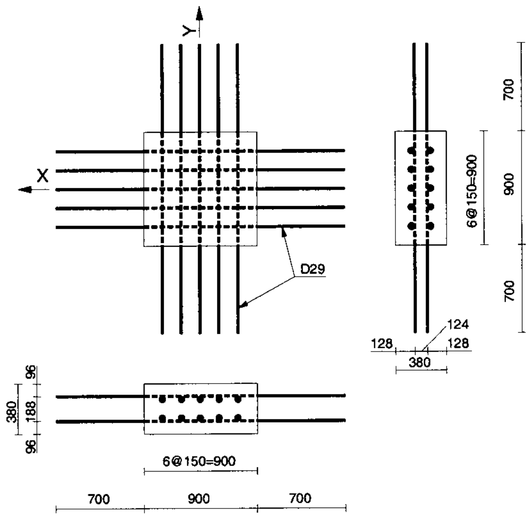
Y
X
D29
700
900
700
6@150=900
124
128
128
380
96
188
96
380
6@150=900
700
900
700

(c) R3 series

Test results

Tensile stress-strain curve of the concrete before a cracking

Prior to an initial cracking, both the reinforcement and concrete behave elastically and the applied tensile force is transferred into each material according to its stiffness. When the externally applied load is P, tensile stress f_t in the concrete corresponding to the tensile strain $\square_t$ is calculated as in Eq (1), by using the force equilibrium. This relation is valid before the reinforcement yields.

$$f_t = \frac{P}{A_c} - \rho E_s \varepsilon_t \qquad (1)$$

Therefore, the tensile stress, corresponding to the tensile strain, follows Eq. (2) through all of the load steps until the first crack occurs, and this relationship can be drawn as a straight line in Figure 5.

$$f_t = E_c \varepsilon_t \qquad (2)$$

where E_c is the modulus of the elasticity of the concrete and contemporarily a slope of that graph.

Table 3 summarizes the results of the tension tests, where U and B indicate the uniaxial and biaxial tests respectively; f_{ck} is the cylindrical compressive strength of the concrete; P_{cr} is the total force applied to the panel member at the first cracking of the concrete; $\square_{cr}$ is the cracking strain of the concrete; f_{cr} is the cracking stress of the concrete.

In Figure 5 and Table 3, the average cracking strain of the concrete is 0.000113, and Eq. (2) can be normalized by dividing f_t and $\square_t$ by f_{ck} and 0.000113, respectively. The following equation is for a normalized tensile stress-strain relationship until a first crack occurrence.

$$\frac{f_t}{f_{cr}} = \frac{\varepsilon_t}{0.000113} \qquad (3)$$

Tensile stress-strain curve of the concrete after a cracking

Eq. (1) could be expanded to calculate the tensile stress f_t in the concrete even after a cracking. Figure 6 and 7 show the average tensile stress-strain curves plotted with the strains measured by the

Figure 5. Stress-strain relationship of the concrete prior to an initial crack

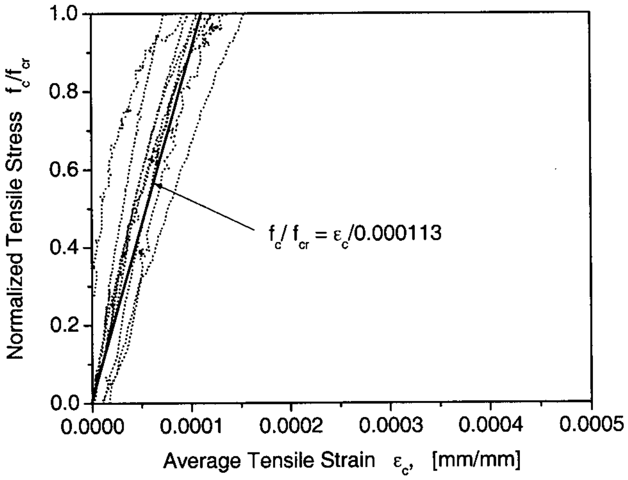

Table 3. Test results for specimens with different reinforcement ratios

Specimen	f_{ck} [MPa]	P_{ck} [kN]	$\square_{cr}$	f_{cr} [MPa]	E_c [MPa]
U-R1-1	44.0	1064	0.000115	1.98	17,228
B-R1-1	44.0	889	0.000098	1.65	16,850
B-R1-2	48.1	966	0.000077	1.86	24,102
B-R1-3	39.1	1131	0.000107	2.14	19,979
U-R2-1	46.2	730	0.000128	1.90	14,808
B-R2-1	36.6	560	0.000116	1.40	12,052
B-R2-2	40.0	673	0.000120	1.74	14,510
B-R2-3	39.1	863	0.000123	2.33	18,942
U-R3-1	46.2	783	0.000121	2.22	18,381
B-R3-1	43.4	777	0.000329	1.29*	3,917*
B-R3-2	36.6	662	0.000126	1.78	14,098
B-R3-3	39.1	1111	0.000303	2.58*	8,510*
B-R3-4**	39.1	1111	0.000117	3.40*	29,028*

* These data were excluded in results because they were proven to be outliers from regression analysis

** Supplementary specimen identical with B-R3-1 strain gages and LVDTs, respectively. As shown in Figure 6, the linearly fitted line (Eq. (4)) is almost the same as the average curve.

$$\frac{f_t}{f_{cr}} = 1 - \frac{\varepsilon_t - \varepsilon_{cr}}{0.0001323 - \varepsilon_{cr}} = 1 - \frac{\varepsilon_t - 0.000113}{0.0001323 - 0.000113} \qquad (4)$$

In Figure 7, a line of Eq. (4), an average curve and an exponentially fitted curve (Eq. (5)) are compared.

$$f_t = f_{cr}\left(\frac{\varepsilon_{cr}}{\varepsilon_t}\right)^c = f_{cr}\left(\frac{0.000113}{\varepsilon_t}\right)^{0.4} \qquad (5)$$

The above type of stress-strain relationship after a cracking was originally proposed by Tamai et al. [12] and Belarbi and Hsu [13,14] verified its validity. Taking the above results into consideration, Eq. (5), obtained from the LVDT measurements, reflects the global behavior of the cracked reinforced concrete member better than Eq. (4) obtained from the strain gages.

Figure 8 shows a comparison of the proposed model with previously proposed models. This graph is a descending part of the tensile stress-strain curve after a cracking, and some models were modified to start from zero on the x-axis. All of these models were obtained from an experimental study but other models (except for this study and Belarbi's) were the results of uniaxial tension tests or shear tests with reinforced concrete panels. On the whole, the stresses resulting from the biaxial tension tests are lower than those from the uniaxial tests and shear tests.

Figure 6. Average stress-strain relationship of the concrete after a crack occurrence (using strain gage data)

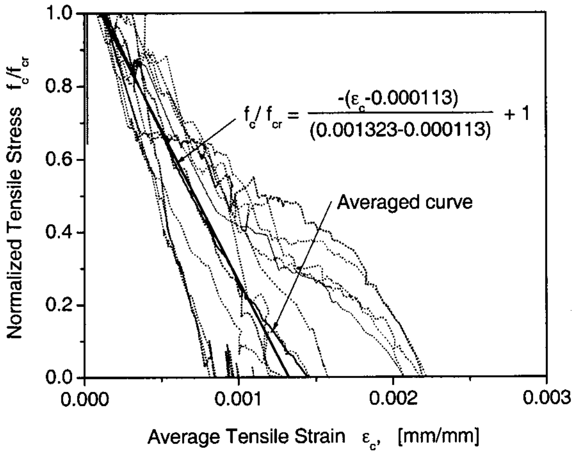

Figure 7. Average stress-strain relationship of the concrete after a crack occurrence (using LVDT data)

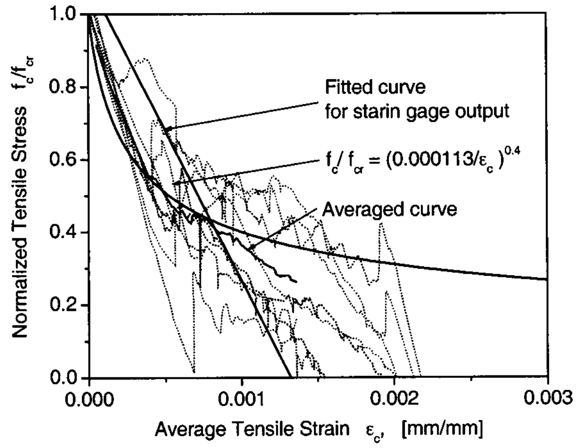

Figure 8. Comparison of the proposed model with other models

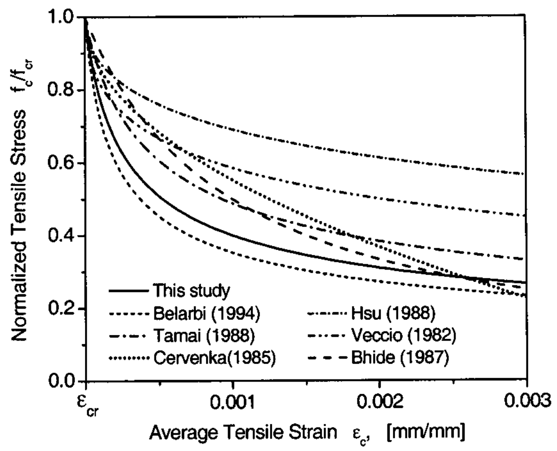

Effects of a liner on the cracking behavior of a containment building

The effects of a liner on the cracking behavior of a concrete containment building were evaluated through the failure test of a wall segment with a liner under tension [9]. The effects of the behavior of a liner on the stress-strain relationship of the concrete were investigated.

Test specimen

Figure 9 and Figure 10 show the test specimen and test setup, respectively. Specimen was designed to be a reinforced concrete of 1,200 x 200 x 2,250 mm with a liner plate 6 mm thick. Vertical stiffeners were welded onto the liner plate. Displacements were simultaneously imposed on both the reinforcement and the liner plate by hydraulic actuators.

Figure 9. Test specimen for liner failure test

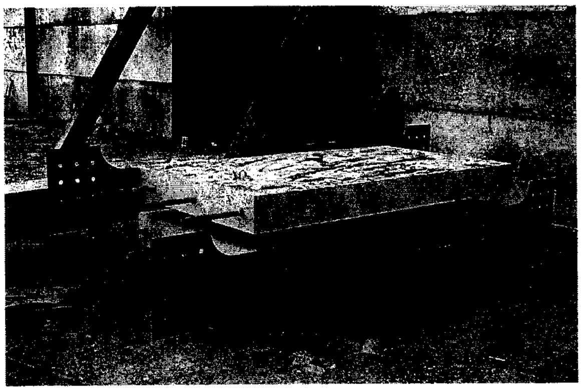

Figure 10. Test setup for liner failure test

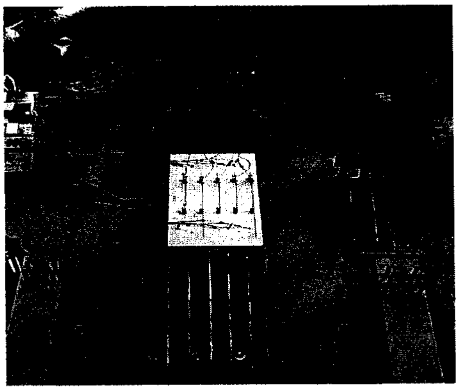

Test results

The through-cracks were formed from the stiffeners welded onto the liner plate as shown in Figure 11. It was demonstrated that when the concrete was totally collapsed, the concrete was separated from the reinforcements and the liner, but the liner did not reach a failure state.

Figure 11. Crack pattern at failure state

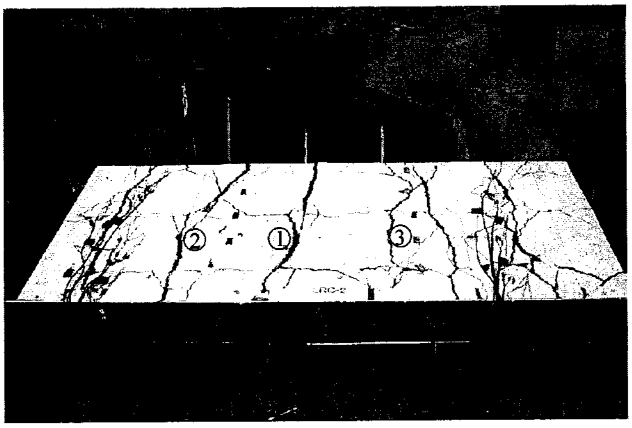

Figure 12 shows the stress-strain relationship of the concrete. The stress-strain curve of the concrete with the liner (legend 'LRC' in figure 12) is slightly lower than that of the concrete without a liner (legend 'RC' figure 12). This means that the liner reduces the concrete tensile strength to sustain the tension forces. The result was based on the experimental observation that the liner locally acts with neither the reinforcement nor the concrete, even though the tensile displacements were simultaneously applied.

Figure 12. Stress-strain relationship of concrete with liner

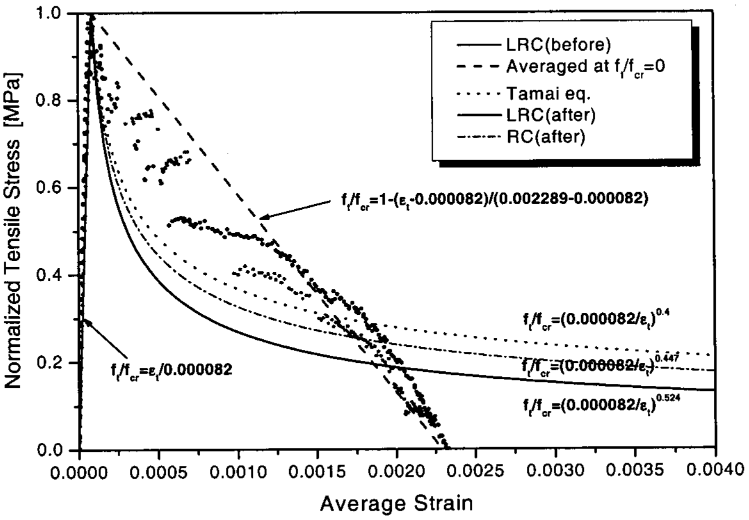

Air leakage characteristics through the cracked concrete

To estimate the leak rate in the concrete containment during a severe accident, the air leakage characteristics through the cracked concrete were experimentally evaluated [9,15].

Test specimen

The overall dimensions of a test specimen and the air chamber are shown in Figure 13. The test specimen represented the containment wall segment with a thickness of 1.2 m and width of 0.2 m. The concrete had a nominal design strength of 40 MPa and the rebar had a yield strength of 400 MPa (SD 40). Three rebars of D29 were embedded into the specimen for a reinforcement in one direction spaced at 0.45m center-to-center. Three steel plates with a dimension of 200 x 75 x 6 mm were embedded into the specimen to simulate the stiffeners of the liner spaced at 0.375 m center-to-center.

An air tight chamber mounted with gas inlet, outlet and pressure gages was manufactured. Contact surfaces on the specimen were sealed with rubber made of urethane to provide airproof conditions. Nitrogen gas was used to impose the air pressure. Input pressure, output pressure and output flow rate were measured with suitable instruments.

Figure 13. Schematic layout of specimen and air chamber

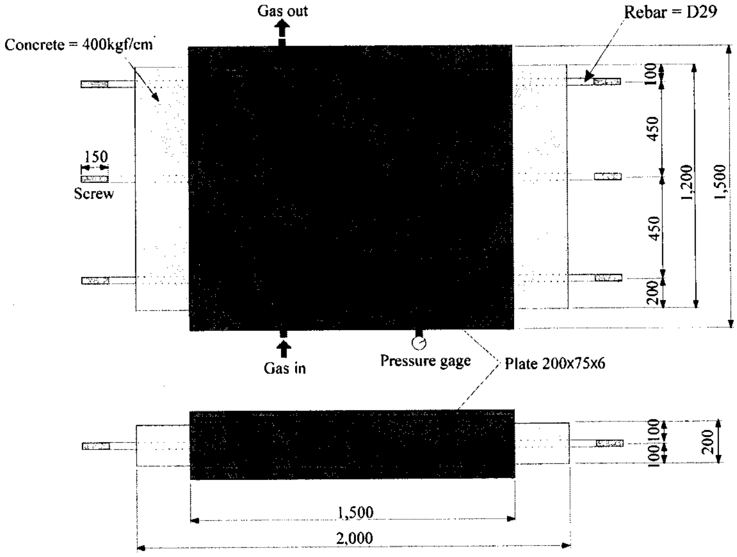
Gas out
Rebar = D29
Concrete = 400kgf/cm
150
Screw
100
450
450
200
1,200
1,500
Gas in
Pressure gage
Plate 200x75x6
100
100
200
1,500
2,000

Test procedure

The test procedure was divided into two steps. During the first step, tension loads were imposed through the reinforcements to make the cracks in test specimen by using hydraulic actuators in a displacement control mode. At this step, the total crack width was measured with vernier callipers. During the second step, by holding the constant displacement state, the air chamber blocks were assembled with a test specimen, and then the air leakage tests were performed. At this step, input and output pressures, and the flow rate at the outlet were measured.

Test results

Figure 14 shows the pressure-flow rate relationship according to the crack width. It was observed that the wider the cracks, the larger the flow rate. It was also found that the flow rate was affected by the total crack width.

Figure 14. Pressure-flow rate curve

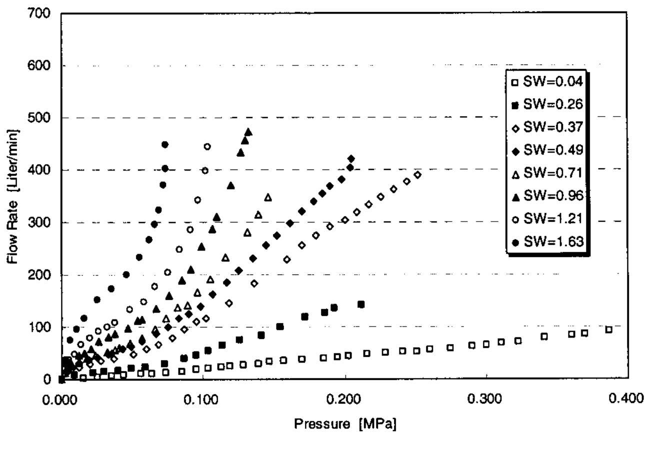

The total flow rate Q_2 through a wall having *j* cracks can be expressed as the sum of the flows through the individual cracks, as described in Eq. (6) [16]. In Eq. (6), 1 and 2 represent the conditions at the beginning and end of a crack; P_1 and P_2 are the input and output pressure; *R* and *T* are the gas constant and the absolute temperature; *k*, □ and *n* are the wall roughness, the dynamic viscosity and the flow coefficient; *L*, *B* and W_i are the crack length (= 1,200 mm), the extent of the crack (= 200 mm) and the crack width, respectively.

$$\frac{P_1^2-P_2^2}{L}=\frac{k^n}{2}\left(\frac{\mu}{2}\right)^n (RT)^{n-1}\left|\frac{P_2Q_2}{B}\right|^{2-n}\frac{1}{\sum W_i^3} \tag{6}$$

Eq. (6) can be simplified as in Eq. (7), where $P''=\left(P_1^2-P_2^2\right)/L$, modified pressure gradient; $C=\left(k^n/2\right)\left(\mu/2\right)^n\left(RT\right)^{n-1}/\sum W_i^3$, a constant; $m=2-n$; and P_2Q_2/B, rate of the flow per unit extent of the crack.

$$P''=C\left|\frac{P_2Q_2}{B}\right|^m \tag{7}$$

Eq. (7) implies a linear relationship between the modified pressure gradient, P'' and the rate of the flow of the air per unit extent of the crack using a log-log scale, as in Eq. (8).

$$\log P''=\log C+m\log\left|\frac{P_2Q_2}{B}\right| \tag{8}$$

Based on the experimental results, a graphical representation of the relationship is shown in

Figure 15. This relationship could be utilized as a criterion for the leakage of a containment wall. The slope of each regression line represents the exponent value of m from which the turbulent coefficient n can be determined. Similarly, k can be calculated from the intersection point on the y-axis. These results are listed in Table 4.

Figure 15. Modified pressure gradient-flow rate

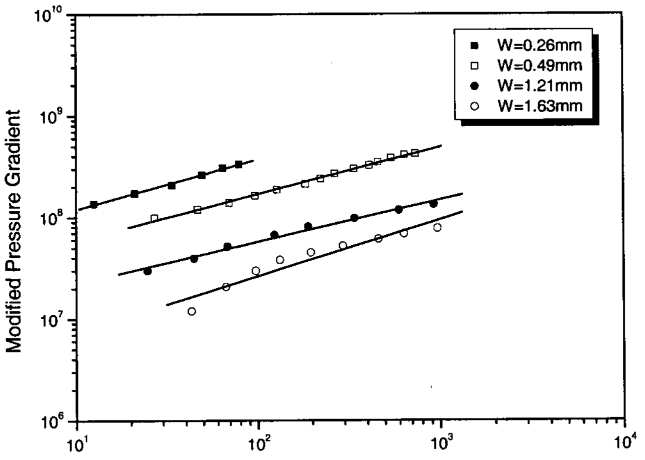

Table 4. Flow coefficient and wall roughness according to the crack width

ΣW_i [mm]	k	n
0.26	30.926	1.5080
0.49	65.749	1.5391
1.21	187.642	1.5882
1.63	210.220	1.4457

Concluding Remarks

This paper introduces a brief summary of the experimental studies on the failure behaviors of a prestressed concrete containment building which have been performed by KAERI. Many of the failure behaviors of a containment building were investigated and verified through various tests. The test results could be utilized to predict the behavior of a containment building and to develop a nonlinear finite element software NUCAS. For a future study, the failure behaviors at a wall-basement junction of a prestressed concrete containment for moment and base shear will be conducted.

References

[1] S. H. Rizkalla, S. H. Simmonds, and J. G. MacGregor, 1979, "Leakage Tests of Wall Segments of Reactor Containments," Structural Engineering Report No. 80, Department of Civil Engineering, University of Alberta, Edmonton, Canada.

[2] S. H. Simmonds, S. H. Rizkalla, and J. G. MacGregor, 1979, "Tests of Wall Segments from Reactor Containments," Structural Engineering Report No. 81, Department of Civil Engineering, University of Alberta, Edmonton, Canada.

[3] J. G. MacGregor, S. H. Rizkalla, and S. H. Simmonds, 1979, "Cracking of Reinforced and Prestressed Concrete Wall Segments," Structural Engineering Report No. 82, Department of Civil Engineering, University of Alberta, Edmonton, Canada.

[4] J. T. Julien, D. M. Schultz, and T. L. Weinmann, 1984, "Concrete Containment Structural Element Tests. Volume 1: Half-thickness Element Tests – Description and Results," EPRI Report, NP-3774, Volume 1, Electric Power Research Institute.

[5] J. T. Julien, D. M. Schultz, and T. L. Weinmann, 1984, "Concrete Containment Structural Element Tests. Volume 2: Half-thickness Element Tests – Detailed Test Data," EPRI Report, NP-3774, Volume 2, Electric Power Research Institute.

[6] M. F. Hessheimer, E. W. Klamerus, L. D. Lambert, and G. S. Rightley, 2003, "Overpressurization Test of A 1:4-Scale Prestressed Concrete Containment Vessel Model," NUREG/CR-6810, SAND2003-0840P, Sandia National Laboratories.

[7] D. S. Horschel, 1992, "Experimental Results From Pressure Testing A 1:6-Scale Nuclear Power Plant Containment," NUREG/CR-5121, Sandia National Laboratories.

[8] Namsik Kim, Namso Cho, and Jaeyeol Cho, 2002, "Structural Member Tests of the Prestressed Concrete Containment," KAERI Research Report, KAERI/CM-493-2001.

[9] Namso Cho, and Hyungtae Kim, 2005, "Structural Member Tests of the Prestressed Concrete Containment," KAERI Research Report, KAERI/CM-777-2004.

[10] Jaeyeol Cho, Namsik Kim, Namso Cho, and Inkil Choi, 2004, "Cracking Behavior of Reinforced Concrete Panel Subjected to Biaxial Tension," *ACI Structural Journal*, Vol. 101, No. 1, Jan.-Feb., pp. 76-84.

[11] Jaeyeol Cho, Namsik Kim, Namso Cho, and Youngsun Choun, 2004, "Stress-Strain Relationship of Reinforced Concrete Subjected to Biaxial Tension," *ACI Structural Journal*, Vol. 101, No. 2, Mar.-Apr., pp. 202-227.

[12] S. Tamai, H. Shima, J. Izumo, and H. Okamura, 1988, "Average Stress-Strain Relationship in Post Yield Range of Steel Bar in Concrete," *Concrete Library*, JSCE, No. 11, pp. 117-129.

[13] A. Belarbi, 1991, "Stress-strain Relationships of Reinforced Concrete in Biaxial Tension-Compression," Ph. D. thesis, University of Houston, Tex.

[14] A. Belarbi and T. T. C. Hsu, 1994, "Constitutive Law of Concrete in Tension and Reinforcing Bar Stiffened by Concrete," *ACI Structural Journal*, Vol. 91, No. 4, July-Aug., pp. 465-474.

[15] Namso Cho, Hyungtae Kim, Youngsun Choun, and Namsik Kim, 2004, "Failure & Leakage Tests of Nuclear Containment for the Evaluation of Structural Integrity," *Proc. KSCE*, Vol. 1A, pp. 296.

[16] S. H. Rizkalla and S. H. Simmonds, 1984, "Air Leakage Characteristics in Reinforced Concrete," *Journal of Structural Engineering*, ASCE, Vol. 110, No. 5, May, pp. 1149-1162.

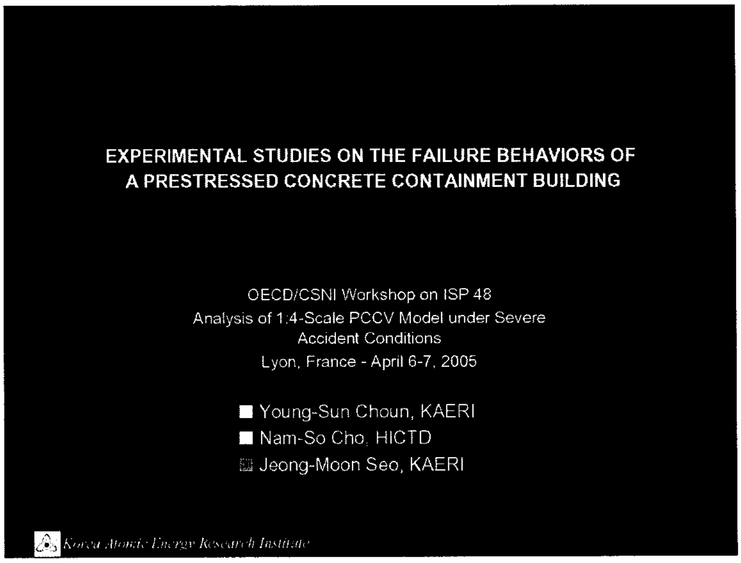

EXPERIMENTAL STUDIES ON THE FAILURE BEHAVIORS OF A PRESTRESSED CONCRETE CONTAINMENT BUILDING

OECD/CSNI Workshop on ISP 48
Analysis of 1:4-Scale PCCV Model under Severe Accident Conditions
Lyon, France - April 6-7, 2005

■ Young-Sun Choun, KAERI
■ Nam-So Cho, HICTD
■ Jeong-Moon Seo, KAERI

Korea Atomic Energy Research Institute

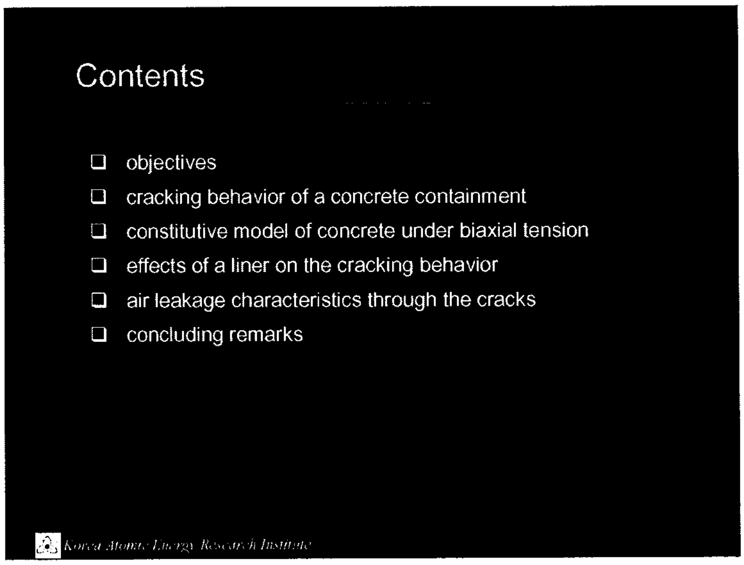

Contents

- ☐ objectives
- ☐ cracking behavior of a concrete containment
- ☐ constitutive model of concrete under biaxial tension
- ☐ effects of a liner on the cracking behavior
- ☐ air leakage characteristics through the cracks
- ☐ concluding remarks

Korea Atomic Energy Research Institute

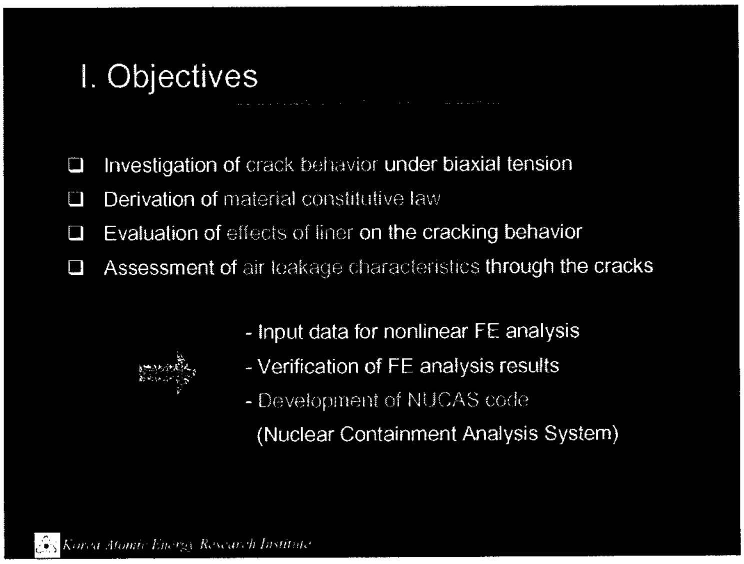

I. Objectives

- ☐ Investigation of crack behavior under biaxial tension
- ☐ Derivation of material constitutive law
- ☐ Evaluation of effects of liner on the cracking behavior
- ☐ Assessment of air leakage characteristics through the cracks

- Input data for nonlinear FE analysis
- Verification of FE analysis results
- Development of NUCAS code
  (Nuclear Containment Analysis System)

Korea Atomic Energy Research Institute

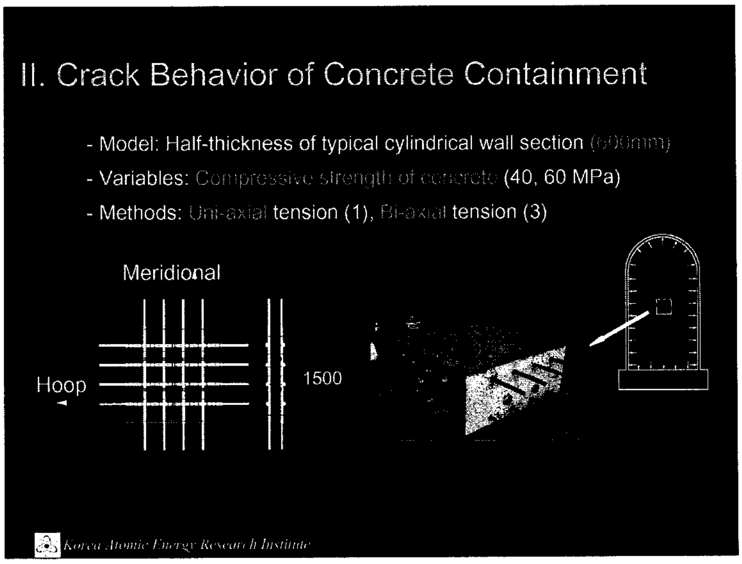

II. Crack Behavior of Concrete Containment

- Model: Half-thickness of typical cylindrical wall section (600mm)
- Variables: Compressive strength of concrete (40, 60 MPa)
- Methods: Uni-axial tension (1), Bi-axial tension (3)

Meridional
Hoop
1500

Korea Atomic Energy Research Institute

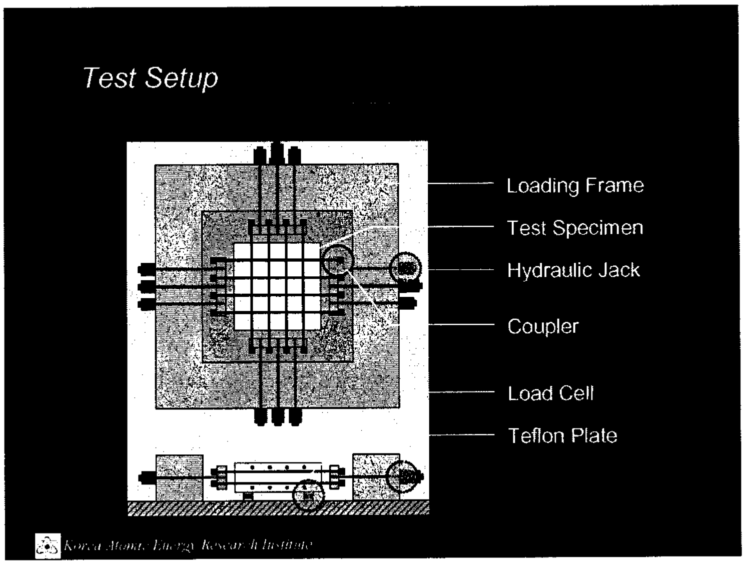

Test Setup

Loading Frame
Test Specimen
Hydraulic Jack
Coupler
Load Cell
Teflon Plate

Korea Atomic Energy Research Institute

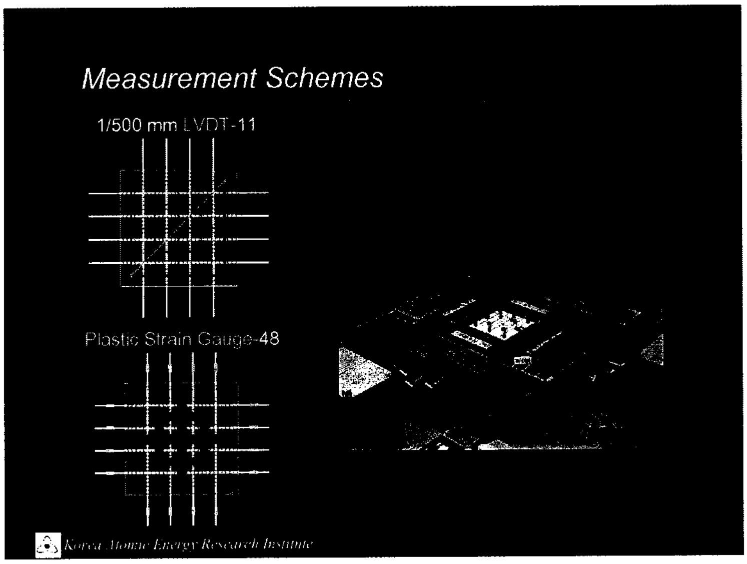

Measurement Schemes

1/500 mm LVDT-11
Plastic Strain Gauge-48

Korea Atomic Energy Research Institute

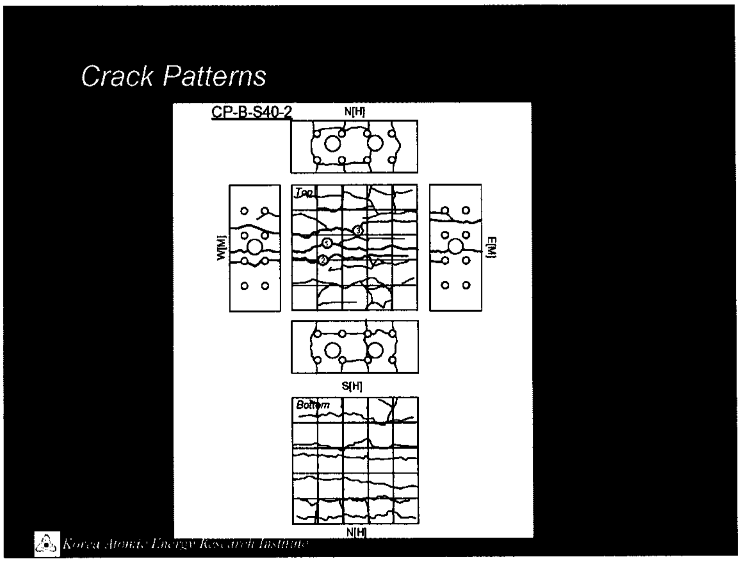

Crack Patterns

Korea Atomic Energy Research Institute

Cracking Forces & Stresses

Specimen	Results of material tests		Load at initial crack			Stress at initial crack	
	$f_{ck}^{(1)}$, MPa	$f_{sp}^{(2)}$, MPa	$P^{(3)}$, kN	$P_c^{(4)}$, kN	$P_s^{(5)}$, kN	$f_c^{(6)}$, MPa	$f_s^{(7)}$, MPa
S40-U	41.2	4.09	1480	1399	81	1.88	193
S40 B1	41.9	2.87	1541	1451	90	1.96	201
S40-B2	41.9	2.87	1598	1505	93	2.03	208
S60-U	61.4	5.00	1612	1520	92	2.05	211
S60-B1	54.5	5.00	1532	1446	86	1.95	200
S60 B2	54.0	5.00	1634	1542	92	2.08	214

Korea Atomic Energy Research Institute

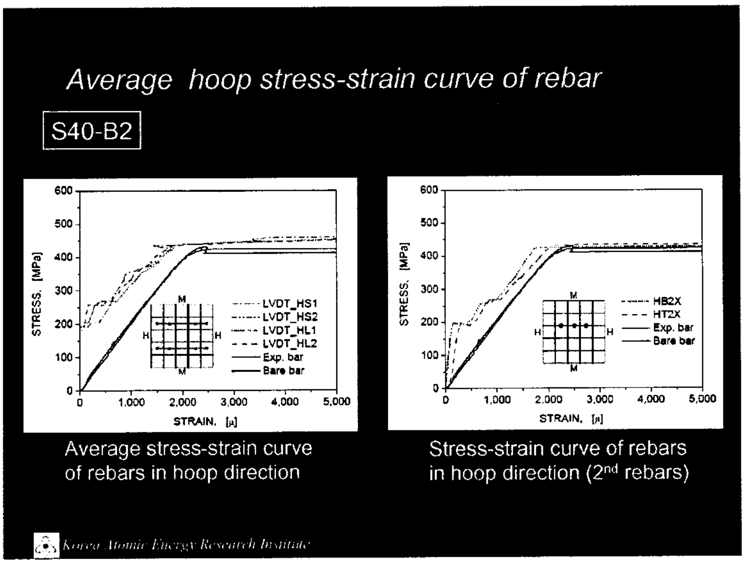

Average hoop stress-strain curve of rebar

S40-B2

Average stress-strain curve of rebars in hoop direction

Stress-strain curve of rebars in hoop direction (2nd rebars)

Korea Atomic Energy Research Institute

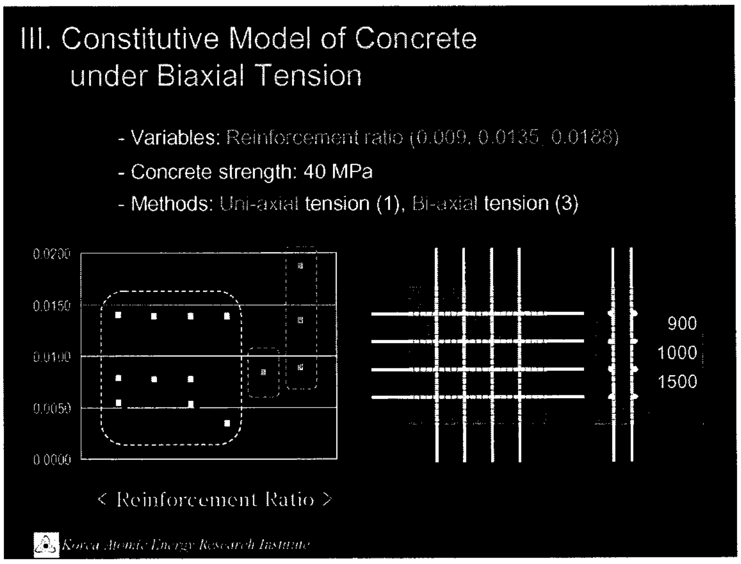

III. Constitutive Model of Concrete under Biaxial Tension

- Variables: Reinforcement ratio (0.009, 0.0135, 0.0188)
- Concrete strength: 40 MPa
- Methods: Uni-axial tension (1), Bi-axial tension (3)

< Reinforcement Ratio >

Korea Atomic Energy Research Institute

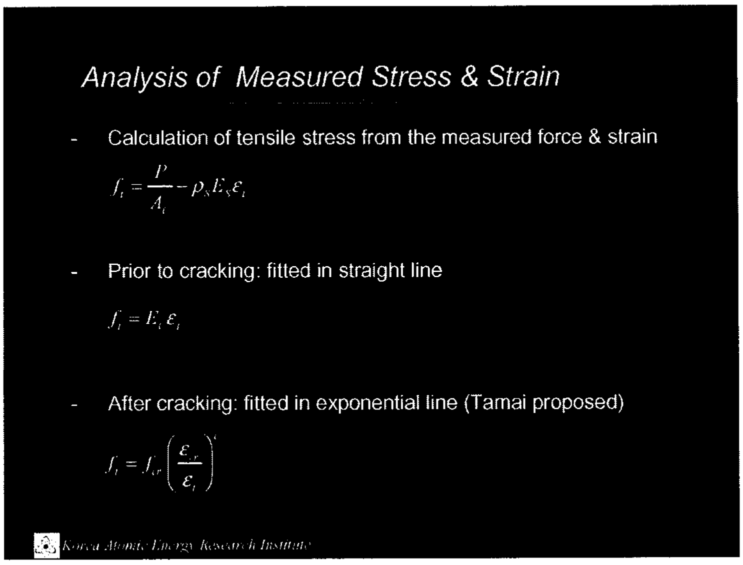

Analysis of Measured Stress & Strain

- Calculation of tensile stress from the measured force & strain

$$f_t = \frac{P}{A_t} - \rho_s E_s \varepsilon_t$$

- Prior to cracking: fitted in straight line

$$f_t = E_c \varepsilon_t$$

- After cracking: fitted in exponential line (Tamai proposed)

$$f_t = f_{cr} \left(\frac{\varepsilon_{cr}}{\varepsilon_t} \right)^c$$

Korea Atomic Energy Research Institute

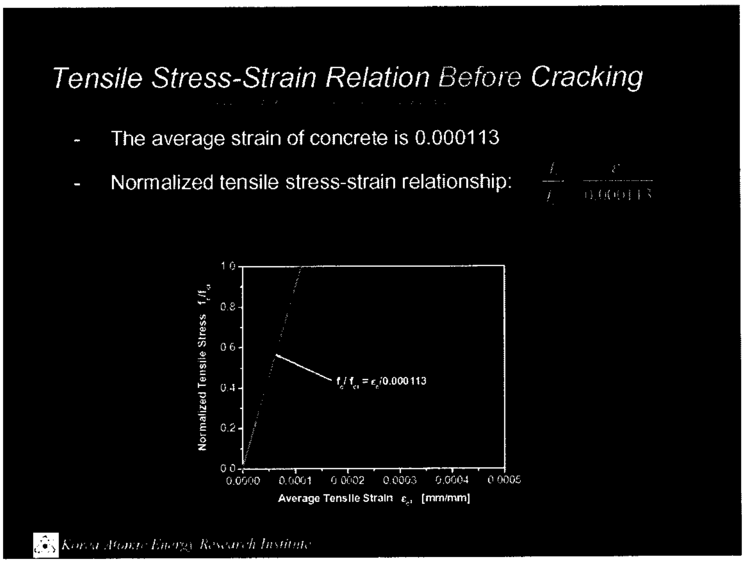

Tensile Stress-Strain Relation Before Cracking

- The average strain of concrete is 0.000113
- Normalized tensile stress-strain relationship: $\frac{f_c}{f_{cr}} = \frac{\varepsilon_c}{0.000113}$

Korea Atomic Energy Research Institute

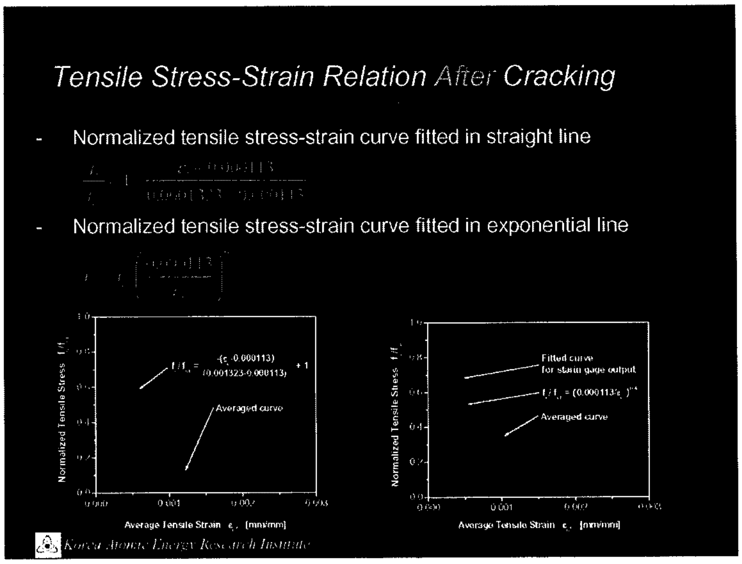

Tensile Stress-Strain Relation After Cracking

- Normalized tensile stress-strain curve fitted in straight line

$$\frac{f_t}{f_{cr}} = 1 - \frac{\varepsilon_t - 0.000113}{0.001323 - 0.000113}$$

- Normalized tensile stress-strain curve fitted in exponential line

$$f_t = f_{cr}\left(\frac{0.000113}{\varepsilon_t}\right)^{0.4}$$

Korea Atomic Energy Research Institute

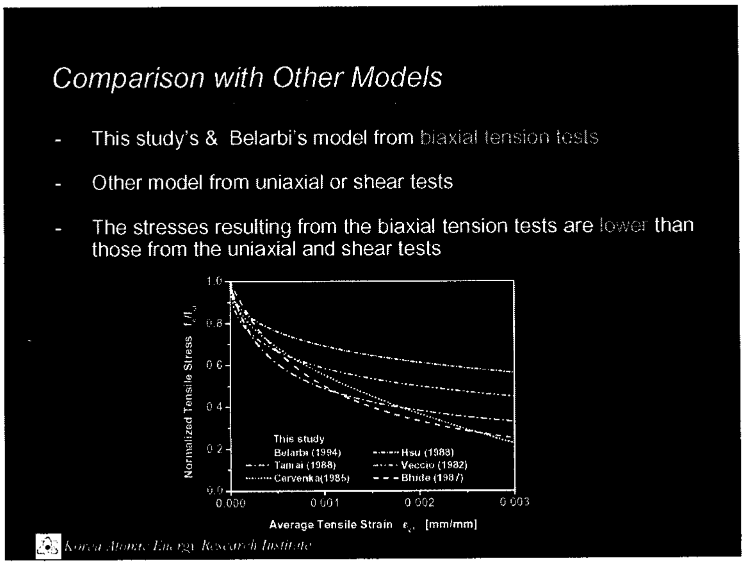

Comparison with Other Models

- This study's & Belarbi's model from biaxial tension tests
- Other model from uniaxial or shear tests
- The stresses resulting from the biaxial tension tests are lower than those from the uniaxial and shear tests

Korea Atomic Energy Research Institute

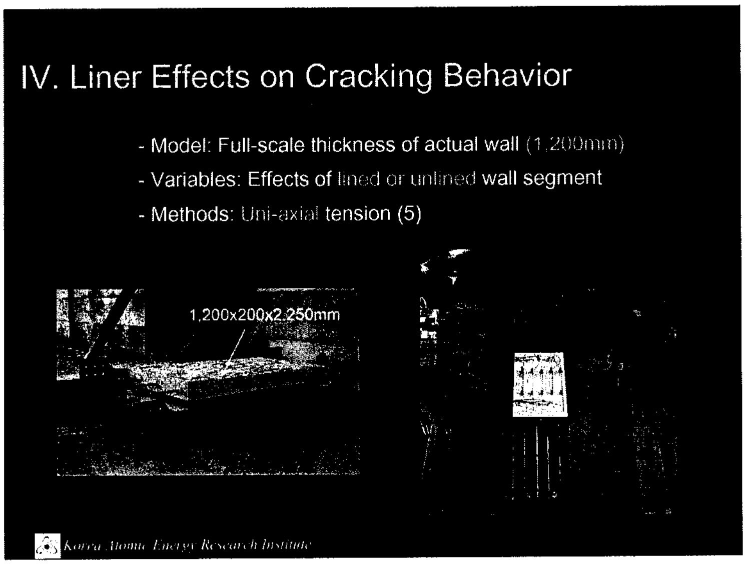

IV. Liner Effects on Cracking Behavior

- Model: Full-scale thickness of actual wall (1,200mm)
- Variables: Effects of lined or unlined wall segment
- Methods: Uni-axial tension (5)

Korea Atomic Energy Research Institute

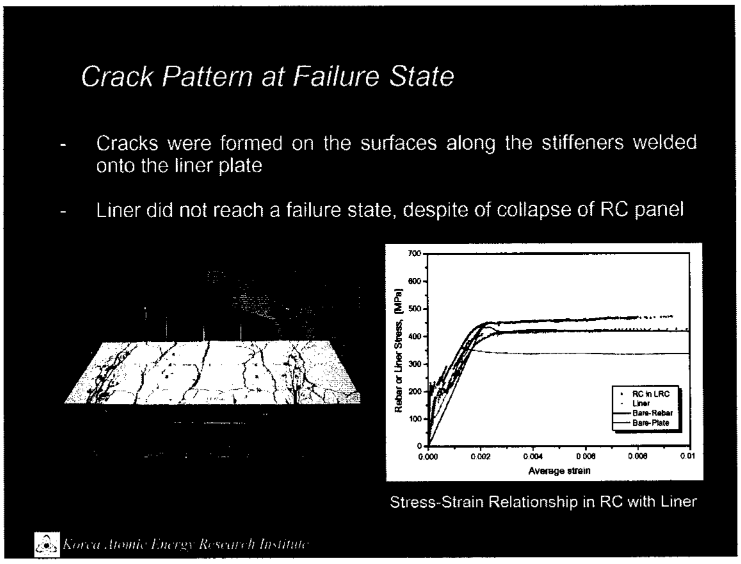

Crack Pattern at Failure State

- Cracks were formed on the surfaces along the stiffeners welded onto the liner plate
- Liner did not reach a failure state, despite of collapse of RC panel

Stress-Strain Relationship in RC with Liner

Korea Atomic Energy Research Institute

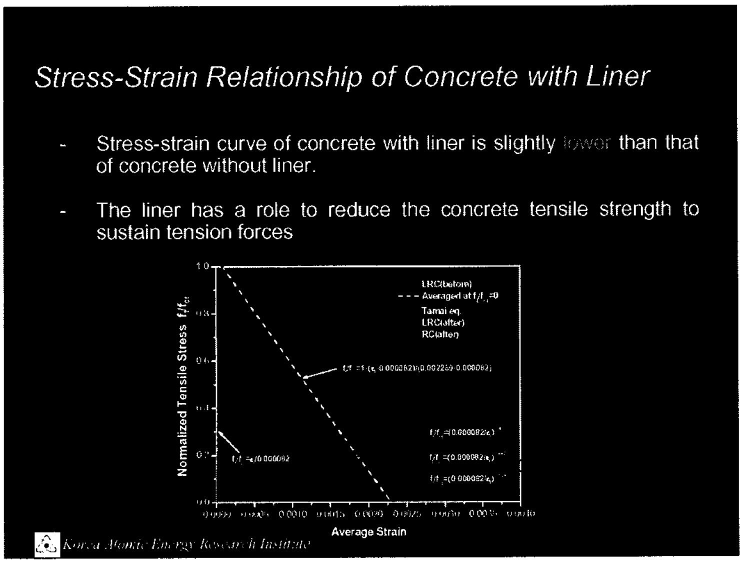

Stress-Strain Relationship of Concrete with Liner

- Stress-strain curve of concrete with liner is slightly lower than that of concrete without liner.
- The liner has a role to reduce the concrete tensile strength to sustain tension forces

Korea Atomic Energy Research Institute

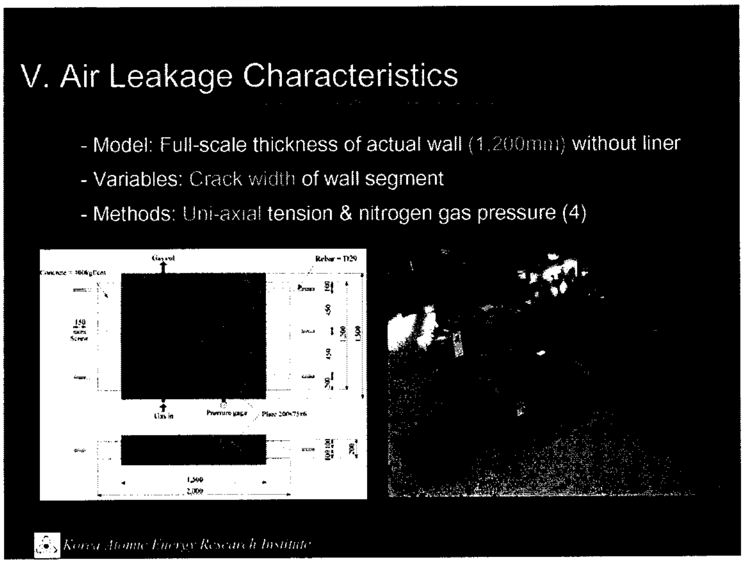

V. Air Leakage Characteristics

- Model: Full-scale thickness of actual wall (1,200mm) without liner
- Variables: Crack width of wall segment
- Methods: Uni-axial tension & nitrogen gas pressure (4)

Korea Atomic Energy Research Institute

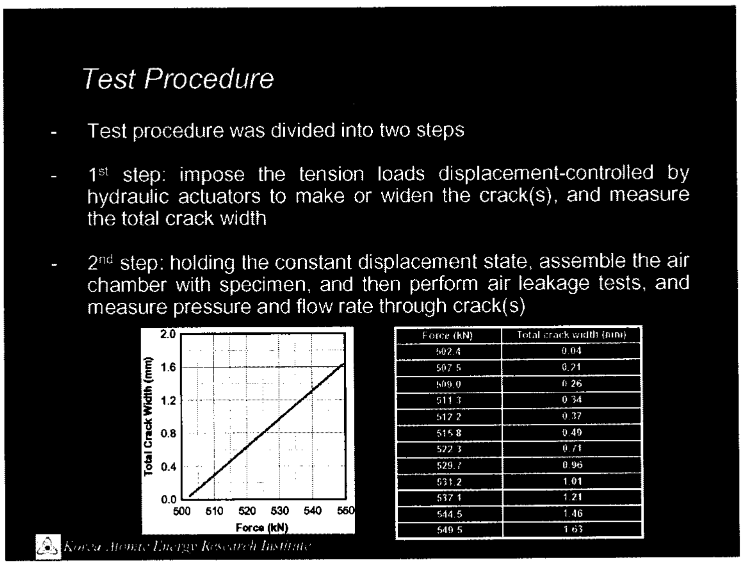
Total Crack Width (mm)
2.0
1.6
1.2
0.8
0.4
0.0
500
510
520
530
540
550
Force (kN)

Test Procedure

- Test procedure was divided into two steps
- 1st step: impose the tension loads displacement-controlled by hydraulic actuators to make or widen the crack(s), and measure the total crack width
- 2nd step: holding the constant displacement state, assemble the air chamber with specimen, and then perform air leakage tests, and measure pressure and flow rate through crack(s)

Force (kN)	Total crack width (mm)
502.4	0.04
507.5	0.21
509.0	0.26
511.3	0.34
512.2	0.37
515.8	0.49
522.3	0.71
529.7	0.96
531.2	1.01
537.1	1.21
544.5	1.46
549.5	1.63

Korea Atomic Energy Research Institute

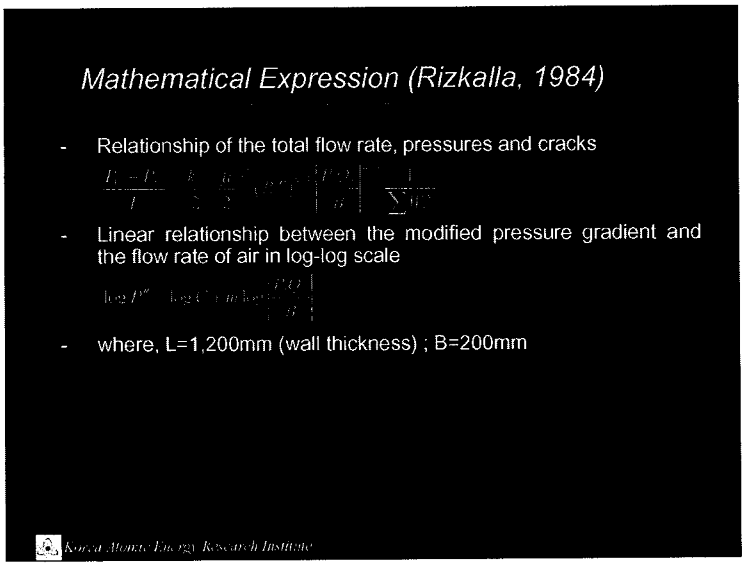

Mathematical Expression (Rizkalla, 1984)

- Relationship of the total flow rate, pressures and cracks
- Linear relationship between the modified pressure gradient and the flow rate of air in log-log scale

$$\log P'' = \log C + m \log\left(\frac{PQ}{B}\right)$$

- where, L=1,200mm (wall thickness) ; B=200mm

Korea Atomic Energy Research Institute

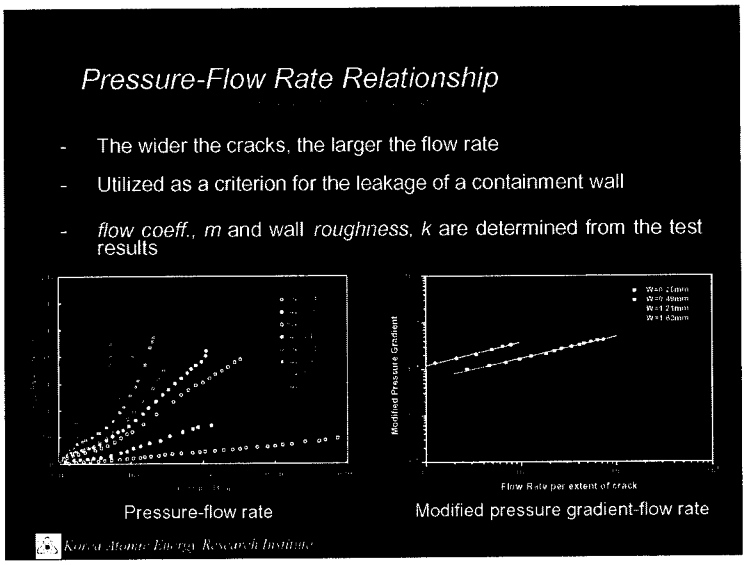
Modified Pressure Gradient
Flow Rate per extent of crack
W=0.26mm
W=0.49mm
W=1.21mm
W=1.63mm

Pressure-Flow Rate Relationship

- The wider the cracks, the larger the flow rate
- Utilized as a criterion for the leakage of a containment wall
- *flow coeff.*, *m* and wall *roughness*, *k* are determined from the test results

Pressure-flow rate

Modified pressure gradient-flow rate

Korea Atomic Energy Research Institute

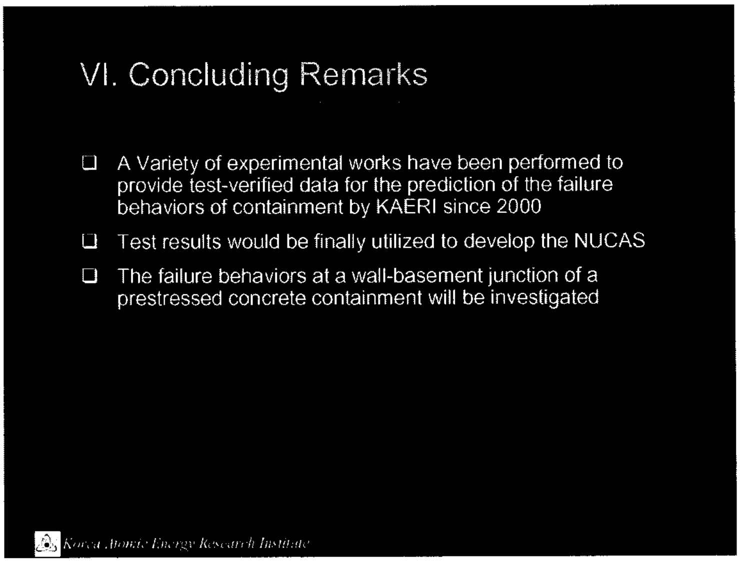

VI. Concluding Remarks

☐ A Variety of experimental works have been performed to provide test-verified data for the prediction of the failure behaviors of containment by KAERI since 2000

☐ Test results would be finally utilized to develop the NUCAS

☐ The failure behaviors at a wall-basement junction of a prestressed concrete containment will be investigated

Korea Atomic Energy Research Institute

A Summary of Complex Evaluation of the Status of Deliveries for the Mochovce NPP Units 3 and 4

Juraj Nozdrovický [1)]
Martin Moravčík [2)]

Abstract:

The purpose of this article is to present the usability evaluation for buildings of, and non-built-in deliveries for the unfinished Mochovce NPP Units 3 and 4 and to assess their potential future use for completion of the plant that was addressed within the project Complex Evaluation of the Status of Deliveries for the Mochovce NPP Units 3 and 4 implemented in 2003 and 2004.

At present, individual buildings and building structures of the Mochovce 3 and 4 are in various degrees of completion. Majority of unfinished buildings and building structures was exposed to long-term weather effects in most cases without final finishing of their internal and external parts.

Since the process of plant erection had been stopped, it was necessary to examine the status of already erected buildings and building structures as well as of deliveries that have not been built in yet.

1. INTRODUCTION

The complex evaluation of the Mochovce NPP Units 3 and 4 taken to possession of SE a.s. includes results of assessments of quality, environmental influences and material ageing as well as results of displacement measurements performed in selected buildings.

Quality was evaluated taking into account the following aspects: quality of individual buildings and building structures, completeness of appendant technical documentation, requirements of current legislation, comparison of the Mochovce 3 and 4 with a reference plant (Mochovce 1 and 2) and with IAEA recommendations.

2. CONCEPT OF EVALUATION OF THE STATUS OF DELIVERIES FOR THE MOCHOVCE NPP 3 AND 4

Based on their future usability, buildings, building structures and deliveries have been divided into three categories as follows:

USABLE ITEMS – items that can be used for the completion of the Mochovce NPP 3 and 4

---

1) Ing. Juraj Nozdrovický,VÚEZ, a.s., Levice, Továrenská 210, 935 28 Tlmače, e-mail: junoz@vuez.sk
2) doc. Ing. Martin Moravčík, PhD., SvF, ŽU Žilina, KSKaM, Komenského 52, 010 26 Žilina, e-mail: martin@fstav.utc.sk

CONDITIONALLY USABLE ITEMS – items which might be used for the completion of the Mochovce NPP 3 and 4 if a certain requirement is fulfilled and its fulfilment is neither time consuming nor costly

NUN-USABLE ITEMS – items that cannot be used for the completion of the Mochovce NPP 3 and 4

Evaluation of individual buildings and building structures complies with the earlier document Principles and Procedures of Complex Evaluation of the Status of Deliveries for the Mochovce NPP Units 3 and 4.

EVALUATION OF THE QUALITY OF MATERIALS IN ERECTED PARTS OF BUILDINGS AND NON-BUILT-IN DELIVERIES PLACED ON STORAGE SITES

To evaluate the quality of buildings and building structures, visual inspections and measurements were used.

Visual inspections

Visual inspections are one of the most effective methods how to establish the actual status since effects of many degradation mechanisms become evident by visible signs or discontinuities on exposed concrete surfaces.

Visual inspections focused on:

- Buildings and building structures (from foundations up to roofing)
- Non-built-in deliveries

Primarily the quality of performed works was examined as well as potential related defects such as technological or static cracks, surface structure of concrete, concrete corrosion and potential signs of reinforcement corrosion.

Checks of parameter measurement

Measurements taken and criteria applied:

- Steel liner corrosion and thickness: Limiting value of liner damage was established to be 20% of the nominal thickness of used sheets.
- Coat thickness: Integrity of coats applied to the liner to prevent corrosion was assessed by dry coat thickness measurements. Coat thickness was not allowed to be below 100 μm.
- Building structures were inspected to disclose cracks in already built-in structural components or non-built-in prefabricated components. The importance to reliable functioning of the concerned structural components was evaluated depending on the crack type:

  - technological cracks – surface cracks that arise as a result of concrete volume changes in the process of manufacture or erection;
  - cracks that arise by activation of microcracks on the surface extending as a result of weather effects (water, frost, etc);
  - static cracks that arise as a result of incidental overloading or improper handling or storage.

- Concrete alkalinity (pH value) and its effects on concrete carbonisation and corrosion rate: A criterion used for evaluation of concrete carbonisation was the progress of carbonisation in cover concrete. Depending on component type, this value ranged from 2 mm to 30 mm.
- Compressive strength test of concrete by a non-destructive method: Design strength and actual strength values of concrete were compared. To provide a sufficient number of values for statistical evaluation, the method was applied to 5 characteristic spots on the given component (e.g. wall). In such a way, all the load-bearing structural components of buildings as well as non-built-in prefabricated components were tested. A rebound hammer type N was used.
- Moisture content in concrete: Presence of moisture in concrete surface layers and its penetration into concrete is another important prerequisite for increased risk of concrete carbonisation and reinforcement corrosion. In individual buildings, water effects on the structure surface were inspected visually and experimental measurements of moisture by weight were performed on samples taken from individual concrete load-bearing components.
- Local leak tests: Underpressure leak tests of weld joints and overpressure leak tests of test volumes were performed. Weld overlaps were considered to be leak-tight if, during an overpressure test (150 kPa), pressure reduction was not observed for a period of 10 minutes.

Each part of a building was quantified by a separate index; by their aggregation, a global parameter was obtained that represents the current information on the status of the evaluated building.

This parameter was used as in input to divide building structures and components into individual categories (USABLE, CONDITIONALLY USABLE or NON-USABLE items).

3. RESULTS OF IN SITU MEASUREMENTS IN THE MOCHOVCE NPP 3 AND 4

In the process of evaluation, the following amounts of buildings have been evaluated:

- in 2003 – 38 buildings, and
- in 2004 –17 buildings.

Based on parameters obtained for individual buildings evaluated using the aforementioned methodology, it can be stated:

1. All the aboveground buildings are USEABLE or CONDITIONALLY USABLE.

2. Only several building structures (underground services with low level of completion and materials that do not meet current requirements for wear and lifetime compared to the reference plant) have been quantified as UNUSABLE.

3. Load-bearing metallic components and structures are in good technical status where preservative treatment has been applied. This is the case of 95% of evaluated building structures. In the other cases, load-bearing steel components and structures are conditionally usable provided that preservation treatment is applied soon.

4. Load-bearing concrete components and structures are in good technical status in all buildings where the degree of completion allowed to close the building. Conditionally usable (provided that intensive preservation treatment is applied) are building structures not protected against weather effects such as SO 580/1-04, SO 580/1-05, SO 580/1-06 (induced draught cooling towers), SO 581/1-05, 06, 07, 08 (natural circulation cooling towers), parts of SO 401/1-02, SO 401/1-03 (piping ducts) that are unfinished and not covered with embankment material. In buildings not protected against weather effects, concrete degradation as a result of external environmental effects is obvious. In some places, the prescribed thickness of cover concrete was not observed, lift joints were improperly situated and as a result surface concrete disintegration has occurred which has been contributed by water effects and rooted vegetation. Reinforcement in unfinished buildings has not been protected and exhibits signs of corrosion. In structural joints of some buildings, disintegration of grouts has occurred as a result of environmental effects – cracks can be observed and even the reinforcement has been exposed to corrosion.

5. Waterproofing systems in the lower parts of buildings (insulation against ground dampness) are completely usable where insulation has been protected against weather effects. In some cases of buildings directly related to the main production building II, only the horizontal insulation is usable. But even in these buildings, taking into account increased moisture content in some locations, in addition to condensation also damaged insulation is likely to occur. Since they have lost their function, these waterproofing systems will need to be completely reconstructed or applied again.

6. In principle, all locksmith structures used to anchor technological equipment are usable if early preservation treatment is applied.

7. Exterior walls are classified as usable and they are in an acceptable technical and functional status. External surfaces of SO 584/1-04 were provided with protective coating and that is why they can be qualified as very good. Some of the panels of the main production building external cladding show signs of mechanical damage (scaled edges and corners of panels). The other buildings were not provided with any protection of the external cladding from outside and repairs of local damages have been also missing which accelerates natural material degradation as a result of weather effects. From inside, the panels were not protected with any surface finish and thus surface cracks have appeared.

8. Majority of joints between the external cladding panels were not filled. In places where this was performed, the joints were not finished in many cases and as a result of weather effects and time they continue to degrade. In case of siporex panels, joints of external walls are usable if both the horizontal and vertical joints are completed.

9. Transparent structures, even if it is the case of simple glazing, are in most evaluated buildings quantified as usable since these are industrial buildings with excessive production of technological heat.

10. All erected lines of sanitary systems, active drains and fire water are quantified as usable.

11. Electrical wiring provided in buildings is temporary and was designed for construction purposes and as such it was not evaluated.

12. Central heating distribution lines can be found in auxiliary buildings and they are in various degrees of completion. They are basically usable if recoated.

13. Electric fire alarm devices for a part of buildings were delivered and have been stored as non-built-in deliveries in storage rooms. The electric fire alarm devices (made by TESLA Liberec) were manufactured in the 70-ies and do not correspond to requirements imposed upon modern systems (exact addressing, registration of the first announcement in time and space, potential co-operation of fire systems); in addition, they do not meet either the requirements that issue from safety improvement measures applied in the reference plant or IAEA recommendations.

14. As to fire protection, it is necessary to stress the requirement for complex solution of the new fire protection system for individual buildings that issues from individual safety improvement measures developed based on IAEA recommendations. This applies to the protection of cable distributions, penetration of individual pipelines through boundaries of fire compartments, automatically controlled fire dampers in pipelines etc.

15. Non-built-in deliveries: parts of some buildings were not completed; deliveries that need to be installed have been marked (date of manufacture, serial number etc) and placed in storage rooms or on external storage sites. Technical status of unprotected deliveries reflects the long-term weather effects.

Furthermore, the individual buildings were assessed from the following standpoints:

A. Completeness of appendant technical documentation

B. Requirements of current legislation and comparison with legislation valid at the time of delivery

C. Comparison of Mochovce 3 and 4 buildings with buildings of the same type in the reference plant, evaluation of safety improvement measures

D. Impacts of IAEA recommendations on upgrading of VVER 440 reactor units

A. Completeness of appendant technical documentation

Completeness of the appendant technical documentation was checked by comparing it with similar documentation for the Mochovce NPP 1 and 2. As to its completeness, no substantial deficiencies were disclosed for the part related to the already erected buildings.

B. Requirements of current legislation

All VVER NPPs were designed in accordance with Soviet (Russian) standards valid at the time of their design.

Design and erection of plant buildings complied with provisions of Building Regulations 50/1976 and ČSN standards valid at that time. At present, the standards have been replaced by STN.

The assessed design documentation (electrical equipment) was elaborated in 1987-1988 and it does not meet current requirements of applicable legislative documents and standards. Prior to starting plant completion, it will be necessary to update the design and detailed design documentation in accordance with legislation that will be valid at the time of plant completion.

When assessing the plant buildings from the standpoint of applicable legislation, no substantial deficiencies were disclosed for the parts related to already erected plant buildings.

C. Comparison with the reference plant

Comparison of Mochovce 3 and 4 buildings with buildings of identical type in the reference plant (Mochovce 1 and 2) was performed for each building and it was included in the complex evaluation of plant buildings.

Compared to the reference plant, no deviations were disclosed that could be evaluated as non-conforming. Proposed or performed changes in buildings of the reference plant are feasible and can be performed within the Mochovce NPP 3 and 4 completion, too.

Based on implemented changes issuing from safety improvement measures for buildings of the Mochovce NPP 1 and 2, it can be stated that they will not have any substantial impact on the completed parts of Mochovce 3 and 4 buildings (except some changes mentioned in relevant protocols). All the changes are feasible.

D. Impacts of IAEA recommendations on upgrading of VVER 440 reactor units

Impacts of IAEA recommendations on upgrading of VVER 440 reactor units were evaluated for each building separately and the evaluation was included in the complex evaluation of individual plant buildings.

No IAEA recommendations that could be considered as non-conformance if not fulfilled by the already completed buildings was indicated. All changes that issue from safety improvement measures can be implemented during the Mochovce 3 and 4 completion.

4. CONCLUSION AND EVALUATION OF RESULTS

In total, 55 plant buildings were evaluated. Usable or conditionally usable are all above-ground buildings and building structures. Only several building structures (underground services with low level of completion and materials that do not meet current requirements for wear and lifetime compared to the reference plant) were qualified as unusable.

From the complex evaluation of buildings, building structures and non-built-in deliveries it follows that the unfinished buildings and building structures are in good technical status and can be used for the Mochovce 3 and 4 completion. Conditionally usable buildings and building structures have deficiencies whose elimination is not either technically or financially demanding. Non-usable items are some non-built-in deliveries (electrical fire alarm devices, lifts, fire doors and some types of prefabricated components) which have been either damaged or are technically or morally obsolete and do not meet requirements of current STN standards. Non-usable deliveries form a negligible percentage of the whole building part.

From the complex evaluation of the plant building part, it follows that all buildings are usable for completion of the Mochovce NPP Units 3 and 4.

-Topical discussions

Contributions:

-Evaluation and modeling of the ageing of the structure over its lifetime - How does finite element analysis fit in an ageing management program?

Moderator: J.P. Touret (Edf, FR) 345
Panel Members: O. Jovall (Scanscot Technology,SWD)......347
P. Lenkei (Paks NPP, HUN)......351

-Suitability of current analytical tools/methods and required model(s) fidelity for realistic capacity estimates - Applicability of standard material test methods for derivation of material constitutive models for large structures subjected to severe damage states. Scale effects between material specimens and structures. Use of laboratory test results for design and performance assessment.

Moderator: N. Prinja (NNC, Ltd, UK) 353
Panel Members: J. Stepan (UJV ReZ, CR) 359
O. Jovall (Scanscot Technology,SWD)......361

-Application of damage or functional performance criteria, e.g. leakage, to numerical simulations. Consensus on surrogate performance/failure criteria, e.g. strain, for statutory performance criteria. Model dependency of surrogate failure criteria.

Moderator: M. Hessheimer (SNL, USA) 363
Panel Members: J-M. Seo (KAERI, KR)...... 369
H. Grebner (GRS, GER)...... 371
JM. Rambach (IRSN, FR)

-Leak vs. Catastrophic rupture: consequences and design implications

Moderator: J. Rashid (ANATECH, USA) 373
Panel Members: J. Gustavsson (Ringhals AB, SWD), J. Curley (NNC, Ltd, UK)......379
P. Varpasuo (Fortum NS, FIN)......381

-Integration of best estimate containment capacity/behavior in PRA models and quantification of uncertainties

Moderator: S. Ali (USNRC, USA) 383
Panel members: S. Basha (NNC, Ltd, UK)......389
N. Lee (KOPEC, KR)......393

-Research needs for advanced and next generation plants, e.g. long term high temperature behavior, confinement (leakage/venting) vs. containment

Moderator: M. Elgohary (AECL, CAN) 395
Panel Members: C. Nyaradi (Paks, HUN), T. Ogata (Obayashi Corp., JPN)......399

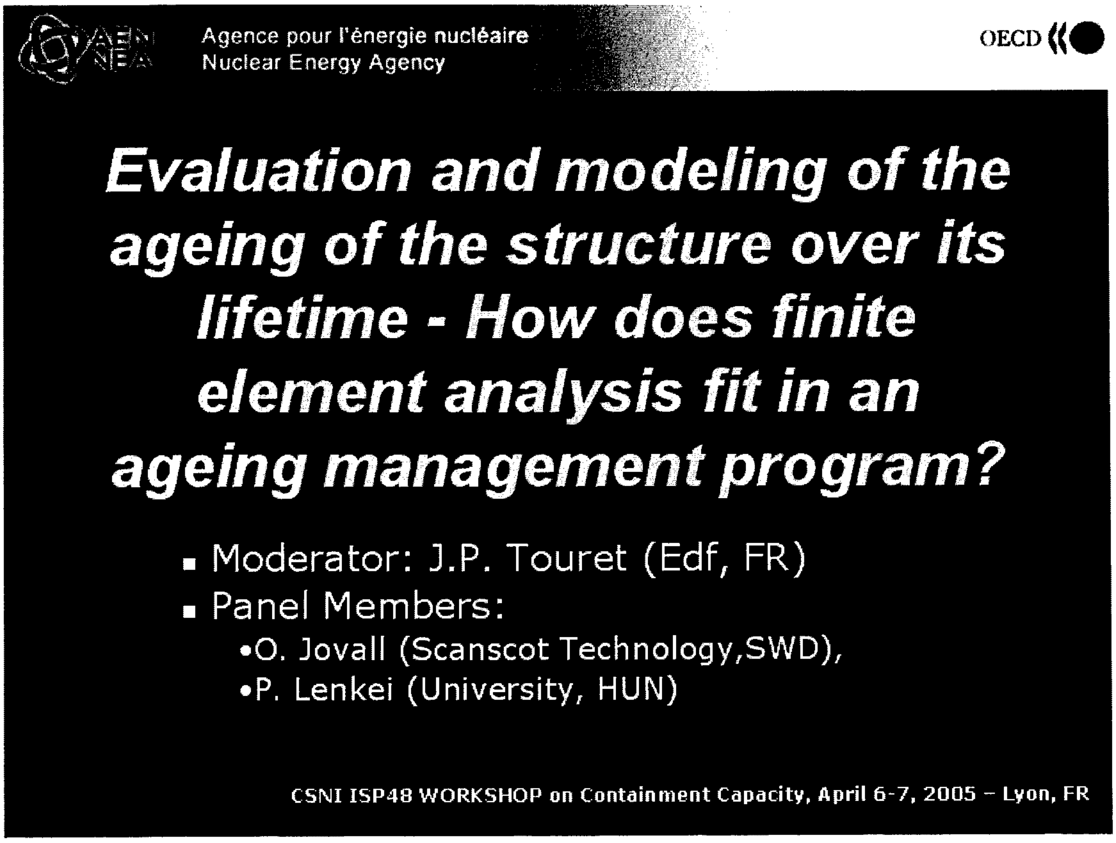

Agence pour l'énergie nucléaire
Nuclear Energy Agency

OECD

Evaluation and modeling of the ageing of the structure over its lifetime - How does finite element analysis fit in an ageing management program?

- Moderator: J.P. Touret (Edf, FR)
- Panel Members:
  - O. Jovall (Scanscot Technology,SWD),
  - P. Lenkei (University, HUN)

CSNI ISP48 WORKSHOP on Containment Capacity, April 6-7, 2005 – Lyon, FR

FEA - ageing

For it to be possible to predict the future condition of a structure it is necessary to construct a PROFILE of that structure.

That means you have to know and understand the present condition of the structure before you can predict the future.

All factors relating to geometry, detailing, condition and ageing together describe the PROFILE of the structure.

FEA - ageing

The PROFILE of the structure is then described by:

- The as-built compliance with design
  - Geometry
  - Positioning of rebars and tendons
  - Unknown defects during construction

- The condition and quality of concrete

- The ageing processes
  - Creep, shrinkage and relaxation
  - Strength gain
  - Deterioration (corrosion, ASR etc)

Defects are very imporant because they can by themeselves be critical, or they initiate and/or accelerate deterioration processes.

FEA - ageing

To state the PROFILE of the structure we can use:

- Monitoring systems
  - Delayed strain
  - Deformations
- Material testing ("destructive" methods)
  - Drilled cores
  - Moisture content in-situ

"INSPECTIONS"

- Non-destructuve testing methods
  - Seismic methods
  - Radar and x-ray (local studies only)
- Other testing
  - Lift-off tests
  - Leak-rate pressure tests
- Theoretical models
  - could or could not be implemented in FE analysis

FEA - ageing

There are several ways in which FEA can be utilized

- Identification of critical parts of the structure for further inspections
- Up-dated FE analysis using input from inspections
- Predictions of inspection response for a known condition at present time
- Prediction of inspection response based on known condition and how this will change in the future due to ageing processes

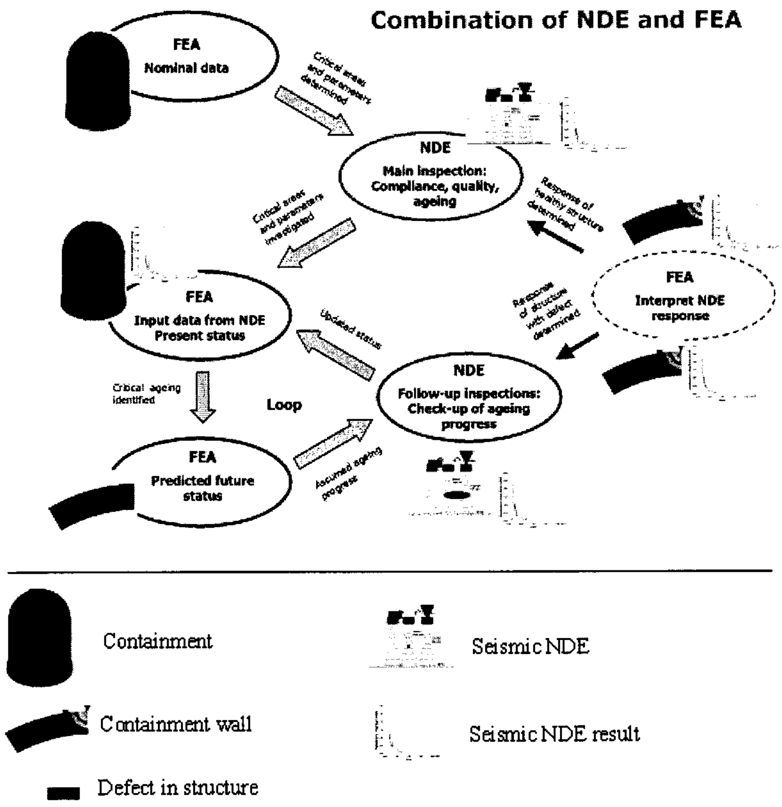
Combination of NDE and FEA
FEA
Nominal data
Critical areas and parameters determined
NDE
Main inspection: Compliance, quality, ageing
Critical areas and parameters investigated
Response of healthy structure determined
FEA
Input data from NDE
Present status
FEA
Interpret NDE response
Response of structure with defect determined
Updated status
NDE
Follow-up inspections: Check-up of ageing progress
Critical ageing identified
Loop
FEA
Predicted future status
Assumed ageing progress
Containment
Seismic NDE
Containment wall
Seismic NDE result
Defect in structure

CSNI Workshop ISP 48

Topical discussion, Thursday, April 7, 2005, 9.00

EVALUATION AND MODELING OF THE AGEING OF THE STRUCTURE OVER ITS LIFETIME - HOW DOES FINITE ELEMENT ANALYSIS FIT IN AN AGEING MANAGEMENT PROGRAM?

Discussion by panel member Peter Lenkei

The concrete ageing problem

At design only the theoretical ageing curve (the variation of the ageing process in time) is available, based on theoretical investigations and corrected by measurements with similar structures.

To check in a given time the state of a concrete structure is simple by the help of the necessary number of NDT and some DT (if possible) tests.

But to estimate a future situation for license renewal or for life time extension is more complex. In case of existing structure this should be based on (desirable regular) previous investigations made during passed life time.

In addition one should take into account, that concrete is a non-homogeneous material, e.g. different FE could have different performance (strength, deformability, ageing curve).

One of the FEM problem is the non-linearity and diversity of the time-dependent real processes like concrete ageing, creep of concrete, relaxation of prestressing devices.

The main problem is which average or which characteristic value should be accepted to model these processes. A conservative simplification might lead to higher costs, mainly when according to the analysis interventions are necessary for limit ageing or for strengthening the often non-accessible structures.

In our days it is generally advised that the easiest and cheapest solution is to choose one grade higher concrete quality during design to increase durability and avoid ageing problems of concrete structures.

It should be mentioned that the use of decontaminatable paints on the concrete surface is also favorable from ageing point of view (preventing carbonization), but the state of the embedded in concrete liners are hard to evaluate.

Agence pour l'énergie nucléaire
Nuclear Energy Agency

OECD

Suitability of current analytical tools/methods and required model(s) fidelity for realistic capacity estimates - Applicability of standard material test methods for derivation of material constitutive models for large structures subjected to severe damage states. Scale effects between material specimens and structures. Use of laboratory test results for design and performance assessment..

- Moderator: N. Prinja (NNC, Ltd, UK)
- Panel Members:
  - J. Stepan (UJV ReZ, CR),
  - O. Jovall, Scanscot, Sweden

CSNI ISP48 WORKSHOP on Containment Capacity, April 6-7, 2005 - Lyon, FR

Agence pour l'énergie nucléaire
Nuclear Energy Agency

OECD

Objective

1. Suitability of current analytical tools/methods and required model(s) fidelity for realistic capacity estimates.
2. Applicability of standard material test methods for derivation of material constitutive models for large structures subjected to severe damage states.
3. Scale effects between material specimens and structures.
4. Use of laboratory test results for design and performance assessment.

CSNI ISP48 WORKSHOP on Containment Capacity, April 6-7, 2005 - Lyon, FR

Agence pour l'énergie nucléaire
Nuclear Energy Agency

OECD

Analytical Tools for Realistic capacity Estimates

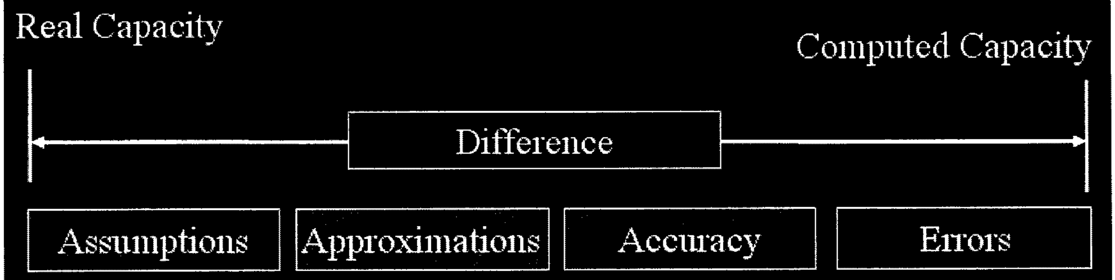

Real Capacity

Computed Capacity

Difference

Assumptions

Approximations

Accuracy

Errors

CSNI ISP48 WORKSHOP on Containment Capacity, April 6-7, 2005 – Lyon, FR

Agence pour l'énergie nucléaire
Nuclear Energy Agency

OECD

Constitutive Models for Analysing Severe Damage States

Numerical fracture mechanics characterisation becomes an important analysis objective

- Highly heterogeneous material, not easily amenable to numerical characterisation.
- Behaviour in tension is vastly different from that in compression.
- bi-axial strength, stress-strain curves, fracture energy for analysis of various grades of concrete.
- The inclusion of reinforcing and pre-stressing elements in practical concrete structures further increases the level of complexity.

CSNI ISP48 WORKSHOP on Containment Capacity, April 6-7, 2005 – Lyon, FR

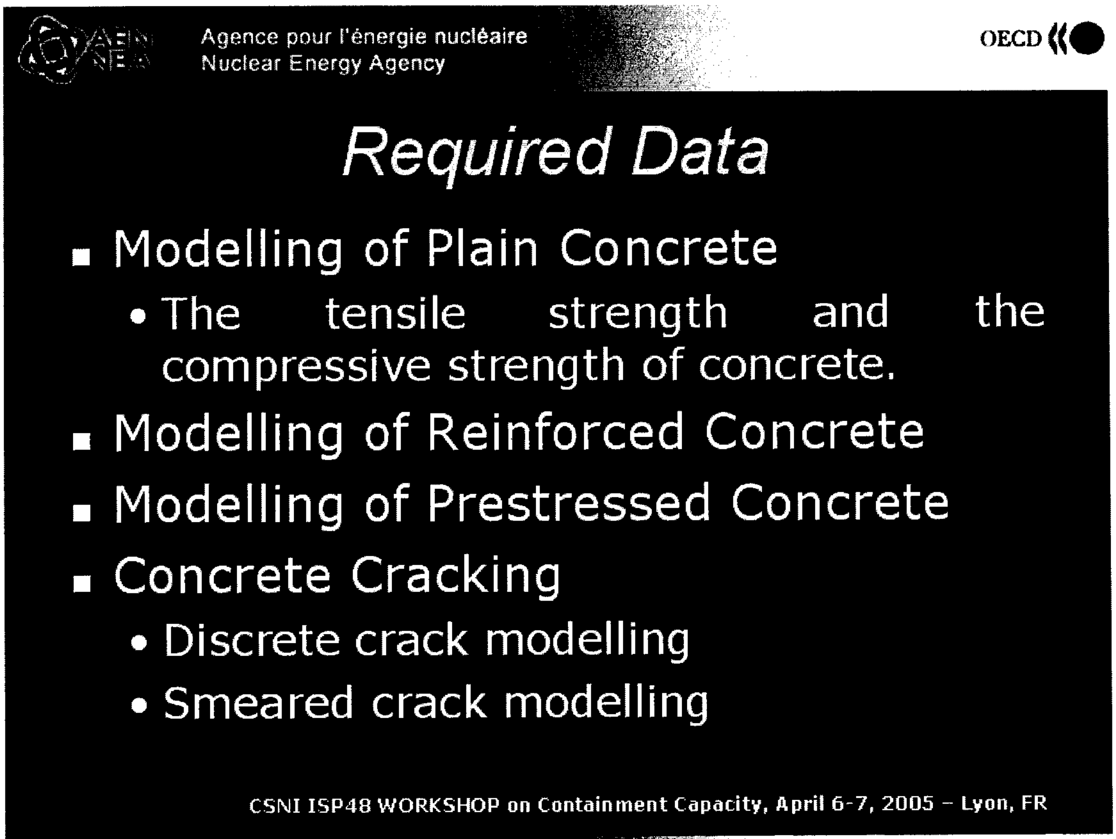

Agence pour l'énergie nucléaire
Nuclear Energy Agency

OECD

Required Data

- Modelling of Plain Concrete
  - The tensile strength and the compressive strength of concrete.
- Modelling of Reinforced Concrete
- Modelling of Prestressed Concrete
- Concrete Cracking
  - Discrete crack modelling
  - Smeared crack modelling

CSNI ISP48 WORKSHOP on Containment Capacity, April 6-7, 2005 - Lyon, FR

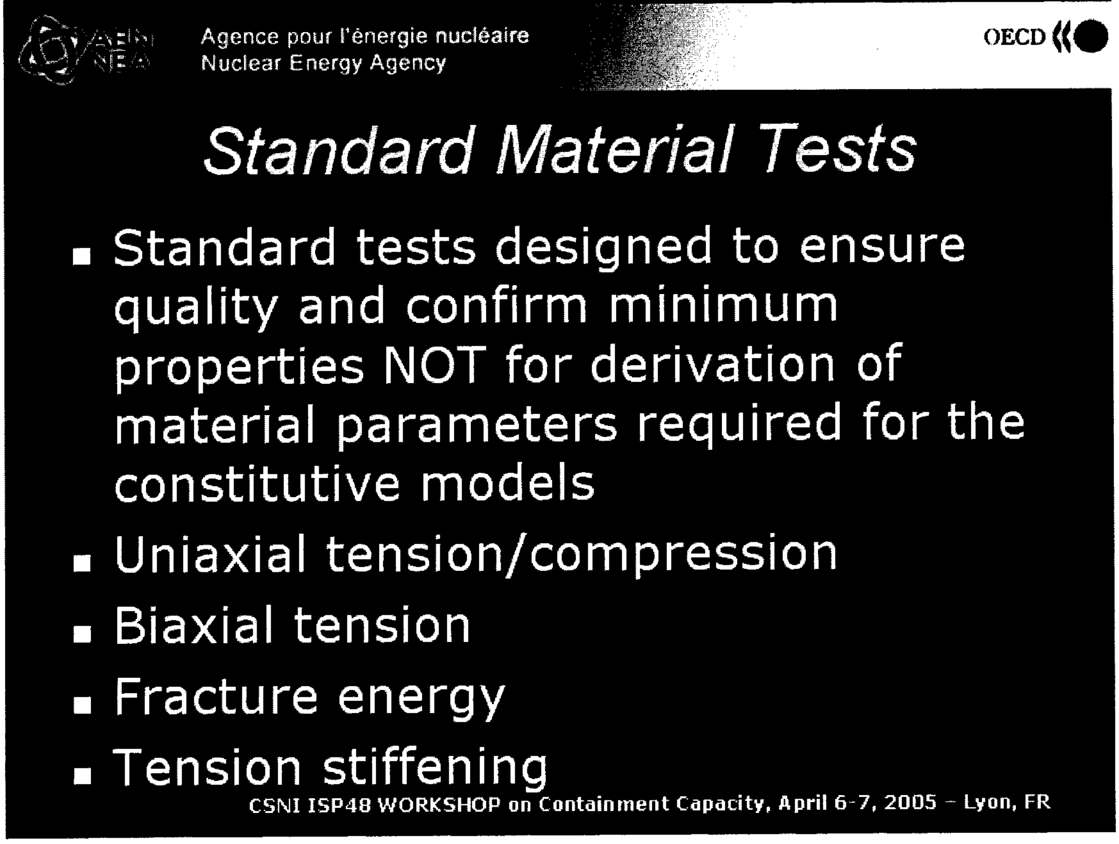

Agence pour l'énergie nucléaire
Nuclear Energy Agency

OECD

Standard Material Tests

- Standard tests designed to ensure quality and confirm minimum properties NOT for derivation of material parameters required for the constitutive models
- Uniaxial tension/compression
- Biaxial tension
- Fracture energy
- Tension stiffening

CSNI ISP48 WORKSHOP on Containment Capacity, April 6-7, 2005 - Lyon, FR

Agence pour l'énergie nucléaire
Nuclear Energy Agency

OECD

Scale Effects

- Mass, dimension and time
- Friction cannot be scaled

CSNI ISP48 WORKSHOP on Containment Capacity, April 6-7, 2005 – Lyon, FR

Agence pour l'énergie nucléaire
Nuclear Energy Agency

OECD

Lab Tests for Design & performance

- **Design**
  - **By rule**
  - **By analysis**
  - **By test**
- **How to satisfy the regulatory bodies**
- **Modelling issues (Bolts, seals and connections)**
- **Validation & verification**

CSNI ISP48 WORKSHOP on Containment Capacity, April 6-7, 2005 – Lyon, FR

Agence pour l'énergie nucléaire
Nuclear Energy Agency

OECD

Conclusions

CSNI ISP48 WORKSHOP on Containment Capacity, April 6-7, 2005 - Lyon, FR

Agence pour l'énergie nucléaire
Nuclear Energy Agency

OECD

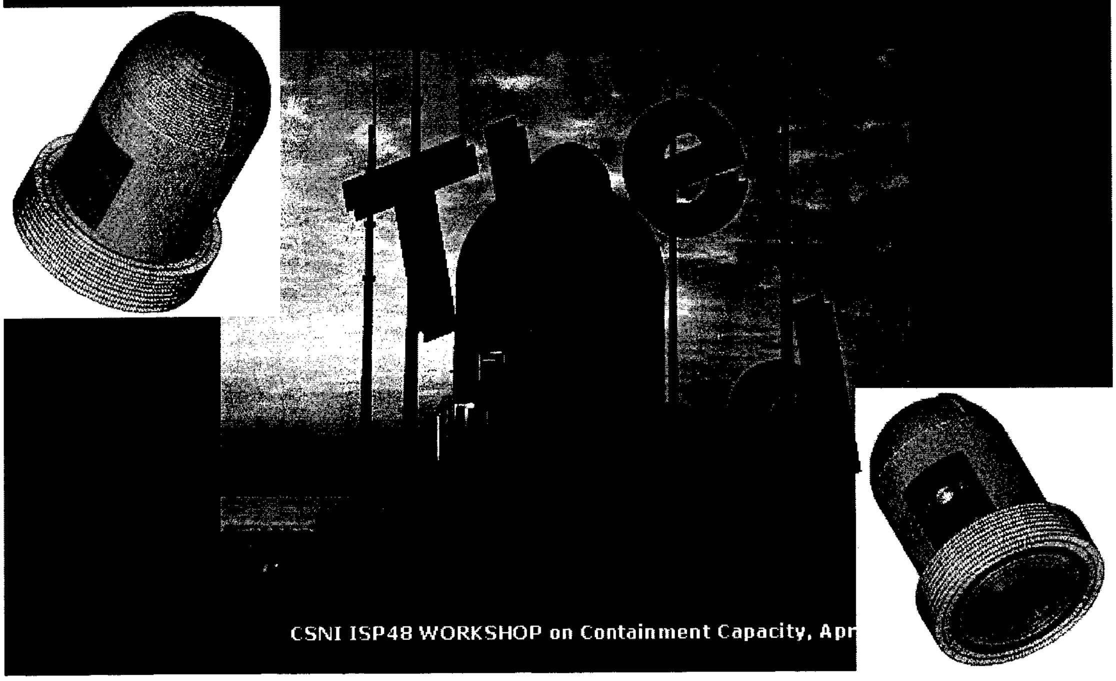

CSNI ISP48 WORKSHOP on Containment Capacity, Apr

Suitability of current analytical tools/methods and required model(s) fidelity for realistic capacity estimates - Applicability of standard material test methods for derivation of material constitutive models for large structures subjected to severe damage states. Scale effects between material specimens and structures. Use of laboratory test results for design and performance assessment.

Jan Stepan

1) Analytical tools and methods

Analytical tools, especially computing tools, are still under continuing evolution. Due to rapid development of computing capacity of computers it is possible to analyze large structures in very complex way including nonlinear behavior. Computing capacity also enables to add new dimension by changing deterministic analyses to probabilistic ones. Despite this fact, the computing analyses are only part of global analysis of structure and although represent simplification of real structure, this simplification is the only one of the series of simplifications which have to be done and then considered in final evaluation of results. Next parts of structure analysis can be for example conversion of real structure to analysis model and evaluation of results and their back application on real structure (exactly these parts of structure analysis are very often source of mistakes and differences in behavior of analysis models). The comparison of ISP48 analyses results shows that, if the input data are same, the results of different analyses are comparable. But, due to lack or uncertainties in knowledge of material failure limits, there are differences in the evaluation of analysis results.

2) Standard material tests

Currently used standard material tests are able to define material parameters needed for nonlinear analyses of structures. Basic condition is to realize test in full range not only in limited scope orientated at one parameter (in case of concrete it is e.g. pressure strength). Disadvantage of material tests is that it is necessary to have material samples taken from real structure for testing (in case of NPP under operation is often difficult to obtain material samples from real structure) and it is needed to have time and money to do tests. Specific problem is case of design of a new structure where the structure exists only in a computer and there is no material to test. The solution could be to extend existent standards with more complex material data – the requirements of probabilistic methods are next reason for this extending.

3) Scale effects between material specimens and structures

Scale effects exist and have to be considered. In case of containments I have experience with two typical examples of scale effect. The first example represents material scale effect - due to cracking of real structure there are differences between tensile strength and modulus of elasticity of concrete in real structure and defined by tests at compact, non cracked, samples. The second example represents change between behavior of single part of the structure and behavior the whole structure – failure capacity of prestressing tendon in containment is lower then sum of load bearing capacity of individual wires in tendon.

4) Use of laboratory test results for design and performance assessment

Laboratory material tests are basic data for analyses and there is no another possibility how obtain this information. In case of more complex tests there are two possible ways of employing of the test results. The first way is to use the test results directly for design of real structure (with considering of the test simplifications). This is typical in case of very complex problems when the test is easier and more demonstrative then analyses. The second way is to use the test results for validation or verification of design methods and analysis tools. Considering the costingness of the complex tests it is advisable to collect and save maximum possible amount of the test result data which enables later reusing or reevaluation of the test results e.g. by using of better analysis tools.

Suitability of current analytical tools... (WS 2)

- In my opinion, if put in the amount of effort needed, we can carry out high quality numerical simulations of reactor containments to predict the reponse of the structure.
- For containments with steel liner, one major issue is how to state acceptance critera for leakage, i.e. liner tearing.
- For containments without liner, i.e. the concrete itself contitutes the major leak-tightness barrier, the acceptance criteria due to leakage is even more difficult to state. In addition, an advance of constitutive models for concrete may be needed.
- It may also be so that material testing methods have to be improved to supply us with more realistic/relevant input data to our analysis.
- We advocate the analysis methodology to use a FE 3D-model to be able to capture the structural response of a reactor containment. Coupled to this model, sub-models in critical areas can be used to study the stress/strain state in more detail to be able to estimate the leak-tightness capacity of the containment.

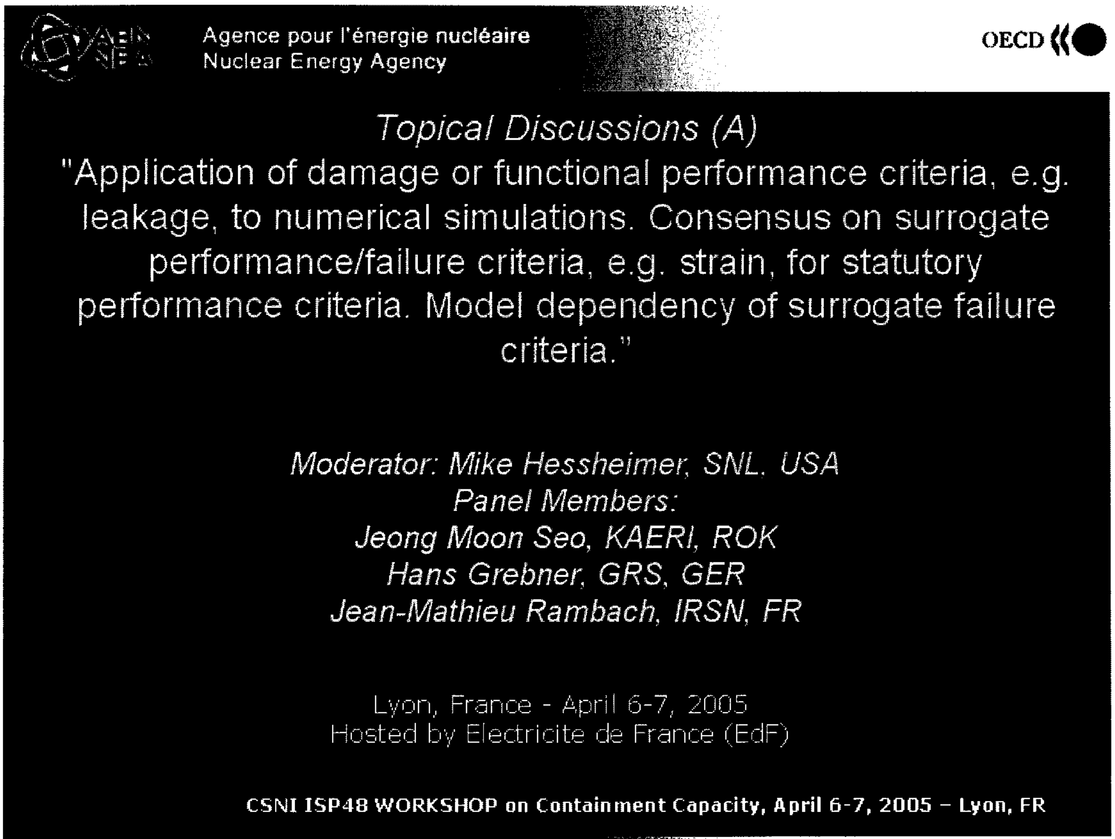

Agence pour l'énergie nucléaire
Nuclear Energy Agency

OECD

Topical Discussions (A)

"Application of damage or functional performance criteria, e.g. leakage, to numerical simulations. Consensus on surrogate performance/failure criteria, e.g. strain, for statutory performance criteria. Model dependency of surrogate failure criteria."

Moderator: Mike Hessheimer, SNL, USA
Panel Members:
Jeong Moon Seo, KAERI, ROK
Hans Grebner, GRS, GER
Jean-Mathieu Rambach, IRSN, FR

Lyon, France - April 6-7, 2005
Hosted by Electricite de France (EdF)

CSNI ISP48 WORKSHOP on Containment Capacity, April 6-7, 2005 – Lyon, FR

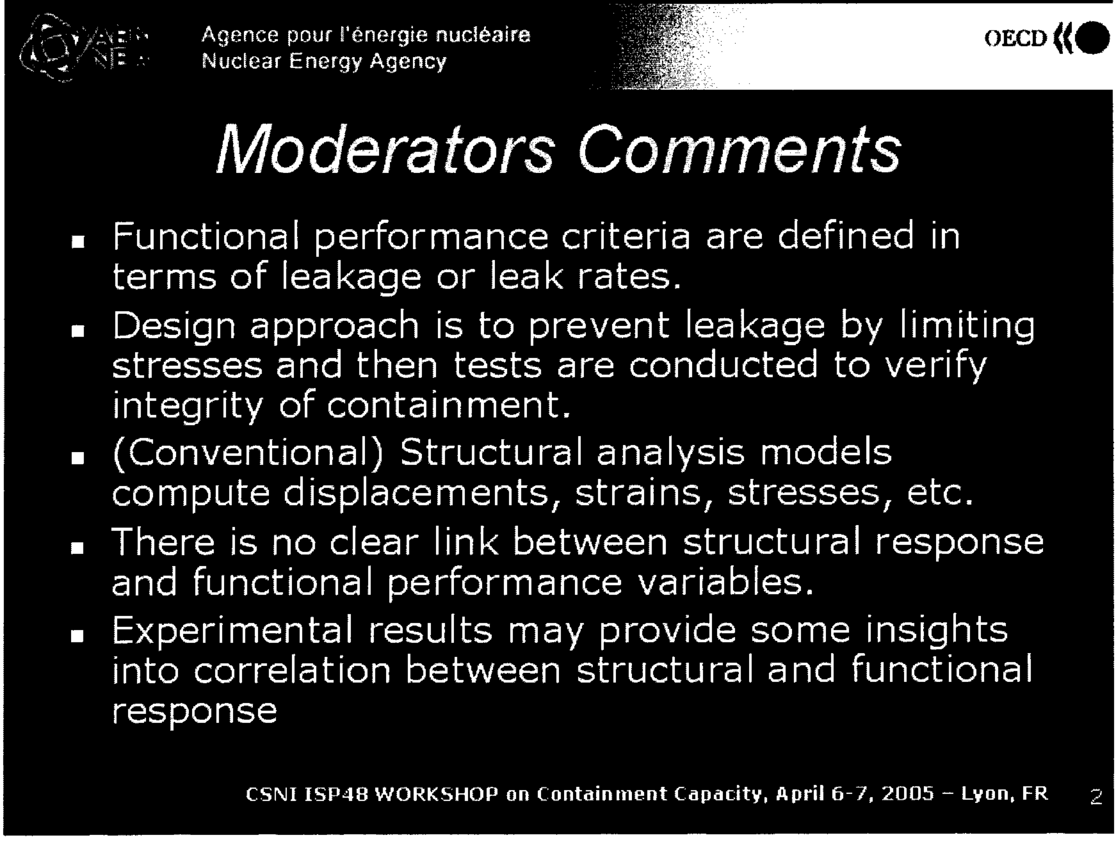

Agence pour l'énergie nucléaire
Nuclear Energy Agency

OECD

Moderators Comments

- Functional performance criteria are defined in terms of leakage or leak rates.
- Design approach is to prevent leakage by limiting stresses and then tests are conducted to verify integrity of containment.
- (Conventional) Structural analysis models compute displacements, strains, stresses, etc.
- There is no clear link between structural response and functional performance variables.
- Experimental results may provide some insights into correlation between structural and functional response

CSNI ISP48 WORKSHOP on Containment Capacity, April 6-7, 2005 – Lyon, FR 2

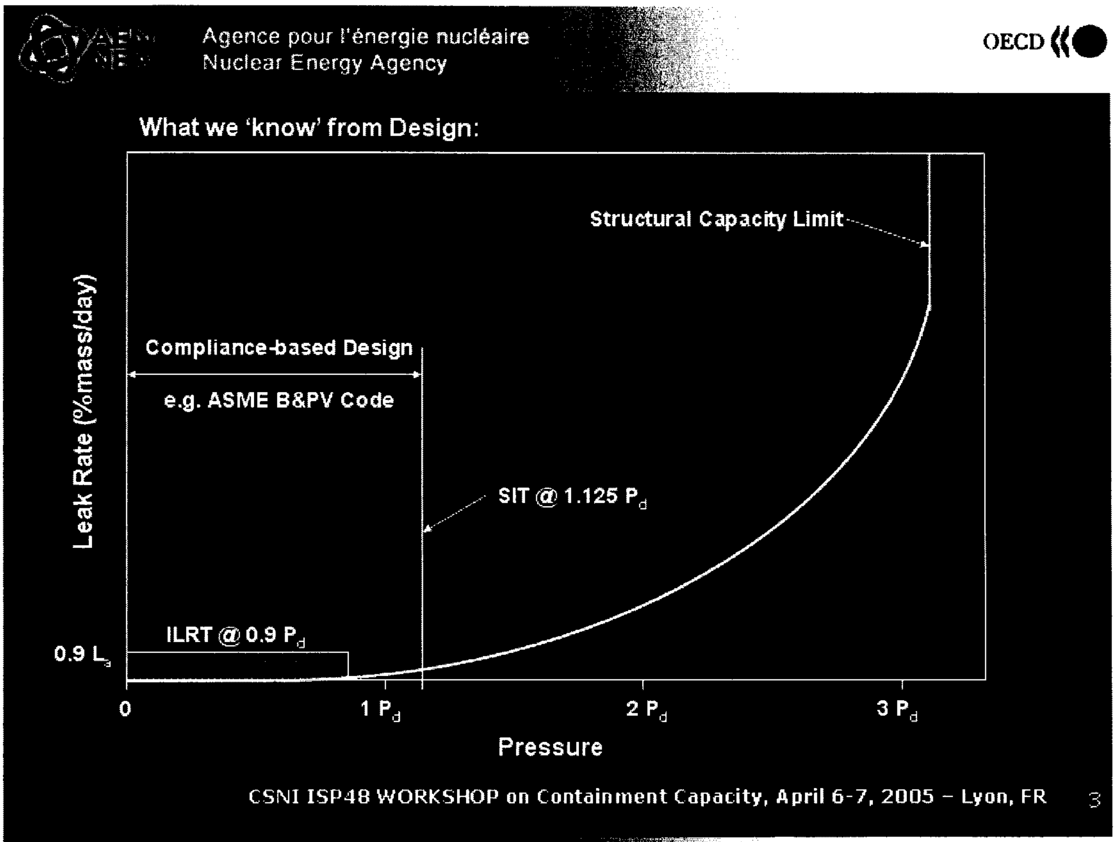

Agence pour l'énergie nucléaire
Nuclear Energy Agency

OECD

What we 'know' from Design:

CSNI ISP48 WORKSHOP on Containment Capacity, April 6-7, 2005 – Lyon, FR 3

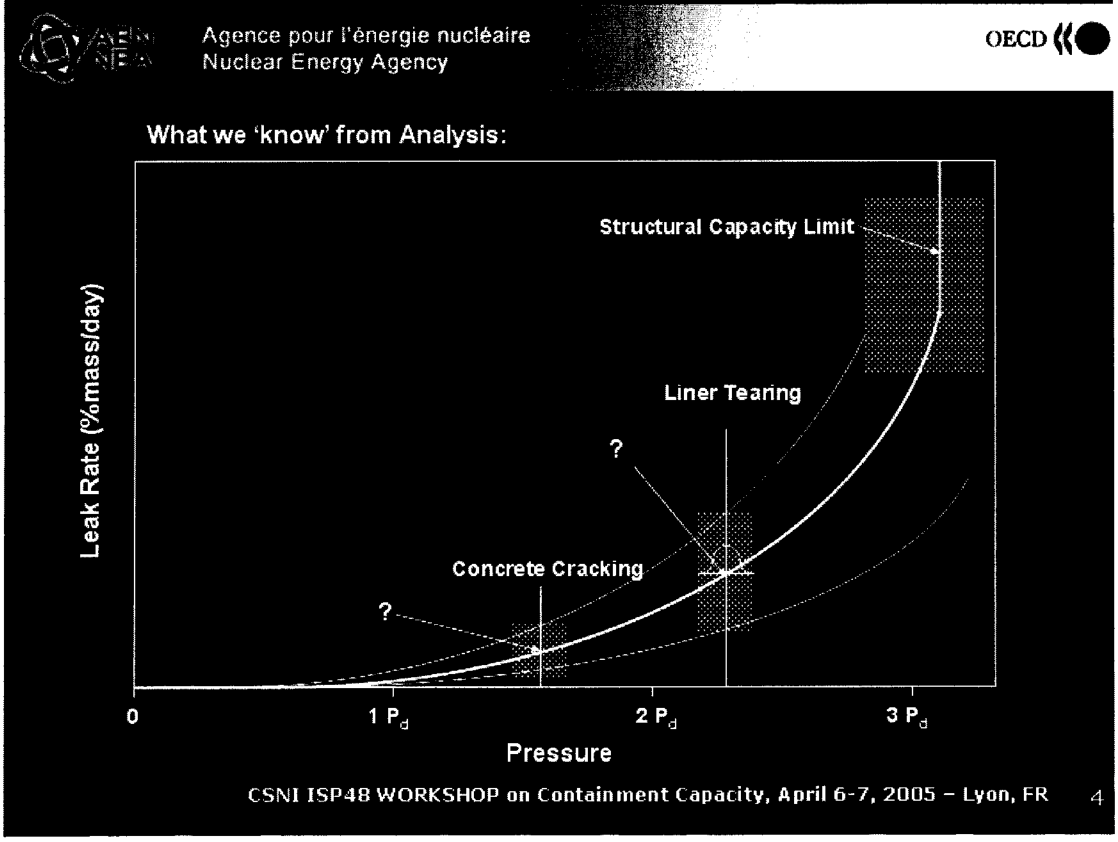

Agence pour l'énergie nucléaire
Nuclear Energy Agency

OECD

What we 'know' from Analysis:

CSNI ISP48 WORKSHOP on Containment Capacity, April 6-7, 2005 – Lyon, FR 4

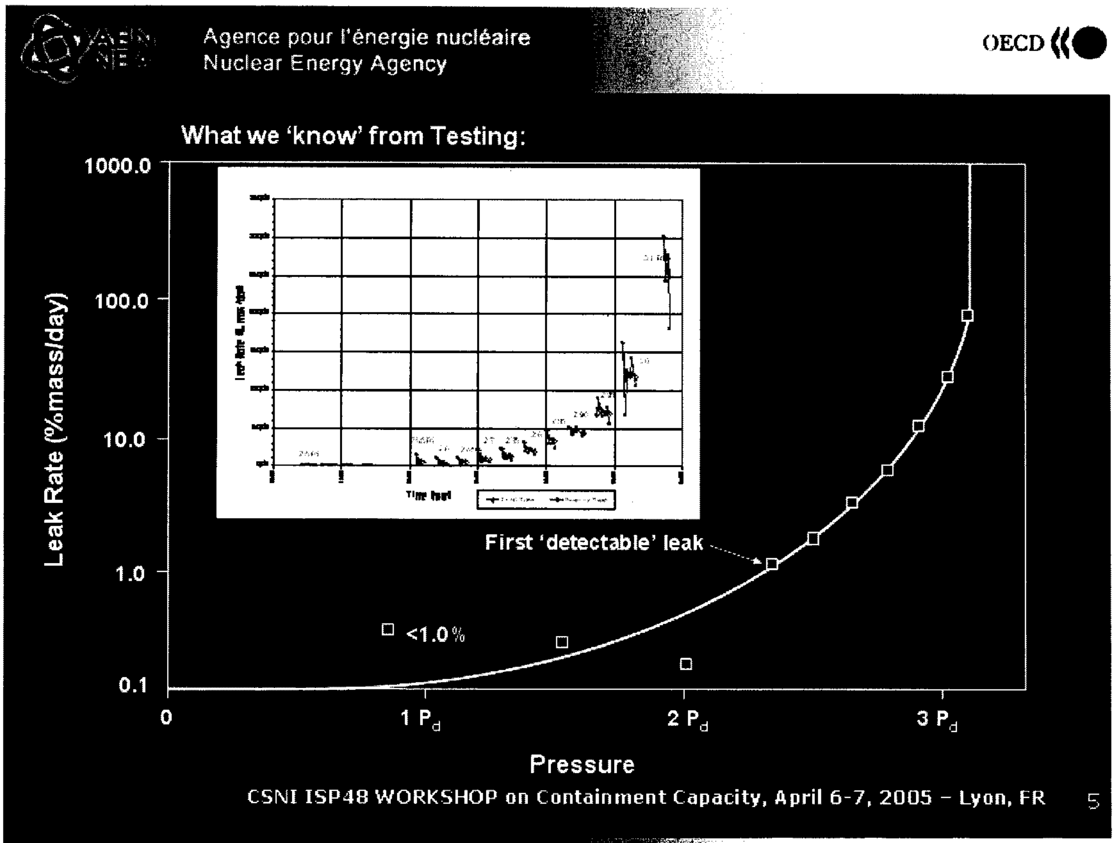

Agence pour l'énergie nucléaire
Nuclear Energy Agency

OECD

What we 'know' from Testing:

CSNI ISP48 WORKSHOP on Containment Capacity, April 6-7, 2005 - Lyon, FR

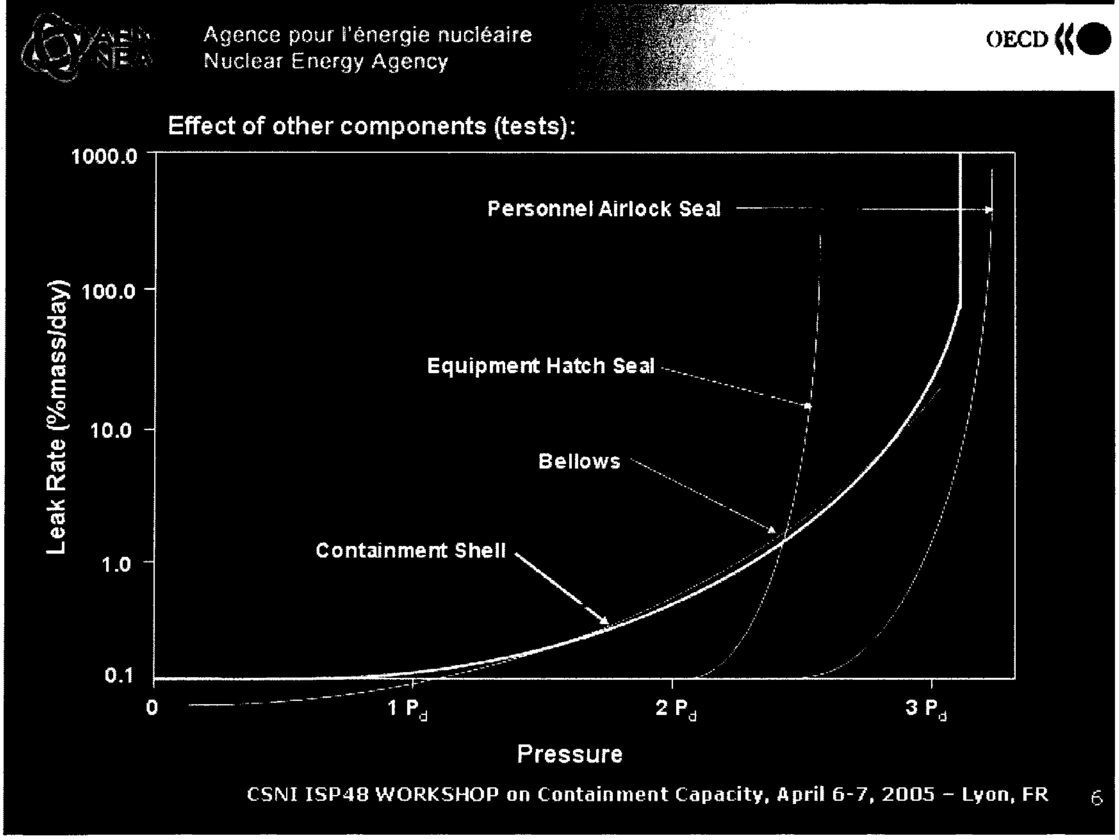

Agence pour l'énergie nucléaire
Nuclear Energy Agency

OECD

Effect of other components (tests):

CSNI ISP48 WORKSHOP on Containment Capacity, April 6-7, 2005 - Lyon, FR

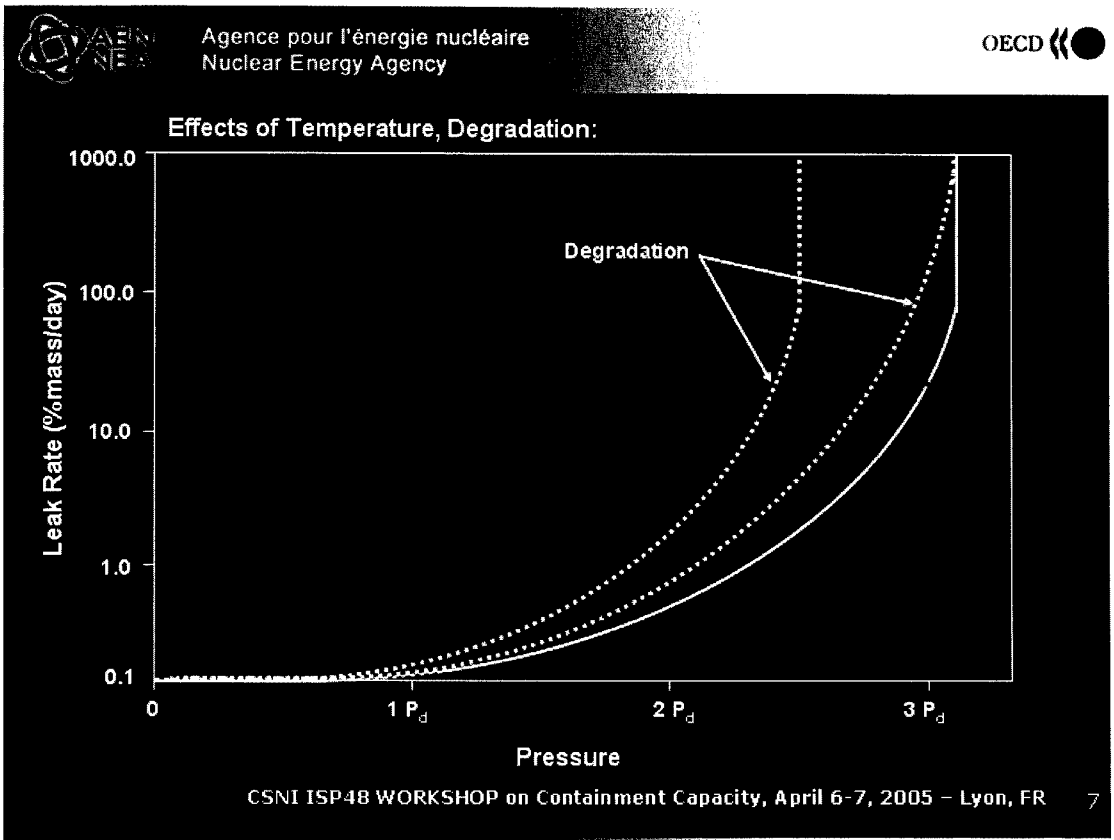

Agence pour l'énergie nucléaire
Nuclear Energy Agency

OECD

Effects of Temperature, Degradation:

CSNI ISP48 WORKSHOP on Containment Capacity, April 6-7, 2005 – Lyon, FR 7

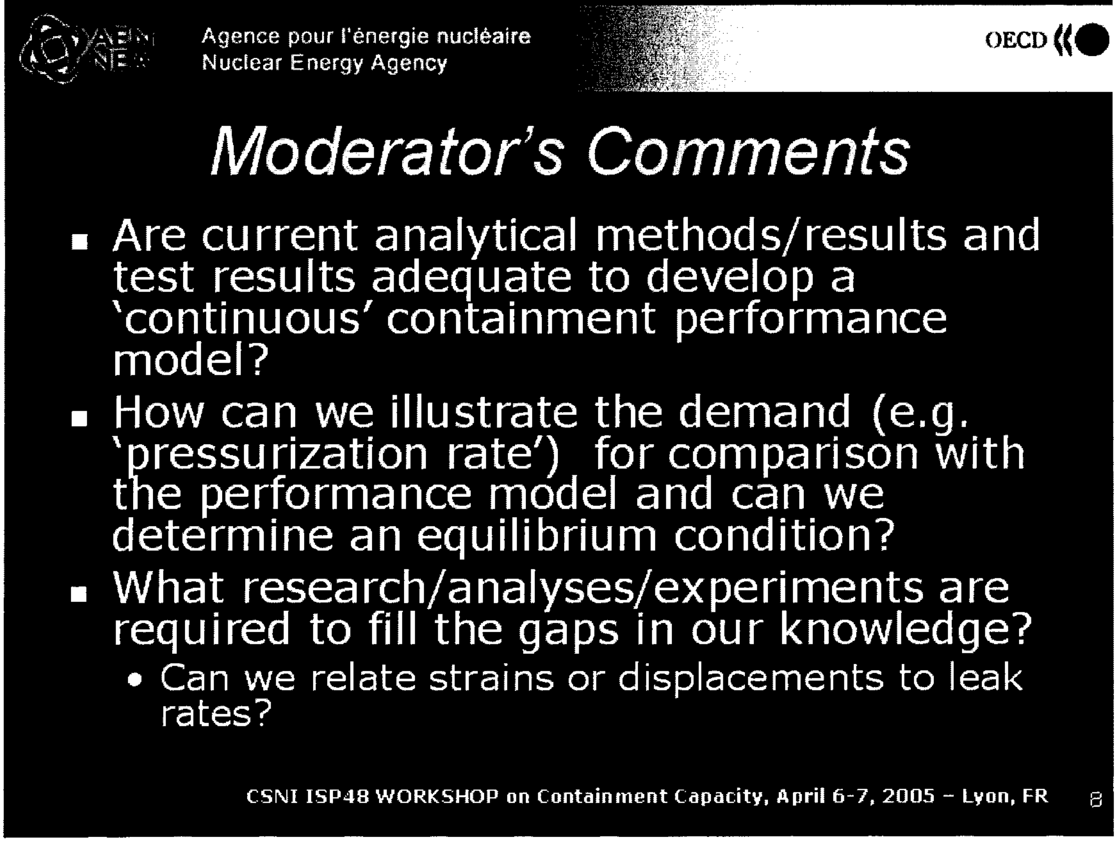

Agence pour l'énergie nucléaire
Nuclear Energy Agency

OECD

Moderator's Comments

- Are current analytical methods/results and test results adequate to develop a 'continuous' containment performance model?
- How can we illustrate the demand (e.g. 'pressurization rate') for comparison with the performance model and can we determine an equilibrium condition?
- What research/analyses/experiments are required to fill the gaps in our knowledge?
  - Can we relate strains or displacements to leak rates?

CSNI ISP48 WORKSHOP on Containment Capacity, April 6-7, 2005 – Lyon, FR 8

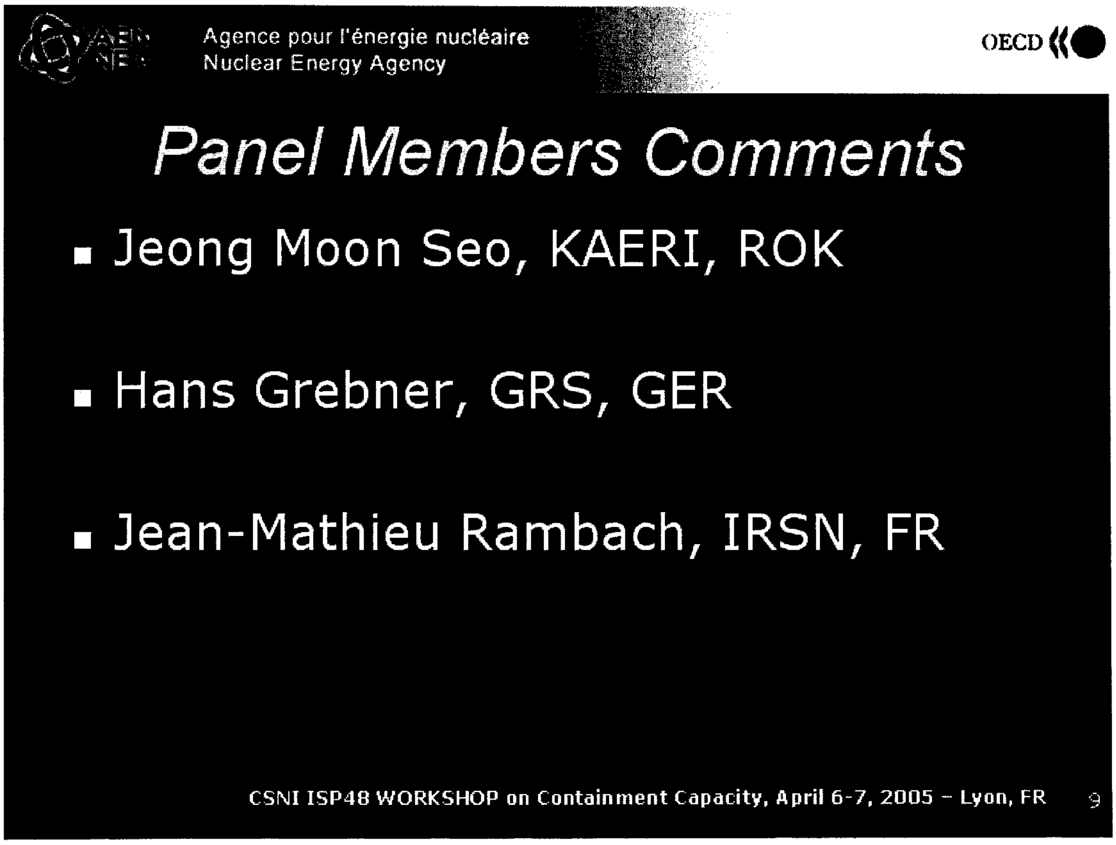

Agence pour l'énergie nucléaire
Nuclear Energy Agency

OECD

Panel Members Comments

- Jeong Moon Seo, KAERI, ROK
- Hans Grebner, GRS, GER
- Jean-Mathieu Rambach, IRSN, FR

Relationship of performance criteria (leakage) with structural response

- We got lots of valuable insights through the ISP 48, both the actual behavior of a PCCV and the ability of the numerical analysis

- Deriving relationship between performance criteria and structural response is desirable, however we need more works;

  ✓ to proportion leakage to each component (containment shell, bellows, E/H seal, Airlock seal). For conservatism, we may assume that all component except containment shell are leaktight.

    - compilation of both test and analysis results are necessary. analysis results presented by IRSN on E/H seal is a good example.

  ✓ to quantify the liner plate tearing in the containment shell

    - liner plate tearing occurs locally and depends much on the design detail and as-built condition (weld defects, geometric imperfection). Effect of these factors needs further study (test and analysis).
    - ISP 48 tests showed that liner plate tearing mostly occurred at the field welds where the liner thickness (before repair) was reduced to ~25% or more.
    - to utilize the ISP 48 test results, it may be worth defining the tensile membrane stain of 0.2 % (0.3%) as the threshold of the local liner tearing as SNL and IRSN suggested.
    - ISP 48 analysis results showed good global containment behavior, however, it gave poor results on the location and extent of the liner tearing. it may be worth analyzing the local behavior of liner using detailed finite element model whether it give similar results to the test one

✓ to quantify the concrete cracking as a function of tensile stress or strain in the containment shell

- cylindrical wall section is subjected to biaxial loads and the reinforcement ratio is the main parameter. Effects of these factors need further study (test and analysis)

  example of KAERI's panel tests:
  -1st through thickness tensile concrete crack occurs at strain of approximately 0.009%
  -liner or rebar yields at strain of 0.2%

- ISP 48 tests showed that cracks occurred at 1.5 ~ 2.0 Pd and visible concrete cracks occurred near the E/H

- ISP 48 analysis: wide spread results in the location and pressure of 1st concrete crack

✓ to quantify the leakage through concrete cracks

- needs further studies (test and analysis) on the variables, analytical models, etc.

  example of KAERI's panel tests:
  -relationship between loads and sum of crack widths
  -relationship between load (or concrete strain) and leakage rate

- ISP 48 test results need to be re-analyzed when the abovementioned relationships are available.

- Compilation of existing test and analysis data maybe worth.

Contribution to topical discussion on „Application of damage or functional performance criteria ...”

Hans Grebner, GRS, Cologne, Germany

Two comments were added to the contribution of M. Hessheimer concerning the use of failure criteria as well as the inclusion of leakage considerations to numerical simulations.

Failure criteria:

From a viewpoint as user of the finite element calculation method it would be desirable to start the definition of failure criteria with measured material data.

- Using measured stress-strain curves, the strain value at uniform elongation might be used as basis for the deduction of a failure strain value.
- The value of the strain at uniform elongation can be decreased by the use of knock-down factors e.g. for
  - the stress triaxiality
  - the material (for instance weldments instead of base material)
  - the analysis accuracy
  - the neglection of geometric details.

An application of these factors to assess the liner tearing was given for instance in the NUREG-report NUREG/CR-6678, appendix C of the pretest round robin analysis of the PCCV model.

Leakage:

Beside the analytical effort to demonstrate the load carrying capacity of containment structures the demonstration of leak tightness is safety relevant. To consider the influence of leakage numerical simulations of the crack formation in concrete structures and the liner, the determination of crack opening due to accident conditions and the calculation of leak rates with consideration of the roughness of the crack faces are necessary.

This is a complex interdisciplinary task, in which an iterative procedure with alternating structural mechanic and thermal hydraulic calculations might be used, and needs adequate effort in development and validation of analytical methods.

For an application in the field of a leaking steel component such an iterative procedure has been studied by GRS for the case of a postulated surge line through wall crack in the coolant loop of a PWR (e.g. in Nuclear Engineering and Design 205 (2001) 219-225).

Panel Discussion o
Leak Before trophic Rupture

Conseque Implications

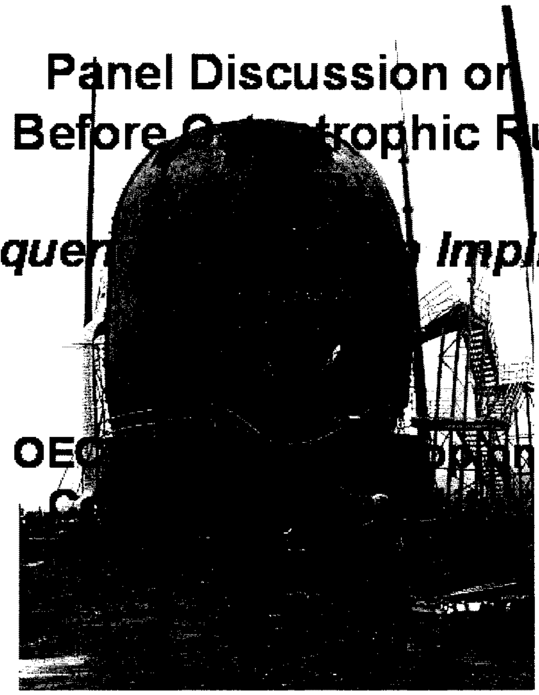

OE
C

Panel Members:
J. Gustavsson (Ringhals AB, SWD),
J. Curley* (NNC, Ltd, UK),
P. Varpasuo (Fortum NS, FIN)

April 6-7, 2005 OECD/CSNI Workshop Lyon

Linking Theory and Practice

Leak vs. Catastrophic rupture: consequences and design implications

- Moderator: J. Rashid (ANATECH, USA)
- Panel Members:
  - **J. Gustavsson (Ringhals AB, SWD),**
  - **J. Curley* (NNC, Ltd, UK),**
  - **P. Varpasuo (Fortum NS, FIN)**

April 6-7, 2005 OECD/CSNI Workshop Lyon

ANATECH
Linking Theory and Practice

Panel Should Attempt to Answer Following Questions

1. Considering current plant safety systems and Post-TMI severe accident studies, is catastrophic rupture a high probability event?
2. If yes, should an engineered LBCR system be imposed on containment design?, or
3. Can we rely on the containment's passive features for LBCR as an alternative?
4. How do we apply lessons learned from ¼-scale model test (and other containment research programs) to answer above questions?

Historical Perspective (Pre & Post-TMI)

- Severe Accident Study WASH-1400, c.1975
  - Simplistic Modeling of "Failure" Modes
  - Defined Containment Performance in terms of Success or Failure to Isolate, with LR as Metric
    - **Design** Leak Rate (LR) = 0.1 v/o /day
    - Containment **Isolation Success** LR ~ 1v/o /day
    - Containment **Isolation Failure** LR ~ 1000 v/o /day

Historical Perspective (Pre/Post-TMI) *(Continued)*

- Severe Accident Study WASH-1400, c.1975
  - A LR of 200 v/o /day Precludes Containment Failure (Catastrophic Rupture)
    - Equivalent to a 10 cm – Diameter Hole
  - Assumes Vessel Breach and Unlimited Water Supply
- NUREG-1150 Updates Accident Sequences and Addresses Accident Management
  - Virtually Precludes Vessel Failure by Maintaining Water in the Vessel

Containment Research Motivated by TMI

- Experimental and Analytical Research by NRC, EPRI, NUPEC and Others in Containment Behavior In the Decade Following TMI
  - NRC/Sandia – 1/6th Scale RC Model
  - EPRI – Structural Elements Tests at CTL
    - Liner-Concrete Interaction
  - Extensive Modeling Work Sponsored by EPRI
    - Led to the Development of Leakage Criteria

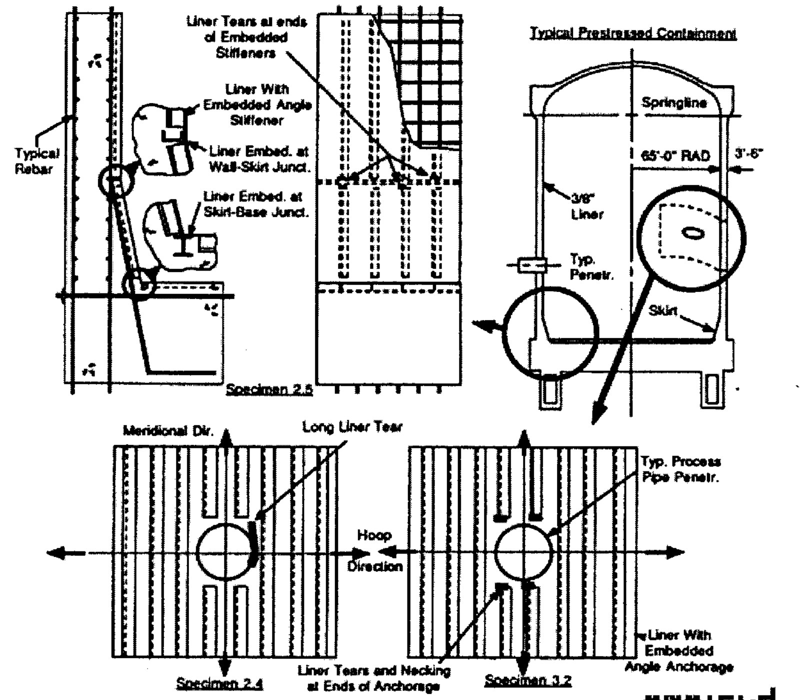
Typical Rebar
Liner Tears at ends of Embedded Stiffeners
Liner With Embedded Angle Stiffener
Liner Embed. at Wall-Skirt Junct.
Liner Embed. at Skirt-Base Junct.
Specimen 2.5
Typical Prestressed Containment
Springline
65'-0" RAD
3'-6"
3/8" Liner
Typ. Penetr.
Skirt
Meridional Dir.
Long Liner Tear
Hoop Direction
Typ. Process Pipe Penetr.
Liner With Embedded Angle Anchorage
Liner Tears and Necking at Ends of Anchorage
Specimen 2.4
Specimen 3.2

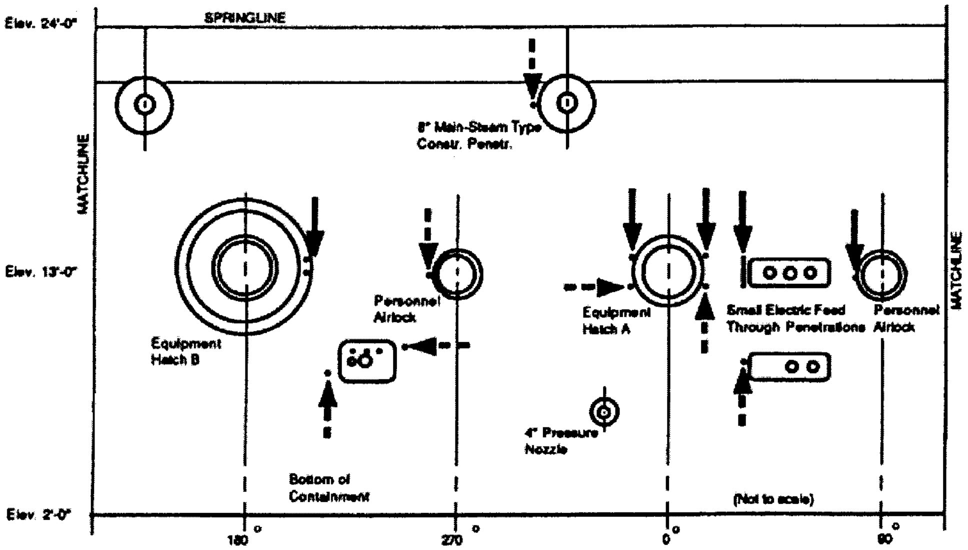
Elev. 24'-0"
SPRINGLINE
MATCHLINE
8" Main-Steam Type Constr. Penetr.
Elev. 13'-0"
Equipment Hatch B
Personnel Airlock
Equipment Hatch A
Small Electric Feed Through Penetrations
Personnel Airlock
MATCHLINE
4" Pressure Nozzle
Bottom of Containment
(Not to scale)
Elev. 2'-0"
180°
270°
0°
90°

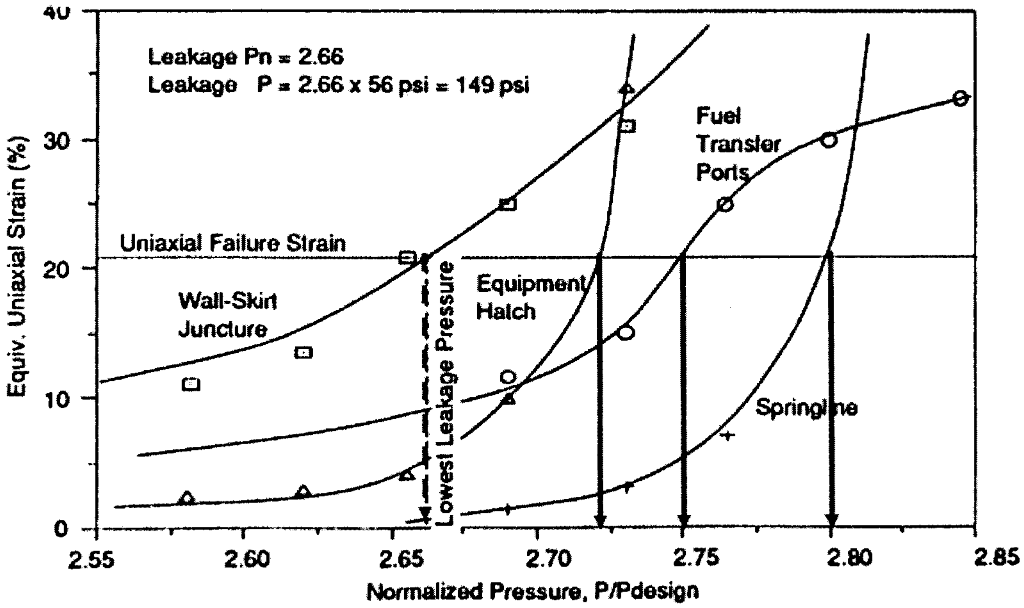

Lessons Learned from 1/4th Scale Model

- Leak Rate = 300v/o /day at 2.5 Design Pressure
  - May have been pre-mature due to liner repair?
  - But would have been inevitable at < 3xDesign ?
  - This would Equilibrate Accident Pressurization Rate
- Unexpectedly Violent Catastrophic Rupture Mode
  - Highly Successful Engineered Failure Mode
  - Water Flashed to Sub-cooled Steam, Enhancing Air-pocket Pressure, Delaying Depressurization and Forming a Water Slug

Design & Operational Implications

- Engineered LBCR Systems
  - **Vents** require operator actions – Not desirable
  - **Rupture discs** require pre-set pressure trigger
    - **Too high could activate pre-mature leakage or CR**
    - **Too low could cause premature release**
  - Both are subject to aging, requiring monitoring and periodic testing
  - Both pose source term issues: rate & concentration
- Passive LBCR
  - Must be Predictable with high degree of certainty
  - Different margins against CR for Pre-stressed and reinforced containments

Leak versus Catastrophic Rupture

Consequences and Design Implications

Contribution by

Panelist J. A. Curley, NNC Ltd

Introduction

- As structural engineers there is no debate. We strive to achieve public safety and the best option is leak before rupture.
- Whether we have leak before rupture is not an engineering issue. We need to raise public awareness of the implications and consequences of striving to design against rupture.

Current Designs

- Leak before rupture is obtained by default and is caused by strain concentration features in the steel liner design and fabrication. There is no engineered control to limit pressure for containments. Thus, there is the possibility of containments of the same design rupturing at different pressures because of fabrication issues.
- Thermal effects: ISP analyses reported margins between liner rupture and catastrophic failure of the containment are either reduced or remain unchanged. No analysis reported an increase in margin. With the current design approach there is no guarantee that as the margins reduce for the range of faults possible in a reactor containment that leakage will remain the initial failure mode.

Analysis of Containments

- The major influences on results are the assumptions in modelling. Participants in the PCCV Round Robin and the ISP have used the same material properties and loads, however large differences are seen in the results obtained. The elastic and early non-linear response is well predicted, but divergence is seen between analysis and test results leading up to containment collapse.
- For confidence in predicting structural response, there is a need to maintain the vessel in an elastic/linear state.

Design Implications

- The functional performance of the containment has to be maintained. The dominant loading in causing containment failure is pressure. Therefore, the maximum achievable pressure should be a design consideration. Hence an engineered pressure controlling system is recommended as the best option.
- Additionally, designing against discontinuities in stiffness for the axisymmetric containment should be considered to alleviate strain concentrations in the steel liner.

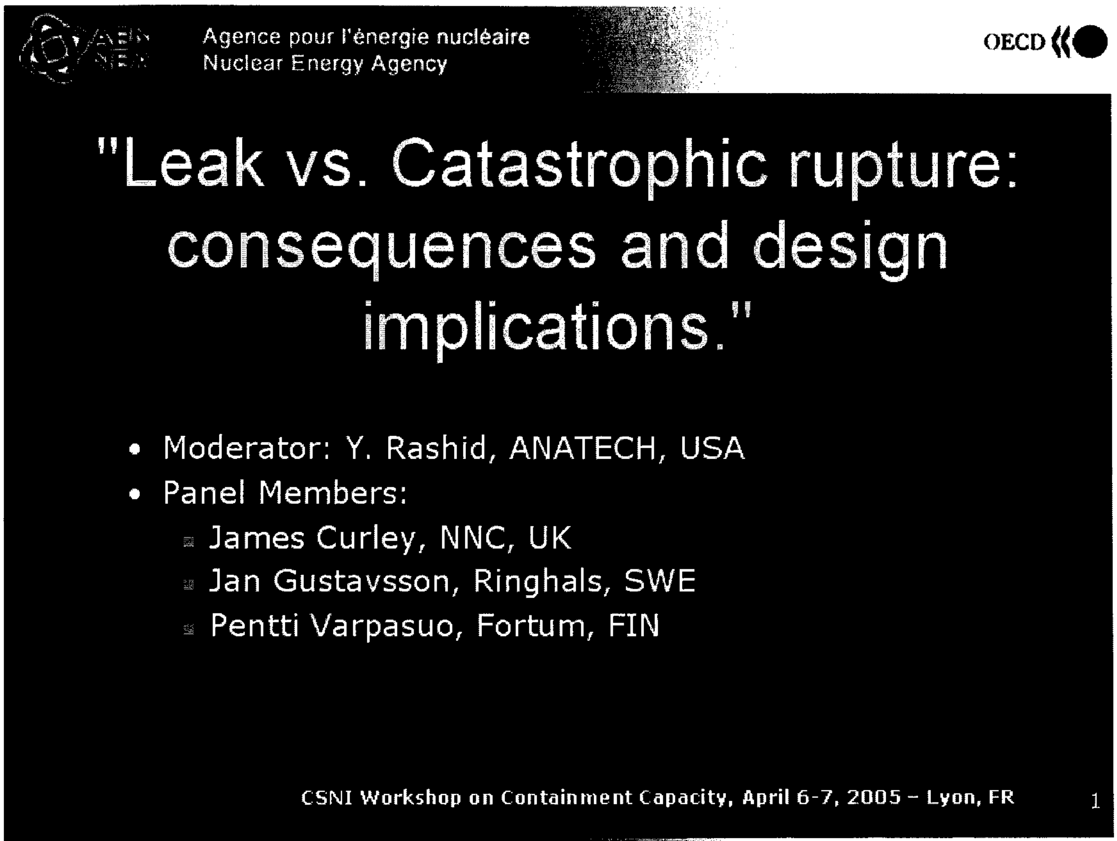

"Leak vs. Catastrophic rupture: consequences and design implications."

- Moderator: Y. Rashid, ANATECH, USA
- Panel Members:
  - James Curley, NNC, UK
  - Jan Gustavsson, Ringhals, SWE
  - Pentti Varpasuo, Fortum, FIN

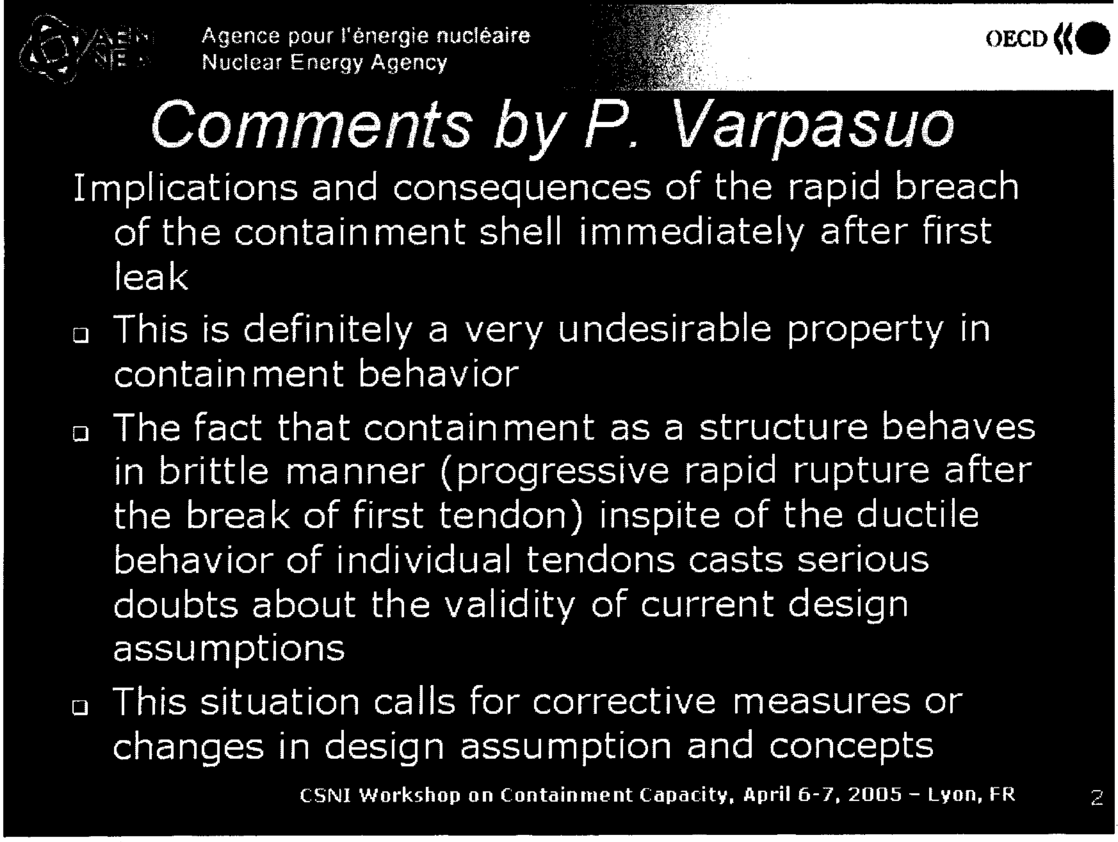

Comments by P. Varpasuo

Implications and consequences of the rapid breach of the containment shell immediately after first leak

- ☐ This is definitely a very undesirable property in containment behavior
- ☐ The fact that containment as a structure behaves in brittle manner (progressive rapid rupture after the break of first tendon) inspite of the ductile behavior of individual tendons casts serious doubts about the validity of current design assumptions
- ☐ This situation calls for corrective measures or changes in design assumption and concepts

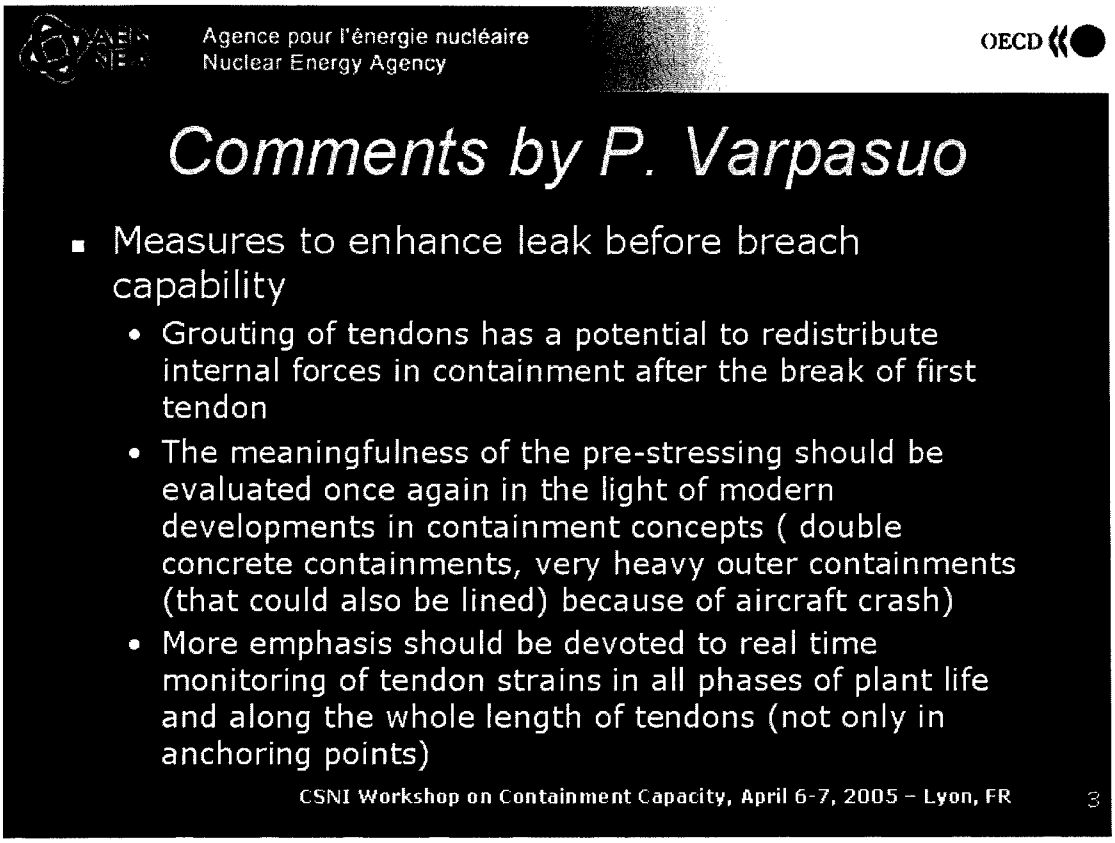

Agence pour l'énergie nucléaire
Nuclear Energy Agency

OECD

Comments by P. Varpasuo

- Measures to enhance leak before breach capability
  - Grouting of tendons has a potential to redistribute internal forces in containment after the break of first tendon
  - The meaningfulness of the pre-stressing should be evaluated once again in the light of modern developments in containment concepts (double concrete containments, very heavy outer containments (that could also be lined) because of aircraft crash)
  - More emphasis should be devoted to real time monitoring of tendon strains in all phases of plant life and along the whole length of tendons (not only in anchoring points)

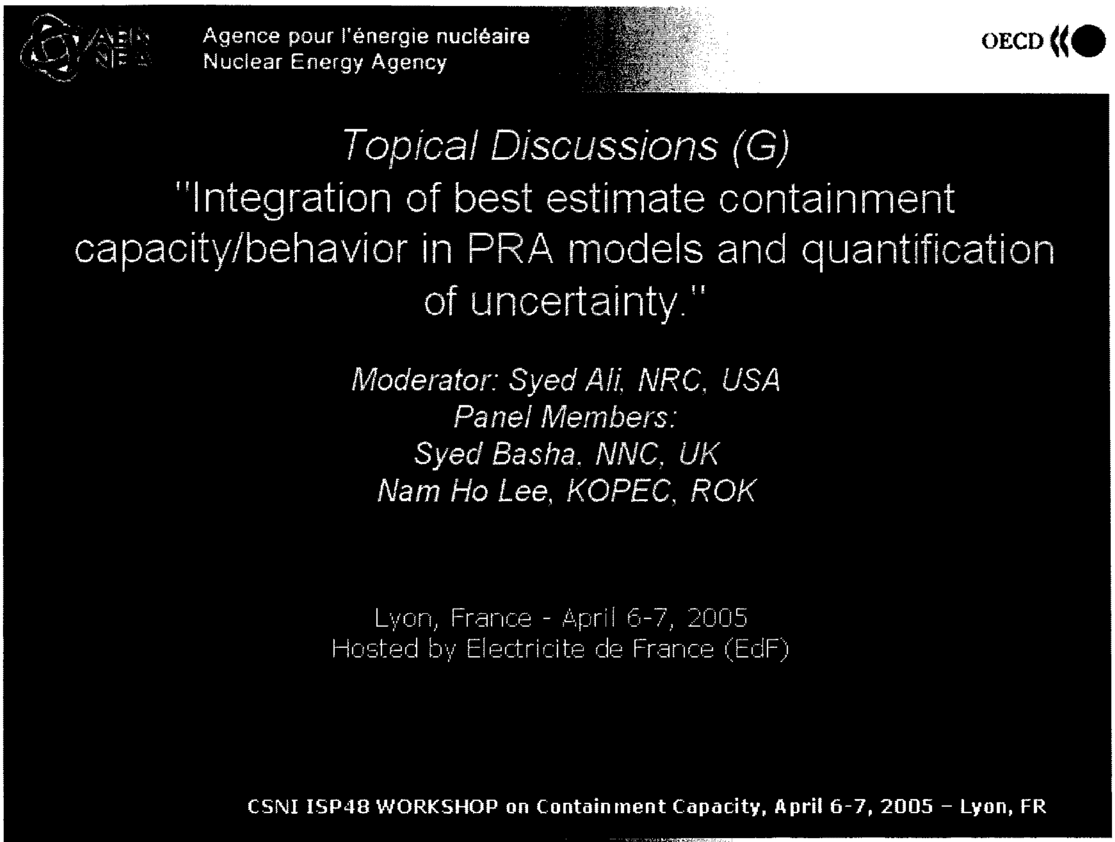

Agence pour l'énergie nucléaire
Nuclear Energy Agency

OECD

Topical Discussions (G)
"Integration of best estimate containment capacity/behavior in PRA models and quantification of uncertainty."

Moderator: Syed Ali, NRC, USA
Panel Members:
Syed Basha, NNC, UK
Nam Ho Lee, KOPEC, ROK

Lyon, France - April 6-7, 2005
Hosted by Electricite de France (EdF)

CSNI ISP48 WORKSHOP on Containment Capacity, April 6-7, 2005 - Lyon, FR

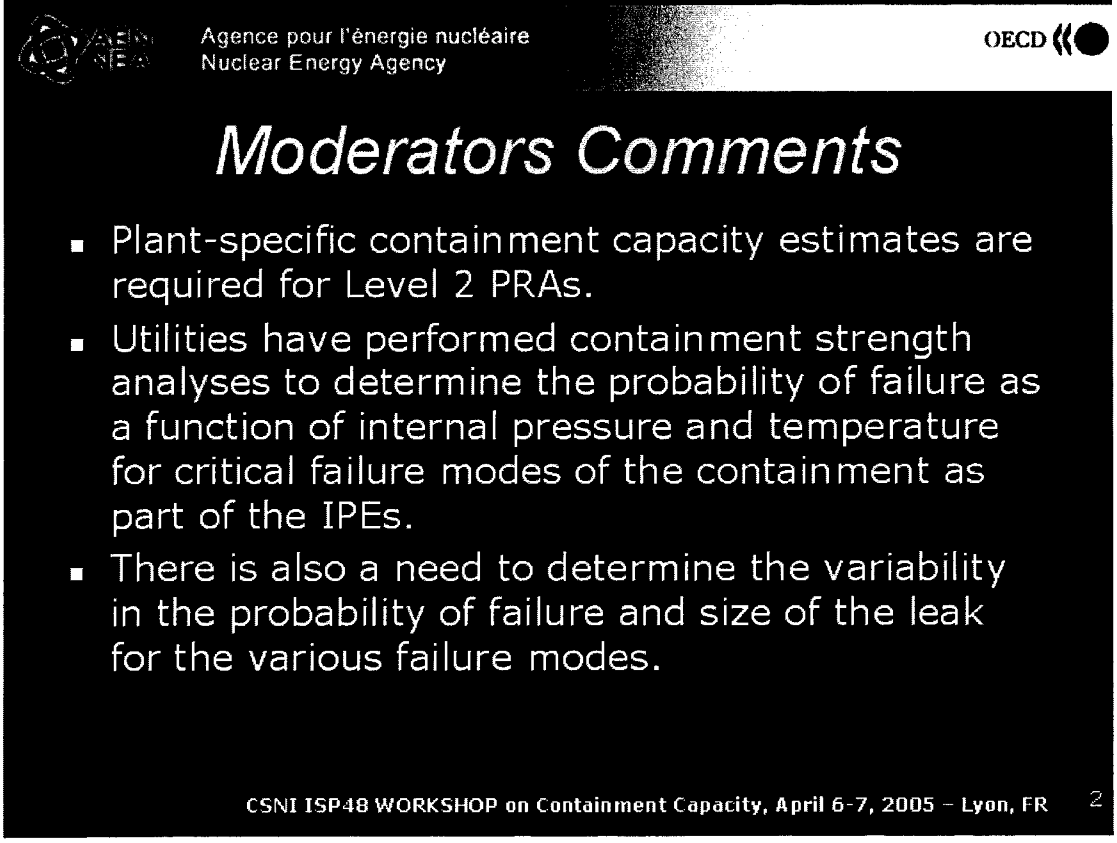

Agence pour l'énergie nucléaire
Nuclear Energy Agency

OECD

Moderators Comments

- Plant-specific containment capacity estimates are required for Level 2 PRAs.
- Utilities have performed containment strength analyses to determine the probability of failure as a function of internal pressure and temperature for critical failure modes of the containment as part of the IPEs.
- There is also a need to determine the variability in the probability of failure and size of the leak for the various failure modes.

CSNI ISP48 WORKSHOP on Containment Capacity, April 6-7, 2005 - Lyon, FR

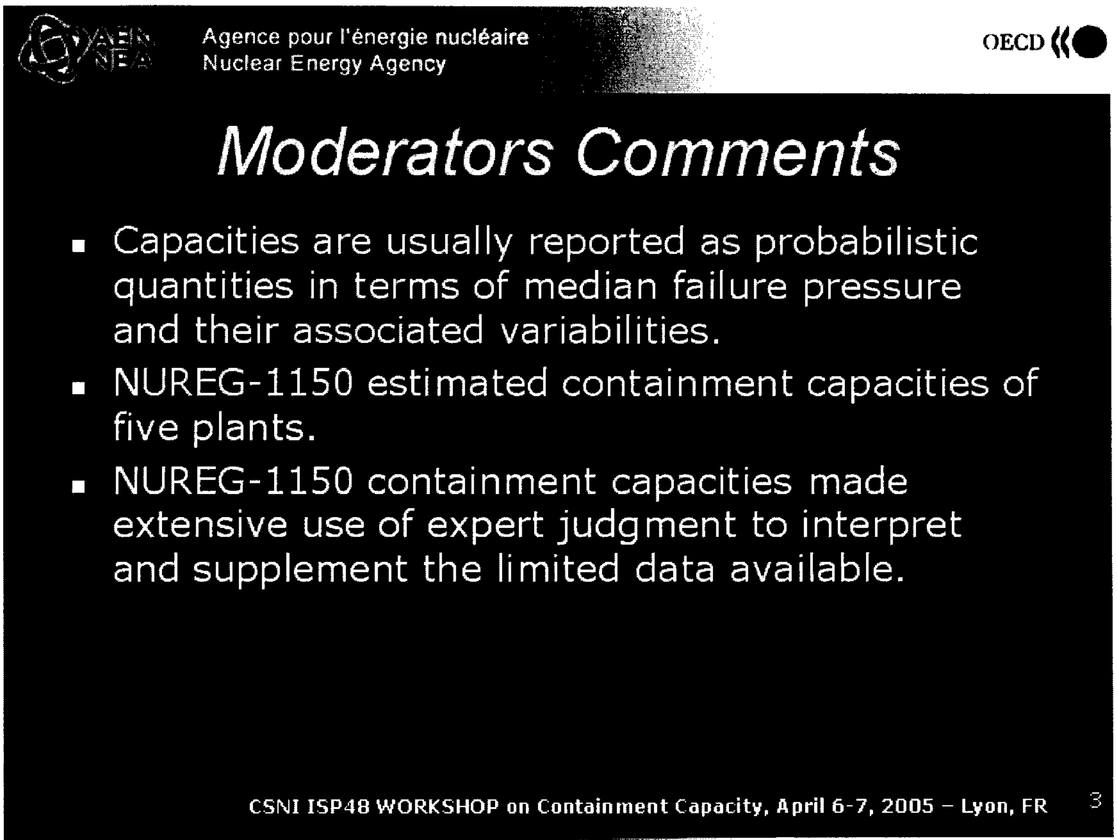

Agence pour l'énergie nucléaire
Nuclear Energy Agency

OECD

Moderators Comments

- Capacities are usually reported as probabilistic quantities in terms of median failure pressure and their associated variabilities.
- NUREG-1150 estimated containment capacities of five plants.
- NUREG-1150 containment capacities made extensive use of expert judgment to interpret and supplement the limited data available.

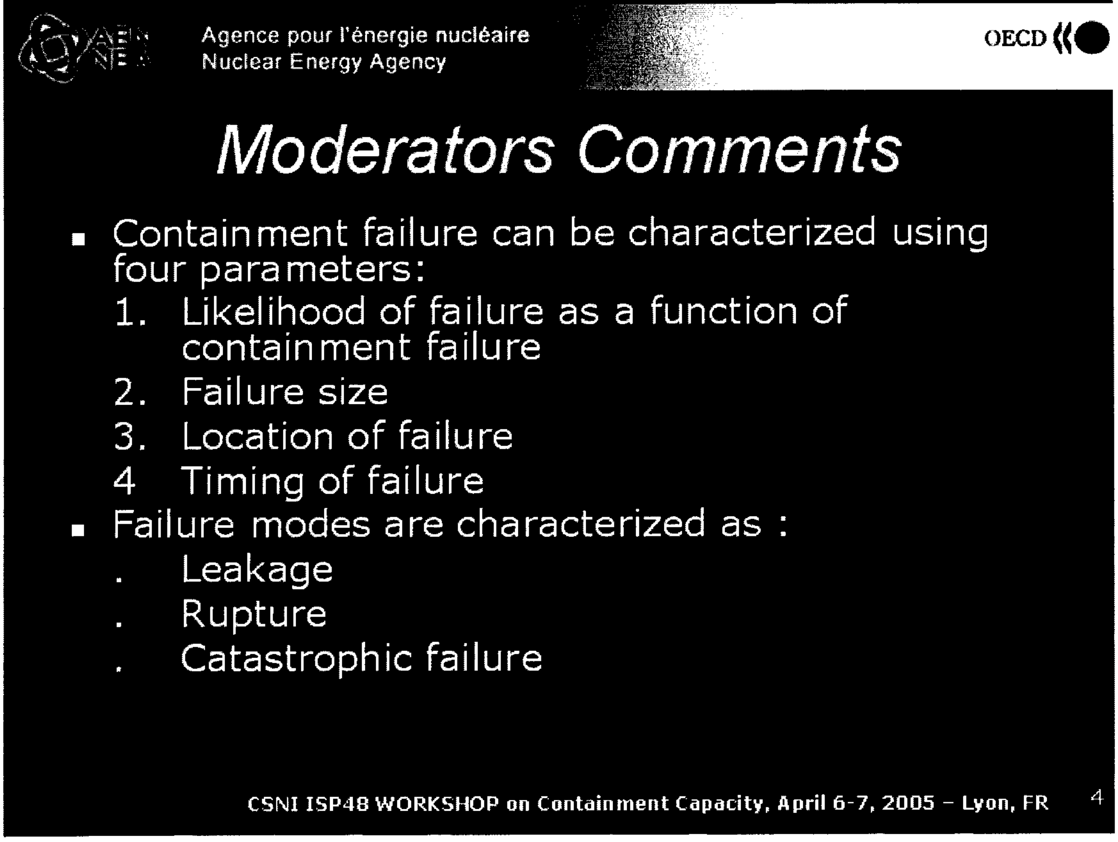

Agence pour l'énergie nucléaire
Nuclear Energy Agency

OECD

Moderators Comments

- Containment failure can be characterized using four parameters:
  1. Likelihood of failure as a function of containment failure
  2. Failure size
  3. Location of failure
  4 Timing of failure
- Failure modes are characterized as :
  . Leakage
  . Rupture
  . Catastrophic failure

Agence pour l'énergie nucléaire
Nuclear Energy Agency

OECD

Moderators Comments

- Sources of uncertainty:
  - . Likelihood of containment failure
  - . Failure size
  - . Location of Failure
  - . Timing of failure
  - . Functional failure mode (leakage, rupture, catastrophic)
  - . Structural failure mode:
    - rebar and tendon failure criteria
    - liner failure criteria
    - steel containment failure criteria

CSNI ISP48 WORKSHOP on Containment Capacity, April 6-7, 2005 - Lyon, FR

Agence pour l'énergie nucléaire
Nuclear Energy Agency

OECD

Moderators Comments

- Areas of future research:

. Develop confirmatory data and analyses on the structural capacity and failure modes for a variety of containment designs.

. Revise regulatory guidance for containment designs to incorporate risk informed approach instead of deterministic approach for design.

CSNI ISP48 WORKSHOP on Containment Capacity, April 6-7, 2005 - Lyon, FR

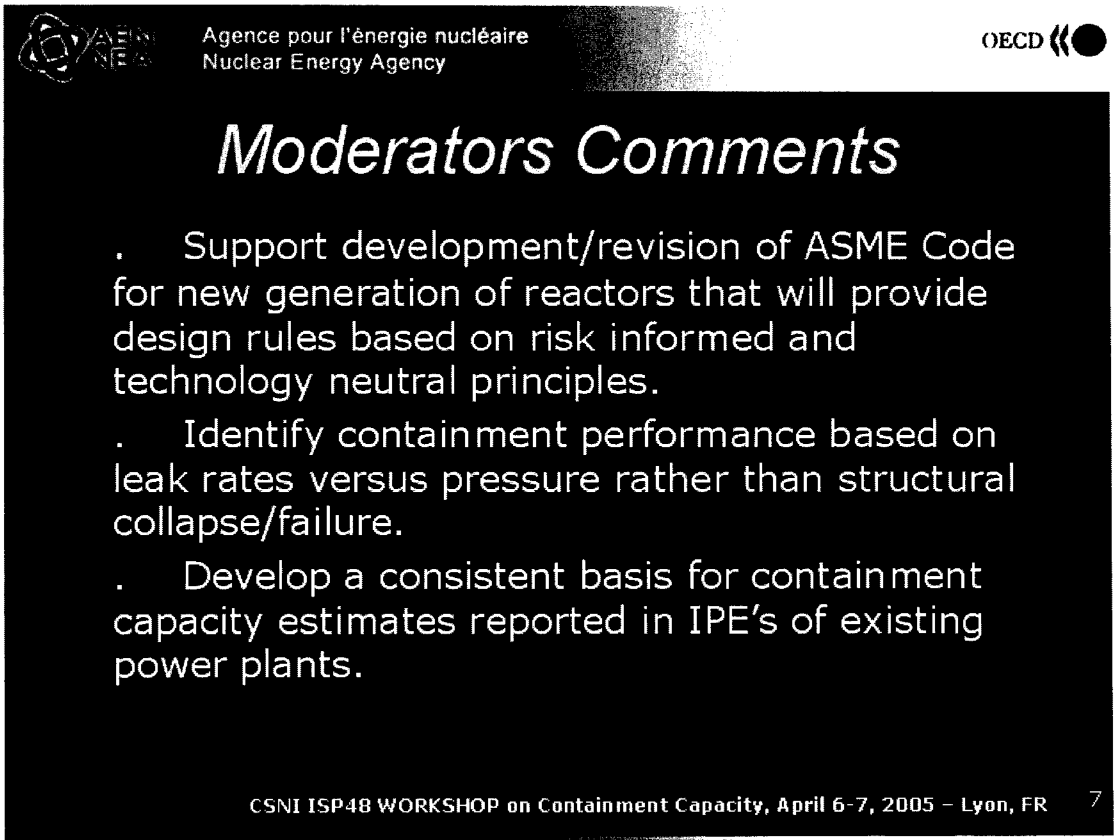

Agence pour l'énergie nucléaire
Nuclear Energy Agency

OECD

Moderators Comments

- Support development/revision of ASME Code for new generation of reactors that will provide design rules based on risk informed and technology neutral principles.
- Identify containment performance based on leak rates versus pressure rather than structural collapse/failure.
- Develop a consistent basis for containment capacity estimates reported in IPE's of existing power plants.

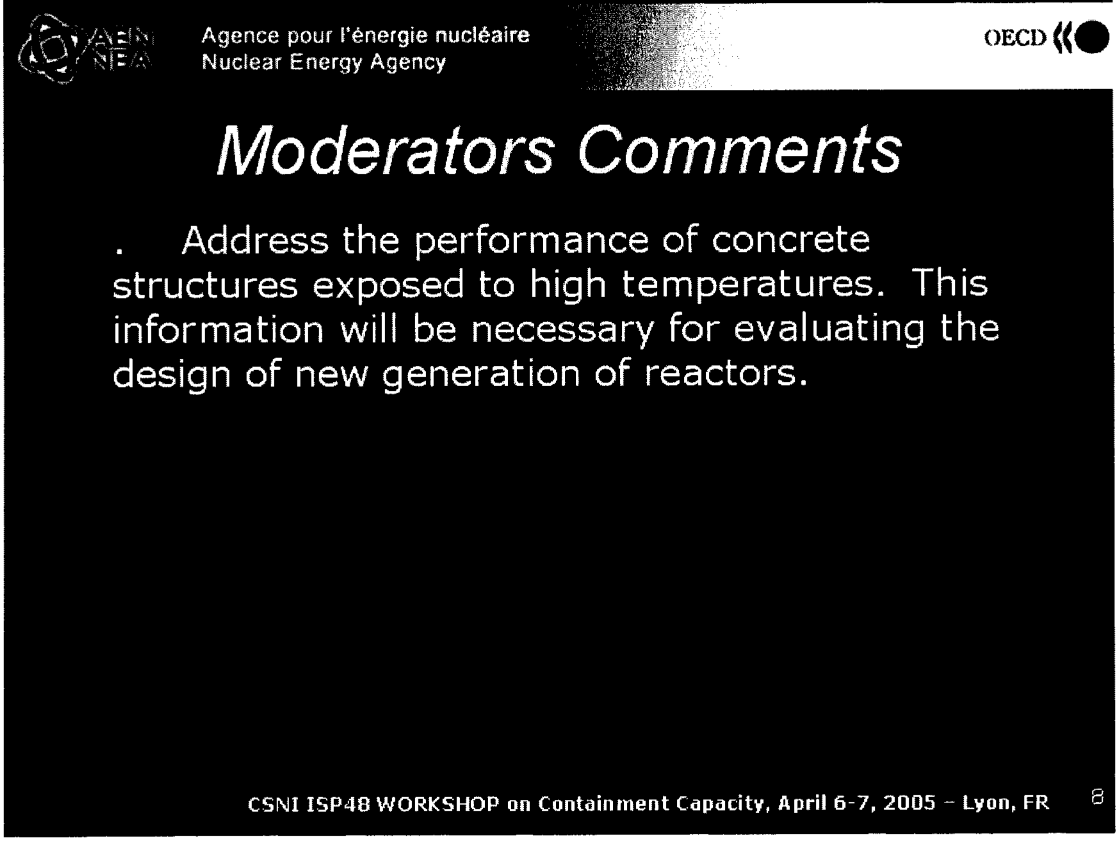

Agence pour l'énergie nucléaire
Nuclear Energy Agency

OECD

Moderators Comments

- Address the performance of concrete structures exposed to high temperatures. This information will be necessary for evaluating the design of new generation of reactors.

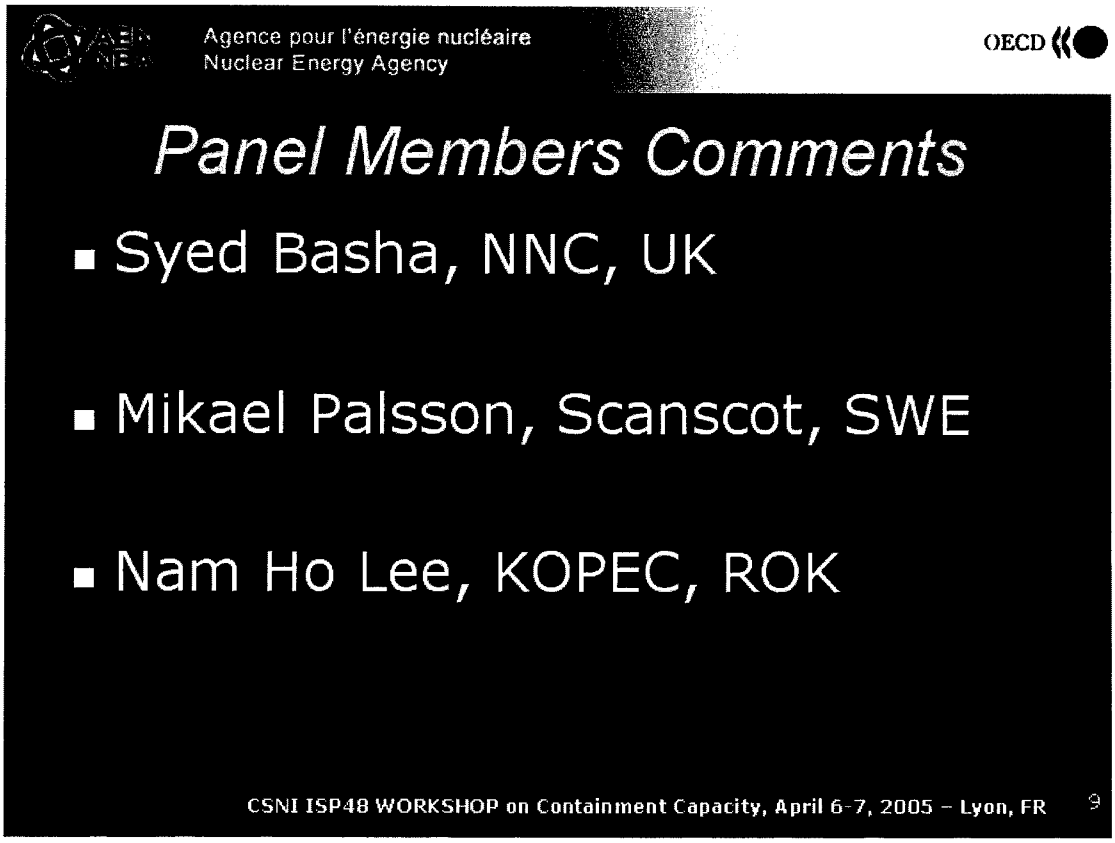

Agence pour l'énergie nucléaire
Nuclear Energy Agency

OECD

Panel Members Comments

- Syed Basha, NNC, UK
- Mikael Palsson, Scanscot, SWE
- Nam Ho Lee, KOPEC, ROK

CSNI ISP48 WORKSHOP on Containment Capacity, April 6-7, 2005 - Lyon, FR

OECD Workshop Topical Discussions

Syed M Basha

Bhabha Atomic Research Centre

Mumbai, India

Engineering Integrity and Performance

Objective

1. **Upper bound – 95% Confidence**
2. **Best Estimate – 95% Confidence**
3. **Lower bound estimate – 95 % Confidence**

No guidance/criteria was SET

Engineering Integrity and Performance

Probabilistic approach

- **Lower bound – Elastic - perfectly plastic material behaviour**
- **Best estimate- Strain hardening material data supplied**
- **Upper bound – Increase in prestressing with containment dilation**
- **6 cases analysed to account for liner material property variation**

Engineering Integrity and Performance

Probabilistic Analysis

- **The COV was very small**

Engineering Integrity and Performance

Entegra-NNC

INDIAN Containment Research Programme

HSE

- **1:4 scaled UNLINED prestressed concrete containment model test**
- **Failure location**
- **Failure mode**
- **Leak size**
- **Planned for 2009**

Engineering Integrity and Performance

CSNI Workshop - International Standard Problem 48

Integration of best estimate containment capacity/behavior in PRA models and quantification of uncertainty

(April 6-7, 2005)

Panel member : Nam Ho Lee, KOPEC, ROK

KOPEC 한국전력기술주식회사

Korea Power Engineering Company, Inc

- **PRA approach determines:**
  - **The median internal pressure at which failure of the containment will occur**
  - **The associated variability from which the conditional probability of failure for a given level of internal pressure can be estimated**
- **Identification of failure modes**
  - **The failure modes may be associated with the structure itself, as in the case of wall failure due to membrane stresses,**

    or with non-structure elements such as major wall penetrations
  - **A careful identification of potential failure modes is necessary to assure that modes governing the risk of radioactive release are properly included in the evaluation**
  - **Required a detailed review of the information on the containment structure, including structural drawings, material test data, containment penetration details, the results of previous containment performance studies, and the available test results**

- **Development of containment fragilities**
  - **To assist in defining the risk associated with any of the postulated overpressure scenarios, compute the fragilities for the postulated containment failure modes, along with their estimated leak areas**
  - **A simplified fragility model formulated as the product of the median internal capacity at failure and a random variable representing uncertainty in the median pressure capacity can be used**
- **Simplified fragility model**
  - **The distribution of containment pressure capacity can be defined in terms of only two quantities:**
    - The median internal pressure capacity : derived from existing analyses, engineering judgement, or additional limit state analyses
    - The lognormal standard deviation associated with uncertainty
  - **Estimate the median centered capacities**

- **Variability in Material Properties**
  - **The median material properties and variabilities of the followings will be used together with stress-strain relations.**
    - **Concrete Compressive Strength**
    - **Reinforcing Steel bars**
    - **Effects of Mechanical Splices**
    - **Prestressing Tendon Strength**
  - **The uncertainties associated with the factor are results of variabilities in the material properties of rebar, concrete, liner and prestressing tendon**

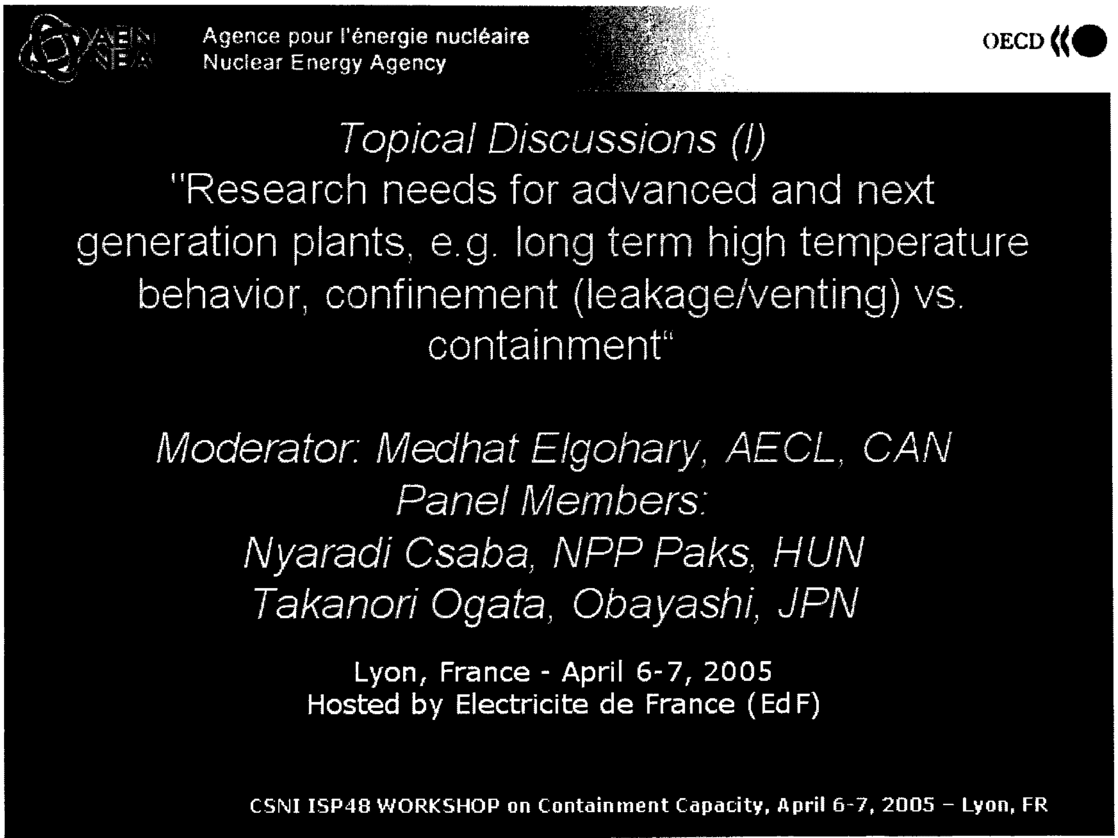

Agence pour l'énergie nucléaire
Nuclear Energy Agency

OECD

Topical Discussions (I)
"Research needs for advanced and next generation plants, e.g. long term high temperature behavior, confinement (leakage/venting) vs. containment"

Moderator: Medhat Elgohary, AECL, CAN
Panel Members:
Nyaradi Csaba, NPP Paks, HUN
Takanori Ogata, Obayashi, JPN

Lyon, France - April 6-7, 2005
Hosted by Electricite de France (EdF)

CSNI ISP48 WORKSHOP on Containment Capacity, April 6-7, 2005 – Lyon, FR

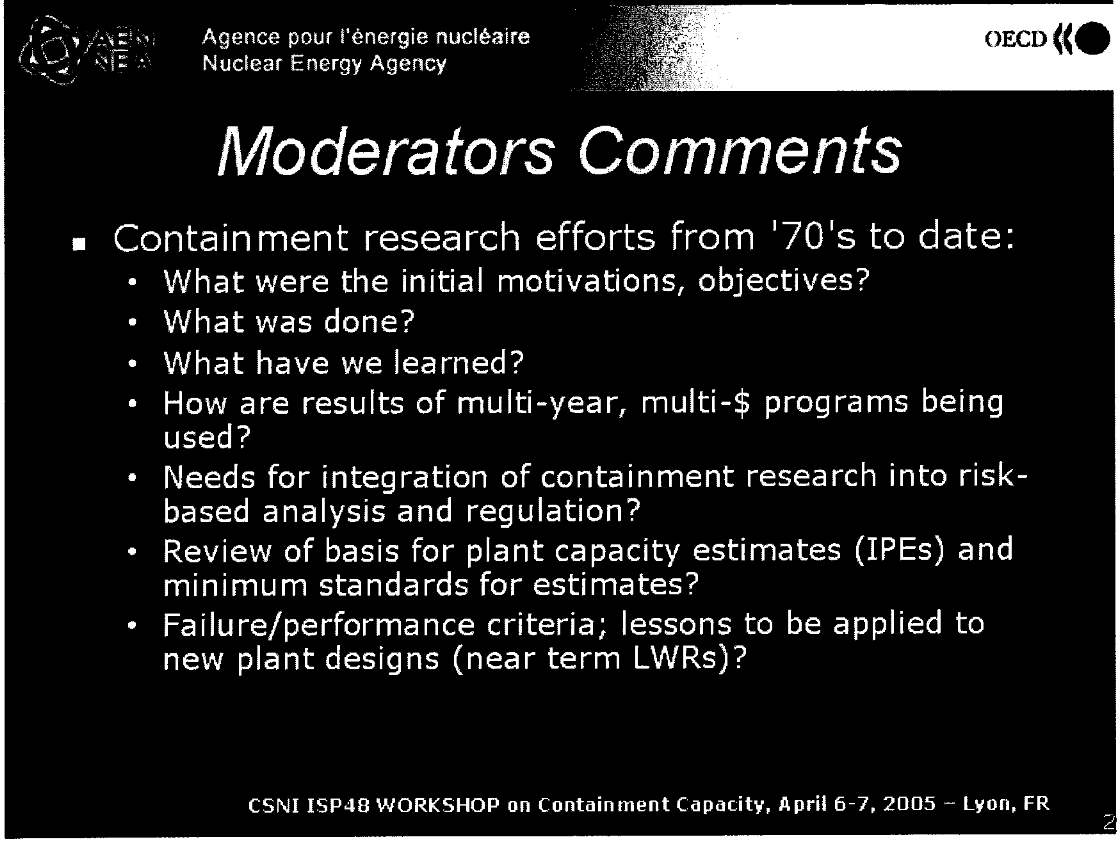

Agence pour l'énergie nucléaire
Nuclear Energy Agency

OECD

Moderators Comments

- Containment research efforts from '70's to date:
  - What were the initial motivations, objectives?
  - What was done?
  - What have we learned?
  - How are results of multi-year, multi-$ programs being used?
  - Needs for integration of containment research into risk-based analysis and regulation?
  - Review of basis for plant capacity estimates (IPEs) and minimum standards for estimates?
  - Failure/performance criteria; lessons to be applied to new plant designs (near term LWRs)?

CSNI ISP48 WORKSHOP on Containment Capacity, April 6-7, 2005 – Lyon, FR

2

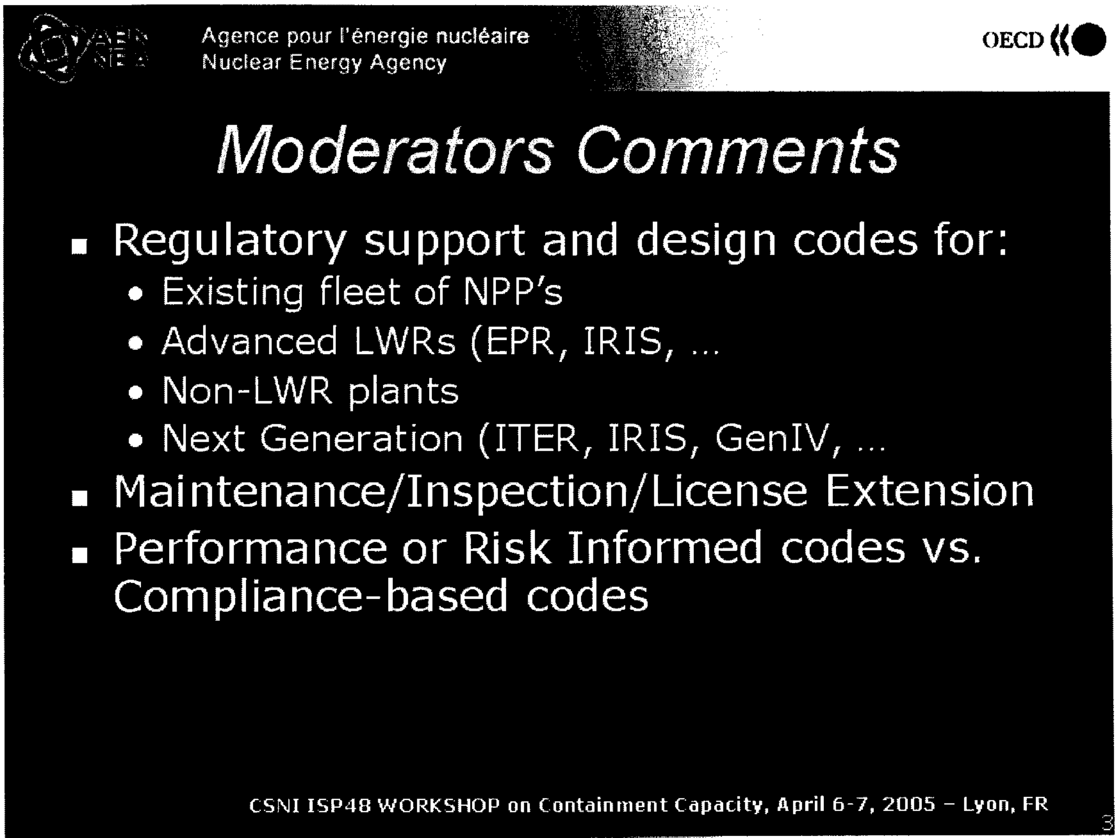

Agence pour l'énergie nucléaire
Nuclear Energy Agency

OECD

Moderators Comments

- Regulatory support and design codes for:
  - Existing fleet of NPP's
  - Advanced LWRs (EPR, IRIS, ...
  - Non-LWR plants
  - Next Generation (ITER, IRIS, GenIV, ...
- Maintenance/Inspection/License Extension
- Performance or Risk Informed codes vs. Compliance-based codes

CSNI ISP48 WORKSHOP on Containment Capacity, April 6-7, 2005 – Lyon, FR

3

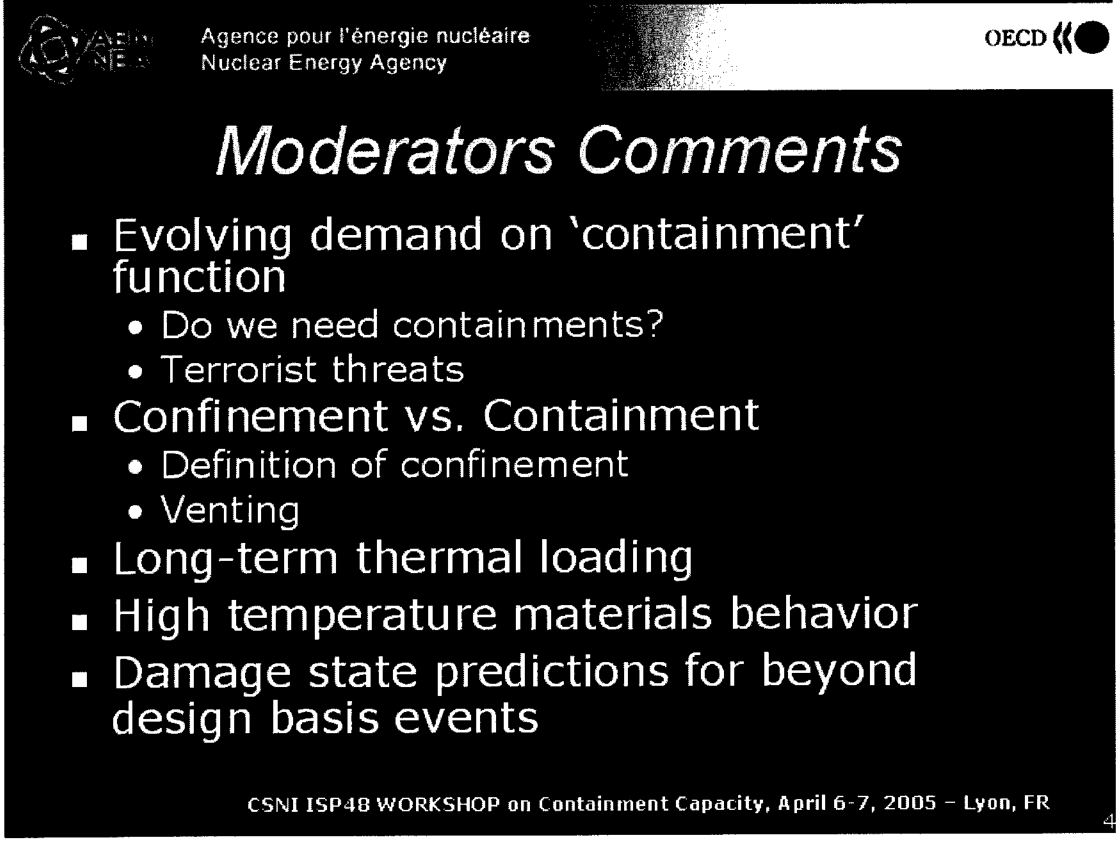

Agence pour l'énergie nucléaire
Nuclear Energy Agency

OECD

Moderators Comments

- Evolving demand on 'containment' function
  - Do we need containments?
  - Terrorist threats
- Confinement vs. Containment
  - Definition of confinement
  - Venting
- Long-term thermal loading
- High temperature materials behavior
- Damage state predictions for beyond design basis events

CSNI ISP48 WORKSHOP on Containment Capacity, April 6-7, 2005 – Lyon, FR

4

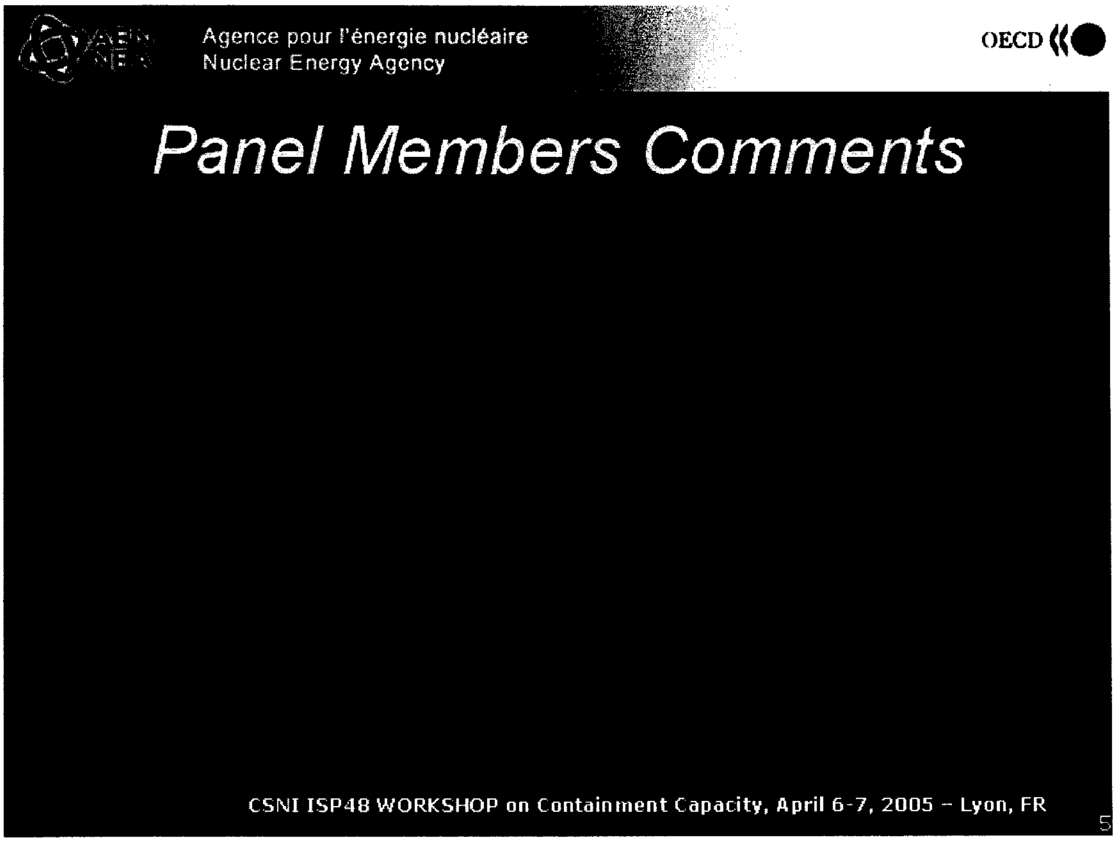

Agence pour l'énergie nucléaire
Nuclear Energy Agency

OECD

Panel Members Comments

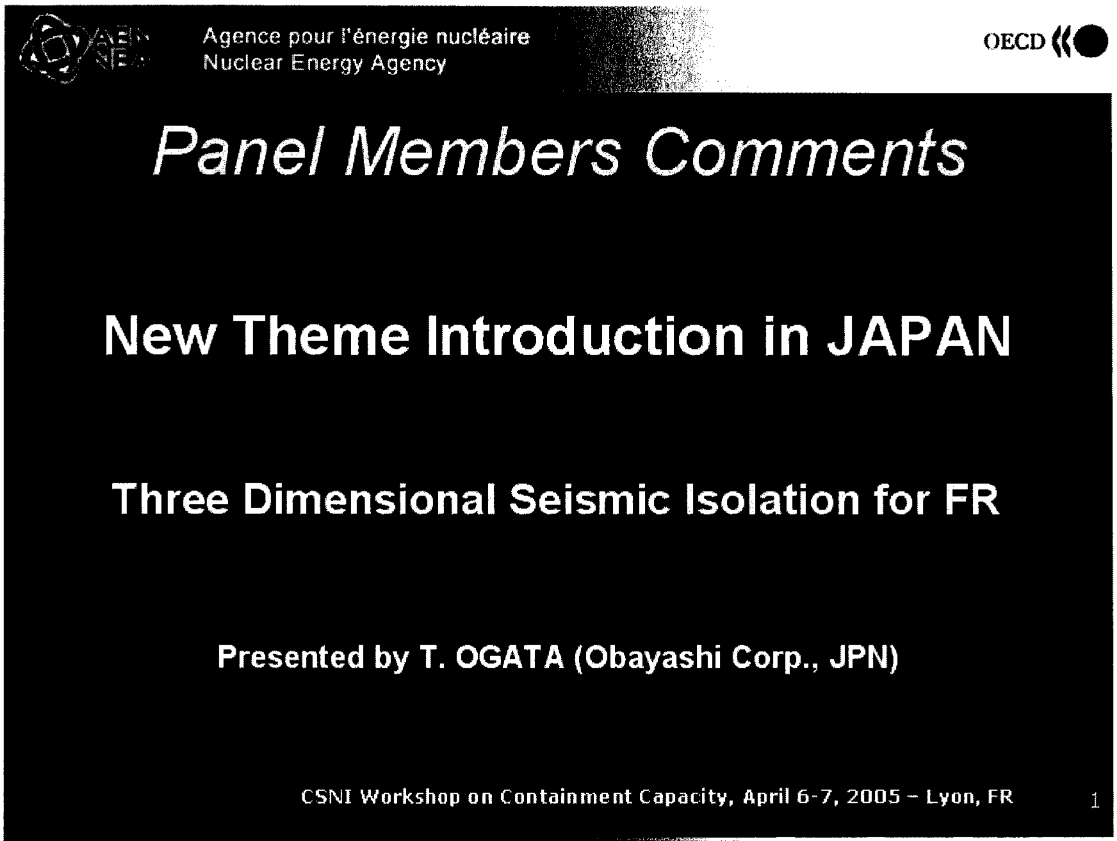

Agence pour l'énergie nucléaire
Nuclear Energy Agency

OECD

Panel Members Comments

New Theme Introduction in JAPAN

Three Dimensional Seismic Isolation for FR

Presented by T. OGATA (Obayashi Corp., JPN)

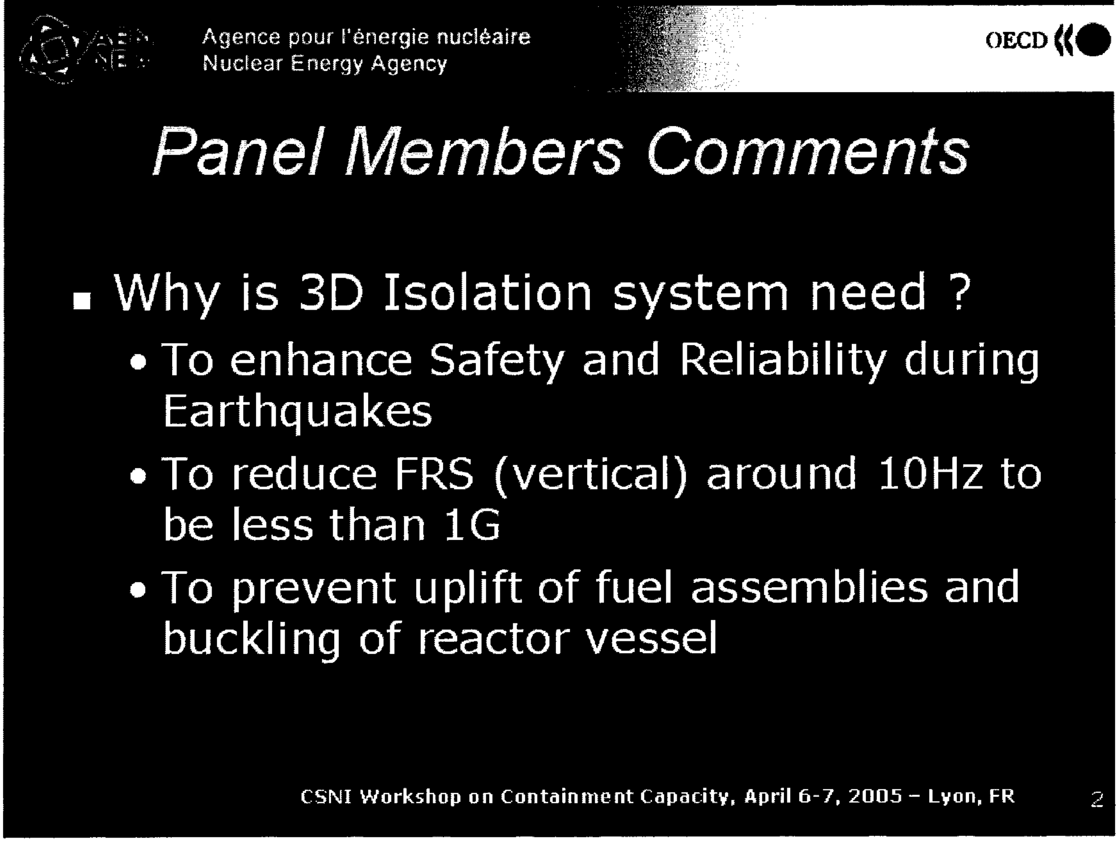

Agence pour l'énergie nucléaire
Nuclear Energy Agency

OECD

Panel Members Comments

- Why is 3D Isolation system need ?
  - To enhance Safety and Reliability during Earthquakes
  - To reduce FRS (vertical) around 10Hz to be less than 1G
  - To prevent uplift of fuel assemblies and buckling of reactor vessel

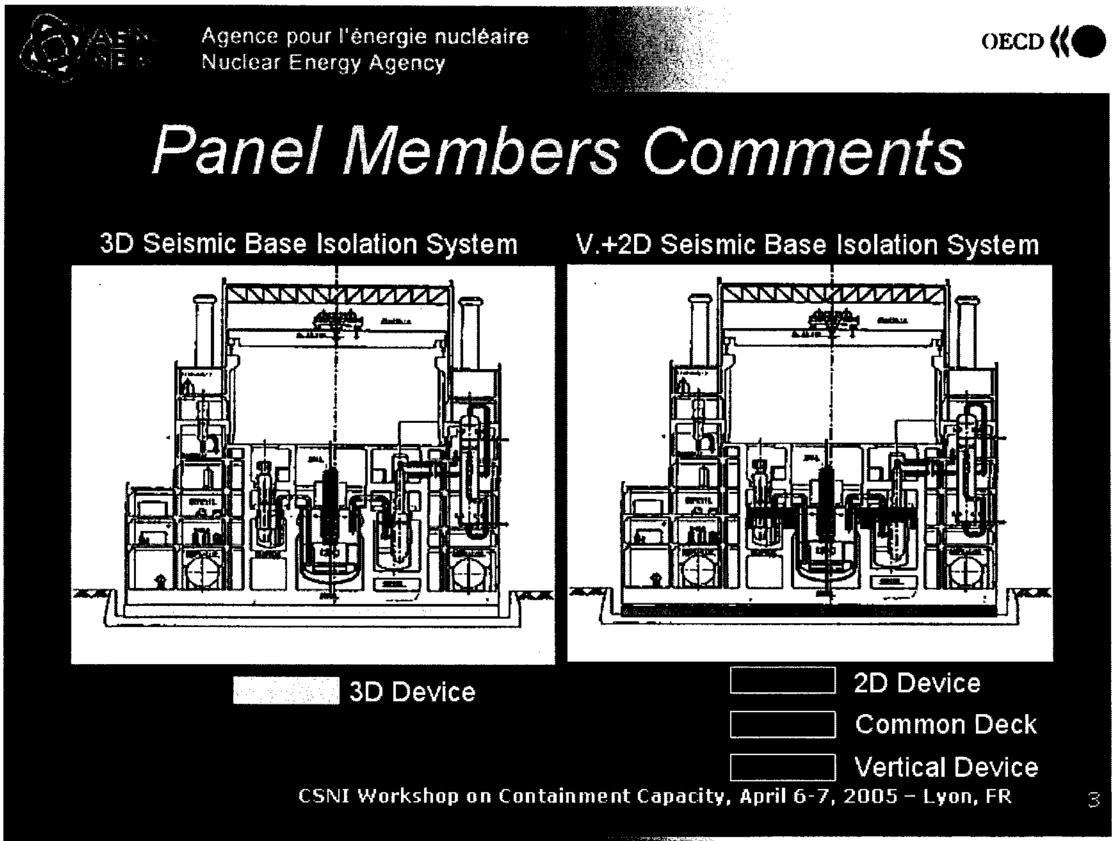

Agence pour l'énergie nucléaire
Nuclear Energy Agency

OECD

Panel Members Comments

3D Seismic Base Isolation System

V.+2D Seismic Base Isolation System

▭ 3D Device

▭ 2D Device

▭ Common Deck

▭ Vertical Device

CSNI Workshop on Containment Capacity, April 6-7, 2005 – Lyon, FR

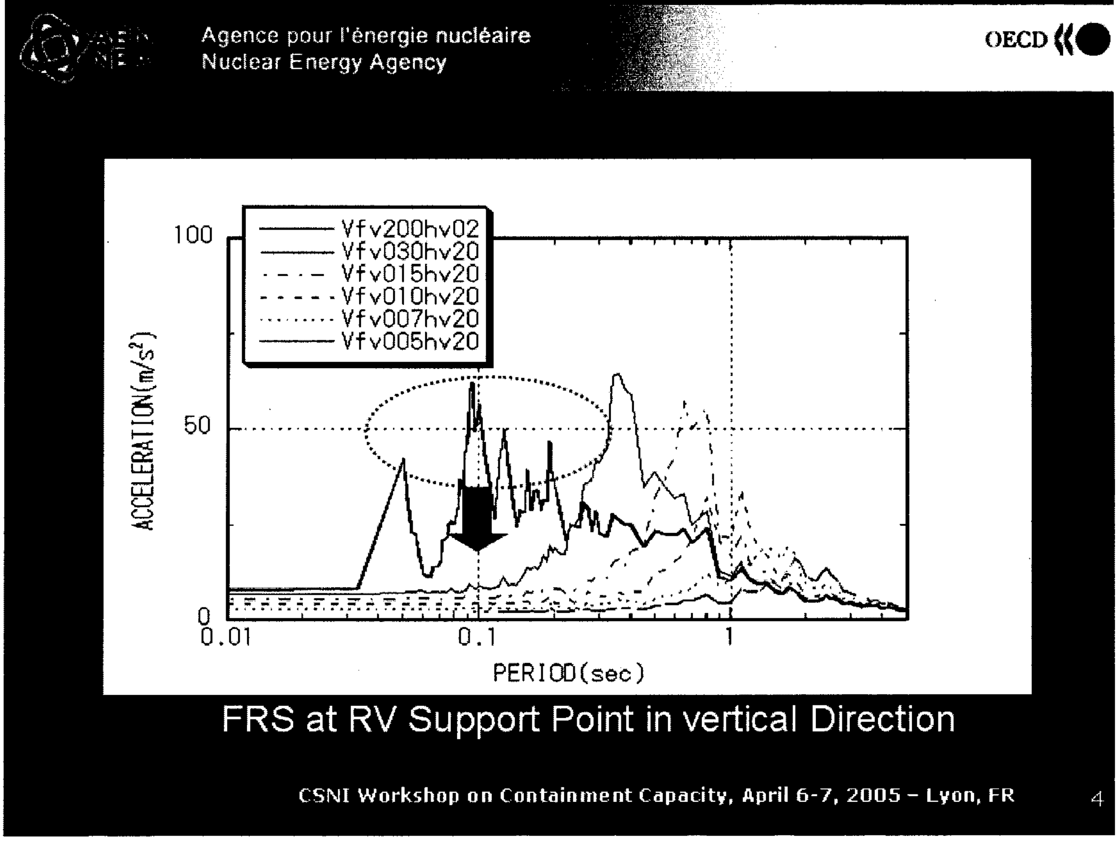

Agence pour l'énergie nucléaire
Nuclear Energy Agency

OECD

FRS at RV Support Point in vertical Direction

CSNI Workshop on Containment Capacity, April 6-7, 2005 – Lyon, FR

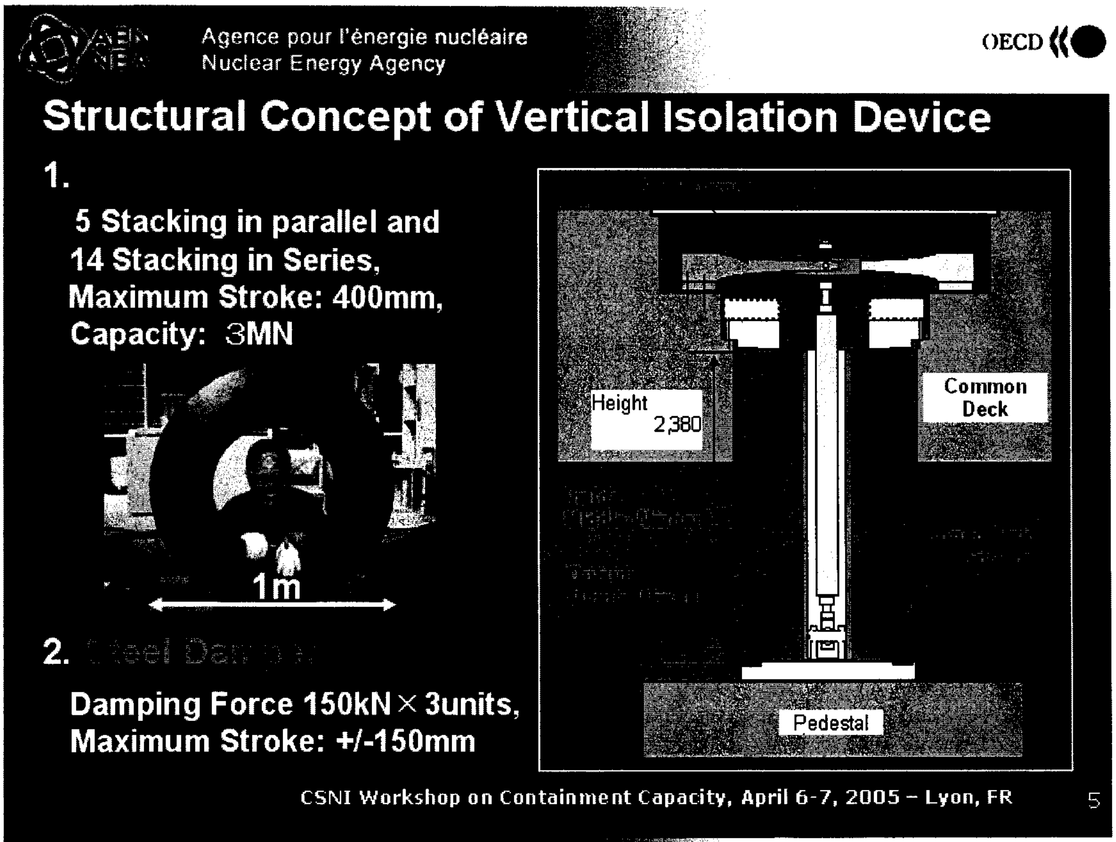

Agence pour l'énergie nucléaire
Nuclear Energy Agency

OECD

Structural Concept of Vertical Isolation Device

1.

5 Stacking in parallel and
14 Stacking in Series,
Maximum Stroke: 400mm,
Capacity: 3MN

2. Steel Damper

Damping Force 150kN × 3units,
Maximum Stroke: +/-150mm

CSNI Workshop on Containment Capacity, April 6-7, 2005 – Lyon, FR

5

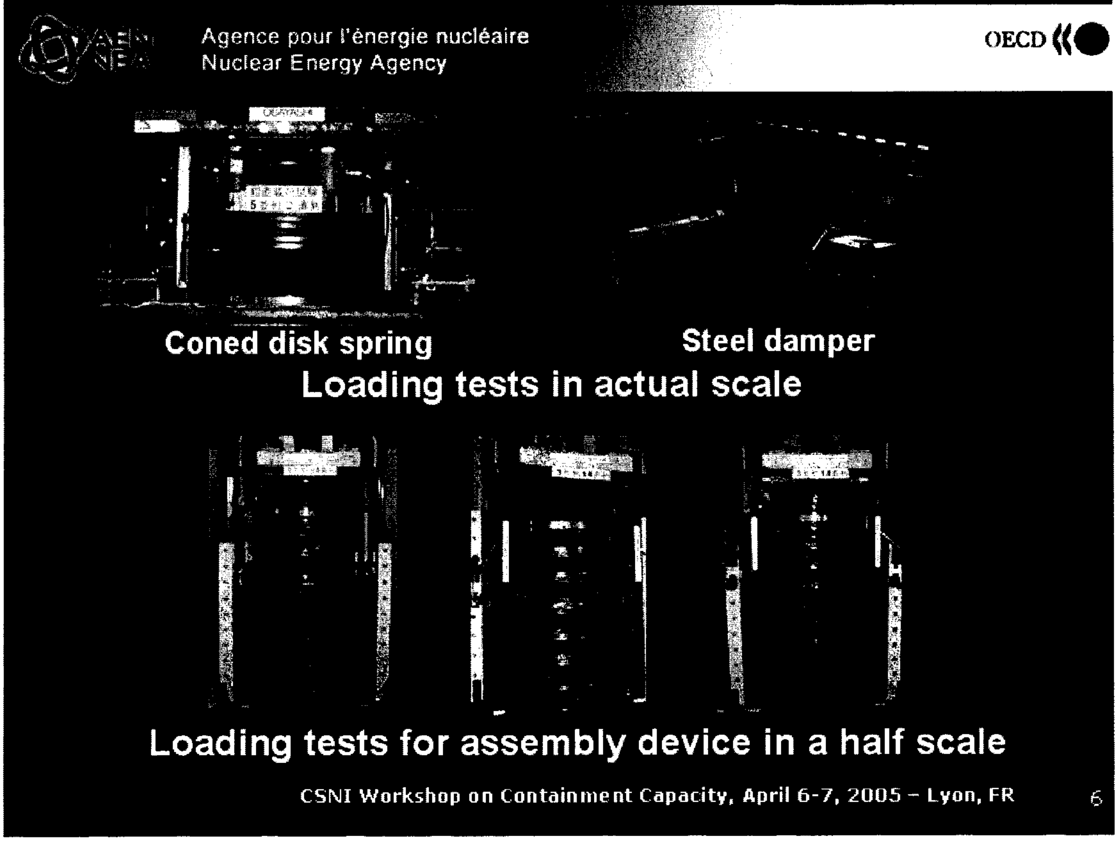

Agence pour l'énergie nucléaire
Nuclear Energy Agency

OECD

Coned disk spring

Steel damper

Loading tests in actual scale

Loading tests for assembly device in a half scale

CSNI Workshop on Containment Capacity, April 6-7, 2005 – Lyon, FR

6

LIST OF PARTICIPANTS

BELGIUM
Mr. Luc DE MARNEFFE
Chief Engineer
TRACTEBEL Engineering
division de SUEZ-TRACTEBEL S.A.
Avenue Ariane 7
1200 Bruxelles

Tel: +32 2 773 81 48
Fax: +32 2 773 89 70
Eml: luc.demarneffe@tractebel.be

CANADA
Mr. Medhat ELGOHARY
Manager of Civil Engineering
AECL
2251 Speakman Drive
MISSISSAUGA, Ont L5K 1B2

Tel: +1 (905) 823 9060 X2135
Fax: +1 (905) 403 7307
Eml: elgoharm@aecl.ca

CZECH REPUBLIC
Mr. Jan STEPAN
UJV Rez div. Energoprojekt Praha
Energoprojekt Praha a.s.
Vyskocilova 3
P.O. Box 158
140 21 Prague 4

Tel: +420 2 4100 6421
Fax: +420 2 41006409
Eml: stepan@egp.cz

FINLAND
Dr. Pentti E. VARPASUO
Principal Engineer
Fortum Nuclear Services Ltd.
POB 10, 00048 Fortum,
Rajatorpantie 8, Vantaa
FIN-01019

Tel: +358 10 45 32223
Fax: +358 10 45 33355
Eml: pentti.varpasuo@fortum.com

Mr. Erkki VESIKARI
Senior Research Scientist
VTT Building and Transport
P.O. Box 1800
FIN-02044 VTT

Tel: +358 20 722 6922
Fax: +358 20 722 7060
Eml: erkki.vesikari@vtt.fi

FRANCE

Mr.BertrandCIREE
IRSN
DES/SAMS
77-83 Avenue du Général de Gaulle
B.P. 17
92265 Fontenay-aux-Roses
Tel: +33(0)1 58357026
Fax: +33(0)1 58351014
Eml: bertrand.ciree@irsn.fr

M. Alexis COURTOIS
EDF
Ingénieur Génie Civil
EDF SEPTEN
Division Génie Civil, Installations et Structures
Groupe Dynamique et Séisme
Tel: +33 472 827324
Fax:+33 472 827713
Eml: alexis.courtois@edf.fr

Mr. Shahrokh GHAVAMIAN
Edf
1 avenue du Général de Gaulle
Boîte postale 408
92141 Clamart cedex
Tel: +33 1.47.65.48.11
Fax:+33 147 654118
Eml: shahrokh.ghavamian@edf.fr

Prof.Pierre LABBE
EDF SEPTEN
12-14 av Dutriévoz
69628 VILLEURBANNE Cedex
Tel: + 33 (4)72827528
Fax:
Eml: Pierre.labbe@edf.fr

M. Bertrand PERRACINO
EDF-SEPTEN
12-14 avenue Dutriévoz
69628 VILLEURBANNE
Tel:
Fax:
Eml: bertrand.perracino@edf.fr

Mr. Jean Mathieu RAMBACH
DSR/SAMS CE FAR
IRSN
77-83 Avenue du General de Gaulle
B.P. 17
92265 Fontenay aux Roses
Tel: +33 (0)1 58 35 8028
Fax: +33 (0)1 58 35 1014
Eml: mathieu.rambach@irsn.fr

Mr Nishizawa TOMOHIRO
Deputy Director
JEPIC
422 rue Saint Honore
75008 Paris
Tel: +33 1-4286-9011
Fax: +33 1-4286-9070
Eml: nishizawa@club.ntt.fr

Mr.Jean-Pierre TOURET
Civil Engineering Expert
EDF/SEPTEN
12-14 Avenue Dutrievoz
69628 VILLEURBANNE Cedex

Tel: +33472 827554
Fax: +33 4 72 82 77 07
Eml: jean-pierre.touret@edf.fr

GERMANY

Dr. Hans GREBNER
Structural Mechanics Dept
Gesellschaft für Anlagen-und
Reaktorsicherheit (GRS) mbH
Schwertnergasse 1
D-50667 KOLN

Tel: +49 221 2068 738
Fax: +49 221 2068 442
Eml: grb@grs.de

HUNGARY

Prof. Dr. Peter LENKEI
Professor Emeritus of Structural Engineering
PÉCS University,
College of Engineering H-7624 PECS
Boszorkany U.2

Tel: +36 72 503 650 ext 3837
Fax: +36 72 503 650 ext 2801
Eml: lenkeip@witch.pmmf.hu

Mr. Csaba NYARADI
Systems Technologist
Nuclear Power Plant Paks
H-7031 PAKS P.O.B. 71

Tel: +36 7550 7054
Fax: +36 7550 7334
Eml: nyaradi@npp.hu

JAPAN

Mr Masaaki OBA
Mitoshiro Bldg.,
1-1, Kanda-Mitoshiro-cho Chiyoda-ku
Tokyo101-0053

Tel: +81 3-4415-6514
Fax: +81 3-4415-6514
Eml: masaaki-ohba@japc.co.jp

Mr Ogata TAKANORI
Manager
Obayashi Corporation
2-15-2, Konan, Minato-ku,
Tokyo 108-8502

Tel: +81 3-5769-2718
Fax: +81 3-5769-1943
Eml: ogata.takanori@obayashi.co.jp

KOREA (REPUBLIC OF)

Dr. Seo JEONG-MOON
Project Manager
Korea Atomic Energy Research Ins.
P.O. Box 105, Yusong, Daejon,
305-600, Korea

Tel: +82 42-868-8371
Fax: +82 42-868-8256
Eml: jmseo@kaeri.re.kr

Dr. Nam-Ho LEE
Engineering Group Supervisor
Civil Engineering Department
Korea Power Engineering Company, Inc.
360-9 Mabuk-ri, Guseong-eup
Yongin-si, Gyeonggi-do 449-713
Tel: +82 31 899 2205
Fax: +82 31 899 2095
Eml: nhlee@kopec.co.kr

Il Hwan MOON
Senior Engineer
Civil Engineering Department
Korea Power Engineering Company, Inc.
360-9 Mabuk-ri, Guseong-eup
Yongin-si, Gyeonggi-do 449-713
Tel: +82 31 899 2251
Fax:
Eml: youmoon@kopec.co.kr

Dr. Jeong-Moon SEO
Project Manager
Korea Atomic Energy Research Institute
Project Manager
Dukjindong 150
Yusongku, Daejon
Tel: +82 42 868 8371
Fax: +82 42 868 8256
Eml: jmseo@kaeri.re.kr

SLOVAK REPUBLIC

Mr. Juraj NOZDROVICKY
Project Manager
VUEZ, a.s.
Hviezdoslavova 35
934 01 LEVICE
Tel: +421 36631 3665
Fax: +421 36631 3663
Eml: junoz@vuez.sk

SLOVENIA

Mr. Bozo KOGOVSEK
Project Manager
IBE Consulting Engineers
Hajdrihova 4
1000 Ljubljana
Tel: +386 1 477 62 03
Fax: +386 1 251 05 27
Eml: bozo.kogovsek@ibe.si

SWEDEN

Mr. Patrick ANDERSON
Division of Structural Engineering
Lund University
P.O. Box 18
SE-22100 LUND
Tel: +46 46 29843
Fax: +46 46 24212
Eml: patrick.anderson@kstr.lth.se

Mr.Jan GUSTAVSSON
Ringhals Nuclear Power Plant
Ringhals AB
S-430 22 VAROBACKA
Tel:+46340 667950
Fax: +46 3 40 66 83 89
Eml: jan.gustavsson@ringhals.se

Mr. OLA JOVALL
Head of Engineering Department
Scanscot Technology AB
Ideon Research Park
SE-223 70 LUND
Tel: +46 46 28 62 338
Fax: +46 46 12 87 45
Eml: jovall@scanscot.com

Mr. Mikael PALSSON
Scanscot Technology AB
Ideon Research Park
SE-223 70 LUND
Tel: +46 2862337
Fax: +46 12 87 45
Eml: palsson@scanscot.com

Mr. Konstantinos XANTHOPOULOS
Swedish Nucler Power Inspectorate
Department of Reactor Technology and
Structural Integrity (SKI)
S 10658 Stockholm
Tel: +46 8 698 84 00
Fax: +46 8 6619086
Eml: Kostas.Xanthopoulos@ski.se

UNITED KINGDOM

Mr James CURLEY
Structural Analyst
NNC Ltd
Booths Hall,
Chelford Road,
Knutsford, Cheshire,
Tel: +44 (0)1565 843195
Fax:
Eml: jim.curley@entegra-nnc.co.uk

Mr Syed MAHABOOB BASHA
Commonwealth Scholar
NNC, Limited
Booths Hall, Chelford Road
Knutsford, Cheshire WA16 8QZ
Tel: +44 1565 843541
Fax: +44 1565 633659
Eml: Syed.Mahaboob-Basha@nnc.co.uk

Dr Nawal PRINJA
Technical Manager
NNC Limited
Booths Hall
Knutsford
Cheshire WA16 8QZ
Tel: +44 (0) 1565 843201
Fax: +44 (0) 1565 843024
Eml: Nawal.Prinja@nnc.co.uk

UNITED STATES OF AMERICA

Dr Syed ALI
U.S. NRC
Senior Advisor for Civil/Structural Issues
Mail Stop T-10 D-20
Washington DC 20555
Tel: +1 301-415-5704
Fax: +1 301-415-5074
Eml: saa3@nrc.gov

Dr. Michael F. HESSHEIMER
Sandia National Laboratories
Dept. 6403
P.O. Box 5800
Albuquerque, NM 87185-0744
Tel: +1 (505) 844 6229
Fax: +1 (505) 844 1648
Eml: mfhessh@sandia.gov

Dr. Joseph RASHID
Chairman
Anatech Research Corp.
5435 Oberlin Drive
San Diego, California
USA 92121
Tel: +1 858 455 6350
Fax: +1 858 455 1094
Eml: joe@anatech.com

International Organisations

OECD Nuclear Energy Agency, Issy-les-Moulineaux
Mr. Eric MATHET
OECD-NEA
Nuclear Safety Division
Le Seine St-Germain
12 bd des Iles
F-92130 ISSY-LES-MOULINEAUX
Tel: +33 1 4524 1057
Fax: +33 1 4524 1129
Eml: eric.mathet@oecd.org